

The Subnuclear Series • Volume 41

Proceedings of the International School of Subnuclear Physics

FROM QUARKS TO BLACK HOLES: PROGRESS IN UNDERSTANDING THE LOGIC OF NATURE

Edited by

Antonino Zichichi

World Scientific

The Subnuclear Series • Volume 41

Proceedings of the International School of Subnuclear Physics

**FROM QUARKS TO BLACK
HOLES: PROGRESS IN
UNDERSTANDING THE
LOGIC OF NATURE**

THE SUBNUCLEAR SERIES

Series Editor: ANTONINO ZICHICHI, European Physical Society, Geneva, Switzerland

1. 1963 STRONG, ELECTROMAGNETIC, AND WEAK INTERACTIONS
2. 1964 SYMMETRIES IN ELEMENTARY PARTICLE PHYSICS
3. 1965 RECENT DEVELOPMENTS IN PARTICLE SYMMETRIES
4. 1966 STRONG AND WEAK INTERACTIONS
5. 1967 HADRONS AND THEIR INTERACTIONS
6. 1968 THEORY AND PHENOMENOLOGY IN PARTICLE PHYSICS
7. 1969 SUBNUCLEAR PHENOMENA
8. 1970 ELEMENTARY PROCESSES AT HIGH ENERGY
9. 1971 PROPERTIES OF THE FUNDAMENTAL INTERACTIONS
10. 1972 HIGHLIGHTS IN PARTICLE PHYSICS
11. 1973 LAWS OF HADRONIC MATTER
12. 1974 LEPTON AND HADRON STRUCTURE
13. 1975 NEW PHENOMENA IN SUBNUCLEAR PHYSICS
14. 1976 UNDERSTANDING THE FUNDAMENTAL CONSTITUENTS OF MATTER
15. 1977 THE WHYS OF SUBNUCLEAR PHYSICS
16. 1978 THE NEW ASPECTS OF SUBNUCLEAR PHYSICS
17. 1979 POINTLIKE STRUCTURES INSIDE AND OUTSIDE HADRONS
18. 1980 THE HIGH-ENERGY LIMIT
19. 1981 THE UNITY OF THE FUNDAMENTAL INTERACTIONS
20. 1982 GAUGE INTERACTIONS: Theory and Experiment
21. 1983 HOW FAR ARE WE FROM THE GAUGE FORCES?
22. 1984 QUARKS, LEPTONS, AND THEIR CONSTITUENTS
23. 1985 OLD AND NEW FORCES OF NATURE
24. 1986 THE SUPERWORLD I
25. 1987 THE SUPERWORLD II
26. 1988 THE SUPERWORLD III
27. 1989 THE CHALLENGING QUESTIONS
28. 1990 PHYSICS UP TO 200 TeV
29. 1991 PHYSICS AT THE HIGHEST ENERGY AND LUMINOSITY:
To Understand the Origin of Mass
30. 1992 FROM SUPERSTRINGS TO THE REAL SUPERWORLD
31. 1993 FROM SUPERSYMMETRY TO THE ORIGIN OF SPACE-TIME
32. 1994 FROM SUPERSTRING TO PRESENT-DAY PHYSICS
33. 1995 VACUUM AND VACUA: The Physics of Nothing
34. 1996 EFFECTIVE THEORIES AND FUNDAMENTAL INTERACTIONS
35. 1997 HIGHLIGHTS OF SUBNUCLEAR PHYSICS: 50 Years Later
36. 1998 FROM THE PLANCK LENGTH TO THE HUBBLE RADIUS
37. 1999 BASICS AND HIGHLIGHTS IN FUNDAMENTAL PHYSICS
38. 2000 THEORY AND EXPERIMENT HEADING FOR NEW PHYSICS
39. 2001 NEW FIELDS AND STRINGS IN SUBNUCLEAR PHYSICS
40. 2002 FROM QUARKS AND GLUONS TO QUANTUM GRAVITY
41. 2004 FROM QUARKS TO BLACK HOLES: PROGRESS IN UNDERSTANDING
THE LOGIC OF NATURE

Volume 1 was published by W. A. Benjamin, Inc., New York; 2-8 and 11-12 by Academic Press, New York and London; 9-10 by Editrice Compositori, Bologna; 13-29 by Plenum Press, New York and London; 30-41 by World Scientific, Singapore.

The Subnuclear Series • Volume 41

Proceedings of the International School of Subnuclear Physics

FROM QUARKS TO BLACK HOLES: PROGRESS IN UNDERSTANDING THE LOGIC OF NATURE

Edited by

Antonino Zichichi

*European Physical Society
Geneva, Switzerland*



NEW JERSEY • LONDON • SINGAPORE • BEIJING • SHANGHAI • HONG KONG • TAIPEI • CHENNAI

Published by

World Scientific Publishing Co. Pte. Ltd.

5 Toh Tuck Link, Singapore 596224

USA office: 27 Warren Street, Suite 401-402, Hackensack, NJ 07601

UK office: 57 Shelton Street, Covent Garden, London WC2H 9HE

British Library Cataloguing-in-Publication Data

A catalogue record for this book is available from the British Library.

**FROM QUARKS TO BLACK HOLES: PROGRESS IN UNDERSTANDING
THE LOGIC OF NATURE**

Proceedings of the International School of Subnuclear Physics

Copyright © 2005 by World Scientific Publishing Co. Pte. Ltd.

All rights reserved. This book, or parts thereof, may not be reproduced in any form or by any means, electronic or mechanical, including photocopying, recording or any information storage and retrieval system now known or to be invented, without written permission from the Publisher.

For photocopying of material in this volume, please pay a copying fee through the Copyright Clearance Center, Inc., 222 Rosewood Drive, Danvers, MA 01923, USA. In this case permission to photocopy is not required from the publisher.

ISBN 981-256-375-X

Printed in Singapore by Mainland Press

PREFACE

During August/September 2003, a group of 94 physicists from 50 laboratories in 14 countries met in Erice to participate in the 41st Course of the International School of Subnuclear Physics. The countries represented by the participants were: Austria, Armenia, Canada, China, Czechoslovakia, France, Germany, Israel, Italy, Mexico, the Netherlands, Mexico, Romania, Russia, South Korea, Spain, Switzerland, United Kingdom, the United States of America and Venezuela.

The School was sponsored by the Academies of Sciences of Estonia, Georgia, Lithuania, Russia and Ukraine; the Chinese Academy of Sciences; the Commission of the European Communities; the European Physical Society; the Italian Ministry of Education, University and Scientific Research; the Sicilian Regional Government; the Weizmann Institute of Science; the World Federation of Scientists and the World Laboratory.

The purpose of the School was to focus attention on the phenomenological and theoretical developments in Gauge Theories, as well as in global and local Supersymmetry, and in all the other sectors of Subnuclear Physics. Experimental highlights from the most relevant sources of new data were presented and discussed, including the latest news from theoretical developments in the progress of understanding the logic of nature, as reported in the contents.

An original feature of the School, introduced in 1996, is a series of special sessions devoted to "New Talents". This is a serious problem in Experimental Physics where collaborations count several hundreds of participants and it is almost impossible for young fellows to be known. Even if with much less emphasis the problem exists also in Theoretical Physics. So we decided to offer the young fellows a possibility to let them be known. 26 "new talents" were invited to present a paper, followed by a discussion. Three were given an award: one for the best presentation; one for an original theoretical work; and one for an original experimental work. These special sessions devoted to New Talents represent the projection of Subnuclear Physics on the axis of the young generation.

As every year, the discussion sessions have been the focal point of the School's activity.

During the organization and the running of this year's Course, I enjoyed the collaboration of my colleague and friend, Gerardus 't Hooft, who shared with me the Directorship of the Course. I would like to thank him, together with the group of invited scientists and all the people who contributed to the success of this year's Course.

I hope the reader will enjoy the book as much as the students attending the lectures and discussion sessions. Thanks to the work of the Scientific Secretaries, the discussions have been reproduced as faithfully as possible. At various stages of my work I have enjoyed the collaboration of many friends whose contributions have been extremely important for the School and are highly appreciated. I thank them most warmly. A final acknowledgement to all those in Erice, Bologna and Geneva, who have helped me on so many occasions and to whom I feel very indebted.

Antonino Zichichi
Geneva, October 2003

CONTENTS

Mini-Courses on Basics

The Latest in Lattice QCD <i>R. D. Kenway</i>	1
Quark-Gluon Plasma Physics <i>F. Karsch</i>	40
String Theory and Exact Results in Quantum Field Theory <i>R. H. Dijkgraaf</i>	51
The Status of Local Supersymmetry <i>M. J. Duff</i>	60

Seminars on Hot Theoretical Topics

Supersymmetry in Nuclei <i>F. Iachello</i>	117
Inflation, Dark Matter, Dark Energy <i>E. W. Kolb</i>	133
How Many Dimensions are Really Compactified? <i>I. Antoniadis</i>	148
Horizons <i>G. 't Hooft</i>	179
Neutrino Oscillations Physics <i>G. Fogli</i>	193
Fundamental Constants and Their Possible Time Dependence <i>H. Fritzsch</i>	210

Experimental Highlights

Highlights from BNL. New Phenomena at RHIC <i>T. W. Ludlam</i>	223
Highlights from BABAR <i>M. A. Giorgi</i>	232

Diffraction Studied with a Hard Scale at HERA <i>G. Wolf</i>	365
The Large Hadron Collider: A Status Report <i>L. Maiani</i>	387
Status of Non-LHC Experiments at CERN <i>W.-D. Schlatter</i>	419
Highlights from Gran Sasso <i>A. Bettini</i>	436
Special Sessions for New Talents	
Fast Automatic Systems for Nuclear Emulsion Scanning: Technique and Experiments <i>C. Bozza</i>	470
Probing the QGP with Charm at ALICE-LHC <i>A. Dainese</i>	478
Magnetic Screening Length in Hot QCD <i>P. Giovannangeli</i>	489
Non-Supersymmetric Deformation of the Klebanov-Strassler Model and the Related Plane Wave Theory <i>S. Kuperstein</i>	498
Holographic Renormalization Made Simple: An Example <i>I. Papadimitriou</i>	508
The KamLAND Impact on Neutrino Oscillations <i>A. M. Rotunno</i>	515
Particle Identification with the ALICE TOF Detector at Very High Multiplicity <i>C. Zampolli</i>	525
Superpotentials of $N = 1$ SUSY Gauge Theories <i>B. M. Gripaios</i>	536
Measurement of the Proton Structure Function F_2 in QED Compton Scattering at HERA <i>V. Lendermann</i>	544

Yang-Mills Effective Action at High Temperature <i>M. Oswald</i>	552
The Time of Flight (TOF) System of the ALICE Experiment <i>G. Sciolì</i>	561
Almost Product Manifolds as the Low Energy Geometry of Dirichlet Branes <i>F. P. Schuller</i>	567
Closing Ceremony	
Diplomas and Awards	579
Participants	583

This page intentionally left blank

The Latest in Lattice QCD

Richard Kenway

School of Physics, University of Edinburgh,
Edinburgh EH9 3JZ, Scotland

1. The Need for Lattice QCD

Beyond small parameters

The purpose of the lattice approach is to extract reliable predictions from a quantum field theory for all values of its input (physical) parameters. This is unlike perturbative approaches, which rely on the assumption that one of these parameters is small. To accomplish this, we need a rigorous definition of the quantum field theory as the limit of a system with a finite number of degrees of freedom, together with a systematically improvable method for computing the properties of the finite system. The idea is to use computer simulation for the finite system over a finite region in parameter space and various types of perturbation theory to extend the solution outside this region.

The finite system is obtained by replacing space-time with a regular four-dimensional lattice of points inside a finite box. In this way, we introduce two unphysical parameters: the lattice spacing, a , and the linear size of the box, L . An essential assumption is that computer simulation is only required over a finite range in each of the parameters (physical and unphysical). Beyond this range, analytical approaches must take over. For the unphysical lattice parameters, this means understanding how to extrapolate results to the continuum ($a \rightarrow 0$) and infinite-volume ($L \rightarrow \infty$) limits. This is possible provided the physical processes being simulated occur only within a finite range of energy scales. For the physical parameters, it means interpolating or extrapolating the results to the experimentally measured parameter values.

A second underlying assumption is that computer speeds will continue to grow exponentially, as they have done for the past 50 years ('Moore's Law'). This is necessary because the simulation cost usually has a power-law dependence on a and L , and so we can expect to explore a finite range of these parameters in linear time.

By far the most progress has been achieved in lattice QCD, although this work has already taken 30 years. Asymptotic freedom allows us to satisfy all the above criteria for QCD in isolation from the other forces and, of course, confinement provides all the motivation required to build up an elaborate computational framework. Until relatively recently, we did not know how to incorporate chiral symmetry correctly in the lattice formulation. Now that we do, lattice QCD is on a very solid footing and we can start to contemplate a lattice approach also for chiral and supersymmetric quantum field theories. Thus, for as long as we continue to describe low-energy physics by quantum field theories, computer simulation is likely to play a central role.

The third methodology

Simulation has become accepted as the third methodology of science, alongside experiment and theory. It is used principally to forecast the behaviours of complex systems. In many applications, the underlying physics is not in question and what matters is the accuracy of the forecast, eg for weather. However, simulation can also be used for discovery when it realises accurately our knowledge and its results differ from those of experiment. The discrepancies may point us in the direction of new physics.

Computer simulation of quantum field theories is a broad cross-disciplinary enterprise. Being limited by computer performance, at one end of the spectrum it requires the design and development of new computer architectures. At the other end, the non-perturbative definition of a quantum field theory on a space-time lattice requires deep understanding of how symmetries are realised and the theory is renormalised. Connecting the two are numerical algorithms. These restrict the lattice models that can be simulated, and their efficient implementation is usually crucial for success. Thus, lattice QCD is dependent on work at the forefront of computer science, mathematics and physics.

Fundamentally, our knowledge advances through experimental falsification of a theory and its replacement by a better one. Simulation plays its part for those theories which give rise to complex emergent phenomena. An example is the mapping from the quark and gluon degrees of freedom of the QCD Lagrangian to the complex low-energy scattering and decays of the hadrons that we observe experimentally. Simulation is a precision tool to achieve this mapping. Already, it has been used to falsify the quenched approximation to QCD. Although this took 17 years to achieve, it represents a significant test of the methodology, demonstrating in principle that simulation can be a discovery tool.

The role of lattice QCD today

It is well known that the Standard Model of elementary particle physics cannot be complete, even with the inclusion of non-zero neutrino masses and mixings. Lots of things point to missing physics: we don't have a quantum theory of gravity; the small neutrino masses imply an unexplained large scale; some 25 free parameters are just too many; and experimental cosmology is demanding new particles (the inflaton, dark matter, quintessence, etc). There is a hint for supersymmetry from the fact that the strong, electromagnetic and weak gauge couplings become equal at very large energies if there are super partners at around the TeV scale, so that their discovery would herald a unified theory.

The search for new physics is our primary goal. There are two ways to proceed: wait for an experimental discovery, eg at the LHC; or look for clues in the comparison between the results of precision Standard Model calculations and experiment. It is the latter which concerns lattice QCD today, because most of these experiments require that we infer quark properties from measurements on hadrons.

You may think of lattice QCD as a 'black box' that relates Standard Model parameters (quark masses, mixing angles and the gauge coupling) to the properties of hadrons – that

this performs a highly non-trivial mapping is suggested because inputting u and d quark masses of just a few MeV generates a proton mass of 938 MeV. In practice, we use the mapping in reverse to infer the parameter values by matching the simulation results for hadrons to experiment.

An important example of this approach is the attempt using B Factories to over-constrain the unitarity triangle, which is a relationship between the quark flavour mixing parameters that holds if there are only three generations. In particular, determination of the sides of the triangle from experiment requires accurate values for QCD matrix elements relating to neutral kaon and neutral B meson mixing, and to the semileptonic decays of B mesons into both charm and light hadrons.

A second example concerns the search for proton decay. Grand Unified Theories (GUTs), in which quarks and leptons are in the same multiplet, typically contain baryon number violating processes that cause protons to decay. Since the transition from quarks to leptons occurs inside a proton, the decay amplitude involves a strong-interaction piece, and can be shown to factorise into a model-dependent part and a QCD part,

$$\text{amplitude} = f(\text{model}, M_X) \times \underbrace{\langle h_2 | O | h_1 \rangle}_{\text{QCD}}. \quad (1.1)$$

The latter comprises a set of matrix elements that may be computed in lattice QCD. The model-dependent factor specifically involves the masses of new particles, X , at the GUT scale. So, the experimental lower bound on the lifetime of the proton places a lower bound on these GUT-scale particle masses, provided we can compute the QCD matrix elements reliably.

2. The Formulation of QCD on a Space-Time Lattice

Discretisation of the classical theory

Lattice QCD uses Monte Carlo methods to evaluate the path integral for QCD. In Minkowski space-time, the integrand is an oscillating function and this makes it very difficult to compute the integral numerically. So the first step is analytic continuation to imaginary time. The entire lattice QCD simulation is performed in four-dimensional Euclidean space, where the path integral

$$\begin{aligned} \langle O \rangle &= \frac{1}{Z} \int DADq D\bar{q} O[A, q, \bar{q}] e^{-S_c[A] + \bar{q}(D[A] + m)q} \\ &= \frac{1}{Z} \int DA \det^{N_f} (D[A] + m) e^{-S_c[A]} O \left[A, \frac{\delta}{\delta \bar{\eta}}, \frac{\delta}{\delta \eta} \right] e^{-\bar{\eta}(D[A] + m)^* \eta} \Big|_{\bar{\eta}, \eta=0} \end{aligned} \quad (2.1)$$

after integration over the Grassmann quark and antiquark fields, may be interpreted as a probability distribution and is suitable for a Monte Carlo approach.

The Euclidean space is approximated by a finite four-dimensional hypercubic lattice. The quark fields, $q(x)$, live on the sites of the lattice and the gauge fields, $U_\mu(x)$, live on the links between neighbouring sites, x and $x+a\hat{\mu}$. The lattice gauge fields are elements of the $SU(3)$ colour gauge group, and are related to the elements of the algebra, $A_\mu(x)$, used in (2.1) by

$$U_\mu(x) = e^{iagA_\mu \left(\frac{x+a\hat{\mu}}{2} \right)}. \quad (2.2)$$

The integral over A_μ in (2.1) is replaced by the integral over the Haar measure of $SU(3)$ and, since the group is compact, these integrals are finite and there is no need to fix a gauge. There is considerable freedom in the definition of the lattice action. The main criterion is that the symmetries of the lattice theory are sufficient to ensure that all the symmetries of the continuum theory are recovered in the limit $a \rightarrow 0$. In particular, the lattice action should satisfy

$$S_{\text{lattice}} = S_{\text{cont}} + O(a). \quad (2.3)$$

Wilson's breakthrough in 1974 (Wilson 1974) was to find a lattice formulation of QCD that preserves exact local gauge invariance at the sites of the lattice. Specifically, the lattice action is invariant under

$$\begin{aligned} q(x) &\rightarrow V(x)q(x) \\ \bar{q}(x) &\rightarrow \bar{q}(x)V^+(x), \quad V(x) \in SU(3) \\ U_\mu(x) &\rightarrow V(x)U_\mu(x)V^+(x+a\hat{\mu}) \end{aligned} \quad (2.4)$$

and this requires that it is built from only two kinds of objects: the trace of the product of the gauge fields around a closed path, called a Wilson loop; and the product of the gauge fields along a path with a quark field at one end and an antiquark field at the other. The simplest Wilson loop is the product of gauge fields around an elementary square on the lattice, called a plaquette. In the continuum limit, the sum of plaquettes over the lattice is proportional to the Yang-Mills action.

The path integral for lattice QCD looks like the partition function for a four-dimensional statistical mechanical system. On a finite lattice, it is a very high-dimensional integral and can be computed using Monte Carlo methods. This approximates the path integral by a sum over N representative gauge field configurations, so that the expectation value of a product of fields is approximated by the average of its value on each configuration. As a result, expectation values have statistical errors that are typically proportional to $1/\sqrt{N}$.

A consequence of the local gauge invariance is that quarks are confined at non-zero lattice spacing. At strong coupling, it can be shown analytically that, at large separations, the potential energy of a massive quark-antiquark pair is proportional to their separation. This is the signal for a confining flux tube – as the quarks separate, the energy in the flux tube grows until it becomes energetically favourable to break into a quark-antiquark pair,

which screen the original colour charges. Monte Carlo simulations confirm this picture at intermediate coupling values and give no indication that there is any phase transition into a deconfined phase in the zero-coupling (continuum) limit. The exact gauge invariance and corresponding colour confinement is the main reason why so much effort has gone into lattice QCD over the past 30 years.

Easily computed quantities

Provided the lattice theory satisfies the Osterwalder-Schrader conditions, then its expectation values can be equated to vacuum expectation values of time-ordered products of operators in a corresponding Euclidean quantum field theory. Expectation values of products of composite fields at two different Euclidean times, 0 and τ , called 2-point functions, ie,

$$\begin{aligned} \langle O^+(\tau)O(0) \rangle &= \langle 0 | T[O^+(\tau)\hat{O}(0)] | 0 \rangle \\ &= \langle 0 | \hat{O}^+ e^{-\hat{H}\tau} \hat{O} | 0 \rangle \\ &= \sum_n |\langle n | \hat{O} | 0 \rangle|^2 \frac{e^{-E_n \tau}}{2E_n} \end{aligned} \quad (2.5)$$

decay exponentially for large τ with the energy of the lightest hadron created by O . If we set the momentum to zero, this energy is the hadron mass. Also, if we choose the composite field O appropriately, from the amplitude of the exponential decay we can extract a pseudoscalar meson decay constant,

$$iM_{\text{PS}} f_{\text{PS}} = Z_A \langle 0 | \bar{q}_1 \gamma_0 \gamma_5 q_2 | \text{PS} \rangle, \quad (2.6)$$

where Z_A is the renormalisation constant for the axial vector current.

Expectation values of products of composite fields at three different Euclidean times, so-called 3-point functions, enable us to compute matrix elements of operators between two hadron states. For example, if $\tau_2 > \tau_1 > 0$,

$$\begin{aligned} \langle \pi(\bar{p}, \tau_2) O(\bar{q}, \tau_1) K(0) \rangle &= \langle 0 | \hat{\pi}(\bar{p}) e^{-\hat{H}(\tau_2 - \tau_1)} \hat{O}(\bar{q}) e^{-\hat{H}\tau_1} \hat{K} | 0 \rangle \\ &= \sum_{n, n'} \underbrace{\langle 0 | \hat{\pi}(\bar{p}) | n \rangle}_{\text{from 2-point functions}} \frac{e^{-E_n(\tau_2 - \tau_1)}}{2E_n} \underbrace{\langle n | \hat{O}(\bar{q}) | n' \rangle}_{\text{from 2-point functions}} \frac{e^{-E_{n'}\tau_1}}{2E_{n'}} \langle n' | \hat{K} | 0 \rangle \end{aligned} \quad (2.7)$$

and for large time separations, $\tau_2 \gg \tau_1 \gg 0$, we can isolate hadronic matrix elements such as

$$\langle \pi(\bar{p}) | \bar{s} \gamma_\mu u(\bar{q}) | K(\bar{p} - \bar{q}) \rangle \quad (2.8)$$

relevant to semileptonic decays.

At the present time, there is no general method for computing matrix elements for which there is more than one hadron in the initial or final state. This may seem like a serious problem, but there are already many useful physical quantities that can be extracted from 2- and 3-point functions alone. Also, note that the hadron masses and matrix elements are obtained directly from the Euclidean-space simulations without having to do analytical continuation back to Minkowski space-time.

Continuum limit of the quantum theory

The lattice action is constructed so that its limit when $a \rightarrow 0$ is the continuum action. This is necessary, but not sufficient for the quantum theory, ie the path integral, to have the correct continuum limit. Two further sets of conditions must be satisfied.

The Osterwalder-Schrader conditions, already mentioned, and specifically a property called reflection positivity, are sufficient for the four-dimensional statistical mechanical system to correspond to a Lorentz-invariant quantum field theory. These have been proved for some but not all of the lattice actions in use today. In particular, it is difficult to prove reflection positivity for improved actions constructed with extra higher dimension operators whose coefficients are tuned so that leading-order discretisation effects cancel out.

Secondly, we have to ensure that all the symmetries of the continuum theory are correctly realised, even though they may be broken at non-zero lattice spacing. Local gauge invariance is preserved on the lattice, but Lorentz invariance obviously is not. It turns out that Lorentz invariance is restored as an accidental symmetry of the continuum limit, simply because it is not possible to write down any relevant operators (of dimension 4 or less) in the lattice theory which break Lorentz invariance. (Higher dimension operators are multiplied by positive powers of a and so vanish in the continuum limit.)

Chiral symmetry plays a central role in QCD, but has proved to be problematic in the lattice formulation. The Nielsen-Ninomiya No-Go Theorem states that if the lattice action is local, bilinear in the fermion fields, translationally invariant, Hermitian, and has continuous chiral symmetry, then the continuum limit contains fermions in opposite chirality pairs. This 'fermion doubling' gives multiple pairs of degenerate quark flavours quite unlike the real world. There are several different remedies.

The first, due to Wilson, is to break chiral symmetry explicitly on the lattice. This creates a tuning problem, because quark masses receive an additive renormalisation and it is necessary to perform simulations over a range of quark masses in order to identify the zero of quark mass (where the pseudoscalar meson mass vanishes). It is also not clear whether Wilson quarks correctly realise chiral symmetry close to zero mass.

The second approach, called staggered fermions, exploits a lattice symmetry to reduce the doubling to a minimum and then regards the extra degenerate quark flavours as being distinguished by a new quantum number called taste. In the improved staggered programme, the lattice action is modified to decouple the non-zero taste quarks as much

as possible and a fractional power of the fermion determinant is used in Equation (2.1) so that effectively only one taste flows around quark loops.

Finally, Ginsparg-Wilson fermions give up ultra-locality, by which I mean that the lattice interactions are of finite range, and replaces it with interactions which are of infinite range (on an infinite lattice), but whose strength falls off exponentially with distance. This formulation possesses an exact lattice version of chiral symmetry, which becomes identical with continuum chiral symmetry as $a \rightarrow 0$.

Exact chiral symmetry on the lattice

The infinitesimal chiral transformation

$$\begin{aligned}\delta\psi &= i\varepsilon\tau\gamma_5\left(1 - \frac{a}{2}D\right)\psi \\ \delta\bar{\psi} &= i\varepsilon\bar{\psi}\left(1 - \frac{a}{2}D\right)\gamma_5\tau\end{aligned}\tag{2.9}$$

where τ is a flavour matrix and D satisfies the Ginsparg-Wilson relation (Ginsparg & Wilson 1982)

$$\gamma_5 D + D\gamma_5 = a D\gamma_5 D\tag{2.10}$$

is a symmetry of the lattice fermion action built from the fermion matrix D , since

$$\delta(\bar{\psi}D\psi) = 0.\tag{2.11}$$

For flavour-singlet transformations ($\tau = 1$), (2.9) is not also a symmetry of the integration measure and the correct anomaly occurs.

From the Ward Identity, it is easily seen that the chiral order parameter is

$$\left\langle \bar{\psi}\left(1 - \frac{a}{2}D\right)\psi \right\rangle\tag{2.12}$$

so the action for massive fermions is

$$S_{GW} = \bar{\psi}D\psi + m\bar{\psi}\left(1 - \frac{1}{2}D\right)\psi.\tag{2.13}$$

Neuberger's overlap construction (Narayanan & Neuberger 1993, Neuberger 1998) is

$$\begin{aligned}D &= 1 + \gamma_5 \text{sgn}(H) \\ H &= \gamma_5(D_W(0) - 1)\end{aligned}\tag{2.14}$$

where $D_W(0)$ is the massless Wilson fermion matrix. It has been proved that this lattice QCD action is local provided the gauge fields are sufficiently smooth (Hernández et al.

1999). In simulations, however, it is necessary to check locality. Also, the Ginsparg-Wilson lattice formulations are $O(\alpha)$ -improved, ie the leading discretisation errors are $O(\alpha^2)$, because there is no dimension-5 chiral-invariant operator.

The computation of the matrix sign function in Equation (2.14) is costly, so that simulations using Ginsparg-Wilson quarks are significantly more computationally demanding than the traditional Wilson or staggered formulations. However, this may not remain true as simulations penetrate deeper into the chiral regime. In any case, Ginsparg-Wilson quarks offer the only known way to realise the chiral symmetry of QCD correctly and they promise for the future the possibility of simulating chiral gauge and supersymmetric theories.

Setting the QCD scale

Computer simulations use dimensionless variables in which the lattice spacing is 1. The quark masses, generically denoted by m , and gauge coupling, g^2 , are varied. In what is referred to as the ‘hadronic scheme’, at each value of g^2 , the quark masses are fixed by matching N_f dimensionless hadron mass ratios to their experimental values (where N_f is the number of flavours). Then, one additional dimensionful quantity fixes the lattice spacing in physical units, eg

$$\frac{\text{nucleon size}}{\text{lattice spacing}} = \frac{M_N^{-1}}{1} \Big|_{\text{computer}} = \frac{(938 \text{ MeV})^{-1}}{\alpha} \Big|_{\text{lab}} . \quad (2.15)$$

If the lattice spacing in physical units, α , is small enough, specifically, if it is smaller than any relevant scale in strong-interaction physics, then the values of dimensionless ratios of physical quantities should become independent of g^2 as it is decreased further. This is called ‘scaling’ and it means that, once our lattice spacing is small enough, we can stop. Furthermore, because asymptotic freedom tells us that the continuum limit of QCD occurs at $g^2 = 0$, we may use perturbation theory to compute the behaviour of physical quantities with g^2 in this limit and, hence, check that our simulations reproduce this behaviour. This is called ‘asymptotic scaling’ and is a stronger condition than scaling, which could set in at larger values of g^2 .

In practice, however, this simple picture is complicated by limited computer power. We must ensure that the physical size of our lattice is large enough not to distort significantly the physics we’re trying to simulate. Just for hadrons built from u , d , s , and c quarks, the range of mass scales which must fit on the lattice is prohibitively large. For instance,

$$L = N\alpha \gg (M_\pi, \dots, M_{J/\psi})^{-1} \gg \alpha \Rightarrow N \gg 20 \quad (2.16)$$

and, even 20^4 lattices are near the limit of what is possible today. Here our ability to vary the quark masses used in our simulations comes to our aid. We compress the quark mass range we simulate so that inequalities like (2.16) are obeyed and then extrapolate our simulation results to the physical regime, using an effective theory.

Effective theories

The parameters which define a lattice QCD simulation are the lattice spacing, a , the linear size of the lattice, L , the lightest quark mass, m_q , and the heaviest quark mass, m_Q . Simulations can only be controlled over a finite range in each of these parameters. The actual range, in each case, depends on the available computer power and algorithmic efficiency. It is essential for the programme that the simulation results can be matched to effective theories which enable us to extrapolate them analytically outside the simulation range. An effective theory describes the relevant degrees of freedom above a particular scale and the interactions between them that model the missing degrees of freedom. For QCD, as sketched in Figure 1, we use Heavy-Quark Effective Theory (HQET), or Non-Relativistic QCD (NRQCD) to extrapolate to large quark mass, and chiral perturbation theory to extrapolate towards zero quark mass. In addition, effective theories due to Symanzik and Lüscher define the lattice-spacing and finite-volume dependences respectively.

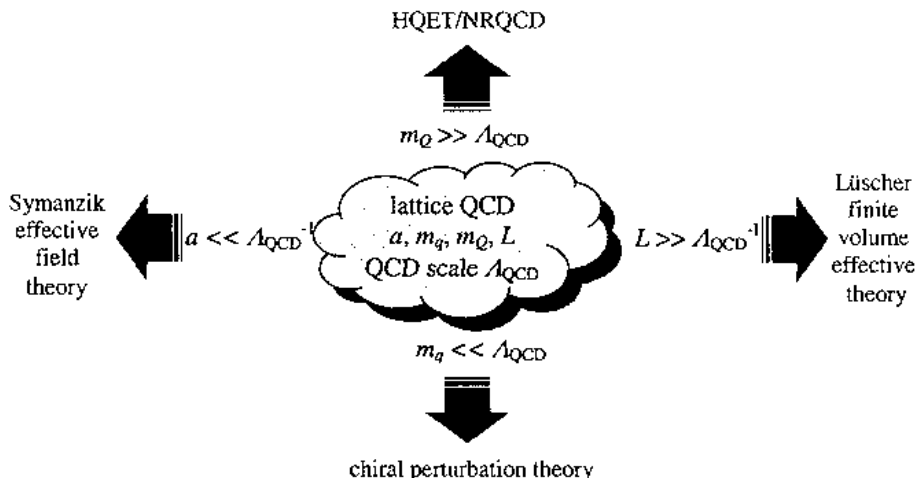


Figure 1. Effective theories that span the range of QCD parameters.

Renormalisation

The hadronic scheme tells us how to fix the parameters in the action to determine spectral quantities. We need a further set of conditions to fix the normalisations of matrix elements. Mass-independent renormalisation conditions are imposed on Green functions at $p^2 = \mu^2$ and $m_0 = 0$,

$$Z_{\text{lat}}^{\text{int}}(\alpha_{\text{lat}}(a), \mu a) \Gamma^{\text{lat}}(pa) \Big|_{p^2 = \mu^2} = \Gamma^{\text{tree}} \quad (2.17)$$

where ‘int’ refers to a scheme in which vertex functions are set equal to the value they would have at tree level in perturbation theory and

$$\alpha_{\text{lat}}(a) = \frac{g_0^2}{4\pi}. \quad (2.18)$$

However, for use in phenomenology, we need matrix elements in a perturbative scheme. The matching between this and the non-perturbative ‘int’ scheme is given by

$$\begin{aligned} \langle O \rangle^{\text{int}}(\mu) &= \underbrace{Z_{\text{lat}}^{\text{int}}(\alpha_{\text{lat}}(a), \mu a)}_{\substack{\text{numerical, provided } \mu \ll \frac{1}{a}}} \langle O \rangle^{\text{lat}}(a) \\ &= \underbrace{Z_{\overline{\text{MS}}}^{\text{int}}\left(\alpha_{\overline{\text{MS}}}(\mu), \frac{\mu}{\Lambda_{\text{QCD}}}\right)}_{\substack{\text{pert theory, provided } \mu \gg \Lambda_{\text{QCD}}}} \langle O \rangle^{\overline{\text{MS}}}(\mu) \end{aligned} \quad (2.19)$$

provided there is a window in which

$$\Lambda_{\text{QCD}} \ll \mu \ll \frac{1}{a}. \quad (2.20)$$

This condition can be problematic on current lattice sizes.

An alternative is to use finite-size scaling by taking the renormalisation scale to be the inverse of the linear box size, $\mu^{-1} = L$, and considering a sequence of intermediate renormalisations at a sequence of box sizes, $L_n = 2^{-n}L_0$,

$$\langle O \rangle(L_n) = \underbrace{\sigma(L_n, L_{n-1})}_{\substack{\text{numerical,} \\ \text{using finite size scaling}}} \langle O \rangle(L_{n-1}) \quad (2.21)$$

where σ is called the step scaling function. Then, by iterating equation (2.21) to a sufficiently small box that perturbation theory is valid inside it, we can compute the renormalisation group invariant (RGI) matrix element from

$$\begin{aligned} \langle O \rangle^{\text{RGI}} &= \lim_{\mu \rightarrow \infty} \langle O \rangle(\mu) \\ &= \underbrace{Z_L^{\text{RGI}}}_{\substack{\text{pert theory,} \\ \text{provided } L^{-1} \gg \Lambda_{\text{QCD}}}} \underbrace{\sigma(L_n, L_{n-1}) \dots \sigma(L_1, L_0)}_{\text{numerical}} \langle O \rangle(L_0). \end{aligned} \quad (2.22)$$

Matching RGI to any perturbative scheme can be done in perturbation theory,

$$\langle O \rangle^{\overline{\text{MS}}}(\mu) = \underbrace{Z_{\text{RGI}}^{\overline{\text{MS}}}(\mu)}_{\substack{\text{pert theory,} \\ \text{provided } \mu \gg \Lambda_{\text{QCD}}}} \langle O \rangle^{\text{RGI}}. \quad (2.23)$$

Computational cost

The way in which the number of arithmetic operations required to simulate QCD with today's best algorithms depends on the input parameters is found empirically to scale according to the following formula,

$$\# \text{ ops (QCD)} \approx L^{4.5-5.0} \left(\frac{1}{a} \right)^{7.0-8.5} \left(\frac{1}{M_{\text{PS}}} \right)^{2.5-3.5}. \quad (2.24)$$

Here M_{PS} , the mass of the pseudoscalar meson, embodies the quark mass dependence. As can be seen, the exponents are not particularly well determined. This is because it is expensive to carry out simulations over a wide range of parameter values close enough to the physical values for the formula to be useful.

The computational cost may be illustrated by observing that a practical test whether a given simulation is close enough to the continuum limit for the results not to depend significantly on the lattice spacing would be to repeat the simulation with a lattice spacing of half the size (with everything else kept fixed). But, according to Equation (2.24), this costs around 500 times more. Hence, even if the original simulation could be carried out on a PC, it takes a supercomputer to check it!

Fortunately, throughout the last 50 years or so, computer speeds have doubled every 18-24 months and this exponential increase, dubbed Moore's Law, shows no sign of abating. Furthermore, QCD simulations parallelise well, simply by splitting the lattice into sub-lattices and assigning adjacent sub-lattices to adjacent microprocessors in an array. The performance that can be achieved grows linearly with the number of microprocessors up to tens of thousands and, potentially, hundreds of thousands. Thus, even without algorithmic improvements, we can look forward to substantially more accurate QCD simulations over the coming years, driven by Moore's Law and massive parallelism.

3. Some Recent Results from Lattice QCD

The steady increase in computer power and advances in the theoretical formulation of lattice QCD have already driven the simulations through several stages. For many years, we were limited to working in quenched QCD, which neglects the effects of virtual quark-antiquark pairs in the vacuum, in order to be able to simulate large enough lattices to have any chance of computing phenomenologically interesting quantities. During the past ten years, we have been able to drop this approximation, although the lattice

formulations used have not correctly realised both the flavour and chiral symmetries of QCD and the quark masses have been restricted to a narrow range between strange and charm. Recently, the rediscovery of the Ginsparg-Wilson relation and the discovery of several implementations of it which correctly realise chiral symmetry at non-zero lattice spacing are promising an era in which all systematic errors are under control. We do not quite have enough computer power yet, but this situation should change for the better over the next five years.

In the following, I will outline some recent results for zero-temperature QCD. All suffer, to a greater or lesser extent, from systematic uncertainties. The dominant cause is that we can only afford to simulate dynamical quarks in a narrow mass range, so that the matching onto effective theories is not properly under control. Nevertheless, some of these results have already been used in experimental data analyses and the resulting determinations of the Standard Model parameters are the most reliable available.

Quenched QCD

As a reference point and because some important physical quantities have only been computed in this approximation, we must start with quenched QCD. The most computationally demanding part of the path integral (2.1) is the fermionic determinant. Solely as an expedient, the quenched approximation sets this to a constant,

$$\int d\bar{q} d\bar{\bar{q}} e^{\bar{q}(\mathcal{D}(U)+m)q} = \det(\mathcal{D}(U) + m) \approx \text{constant.} \quad (3.1)$$

This is equivalent to taking the quark mass in loops to infinity. There is no good reason why this theory, which is not even unitary, should be a close approximation to QCD. However, it is. In one of the earliest lattice simulations, Hamber and Parisi used it to estimate the nucleon mass and found $M_N = 900$ (100) MeV (Hamber & Parisi 1982). It took a further 15 years or so for the simulation accuracy to improve to the point where the uncertainty in the quenched nucleon mass was small enough to expose a discrepancy with the experimental value.

The results of the CP-PACS Collaboration (CP-PACS 2000) which definitively showed that the light hadron spectrum in quenched QCD disagreed with experiment are shown in Figure 2. They reveal two interesting facts. First, quenched QCD gives inconsistent results when the strange quark mass is fixed from different hadron masses – a clear signal that the theory is wrong. But second, the deviation of the spectrum from experiment is only about 10% – quenched QCD is actually rather a good approximation for some quantities. This explains why it took so long for simulations to falsify quenched QCD, but it also indicates that quenched QCD is a useful model of strong interaction physics. Part of the reason for this is that the hadronic scheme absorbs some of the quark loop effects into a renormalisation of the quark-gluon coupling. It is important to bear this in mind when interpreting results for more complicated quantities where only quenched results are available.

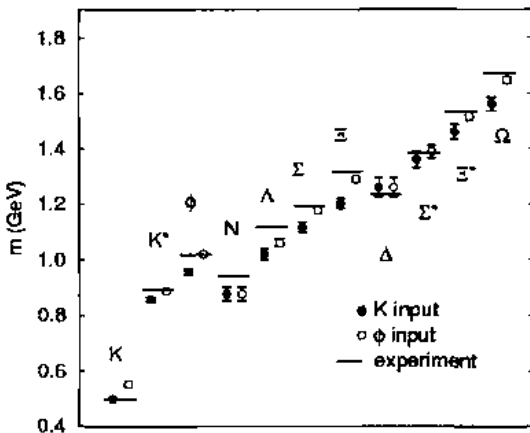


Figure 2. The light hadron spectrum in quenched QCD obtained by CP-PACS (CP-PACS 2000). The horizontal lines are the experimental mass values and the two sets of data correspond to fixing the strange quark mass from the kaon mass or from the ϕ meson mass.

Quark masses

The quark masses are fundamental parameters of the Standard Model that are encoded in the hadron spectrum by QCD. Lattice QCD is the only method we have to extract the quark masses from the spectrum and this is an important application of the method, because the running quark masses in a perturbative scheme play an important part in phenomenology. The matching relationship between the lattice and perturbative masses is

$$\underbrace{m_q^{\overline{\text{MS}}(\mu)}}_{\text{perturbative scheme}} = Z_m^{\overline{\text{MS}}, \text{lat}}(\mu a) \underbrace{m_q(a)}_{\text{hadronic scheme}} \quad (3.2)$$

where there are several convenient ways to define the lattice mass, $m_q(a)$, and the corresponding matching coefficient, Z_m .

The Vector Ward Identity (VWI) mass is given by

$$m_q^{\text{VWI}}(a)a = \frac{1}{2\kappa_q} - \frac{1}{2\kappa_{\text{crit}}} \quad (3.3)$$

in the Wilson quark formulation where κ_q is the hopping parameter (essentially the inverse bare quark mass) and κ_{crit} is the hopping parameter value at which the pseudoscalar meson mass vanishes (interpreted as the zero of quark mass). Since the conserved vector current is not renormalised, the vector Ward identity shows that

$$\begin{aligned}\langle \partial_\mu V_\mu^a(x) O(0) \rangle &= \left(\frac{1}{2\kappa_2} - \frac{1}{2\kappa_1} \right) \langle S^a(x) O(0) \rangle(a) \\ &= \left(\frac{1}{2\kappa_2} - \frac{1}{2\kappa_1} \right) \frac{\langle S^a(x) O(0) \rangle(\mu)}{Z_S^{\overline{\text{MS}},\text{lat}}(\mu a)}\end{aligned}$$

so that

$$m_q^{\overline{\text{MS}}}(\mu) = \left(Z_S^{\overline{\text{MS}},\text{lat}}(\mu a) \right)^{-1} m_q^{\text{VWI}}(a). \quad (3.4)$$

Alternatively, the Axial-vector Ward Identity (AWI) mass is given by

$$(m_l + m_2)^{\text{AWI}}(a) = \frac{\langle \partial_\mu A_\mu^a(x) O(0) \rangle(a)}{\langle P^a(x) O(0) \rangle(a)}$$

so that

$$m_q^{\overline{\text{MS}}}(\mu) = \frac{Z_A^{\overline{\text{MS}},\text{lat}}}{Z_P^{\overline{\text{MS}},\text{lat}}(\mu a)} m_q^{\text{AWI}}(a). \quad (3.5)$$

Simulations of QCD with two degenerate flavours, interpreted as the u and d quarks, by the CP-PACS Collaboration (CP-PACS 2002) obtain estimates of the common quark mass, m_{ud} , using both the VWI and AWI definitions, at various lattice spacings, as shown in Figure 3. These estimates are based on chiral extrapolation from sea-quark masses corresponding to $M_{\text{PS}}/M_V \geq 0.6$ in a $(2.5 \text{ fm})^3$ box.

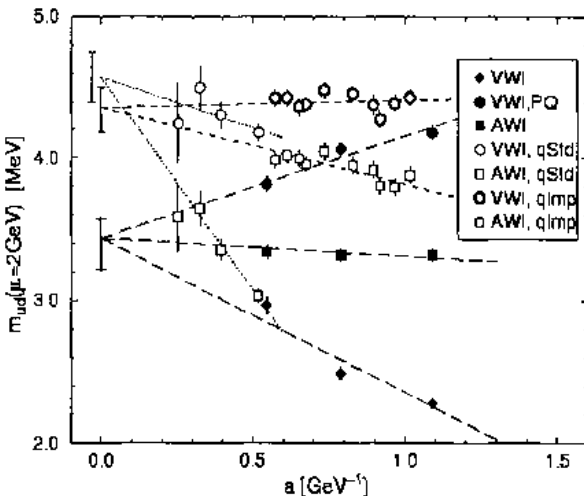


Figure 3. Estimates of the common u and d quark mass as a function of lattice spacing in quenched (open symbols) and 2-flavour (solid symbols) QCD, obtained by the CP-PACS Collaboration (CP-PACS 2002).

It is encouraging that, although the chiral extrapolation is rather long, the different definitions at non-zero lattice spacing have consistent continuum extrapolations. The continuum values are (CP-PACS 2002)

$$\begin{aligned} \bar{m}_{ud}^{\overline{\text{MS}}} (2 \text{ GeV}) &= 4.36^{+0.14}_{-0.17} \text{ MeV} \quad (N_f = 0) \\ \bar{m}_{ud}^{\overline{\text{MS}}} (2 \text{ GeV}) &= 3.44^{+0.14}_{-0.22} \text{ MeV} \quad (N_f = 2). \end{aligned} \quad (3.6)$$

Clearly, there is a big quenching error that tends to overestimate the quark mass. A recent result from a simulation at fixed lattice spacing ($a^{-1} = 2 \text{ GeV}$) including a dynamical strange quark supports this trend that dynamical quark effects decrease the mass estimate (CP-PACS & JLQCD 2003a),

$$\bar{m}_{ud}^{\overline{\text{MS}}} (2 \text{ GeV}) = 2.89(6) \text{ MeV} \quad (N_f = 2+1) \quad (3.7)$$

although the lattice size was quite small, $(1.6 \text{ fm})^3$, and the chiral extrapolation was again quite long (from data with $M_{\text{PS}}/M_V \geq 0.64$).

We have already seen that the strange quark mass cannot be determined unambiguously in quenched QCD (CP-PACS 2000). Nevertheless, it is convenient to have a value to compare the dynamical results with, and the most precise value obtained so far from the kaon mass is (Alpha & UKQCD 1999),

$$\bar{m}_s^{\overline{\text{MS}}} (2 \text{ GeV}) = 97(4) \text{ MeV} \quad (N_f = 0, K \text{ mass input}). \quad (3.8)$$

In simulations of 2-flavour QCD with the strange quark still treated in the quenched approximation (CP-PACS 2002), the inconsistency in the strange quark mass disappears, at least within the 10% uncertainty of the results, as can be seen in Figure 4.

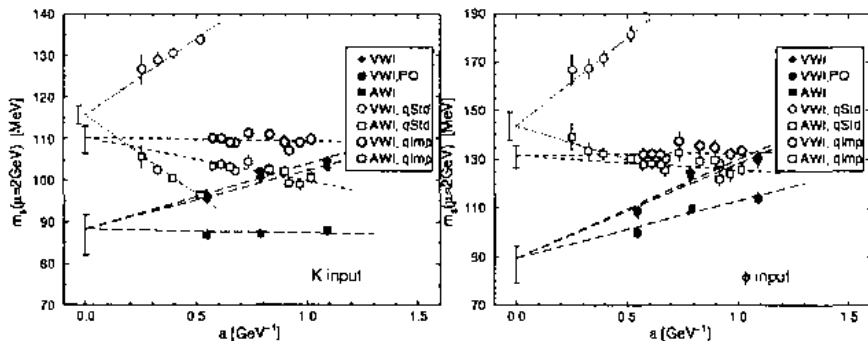


Figure 4. Estimates of the strange quark mass as a function of the lattice spacing in quenched (open symbols) and 2-flavour (solid symbols) QCD, using the kaon mass (left) and the ϕ meson (right) as input (CP-PACS 2002).

The resulting continuum value for the strange quark mass from the kaon mass (CP-PACS 2002) is

$$m_s^{\overline{\text{MS}}}(2 \text{ GeV}) = 88_{-6}^{+4} \text{ MeV } (N_f = 2) \quad (3.9)$$

some 10% lower than the quenched result. A low strange quark mass increases the Standard Model estimate for ϵ'/ϵ and so this result may have important consequences for our understanding of CP violation. The result at fixed lattice spacing for a dynamical strange quark, corresponding to Equation (3.7) is (CP-PACS & JLQCD 2003a)

$$m_s^{\overline{\text{MS}}}(2 \text{ GeV}) = 75.6(3.4) \text{ MeV } (N_f = 2 + 1). \quad (3.10)$$

From Equations (3.7) and (3.10), the ratio $m_s/m_{ud} = 26.2(1.0)$ compared with the chiral perturbation theory prediction of 24.4(1.5).

Estimates for the charm and bottom quark masses have only been obtained in quenched QCD. Two recent calculations of the charm quark mass, which employ the fully non-perturbative step-scaling renormalisation, (Rolf & Sint 2002 and de Divitiis et al. 2003b) are in excellent agreement. The latter obtains

$$m_c^{\overline{\text{MS}}}(m_c) = 1.319(28) \text{ GeV } (N_f = 0) \quad (3.11)$$

and for the bottom quark mass

$$m_b^{\overline{\text{MS}}}(m_b) = 4.33(10) \text{ GeV } (N_f = 0). \quad (3.12)$$

Given m_c and m_b , we can predict the B_c meson mass (de Divitiis et al. 2003b)

$$\begin{aligned} M_{B_c} &= 6.46(15) \text{ GeV } (N_f = 0) \\ &= 6.40(39)(13) \text{ GeV (expt)}. \end{aligned} \quad (3.13)$$

Preliminary 2-flavour results for m_c are consistent with, but not yet precise enough to compare with the quenched results.

The D_s meson spectrum

A story which illustrates how lattice QCD has supplanted QCD-inspired potential models was played out earlier this year. In April, BaBar announced a narrow $J^P = 0^+$ resonance in $D_s^+\pi^0$ at 2.32 GeV. In May, CLEO confirmed the 2.32 GeV state and announced a narrow $J^P = 1^+$ resonance in $D_s^{*,+}\pi^0$ at 2.46 GeV. Potential models predict that the candidate 3P_0 scalar meson has a mass around 2.48 GeV, which is above the DK threshold and is therefore broad. This observation led to several exotic explanations for the new states.

However, models can be deceiving, whereas QCD removes the puzzle (at least, for now). In the heavy-quark and chiral-symmetry limits of QCD, the heavy-light multiplets $\{0^-, 1^-\}$ and $\{0^+, 1^+\}$ are degenerate, because the spin of the heavy quark decouples.

Spontaneous chiral symmetry breaking splits the parity partners so that the $1^+ - 1^-$ and $0^+ - 0^-$ mass splittings are equal. CLEO sees 351(2) and 350(1) MeV for these respectively. Results from lattice QCD in the quenched continuum limit and for two flavours at fixed lattice spacing (UKQCD 2003) confirm this equality. The spectrum obtained from the simulations is shown in Figure 5 and is consistent with experiment, although the uncertainties are still rather large. Evidently, at the present level of precision, QCD is consistent with the new states being conventional mesons with masses below the DK threshold and hence narrow. No exotic explanations are required (yet).

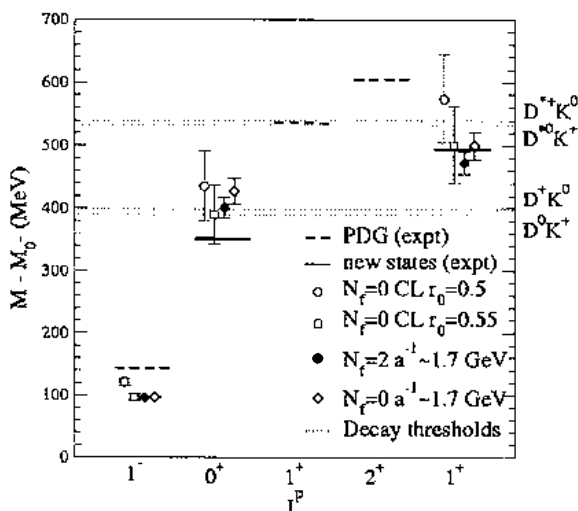


Figure 5. The spectrum of D_s mesons obtained in lattice QCD (UKQCD 2003) compared with experiment. Results at two different values of r_0 , correspond to two ways of setting the scale in quenched QCD.

Neutral kaon mixing and $K \rightarrow \pi\pi$

CP violation in non-leptonic neutral kaon decays may occur through two mechanisms: 'direct' CP violation is when the CP odd component of K_L decays into the CP even two-pion final state, with strength ϵ' ; and 'indirect' CP violation is due to the admixture of a CP even component in the K_L state, with weight ϵ .

$$\begin{aligned}
 K_L &= K^{CP \text{ odd}} + \epsilon K^{CP \text{ even}} \\
 \epsilon' \downarrow &\qquad \downarrow \\
 \text{direct} &\qquad \text{indirect}
 \end{aligned} \tag{3.14}$$

Indirect CP violation is proportional to the matrix element of a 4-quark operator,

$$\begin{aligned}\varepsilon &\approx \left\langle \bar{K}^0 \left| \bar{s} \gamma_\mu (1 - \gamma_5) d \right. \bar{s} \gamma_\mu (1 - \gamma_5) d \right| K^0 \right\rangle \\ &= \frac{8}{3} f_K^2 M_K^2 B_K(\mu).\end{aligned}\quad (3.15)$$

This is the best determined matrix element in continuum quenched QCD. Consistent high-precision results have been obtained from different lattice actions, including the effects of operator mixing (due to the lack of chiral symmetry in the Wilson quark formulation). The best estimate is (JLQCD 1998)

$$B_K^{\overline{\text{MS}}} (2 \text{ GeV}) = 0.63(4) \quad (3.16)$$

but the quenching error is unknown, although it is usually assumed to be around 15%.

The calculation of the matrix elements contributing to direct *CP* violation is much more challenging. Apart from being technically more difficult, there may be significant cancellations so that the estimates are noisy,

$$\varepsilon' = \frac{\text{Re } A_2}{\text{Re } A_0} \underbrace{\left(\frac{\text{Im } A_2}{\text{Re } A_2} - \frac{\text{Im } A_0}{\text{Re } A_0} \right)}_{\text{cancellation can be -ve}}. \quad (3.17)$$

The direct lattice method involves tuning the lattice volume so that one of the (discrete) energy levels of two pions at rest equals the kaon mass. It is then possible to relate the transition matrix element to the decay rate in infinite volume (Lellouch & Lüscher 2001). However, in order to work at the kaon mass, the lattice size must be at least 5 fm, which is very expensive even for quenched QCD.

The indirect lattice method, and the only one employed to date, uses chiral perturbation theory to relate the desired matrix elements to $K \rightarrow \pi$ and $K \rightarrow$ vacuum matrix elements, which are easier to calculate. The results are only for quenched QCD and it is not yet understood whether all the relevant matrix elements have been included. Two groups have published results for ε'/ε , both negative (RBC 2001, CP-PACS 2003). The data from the former group are shown in Figure 6. Although the final results are similar, there are significant differences between the two calculations. For instance, the results for the $\Delta I = \frac{1}{2}$ rule are

$$\begin{aligned}\omega^{-1} &= \frac{\text{Re } A_0}{\text{Re } A_2} \approx 22 \text{ (expt)} \\ &= 25.3 \pm 1.8 \pm \text{syst (RBC)} \\ &= 9.5^{+3.2}_{-1.8} \pm \text{syst (CP - PACS)}.\end{aligned}\quad (3.18)$$

Despite the puzzling values obtained, these computations represent a substantial advance in showing that the cancellation between matrix elements can be controlled. It remains a considerable challenge to understand all the systematic effects, but we can be hopeful that this long-standing problem in strong-interaction physics will eventually be resolved by lattice QCD.

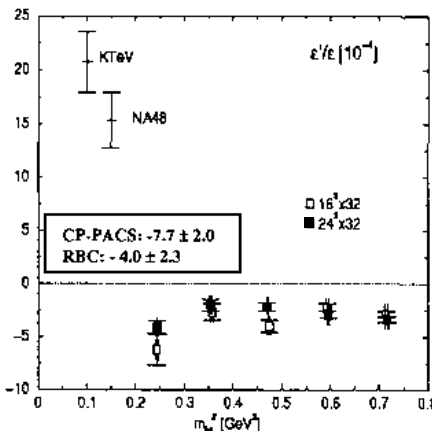


Figure 6. CP-PACS results for ϵ'/ϵ (CP-PACS 2003) compared with experiment (KTeV and NA48) and the RBC result (RBC 2001).

Leptonic decays of heavy-light mesons

The neutral B_q meson mass difference is given by

$$\Delta M_q = \frac{G_F^2}{6\pi^2} M_W^2 \eta_B S_0 \left(m_t^2 / M_W^2 \right) \left| V_{tq} V_{tb}^* \right|^2 M_{B_q} f_{B_q}^2 \hat{B}_{B_q}. \quad (3.19)$$

ΔM_d is measured to within 4% and ΔM_s will be measured in another year. If the leptonic decay constants, f_{Bq} , and B-parameters, B_{Bq} , can be computed, then these measurements will allow the determination of the CKM matrix elements V_{tq} , since the other parameters in Equation (3.19) are known.

The leptonic decay constants

$$\langle 0 | A_\mu(0) | B_q(p) \rangle = i f_{B_q} p_\mu \quad (3.20)$$

are easily obtained from 2-point functions (see Equations (2.5) and (2.6)), although the B meson presents a challenge because it requires that we are able to simulate a wide range of mass scales.

f_{D_s} provides the only direct comparison with experiment that can be used to test the lattice method. Two groups (Jüttner & Rolf 2003, de Divitiis et al. 2003a) have used the step-scaling method to control all the uncertainties in the lattice calculation except quenching. They obtain

continuum quenched QCD	experiment
$f_{D_s} = 252(9)$ MeV (Juettner & Rolf)	$f_{D_s} = 280(17)(25)(34)$ MeV (CLEO 98)
$= 240(5)(5)$ MeV (de Divitiis et al.)	$= 285(19)(40)$ MeV (ALEPH 02) (3.21)

At present the experimental measurement is not precise enough to expose any quenching effect. However, CLEO-c aims to determine the D and D_s leptonic and semileptonic decays to 2% accuracy, so this will eventually become a benchmark for lattice QCD.

We cannot simulate the b quark directly on current lattices without large systematic effects. The Alpha Collaboration (Alpha 2003) obtains f_B , by interpolating between charm data and the static limit (leading order in Heavy Quark Effective Theory (HQET)). de Divitiis et al. (2003a) achieve better control by simulating the b quark directly in a small box (0.4 fm) with a fine lattice ($m_b a \ll 1$) and then using finite-size scaling. Their results for continuum quenched QCD are

$$\begin{aligned} f_B &= 206(10) \text{ MeV (Alpha 2003)} \\ &= 192(6)(4) \text{ MeV (de Divitiis et al. 2003a)} \end{aligned} \quad (3.22)$$

are in good agreement, but again we have no idea how big the quenching effect is. de Divitiis et al. (2003a) also estimate the decay constants for other B mesons,

$$\begin{aligned} f_B &= 171(8)(4) \text{ MeV} \\ \frac{f_{B_s}}{f_B} &= 1.12(2)(1) \\ f_{B_c} &= 347(5)(8) \text{ MeV} \end{aligned} \quad (3.23)$$

although the chiral extrapolation is probably not yet under control and it will be essential to rectify this before we can quantify the quenching effects. The range of light quark masses used in the simulations does not penetrate sufficiently into the chiral regime to distinguish different forms for the chiral extrapolation. In particular, the decay constants vary by 10-20% depending on the scale assumed in the quenched chiral logarithms. For this reason, JLQCD quotes a large upward error on the SU(3) flavour breaking (JLQCD 2003)

$$\begin{aligned} \xi &= \frac{f_{B_s} \sqrt{\hat{B}_{B_s}}}{f_B \sqrt{\hat{B}_B}} \\ &= 1.14(3)^{+13}_{-2} (N_f = 2) \end{aligned} \quad (3.24)$$

and

$$B_{B_s}/B_{B_d} = 1.017(16)^{+56}_{-17}. \quad (3.25)$$

Perils of chiral extrapolation

Now that Ginsparg-Wilson formulations are beginning to be used in simulations, it is becoming possible to test chiral extrapolations. In quenched QCD, the absence of quark loops means that the flavour-singlet pseudoscalar meson propagator yields a double pole and not the full η' mass. Hence there are nine pseudo-Goldstone bosons and this leads to additional quenched chiral logarithms compared with the unquenched theory, eg

$$M_\pi^2 = Am \left\{ 1 - \delta \left[\ln \left(\frac{Am}{\Lambda_\chi^2} \right) + 1 \right] \right\} + O(m^2) \quad (3.26)$$

where δ determines the size of the contribution from the quenched terms and Λ_χ the scale below which they set in.

Simulations of quenched QCD with overlap quark masses down to $M_{\text{PS}} = 180$ MeV (Dong et al. 2003) show that 1-loop chiral perturbation theory, such as Equation (3.26), for $M_m f_n$ and M_N is valid up to $M_{\text{PS}} = 300$ MeV. More importantly, it is not possible to fit the chiral behaviour correctly if data above 300 MeV is included. While nothing can be concluded from this about QCD with dynamical quarks, nevertheless, it provides a stern warning that it may be necessary to push QCD simulations to lighter quark masses than have been possible until very recently for quenched QCD, before we can be sure that we have the correct behaviour to match onto chiral perturbation theory.

Exclusive semileptonic decays

In principle, lattice QCD can provide model-independent form factors for semileptonic b decays to charm and light quarks. These involve computing 3-point functions, as we have seen in Equations (2.7) and (2.8), from which we can extract matrix elements such as

$$\langle \pi(p') | V^\mu | B(p) \rangle = \frac{M_B^2 - M_\pi^2}{q^2} q^\mu F_0(q^2) + \left(p^\mu + p'^\mu - \frac{M_B^2 - M_\pi^2}{q^2} q^\mu \right) F_+(q^2) \quad (3.27)$$

$$q = p - p', \quad V^\mu = \bar{b} \gamma^\mu u.$$

These form factors are extremely valuable input to data analyses by B Factories seeking to extract precise values for the poorly-known CKM matrix elements, $|V_{ub}|$ and $|V_{cb}|$, in order to test the consistency of the Standard Model. However, they present a new challenge for lattice QCD. In addition to the usual problem of controlling the chiral and heavy-quark mass extrapolations, all the hadron momenta must be small to minimise discretisation errors. This typically means that the matrix elements are obtained at large transverse momenta and may have to be extrapolated in transverse momentum in order to reach the experimentally accessible kinematic regime. These extrapolations introduce some model dependence.

A good testing ground for lattice QCD will be semileptonic D decays to π or $K\nu$, because c and s quarks may be simulated directly on currently available lattices, $|V_{cs}|$ is well measured, and there will be an opportunity for a precision test of the lattice form factors when CLEO-c measures the decay rates to a few percent. A recent simulation in 2+1-flavour QCD at fixed lattice spacing (Okamoto et al. 2003) obtained

$$\begin{aligned} F_+^{D \rightarrow \pi}(0) &= 0.69(5) \text{ cf expt } 0.73(13) \\ F_+^{D \rightarrow K}(0) &= 0.76(4) \text{ cf expt } 0.73(2) \end{aligned} \quad (3.28)$$

using the Particle Data Group 2002 values,

$$\begin{aligned} |V_{cs}| &= 0.996(13) \\ |V_{cd}| &= 0.224(16). \end{aligned} \quad (3.29)$$

This is an encouraging start, but it will require a lot more work to reduce the lattice uncertainty to a few percent.

Semileptonic B decays have been studied quite extensively in quenched QCD. Although little is known about quenching effects (these are usually assumed to be at the 10% level), the techniques developed will work for dynamical quarks, so these studies are a hint of what should be possible with more powerful computers.

For $b \rightarrow c$ decays the recoil is relatively small, so the lattice can cover the entire kinematic range and the form factors can be computed from first principles. However, this is not as useful as you might think, because HQET determines the normalisation of the form factors at zero recoil and, to the extent that HQET applies, this enables $|V_{cb}|$ to be determined by extrapolating the $B \rightarrow D^* \ell \nu$ differential decay rate to zero recoil. To make a significant contribution, lattice QCD must quantify the deviations from HQET at the physical b and c masses, for which few-percent accuracy is required. The Fermilab group has shown how the statistical and systematic errors approximately cancel in a particular ratio of matrix elements, in order to estimate the deviation of the form factor from the HQET limit, obtaining (FNAL 2002),

$$F_{B \rightarrow D^* \ell \nu}(1) = 1 - 0.087^{+34}_{-29} \quad (3.30)$$

demonstrating that precision lattice calculations are indeed possible.

The Isgur-Wise function may be extracted from both the $B \rightarrow D$ and the $B \rightarrow D^*$ form factors. In quenched QCD, the functions obtained from these decays at quark masses around charm agree and have no significant dependence on the lattice spacing (over the small range available). This suggests that the HQET picture applies at the charm mass and above. Furthermore, the recoil dependence matches CLEO data with a value of $|V_{cb}|$ consistent with the world average (UKQCD 2002).

For $b \rightarrow u$ decays there is no heavy-quark symmetry to help and lattice QCD comes into its own as the only method that can fix the normalisation of the form factors in a model-independent way. However, because the mass difference between the B meson and the pion is large and the kinematic range of the lattice calculation is restricted to near zero recoil, the form factors can only be computed directly at high q^2 . So, either a model-dependent extrapolation must be used to obtain the full kinematic range, or the differential decay rate must be measured experimentally to extract $|V_{ub}|$. There is a good prospect of the latter happening, as can be seen in Figure 7.

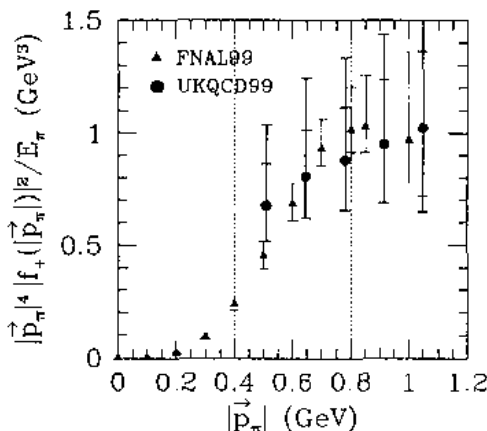


Figure 7. The form factor for $B \rightarrow \pi \bar{\nu}$ decays (Lellouch 1999) computed in quenched QCD by two groups (FNAL 2000, UKQCD 2000). The region between the vertical dashed lines should be accessible to experimental measurement and, if measured, should match the lattice results up to a factor of $|V_{ub}|^2$.

4. Prospects for Physics Beyond the Standard Model

An exciting target for lattice quantum field theory is non-perturbative physics beyond the Standard Model. I will mention two approaches. The first is to compute QCD matrix elements which, in conjunction with experimental data, can be used to estimate, or constrain physics beyond the Standard Model. The second is to extend numerical simulation to supersymmetric field theories.

Rare B decays

Rare decays such as $b \rightarrow s$, which only occur through quantum loops, offer the possibility of glimpsing physics beyond the Standard Model. For instance, the decay $B \rightarrow K^* \gamma$ has been observed and could receive contributions from virtual supersymmetric particles in an extension of the Standard Model, as shown in Figure 8. If we can compute the

Standard Model amplitude, then any difference with experiment can be identified with physics beyond the Standard Model.

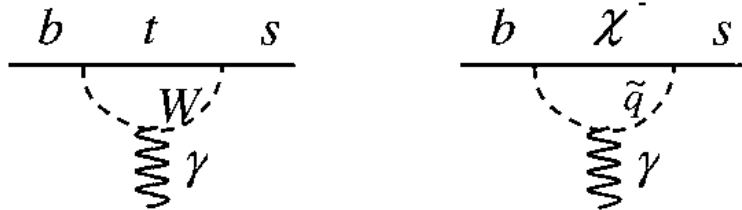


Figure 8. The leading order diagram contributing to $B \rightarrow K^*\gamma$ decay in the Standard Model (left) and a possible contribution from virtual sparticles in a supersymmetric extension of the Standard Model (right).

The lattice calculation involves computing the matrix element

$$\langle K^*(p') | \bar{s} \sigma_{\mu\nu} (1 + \gamma_5) b | B(p) \rangle = \sum_{i=1}^3 c_{\mu\nu}^{(i)} T_i(q^2) \quad (4.1)$$

where now the form factors must be extrapolated from high q^2 to $q^2 = 0$ since the photon is real. The result for the branching ratio obtained in quenched QCD (Becirevic 2002), compared with experiment is

$$\begin{aligned} \text{BR}(B \rightarrow K^*\gamma) &= 0.29(16) \times 10^{-4} \text{ (lattice)} \\ &= 0.42(4) \times 10^{-4} \text{ (expt)} \end{aligned} \quad (4.2)$$

which is, again, encouraging for the lattice method, although a lot remains to be done to get the lattice uncertainties under control and small enough to claim any discrepancy with experiment.

Proton decay

SuperKamiokande, with 79 kt years of observation, has placed the following limits on the proton lifetime for the two most likely decay modes:

$$\begin{aligned} \tau(p \rightarrow K^+ \bar{\nu}) &> 1.6 \times 10^{33} \text{ years} \\ \tau(p \rightarrow \pi^0 e^+) &> 5 \times 10^{33} \text{ years.} \end{aligned} \quad (4.3)$$

These bounds should be pushed at least an order of magnitude higher over the next 5-10 years. Already, they are starting to constrain GUT models and supersymmetric (SUSY) extensions.

In SUSY GUT models, R parity (which requires that sparticles are produced in pairs) forbids dangerous dimension-4 Yukawa-like couplings that would lead to much too rapid

proton decay. At dimension 5, colour-triplet Higgsino exchange can mediate proton decay through the diagrams in Figure 9, when the effective four-point interaction is dressed by sparticles, as in Figure 10. The superfield formalism shows that the four-point interaction must be totally symmetric so that, being colour-antisymmetric requires that it is flavour antisymmetric. Thus, the dominant decay mode is into strange mesons.

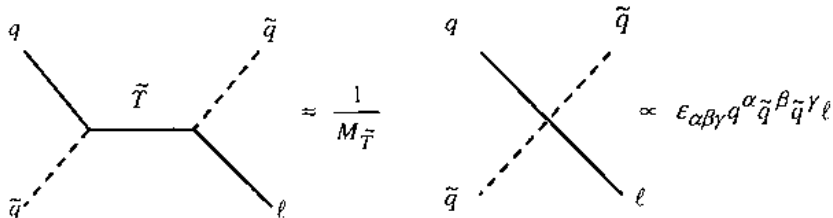


Figure 9. Leading-order colour-triplet Higgsino exchange diagram, which generates a flavour-antisymmetric four-point interaction at low energies.

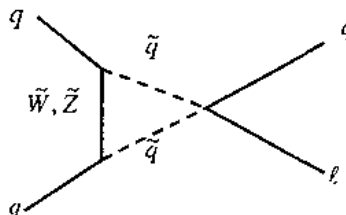


Figure 10. Leading-order diagram mediating proton decay to strange mesons.

These dimension-5 SUSY-GUT interactions, as well as the dimension-6 vector boson exchange interactions in non-SUSY GUTs, all give rise to effective dimension-6 baryon-number violating operators at low energies. The QCD matrix elements of all these operators can be computed in lattice QCD and provide model-independent input to (SUSY-)GUT estimates of the proton lifetime, as noted in Equation (1.1). The matrix elements have been computed at fixed lattice spacing in quenched QCD. To simplify the analysis, chiral perturbation theory may be used to relate them to a single matrix element, which has been computed in the continuum limit of quenched QCD (CP-PACS & JLQCD 2003b),

$$\beta_{\text{latt}} = \langle 0 | \bar{q} q q | p \rangle = 0.0094(19) \text{ GeV}^3. \quad (4.4)$$

The resulting proton lifetime in a particular SUSY-GUT is

$$\tau(p \rightarrow K^+ \bar{\nu}) = 1.6 \times 10^{33} \text{ years} \left(\frac{0.0094 \text{ GeV}^3}{\beta_{\text{latt}}} \right)^2 \left(\frac{M_{\tilde{T}}}{3 \times 10^{19} \text{ GeV}} \right)^2 \quad (4.5)$$

and it is clear that the lower bound on the lifetime places a lower bound on the mass of the colour-triplet Higgsino. This already rules out the minimal SU(5) SUSY-GUT and is within an order of magnitude of ruling out SO(10). The uncertainty in the lattice QCD scale, which enters to the sixth power in Equation (4.5), could easily render the lifetime uncertain by an order of magnitude, while experiment is steadily raising the lower bound. So, achieving greater precision in the lattice QCD matrix element calculation soon could be decisive in setting constraints on particle masses at the GUT scale.

Lattice supersymmetry

There may be important non-perturbative SUSY physics, but is there a non-perturbative regulator? At first sight, a lattice approach seems hopeless. The SUSY algebra says that the anticommutator of two supercharges,

$$\{Q, Q\} = 2P, \text{ the generator of translations} \quad (4.6)$$

and the lattice breaks translation invariance, so there can be no SUSY on the lattice. But, Poincaré symmetry arises as an accidental symmetry in the infrared limit of lattice QCD, because there are no relevant Poincaré-symmetry violating operators. So, perhaps SUSY can arise as an accidental symmetry?

An example of this would be $N = 1$ Super Yang Mills (SYM) in 3+1 dimensions. This model comprises gauge bosons and gauginos, and (in the continuum) has an exact chiral symmetry. As we have seen in Section 2, chiral symmetry can be realised exactly on the lattice and it turns out that, in this case, there are no SUSY-violating operators consistent with the chiral and gauge symmetries. However, simulating this theory is beyond current technology, because it is necessary to simulate both gauge and fermion loops. Unfortunately, this approach doesn't work for SUSY theories with scalar fields, because there is nothing to stop the generation of scalar mass terms which violate the SUSY.

Recently, Kaplan et al. (2003) have proposed an orbifolding method to construct lattice SUSY theories. They start with a matrix model in 0+1 dimensions with a large gauge group $U(kN^d)$ and global symmetry G_R (the so-called 'mother theory'). Then they identify a $(Z_N)^d$ subgroup of $U(kN^d) \times G_R$ and remove from the matrix model any field which transforms non-trivially under $(Z_N)^d$ (this is 'orbifolding'). The resulting matrix model is an N^d site lattice possessing a $U(k)$ gauge symmetry. By this method, Kaplan et al. have constructed SYM lattice models in 1, 2, 3 and 4 Euclidean dimensions with exact SUSY on the lattice to protect them from radiative corrections. The lattice models have complex geometries, some fermion determinants have sign problems which may make them very expensive to simulate and, of course, they all need dynamical massless fermions. So this is not yet a practical approach, but it could become so with more work, if there is sufficient motivation, such as LHC discovering that the world really does possess supersymmetry!

5. Conclusions

Recent theoretical progress has shifted the goal posts compared with the original vision of lattice QCD 30 years ago. We now have exact lattice chiral symmetry and non-perturbative renormalisation giving, in principle, an unforeseen degree of control over the systematics of lattice simulations. This is tempting us to ask harder questions of lattice QCD, involving computing complicated matrix elements and demanding that the lattice results match smoothly onto those of effective theories. It is also expanding the range of quantum field theories that are accessible to non-perturbative study, eg to chiral and SUSY gauge theories. We are increasing the reach of lattice phenomenology with the prospect that precision low-energy computations may constrain physics beyond the Standard Model. The computational cost of all of this is much higher than originally expected. Fortunately, algorithmic improvements and the relentless advance in computer power will continue to sustain this ambitious programme.

References

- Alpha 2003, Della Morte, M., et al., Lattice HQET with exponentially improved statistical precision (arXiv:hep-lat/0307021).
- Becirevic, D.. 2002, Lattice results relevant to the CKM matrix determination (arXiv:hep-ph/0211340).
- CP-PACS 2000, Aoki, S., et al., Phys. Rev. Lett. 84 (2000) 238 (arXiv:hep-lat/9904012).
- CP-PACS 2002, Ali Khan, A., et al., Phys. Rev. D65 (2002) 054505 (arXiv:hep-lat/0105015).
- CP-PACS 2003, Noaki, J., et al., Phys. Rev. D68 (2003) 014501 (arXiv:hep-lat/0108013).
- CP-PACS & JLQCD 2003a, Kaneko, T., et al., Light hadron spectrum in three-flavor QCD with O(a)-improved Wilson quark action (arXiv:hep-lat/0309137).
- CP-PACS & JLQCD 2003b, Tsutsui, N., et al., Continuum limit of proton decay matrix elements in quenched lattice QCD (arXiv:hep-lat/0309139).
- de Divitiis, G. M., et al. 2003a, Nucl. Phys. B672 (2003) 372 (arXiv:hep-lat/0307005).
- de Divitiis, G. M., et al. 2003b, Nucl. Phys. B675 (2003) 309 (arXiv:hep-lat/0305018).
- Dong, S.J., et al. 2003, Chiral logs in quenched QCD (arXiv:hep-lat/0304005).
- FNAL 2000, Ryan, S. M., et al., Nucl. Phys. Proc. Suppl. 83 (2000) 328 (arXiv:hep-lat/9910010).

- FNAL 2002, Hashimoto, S., et al., Phys. Rev. D66 (2002) 014503 (arXiv:hep-ph/0110253).
- Ginsparg, P. H., & Wilson, K. G., 1982, Phys. Rev. D25 (1982) 2649.
- Hamber, H., & Parisi, G., 1982, Phys. Rev. Lett. 47 (1982) 1792.
- Hernández, P., et al. 1999, Nucl. Phys. B552 (1999) 363 (arXiv:hep-lat/9809010).
- JLQCD 1998, Aoki, S., et al., Phys. Rev. Lett. 80 (1998) 5271 (arXiv:hep-lat/9710073).
- JLQCD 2003, Aoki, S., et al., B-Bbar mixing in unquenched lattice QCD (arXiv:hep-ph/0307039).
- Jüttner, A., & Rolf, J., 2003, Phys. Lett. B560 (2003) 59 (arXiv:hep-lat/0302016).
- Kaplan, D. B., et al. 2003, JHEP 0305 (2003) 037 (arXiv:hep-lat/0206019).
- Lellouch, L., 1999, Exclusive semileptonic B decays: lattice results and dispersive bounds (arXiv:hep-ph/9912353).
- Lellouch, L., & Lüscher, M., 2001, Commun. Math. Phys. 219 (2001) 31 (arXiv:hep-lat/0003023).
- Narayanan, R., & Neuberger, H., 1993, Phys. Lett. B302 (1993) 62.
- Neuberger, H., 1998, Phys. Lett. B417 (1998) 141 (arXiv:hep-lat/9707016); Phys. Lett. B427 (1998) 353 (arXiv:hep-lat/9801031).
- Okamoto, M., et al. 2003, Semileptonic decays of D mesons in unquenched lattice QCD (arXiv:hep-lat/0309107).
- RBC 2001, Blum, T., et al., Kaon matrix elements and CP-violation from quenched lattice QCD: (I) the 3-flavour case (arXiv:hep-lat/0110075).
- Rolf, J., & Sint, S., 2002, JHEP 0212 (2002) 007 (arXiv:hep-ph/0209255).
- UKQCD 2000, Bowler, K. C., et al., Phys. Lett. B486 (2000) 111 (arXiv:hep-lat/9911011).
- UKQCD 2002, Bowler, K. C., et al., Nucl. Phys. B637 (2002) 293 (arXiv:hep-lat/0202019).
- UKQCD 2003, Dougall, A., et al., Phys. Lett. B569 (2003) 41 (arXiv:hep-lat/0307001).
- Wilson, K. G., 1974, Phys. Rev. D10 (1974) 2445.

CHAIRMAN: R. D. KENWAY

Scientific Secretaries: W. Menges, M. Rotaev.

DISCUSSION 1

- *Bozza:*

Do you use lattice QCD in SUSY processes for the hadronization only or also for SUSY fields?

- *Kenway:*

Up to now, not so much has been done using lattice calculations for supersymmetry. There has been some progress recently in formulating certain supersymmetric gauge theories on the lattice with a well-defined continuum limit. There have been some initial simulations of a N=1 Super Yang-Mills theory which has a gauge boson and a gaugino, but no scalar fields, because they can cause problems with the continuum limit. Some correlation functions were measured to determine the spectrum of bound states. The statistics were low, and the spectrum does not look like what is expected. The main difficulty of these simulations is to treat fermions and bosons equally, but fermions are expensive to simulate. Often in lattice QCD the quenched approximation is made, where no fermion loops are included in the vacuum. This is not a good way to treat supersymmetry on the lattice and more powerful computers will be needed for these simulations.

- *Sykora:*

Can you test QED on the lattice?

- *Kenway:*

Yes, we can formulate QED on the lattice. Not surprisingly, this formulation is just the same as for QCD. Where there is a difference is how you approach the continuum limit. In QCD, essentially because of asymptotic freedom, you know that the continuum limit occurs near $g^2=0$, where you have perturbation theory to rely on, that can tell you how physical quantities should behave as functions of g^2 .

The problem in QED, as you know, is that there is no asymptotic freedom. The coupling runs in the opposite way, so that to decrease the lattice spacing you are driven towards strong coupling, specifically the Landau pole, where perturbation theory breaks down. There may be critical points in the electric charge – electron mass plane, where you can define a continuum limit, but this may look nothing like perturbative QED. These problems may go away when QED is embedded in electroweak theory.

- *Sykora:*

In principle, maybe we do not need the continuum limit? Maybe it is our mistake?

- *Kenway:*

This is an option if you want to take QED on its own. You could regard QED as an effective theory with a cut-off, which is just a small lattice spacing. What has stopped people attempting to do this is simply that the sizes of the lattices you need are very much bigger than it is possible to compute with today.

- *Sykora:*

Is it necessary to keep Lorentz invariance? The violation is, as you said, proportional to the lattice spacing “ a ”, and it can be also a way to study a non-commutative QFT.

- *Kenway:*

In general, there are two possibilities on the lattice which protect you from generating a term that could break Lorentz invariance. One is that the lattice theory possesses symmetry which prevents the generation of such terms. The other is that the continuum symmetry you are looking for appears accidentally, because there is no relevant operator, which could break the symmetry. I am not sure in the case of non-commutative geometry whether such possibilities arise, but the continuum limit will be determined by the symmetries which are recovered (and the dimension). Some people are starting to simulate lattice non-commutative geometries in low dimensions, so there may be some results relevant to your question soon.

- *Krotov:*

What is the method that is used to evaluate the integral for the partition function? How do we determine the measure, boundary conditions, how do we deal with the gauge invariance?

- *Kenway:*

First of all, if you are only interested in calculating expectation values of gauge invariant quantities, like hadron correlation functions, then you do not need to fix a gauge. The main breakthrough Wilson made when he reformulated QCD on the lattice was to realize that, instead of using the fields A_μ that you use in the continuum which are elements of the algebra, you can formulate the lattice theory in terms of the elements of the gauge group SU(3). This is a compact group, and the integration over the group manifold is finite. You may recall something about parallel transport of colour. If I want to transport a quark field, which is a coloured object, from some point X to another point Y and preserve local gauge invariance, then I must multiply it by the exponential of the line integral of the gauge field from X to Y. That is familiar from the continuum gauge theory. This factor is an element of the gauge group, so if X and Y are neighbouring sites of the lattice, then we can use this factor in a discrete form for the lattice gauge field. The path integral becomes a multiple integral over the elements of the group on each link of the lattice. As I said this morning, the quark fields that sit on the lattice sites are Grassmann variables, so it is problematic to integrate them numerically. It is possible only for low dimensional

systems. Fortunately, the Grassmann integrals that you have to do involve only the exponential of a quadratic form, the lattice Dirac action, and this can be done analytically, giving the determinant of the Dirac matrix. Finally, the integrals over the Haar measure of the gauge group are performed by Monte Carlo.

- *Gripaios:*

Why do scalar fields pose a problem for the continuum limit of lattice supersymmetric gauge theory?

- *Kenway:*

The point is that there is nothing to stop the production of scalar field mass terms unless there is a chiral symmetry in the lattice theory, which prevents it. The scalar field mass term breaks the supersymmetry. In the continuum limit you could try to tune the scalar mass to zero, but you cannot guarantee that your limit recovers the supersymmetry, because operators which transform differently under supersymmetry could mix in a complicated way on the lattice.

- *Oswald:*

We know that chiral symmetry breaking is associated with an order parameter. But we also need the infinite volume limit for that. If you take the limit $a \rightarrow 0$, how can you make sure that you get a correct order parameter with correct properties?

- *Kenway:*

A continuous symmetry in a finite system cannot have a non-zero expectation value. This occurs often in statistical mechanics. So the technique used in statistical mechanics is the same as we use here: you have to put in explicitly a mass term, which couples to the order parameter, to give it a non-zero value. In statistical mechanics language, this is called an external field. Then you take the infinite volume limit before taking the external field to zero. In brief, it is the order of the limits which matters.

- *Papadimitriou*

How can you trust what the lattice calculation tells you in the continuum limit? In particular, there could be a second order phase transition which prevents you from obtaining confinement in the continuum limit.

- *Kenway:*

The theory on the lattice has been shown rigorously to be confining and all simulations so far show no indication of a phase transition in the continuum limit into a deconfined phase. But this is not a proof, only a practical demonstration. However, the evidence for confinement is very compelling.

- *Markov:*

Could lattice QCD help us to identify the effective degrees of freedom. If yes, what calculations must be carried out?

- *Kenway:*

There is a long-term hope that simulating the low energy properties of QCD will enable us to get some idea of what an effective theory would be, that encapsulates the most important degrees of freedom. This certainly has not been delivered so far. I think, the approach, which is more likely to work, is to start from the other direction and say: for theoretical reasons some model seems to be a good approximation, for instance a gas of instantons, and attempt within your simulation to match the parameters of that model. To the extent that this makes sense, perhaps it can give you the answer to your question, telling you that these particular topological excitations, or whatever, somehow play a significant role.

People who are trying to understand the confinement mechanism are doing this. They are trying to understand what topological excitations are playing a dominant role in generating the linear potential between quarks.

- *Markov:*

What is the force between gluons in pure gluodynamics at large distances?

- *Kenway:*

The potential between coloured objects is linear at large distances. You can compute the potentials in lattice QCD between colour sources in various representations and extract the corresponding values for the string tension (see papers by Michael).

- *Lysov:*

What is the non-perturbative formulation of lattice QCD? Can you write down the action ?

- *Kenway:*

The $F_{\mu\nu}F^{\mu\nu}$ term in the action comes from taking the trace of the product of the link variables around an elementary plaquette. As $a \rightarrow 0$, this gives you the Yang-Mills action plus corrections proportional to a^2 . The fermionic part of the action is obtained by using a finite difference approximation for the covariant derivative in the Dirac action, although you have to be careful because of the Nielsen-Ninomiya No-Go Theorem, as I explained this morning.

- *Lysov:*

And what about the linear term in F ?

- *Kenway:*

There is no linear term in F due to the trace.

- *Lysov:*

Does this action work only in D=4?

- *Kenway:*

This works in any dimension.

- *Kuperstein:*

Do we have to fix the gauge freedom in the lattice gauge theory?

- *Kenway:*

No, provided you only want to calculate gauge invariant quantities. The entire formulation is gauge invariant and the integrals over the gauge group for each link variable are finite, so you never need to fix the gauge. You may ask, what happens if I try to calculate the correlation functions for quark or gluon fields? Then I do have to fix the gauge on the lattice, otherwise the result is zero, and you get into all the problems of gauge dependence familiar in the continuum. It is difficult to interpret results in a fixed gauge, but there are some instances where it is useful to do that. However, generally speaking, what I will be talking about is the calculation of physical matrix elements or hadron masses and they all involve working in a gauge invariant way, so we do not have to worry about fixing the gauge.

- *Kuperstein:*

You made a remark that one of the latest directions in lattice QCD is to introduce a non-local interaction. Does this non-locality disappear in the continuum limit?

- *Kenway:*

The lattice formulations which implement chiral symmetry exactly give up ultralocality. That is, instead of the interaction terms in the action being non-zero only over a finite (usually small) number of sites, they extend across the whole lattice, but their strength falls exponentially with distance. This is sufficient to ensure a local field theory is obtained in the continuum limit. However, this exponential locality of interactions is not guaranteed for all parameter values in the lattice action and must be checked in practice.

- *Rotaev:*

How does the lattice parameter "a" relate to the renormalization parameter Λ ?

- *Kenway:*

It is the usual dimensional transmutation in which, by taking the cut-off away, you dynamically generate the scale Λ in QCD. In this respect, the lattice spacing is just like the (inverse of) the momentum cut-off you introduce to regularise QCD in perturbation theory.

CHAIRMAN: R.D. KENWAY

Scientific secretaries: D. Krotov, V. Lysov

DISCUSSION II

- *Gripaios:*

In lattice estimates of quark masses, adding dynamical quarks always pushes down the estimate of the quark mass. Is there an explanation of this?

- *Kenway:*

No. This is the lattice telling us something about the real world. It is quite significant, particularly for the strange quark mass. The theoretical value for ϵ'/ϵ is inversely proportional to the square of the strange quark mass. Early estimates of the strange quark mass were much higher than the value of about 100 MeV, which is coming from simulations. This has the effect of boosting the theoretical prediction for ϵ'/ϵ . Now we have good experimental measurements, that boost seems to be needed. So there is really quite important physics here, not just the calculation of SM parameters.

- *Cerri:*

What is the computational power required?

- *Kenway:*

The cost of the calculations depends on such parameters as the lattice spacing, the number of lattice sites, the quark mass parameters, and so on.

It is a challenge to pin down the formula for how the cost depends on the lattice parameters, because this requires testing algorithms in regimes where the cost is high. Although the lattice community believes these studies are important, it is difficult to divert enough computer resources, or human effort, from more interesting physics to do this work. Currently, our best estimate is that the number of arithmetic operations depends on the linear size of the box to some power which is between 4 and 5, the inverse of the lattice spacing to some power between 7 and 9 and on the mass of the lightest quark through the inverse of the corresponding pseudoscalar meson mass to a power between 2 and 3.

A simple thing you want to do during your calculations, if you are calculating the properties of some hadron on a particular lattice, is to check whether your result depends on the lattice spacing. You might repeat the calculation with half the lattice spacing and all other parameters fixed, but to do this you need 500 times more computer power. So, even if the first calculation was done on a PC, checking it requires a much higher performance machine. There are two things which come to our rescue: computer speeds grow exponentially and double every 18-24 months; and due to translation invariance, you can distribute the calculations efficiently over many

microprocessors, one piece of the lattice on each, and you can just build larger and larger machines, with more and more microprocessors.

- *Cerri:*

Are there plans/predictions available for inclusive properties of the semileptonic b-decays?

- *Kenway:*

The computation of inclusive quantities is rather challenging. Most work has concentrated on exclusive quantities, because they are more easily computable. Work on inclusive properties is still at a technical stage and the numerical results are rather preliminary.

- *Rotaev:*

The uncertainties in computer simulations play a crucial role in incorporation with experiment. What are the general ideas for computation of error estimates?

- *Kenway:*

Generally, the statistical errors can be reduced by applying more computer power. The set of input parameters, the quark masses, the lattice size and lattice spacing in physical units, control the systematic uncertainties. Because the hadron has a size of around one fermi, the lattice spacing must be much smaller than one fermi, and the linear size of the lattice must be significantly bigger than one fermi. Then all the lattice effects are small and we can model the dependence on the lattice spacing and the finite volume using various effective theories. Large quark masses take the theory into the regime where heavy quark effective theory works. Small quark masses take it to the regime where chiral perturbation theory works. For relatively large boxes, the volume effects fall exponentially. Typically, lattices are now sufficiently large that the finite volume effect does not influence the phenomenological predictions much. Symanzik quantified the discretisation errors with an effective theory order by order in powers of the lattice spacing. The lattice spacing effects are now so well understood that people add irrelevant terms to the action to explicitly cancel the leading lattice spacing effects.

The big problem today is the connection with chiral perturbation theory. Only now are we starting to be able to simulate with chiral invariant actions at small quark masses where chiral perturbation theory is effective.

Once we are able to match the lattice QCD simulation onto an effective theory, in whatever direction we vary the input parameters away from the regime where the simulations are under control, then we are finished.

- *Bozza:*

Is it possible to use lattice QCD to compute only static observables such as masses, or can you also model dynamic situations such as colliding nuclei?

- *Kenway:*

The difficulty is that the theory is formulated in Euclidean space and we do not have a good way to analytically continue the numerical results back to Minkowski space. The quantities, such as hadron masses and matrix elements given by two and three point correlation functions, do give you quite a lot, but unfortunately not everything.

- *Skinner:*

Do you think there is much prospect for improved algorithms, or should one wait for better computer power to get more precise results in lattice QCD?

- *Kenway:*

Over the past 20 years or so, the improvement in precision has been as much due to algorithmic improvements as to increased computer power. The problem is that progress in algorithms happens suddenly and unexpectedly. All the algorithms which we use rely on local updating of the fields. Step by step, we change the fields at each lattice site in order to get a new field configuration. It is well known in statistical mechanics that you should exploit the collective behaviour and update some big structure in one operation. This type of algorithm can reduce the exponent in the cost formula and result in big savings. But nobody knows how to formulate these cluster updates for gauge theories.

- *Casalderrey-Solana:*

Are instantons included in the lattice calculations? If they are, is it possible to disentangle their contribution? If not, why?

- *Kenway:*

Instantons are contained in the QCD simulations, because we are simulating the QCD vacuum from first principles. The problem arises in trying to disentangle topological excitations from everything else in the configuration. The usual way is to modify the configurations by cooling them to remove small scale fluctuations, or going into a gauge where the topological excitations can be easily identified, but you do not know whether, in doing this, you are left with the correct physics. It is a difficult area, but there has been a lot of work and some understanding is emerging. You should refer to Mike Teper's lectures here last year to find out more.

- *Markov:*

What is the constituent quark mass from the point of view of the lattice?

- *Kenway:*

It is difficult to define the constituent quark mass uniquely in lattice QCD. You could take it to be the pole in the quark propagator in a fixed gauge and, of course, you can compare the excitation spectrum for hadrons with the results of quark

potential models. But I do not think the concept of constituent quark is helpful in lattice QCD.

- *Oswald:*

Do you think that you will profit from quantum computers one day?

- *Kenway:*

Feynman first had the idea to use quantum computers to simulate quantum systems directly. Will one ever use this idea in my lifetime? I do not know. There has been a lot of technological progress, but I think it will still be many years before we have quantum computers which are more powerful than classical computers.

- *Sykora:*

People invented lattice calculations since they were not able to solve models non-perturbatively. For example, for airplanes we construct models since we are not able to calculate anything. Where is the border of your methods? I mean, maybe in some cases it would be easier to build an accelerator than to use lattice calculations.

- *Kenway*

We do not know what the limit is for the chirally symmetric formulation of lattice QCD. With the older formulations, we expected that we could solve QCD using a few hundred teraflops computers. A teraflops is 10^{12} operations per second. Now we are near to having a computer with 5 teraflops, but we have invented a new formulation which allows us to make much more sophisticated calculations - perhaps we need another factor of 100. We expect that in 2005 there will be a computer capable of over 100 teraflops. For lattice QCD, the limit is money. And the money we allocate to lattice QCD is much less than the money we spend on detectors. For example, the 5 teraflops machine which we are building costs about 7 million euros.

- *Cifarelli:*

Could you tell us something about the most powerful computers which are used in QCD simulations? I know about the Columbia project and the Italian one.

- *Kenway:*

UKQCD is working with Columbia University and Brookhaven National Lab to develop a specialised microprocessor for QCD using standard IBM components. This is called QCDOC, "QCD on a chip", and we are now testing the first chips. The most important optimization is fast on-chip memory, because it is memory accesses which usually limit the performance of QCD codes. Each microprocessor has all the functionality of a computer and communications links which will enable us to connect 10000 microprocessors into a 6 dimensional mesh. This should give us a computer in 2004 that is 10 times faster than anything available for QCD today. There are two other projects relevant to QCD. One is the apeNEXT project in Europe which is similar to QCDOC, but aims to build less powerful machines. The second is the Earth

Simulator which was built in Japan. It cost about half a billion dollars and sustains 26 teraflops for some climate codes. In fact, QCD performs badly on this computer, because of the slow communication between processors.

- *Baldini*:

You did not mention glueballs; because of the lack of time or are there some problems with this?

- *Kenway*:

I was asked to talk about the latest results and there has been no news on glueballs for several years. The glueball spectrum was computed in pure Yang-Mills theory 3-4 years ago using a special technique which gave very precise results in the continuum limit. The problem is that the glueballs must mix with the light quarks and you need to have the light dynamical quarks in the simulations. Until we can simulate light quarks, it is pointless to try to improve the quenched results. Current simulations, in which the masses of the dynamical quarks are too large, do see small effects, but we are really waiting for simulations with a chirally symmetric action with much lighter quarks.

- *Nikolaev*:

Is it possible to use chemical computations for QCD?

- *Kenway*:

The chemical computations concern quantum mechanical problems, and we are trying to investigate a quantum field theory. So, I do not see how these methods can be used.

- *Rotaev*:

Are there any attempts to simulate higher dimensional theories just to check some theoretical predictions?

- *Kenway*:

There has not been much work since some early simulations of Yang-Mills in higher dimensions. It is expensive because the number of calculations grows with the lattice volume. Four-dimensional chirally symmetric QCD can be formulated on a five-dimensional lattice, so we are simulating higher dimensions in that context, but this is really to simplify the algorithm and probably does not have a deep physical significance.

- *Papadimitriou*:

Spinor properties are different for Euclidean and Minkowski signature. The lattice results cannot be Wick rotated. Can you make any conclusions about chirality in Minkowski space?

- *Kenway:*

There is no well-defined way to analytically continue numerical data into Minkowski space. So we cannot say anything.

- *Papadimitriou:*

But if you want to measure some physical quantities, you should make a Wick rotation.

- *Kenway:*

Not for all quantities. We can extract some physical matrix elements and hadron masses from the Euclidean space calculation without any Wick rotation, as I showed yesterday.

- *Krotov and Lysov:*

Are there any attempts to compare the lattice simulations with some exactly solvable models, just to investigate the method of lattice calculations?

- *Kenway:*

There are statistical mechanical models in two dimensions for which there are exact results, for example the Ising model. These have been simulated on very large lattices and the agreement with the exact results is perfect.

- *Krotov and Lysov:*

And is it possible to simulate some kind of a quantum field theory in two dimensions, for example, since several of them have analytical solutions too?

- *Kenway:*

Two-dimensional sigma models can be simulated on the lattice and the results agree precisely with the analytical predictions.

Quark-Gluon Plasma Physics

F. Karsch
Bielefeld University

Only the discussions are reported here,
since the camera-ready copy of the contribution
did not arrive in time.

CHAIRMAN: F. KARSCH

Scientific Secretaries: J. Casalderrey-Solana, D. d'Enterria

DISCUSSION 1

- *Galletly:*

You studied a system where the fermions transformed in the adjoint representation as opposed to the fundamental representation. What do you gain from this?

- *Karsch:*

We wanted to show that there are gauge theories which actually have two different phase transitions (confinement-deconfinement and chiral symmetry restoration) at two different temperatures. This is not the case in QCD, where the fermions are in the fundamental representation; but when you take a quite similar theory with fermions in the adjoint representation, you can really get thermal systems which have two different phase transitions. The reason for this is that in the adjoint representation, fermions are blind to the centre of the SU(3) group; so you still have an exact Z_3 symmetry in the fermion sector which you do not have in QCD. Therefore you can break two different symmetries at two different temperatures.

- *Gripaios:*

It is very interesting that we have two theories, one with fundamental fermions where deconfinement and chiral symmetry restoration coincide, and one with adjoint fermions where they do not. Are there other theories in which this has been studied?

- *Karsch:*

There are some older calculations by J. Kogut and collaborators where they consider fermions in other (higher) representations. These calculations, however, have been performed only in the quenched approximation.

- *Skinner:*

Can one treat a finite T gauge theory as a dimensionally reduced theory at high T – there seems to be a conflict between requiring high T and having only low energy modes in the theory?

- *Karsch:*

In fact, it is quite common to analyse properties of gauge theories in the high temperature limit in terms of a dimensionally reduced theory. In this case one does, however, not focus on properties of the high energy modes, which are integrated out and show up only in the couplings of the reduced theory, but focuses on properties of the low momentum modes.

- *Oswald:*

You showed a plot of $\langle L \rangle$ versus temperature which goes from zero to some finite number, which is usually smaller than one on the lattice. If one increases the number of time-steps, N_τ , then this number gets smaller, so that eventually for very large N_τ the expectation value becomes zero for all temperatures. How does one take account for this renormalization problem on the lattice?

- *Karsch:*

The Polyakov loop as such is indeed an ultraviolet divergent quantity and one has to renormalize it properly. The way we have done it in recent times is by defining it through the long distance behaviour of the two-point correlation function. We take the two-point correlation function at infinite distance and the square root of that is the Polyakov loop expectation value. In order to renormalize the two-point correlation function itself, we match the associated free energy to the corresponding zero temperature heavy quark potential. Indeed, at short distances, even at finite temperatures, the free energy of the quark-antiquark system is nothing else but the zero temperature potential energy, because the $q\bar{q}$ system does not see the medium where it lives at all. Having done this renormalization at short distances, the long distance behaviour is controlled and one obtains a renormalized Polyakov loop which is well defined for all different lattice spacings and of course stays finite in the continuum limit.

- *Lendermann:*

In thermodynamics, the concept of temperature usually applies to an equilibrium state. Is there a characteristic time in a heavy-ion collision necessary to attain thermal equilibrium? What is this time in modern experiments?

- *Karsch:*

In a Heavy Ion Collision you start from a situation that is far from equilibrium and you have to establish equilibrium for the quantities you want to describe by thermal models. This equilibration will set in at different time scales for the different energy modes you are interested in. As for the typical equilibration time, calculations that describe, for instance, elliptic flow require very short equilibration times of the order of a fraction of a fm, whereas the lifetime of the system is of several fm.

- *Lendermann:*

Are there any significant corrections due to electromagnetic effects in the description of QGP?

- *Karsch:*

For the thermodynamics of QCD it does not matter at all.

- *Giovannangeli:*

You have shown that $T_c(\text{chiral restoration}) = T_c(Z(N) \text{ breaking})$. Are there any theoretical reasons for that?

- *Karsch:*

There seems to be no deep argument why the two temperatures should coincide. More or less strict arguments tell us that deconfinement should happen before or at chiral symmetry restoration. Looking at the quark mass dependence in the heavy quark limit, deconfinement happens at a higher temperature (something like 270 MeV) whereas in QCD with light quarks the transition takes place at 170 MeV. This could mean that chiral symmetry would not play a role in QCD, deconfinement would happen at 270 MeV. However, chiral symmetry restoration sets in earlier and then, deconfinement is forced by chiral symmetry restoration to take place at the same temperature.

- *Papadimitriou:*

Is there a competing semi-analytical method for evaluating the Polyakov loop on the lattice? If yes, does it give reliable information in the continuum limit?

- *Karsch:*

I only know about perturbative calculations of the Polyakov loop at high temperature. There are also effective models constructed in terms of Polyakov loops which you can use to get some understanding of the phase transition. However, this is not a direct calculation of the Polyakov loop expectation value.

- *Rotaev:*

What is the influence of finite size effects in the quark-gluon plasma phase transition?

- *Karsch:*

As far as thermodynamics on the lattice is concerned, a system which is of the order of 2 to 3 times larger than the inverse temperature has to be considered as a large system. Therefore, with the relevant temperatures being of the order of 200 MeV, systems with a spatial extent of the order of 2 or 3 fm can be considered for all practical purposes as infinitely large and you do not have to worry about strong finite size effects in such a system.

- *Sykora:*

What parts of the QCD phase diagram have been investigated on the lattice ?

- *Karsch:*

Since the first calculations, about 20 years ago, the region most studied is that of vanishing chemical potential and rather high temperatures. These calculations have been recently extended up to finite chemical potentials which are of the order of the

temperatures itself. Namely, for values of $\mu_q \sim 200$ MeV corresponding to $\mu_{\text{baryon}} \sim 600$ MeV, somehow larger than half the value of the nucleon mass. This brings us close to the interesting chiral critical point where the system undergoes a 2nd order phase transition.

- *Lysov:*

Could you say something more about the 3rd phase of the QCD phase diagram: the colour superconductor phase?

- *Karsch:*

This sector of the phase diagram found much attention recently and a lot of work has been performed to explore properties of QCD in this regime. There are various colour superconducting phases discussed at length in recent reviews like those of e.g. F. Wilczek and K. Rajagopal, E. Shuryak, T. Schäfer, M. Alford...

- *Markov:*

$T > 0$ breaks Lorentz symmetry. Does the QCD thermodynamics depend on the reference system you are in?

- *Karsch:*

Yes, of course. When one writes down the partition function itself, one has chosen a preferred rest frame for the thermodynamical system, whose overall momentum is zero. In a heavy-ion reaction this would correspond to the mid-rapidity region.

- *Krotov:*

Why do we need LHC to study the QGP if the temperature of the QCD phase transition is as low as 170 MeV?

- *Karsch:*

Heavy-ion collisions at LHC will create a system at much higher energy density in the initial state than those created at lower energy accelerators. Already at RHIC there are experimental indications that the attained energy densities at the beginning of the reaction are much larger than the critical QCD value. These systems expand and cool down rapidly, so at LHC they will stay for much longer time in the plasma phase and, thus, we will have much better possibilities for equilibrating them. In this way, we can hope to get much cleaner signals of the QGP.

- *Dainese:*

Can you comment on the fact that $T_c \sim m_\pi \sim \Lambda_{\text{QCD}}$?

- *Karsch:*

The fact that T_c is close to the pion mass is accidental. I will discuss this tomorrow in my presentation.

- *'t Hooft:*

When there is a first order phase transition, there will be a surface layer separating these phases. Have such surfaces been studied and is there a way to detect them experimentally?

- *Karsch:*

Indeed such surfaces should exist if the phase transition is 1st order and they have been studied in lattice QCD, where for instance, the surface tension has been computed. Pure SU(3) gauge theory has such surfaces between the partonic and hadronic phases. But in the real world, with quarks, there is no first order phase transition, so one cannot talk about such surfaces.

- *d'Enterria:*

We learned from Kenway's lectures that the most advanced way to realize exact chiral symmetry on the lattice is using "Ginsparg-Wilson" fermions. All recent QCD thermodynamics calculations on the lattice that I know of, have been done with staggered fermions. Are there any calculations using Ginsparg-Wilson fermions?

- *F. Karsch:*

There are calculations with Wilson fermions and with staggered fermions which agree, for instance, on the value of the critical temperature. The Wilson fermions have more problems with discretization errors as well as realizing continuous symmetries on the lattice. There are studies with domain-wall fermions, which are a variant of the "overlap" or Ginsparg-Wilson fermions, by the Columbia group. The value of T_c that they obtain agrees with that obtained by using the other methods. However, the amount of computational power one needs to run such studies is huge and thus one needs supercomputers in the Teraflops regime to do calculations that, with staggered fermions, one could do already on rather small PC clusters. It is good to have the exact symmetries in the lattice formulation but so far it requires probably too much effort to use this implementation of chiral fermions in thermodynamic studies.

CHAIRMAN: F. KARSCH

Scientific Secretaries: A. de Freitas, P. Otiougov, O. Shekhtovtsova

DISCUSSION II

- *D'Enterria:*

- 1: On the lattice, the high temperature behaviour of the equation-of-state (EOS) does not reach the Stefan-Boltzmann ideal gas limit. What is the physical reason for this?
- 2: If one fits phenomenologically the density of hadronic resonance states to the Hagedorn spectrum independently for baryons and for mesons, one gets two different temperatures. Is this observation reproduced on the lattice?
- 3: What limits the lattice calculations of the EOS at low temperatures ($T < T_c$)?

- *Karsch:*

1. As you correctly noticed on the graph I have shown for the energy density, the Stefan-Boltzmann limit is not reached at temperatures a few times the transition temperature. However, we do not expect the QGP to be a simple ideal gas at these temperatures. There are perturbative corrections as well as non-perturbative effects arising; for instance, from the generation of a thermal (Debye) mass for the gluons. The Stefan-Boltzmann limit will be reached at very high temperatures. However, because of asymptotic freedom, thermodynamic quantities like the energy density will approach this limit very slowly (the running coupling decreases only logarithmically with increasing T).

This has not been checked in direct simulations of QCD in (3+1)-dimensions. The logarithmic approach to the Stefan-Boltzmann limit has, however, been studied in dimensionally reduced, 3-dimensional QCD.

2. When comparing lattice results with resonance gas models we have used the experimentally measured resonances rather than a fit to them. The lattice calculations thus cannot directly be compared to fits for the hadron spectra in the meson and baryon sectors.

3. The fact that in the low temperature phase only massive particles (hadrons) contribute to the thermodynamics leads to an exponential decrease of the energy density at small temperatures. The statistical accuracy of the lattice calculations thus rapidly is lost below T_c . This problem is enhanced due to the fact that current simulations are not performed at the physical values of the quark masses. For this reason even the pion is a rather heavy hadron with a mass about 3 to 4 times larger than in nature.

All this limits current studies of the thermodynamics in the low temperature phase to $T > 0.5T_c$.

- *Casalderrey-Solana:*

- Is it possible to study the transition temperature at different values of the chiral condensate?

- *Karsch:*

The chiral condensate always vanishes at the phase transition point. One starts with the zero temperature theory which has a certain value of the chiral condensate. As you increase the temperature, the chiral condensate will become smaller. It thus is always temperature dependent. You cannot fix it to a certain value and then change the temperature.

- *Giovannangeli:*

You have told us that, according to recent lattice calculations, J/Ψ suppression sets in only above $T=1.5T_c$. Is there some correlation between that temperature and the Debye length at $T=1.5T_c$? Can the lattice give us a more quantitative explanation?

- *Karsch:*

Yes, there certainly is a relation between the value of the Debye mass or the Debye screening length and the temperature at which heavy quark bound states disappear. The Debye mass controls the screening of the heavy quark potential above T_c . The larger the Debye mass, the stronger is the screening effect and the earlier the heavy quark bound states will disappear.

One would expect that in QCD with light quarks, the Debye mass is larger than in QCD with heavier quarks or in pure SU(3) gauge theory. One thus could study the dependence of the dissolution of heavy quarks bound states as a function of the dynamical (light) quark masses and thus also as a function of the Debye screening length. At present, however, direct calculations based on studies of spectral functions have only been performed in the pure gauge theory. To some extent this problem has been studied in the past using the Schrödinger equation approach. In these calculations one finds, of course, a direct relation between the Debye mass and the temperature at which heavy quark bound states dissolve.

- *Krotov:*

What is the technique used for the analytic continuation of a set of numbers obtained in a lattice calculation? What is the physical motivation for using a particular ansatz?

- *Karsch:*

When doing lattice calculation with large imaginary chemical potential, one generally does not know the analytic structure of the function that describes the observables one wants to analyze. This is the reason why also this approach is limited to small values of the chemical potential. One then can use a polynomial ansatz to perform the analytic continuation. We know some constraints for such an ansatz. For instance, the symmetry of the partition function under exchange of particles and anti-particles tells us that thermodynamic observables are functions of even powers of the chemical potential.

- *Skinner:*

In the $\mu=0$ limit, $\epsilon_c \sim 0.9$ GeV fm⁻³. You claimed that the lightest 20 hadrons only contribute to about 1/2 of the energy density. Why should heavy hadrons be so important at this low energy?

- *Karsch:*

Simply because there are so many of them. It is the exponentially rising mass spectrum, which also leads to a large contribution from many heavy degrees of freedom.

- *Oswald:*

Today you showed lattice results for the critical temperature over square root of sigma. Why are these numbers so similar for SU(2) and SU(3)?

- *Karsch:*

Indeed the results I have shown for SU(2) and SU(3) are very similar, $T_c = 0.69$ and 0.63 for SU(2) and SU(3) in three space dimensions. While the critical temperature depends strongly on the space dimension, it seems to change only little with the number of colours. This is consistent with the string model results I have discussed.

- *Galeatty:*

Most of the methods you have described to model non-zero chemical potential rely on the chemical potential being small. Is it possible to simulate far enough into the phase diagram to study the QGP, colour-superconductivity phase transition?

- *Karsch:*

None of the methods used today can reach the interesting low temperature, high density regime. In fact, a variant of the reweighting technique used today at high temperature has been used in the past also at low temperature (Glasgow method). This approach failed because the gauge field configuration most relevant for the physics at the point where simulations are performed ($\mu \approx 0$, $T \approx 0$) and at points with $\lambda > 0$ are too different.

- *Dainese:*

Why $T_c \sim \Lambda_{\text{QCD}}$? Can you say some words on the curve for ϵ/T^4 shown for the "2+1 flavour" case in your figure for energy densities in QCD with different numbers of light flavours? Why in this case does the curve interpolate between the two and three flavour cases?

- *Karsch:*

Indeed, T_c is numerically close to Λ_{QCD} . I tried to explain in my lecture that also heavy hadronic resonances play a role in understanding the quantitative value of the transition temperature. Why this leads to $T_c \sim \Lambda_{\text{QCD}}$ is indeed not evident.

What is shown in the figure for the energy density are results for 2 and 3 flavour QCD obtained with quarks of finite mass where the mass is held fixed in units of the

temperature, $m/T = 0.4$. The quark masses are small enough so that these curves are a good approximation for QCD with massless quarks.

Eventually we want to obtain the energy density for QCD with realistic values of the quark mass, i.e. two nearly massless u,d quarks and a heavier strange quark mass, $m_s \sim T_c$. In this case, the energy density will approach the value of massless 3-flavour QCD at high temperature ($m_s/T \rightarrow 0$) whereas close to T_c the strange quark is too heavy to contribute to the thermodynamics and the energy density will be close to that of 2-flavour QCD. The interpolation between these two limits is indicated by the crosses shown in the figure for the energy density.

- *Sykora:*

Does one see other stable hadrons made of more than three quarks in lattice calculations? Say, big molecules? If yes, at which scale?

- *Karsch:*

This is really a question for people studying the hadron spectrum at $T = 0$. At finite temperature, one has not looked at such kind of states. At $T = 0$, one did look at states that contain more quarks. One of the states which has been analyzed is the H-baryon, a hadron containing six quarks. In lattice calculations this came out either unbound or very weakly bound. Now interest comes up to look at penta-quark states. Although I do not know any definite results so far, several groups are working on it.

- *Casalderrey-Solana:*

What happens with the transition temperature when you consider QCD with even more light quark flavours?

- *Karsch:*

The tendency is that by increasing the number of flavours, the transition temperature becomes smaller. For 2-flavour QCD, the transition temperature is around 170MeV, for 3-flavour QCD, it is around 155MeV. There are some calculations for 4-flavour QCD which indicate a transition temperature around 100-120MeV. 4-flavour QCD has not been studied that extensively, but the tendency that the transition temperature decreases is clear. At some point you hit, of course, problems. For more than 12 flavours you lose asymptotic freedom.

- *Baldini:*

You said that J/Ψ is deconfined close to T_c . Should the Φ be deconfined?

- *Karsch:*

Yes, I think so. First studies of spectral functions with light quarks indicate that these bound states disappear above T_c .

- *Lipatov:*

In your opinion, what happens to the Regge trajectories of hadrons? They simply disappear or their parameters (slope and intercept) are changed?

- *Karsch:*

This question is related to the question of what happens to hadron masses at finite temperature: will their mass change or will they just become broader resonances. So far studies of spectral functions did not show evidence for significant mass shifts. I thus expect that the dominant thermal effect will be the broadening of resonances.

- *Levy:*

How strongly do you actually in your calculations depend on the existence of glueballs?

- *Karsch:*

The lattice calculations as such do not at all depend on the existence of glueballs. The thermodynamic quantities (T_c , ϵ/T^4 , ...) are calculated from the QCD partition function which does not care about the existence of certain bound states.

- *Ludlam:*

Is it likely that the quark mass dependence of T_c , which is "astonishingly weak" at $\mu_B=0$, will be quite different at large values of μ_B ?

- *Karsch:*

At large values of μ_B , the transition temperature will drop to zero. On the other hand, at any fixed value of μ_B , the transition temperature will again approach the pure gauge theory value of about 270 MeV when one increases the quark masses to infinity. In this sense the quark mass dependence can become stronger at non-zero μ_B .

- *Dainese:*

What is your view of the experimental situation on QGP search? Do you think we have sufficient evidence for existence of the phase transition? What is missing?

- *Karsch:*

What is really missing is a clear-cut signal which tells us unambiguously that a QGP has been created. The J/Ψ suppression has been considered as such a signal. However, there exist also various other explanations for the occurrence of J/Ψ suppression in heavy ion collisions so that this signature has to be discussed together with other signals which give evidence for the creation of hot and dense matter in heavy ion collisions. The observation of elliptic flow and jet quenching at RHIC seem to point in this direction.

Although there is at present no single clear-cut signal, I believe that the combination of a careful analysis of various observables will, in the coming years, lead to a unique picture about the properties of matter created in heavy ion collisions.

String Theory and Exact Results in Quantum Field Theory

R.H. Dijkgraaf
Amsterdam University

Only the discussions are reported here,
since the camera-ready copy of the contribution
did not arrive in time.

CHAIRMAN: R. DIJKGRAAF

Scientific secretaries: B. Durin, P. Giovannangeli, M. Oswald

DISCUSSION

- *Gripaios:*

One would very much like to study spontaneous breaking of SUSY using the matrix model correspondence. For this one needs massless chiral matter, but the arguments you presented only apply for massive matter. One could still do the calculation for the massive case and take the limit in which the mass goes to zero in the end. If one does this, does the superpotential simply blow up?

- *Dijkgraaf:*

The problem of massless matter is completely open. You have to be very careful with everything I was saying, in particular for the chiral ring and the fact that you have this factorization. For instance, a very good analog could be to first look at the 2d sigma models because they have very much similar properties. We know, for instance, that if we have a massive sigma model in 2 dimensions, we have similar properties, we have this chiral ring, we can factorize it. But then if you do superconformal field theory, that is a very rich structure. I guess very little actual results have been obtained but I think that is very worthwhile to investigate. I should also say that is part of a conjecture we made, because a related question is "to which extent do these computations that I did today fix the theory completely?" I made only a statement about F-terms but nothing can be said about the other terms in the effective action. Going back to the two-dimensional, massless, conformal case, F-terms and conformal invariance fix completely the effective Lagrangian. We make the conjecture that it is also true in four dimensions and this conjecture is motivated by duality in four-dimensional (super)conformal fields theory and string theory backgrounds.

Little has been done. It is very interesting. In some sense the superconformal field theory could be a starting point of any investigation. One could dream that one could fix everything. And one would understand massive theories by perturbations around the superconformal fixpoint. There has been some work done on the Argyres-Douglas point where one can actually follow what happens in the matrix model. But this is still somehow an open question.

- *Papadimitriou:*

Can you explain what is the relation of the dimension of \tilde{N} of the matrix model to the rank of the original gauge group?

- *Dijkgraaf:*

In the perturbative expansion of the gauge theory, we can approximate string theory diagrams by fishnet-like double line diagrams. And then for every hole in the Riemann surface, you have one factor of S , because essentially, there are precisely two gluino insertions on every boundary which make one factor of gluino condensate S . At some point you will have to sum over all Feynman diagrams, where you weigh a diagram with h holes with a factor S^h . For the question "How do you do this, how do you suppress the non-planar diagrams?", you use the 't Hooft trick, and introduce the auxiliary rank of \tilde{N} such that the 't Hooft coupling $1/(g^2 \tilde{N}) = S$ and take this \tilde{N} to infinity. You only get the planar diagrams. In this sense, the expansion is not the usual one in $1/N$. In fact the thing you compute depends little on N at all. But then you have another parameter which is the condensate, which plays exactly the same role as N in the $1/N$ expansion. So you introduce an auxiliary kind of rank of the matrix to simulate this condensate S .

- *Skinner:*

You explained how one could pick an arbitrary polynomial for the holomorphic superpotential $W(\phi)$, and that one should consider the extension of this over the complex plane. Does the choice of the holomorphic part not impose some constraint on the anti-holomorphic part? Later on you said they could be treated independently.

- *Dijkgraaf:*

This is an important point. In a physical theory, you think for example of the mass parameter. Mass, in the superconformal field theory, becomes a complex variable. So m appears in the superpotential and \bar{m} appears in the antiholomorphic superpotential. Of course \bar{m} is the complex conjugate of m . You have some kind of reality condition that \bar{m} is the complex conjugate. This is in the physical theory. But certain quantities only depend on m and not on \bar{m} just because they are holomorphic in the coupling constant for any F-term in the effective theory. This is for the following reason: we know that if we have an F-term it can only depend on the chiral fields. So if you have a constant in your Lagrangian, it is a holomorphic quantity, then you can think of it as a vacuum expectation value of a holomorphic field. Just make it into a spacetime-dependant variable and think of it as being fixed, given a certain VEV. So anything you compute, any F-term, can only be holomorphic in these quantities. Another point is if we think of the path integral, we integrate over ϕ and $\bar{\phi}$ which are each other's complex conjugate. It is like integrating over the complex plane in terms of z and \bar{z} . In many cases, you can write this as a separate integral over a holomorphic and a separate integral over the antiholomorphic quantity. So it is more like writing this as two contour integrals. Then you can think of the path integral as being over contour in complexified field space. For instance, if you want to do saddle point approximation, you pick the contour in a convenient way.

As for these F-term computations, the integrals over chiral and antichiral fields are independent and then you can make m and \bar{m} completely independent: you put one to

0. You can relax the physical reality condition as far as the computation of these F-terms is concerned.

- *Skinner:*

Are you saying that in some sense the superpotential is not well defined, but it somehow does not affect just these particular terms?

- *Dijkgraaf:*

Yes, it is more like a contour integral. Therefore it is a holomorphic quantity and you can just treat it independently of the antiholomorphic variables. I should make one remark here. There is still an open question related to the fact that if you look at the string theory computation, actually there is a so-called holomorphic anomaly. This tells you that many quantities that naïvely are holomorphic have a secret antiholomorphic dependence. This might mess things up. But in the field theory we have not yet found this behaviour. Today I only did the perturbation, we can ask that for instance in these matrix models: "are they also non-perturbatively defined?" That depends very much on the contour and in particular how the contour behaves at infinity. I think there is certainly room for antiholomorphic dependence. But I do not think it would enter the superpotential, which is believed to be holomorphic.

- *Krotov:*

Could you explain what a chiral ring is and what its properties are?

- *Dijkgraaf:*

The technical definition is the following. You take all the operators of the theory; we have essentially the supercharges split in two parts, the chiral and the antichiral Q and \bar{Q} . Look at all the operators that are annihilated by \bar{Q} , which means they are invariant if you take the commutator with \bar{Q} and use essentially that this operation of taking the commutator with \bar{Q} squares to 0. It is very much like a BRST operator. You can compute its cohomology. You look at the things that are kind of \bar{Q} -closed (killed by \bar{Q}) and you make them equivalent if they differ by something which is \bar{Q} -exact. It is very similar to BRST and you have something which is mathematically called cohomology, so things which are BRST-closed modulo BRST-exact. The statement is that this is a vector space of operators which close among themselves in the operator product. In the end, you just have to give the generators and the relations they satisfy. And the chiral ring is capturing the structure of the vacua of the theory.

- *Krotov:*

As far as I know, there is a big science around the chiral ring

- *Dijkgraaf:*

It is one of the few thing which you can explicitly compute. Knowledge of the chiral rings is equivalent to knowing precisely the properties of the vacua. In a bosonic theory, you have a vacuum and all the physical states, but in supersymmetric

theories, there is something in between. There is a bunch of operators which are almost like the identity operator in the sense that they do not depend on spacetime coordinates, they close among themselves and they form a finite algebra. But yet you have non-trivial relations. These are protected operators which you can expect to compute exactly. And the rest of it, for example the mass spectrum and everything which sits in the D-terms, is as difficult in a SUSY theory as in a bosonic theory.

- *Lysov:*

If you look at the effective action, why is S playing the role of the effective scale in this theory?

- *Dijkgraaf:*

A dimensional argument fixes that the power of the superpotential should be 1. So you have to write some function in S which you know is first order. In the usual Yang-Mills action it is just S . You also know that you have this multi-valuedness. So that is the assumption that fixes $S \log S$.

Besides, it looks very much like a Coleman-Weinberg effective action. But it is really an open question of finding the right effective action, from first principle, by just integrating out the fluctuations of the gauge field. That is still something, I guess, to be found. We have indirect arguments but not direct field theory arguments for that result.

- *Rotaev:*

My question is about the Konishi anomaly. What is it and why does it prevent us from taking the limit of zero mass?

- *Dijkgraaf:*

First something about the Konishi anomaly. You should be very careful not to confuse it with the chiral anomaly, which is a phase rotation of the fermions. The Konishi anomaly acts on the full superfield, Φ , which is a complex field. Thus we can make a phase rotation of Φ and if you wish, another phase rotation of $\bar{\Phi}$. Phase rotation of Φ is not a U(1) R-symmetry, which is not commuting with supersymmetry. This phase rotation commutes with supersymmetry, and rotates both the fermions and the bosons at the same rate. Since it is rotating the fermions, it has an anomaly that you can compute. This anomaly tells you that, if you rotate Φ and do not rotate $\bar{\Phi}$, i.e. just make a chiral rotation of your fields, you pick an anomaly which is proportional to $F\bar{F}$, the usual anomaly contribution. But you can extend that anomaly, you can say "what if I just do not a phase rotation of Φ , but I make a general field redefinition of Φ ?" For instance, I have the variation of Φ not being proportional to Φ , but to Φ^n and you can compute again a similar anomaly.

- *Rotaev:*

I am speaking about general transformation of Φ , not only like Lorentz rotations

Dijkgraaf:

That is not a Lorentz rotation, it is phase rotation of the fields. But you can try to write down nonlinear transformations, they are still anomalous, and the form of the anomaly is a bit more complicated in the sense that it just contains the field itself in addition to the usual $F\bar{F}$. But this will express in some sense the dependence on Φ and on the coupling constant together with the gauge field.

- Kuperstein:

Is it correct that the calculations you have performed require large N limit? If the answer is positive, what is the physical meaning of the finite N corrections?

- Dijkgraaf:

We can rephrase that question directly in the gauge theory and forget about this N because it is just a way to simulate the S dependence. Another way of rephrasing is to ask about nonplanar diagrams. If you do not take this $N \rightarrow \infty$ limit, you also get the nonplanar diagrams. What is the role of nonplanar diagrams? Here you have to work for fixed topology, the planar diagrams have genus 0 and then you could move up to genus 1. And these genus 1 diagrams appear if you put this 4D gauge theory on a curved 4-manifold. Then there is an induced gravitational term for the gauge theory which will react to the curvature and produce a curvature squared term. So I can compute the coefficient in front of this curvature squared, and that coefficient is computed in terms of genus 1 diagrams. There are more complicated behaviour terms which are computed from higher genus terms. The non-planar diagrams encode the gravitational backreaction of this 4D gauge theory. So the question is: "What does this compute?"

- Zichichi:

I think that gravitational effects should be negligible in this case. The planar remains the dominant part, if I understand your philosophy.

- Dijkgraaf:

If you just work in flat space, yes. The question is, what do you gain by putting the theory on a curved 4D manifold? You can think of this coefficient as measuring the number of degrees of freedom in your theory, because everything couples to gravity. So the coefficient in front of this induced gravitational term is keeping track precisely of the number of the degrees of freedom in your theory. What is interesting is that, just from the answer, you can have some hint of confinement. For instance, you will expect naively, if you have an abelian gauge theory of rank N , that the total degrees of freedom couple to gravity like N^2 , which is indeed somehow the behaviour of planar diagrams. But since it is non-planar diagrams, the coefficients of this term are actually of order one. It is like in two dimensions where you have two points of view: you can put the conformal theory on flat space, you look at local operators or you put it on a curved manifold and you look how it reacts to it. And the coefficient of how it interacts is the central charge which measures the total number of degrees of

freedom. So this coefficient is just as it is the case if one puts the central charge of the 4D gauge theory, and so it is just a trick to see the number of the degrees of freedom, to put the theory in a box with compactified time to measure the thermal partition function. This is one application of this idea to put it on a curved manifold.

- *Zichichi:*

What we want to do is Physics. If I want to compute the cross section A+B to final state, what is the result?

- *Dijkgraaf:*

I agree that for this you do not need it.

- *Kuperstein:*

Can you elaborate more on the relation between the model you have described this morning and the string theory?

- *Dijkgraaf:*

The question is how to make an $N=1$ gauge theory in string theory. One nice way to do this is to take a collection of branes. Branes have open strings on them; in the limit where the string tension becomes infinite, you get just Yang-Mills degrees of freedom. String theory suggests that there is a dual description of the branes which is part of the AdS/CFT duality, that is a dual description of the same system just in terms of curved manifolds. This suggests that there are two ways to describe theories with $N=1$ supersymmetry, either in terms of this gauge theory, or, if you are just on the level of the effective action, you can describe the same effective action in terms of a curved manifold. This curved manifold is essentially the Seiberg-Witten curve. So string theory suggests that there is an effective gravitational description of the gauge theory system. In some sense our argument summing all these planar diagrams shows how this gravitational system emerges from the field theory.

- *Papadimitriou:*

Can you explain what the connection between $N=2$ SYM and the Seiberg-Witten curve is?

- *Dijkgraaf:*

The model we consider has $N=1$, so we have a superpotential. We have a field ϕ and picking a potential, at least classically, will give a VEV to the field ϕ thus fixing it to a particular form. Starting from $N=2$, you break the symmetry down to $N=1$ introducing a superpotential W .

In $N=2$ there is a supersymmetry connecting the gauge field A as a multiplet together with the matter multiplet ϕ . So naïvely, if you put a small coefficient ϵ in front of the superpotential and take the limit ϵ to zero, you recover the $N=2$ SUSY theory. In $N=2$, the theory does not have an isolated vacuum, it has moduli space of vacua, which are parametrized by the value of the VEV of the field ϕ . In the end you

want to compute something, the gauge coupling as a function of this VEV. Now you can introduce a potential W . By picking this W in a clever way, you can fix the VEV of ϕ . Now the field ϕ is sitting in the minimum and we can tune ϵ to zero. Depending on what you compute, things go either to zero or blow up. It is not difficult to see that the gauge coupling τ , which is the second derivative of F w.r.t. S , and if you look just at the formula of this, just in terms of Feynman diagrams, you see that they are all of order ϵ^0 . It is precisely this term, and only this term, which has no dependence on ϵ .

You now lift the theory from $N=1$ to $N=2$. You have localized your theory at this particular point of the moduli space, and you compute a gauge coupling at this position. What this does for you is that it takes the spectral curve which comes out from the summation of the planar diagrams, and makes it into the Seiberg-Witten curve. Changing the potential, you sweep over this moduli space, compute the gauge coupling as a function of the position in this space, and then recover the $N=2$ gauge theory. We can do something similar for the $N=4$ theory, which is even more interesting because of the τ to $1/\tau$ symmetry. Again there is a Riemann surface coming out from the theory, and that precisely is a 2-torus curve which has the correct symmetry for the coupling constant.

I should stress that our aim is not to reproduce the answer of $N=2$ gauge theory, but this is just a consistency check. Starting from $N=1$ theory, we can get $N=2$ or $N=4$ by adding one or three adjoints. The case of two adjoints is not an extended supersymmetry, but also there you have closed solutions.

- *Nikolaev:*

If I put a heavy quark with magnetic charge near a domain wall, could I receive a string-like flux from the quark to the domain wall? Does screening exist?

- *Dijkgraaf:*

The only thing I can say is that this theory has a very complicated vacuum structure. You can determine its vacuum. What is the particle with the lowest charges which can condensate? E.g. for $U(2)$ theory it has 2 vacua, one where there is a magnetic monopole condensate, that confines the electric charge, and there is another vacuum, where you have a dyon condensing. You can physically distinguish between the two vacua. In general, if you have much more complicated symmetry breaking, you can determine exactly the magnetic and electric charges of the condensing objects.

- *Nikolaev:*

I think that in the vacuum, electric charge of quarks get screened, and magnetic flux should go to the domain wall. Am I right?

- *Dijkgraaf:*

I do not really know how to answer this question.

- *Nikolaev:*

Does this domain wall look like a D-brane?

- *Dijkgraaf:*

Yes, in string theory the domain walls which separate the vacua have an interpretation as D-branes. They are two-dimensional in space, and they have internal dimensions too. In string theory, you have these six internal dimensions which are rolled up into a Calabi-Yau manifold. In principle this Calabi-Yau manifold and all the six dimensions of it are visible just by looking at the Feynman diagrams of the field theory. Then you can think indeed of the domain walls as being certain branes which wrap around certain cycles in this internal space.

- *Lysov:*

We know the properties of the chiral ring for the vacuum expectation values. How could we extend these properties to the operator product?

- *Dijkgraaf:*

The chiral ring is some kind of limit of the full operator product: elements of the chiral ring have finite operator products. If you put two operators together, there is no singularity, because there is no space-time dependence, contrary to the usual case. Chiral operators are very much like the identity operator. To go beyond that, to really find the full operator product expansion, we can do either weak or strong coupling expansion but there is no full analytic answer.

- *Lipatov:*

In the beginning of your lecture you said that for the planar diagram the perturbation theory is convergent, but there are different reasons for a divergence of the perturbation theory. One of them is the existence of renormalons. Is it correct that the observables which you investigate do not contain renormalon diagrams?

- *Dijkgraaf:*

Essentially because these Feynman diagrams have the miraculous property that they are finite. Even for a non-renormalizable field theory, if you just compute these diagrams you get nice finite numbers. There is no need for renormalization. In fact, in this case, just by inspection, the theory of these diagrams is analytic and does converge with a finite radius of convergence. It has very non-trivial analytic properties but if you look at it as a function of the coupling, the various branch cuts and other things, it is not taking values in a plane, it takes values on a non-trivial Riemann surface. And that is very interesting. It is also because it has these nice holomorphic properties.

The status of local supersymmetry¹

M. J. Duff²

Michigan Center for Theoretical Physics

*Randall Laboratory, Department of Physics, University of Michigan
Ann Arbor, MI 48109 1120, USA*

Abstract

In the first lecture we review the current status of local supersymmetry. In the second lecture we focus on D=11 supergravity as the low-energy limit of M-theory and pose the questions: (1) What are the D=11 symmetries? (2) How many supersymmetries can M-theory vacua preserve?

¹Research supported in part by DOE Grant DE-FG02-95ER40899.

²mduff@umich.edu

Contents

1 Local supersymmetry in supergravity, superstrings and M-theory	2
1.1 Supergravity	2
1.2 String theory	4
1.3 M-theory	5
2 Simple supersymmetry in four dimensions	7
2.1 The algebra	7
2.2 Wess-Zumino model	7
2.3 Super Yang-Mills	8
2.4 Simple supergravity	8
2.5 Off-shell versus on-shell	9
2.6 Particle phenomenology	10
3 Extended supersymmetry	11
3.1 The algebra	11
3.2 Multiplets	12
3.3 Auxiliary fields?	12
4 Eleven dimensions	14
4.1 The algebra	14
4.2 The multiplet	15
4.3 D=11 supergravity	16
5 Hidden spacetime symmetries in D=11	20
5.1 Spacelike, null and timelike reductions	20
5.2 The complete uncompactified D=11 theory	23
6 Counting supersymmetries of D=11 vacua	26
6.1 Holonomy and supersymmetry	26
6.2 Generalized holonomy	28
6.3 Specific examples	31
6.4 The full M(only)?	33

1 Local supersymmetry in supergravity, superstrings and M-theory

Gravity exists, so if there is any truth to supersymmetry then any realistic supersymmetry theory must eventually be enlarged to a supersymmetric theory of matter and gravitation, known as supergravity. Supersymmetry without supergravity is not an option, though it may be a good approximation at energies below the Planck Scale.

Steven Weinberg, The Quantum Theory of Fields, Volume III, Supersymmetry

1.1 Supergravity

The organizers of the school requested that I review the status of “local supersymmetry”. Since local supersymmetry represents a large chunk of the last 25 years of research in theoretical high energy physics, I will necessarily be selective. Local supersymmetry appears in supergravity, superstrings, supermembranes and M-theory. A complete treatment of strings, branes and M-theory is beyond the scope of these lectures and they will deal mostly with supergravity. In my opinion there are currently four reasons why supergravity is interesting:

- 1) Ten dimensional and eleven dimensional supergravity respectively describe the low energy limits of string theory and M-theory, which represent our best hope for a unification of all fundamental phenomena: particle physics, black holes and cosmology. Supergravities in lower dimensions are also important for discussing compactifications. Pending such a final theory there are less sweeping but more tractable uses of supergravity such as:
- 2) The gauge-theory/supergravity correspondence allows us to use our knowledge of weakly coupled five-dimensional supergravity to probe strongly coupled four-dimensional gauge theories such as QCD.
- 3) Cosmological solutions of supergravity hold promise of explaining inflation and the current acceleration of the universe.
- 4) There is still no direct experimental evidence for supersymmetry but it might be the panacea for curing the ills of non-supersymmetric theories of particles and cosmology:

The gauge hierarchy problem

Electroweak symmetry breaking

Gauge coupling unification

Cold dark matter

Baryon asymmetry

Let us recall that global supersymmetry unifies bosons and fermions by requiring that our equations be invariant under a transformation involving a constant fermionic parameter ϵ which converts boson fields B to fermion fields F and vice versa. Symbolically

$$\delta F = \partial B \epsilon \quad \delta B = \bar{\epsilon} F \quad (1)$$

Here B is commuting while F and ϵ are anticommuting. There can be up to 4 such supersymmetries in four spacetime dimensions: simple $N = 1$ and extended $N = 2,4$. The maximum spin allowed is $s = 1$. The maximum spacetime dimension allowed is $D = 10$ corresponding to 16 spinor components.

Local supersymmetry means that we allow ϵ to be a function of the spacetime coordinates. The massless gauge field associated with local supersymmetry is a spin 3/2 fermion, the gravitino. Interestingly enough, local supersymmetry necessarily implies invariance under general coordinate transformations and so, as its name implies, the gravitino is the superpartner of the graviton. There can be up to 8 such supersymmetries in four spacetime dimensions: simple $N = 1$ and extended $N = 2,3,4,5,6,8$. The maximum spin allowed is $s = 2$. The maximum spacetime dimension allowed is $D = 11$ corresponding to 32 spinor components.

The status of local supersymmetry is largely the status of supergravity: the supersymmetric version of general relativity discovered in 1976. This is the original reason for the popularity of supergravity: it provides a natural framework in which to unify gravity with the strong, weak and electromagnetic forces. This is the top-down approach.

Local supersymmetry played a major part in many subsequent developments such as matter coupling to supergravities, the super Higgs mechanism, anti de Sitter supergravities, BPS black holes and supersymmetric sigma-models. Many of these contributed to the phenomenological application of supergravity-induced supersymmetry breaking in the physics beyond the standard model, as well as to the connection between Yang-Mills theories and supergravity via the AdS/CFT correspondence.

It is important not only as supersymmetric extension of gravity but has also had a significant impact on other fields. In standard general relativity it has given rise to positive energy theorems and to new results in the study of black holes, extra spacetime dimensions

and cosmology.

Since local supersymmetry places an upper limit on the dimension of spacetime, it naturally suggests that we incorporate the Kaluza-Klein idea that our universe may have hidden dimensions in addition to the familiar three space and one time.

Since my job is to evaluate the status of local supersymmetry, I shall not spend much time with introductions. Rather I wish in this first lecture to explain where it stands in the grand scheme of things and to what extent the top-down approaches enumerated in (1)-(3) above and bottom-up approaches of (4) are compatible. In this connection, we note that the criterion of chirality in four dimensions means that only simple $N = 1$ supersymmetry could be directly relevant to observed particles. However, such models can emerge from both simple and extended theories in higher dimensions.

Early discussions of local supersymmetry may be found in the papers of Volkov and Soroka [1, 2]. Supergravity was introduced by Ferrara, Freedman and van Nieuwenhuizen [3] and by Deser and Zumino [4]. Introductions to supersymmetry and supergravity may be found in the books by Bagger and Wess [5], Gates, Grisaru, Rocck and Siegl [6], Srivastava [7], West [8], Freund [9], Bailin and Love [10] and Weinberg [11]. See also the Physics Reports of Sohnius [12], van Nicuwenhuizen [13] and Fayet and Ferrara [14] and the review by Lykken [15].

For phenomenological applications of local supersymmetry see the lecture of Ellis [19] and the Physics Reports by Nilles [17], Nanopoulos [16], Haber and Kane [18], and Chung, Everett, Kane, King, Lykken and Wang [20]. See also the TASI lectures of Dine [21], the Les Houches lectures of Ross [22] and the review by Raby [23].

For Kaluza-Klein theories and supergravity, see the Shelter Island lectures of Witten [28], the Physics Reports by Duff, Nilsson and Pope [29], the reprint volume by Appelquist, Chodos and Freund [30], the books by Castellani, D'Auria and Fre [31] and Salam and Sezgin [32] and the reviews by Duff [33, 34].

1.2 String theory

To paraphrase Weinberg:

Supergravity is itself only an effective nonrenormalizable theory which breaks down at the Planck energies. So if there is any truth to supersymmetry then any realistic theory must eventually be enlarged to superstrings which are ultraviolet finite. Supersymmetry without strings is a vacuous concept.

superstrings is not an option.

Following the 1984 superstring revolution, the emphasis in the search for a final theory shifted away from the spacetime aspects of supergravity towards the two-dimensions of the string worldsheet. The five consistent superstrings: Type I, Type IIA, Type IIB, Heterotic $E_8 \times E_8$ and Heterotic $SO(32)$ all feature spacetime local supersymmetry in ten dimensions. It plays a crucial part in discussions of superstring compactification from ten to four dimensions and, *inter alia*, has also stimulated research in pure mathematics, for example Calabi-Yau manifolds and manifolds of exceptional holonomy.

Introductions to string theory may be found in the books by Green, Schwarz and Witten [35] and Polchinski [36].

1.3 M-theory

To paraphrase Weinberg again:

Superstring theory is itself only a perturbative theory which breaks down at strong coupling. So if there is any truth to supersymmetry then any realistic theory must eventually be enlarged to the non-perturbative M-theory, a theory involving higher dimensional extended objects: the super p-branes. Supersymmetry without M-theory is not an option.

In 1995 it was realized that a non-perturbative unification of the five consistent superstring theories is provided by M-theory, whose low-energy limit is eleven-dimensional supergravity. In addition to strings, M-theory involves p-dimensional extended objects, namely the p-branes which couple to the background fields of D=11 supergravity. This resolved the old mystery of why local supersymmetry allows a maximum of eleven dimensions while superstrings stop at ten. Indeed, many of the p-branes were first understood as classical solutions of the supergravity field equations. As a result, supergravity has returned to center stage.

M-theory is regarded by many as the dreamed-of final theory and has accordingly received an enormous amount of attention. It is curious, therefore, that two of the most basic questions of M-theory have until now remained unanswered:

- i) *What are the D=11 symmetries?*

In the section 5 we will argue that the equations of M-theory possess previously unidentified hidden spacetime (timelike and null) symmetries in addition to the well-known hidden internal (spacelike) symmetries. For $11 \geq d \geq 3$, these coincide with the general-

ized structure groups discussed below and take the form $\mathcal{G} = \text{SO}(d-1, 1) \times G(\text{spacelike})$, $\mathcal{G} = \text{ISO}(d-1) \times G(\text{null})$ and $\mathcal{G} = \text{SO}(d) \times G(\text{timelike})$ with $1 \leq d < 11$. For example, $G(\text{spacelike}) = \text{SO}(16)$, $G(\text{null}) = [\text{SU}(8) \times \text{U}(1)] \ltimes \mathbb{R}^{56}$ and $G(\text{timelike}) = \text{SO}^*(16)$ when $d = 3$. The nomenclature derives from the fact that these symmetries also show up in the spacelike, null and timelike dimensional reductions of the theory. However, we emphasize that we are proposing them as background-independent symmetries of the full unreduced and untruncated $D = 11$ equations of motion, not merely their dimensional reduction. Although extending spacetime symmetries, there is no conflict with the Coleman-Mandula theorem. A more speculative idea is that there exists a yet-to-be-discovered version of $D = 11$ supergravity or M -theory that displays even bigger hidden symmetries corresponding to \mathcal{G} with $d \leq 3$ which could be as large as $SL(32, R)$.

ii) *How many supersymmetries can vacua of M-theory preserve?*

The equations of M-theory display the maximum number of supersymmetries $N=32$, and so n , the number of supersymmetries preserved by a particular vacuum, must be some integer between 0 and 32. But are some values of n forbidden and, if so, which ones? For quite some time it was widely believed that, aside from the maximal $n = 32$, n is restricted to $0 \leq n \leq 16$ with $n = 16$ being realized by the fundamental BPS objects of M-theory: the M2-brane, the M5-brane, the M-wave and the M-monopole. The subsequent discovery of intersecting brane configurations with $n = 0, 1, 2, 3, 4, 5, 6, 8, 16$ lent credence to this argument. On the other hand, it has been shown that all values $0 \leq n \leq 32$ are in principle allowed by the M-theory algebra discussed in section 4.1, and examples of vacua with $16 < n < 32$ have indeed since been found. In fact, the values of n that have been found “experimentally” to date are: $n = 0, 1, 2, 3, 4, 5, 6, 8, 10, 12, 14, 16, 18, 20, 22, 24, 26, 28, 32$.

In M-theory vacua with vanishing 4-form $F_{(4)}$, one can invoke the ordinary Riemannian holonomy $H \subset \text{SO}(10, 1)$ to account for unbroken supersymmetries $n = 1, 2, 3, 4, 6, 8, 16, 32$. To explain the more exotic fractions of supersymmetry, in particular $16 < n < 32$, we need to generalize the notion of holonomy to accommodate non-zero $F_{(4)}$. In section 6 we show that the number of supersymmetries preserved by an M-theory vacuum is given by the number of singlets appearing in the decomposition of the 32-dimensional representation of \mathcal{G} under $\mathcal{G} \supset \mathcal{H}$ where \mathcal{G} are generalized structure groups that replace $SO(1, 10)$ and \mathcal{H} are generalized holonomy groups. In general we require the maximal \mathcal{G} , namely $SL(32, R)$, but smaller \mathcal{G} appear in special cases such as product manifolds.

Reviews of M -theory may be found in the paper by Schwarz [38], the paper by Duff [39], the book by Duff [40], the lectures of Townsend [41] and the books by Kakı [42, 43]. Reviews on supermembranes are given in the Physics reports of Duff, Khuri and Lu [37], the TASI lectures by Duff [46] and the papers by Duff [44, 45] and Stelle [47], the books by Polchinski [36], Johnson [48] and Ortin [49].

2 Simple supersymmetry in four dimensions

2.1 The algebra

The $N = 1$ supersymmetry algebra takes the form

$$\begin{aligned}\{Q_\alpha, Q_\beta\} &= 2(\gamma_a C)_{\alpha\beta} P^\mu \\ [Q_\alpha, P_\mu] &= 0 \\ [Q_\alpha, J_{\mu\nu}] &= \frac{1}{2}(\sigma_{\mu\nu})_\alpha^\beta Q_\beta \\ [Q_\alpha, R] &= i(\gamma_5)_\alpha^\beta Q_\beta\end{aligned}\tag{2}$$

together with the commutation relations of the Poincaré group.

2.2 Wess-Zumino model

The simplest representation of this algebra is provided by the Wess-Zumino multiplet which consists of 2 scalars A and B , a 4-component fermion χ and two auxiliary fields F and G . The free Wess-Zumino Lagrangian is given by

$$\mathcal{L}_{WZ} = -\frac{1}{2} \left[(\partial_\mu A)^2 + (\partial_\mu B)^2 + \bar{\chi} \gamma^\mu \partial_\mu \chi - F^2 - G^2 \right]$$

The action is invariant under the supersymmetry transformations

$$\begin{aligned}\delta A &= \frac{1}{2}\bar{\epsilon}\chi \\ \delta B &= -\frac{1}{2}\bar{\epsilon}\gamma_5\chi \\ \delta\chi &= \frac{1}{2}[\gamma^\mu \partial_\mu(A - i\gamma_5 B) + (F + i\gamma_5 G)]\epsilon \\ \delta F &= \frac{1}{2}\bar{\epsilon}\gamma^\mu \partial_\mu \chi\end{aligned}$$

$$\delta G = \frac{1}{2} \bar{\epsilon} \gamma_5 \gamma^\mu \partial_\mu \chi \quad (3)$$

It is now easy to see why supersymmetry is sometimes called “the square root of a translation”. For example

$$[\delta_1, \delta_2] A = a^\mu \partial_\mu A \quad (4)$$

where

$$a^\mu = \bar{\epsilon}_1 \gamma^\mu \epsilon_2 \quad (5)$$

2.3 Super Yang-Mills

Another representation is provided by the vector multiplet which consists of a set of vectors A_μ^i , fermions λ^i and auxiliary fields D^i . The Yang-Mills Lagrangian is given by

$$\mathcal{L}_{YM} = -\frac{1}{4} (F_{\mu\nu}^i)^2 - \frac{1}{2} \bar{\lambda}^i \not{D} \lambda^i + \frac{1}{2} (D^i)^2 \quad (6)$$

The action is invariant under the supersymmetry transformations

$$\begin{aligned} \delta A_\mu^i &= \bar{\epsilon} \gamma_\mu \lambda^i \\ \delta \lambda^i &= \left(-\frac{1}{2} \sigma^{\mu\nu} F_{\mu\nu}^i + i \gamma_5 D^i \right) \epsilon \\ \delta D^i &= i \bar{\epsilon} \gamma_5 \not{D} \lambda^i \end{aligned} \quad (7)$$

where

$$F_{\mu\nu}^i = \partial_\mu A_\nu^i - \partial_\nu A_\mu^i - g c_{jk}^i A_\mu^j A_\nu^k \quad (8)$$

2.4 Simple supergravity

Finally we come to the tensor multiplet consisting of a vierbein e_a^μ , a gravitino ψ_μ and auxiliary fields b_μ , M and N . The supergravity lagrangian is

$$\mathcal{L}_{SUGRA} = \frac{e}{2\kappa^2} R - \frac{1}{2} \bar{\psi}_\mu R^\mu - \frac{1}{3} e (M^2 + N^2 - b_\mu b^\mu) \quad (9)$$

where

$$R = R_{\mu\nu}^{ab} e_a^\mu e_b^\nu \quad (10)$$

and

$$\frac{1}{4} R_{\mu\nu}^{ab} \sigma_{ab} = [D_\mu, D_\nu] \quad (11)$$

The transformations are now those of local supersymmetry where $\epsilon = \epsilon(x)$:

$$\begin{aligned}\delta e_\mu^a &= \kappa \bar{\epsilon} \gamma^a \psi_\mu \\ \delta \psi_\mu &= 2\kappa^{-1} D_\mu(w(e, \psi)) \epsilon + i\gamma_5 \left(b_\mu - \frac{1}{3} \gamma_\mu \psi \right) \epsilon - \frac{1}{3} \gamma_\mu (M + i\gamma_5 N) \epsilon \\ \delta M &= -\frac{1}{2} e^{-1} \bar{\epsilon} \gamma_\mu R^\mu - \frac{\kappa}{2} i\bar{\epsilon} \gamma_5 \psi_\nu b^\nu - \kappa \bar{\epsilon} \gamma^\nu \psi_\nu M + \frac{\kappa}{2} \bar{\epsilon} (M + i\gamma_5 N) \gamma^\mu \psi_\mu \\ \delta N &= -\frac{e^{-1}}{2} i\bar{\epsilon} \gamma_5 \gamma_\mu R^\mu + \frac{\kappa}{2} \bar{\epsilon} \psi_\nu b^\nu - \kappa \bar{\epsilon} \gamma^\nu \psi_\nu N - \frac{\kappa}{2} i\bar{\epsilon} \gamma_5 (M + i\gamma_5 N) \gamma^\mu \psi_\mu \\ \delta b_\mu &= \frac{3i}{2} e^{-1} \bar{\epsilon} \gamma_5 \left(g_{\mu\nu} - \frac{1}{3} \gamma_\mu \gamma_\nu \right) R^\nu + \kappa \bar{\epsilon} \gamma^\nu \psi_\nu b_\mu - \frac{\kappa}{2} \bar{\epsilon} \gamma^\nu \psi_\nu b_\mu - \frac{\kappa}{2} i\bar{\psi}_\mu \gamma_5 (M + i\gamma_5 N) \epsilon - \frac{i\kappa}{4} \epsilon_\mu^{bcd} b_b \bar{\epsilon} \gamma_5 \gamma_c \psi_d\end{aligned}\tag{12}$$

where

$$R^\mu = \epsilon^{\mu\nu\rho\kappa} i\gamma_5 \gamma_\nu D_\rho(w(e, \psi)) \psi_\kappa\tag{13}$$

$$D_\mu(w(e, \psi)) = \partial_\mu + \frac{1}{4} w_{\mu ab} \sigma^{ab}\tag{14}$$

and

$$\begin{aligned}w_{\mu ab} &= \frac{1}{2} e^\nu_a (\partial_\mu e_{b\nu} - \partial_\nu e_{b\mu}) - \frac{1}{2} e^\nu_b (\partial_\mu e_{a\nu} - \partial_\nu e_{a\mu}) \\ &\quad - \frac{1}{2} e_a^\rho e_b^\sigma (\partial_\rho e_{\sigma c} - \partial_\sigma e_{\rho c}) e_\mu^c \\ &\quad + \frac{\kappa^2}{4} (\bar{\psi}_\mu \gamma_a \psi_b + \bar{\psi}_a \gamma_\mu \psi_b - \bar{\psi}_\mu \gamma_b \psi_a)\end{aligned}\tag{15}$$

2.5 Off-shell versus on-shell

Since the auxiliary fields F , G , D^i , b_μ , M and N enter only algebraically in the Lagrangians, they may be eliminated by their equations of motion, if so desired. With the auxiliary fields, however, the algebra closes off-shell whereas it closes only on-shell without them. It is useful to count the number of degrees of freedom in both cases.

Off-shell: For the Wess-Zumino multiplet, A and B each count 1, χ counts 4 and F and G each count 1, making 4 bose and 4 fermi in total. For the vector multiplet, A_μ counts 3, λ counts 4 and D counts 1, making 4 bose and 4 fermi in total. For the supergravity multiplet, e^μ_a counts $16 - 10 = 6$, ψ_μ counts $16 - 4 = 12$, b_μ counts 4 and M and N each count 1, making 12 bose plus 12 fermi in total.

On-shell: For the Wess-Zumino multiplet, A and B each count 1, χ counts 2 and F and G each count 0, making 2 bose and 2 fermi in total. For the vector multiplet, A_μ counts 2, λ

counts 2 and D counts 0, making 2 bose and 2 fermi in total. For the supergravity multiplet, e^μ_a counts 2, ψ_μ counts 2, b_μ counts 0 and M and N each count 0, making 2 bose plus 2 fermi in total.

Note that supersymmetry always requires equal number of bose and fermi degrees of freedom both off-shell and on-shell.

2.6 Particle phenomenology

The requirement of chirality limits us to $N = 1$ and the most general such theory consists of $N = 1$ supergravity coupled to $N = 1$ Yang-Mills and $N = 1$ chiral multiplets. This theory is characterized by three functions of the chiral multiplets: the superpotential W , the Kahler potential K and the gauge function f . The function f is real while W and K are holomorphic.

Within this framework, one might wish to embed the standard model gauge groups $SU(3) \times SU(2) \times U(1)$ and three families of quarks and leptons. Of course this immediately doubles the number of elementary particles, since every particle we know of acquires a superpartner, none of which can be identified with a known particle. These have names like gauginos (winos, zinos, photinos and gluinos), higgsinos, squarks and sleptons. Moreover, unbroken supersymmetry implies that these superpartners are degenerate in mass with the known particles in obvious disagreement with experiment. In any realistic theory, therefore, supersymmetry must be broken. Since the equations of motion of the only known quantum consistent theories of gravity are supersymmetric, this breaking must be spontaneous. However, the resulting low-energy theory can be represented by a globally supersymmetric Lagrangian $\mathcal{L}_{\text{soft}}$ with explicit but soft breaking terms. By soft we mean operators of dimensions 2 or 3. The bottom-up approach is thus to write down such a minimal supersymmetric standard model (MSSM) with mass parameters that are typically of the order of the electroweak to TeV scale. Counting the masses, coupling constants and phases, the most general such model has 124 parameters. Of course, experiment can provide constraints. Its claimed successes include resolutions of: the technical gauge hierarchy problem, the electroweak symmetry breaking problem, the gauge coupling unification problem, the cold dark matter problem and the baryon asymmetry problem.

In the literature, there is a plethora of different top-down proposals for how this spontaneous supersymmetry breaking may come about. The obvious tree-level TeV breaking in

which either the F or D auxiliary fields acquire vacuum expectation values seems to be ruled out by experiment. One alternative is the hidden sector framework where the theory can be split into two sectors with no renormalizable couplings between them: an observable sector containing the SM model particles and their superpartners, and hidden sector in which supersymmetry is broken by a dynamical mechanism such as gaugino condensation. The scale of supersymmetry breaking M_S is hierarchically higher than a TeV.

There are various versions of these hidden sector models: gravity mediated models, gauge mediated models, bulk mediated models. In the latter scenario, the observable and hidden sectors reside on different branes embedded in a bulk spacetime of higher dimension.

Another alternative is D-term breaking which arises in extensions of the MSSM to GUTs or strings.

The hope, of course, is that the correct mechanism will be selected by the fundamental theory but owing to the vacuum degeneracy problem, there has been very little progress in this respect. In fact, neither string theory nor M-theory has yet been able to fix any of the 124 parameters.

3 Extended supersymmetry

3.1 The algebra

To discuss extended supersymmetry, it is more convenient to rewrite the (anti)commutation relations (2) in terms of two-component Weyl spinors Q_α and $\bar{Q}_{\dot{\alpha}}$

$$\begin{aligned} \{Q_\alpha, Q_\beta\} &= \{\bar{Q}_{\dot{\alpha}}, \bar{Q}_{\dot{\beta}}\} = 0 \\ \{Q_\alpha, \bar{Q}_{\dot{\beta}}\} &= 2\sigma_{\alpha\dot{\beta}}^\mu P_\mu \\ [Q_\alpha, P_\mu] &= [\bar{Q}_{\dot{\alpha}}, P_\mu] = 0 \end{aligned} \tag{16}$$

in which dotted and undotted indices take the values $\alpha, \dot{\alpha} = 1, 2$.

We now allow for a set of Q_α , labelled by an index L , which transform according to some representation of a compact Lie group G , and $\bar{Q}_\alpha^L = (Q_\alpha^L)^*$ which transform according to the complex conjugate representation. The simple supersymmetry algebra (16) now generalizes to the extended supersymmetry algebra

$$\{Q_\alpha^L, Q_\beta^M\} = \epsilon_{\alpha\beta} Z^{LM}$$

N					
Spin	1	1	2	2	4
Spin 1	—	1	1	—	1
Spin $\frac{1}{2}$	1	1	2	2	4
Spin 0	2	—	2	4	6

Table 1: Multiplicities for massless irreducible representations with maximal helicity 1 or less

$$\begin{aligned}
 \{\bar{Q}_{\alpha}^L, \bar{Q}_{\beta}^M\} &= \epsilon_{\alpha\beta} Z^{LM} \\
 \{Q_{\alpha}^L, \bar{Q}_{\beta}^M\} &= 2\delta^{LM} \sigma_{\alpha\beta}^{\mu} P_{\mu} \\
 [Q_{\alpha}^L, P_{\mu}] &= [\bar{Q}_{\alpha}^L, P_{\mu}] = 0 \\
 [Q_{\alpha}^L, B_l] &= iS_l^{LM} Q_{\alpha}^M \\
 [B_l, B_m] &= if_{lmk} B_k
 \end{aligned} \tag{17}$$

where S_l^{LM} are the hermitian matrices of the representation containing the Q_{α}^L and the B_k are the generators of the internal symmetry group G . The Z^{LM} are central charges which commute with all the other generators.

3.2 Multiplets

We shall not detail the representation theory of the extended supersymmetry algebra (17) but simply quote some results. Massless irreducible representations with maximum helicity 1 and 2 are tabulated in Tables 1 and 2, respectively. Some massive representations with and without central charges are tabulated in Tables 3 and 4.

Discussions of representations of extended supersymmetry may be found in the Trieste Lectures of Ferrara and Savoy [51] and in the review of Strathdee [50].

3.3 Auxiliary fields?

When we come to extended supersymmetry and higher dimensions, the off-shell formalism is not always available. In $D = 4$, the finite set of auxiliary fields has been worked out only for $N = 1$ and $N = 2$ multiplets and some $N = 4$ supergravity/matter combinations. No

N								
Spin	1	2	3	4	5	6	7	8
Spin 2	1	1	1	1	1	1	1	1
Spin $\frac{3}{2}$	1	2	3	4	5	6	8	8
Spin 1		1	3	6	10	16	28	28
Spin $\frac{1}{2}$			1	4	11	26	56	56
Spin 0			2	10	30	70	70	

Table 2: Multiplicity for massless on-shell representations with maximal helicity 2.

N						
Spin	1	2	3	4		
Spin 2		1		1		1
Spin $\frac{3}{2}$		1 2	1	4	1	6
Spin 1	1 2 1	1 4	5 + 1	6 14 + 1	27	
Spin $\frac{1}{2}$	1 2 1	4 5 + 1	4	14 14' + 6	48	
Spin 0	2 1	5 4	1	14' 14	42	

Table 3: Some massive representations (without central charges) labelled in terms of the $U\mathcal{S}p(2N)$ representations.

theory beyond half-maximal has an off-shell formulation with a finite number of auxiliary fields. Harmonic superspace can extend the range but at the price of an infinite number. There is no known off-shell formulation for the maximally supersymmetric theories. This is a drawback since non-renormalization theorems are most transparent in the off-shell formalism. For example, the finiteness of the maximally supersymmetric $N=4$ Yang-Mills theory leads one to wonder whether the maximally supersymmetric $N=8$ supergravity might also have some peculiar ultraviolet properties.

The absence of a complete off-shell formalism also remains something of a mystery: is there some deeper meaning to all this?

Early discussions of ultraviolet divergences in extended supergravity may be found in the Trieste Lectures by Duff [24] and the paper by Howe and Lindstrom [25], and up-to-date

N				
Spin	2	4	6	8
Spin 2			1	1
Spin $\frac{3}{2}$		1	1 6	8
Spin 1	1	1 4	6 14 + 1	27
Spin $\frac{1}{2}$	1 2	4 5 + 1	14 14' + 6	48
Spin 0	2 1	5 4	14' 14	42

Table 4: Some massive representations with one central charge ($|Z| = m$). All states are complex.

ones in the review by Bern et al [26] and the paper by Howe and Stelle [27].

4 Eleven dimensions

4.1 The algebra

Eleven is the maximum spacetime dimension in which one can formulate a consistent supersymmetric theory, as was first recognized by Nahm in his classification of supersymmetry algebras. The easiest way to see this is to start in four dimensions and note that one supersymmetry relates states differing by one half unit of helicity. If we now make the reasonable assumption that there be no massless particles with spins greater than two, then we can allow up to a maximum of $N = 8$ supersymmetries taking us from helicity -2 through to helicity $+2$. Since the minimal supersymmetry generator is a Majorana spinor with four off-shell components, this means a total of 32 spinor components. Now in a spacetime with D dimensions and signature $(1, D - 1)$, the maximum value of D admitting a 32 component spinor is $D = 11$. (Going to $D = 12$, for example, would require 64 components.) See Table 5³. Furthermore, $D = 11$ emerges naturally as the maximum dimension admitting supersymmetric extended objects.

³Conventions differ on how to count the supersymmetries and the more usual conventions are that $N_{\max} = 8$ in $D = 5$ and $N_{\max} = 4$ in $D = 7$.

Dimension (D or d)	Minimal Spinor (M or m)	Supersymmetry (N or n)
11	32	1
10	16	2, 1
9	16	2, 1
8	16	2, 1
7	16	2, 1
6	8	4, 3, 2, 1
5	8	4, 3, 2, 1
4	4	8, ..., 1
3	2	16, ..., 1
2	1	32, ..., 1

Table 5: Minimal spinor components and supersymmetries.

The full D=11 supertranslation algebra is

$$\{Q_\alpha, Q_\beta\} = (C\Gamma^M)_{\alpha\beta} P_M + (C\Gamma_{MN})_{\alpha\beta} Z^{MN} + (C\Gamma_{MNPQR})_{\alpha\beta} Z^{MNPQR}. \quad (18)$$

Note that the total number of algebraically independent charges that could appear on the right hand side is 528. The number actually appearing is

$$11 + 55 + 462 = 528 \quad (19)$$

so the algebra (18) is ‘maximally extended’. The three types of charge appearing on the right hand side are those associated with the supergraviton, the supermembrane and the superfivebrane, which are the three basic ingredients of M-theory. The time components Z_{0I} and Z_{0IJKL} are associated with the 8-brane and 6-brane of Type IIA theory that arise on compactification to D=10.

The M-theory algebra is treated in the papers by Townsend[53] and Gauntlett and Hull [52].

4.2 The multiplet

Not long after Nahm’s paper, Cremmer, Julia and Scherk realized that supergravity not only permits up to seven extra dimensions but in fact takes its simplest and most elegant

<i>d-bein</i>	$e_M{}^A$	$D(D-3)/2$
<i>gravitino</i>	Ψ_M	$2^{(\alpha-1)}(D-3)$
<i>p-form</i>	$A_{M_1 M_2 \dots M_p}$	$\binom{D-2}{p}$
<i>spinor</i>	χ	$2^{(\alpha-1)}$

Table 6: On-shell degrees of freedom in D dimensions. $\alpha = D/2$ if D is even, $\alpha = (D-1)/2$ if D is odd. We assume Majorana fermions and divide by two if the fermion is Majorana-Weyl. Similarly, we assume real bosons and divide by two if the tensor field strength is self-dual.

form when written in its full eleven-dimensional glory. The unique $D = 11, N = 1$ supermultiplet is comprised of a graviton g_{MN} , a gravitino ψ_M and 3-form gauge field A_{MNP} with 44, 128 and 84 physical degrees of freedom, respectively. For a counting of on-shell degrees of freedom in higher dimensions, see Table 6. The theory may also be formulated in superspace. Ironically, however, these extra dimensions were not at first taken seriously but rather regarded merely as a useful device for deriving supergravities in four dimensions. Indeed $D = 4, N = 8$ supergravity was first obtained by Cremmer and Julia via the process of *dimensional reduction* i.e. by requiring that all the fields of $D = 11, N = 1$ supergravity be independent of the extra seven coordinates.

4.3 D=11 supergravity

For future reference we record the bosonic field equations

$$R_{MN} = \frac{1}{12} \left(F_{MPQR} F_N{}^{PQR} - \frac{1}{12} g_{MN} F^{PQRS} F_{PQRS} \right) \quad (20)$$

and

$$d * F_{(4)} + \frac{1}{2} F_{(4)} \wedge F_{(4)} = 0, \quad (21)$$

where $F_{(4)} = dA_{(3)}$. The supersymmetry transformation rule of the gravitino reduces in a purely bosonic background to

$$\delta \Psi_M = \mathcal{D}_M \epsilon, \quad (22)$$

where the parameter ϵ is a 32-component anticommuting spinor, and where

$$\mathcal{D}_M = D_M - \frac{1}{288} (\Gamma_M{}^{NPQR} - 8\delta_M^N \Gamma^{PQR}) F_{NPQR}, \quad (23)$$

where Γ^A are the $D = 11$ Dirac matrices and $\Gamma_{AB} = \Gamma_{[A}\Gamma_{B]}$. Here D_M is the usual Riemannian covariant derivative involving the connection ω_M of the usual structure group $\text{Spin}(10, 1)$, the double cover of $\text{SO}(10, 1)$,

$$D_M = \partial_M + \frac{1}{4}\omega_M{}^{AB}\Gamma_{AB} \quad (24)$$

For many years the Kaluza-Klein idea of taking extra dimensions seriously was largely forgotten but the arrival of eleven-dimensional supergravity provided the missing impetus. The kind of four-dimensional world we end up with depends on how we *compactify* these extra dimensions: maybe seven of them would allow us to give a gravitational origin, a la Kaluza-Klein, to the strong and weak forces as well as the electromagnetic. In a very influential paper, Witten drew attention to the fact that in such a scheme the four-dimensional gauge group is determined by the *isometry* group of the compact manifold \mathcal{K} . Moreover, he proved (what to this day seems to be merely a gigantic coincidence) that seven is not only the maximum dimension of \mathcal{K} permitted by supersymmetry but the minimum needed for the isometry group to coincide with the standard model gauge group $SU(3) \times SU(2) \times U(1)$.

In the early 80's there was great interest in four-dimensional N -extended supergravities for which the global $SO(N)$ is promoted to a gauge symmetry. In these theories the underlying supersymmetry algebra is no longer Poincaré but rather anti-de Sitter (AdS_4) and the Lagrangian has a non-vanishing cosmological constant Λ proportional to the square of the gauge coupling constant g :

$$G\Lambda \sim -g^2 \quad (25)$$

where G is Newton's constant. The $N > 4$ gauged supergravities were particularly interesting since the cosmological constant Λ does not get renormalized and hence the $SO(N)$ gauge symmetry has vanishing β -function⁴. The relation (25) suggested that there might be a Kaluza-Klein interpretation since in such theories the coupling constant of the gauge group arising from the isometries of the extra dimensions is given by

$$g^2 \sim Gm^2 \quad (26)$$

⁴For $N \leq 4$, the *beta* function (which receives a contribution from the spin 3/2 gravitinos) is positive and the pure supergravity theories are not asymptotically free. The addition of matter supermultiplets only makes the β function more positive and hence gravitinos can never be confined.

Compactification	Supergroup	Bosonic subgroup
$AdS_4 \times S^7$	$OSp(4 8)$	$SO(3, 2) \times SO(8)$
$AdS_5 \times S^5$	$SU(2, 2 4)$	$SO(4, 2) \times SO(6)$
$AdS_7 \times S^4$	$OSp(6, 2 4)$	$SO(6, 2) \times SO(5)$

Table 7: Compactifications and their symmetries.

where m^{-1} is the size of the compact space. Moreover, there is typically a negative cosmological constant

$$\Lambda \sim -m^2 \quad (27)$$

Combining (26) and (27), we recover (25). Indeed, the maximal ($D = 4, N = 8$) gauged supergravity was seen to correspond to the massless sector of ($D = 11, N = 1$) supergravity compactified on an S^7 whose metric admits an $SO(8)$ isometry and 8 Killing spinors. An important ingredient in these developments that had been insufficiently emphasized in earlier work on Kaluza-Klein theory was that the $AdS_4 \times S^7$ geometry was not fed in by hand but resulted from a *spontaneous compactification*, i.e. the vacuum state was obtained by finding a stable solution of the higher-dimensional field equations. The mechanism of spontaneous compactification appropriate to the $AdS_4 \times S^7$ solution of eleven-dimensional supergravity was provided by the Freund-Rubin mechanism in which the 4-form field strength in spacetime $F_{\mu\nu\rho\sigma}$ ($\mu = 0, 1, 2, 3$) is proportional to the alternating symbol $\epsilon_{\mu\nu\rho\sigma}$:

$$F_{\mu\nu\rho\sigma} \sim \epsilon_{\mu\nu\rho\sigma} \quad (28)$$

By applying a similar mechanism to the 7-form dual of this field strength one could also find compactifications on $AdS_7 \times S^4$ whose massless sector describes gauged maximal $N = 4$, $SO(5)$ supergravity in $D = 7$. Type IIB supergravity in $D = 10$, with its self-dual 5-form field strength, also admits a Freund-Rubin compactification on $AdS_5 \times S^5$ whose massless sector describes gauged maximal $N = 8$ supergravity in $D = 5$.

In the three cases given above, the symmetry of the vacuum is described by the supergroups $OSp(4|8)$, $SU(2, 2|4)$ and $OSp(6, 2|4)$ for the S^7 , S^5 and S^4 compactifications respectively, as shown in Table 7. Each of these groups is known to admit the so-called singleton, doubleton or triplet⁵ supermultiplets as shown in Table 8. We recall that sin-

⁵Our nomenclature is based on the AdS_4 , AdS_5 and AdS_7 groups having ranks 2, 3 and 4, respectively, and differs from that of Gunaydin.

Supergroup	Supermultiplet	Field content
$OSp(4 8)$	($n = 8, d = 3$) singleton	8 scalars, 8 spinors
$SU(2, 2 4)$	($n = 4, d = 4$) doubleton	1 vector, 8 spinors, 6 scalars
$OSp(6, 2 4)$	(($n_+, n_- = (2, 0), d = 6$) tripleton	1 chiral 2-form, 8 spinors, 5 scalars

Table 8: Superconformal groups and their singleton, doubleton and triplet representations.

gletons are those strange representations of AdS first identified by Dirac which admit no analogue in flat spacetime. They have been much studied by Fronsdal and collaborators.

This Kaluza-Klein approach to $D = 11$ supergravity eventually fell out of favor for three reasons. First, in spite of its maximal supersymmetry and other intriguing features, eleven dimensional supergravity was, after all, still a *field theory* of gravity with all the attendant problems of non-renormalizability. The resolution of this problem had to await the dawn of M -theory, since we now regard $D = 11$ supergravity not as a fundamental theory in its own right but the effective low-energy Lagrangian of M -theory. Second, as emphasized by Witten, it is impossible to derive by the conventional Kaluza-Klein technique of compactifying on a manifold a *chiral theory* in four spacetime dimensions starting from a non-chiral theory such as eleven-dimensional supergravity. Ironically, Horava and Witten were to solve this problem years later by compactifying M -theory on something that is not a manifold, namely S^1/Z_2 . Thirdly, these AdS vacua necessarily have non-vanishing cosmological constant unless cancelled by fermion condensates and this was deemed unacceptable at the time. However, AdS is currently undergoing a renaissance thanks to the AdS/CFT correspondence.

A discussion of spinors and Dirac matrices in D spacetime dimensions may be found in the reprint volume of Salam and Sezgin [32] and the book by West [8]. $D = 11$ supergravity is discussed in the paper of Cremmer, Julia and Scherk [64]. A summary of the S^7 and other X^7 compactifications of $D = 11$ supergravity down to AdS_4 may be found in the Physics Report of Duff, Nilsson and Pope [29].

Discussions of anti-de Sitter space and singlettes in supergravity may be found in the Physics Reports by Duff, Nilsson and Pope [29], the review by Gunaydin in proceedings of the 1989 Trieste supermembrane conference [85], the book by Salam and Sezgin [32], and the TASI lectures by Duff [87].

A review of the AdS/CFT correspondence may be found in Physics Reports of Aharony,

Gubser, Maldacena, Ooguri and Oz [88] and the TASI lectures of Maldacena [89].

5 Hidden spacetime symmetries in D=11

5.1 Spacelike, null and timelike reductions

Long ago, Cremmer and Julia pointed out that, when dimensionally reduced to d dimensions, $D = 11$ supergravity exhibits hidden symmetries. For example $E_7(\text{global}) \times \text{SU}(8)(\text{local})$ when $d = 4$ and $E_8(\text{global}) \times \text{SO}(16)(\text{local})$ when $d = 3$. Cremmer and Julia concentrated on the case where all extra dimensions are spacelike. Here we shall consider timelike and null reductions as well. The global symmetries remain the same but we shall focus on the local symmetries.

In fact, in anticipation of applications to vacuum supersymmetries in section 6, we shall focus particularly on the supercovariant derivative (23) as it appears in the gravitino variation of the dimensionally reduced theory. One finds that, after making a $d/(11-d)$ split, the Lorentz subgroup $G = \text{SO}(d-1, 1) \times \text{SO}(11-d)$ can be enlarged to the generalized structure groups $\mathcal{G} = \text{SO}(d-1, 1) \times G(\text{spacelike})$, $\mathcal{G} = \text{ISO}(d-1) \times G(\text{null})$ and $\mathcal{G} = \text{SO}(d) \times G(\text{timelike})$ arising in the spacelike, null and timelike dimensional reduction, respectively. As we shall see, these generalized structure groups are the same as the hidden symmetries for $d \geq 3$ but differ for $d < 3$.

First we consider a spacelike dimensional reduction corresponding to a $d/(11-d)$ split. Turning on only d -dimensional scalars, the reduction ansatz is particularly simple

$$g_{MN}^{(11)} = \begin{pmatrix} \Delta^{-1/(d-2)} g_{\mu\nu} & 0 \\ 0 & g_{ij} \end{pmatrix}, \quad A_{ijk}^{(11)} = \phi_{ijk}, \quad (29)$$

where $\Delta = \det g_{ij}$. For $d \leq 5$, we must also consider the possibility of dualizing either $F_{(4)}$ components or (for $d = 3$) Kaluza-Klein vectors to scalars. We will return to such possibilities below. But for now we focus on $d \geq 6$. In this case, a standard dimensional reduction of the $D = 11$ gravitino transformation (22) yields the d -dimensional gravitino transformation

$$\delta\psi_\mu = \hat{D}_\mu \epsilon \quad (30)$$

where

$$\hat{D}_\mu = \partial_\mu + \omega_\mu{}^{\alpha\beta} \gamma_{\alpha\beta} + Q_\mu{}^{ab} \Gamma_{ab} + \frac{1}{3!} \epsilon^{ia} \epsilon^{jb} \epsilon^{kc} \partial_\mu \phi_{ijk} \Gamma_{abc}. \quad (31)$$

Here γ_α are $\text{SO}(d-1,1)$ Dirac matrices, while Γ_a are $\text{SO}(11-d)$ Dirac matrices. For completeness, we also note that the d -dimensional dilatinos transform according to

$$\delta\lambda_i = -\frac{1}{2}\gamma^\mu[P_{\mu ij}\Gamma^j - \frac{1}{36}(\Gamma_i^{jkl} - 6\delta_i^j\Gamma^{kl})\partial_\mu\phi_{jkl}]\epsilon. \quad (32)$$

In the above, the lower dimensional quantities are related to their $D = 11$ counterparts through

$$\begin{aligned} \psi_\mu &= \Delta^{\frac{1}{4(d-2)}} \left(\Psi_\mu^{(11)} + \frac{1}{d-2} \gamma_\mu \Gamma^i \Psi_i^{(11)} \right), & \lambda_i &= \Delta^{\frac{1}{4(d-2)}} \Psi_i^{(11)}, \\ \epsilon &= \Delta^{\frac{1}{4(d-2)}} \epsilon^{(11)}, \\ Q_\mu^{ab} &= e^{i[a} \partial_\mu e_i^{b]}, & P_{\mu ij} &= e_i^a \partial_\mu e_j)_a. \end{aligned} \quad (33)$$

This decomposition is suggestive of a generalized structure group with connection given by \hat{D}_μ . However one additional requirement is necessary before declaring this an enlargement of $\text{SO}(d-1,1) \times \text{SO}(11-d)$, and that is to ensure that the algebra generated by Γ_{ab} and Γ_{abc} closes within itself. Along this line, we note that the commutators of these internal Dirac matrices have the schematic structure

$$[\Gamma^{(2)}, \Gamma^{(2)}] = \Gamma^{(2)}, \quad [\Gamma^{(2)}, \Gamma^{(3)}] = \Gamma^{(3)}, \quad [\Gamma^{(3)}, \Gamma^{(3)}] = \Gamma^{(6)} + \Gamma^{(2)}. \quad (34)$$

Here the notation $\Gamma^{(n)}$ indicates the antisymmetric product of n Dirac matrices, and the right hand sides of the commutators only indicate what possible terms may show up. The first commutator above merely indicates that the Γ_{ab} matrices provide a representation of the Riemannian $\text{SO}(11-d)$ structure group.

For $d \geq 6$, the internal space is restricted to five or fewer dimensions. In this case, the antisymmetric product $\Gamma^{(6)}$ cannot show up, and the algebra clearly closes on $\Gamma^{(2)}$ and $\Gamma^{(3)}$. Working out the extended structure groups for these cases results in the expected Cremmer and Julia groups listed in the first four lines in the second column of Table 9. A similar analysis follows for $d \leq 5$. However, in this case, we must also dualize an additional set of fields to see the hidden symmetries. For $d = 5$, an additional scalar arises from the dual of $F_{\mu\nu\rho\sigma}$; this yields an addition to (31) of the form $\hat{D}_\mu^{\text{additional}} = \frac{1}{4!} \epsilon_\mu^{\nu\rho\sigma\lambda} F_{\nu\rho\sigma\lambda} \Gamma_{123456}$. This $\Gamma^{(6)}$ term is precisely what is necessary for the closure of the algebra of (34). Of course, in this case, we must also make note of the additional commutators

$$[\Gamma^{(2)}, \Gamma^{(6)}] = \Gamma^{(6)}, \quad [\Gamma^{(3)}, \Gamma^{(6)}] = \Gamma^{(7)} + \Gamma^{(3)}, \quad [\Gamma^{(6)}, \Gamma^{(6)}] = \Gamma^{(10)} + \Gamma^{(6)} + \Gamma^{(2)}. \quad (35)$$

However neither $\Gamma^{(7)}$ nor $\Gamma^{(10)}$ may show up in $d = 5$ for dimensional reasons.

The analysis for $d = 4$ is similar; however here $\hat{D}_\mu^{\text{additional}} = \frac{1}{3!} \epsilon_\mu^{\nu\rho\sigma} e^{ia} F_{\nu\rho\sigma i} \Gamma_a \Gamma_{1234567}$. Closure of the algebra on $\Gamma^{(2)}$, $\Gamma^{(3)}$ and $\Gamma^{(6)}$ then follows because, while $\Gamma^{(7)}$ may in principle arise in the middle commutator of (35), it turns out to be kinematically forbidden. For $d = 3$, on the other hand, in addition to a contribution $\hat{D}_\mu^{\text{additional}} = \frac{1}{2!2!} \epsilon_\mu^{\nu\rho} e^{ia} e^{jb} F_{\nu\rho j} \Gamma_{ab} \Gamma_{12345678}$, one must also dualize the Kaluza-Klein vectors g_μ^i . Doing so gives rise to a $\Gamma^{(7)}$ in the generalized connection which, in addition to the previously identified terms, completes the internal structure group to $\text{SO}(16)$.

The remaining three cases, namely $d = 2$, $d = 1$ and $d = 0$ fall somewhat outside the framework presented above. This is because in these low dimensions the generalized connections \hat{D}_μ derived via reduction are partially incomplete. For $d = 2$, we find

$$\hat{D}_\mu^{(d=2)} = \partial_\mu + \omega_\mu^{\alpha\beta} \gamma_{\alpha\beta} + Q_\mu^{ab} \Gamma_{ab} + \frac{1}{9} (\delta_\mu^\nu - \frac{1}{2} \gamma_\mu^\nu) e^{ia} e^{jb} e^{kc} \partial_\nu \phi_{ijk} \Gamma_{abc}, \quad (36)$$

where $\gamma_{\mu\nu} = -\frac{1}{2} \epsilon_{\mu\nu} (\epsilon^{\alpha\beta} \gamma_{\alpha\beta})$ is necessarily proportional to the two-dimensional chirality matrix. Hence from a two-dimensional point of view, the scalars from the metric enter non-chirally, while the scalars from $F_{(4)}$ enter chirally. Taken together, the generalized connection (36) takes values in $\text{SO}(16)_+ \times \text{SO}(16)_-$, which we regard as the enlarged structure group. However not all generators are present because of lack of chirality in the term proportional to Q_μ^{ab} . Thus at this point the generalized structure group deviates from the hidden symmetry group, which would be an infinite dimensional subgroup of affine E_8 . Similarly, for $d = 1$, closure of the derivative $\hat{D}_\mu^{(d=1)}$ results in an enlarged $\text{SO}(32)$ structure group. However this is not obviously related to any actual hidden symmetry of the 1/10 split. The $d = 0$ case is subject to the same caveats as the $d = 1$ and $d = 2$ cases: not all group generators are present in the covariant derivative. $\text{SL}(32, \mathbb{R})$ requires $\{\Gamma^{(1)}, \Gamma^{(2)}, \Gamma^{(3)}, \Gamma^{(4)}, \Gamma^{(5)}\}$ whereas only $\{\Gamma^{(2)}, \Gamma^{(3)}, \Gamma^{(5)}\}$ appear in the covariant derivative.

Next we consider a timelike reduction for which we simply interchange a time and a space direction in the above analysis. This results in an internal Clifford algebra with signature $(10-d, 1)$, and yields the extended symmetry groups indicated in the fourth column of Table 9. The same caveats concerning $d = 2, 1, 0$ apply in the timelike case.

Turning finally to the null case, we may replace one of the internal Dirac matrices with Γ_+ (where $+, -$ denote light-cone directions). Since $(\Gamma_+)^2 = 0$, this indicates that the extended structure groups for the null case are contractions of the corresponding spacelike (or timelike)

groups. In addition, by removing Γ_+ from the set of Dirac matrices, we essentially end up in the case of one fewer compactified dimensions. As a result, the $G(\text{null})$ group in d -dimensions must have a semi-direct product structure involving the $G(\text{spacelike})$ group in $(d+1)$ -dimensions. Of course, these groups also contain the original $\text{ISO}(10-d)$ structure group as a subgroup. The resulting generalized structure groups are given in the third column of Table 9. Once again, the same caveats concerning $d = 2, 1, 0$ apply.

Spacelike reductions of D=11 supergravity may be found in the paper of Cremmer and Julia [65], null reductions in the paper of Duff and Liu [55] and timelike reductions in the paper of Hull and Julia [66]. Some of the noncompact groups appearing in the Table may be unfamiliar, but a nice discussion of their properties may be found in the book by Gilmore [67].

5.2 The complete uncompactified D=11 theory

Following Cremmer and Julia's spacelike reduction, the question was then posed: do these symmetries appear magically only after dimensional reduction, or were they already present in the full uncompactified and untruncated $D = 11$ theory? The question was answered by de Wit and Nicolai who made a $d/(11-d)$ split and fixed the gauge by setting to zero the off-diagonal components of the elfbein. They showed that in the resulting field equations the local symmetries are indeed already present, but the global symmetries are not. For example, after making the split $\text{SO}(10, 1) \supset \text{SO}(3, 1) \times \text{SO}(7)$, we find the enlarged symmetry $\text{SO}(3, 1) \times \text{SU}(8)$. There is no global E_7 invariance (although the 70 internal components of the metric and 3-form may nevertheless be assigned to an $E_7/\text{SU}(8)$ coset). Similar results were found for other values of d : in each case the internal subgroup $\text{SO}(11-d)$ gets enlarged to some compact group $G(\text{spacelike})$ while the spacetime subgroup $\text{SO}(d-1, 1)$ remains intact⁶. Here we ask instead whether there are hidden *spacetime* symmetries. This is a question that could have been asked long ago, but we suspect that people may have been inhibited by the Coleman-Mandula theorem which forbids combining spacetime and internal symmetries. However, this is a statement about Poincare symmetries of the S-matrix and here we are concerned with Lorentz symmetries of the equations of motion, so there will be no conflict.

⁶We keep the terminology "spacetime" and "internal" even though no compactification or dimensional reduction is implied.

$d/(11-d)$	$G(spacelike)$	$G(null)$	$G(timelike)$
11/0	{1}	{1}	{1}
10/1	{1}	{1}	{1}
9/2	$SO(2)$	R	$SO(1,1)$
8/3	$SO(3) \times SO(2)$	$ISO(2) \times R$	$SO(2,1) \times SO(1,1)$
7/4	$SO(5)$	$[SO(3) \times SO(2)] \ltimes R_{(3,2)}$	$SO(3,2)$
6/5	$SO(5) \times SO(5)$	$SO(5) \ltimes R_{(10)}^{10}$	$SO(5,C)$
5/6	$USp(8)$	$[SO(5) \times SO(5)] \ltimes R_{(4,4)}^{16}$	$USp(4,4)$
4/7	$SU(8)$	$USp(8) \ltimes R_{(27)}^{27}$	$SU^*(8)$
3/8	$SO(16)$	$[SU(8) \times U(1)] \ltimes R_{(28_{1/2},\bar{28}_{-1/2})}^{56}$	$SO^*(16)$
2/9	$SO(16) \times SO(16)$	$SO(16) \ltimes R_{(120)}^{120}$	$SO(16,C)$
1/10	$SO(32)$	$[SO(16) \times SO(16)] \ltimes R_{(16,16)}^{256}$	$SO(16,16)$
0/11	$SL(32,R)$	$SL(32,R)$	$SL(32,R)$

Table 9: The generalized structure groups are given by $\mathcal{G} = SO(d-1,1) \times G(spacelike)$, $\mathcal{G} = ISO(d-1) \times G(null)$ and $\mathcal{G} = SO(d) \times G(timelike)$.

The explicit demonstration of $G(spacelike)$ invariance by de Wit and Nicolai is very involved, to say the least. However, the result is quite simple: one finds the same $G(spacelike)$ in the full uncompactified $D=11$ theory as was already found in the spacelike dimensional reduction of Cremmer and Julia. Here we content ourselves with the educated guess that the same logic applies to $G(timelike)$ and $G(null)$: they are the same as what one finds by timelike and null reduction, respectively. The claim that the null and timelike symmetries are present in the full theory and not merely in its dimensional reductions might be proved by repeating the spacelike calculations of de Wit and Nicolai with the appropriate change of Γ matrices. So we propose that, after making a $d/(11-d)$ split, the Lorentz subgroup $G = SO(d-1,1) \times SO(11-d)$ can be enlarged to the generalized structure groups $\mathcal{G} = SO(d-1,1) \times G(spacelike)$, $\mathcal{G} = ISO(d-1) \times G(null)$ and $\mathcal{G} = SO(d) \times G(timelike)$.

As we have seen, for $d > 2$ the groups $G(spacelike)$, $G(timelike)$ and $G(null)$ are the same as those obtained from dimensional reductions. For the purposes of this section, however, their physical interpretation is very different. They are here proposed as symmetries of the full $D=11$ equations of motion; there is no compactification involved, whether toroidal or

otherwise. (Note that by postulating that the generalized structure groups survive as hidden symmetries of the full uncompactified theory, we avoid the undesirable features associated with compactifications including a timelike direction such as closed timelike curves.)

For $d \leq 2$ it is less clear whether these generalized structure groups are actually hidden symmetries. Yet one might imagine that there exists a yet-to-be-discovered formulation of M-theory in which the $d = 2$ and $d = 1$ symmetries are realized. This would still be in keeping with the apparent need to make a non-covariant split and to make the corresponding gauge choice before the hidden symmetries emerge. A yet bolder conjecture, due to Hull, requiring no non-covariant split or gauge choice since $d = 0$ is that there exists a formulation of M-theory with the full $SL(32, R)$. This proposal is nevertheless very attractive since $SL(32, R)$ contains all the groups in Table 9 as subgroups and would thus answer the question of whether all these symmetries are present at the same time. This is an important issue deserving of further study.

We can apply similar logic to theories with fewer than 32 supersymmetries. Of course, if M-theory really underlies all supersymmetric theories then the corresponding vacua will all be special cases of the above. However, it is sometimes useful to focus on such a sub-theory, for example the Type I and heterotic strings with $N = 16$. Here $G(\text{spacelike}) = SO(d) \times SO(d)$, $G(\text{null}) = ISO(d - 1) \times ISO(d - 1)$ and $G(\text{timelike}) = SO(d - 1, 1) \times SO(d - 1, 1)$.

Finally, we emphasize that despite the $d/(11 - d)$ split these symmetries refer to the full equations of motion and not to any particular background such as product manifolds. This issue of specific solutions of these equations is the subject of the next section.

Note that we have not considered the global symmetries such as E_7 for $d=4$, E_8 for $d=3$ and their infinite dimensional generalizations E_{11-d} for $d \leq 2$. These appear after dimensional reduction but, according to de Wit and Nicolai, not even the finite dimensional examples are symmetries of the full uncompactified theory. Discrete subgroups, known as U-dualities, do appear in M-theory, but so far only as symmetries of toroidally compactified vacua, not as background-independent symmetries of the equations of motion.

Hidden symmetries of the uncompactified $D = 11$ equations, as opposed to their dimensional reduction, are discussed in the papers by Duff [68], de Wit and Nicolai [69, 70], Duff and Liu [55], Hull [56] and Keurentjes [61, 62].

U-duality conjectures in membrane and M-theory may be found in the papers of Duff and Liu [98] and Hull and Townsend [99]. For a recent discussion of E_{11} see the paper by

West [100].

6 Counting supersymmetries of D=11 vacua

6.1 Holonomy and supersymmetry

The equations of M-theory display the maximum number of supersymmetries $N = 32$, and so n , the number of supersymmetries preserved by a particular vacuum, must be some integer $0 \leq n \leq 32$. In vacua with vanishing 4-form $F_{(4)}$, it is well known that n is given by the number of singlets appearing in the decomposition of the 32 of $\mathrm{SO}(1, 10)$ under $H \subset \mathrm{SO}(1, 10)$ where H is the holonomy group of the usual Riemannian connection (24). This connection can account for vacua with $n = 0, 1, 2, 3, 4, 6, 8, 16, 32$.

Vacua with non-vanishing $F_{(4)}$ allow more exotic fractions of supersymmetry, including $16 < n < 32$. Here, however, it is necessary to generalize the notion of holonomy to accommodate the generalized connection (23) that results from a non-vanishing $F_{(4)}$. As discussed by Duff and Liu, the number of M-theory vacuum supersymmetries is now given by the number of singlets appearing in the decomposition of the 32 of \mathcal{G} under $\mathcal{H} \subset \mathcal{G}$ where \mathcal{H} is the generalized holonomy group and \mathcal{G} is the generalized structure group.

In subsequent papers by Hull and by Papadopoulos and Tsypis it was shown that \mathcal{G} may be as large as $\mathrm{SL}(32, \mathbb{R})$ and that an M-theory vacuum admits precisely n Killing spinors iff

$$\mathrm{SL}(31 - n, \mathbb{R}) \ltimes (n + 1)\mathbb{R}^{(31-n)} \not\subseteq \mathcal{H} \subseteq \mathrm{SL}(32 - n, \mathbb{R}) \ltimes n\mathbb{R}^{(32-n)}, \quad (37)$$

i.e. the generalized holonomy is contained in $\mathrm{SL}(32 - n, \mathbb{R}) \ltimes n\mathbb{R}^{(32-n)}$ but is not contained in $\mathrm{SL}(31 - n, \mathbb{R}) \ltimes (n + 1)\mathbb{R}^{(31-n)}$.

We recall that the number of supersymmetries preserved by an M-theory background depends on the number of covariantly constant spinors,

$$\mathcal{D}_M \epsilon = 0, \quad (38)$$

called *Killing* spinors. It is the presence of the terms involving the 4-form $F_{(4)}$ in (23) that makes this counting difficult. So let us first examine the simpler vacua for which $F_{(4)}$ vanishes. Killing spinors then satisfy the integrability condition

$$[D_M, D_N]\epsilon = \frac{1}{4}R_{MN}{}^{AB}\Gamma_{AB}\epsilon = 0, \quad (39)$$

$d/(11-d)$	$H \subset \text{SO}(11-d) \subset \text{Spin}(10)$	n
7/4	$\text{SU}(2) \cong \text{Sp}(2)$	16
5/6	$\text{SU}(3)$	8
4/7	G_2	4
3/8	$\text{SU}(2) \times \text{SU}(2)$	8
	$\text{Sp}(4)$	6
	$\text{SU}(4)$	4
	$\text{Spin}(7)$	2
1/10	$\text{SU}(2) \times \text{SU}(3)$	4
	$\text{SU}(5)$	2

Table 10: Holonomy of static M-theory vacua with $F_{(4)} = 0$ and their supersymmetries.

where R_{MN}^{AB} is the Riemann tensor. The subgroup of $\text{Spin}(10, 1)$ generated by this linear combination of $\text{Spin}(10, 1)$ generators Γ_{AB} corresponds to the *holonomy* group H of the connection ω_M . We note that the same information is contained in the first order Killing spinor equation (38) and second-order integrability condition (39). One implies the other, at least locally. The number of supersymmetries, n , is then given by the number of singlets appearing in the decomposition of the 32 of $\text{Spin}(10, 1)$ under H . In Euclidean signature, connections satisfying (39) are automatically Ricci-flat and hence solve the field equations when $F_{(4)} = 0$. In Lorentzian signature, however, they need only be Ricci-null so Ricci-flatness has to be imposed as an extra condition. In Euclidean signature, the holonomy groups have been classified. In Lorentzian signature, much less is known but the question of which subgroups H of $\text{Spin}(10, 1)$ leave a spinor invariant has been answered by Bryant. There are two sequences according as the Killing vector $v_A = \bar{\epsilon} \Gamma_A \epsilon$ is timelike or null. Since $v^2 \leq 0$, the spacelike v_A case does not arise. The timelike v_A case corresponds to static vacua, where $H \subset \text{Spin}(10) \subset \text{Spin}(10, 1)$ while the null case to non-static vacua where $H \subset \text{ISO}(9) \subset \text{Spin}(10, 1)$. It is then possible to determine the possible n -values and one finds $n = 2, 4, 6, 8, 16, 32$ for static vacua, and $n = 1, 2, 3, 4, 8, 16, 32$ for non-static vacua as shown in Table 10, and $n = 1, 2, 3, 4, 8, 16, 32$ for non-static vacua, as shown in Table 11.

The allowed n values for Riemannian connections may be found in the papers of Acharya et al [74, 75] and by Figueroa-O'Farrill [71].

$d/(11-d)$	$H \subset \text{ISO}(d-1) \times \text{ISO}(10-d) \subset \text{Spin}(10,1)$	n
10/1	\mathbb{R}^9	16
6/5	$\mathbb{R}^5 \times (\text{SU}(2) \ltimes \mathbb{R}^4)$	8
4/7	$\mathbb{R}^3 \times (\text{SU}(3) \ltimes \mathbb{R}^6)$	4
3/8	$\mathbb{R}^2 \times (\text{G}_2 \ltimes \mathbb{R}^7)$	2
2/9	$\mathbb{R} \times (\text{SU}(2) \ltimes \mathbb{R}^4) \times (\text{SU}(2) \ltimes \mathbb{R}^4)$	4
	$\mathbb{R} \times (\text{Sp}(4) \ltimes \mathbb{R}^8)$	3
	$\mathbb{R} \times (\text{SU}(4) \ltimes \mathbb{R}^8)$	2
	$\mathbb{R} \times (\text{Spin}(7) \ltimes \mathbb{R}^8)$	1

Table 11: Holonomy of non-static M-theory vacua with $F_{(4)} = 0$ and their supersymmetries.

6.2 Generalized holonomy

In general we want to include vacua with $F_{(4)} \neq 0$. Such vacua are physically interesting for a variety of reasons. In particular, they typically have fewer moduli than their zero $F_{(4)}$ counterparts. Now, however, we face the problem that the connection in (23) is no longer the spin connection to which the bulk of the mathematical literature on holonomy groups is devoted. In addition to the $\text{Spin}(10,1)$ generators Γ_{AB} , it is apparent from (23) that there are terms involving Γ_{ABC} and Γ_{ABCDE} . In fact, the generalized connection takes its values in $\text{SL}(32, \mathbb{R})$. Note, however, that some generators are missing from the covariant derivative. Denoting the antisymmetric product of k Dirac matrices by $\Gamma^{(k)}$, the complete set of $\text{SL}(32, \mathbb{R})$ generators include $\{\Gamma^{(1)}, \Gamma^{(2)}, \Gamma^{(3)}, \Gamma^{(4)}, \Gamma^{(5)}\}$ whereas only $\{\Gamma^{(2)}, \Gamma^{(3)}, \Gamma^{(5)}\}$ appear in the covariant derivative. Another way in which generalized holonomy differs from the Riemannian case is that, although the vanishing of the covariant derivative of the spinor implies the vanishing of the commutator, the converse is not true, as discussed below.

This generalized connection can preserve exotic fractions of supersymmetry forbidden by the Riemannian connection. For example, M-branes at angles include $n=5$, 11-dimensional pp-waves include $n = 18, 20, 22, 24, 26$, squashed $N(1,1)$ spaces and M5-branes in a pp-wave background include $n = 12$ and Godel universes include $n = 14, 18, 20, 22, 24$. However, we can attempt to quantify this in terms of generalized holonomy groups⁷.

⁷In these lectures we focus on $D = 11$ but similar generalized holonomy can be invoked to count n in Type IIB vacua, which include pp-waves with $n = 28$.

Generalized holonomy means that one can assign a holonomy $\mathcal{H} \subset \mathcal{G}$ to the generalized connection appearing in the supercovariant derivative \mathcal{D} where \mathcal{G} is the generalized structure group. The number of unbroken supersymmetries is then given by the number of \mathcal{H} singlets appearing in the decomposition of the 32 dimensional representation of \mathcal{G} under $\mathcal{H} \subset \mathcal{G}$.

For generic backgrounds we require that \mathcal{G} be the full $SL(32, R)$ while for special backgrounds smaller \mathcal{G} are sufficient. To see this, let us write the supercovariant derivative as

$$\mathcal{D}_M = \hat{D}_M + X_M, \quad (40)$$

for some other connection \hat{D}_M and some covariant 32×32 matrix X_M . If we now specialize to backgrounds satisfying

$$X_M \epsilon = 0, \quad (41)$$

then the relevant structure group is $\hat{\mathcal{G}} \subseteq \mathcal{G}$.

Consider, for example, the connection \hat{D} arising in dimensional reduction of $D = 11$ supergravity (31). The condition (41) is just $\delta\lambda_i = 0$ where λ_i are the dilatinos of the dimensionally reduced theory. In this case, the generalized holonomy is given by $\hat{\mathcal{H}} \subseteq \hat{\mathcal{G}}$ where the various $\hat{\mathcal{G}}$ arising in spacelike, null and timelike compactifications are tabulated in Table 9 for different numbers of the compactified dimensions.

Another way in which generalized holonomy differs from Riemannian holonomy is that, although the vanishing of the covariant derivative implies the vanishing of the commutator, the converse is not true. Consequently, the second order integrability condition alone may be a misleading guide to the generalized holonomy group \mathcal{H} .

To illustrate this, we consider Freund-Rubin vacua with $F_{(4)}$ given by

$$F_{\mu\nu\rho\sigma} = 3m\epsilon_{\mu\nu\rho\sigma}, \quad (42)$$

where $\mu = 0, 1, 2, 3$ and m is a constant with the dimensions of mass. This leads to an $AdS_4 \times X^7$ geometry. For such a product manifold, the supercovariant derivative splits as

$$\mathcal{D}_\mu = D_\mu + m\gamma_\mu\gamma_5 \quad (43)$$

and

$$\mathcal{D}_m = D_m - \frac{1}{2}m\Gamma_m, \quad (44)$$

and the Killing spinor equations reduce to

$$\mathcal{D}_\mu\epsilon(x) = 0 \quad (45)$$

and

$$\mathcal{D}_m \eta(y) = 0. \quad (46)$$

Here $\epsilon(x)$ is a 4-component spinor and $\eta(y)$ is an 8-component spinor, transforming with Dirac matrices γ_μ and Γ_m respectively. The first equation is satisfied automatically with our choice of AdS_4 spacetime and hence the number of $D = 4$ supersymmetries, $0 \leq N \leq 8$, devolves upon the number of Killing spinors on X^7 . They satisfy the integrability condition

$$[\mathcal{D}_m, \mathcal{D}_n]\eta = -\frac{1}{4}C_{mn}^{ab}\Gamma_{ab}\eta = 0, \quad (47)$$

where C_{mn}^{ab} is the Weyl tensor. Owing to this generalized connection, vacua with $m \neq 0$ present subtleties and novelties not present in the $m = 0$ case, for example the phenomenon of *skew-whiffing*. For each Freund-Rubin compactification, one may obtain another by reversing the orientation of X^7 . The two may be distinguished by the labels *left* and *right*. An equivalent way to obtain such vacua is to keep the orientation fixed but to make the replacement $m \rightarrow -m$ thus reversing the sign of F_4 . So the covariant derivative (44), and hence the condition for a Killing spinor, changes but the integrability condition (47) remains the same. With the exception of the round S^7 , where both orientations give $N = 8$, at most one orientation can have $N \geq 0$. This is the *skew-whiffing theorem*.

The squashed S^7 provides a non-trivial example : the left squashed S^7 has $N = 1$ but the right squashed S^7 has $N = 0$. Other examples are provided by the left squashed $N(1,1)$ spaces, one of which has $N = 3$ and the other $N = 1$, while the right squashed counterparts both have $N = 0$. (Note, incidentally, that $N = 3$ i.e. $n = 12$ can never arise in the Riemannian case.)

All this presents a dilemma. If the Killing spinor condition changes but the integrability condition does not, how does one give a holonomic interpretation to the different supersymmetries? We note that in (44), the $SO(7)$ generators Γ_{ab} , augmented by the presence of Γ_a , together close on $SO(8)$. Hence the generalized holonomy group satisfies $\mathcal{H} \subset SO(8)$. We now ask how the 8 of $SO(8)$ decomposes under \mathcal{H} . In the case of the left squashed S^7 , $\mathcal{H} = SO(7)^-, 8 \rightarrow 1 + 7$ and $N = 1$, but for the right squashed S^7 , $\mathcal{H} = SO(7)^+, 8 \rightarrow 8$ and $N = 0$. From the integrability condition alone, however, we would have concluded naively that $\mathcal{H} = G_2$ and that both orientations give $N = 1$.

Another context in which generalized holonomy may prove important is that of higher loop corrections to the M-theory Killing spinor equations with or without the presence of

non-vanishing $F_{(4)}$. Higher loops yield non-Riemannian corrections to the supercovariant derivative, even for vacua for which $F_{(4)} = 0$, thus rendering the Berger classification inapplicable. Although the Killing spinor equation receives higher order corrections, so does the metric, ensuring, for example, that $H = G_2$ Riemannian holonomy 7-manifolds still yield $N = 1$ in $D = 4$ when the non-Riemannian corrections are taken into account. This would require a generalized holonomy \mathcal{H} for which the decomposition $8 \rightarrow 1 + 7$ continues to hold.

Generalized holonomy is discussed in the papers of Duff and Stelle [97], Duff [54], Duff and Liu [55], Hull [56], Papadopoulos and Tsimpis [57, 58], Batrachenko, Duff, Liu and Wen [59], Bandos, de Azcarraga, Izquierdo, Lukierski, Picon and Varela [60, 76] and Keurentjes [61, 62].

Skew-whiffing is discussed in the paper and Physics Report by Duff, Nilsson and Pope [91, 29] and the paper of van Nieuwenhuizen and Warner [90]. The squashed S^7 may be found in the papers of Awada, Duff and Pope [92] and Duff, Nilsson and Pope [91]. For the result that $SO(7)$ generators Γ_{ab} , augmented by presence of Γ_a , together close on $SO(8)$ see the paper by Castellani, D'Auria, Fre and van Nieuwenhuizen [93].

Higher loop corrections to the Killing spinor equation are treated in the paper by Lu, Pope, Stelle and Townsend [94].

6.3 Specific examples

In Table 12 we tabulate the results of computations of this generalized holonomy for the $n = 16$ examples of the M2-brane, the M5-brane, the M-wave (MW) and the M-monopole (MK), and for a variety of their $n = 8$ intersections: M5/MK, M2/MK/MK, M2/MK, M2/MW, M5/MW, MW/MK and M2/M5. As we can see, the generalized holonomy of M-theory solutions takes on a variety of guises. We make note of two features exhibited by these solutions. Firstly, it is clear that many generalized holonomy groups give rise to the same number n of supersymmetries. This is a consequence of the fact that while \mathcal{H} must satisfy the condition (37), there are nevertheless many possible subgroups of $SL(32 - n, \mathbb{R}) \ltimes n\mathbb{R}^{(32-n)}$ allowed by generalized holonomy. Secondly, as demonstrated by the plane wave solutions, knowledge of \mathcal{H} by itself is insufficient for determining n ; here $\mathcal{H} = \mathbb{R}^9$, while n may be any even integer between 16 and 26.

What this indicates is that, at least for counting supersymmetries, it is important to understand the embedding of \mathcal{H} in \mathcal{G} . In contrast to the Riemannian case, different embed-

n	Background	Generalized holonomy
32	$E^{1,10}$, $AdS_7 \times S^4$, $AdS_4 \times S^7$, Hpp	$\{1\}$
18, ..., 26	plane waves	R^9
16	M5	$SO(5) \ltimes 6R^{4(4)}$
16	M2	$SO(8) \ltimes 12R^{2(8)}$
16	MW	R^9
16	MK	$SU(2)$
8	M5/MK	$[SO(5) \times SU(2)] \ltimes 6R^{2(4,1)+(4,2)}$
8	M2/MK/MK	$[SO(8) \times SU(2) \times SU(2)] \ltimes 3R^{(8,2,2)} \ltimes 6R^{2(8,1,1)}$
8	M2/MK	$[SO(8) \times SU(2) \ltimes 3R^{2(8,2)}] \ltimes 6R^{2(8,1,1)}$
8	M2/MW	$[SO(8) \times SL(16, R) \ltimes R^{(8,16)}] \ltimes 8R^{(8,1)+(1,16)}$
8	M5/MW	$[SO(5) \times SU^*(8) \ltimes 4R^{(4,8)}] \ltimes 8R^{2(4,1)+2(1,8)}$
8	MW/MK	$R^5 \times (SU(2) \ltimes R^{2(2)})$
8	M2/M5	$SL(24, R) \ltimes 8R^{24}$

Table 12: Generalized holonomies of the objects investigated in the text. For $n = 16$, we have $\mathcal{H} \subseteq SL(16, R) \ltimes 16R^{16}$, while for $n = 8$, it is instead $\mathcal{H} \subseteq SL(24, R) \ltimes 8R^{24}$.

dings of \mathcal{H} yield different possible values of n . Although this appears to pose a difficulty in applying the concept of generalized holonomy towards classifying supergravity solutions, it may be possible that a better understanding of the representations of non-compact groups will nevertheless allow progress to be achieved in this direction.

While the full generalized holonomy involves several factors, the transverse (or \hat{D}) holonomy is often simpler, *e.g.* $SO(5)$ for the M5 and $SO(8)$ for the M2. The results summarized in table 12 are suggestive that the maximal compact subgroup of \mathcal{H} , which must be contained in $SL(32 - n, R)$, is often sufficient to determine the number of surviving supersymmetries. For example, the M2/MK/MK solution may be regarded as a 3/8 split, with a hyper-Kahler eight-dimensional transverse space. In this case, the \hat{D} structure group is $SO(16)$, and the 32-component spinor decomposes under $SO(32) \supset SO(16) \supset SO(8) \times SU(2) \times SU(2)$ as $32 \rightarrow 2(16) \rightarrow 2(8,1,1) + 2(1,2,2) + 8(1,1,1)$ yielding eight singlets. Similarly, for the M5/MW intersection, we consider a 2/9 split, with the wave running along the two-dimensional longitudinal space. Since the \hat{D} structure group is $SO(16) \times SO(16)$ and the maximal compact subgroup of $SU^*(8)$ is $USp(8)$, we obtain the decomposition $32 \rightarrow$

$(16, 1) + (1, 16) \rightarrow 4(4, 1) + (1, 8) + 8(1, 1)$ under $\mathrm{SO}(32) \supset \mathrm{SO}(16) \times \mathrm{SO}(16) \supset \mathrm{SO}(5) \times \mathrm{USp}(8)$. This again yields $n = 8$. Note, however, that this analysis fails for the planck waves, as \mathbb{R}^9 has no compact subgroups.

Ultimately, one would hope to achieve a complete classification of M-theory vacua, either through generalized holonomy or other means. In this regard, one must also include the effects of higher order corrections and perhaps additional contributions beyond the supergravity itself.

6.4 The full M(only)?

In sections 5 and 6 we have focused on the low energy limit of M-theory, but since the reasoning is based mainly on group theory, it seems reasonable to promote it to the full M-theory. Similar reasoning can be applied to M-theory in signatures $(9,2)$ and $(6,5)$, the so-called M' and M^* theories, but the groups will be different. When counting the n value of a particular vacuum, however, we should be careful to note the phenomenon of *supersymmetry without supersymmetry*, where the supergravity approximation may fail to capture the full supersymmetry of an M-theory vacuum. For example, vacua related by T-duality and S-duality must, by definition, have the same n values. Yet they can appear to be different in supergravity if one fails to take into account winding modes and non-perturbative solitons. So more work is needed to verify that the n values found so far in $D = 11$ supergravity exhaust those of M-theory.

A different approach to supersymmetric vacua in M-theory is through the technique of G -structures. Hull has suggested that G -structures may be better suited to finding supersymmetric solutions whereas generalized holonomy may be better suited to classifying them. In any event, it would be useful to establish a dictionary for translating one technique into the other.

Ultimately, one would hope to achieve a complete classification of vacua for the full M-theory. In this regard, one must at least include the effects of M-theoretic corrections to the supergravity field equations and Killing spinor equations and perhaps even go beyond the geometric picture altogether. It seems likely, however, that counting supersymmetries by the number of singlets appearing in the decomposition 32 of $\mathrm{SL}(32, \mathbb{R})$ under $\mathcal{H} \subset \mathrm{SL}(32, \mathbb{R})$ will continue to be valid.

The various spacetime signatures in which M-theory can be formulated is discussed in the

paper by Blencowe and Duff [95]. M' and M^* theories are treated in [96]. Supersymmetry without supersymmetry may be found in the papers of Duff, Lu and Pope [82, 83]. For G-structures, see the papers by Gauntlett, MartelliPakis, Sparks and Waldram [77, 78, 79, 80, 81] and by Hull [56]. Connections between generalized holonomy and G-structures in theories with 8 supercharges are discussed in the paper by Batrachenko and Wen [101].

Acknowledgements

The first lecture has benefitted from useful conversations with Gordy Kane and correspondence with Kelly Stelle. The second lecture is based on work written with my collaborators Alex Batrachenko, Jim Liu and Steve Wen. Thanks to Arthur Greenspoon, who suggested several improvements to the manuscript. I am grateful to organizers of the school, Gerard 't Hooft and Nino Zichichi, for their kind hospitality in Erice.

References

- [1] D.V. Volkov and V.A. Soroka, *Higgs effect for Goldstone particles with spin 1/2*, JETP Lett. 18 (1973) 312.
- [2] D.V. Volkov and V.A. Soroka, *Gauge fields for symmetry group with spinor parameters*, Theor. Math. Phys. 20 (1974) 829.
- [3] S. Ferrara, D. Z. Freedman and P. van Nieuwenhuizen, *Progress toward a theory of supergravity*, Phys. Rev. D13 (1976) 3214.
- [4] S. Deser and B. Zumino, *Consistent supergravity*, Phys. Lett. B62 (1976) 335.
- [5] J. Wess and J. Bagger, *Supersymmetry and supergravity*, Princeton University Press (1983).
- [6] S. J. Gates, Jr., M. T. Grisaru, M. Rocek and W. Siegel, *Superspace or one thousand and one lessons in supersymmetry*, Benjamin Cummings (1983).
- [7] Prem P. Srivastava, *Supersymmetry, superfields and supergravity*, Adam Hilger (1986).
- [8] P. West, *Introduction to supersymmetry and supergravity*, World Scientific (1986).
- [9] P. G. O. Freund, *Introduction to supersymmetry* C. U. P. (1988).
- [10] D. Bailin and A. Love, *Supersymmetric gauge field theory and string theory*, I. O. P. (1994).
- [11] S. Weinberg, *The Quantum Theory of Fields, Volume III, Supersymmetry*, C. U. P. (2000).
- [12] M. Sohnius, *Introducing Supersymmetry*, Phys. Rept. 128, 39 (1985).
- [13] P. Van Nieuwenhuizen, *Supergravity*, Phys. Rept. 68 (1981) 189.
- [14] P. Fayet and S. Ferrara, *Supersymmetry*, Phys. Rept. 32, 249 (1977).
- [15] J. D. Lykken, *Introduction to supersymmetry*, arXiv:hep-th/9612114.
- [16] D. Nanopoulos, *Supersymmetric GUTS* Phys. Rept. 105, 71 (1984).

- [17] H. Nilles, *Supersymmetry, supergravity and particle physics*, Phys. Rept. **110**, 1 (1984).
- [18] H. E. Haber and G. L. Kane, *The Search For Supersymmetry: Probing Physics Beyond The Standard Model*, Phys. Rept. **117**, 75 (1985).
- [19] J. Ellis, *Supersymmetry and grand unification*, hep-th/9512335.
- [20] D. J. H. Chung, L. L. Everett, G. L. Kane, S. F. King, J. Lykken and Lian-Tao Wang, *The soft supersymmetry-breaking lagrangian: theory and applications*, MCTP-03-39.
- [21] M. Dine, *TASI lectures on M Theory phenomenology*, hep-th/0003175.
- [22] G. G. Ross, *Supersymmetric models*, *Prepared for Les Houches Summer School in Theoretical Physics, Session 68: Probing the Standard Model of Particle Interactions, Les Houches, France, 28 Jul - 5 Sep 1997*
- [23] S. Raby, *Desperately seeking supersymmetry*, hep-ph/0401169.
- [24] M. J. Duff, *Ultraviolet divergences in extended supergravity*, CERN-TH-3232, *Lectures given at Spring School on Supergravity, Trieste, Italy, Apr 22 - May 6, 1981*.
- [25] P. S. Howe and U. Lindstrom, *Higher order invariants in extended supergravity*, Nucl. Phys. B **181**(1981) 487.
- [26] Z. Bern *et al.*, *Counterterms in supergravity*, hep-th/0012230.
- [27] P.S. Howe and K.S. Stelle, *Supersymmetry counterterms revisited*, Phys. Lett. **B554** (2003) 190.
- [28] E. Witten, *Fermion quantum numbers in Kaluza-Klein theory*, in Proceedings of the Shelter Island II conference (1983) 227, eds Khuri, Jackiw, Weinberg and Witten (M. I. T. Press, 1985).
- [29] M. J. Duff, B. E. W. Nilsson and C. N. Pope, *Kaluza-Klein supergravity*, Phys. Rep. **130** (1986) 1.
- [30] T. Appelquist, A. Chodos and P. G. O. Freund, *Modern Kaluza-Klein theories*, (Addison-Wesley, 1987).

- [31] L. Castellani, R. D'Auria and P. Fre, *Supergravity and superstrings: a geometric perspective*, (in 3 volumes, World Scientific 1991).
- [32] Abdus Salam and Ergin Sezgin, *Supergravities in diverse dimensions*, (World Scientific, 1989).
- [33] M. J. Duff, *Kaluza-Klein theory in perspective*, in the Proceedings of the Nobel Symposium *Oskar Klein Centenary*, Stockholm, September 1994, (Ed Lindstrom, World Scientific, 1995), hep-th/9410046.
- [34] M. J. Duff, *The world in eleven dimensions: a tribute to Oskar Klein*, hep-th/0111237.
- [35] M. B. Green, J. H. Schwarz and E. Witten, *Superstring theory*, Cambridge University Press (1987).
- [36] J. Polchinski, *String Theory*, Volumes I and II, Cambridge University Press, (1998).
- [37] M. J. Duff, R. R. Khuri and J. X. Lu, *String solitons*, Phys. Rep. **259** (1995) 213.
- [38] J. H. Schwarz, *The power of M-theory*, Phys. Lett. **B360** (1995) 13.
- [39] M. J. Duff, *M-theory: the theory formerly known as strings*, Int. J. Mod. Phys. A11 (1996) 5623-5642, hep-th/9608117.
- [40] M. J. Duff, *The World in Eleven Dimensions: Supergravity, Supermembranes and M-theory*, Institute of Physics Publishing (1999).
- [41] P. K. Townsend, *Four lectures on M-theory*, hep-th/9612121.
- [42] M. Kaku, *Introduction to superstrings and M-theory*, (Springer, 1999).
- [43] M. Kaku, *Strings, conformal fields and M-theory*, (Springer, 1999).
- [44] M. J. Duff, *Supermembranes: The first fifteen weeks*, Class. Quant. Grav. **5**, 189 (1988).
- [45] M. J. Duff, *Classical and quantum supermembranes*, Class. Quant. Grav. **6**, 1577 (1989).
- [46] M. J. Duff, *Supermembranes*, Lectures given at the Theoretical Advanced Study Institute in Elementary Particle Physics (TASI 96), Boulder, 1996, hep-th/9611203.

- [47] K. S. Stelle, *An introduction to p-branes*, In *Seoul/Sokcho 1997, Dualities in gauge and string theories 39-104.
- [48] C. Johnson, D-branes, C. U. P. 2003.
- [49] T. Ortin, *Gravity and strings*, C. U. P. 2004.
- [50] J. Strathdee, *Extended Poincare supersymmetry*, Int. J. Mod. Phys. **A2** (1987) 273.
- [51] S. Ferrara and C. A. Savoy, *Representations of extended supersymmetry on one and two particle states*, in Supergravity 81, (Eds. Ferrara and Taylor, C. U. P, 1982).
- [52] J. P. Gauntlett and C. M. Hull, *BPS states with extra supersymmetry*, JHEP **0001**, 004 (2000) [hep-th/9909098].
- [53] P. K. Townsend, *M-theory from its superalgebra*, hep-th/9712004.
- [54] M. J. Duff, *M-theory on manifolds of G_2 holonomy: the first twenty years*, hep-th/0201062.
- [55] M. J. Duff and J. T. Liu, *Hidden spacetime symmetries and generalized holonomy in M-theory*, hep-th/0303140.
- [56] C. Hull, *Holonomy and symmetry in M-theory*, hep-th/0305039.
- [57] G. Papadopoulos and D. Tsimpis, *The holonomy of the supercovariant connection and Killing spinors*, JHEP **0307**, 018 (2003) [hep-th/0306117].
- [58] G. Papadopoulos and D. Tsimpis, *The holonomy of IIB supercovariant connection*, hep-th/0307127.
- [59] A. Batrachenko, M. J. Duff, J. T. Liu and W. Y. Wen, *Generalized holonomy of M-theory vacua*, hep-th/0312165.
- [60] I. A. Bandos, J. A. de Azcarraga, J. M. Izquierdo, M. Picon and O. Varela, *On BPS preons, generalized holonomies and $D = 11$ supergravities*, hep-th/0312266.
- [61] A. Keurentjes, *The topology of U-duality (sub-)groups*, hep-th/0309106.
- [62] A. Keurentjes, *U-duality (sub-)groups and their topology*, hep-th/0312134.

- [63] E. Witten, *Search for a realistic Kaluza-Klein theory*, Nucl. Phys. **B186** (1981) 412-428.
- [64] E. Cremmer, B. Julia and J. Scherk, *Supergravity theory in eleven-dimensions*, Phys. Lett. **B76** (1978) 409.
- [65] E. Cremmer and B. Julia, *The $SO(8)$ supergravity*, Nucl. Phys. **B159** (1979) 141.
- [66] C. Hull and B. Julia, *Duality and moduli spaces for time-like reductions*, Nucl. Phys. B **534**, 250 (1998) [hep-th/9803239].
- [67] R. Gilmore, *Lie groups, Lie algebras and some of their applications* (Wiley, New York, 1974).
- [68] M. J. Duff, *$E_8 \times SO(16)$ Symmetry of $d = 11$ Supergravity?*, in *Quantum Field Theory and Quantum Statistics, Essays in Honor of E. S. Fradkin*, Batalin, Isham and Vilkovisky, eds. (Adam Hilger, 1986).
- [69] B. de Wit and H. Nicolai, *$D = 11$ supergravity with local $SU(8)$ invariance*, Nucl. Phys. B **274**, 363 (1986).
- [70] H. Nicolai, *$D = 11$ supergravity with local $SO(16)$ invariance*, Phys. Lett. B **187**, 316 (1987).
- [71] J. Figueroa-O'Farrill, *Breaking the M-waves*, Class. Quant. Grav. **17**, 2925 (2000) [hep-th/9904124].
- [72] M. Berger, *Sur les groupes d'holonomie homogène des variétés à connexion affine et des variétés riemanniennes*, Bull. Soc. Math. France **83** (1955) 225.
- [73] R. L. Bryant, *Pseudo-Riemannian metrics with parallel spinor fields and non-vanishing Ricci tensor*, math.DG/0004073.
- [74] B. S. Acharya, J. M. Figueroa-O'Farrill and B. Spence, *Planes, branes and automorphisms. I: Static branes*, JHEP **9807**, 004 (1998) [hep-th/9805073].
- [75] B. S. Acharya, J. M. Figueroa-O'Farrill, B. Spence and S. Stanciu, *Planes, branes and automorphisms. II: Branes in motion*, JHEP **9807**, 005 (1998) [hep-th/9805176].

- [76] I. A. Bandos, J. A. de Azcarraga, J. M. Izquierdo and J. Lukierski, *BPS states in M-theory and twistorial constituents*, Phys. Rev. Lett. **86**, 4451 (2001) [hep-th/0101113].
- [77] J. P. Gauntlett and S. Pakis, *The geometry of $D = 11$ Killing spinors*, JHEP **0304**, 039 (2003) [hep-th/0212008].
- [78] J. P. Gauntlett, J. B. Gutowski and S. Pakis, *The geometry of $D = 11$ null Killing spinors*, JHEP **0312** (2003) 049. [hep-th/0311112].
- [79] J. P. Gauntlett, D. Martelli, J. Sparks and D. Waldram, *Supersymmetric $AdS(5)$ solutions of M-theory*, arXiv:hep-th/0402153.
- [80] J. P. Gauntlett, D. Martelli, S. Pakis and D. Waldram, *G-structures and wrapped NS5-branes*, Commun. Math. Phys. **247** (2004) 421. [arXiv:hep-th/0205050].
- [81] D. Martelli and J. Sparks, *G-structures, fluxes and calibrations in M-theory*, Phys. Rev. D **68**, 085014 (2003) [arXiv:hep-th/0306225].
- [82] M. J. Duff, H. Lu and C. N. Pope, *Supersymmetry without supersymmetry*, Phys. Lett. B **409**, 136 (1997) [hep-th/9704186].
- [83] M. J. Duff, H. Lu and C. N. Pope, *$AdS_5 \times S^5$ untwisted*, Nucl. Phys. B **532**, 181 (1998) [hep-th/9803061].
- [84] M. J. Duff, *Ultraviolet divergences in extended supergravity*, in Proceedings of the 1981 Trieste Conference “Supergravity 81”, eds. Ferrara and Taylor, C. U. P. 1982.
- [85] M. Gunaydin, *Singleton and doubleton supermultiplets of space-time supergroups and infinite spin superalgebras*, in Proceedings of the 1989 Trieste Conference “Supermembranes and Physics in 2 + 1 Dimensions”, eds Duff, Pope and Sezgin, World Scientific 1990.
- [86] E. Sezgin, *The spectrum of the eleven dimensional supergravity compactified on the round seven sphere*, Trieste preprint, 1983, in Supergravity in Diverse Dimensions, vol. 2, 1367, (eds A. Salam and E. Sezgin World Scientific, 1989); Fortschr. Phys. **34** (1986) 217.

- [87] M. J. Duff, *TASI lectures on branes, black holes and anti-de Sitter space*, hep-th/9912164.
- [88] O. Aharony, S. S. Gubser, J. M. Maldacena, H. Ooguri and Y. Oz, *Large N field theories, string theory and gravity*, *Phys. Rept.* **323**, 183 (2000), [arXiv:hep-th/9905111].
- [89] J. Maldacena, *TASI lectures on AdS/CFT*, hep-th/0309246.
- [90] P. van Nieuwenhuizen and N. Warner, *Integrability conditions for Killing spinors*, *Commun. Math. Phys.* **93** (1984) 277.
- [91] M. J. Duff, B. E. W. Nilsson and C. N. Pope, *Spontaneous supersymmetry breaking by the squashed seven-sphere*, *Phys. Rev. Lett.* **50** (1983) 2043.
- [92] M. A. Awada, M. J. Duff and C. N. Pope, *$N = 8$ supergravity breaks down to $N = 1$* , *Phys. Rev. Lett.* **50** (1983) 294.
- [93] L. Castellani, R. D'Auria, P. Fre and P. van Nieuwenhuizen, *Holonomy groups, sesquidual torsion fields and $SU(8)$ in $d = 11$ supergravity*, *J. Math. Phys.* **25** (1984) 3209.
- [94] H. Lu, C. N. Pope, K. S. Stelle and P. K. Townsend, *Supersymmetric deformations of G_2 manifolds from higher-order corrections to string and M-theory*, hep-th/0312002.
- [95] M. P. Blencowe and M. J. Duff, *Supermembranes and the signature of space-time*, *Nucl. Phys. B* **310** (1988) 387.
- [96] C. M. Hull, *Duality and the signature of space-time*, *JHEP* **9811**(1998) 017, hep-th/9807127.
- [97] M. J. Duff and K. Stelle, *Multimembrane solutions of $d = 11$ supergravity*, *Phys. Lett. B* **253** (1991) 113.
- [98] M. J. Duff and J. X. Lu, *Duality Rotations In Membrane Theory*, *Nucl. Phys. B* **347**, 394 (1990).
- [99] C. M. Hull and P. K. Townsend, *Unity of superstring dualities*, *Nucl. Phys. B* **438**, 109 (1995) [arXiv:hep-th/9410167].

- [100] P. West, *The IIA, IIB and eleven dimensional theories and their common E(11) origin*, hep-th/0402140.
- [101] A. Batrachenko and W. Y. Wen, *Generalized holonomy of supergravities with 8 real supercharges*, hep-th/0402141.

CHAIRMAN: M. J. DUFF

Scientific Secretaries: S. Kuperstein, I. Papadimitriou

DISCUSSION I

- *Gripaios:*

You mentioned that by compactifying 11d SUGRA on S^1 , one obtains Type IIA SUGRA in 10d, suggesting that Type IIA strings come from M-theory. How do I obtain other limits, e.g. Type IIB, Type I etc?

- *Duff:*

Type IIA compactified on a circle of radius R is equivalent to Type IIB compactified on a circle of radius $1/R$. So M-theory on a two-dimensional torus yields Type IIB on shrinking the area of the torus to zero. Now what about the heterotic side? This side is in a certain sense more interesting, because you may recall I quoted a theorem of Witten that if you start with $D=11$ supergravity and you compactify it on a smooth manifold, you will never get a $D=4$ theory that is chiral. So having put the final nail in the coffin, it was ironic that Witten was to pull it out again by showing that if you compactify on something which is not a manifold, such as this singular space S^1/Z_2 , which is fact the real line, you get the $E_8 \times E_8$ string. This is work of Horava and Witten, actually. If you put M-theory on a real line, the manifold consists of an 11d bulk with two 10d boundaries, and the 11th dimension is the distance between these two boundaries. Remarkably, they were able to demonstrate that what we usually think of as the $E_8 \times E_8$ string is the $R \rightarrow 0$ limit of this M-theory configuration: one E_8 lives on one boundary and the other E_8 on the other. (Incidentally, this is the prototype of the parallel universe braneworld idea that we live on one brane and there is a hidden sector living on the other brane. There have been many variations on this theme lately. One possibility is that dark matter lives on one brane and since we communicate only gravitationally between the branes, we do not see it, but we feel it.) So that is the $E_8 \times E_8$ scenario and the wonderful thing, of course, is that the $E_8 \times E_8$ string is chiral, so that the no-go theorem is circumvented and the 11d starting point is now a good one. So just as the Type IIA and Type IIB strings are known to be related by T-duality, so the $E_8 \times E_8$ and the $SO(32)$ heterotic strings are also related by T-duality. So if you go down to nine dimensions and up again on a circle of radius $1/R$, you get the $SO(32)$ string. Now the one that is missing from this picture is the Type I string whose gauge group is also $SO(32)$. It is an open string which makes it different from all others, but it is related is by what is called S-duality. This $SO(32)$ string has a coupling constant that tells you how strongly the strings interact at the vertex. And it turns out that the strong coupling limit of the heterotic $SO(32)$ string is the weak coupling limit of Type I $SO(32)$ string.

So in this way we have managed to link together all the five consistent superstring theories by giving them this 11d origin. Witten also told us how to relate the coupling constant to the radius of the extra dimension: the bigger the radius, the bigger the coupling constant. The illusion that we are living in 10d just came about from the weak coupling limit of string theory. In the perturbative string theory, this eleventh dimension was small and that is why we did not see it. It is only when we go to the strong coupling regime of the string theory that this eleventh dimension opens up. Incidentally, Witten also made an interesting observation in connection with this eleventh dimension to do with the coupling constant. We know that in the supersymmetric Standard Model, strong, electromagnetic and weak couplings converge at some 10^{16} GeV. However, if we look at the gravitational dimensionless constant, which is Newton's constant times energy squared, it almost meets the other three, but not quite. This makes you wonder if there is some sort of connection. Witten pointed it out that when this eleventh dimension kicks in, it changes the running of the gravitational constant at around 10^{15} GeV and you can tune the radius so that it actually meets the other three. So then all the four forces come together at a common scale. The interesting thing is that it is much lower than the traditional Planck scale, 10^{19} GeV: it is more like the GUT scale.

So if this picture was correct (this is just one picture of course) then the quantum gravity effects are much closer than we previously thought. There have even been more extreme versions of this scenario.

- *Gripaios:*

Do you have any idea what any of the other compactifications of eleven dimensions might correspond to at the membrane level?

- *Duff:*

This opens up a whole can of worms. For example, one of the earliest compactifications of eleven dimensions that were studied after the 7-torus was the seven-dimensional sphere. The theory admits a solution in which the spacetime is a four-dimensional anti-de Sitter space and the extra seven dimensions are a sphere, and this configuration has recently featured in the AdS/CFT correspondence. According to Maldacena, supergravity on anti-de Sitter spacetime is dual to a conformal field theory that lives in a spacetime of dimension one, less what resides on the boundary of that spacetime. In fact that is an example of what is called "holography", namely that you can encode the information of a gravitational theory in D dimensions via a non-gravitational theory in D-1 dimensions. So, there is an example where a compactification of M-theory has some interesting consequences. Now there are many variations on that: you can take a squashed 7-sphere, which interestingly enough has G_2 holonomy giving $N=1$ supersymmetry in four dimensions, and one supersymmetry is what we need to do phenomenology. Now, if you just do the supergravity on the squashed 7-sphere, the resulting theory is not very realistic (it is a vector-like theory) but just recently, by promoting the theory to M-theory, you can

imagine compactifying on singular manifolds of G2 holonomy and that way you can get four-dimensional theories with $N=1$ supersymmetry, realistic gauge groups and chiral fermions, so that is a whole industry by itself. Another example is Type IIA string compactified on a K3 manifold which has SU(2) holonomy, and so you get half as much supersymmetry as you would if you compactified it on a 4-torus. That gives you an $N=2$ theory in six dimensions, and if you compactify the heterotic string on a 4-torus, you also get an $N=2$ theory in six dimensions and the remarkable thing is that these are actually the same theory; the heterotic string on a 4-torus is dual to the Type IIA string on a K3 manifold. And there are many more examples of theories compactified on manifolds which can be dual to apparently very different looking theories. The heterotic string compactified on a six-dimensional circle has an $SL(2, \mathbb{Z})$ symmetry which acts as an electromagnetic or strong-weak coupling duality, so that is an example of a theory which is self-dual. There is a whole lot of dualities that relate theory A on manifold X to theory B on manifold Y. If they have the same supersymmetries and the same bosonic symmetries you might expect that these theories have the same physics and this is often what happens.

- *Skinner:*

Could you explain the difference between gravity-mediated SUSY breaking and bulk-mediated SUSY breaking? Is one just a geometrical picture of the other?

- *Duff:*

Let us go back to SUSY breaking. The simplest version does not involve branes at all, it only involves two sectors of the theory that communicate with each other only gravitationally (or in some other weak way) and you imagine that supersymmetry is broken in the hidden sector typically by some non-perturbative effect like gaugino condensation and then that gets fed back into the visible sector on a much smaller scale. Now the bulk mediation is similar in spirit to that: there is a hidden sector and an observable sector, but it is more in the Horava-Witten scenario where the hidden sector lives on one brane and the observable sector on the other brane. So the overall effect might be similar but the underlying mechanism is quite different.

- *Skinner:*

But if you are at energy below the resolution of the orbifold, you cannot tell the difference, is that true?

- *Duff:*

Yes. The people who look at the low-energy globally supersymmetric Lagrangian with soft supersymmetry breaking terms, that could represent either one of the different scenarios, would not be able to tell the difference very easily.

- *Bozza:*

Is there any theory that predicts the existence of “structures” in the bulk that could eventually show up in the visible sector?

- *Duff:*

Yes, there are many variations on this brane-world. In some of them, the Standard Model fields live on the brane and only gravity lives in the bulk. But there are also variations of that where matter can also live in the bulk and get trapped on the brane and have some effect on the visible sector.

- *Durin:*

1. Why is $d=11$ the highest dimension where supersymmetry is possible?
2. In supersymmetric theories branes are D-branes. How do branes appear in M-theory as we have only 11-dimensional low energy SUGRA?

- *Duff:*

To answer the first question, why eleven is the maximal dimension, there are two arguments. The first one is the field theory argument. Let us assume (as is generally believed, but not proved) that there are no consistent quantum field theories with massless particles whose spin is greater than two. So if we have spin less than or equal to two and we have supersymmetry relating helicities of one half unit, then we have $-2, -3/2, -1, 0, 1/2, 1, 3/2, 2$ and if you count the number of steps it should be eight in $D=4$, so $N_{\text{max}}=8$. In four dimensions, the supersymmetry parameter is a four-component spinor, so the maximal number spinor components is 32. We can translate this statement to higher dimension by asking what is the maximal space-time dimension with a 32-component spinor. From the properties of Clifford algebra, it is 11 (at least in the usual signature, one time ten space, then eleven is the maximum, because in $D=12$ the minimum number of spinor components is 64, which is too many). So at least in space-times with the usual signature, eleven is the bound. If you instead imagine a world with two time-like dimensions, the argument changes and you can tolerate up to twelve dimensions and still only have a 32 component spinor, because in twelve dimensions with that particular signature, $s-t$ is eight and that means that you can have a spinor that is both Majorana and Weyl, so it reduces the number of components. This is a tantalizing observation, but so far I think it has never really taken off. I do not really have a good answer whether this is significant or not.)

Another way of understanding the $D=11$ limit is a "braney" one. Remember we required that on the world-volume of the brane, the number of bosonic degrees of freedom, which is the space-time dimension minus the brane dimension, must equal the number of fermions, which is given by $MN/4$, where M is the dimension of the minimal spinor and N is the number of supersymmetries. And once again you see that the maximum spacetime dimension in which this equation has a solution is 11. It corresponds to $M=32$, $N=1$, so it describes a three-dimensional membrane world-volume with 8+8 propagating degrees of freedom. So that is another reason why we believe 11 is the maximum.

As for your second question, let us talk about D-branes. They were introduced by Polchinski as surfaces of dimension p where open strings can end and they also carry the so-called Ramond-Ramond charge. In fact, we have already been dealing with

these branes, before we called them D-branes. In ordinary four-dimensional electromagnetism, we are used to the idea that a charged-point particle couples to a vector potential, the Maxwell potential. This generalizes to higher dimensional objects in higher spacetime dimensions. A p-branes couples to a p+1 form, so a string couples to a rank 2 tensor, a membrane couples to a rank 3 tensor. (Incidentally, remember that the tensor that appears in 11d supergravity is of rank 3, which is another hint that 11d SUGRA is related to membranes.) So this potential has a field strength F which is a p+2 form, and then in D spacetime dimensions it has a magnetic dual, \tilde{F} , which is a D-p-2 form. So, a brane can carry two types of charge, an electric charge and a magnetic charge and, just as for magnetic monopoles in four dimensions, there is a Dirac quantization condition. Of particular interest are the BPS branes whose tension is equal to the charge, and all the supersymmetric branes that I showed you on the "brane-scan" are BPS; the converse is not true, however, you can have BPS branes that are not supersymmetric. So let us look at some examples. In the ten-dimensional Heterotic string, there is a two form which has a three form field strength and so its dual is a seven form and that corresponds to a six form potential and a six form potential couples to a five brane. So the natural magnetic dual of the Heterotic string is the Heterotic five brane. But notice it has the interpretation of a soliton, you start with the elementary string and the electric excitation is the string itself, and then you discover in the spectrum there is also a five brane, which is the magnetic solitonic quantity. Now the Type IIA and Type IIB strings and their supergravities have a whole wealth of p-forms. In Type IIA you have the even p-forms, in Type IIB you have the odd ones, so there is a variety of different branes that show up in Type II. In 11 dimensions, the dual of a two brane is also a five brane. So in fact that brane scan I showed you is only part of the story; there is a richer spectrum of objects. In addition to all the elementary branes, there are also the solitonic branes. Why didn't we see these solitonic objects from our previous argument? Well, the argument that led to the elementary branes was a superspace argument, that is we assumed that there were only scalar supermultiplets living on the branes. However, it turns out that these solitonic branes have higher spin fields on their world volume, such as vector supermultiplets and antisymmetric tensor supermultiplets. So the Type II solitonic branes which exist in 10 dimensions, as it turns out, correspond to what Polchinski called Dirichlet branes.

In 11 dimensions, in addition to the elementary membrane, there is a solitonic five brane. Its world volume fields include an antisymmetric tensor two form whose field strength is self-dual, and so it is a chiral theory, which is rather unusual. You start from 11d theory and it admits as a solution a chiral brane. Now, being chiral is potentially anomalous. In fact if you look at the fields living on the brane, they appear to lead to a gravitational anomaly, but the whole theory must be anomaly-free. What happens is that there is a trade-off between the fields in the bulk and the fields on the brane, and you get an anomaly-free theory but at the price of making additions to the

11d supergravity theory. There are terms which you did not know were there before, which are intrinsically M-theoretic terms.

- *'t Hooft:*

You said that if two theories are mathematically equivalent, they also share the same physics, but in a physical world you might expect one particular value say of radius R . So if you map that to $1/R$, I would say this is a different physical theory. And of course it gets much worse if you consider those Calabi-Yau spaces. So, is it not more fair to say that there are billions of physically distinct theories in nature, not just one?

- *Duff:*

Let us take the simple case of $1/R$. What we are saying is that R is not an observable. Because, given a spectrum of states with certain quantum numbers, we cannot tell by looking at this spectrum if it comes from a Type IIA string on a circle of radius R or a Type IIB string on a circle of radius $1/R$. They are the same. So it is not meaningful to say "big R " or "small R ". As an interesting consequence, if you think of the Big Crunch with the universe shrinking below the Planck scale, we imagine that all sorts of weird things happen. But if there is a kind of duality that I just described, it could be that a shrinking universe is operationally indistinguishable from an expanding one. Similar remarks apply to more complicated cases like Calabi-Yau spaces. There is work by Green and Strominger and other people who showed that a large class of Calabi-Yau manifolds that were classically topologically inequivalent, in M-theory can be continuously connected. The way it happens is that these Calabi-Yau manifolds have holes like some higher dimensional Swiss cheese. The various dimensional branes can wrap around these holes with the four-dimensional interpretation of black holes, in fact. And as the size of this brane shrinks to zero, the mass of the black hole goes to zero and this massless state changes the quantum theory. You discover that what you thought were disconnected Calabi-Yau manifolds with different Hodge numbers and so on are actually smoothly connected to one another. So we have traded one problem for another one. Instead of asking what topology do we live in, we are left with the question of which corner of this supertopology do we occupy. We do not have an answer to this question, but it may have a dynamical solution.

- *'t Hooft:*

But could it be dynamically determined in which of these corners we are going to sit eventually?

- *Duff:*

Yes. Ideally, which corner we are in will tell us the masses of quarks, the mixing angles and all the rest of the parameters. But at the moment we have no way of discriminating between all these solutions. This is the reason why string theory has not been able to make any concrete experimental predictions. It is frequently thought

that the inability of string theory or M-theory to make concrete experimental predictions has something to do with the fact that it is formulated at the Planck scale, or that it has extra dimensions. Neither of those reasons is an obstacle. The real obstacle is this vacuum degeneracy. My own thinking is that doing string phenomenology is rather premature until we have resolved these theoretical issues about what the right vacuum is.

- *D'Enterria:*

You mentioned that supergravity can provide hints on strongly coupled theories like QCD. Can M-theory explain or at least address the problem of confinement, namely the fact that quarks and gluons do not appear as free states in nature?

- *Duff:*

It can explain confinement in these supersymmetric gauge theories, which is not the real QCD. So, as far as I know, no one has explained real confinement from M-theory. But in these toy theories of supersymmetric gauge theories, Seiberg and Witten have proved quark confinement.

- *Casalderrea-Solana:*

If no supersymmetric partners are ever found, what are the consequences for theories with extended objects? In other words, is it possible to construct theories with extended objects and fermions but without supersymmetry?

- *Duff:*

I do not have an existing proof that you can never do it, but so far no one has succeeded in constructing a consistent, anomaly-free theory without supersymmetry. Supersymmetry has all those wonderful properties that save us from a potentially inconsistent theory. So, to answer your question, I would say it is the supersymmetry which is the underlying reason. But it is rather risky for me to say that there is no other theory that could do it.

- *Bei:*

I would like to know whether it is reasonable to assume that local supersymmetry coupled to gravity should preserve the CPT theorem, or better said, is it not natural to assume that the action of gravity might cause local violation of the CPT theorem?

- *Duff:*

I believe I am right in saying that the Wightman proof of the CPT does not go through in curved spacetimes. So you have to look at the whole question afresh. There have been some papers looking at stringy configurations that might violate CPT. I do not know how reliable those theories are, but certainly the possibility of CPT violation has been entertained, because there is no theorem forbidding it.

- *Rotaev:*

There are two ways to quantize strings: the path integral way and the operator formalism. The troubles of quantization of high dimensional objects (branes) are manifested when we try to use the path integral way. What kind of problems exist in operator formalism in dealing with high dimensional objects (branes)?

- *Duff:*

In the path integral formalism of strings, the loop expansion is an expansion in the number of holes in the Riemann surface, in Euclidean worldsheet signature. That is a well-defined perturbation expansion. As you point out, it is to be hoped that this is not the right thing to do for branes, because there are mathematical theorems telling us that we can never classify all three dimensional topologies, so summing over them would be rather difficult. But it is not clear that this is the right thing to do anyway, because there is no connection as far as we know between summing over membrane topologies and perturbation theory. Of all the extended objects, strings are unique in admitting a perturbation expansion. The branes are somehow intrinsically non-perturbative objects.

When you come to the operator formalism, a similar problem arises. We can go to a gauge on the string worldsheet where the equations of motion are free, but there is no such gauge for higher-dimensional objects that renders the equations free equations. They are intrinsically non-linear. So we have to find cleverer ways of extracting information. At the moment we proceed via conjecture and refutation. You make some non-perturbative conjecture which you cannot actually prove, but then you do a series of consistency checks in order to try and disprove it. What we have found after eight years of M-theory is that everything turns out to be consistent.

CHAIRMAN: M. J. DUFF

Scientific Secretaries: M. Rotaev and D. Skinner.

DISCUSSION II

- *Gripaios:*

You told us that the main problem in using string theory to make physical predictions was the vacuum degeneracy problem. We now know a lot about Calabi-Yau manifolds, appropriate for string compactifications. How much do we know about the manifolds of G_2 holonomy, which are relevant for M-theory compactifications?

- *Duff:*

The first example of a compactification on a manifold of G_2 holonomy was in 1982 when Awada, Pope and I considered supergravity on a squashed seven sphere, which gave $N=1$ supersymmetry in four dimensions. Unfortunately, Witten proved that if you compactify supergravity on a smooth manifold, the low energy theory cannot contain chiral fermions. However, recent progress in M-theory allows us to compactify on singular manifolds and there are examples of singular manifolds with G_2 holonomy, which have realistic gauge groups and chiral fermions, and Witten is even considering using these to solve the doublet-triplet splitting problem and other phenomenological issues. Interestingly enough, M-theory on certain singular G_2 manifolds is dual to heterotic string theory on certain Calabi-Yau manifolds, which was the original way of obtaining $N=1$ supersymmetry in four dimensions with chiral fermions from theories like the $E_8 \times E_8$ string theory in ten dimensions. So, it turns out that, at least in some cases, these different ways of getting realistic four-dimensional phenomenology are dual to one another.

- *Bulbinot:*

Among the major successes of M-theory, you mentioned the derivation of the Bekenstein-Hawking formula for the entropy of black holes; originally Strominger and Vafa's proof was given for extremal black holes by counting *BPS* states. What is known about more realistic black holes, such as the Schwarzschild one?

- *Duff:*

The short answer is nothing! My understanding is that you can still do calculations for near-extremal black holes, but you cannot go so far from extremality as to reach the Schwarzschild case.

- *Bulbinot:*

Just as a comment, if one evaluates the Hawking entropy numerically for a Schwarzschild black hole, the number you obtain is many orders of magnitude larger than the entropy of, say, the collapsing dust cloud which may have formed the black hole astrophysically. So, for me, the real meaning of the Hawking entropy is still very mysterious.

- *Duff:*

You have touched on another very interesting aspect of black holes, which is that they have no memory of whatever it was that went in to forming them. You can measure only their mass, charge and angular momentum, so there is a puzzle if you consider throwing in a copy of the "Encyclopaedia Britannica", because, according to Hawking, this information cannot then be retrieved. This view is controversial, because it would mean abandoning the usual formulation of quantum mechanics. An alternative view, as advocated by 't Hooft, would be that information is not lost and so the unitarity of quantum mechanics can be preserved. This issue is still being hotly debated!

- *Lysov:*

Could you describe the situation for calculations of higher-loop amplitudes in superstring theory? What is known about two and three loop calculations?

- *Duff:*

I am not sure how many loops have been calculated in string theory now. I am pretty sure that two loops have been done, but not three. In principle we know how to calculate arbitrarily high loops, but, as in quantum field theory, the higher loops you go to, the more difficult the integral you have to do becomes. People get daunted by this eventually.

- *Markov:*

How many scalar fields does string theory predict in four dimensions? What is the typical inflationary potential derived from superstrings?

- *Duff:*

Typical string and M-theory compactifications have dozens of light scalars, and this is in fact a problem because many of these scalars have flat potentials, leading to many undetermined parameters in the low energy theory. The belief is that when we understand the non-perturbative aspects of the theory better, these scalars will acquire non-trivial potentials, for example the dilaton may acquire a potential related to supersymmetry breaking. But this is all in the realm of speculation and there are no generic predictions – one has to examine each compactification case by case. In a recent paper, Linde *et al* claim that you can generate a potential with some parameters that, if you fine-tune these parameters in a rather extreme way, is compatible with slow-roll inflation, but I do not think this arises in any natural way. Until we

understand supersymmetry breaking, it is difficult to say what the scalar potential should be.

- *Kuperstein:*

Is there any progress in understanding the M-theoretic origin of the *D*8-brane in type IIA supergravity?

- *Duff:*

I explained in the lectures how to obtain the string from membranes in eleven dimensions, and you can explain many of the type IIA branes in this way, but one apparent exception is the *D*8-brane. There have been suggestions that there is an M-theory 9-brane, but this idea never really made much progress. An alternative explanation, which I think is correct, is that the 8-brane is not a solution of ordinary type IIA supergravity, but rather of Romans' massive type IIA supergravity, which does not have any direct link to eleven-dimensional supergravity. However, there is some work by Pope *et al.* which shows that if you perform a Scherk-Schwarz compactification of eleven-dimensional supergravity, and an ordinary compactification of Romans' theory, then they coincide in lower dimensions. It is a little like the type IIB theory: in order to see its relation to the eleven-dimensional theory, you have to go "down then up again". So, the existence of the D8-brane and Romans' massive supergravity, although not directly linked to eleven dimensions, does have an indirect connection.

- *Krotov:*

Is there any candidate for the theory of everything except M-theory? In particular, I refer to the quantization method of Berkovits, where he considers the physical fields to be given by the cohomological classes of a certain special operator.

- *Duff:*

Just to give a little background: we can quantize string theory in a non-covariant way, or consider a covariant classical theory, but problems arise when trying to quantize the theory covariantly. In particular, the Ramond-Ramond sector presents certain technical difficulties, and Berkovits spent a lot of time trying to overcome this. I am not sure everyone agrees that he has succeeded, but even if he has, the string theories are only special points in the M-theory parameter space, so his quantization method cannot be the whole story.

- *Krotov:*

What about approaches by people other than Berkovits?

- *Duff:*

The only other well-known method is the loop quantum gravity approach of Ashtekar, which is a very different approach, a little analogous to Polyakov loops in a gauge theory. Unfortunately (or perhaps fortunately!) the loop quantum gravity

people and string theorists do not often talk to one another, so I cannot tell you much about the progress of this approach. However, even if this program succeeds, this is only a theory of gravity, whereas M-theory is much more ambitious because it attempts to describe the other forces as well.

- *Krotov:*

But isn't it true that one of the main attractions of string theory is that it might be a consistent theory of quantum gravity?

- *Duff:*

Yes, and this was one of the main reasons that everyone was so excited by string theory in the 1980's, and this continues to be true.

- *Rotaev:*

In the first lecture, you explained that higher dimensional theories could contain not just strings with a two dimensional world-sheets, but also branes. Could it be that the groups of the known string theories, such as E_8 , are specific to strings, and that theories with branes could contain many other gauge groups?

- *Duff:*

To avoid confusion, the group E_8 occurred in two different ways during my lectures. Firstly, the requirement of anomaly freedom fixes the gauge group of one of the ten-dimensional string theories to be $E_8 \times E_8$, and these E_8 's are compact. An entirely different place where E_8 occurred was as a hidden global symmetry of eleven-dimensional supergravity, first identified by Cremmer and Julia, at least in the dimensionally reduced equations. This E_8 is non-compact, and as far as we know, it is unrelated to the previous E_8 gauge group. Hull and Townsend have provided powerful evidence that a discrete version of this non-compact E_8 (where the elements are restricted to the integers) is a symmetry of the full M-theory, provided you compactify it on a torus. In this case, the discrete E_8 becomes the U -duality group of the theory, where U -duality is a transformation which combines the strong-weak S -duality of electromagnetism with the large-small radius T -duality. So this E_8 certainly seems to be connected to eleven-dimensional supergravity and M-theory, whereas the other E_8 as a gauge group was specific to a particular string theory. As far as I know, there is no connection between the two.

- *Cerri:*

You mentioned substantial problems, such as vacuum selection, that need to be overcome before we can make string theory predictive, in the sense that an experimentalist would be able to return to the laboratory and systematically check them. How far do you think we are from this?

- *Duff:*

I wish I could say that we have made much progress on this front, but unfortunately this is not true, so I do not really know the answer to your question. Of course, people do not just give up at this point, but instead try to imagine what the theory should have to look like if we were clever enough to solve it. For example, you make the plausible assumptions that we should only concentrate on compactifications down to four dimensions, and then only those compactifications that include $SU(3)$, $SU(2)$, $U(1)$ with three generations and dilaton that acquires a potential of the right form to break supersymmetry. Once you have made assumptions like these, you start to make contact with the “bottom up” approach of globally supersymmetric theories with soft breaking terms. The only trouble, of course, is that if it does not work, you cannot tell if it is the theory that is wrong, or just one of your assumptions. While this is the best we can do, it is certainly worth trying, but it seems to me to be a very difficult problem and I would not like to suggest a timescale in which it will be finished.

However, I would like to make a comment about how worried we should be that string theory does not yet make any testable predictions. At present, experimentalists are searching for extra dimensions, which were proposed in the 1920’s, the Higgs boson, which was put forward in the 1960’s, and supersymmetry, which was proposed in the 1970’s, while cosmologists are searching for inflation, which was suggested in the 1980’s. Even if these ideas work out, there is a large delay between the theory and its experimental confirmation. M-theory purports to be a Theory of Everything, and so is more ambitious than any of these ideas, so I do not expect the timescale to be any shorter. We should just be patient!

- *Bei:*

I did not understand how we might approach the issue of vacuum degeneracy. Could you explain this a little further? How much might it depend on the property of having a spacelike action?

- *Duff:*

I have discussed the vacuum degeneracy problem a few minutes ago, and I think the basic answer is that nobody knows the solution: it is one of the most important unsolved problems in string theory.

- *Sykora:*

What are the restrictions on the number of timelike dimensions? How would the theory be changed in the case of more timelike dimensions? Can M-theory give us an answer to the question of the origin of the time?

- *Duff:*

The issue of why our world should have only one timelike dimension is very interesting. Supersymmetry restricts the number of timelike dimensions, but it does not say there can be only one, for example, in eleven dimensions you can have (10,1)

or (9,2) or (6,5) etc. Obviously, one can then ask if these choices are simply mathematical curiosities, or have some physical significance. Hull points out that if you are willing to consider compactified timelike dimensions, there is a T -duality which relates this to a theory of different signature. This idea is interesting because it is radical in forcing you to think about theories with more than one time dimension, but at the same time conservative because it restricts you to those theories which are dual to familiar ones with only one time dimension. If true, this would remove the question of which one does nature pick – they are all right! An objection to his idea is that it introduces closed timelike curves, so a particle would be able to travel into its own past. However, there are many recent papers which are concerned with the so-called “Chronology Protection Conjecture” which discusses whether these closed timelike curves are really problematic. This area is still very uncertain, but if correct, it would evade the question of which signature did nature pick. I do not know whether this will give us a deeper understanding of the nature of time.

- *'t Hooft:*

A question I have also asked to other advocates of M-theory: suppose you were given a computer with unlimited power and speed. Would you, in principle, be able to program it to simulate M-theory as is done for example with lattice gauge theories?

- *Duff:*

There are still very fundamental problems that obstruct this. In particular, we do not yet understand what exactly the degrees of freedom are – strings, branes or matrices for example. Therefore, it is more than just a technical issue about solving difficult equations: we do not yet know what the equations are.

- *Korthals Altes:*

You discussed S -duality as a map from weak to strong coupling. This is a known mapping in certain field theories, and is there accompanied by a mapping of the group into its dual, for example $U(1)$ into Z , the group of integers. How does this work with the groups in S -dual string theories?

- *Duff:*

It depends on whether you have exact or effective dualities. The canonical example of a theory with exact S -duality is $N=4$ SYM theory. This theory is self-dual: the electric and magnetic charges are mapped onto each other, while g^2 goes to $1/g^2$. For theories with less supersymmetry, such as $N=2$ Seiberg-Witten theory, or $N=1$ SYM as studied by Seiberg, the duality is only effective and the mapping can be very complicated. For example, the two duality-related theories may contain different gauge groups with different fermionic representations. These have to be studied case by case.

SUPERSYMMETRY IN NUCLEI

FRANCESCO IACHELLO

*Center for Theoretical Physics, Sloane Physics Laboratory,
Yale University, New Haven, CT 06520-8120*

The concept of spectrum generating superalgebras and associated dynamic supersymmetries is introduced and placed within the general context of symmetry in physics. The discovery of dynamic supersymmetry in nuclei and its recent confirmation in ^{196}Au is presented.

1. Introduction

In the last 40 years the concept of spectrum generating algebras and dynamic symmetries has been extensively used to study physical systems. In the late 1970's this concept was enlarged to spectrum generating superalgebras and associated supersymmetries. In this lecture, dynamic symmetries are first placed within the context of symmetries in physics and applications to the structure of atomic nuclei are reviewed (Sects.2 and 3). Subsequently, the concept of dynamic supersymmetries is introduced and placed within the context of supersymmetry in physics (Sect.4). Applications to the study of spectra of nuclei are reviewed. The discovery of supersymmetry in nuclei and its recent confirmation is presented (Sect.5).

2. Symmetries

Symmetry is a wide-reaching concept used in a variety of ways.

2.1. Geometric symmetries

These symmetries are the first to be used in physics. They describe the arrangement of constituent particles into a structure. An example of symmetries of this type is the arrangement of atoms in a molecule. The mathematical framework needed to describe these symmetries is finite groups, sometimes called point groups. In Fig.1, the molecule C_{60} is shown as an example. The symmetry of this molecule is I_h . Geometric symmetries are used to reduce the complexity of the equations describing the system through the construction of a symmetry adapted basis. The Hamiltonian matrix in this basis is block diagonal.

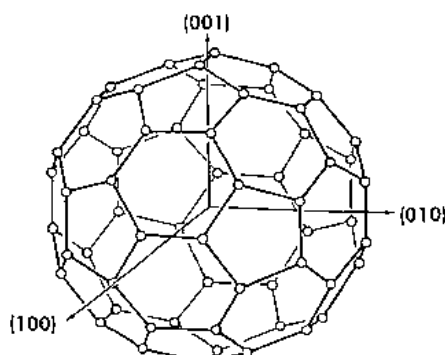


Figure 1. The fullerene molecule C_{60} is shown as an example of geometric symmetry, I_h .

2.2. Space-time symmetries

These symmetries fix the form of the equations governing the motion of the constituent particles. An example is provided by Lorentz invariance that fixes the form of the Dirac equation to be

$$(i\gamma^\mu \partial_\mu - m)\psi(x) = 0. \quad (1)$$

The mathematical framework needed to describe these symmetries is continuous groups, in particular Lie groups, here the Lorentz group $SO(3,1)$.

2.3. Gauge symmetries

These symmetries fix the form of the interaction between constituent particles and/or with external fields. An example is provided by the QCD Lagrangian

$$\begin{aligned} \mathcal{L} &= \frac{1}{4} G_{\mu\nu}^i G_{\mu\nu}^i - \bar{\psi}^a (\gamma_\mu D_\mu + m_a) \psi^a \\ G_{\mu\nu}^i &= \partial_\mu A_{\nu}^i - \partial_\nu A_{\mu}^i + g [A_\mu, A_\nu]_i^j \\ D_\mu \psi_i^a &= \partial_\mu \psi_i^a + g A_{\mu}^j \psi_j^a. \end{aligned} \quad (2)$$

Also here the mathematical framework is Lie groups, in QCD $SU_c(3)$. In view of the fact that the strong and weak forces appear to be guided by gauge principles, gauge symmetries have become in recent years, one of the most important tools in physics.

2.4. Dynamic symmetries

These symmetries fix the interaction between constituent particles and/or external fields (hence the name dynamic). They determine the spectral properties of quantum systems (patterns of energy levels). They are described by Lie groups.

The earliest example of this type of symmetry is provided by the non-relativistic hydrogen atom. The Hamiltonian of this system can be written in terms of the quadratic Casimir operator C_2 of $SO(4)$ as¹

$$\begin{aligned} H &= \frac{p^2}{2m} - \frac{e^2}{r} \\ &= -\frac{A}{C_2(SO(4)) + 1}, \end{aligned} \quad (3)$$

where A is a constant that depends on m and e . As a result, the energy eigenvalues can be written down explicitly in terms of quantum numbers

$$E(n, \ell, m) = -\frac{A}{n^2} \quad (4)$$

providing a straightforward description of the spectrum, Fig.2.

Another example is provided by hadrons. These can be classified in terms of a flavor $SU_f(3)$ symmetry^{2,3}. The mass operator for hadrons can be written in terms of the Casimir operators of isospin, $SU(2)$, and hypercharge, $U(1)$, as

$$M = a + b [C_1(U(1))] + c \left[C_2(SU(2)) - \frac{1}{4} C_1^2(U(1)) \right] \quad (5)$$

leading to the mass formula⁴

$$M(Y, I, I_3) = a + bY + c[I(I+1) - \frac{1}{4} Y^2]. \quad (6)$$

This mass formula provides a very realistic description of hadron spectra, Fig.3.

The concept of dynamic symmetry was introduced implicitly by Pauli in the above mentioned paper¹, expanded by Fock⁵, and, reintroduced in explicit form, by Dothan, Gell-Mann and Ne'emann⁶ and Barut

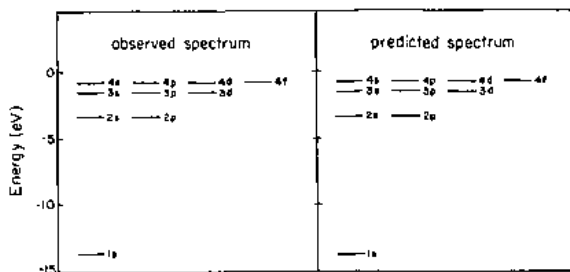


Figure 2. The spectrum of the non-relativistic hydrogen atom is shown as an example of dynamic symmetry of the Schrödinger equation, $SO(4)$.

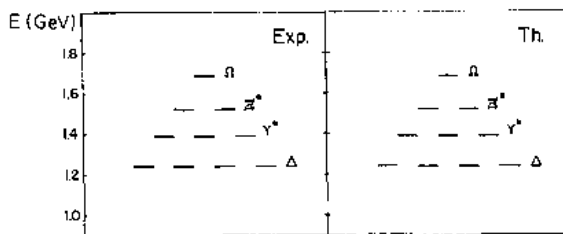


Figure 3. The spectrum of the baryon decuplet is shown as an example of dynamic symmetry of the mass operator, $SU_f(3)$.

and Böhm⁷. It has been used extensively in the last 25 years and has produced many important discoveries. A mathematical definition is given in⁸.

A dynamic symmetry is that situation in which:

(i) The Hamiltonian H is written in terms of elements, G_α , of an algebra G , called spectrum generating algebra (SGA), $G_\alpha \in G$.

(ii) H contains only invariant (Casimir) operators, C_i , of a chain of algebras $G \supset G' \supset G'' \supset \dots$

$$H = f(C_i). \quad (7)$$

When a dynamic symmetry occurs, all observables can be written in explicit analytic form. For example, the energy levels are

$$E = \langle H \rangle = \alpha_1 \langle C_1 \rangle + \alpha_2 \langle C_2 \rangle + \dots \quad (8)$$

One of the best studied cases is that of atomic nuclei, to be described in the following section.

3. Dynamic symmetries of the Interacting Boson Model

Atomic nuclei with an even number of nucleons can be described as a collection of correlated pairs with angular momentum $J = 0$ and $J = 2$. When the pairs are highly correlated they can be treated as bosons, called s and d . The corresponding model description is called Interacting Boson Model⁹. The spectrum generating algebra (SGA) of the Interacting Boson Model can be easily constructed by introducing six boson operators

$$b_\alpha (\alpha = 1, \dots, 6) \equiv s, d_\mu (\mu = 0, \pm 1, \pm 2) \quad (9)$$

which span a six-dimensional space. The corresponding algebraic structure is that of $U(6)$. The elements of $U(6)$ can be written as bilinear products of creation and annihilation operators

$$G_{\alpha\beta} = b_\alpha^\dagger b_\beta \quad (\alpha, \beta = 1, \dots, 6). \quad (10)$$

Since we are dealing with a system of bosons, the basis \mathcal{B} is the totally symmetric irreducible representation of $U(6)$ with Young tableau

$$[N] \equiv \square \square \dots \square \quad (11)$$

where N is the total number of bosons (pairs).

The model Hamiltonian and other operators are written in terms of creation and annihilation operators

$$H = E_0 + \sum_{\alpha\beta} \varepsilon_{\alpha\beta} b_\alpha^\dagger b_\beta + \sum_{\alpha\alpha'\beta\beta'} v_{\alpha\alpha'\beta\beta'} b_\alpha^\dagger b_\alpha' b_\beta b_{\beta'}, \quad (12)$$

It can be rewritten in terms of elements of $U(6)$ as

$$H = E_0 + \sum_{\alpha\beta} \varepsilon'_{\alpha\beta} G_{\alpha\beta} + \sum_{\alpha\alpha'\beta\beta'} v_{\alpha\alpha'\beta\beta'} G_{\alpha\beta} G_{\alpha'\beta'}, \quad (13)$$

The fact that $U(6)$ is the SGA of this problem becomes then obvious.

The dynamic symmetries of the Interacting Boson Model can be constructed by considering all possible breakings of $U(6)$.

There are three and only three dynamic symmetries that include the angular momentum algebra $SO(3)$ as a subalgebra, corresponding to the breakings:

$$\begin{aligned} U(6) &\supset U(5) \supset O(5) \supset O(3) \supset O(2) \quad (I), \\ U(6) &\supset SU(3) \supset O(3) \supset O(2) \quad (II), \\ U(6) &\supset O(6) \supset O(5) \supset O(3) \supset O(2) \quad (III). \end{aligned} \quad (14)$$

When a dynamic symmetry occurs, all properties can be calculated in explicit analytic form. In particular, the energies of the states are given in terms of quantum numbers by ^{10,11,12}

$$\begin{aligned} E^{(I)}(N, n_d, v, n_\Delta, L, M_L) &= E_0 + \varepsilon n_d + \alpha n_d(n_d + 4) + \beta v(v + 3) + \gamma L(L + 1) \\ E^{(II)}(N, \lambda, \mu, K, L, M_L) &= E_0 + \kappa(\lambda^2 + \mu^2 + \lambda\mu + 3\lambda + 3\mu) + \kappa'L(L + 1) \\ E^{(III)}(N, \sigma, \tau, \nu_\Delta, L, M_L) &= E_0 + A\sigma(\sigma + 4) + B\tau(\tau + 3) + CL(L + 1) \end{aligned} \quad (15)$$

where the various terms are the eigenvalues of the Casimir operators in the appropriate irreducible representations.

Several examples of dynamic symmetries in nuclei have been found. Three of these examples are shown in Figs. 4, 5, 6. In the last 25 years, the symmetries of the Interacting Boson Model have provided a classification of spectra of even-even nuclei.

4. Supersymmetry

In the 1970's a new concept, supersymmetry, was introduced in physics, originally for applications to particle physics. This concept was implicitly introduced by Miyazawa ¹³. Later Ramond ¹⁴ and Neveu and Schwartz ¹⁵ introduced it within the context of dual models. The concept became very popular after the work of Volkov and Akulov ¹⁶ and, especially, Wess and Zumino ¹⁷. Supersymmetry, a symmetry that involve bosons and fermions, has become in the last 20 years one of the most important concepts in physics and has today wide reaching applications.

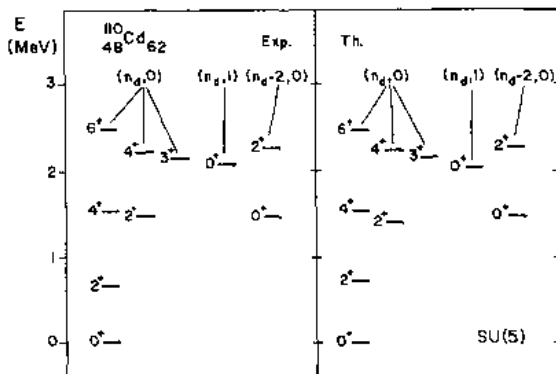


Figure 4. An example of $U(5)$ dynamic symmetry in nuclei: ^{110}Cd .

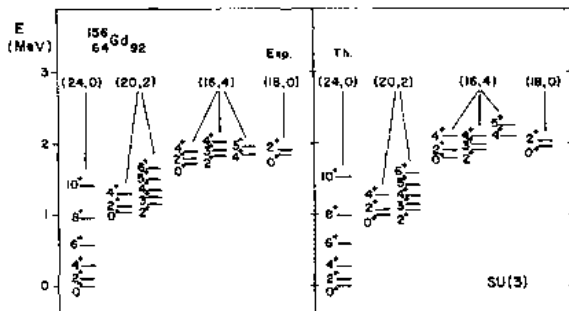


Figure 5. An example of $SU(3)$ dynamic symmetry in nuclei: ^{156}Gd .

4.1. Geometric supersymmetries

Contrary to the case of geometric symmetries, this subject has not been much studied. An example is the introduction of a superlattice¹⁸. The mathematical framework to describe it is point supergroups, that is discrete subgroups of supergroups.

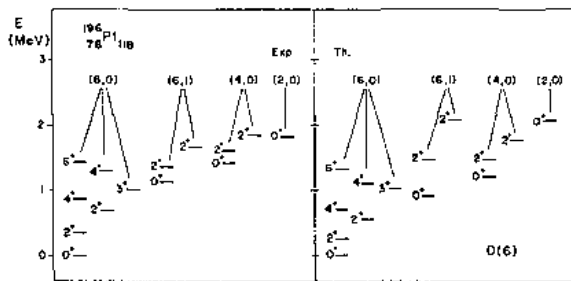


Figure 6. An example of $SO(6)$ dynamic symmetry in nuclei: ^{196}Pt .

4.2. Space-time supersymmetries

These supersymmetries fix the form of the equation governing the motion of mixed systems of bosons and fermions. An example is the original Wess-Zumino Lagrangian¹⁷

$$\begin{aligned} \mathcal{L} = & -\frac{1}{2}(\partial_\mu A(x))^2 - \frac{1}{2}(\partial_\mu B(x))^2 - \frac{1}{2}i\psi(x)\gamma^\mu\partial_\mu\psi(x) \\ & -\frac{1}{2}m^2[A^2(x) + B^2(x)] - \frac{1}{2}im\bar{\psi}(x)\psi(x) \\ & -gmA(x)[A^2(x) + B^2(x)] - \frac{1}{2}g^2[A^2(x) + B^2(x)] \\ & -ig\bar{\psi}(x)[A(x) - \gamma_5B(x)]\psi(x). \end{aligned}$$

The mathematical framework here is continuous supergroups, as for example the SuperPoincare¹ group.

4.3. Gauge supersymmetries

These fix the form of interactions. For example in a supersymmetric gauge theory one has the occurrence of both bosonic and fermionic gauge fields with related properties.

4.4. Dynamic supersymmetries

These symmetries fix the interaction between constituent particles. They produce patterns of energy levels for mixed systems of bosons and fermions. They are a very ambitious unifying concept. A mathematical definition of dynamic supersymmetries is given in¹⁹.

A dynamic supersymmetry is that situation in which:

(i) The Hamiltonian H is written in terms of elements G_α^* of a graded algebra G^* .

(ii) H contains only Casimir operators of a chain of algebras $G^* \supset G'' \supset G''' \supset \dots$. The subalgebras can be either graded or not.

One of the best studied cases is again that of atomic nuclei, where supersymmetries were introduced in 1980¹⁹, as described in the following section.

5. Dynamic Supersymmetries of the Interacting Boson-Fermion Model

In nuclei with an odd number of nucleons at least one is unpaired. Furthermore at higher excitation energies, some of the pairs may be broken. A comprehensive description of nuclei requires a simultaneous treatment

of correlated pairs (bosons) and of fermions²⁰. The corresponding model has been called Interacting Boson-Fermion Model²¹. The building blocks in this model are:

$$\begin{aligned} \text{Bosons : } & s(J=0); d_\mu(J=2; \mu=0, \pm 1, \pm 2) \\ \text{Fermions : } & a_{\alpha m}(m=\pm j, \pm(j-1), \dots, \pm \frac{1}{2}) \end{aligned} \quad (16)$$

The model Hamiltonian can be written as

$$H = H_B + H_F + V_{BF} \quad (17)$$

with

$$\begin{aligned} H_B &= E_0 + \sum_{\alpha\beta} \epsilon_{\alpha\beta} b_\alpha^\dagger b_\beta + \sum_{\alpha\alpha' \beta\beta'} v_{\alpha\alpha'\beta\beta'} b_\alpha^\dagger b_{\alpha'}^\dagger b_\beta b_{\beta'} \\ H_F &= E'_0 + \sum_{ik} \eta_{ik} a_i^\dagger a_k + \sum_{i'k'k''} u_{i'k'k''} a_i^\dagger a_{i'}^\dagger a_{k'} a_{k''} \\ V_{BF} &= \sum_{\alpha\beta i k} w_{\alpha\beta i k} b_\alpha^\dagger b_\beta a_i^\dagger a_k. \end{aligned} \quad (18)$$

In order to study the possible symmetries of a mixed system of bosons and fermions, a new mathematical framework is needed, namely that of graded Lie algebras (also called superalgebras).

A set of elements G_α, F_i forms a Lie superalgebra if they satisfy the following commutation relations

$$\begin{aligned} [G_\alpha, G_\beta] &= c_{\alpha\beta}^{\gamma} G_\gamma \\ [G_\alpha, F_i] &= d_{\alpha i}^j F_j \\ \{F_i, F_j\} &= g_{ij}^\alpha G_\alpha \end{aligned} \quad (19)$$

plus super Jacobi identities. [Graded semisimple Lie algebras with Z_2 grading have been classified by V. Kac²²]. By inspection of Eq.(18) one can see that the combined boson-fermion Hamiltonian can be written in terms of elements of the graded superalgebra $G^* \equiv U(n/m)$

$$\begin{aligned} G_{\alpha\beta} &= b_\alpha^\dagger b_\beta \\ G_{ij} &= a_i^\dagger a_j \\ F_{\alpha i}^\dagger &= b_\alpha^\dagger a_i \\ F_{ia} &= a_i^\dagger b_\alpha \end{aligned} \quad (20)$$

These elements can be arranged in matrix form

$$\begin{pmatrix} b_\alpha^\dagger b_\beta & b_\alpha^\dagger a_i \\ a_i^\dagger b_\alpha & a_i^\dagger a_j \end{pmatrix}. \quad (21)$$

The basis upon which the elements act is the totally supersymmetric irrep of $U(n/m)$ with Young supertableau

$$[\mathcal{N}] \equiv \boxtimes \boxtimes \dots \boxtimes \quad (22)$$

For applications to Nuclear Physics, $\mathcal{N} = N_B + N_F$, $n = 6$ and $m = \sum_j (2j+1) \equiv \Omega$, where Ω is the total degeneracy of the fermionic shell. A dynamic supersymmetry occurs whenever the Hamiltonian of Eq.(18) can be written in terms only of the Casimir operators of $U(n/m)$ and its subalgebras.

5.1. Supersymmetry in nuclei found

One of the consequences of supersymmetry is that if bosonic states are known, one can predict fermionic states. Both are given by the same energy formula. Indeed all properties of the fermionic system can be found from a knowledge of those of the bosonic system. Supersymmetry has thus a predictive power that can be tested by experiment. After its introduction in the 1980's, several examples of spectra with supersymmetric

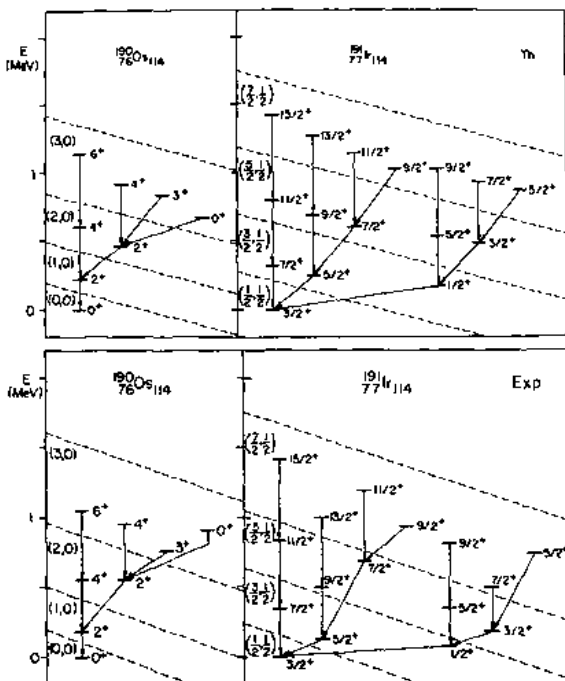


Figure 7. An example of supersymmetry in nuclei: the pair of nuclei $^{190}\text{Os} - ^{191}\text{Ir}$, $U(6/4)$.

properties were found, relating spectra of even-even nuclei with those of odd-even nuclei (odd proton or odd neutron). In the first example, $j = 3/2$ fermions were coupled to s and d bosons. States were classified then in terms of the group $U(6/4)$ ²³. An example is shown in Fig.7, referring to the pair of nuclei Os-Ir. Other cases were subsequently found, for example $j = 1/2, 3/2, 5/2$ fermions with s and d bosons, described algebraically by $U(6/12)$ ²⁴.

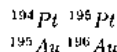
5.2. Supersymmetry in nuclei confirmed

Supersymmetry in nuclei has been recently confirmed in a series of experiments involving several laboratories. The confirmation relates to an improved description of nuclei in which proton and neutron degrees of freedom are explicitly introduced. The model with proton and neutron bosons is called Interacting Boson Model-2. The basic building blocks of this model are boson operators

$$\begin{aligned} b_{\alpha\pi} (\alpha = 1, \dots, 6) &\equiv s_\pi, d_{\pi,\mu} (\mu = 0, \pm 1, \pm 2) \\ b_{\alpha\nu} (\alpha = 1, \dots, 6) &\equiv s_\nu, d_{\nu,\mu} (\mu = 0, \pm 1, \pm 2) \end{aligned} \quad (23)$$

where the index $\pi(\nu)$ refers to proton (neutron). The boson operators span a (six+six)-dimensional space with algebraic structure $U_\pi(6) \oplus U_\nu(6)$. Consequently, when going to nuclei with unpaired particles, one has a model with two types of bosons (proton and neutron) and two types of fermions (proton and neutron), called Interacting Boson-Fermion Model-2. If supersymmetry occurs for this very complex system one expects now

to have supersymmetric partners composed of a quartet of nuclei, even-even, even-odd, odd-even and odd-odd, for example



Spectra of even-even and even-odd nuclei have been known for some time. However, spectra of odd-odd nuclei are very difficult to measure, since the density of states in these nuclei is very high and the energy resolution of most detectors is not sufficiently good. In a major effort that has involved several laboratories for several years it has now been possible to measure spectra of odd-odd nuclei. In particular, the magnetic spectrometer at the Ludwig-Maximilians Universität in München, Germany can separate levels only a few keV apart. It has thus been possible to measure the spectrum of ^{196}Au , the missing supersymmetric partner of ^{194}Pt , ^{195}Pt and ^{196}Au ^{25,26,27}. The spectrum of ^{196}Pt follows very closely the pattern predicted by the supersymmetry $U_{\pi}(6/4) \oplus U_{\nu}(6/12)$. Most of the states predicted by supersymmetry have been observed.

6. Implications of supersymmetry in nuclei

(a) Particle Physics

Supersymmetry has been sought in Particle Physics for decades. The confirmation of supersymmetry in nuclei indicates that this very complex type of symmetry can occur in Nature. It gives hope that, although badly broken, supersymmetry may occur in particle physics. However, supersymmetry in nuclear physics is a symmetry that relates composite objects (pairs) with fundamental objects (nucleons). Can it be the same in particle physics?

(b) Condensed matter physics

Some supersymmetric theories have been constructed in condensed matter physics²⁸. Nambu has suggested that supersymmetry may occur in Type II superconductors²⁹.

Recently, it has been suggested that cuprate materials (high- T_c superconductors) may display supersymmetry. This case is being investigated at the present time³⁰.

7. Conclusions

A form of supersymmetry has been found and confirmed in Nuclei!

8. Acknowledgements

This work was supported in part under USDOE Contract No. DE-FG-02-91ER-40608.

References

1. W. Pauli, *Z. Physik* **36**, 336 (1926).
2. M. Gell-Mann, *Phys. Rev.* **125**, 1067 (1962).
3. Y. Ne'eman, *Nucl. Phys.* **26**, 222 (1962).
4. S. Okubo, *Progr. Theor. Phys.* **27**, 949 (1962).
5. V. Fock, *Z. Physik* **98**, 145 (1935).
6. Y. Dothan, M. Gell-Mann, and Y. Ne'eman, *Phys. Lett.* **17**, 148 (1965).
7. A.O. Barut and A. Böhm, *Phys. Rev. B* **139**, 1107 (1965).
8. F. Iachello, in *Group Theoretical Methods in Physics*, Lecture Notes in Physics, Vol. **94**, A. Böhm ed., Springer, Berlin, p.420-429 (1979).
9. For a review, see F. Iachello and A. Arima, *The Interacting Boson Model*, Cambridge University Press, Cambridge, England (1987).
10. A. Arima and F. Iachello, *Ann. Phys. (N.Y.)* **99**, 253 (1976).
11. A. Arima and F. Iachello, *Ann. Phys. (N.Y.)* **111**, 201 (1978).
12. A. Arima and F. Iachello, *Ann. Phys. (N.Y.)* **123**, 468 (1979).

13. H. Miyazawa, *Prog. Theor. Phys.* **36**, 1266 (1966).
14. P. Ramond, *Phys. Rev. D* **3**, 2415 (1971).
15. A. Neveu and J. Schwarz, *Nucl. Phys. B* **31**, 86 (1971).
16. D.V. Volkov and V.P. Akulov, *Phys. Lett.* **46B**, 109 (1973).
17. J. Wess and B. Zumino, *Nucl. Phys.* **70**, 39 (1974).
18. V. A. Kostelecky and J. M. Rabin, in *Supersymmetry in Physics*, edited by V.A. Kostelecky and D.K. Campbell, *Physica D* **15**, 213 (1985).
19. F. Iachello, *Phys. Rev. Lett.* **44**, 772 (1980).
20. For a review see, F. Iachello and P. van Isacker, *The Interacting Boson-Fermion Model*, Cambridge University Press, Cambridge, England (1991).
21. F. Iachello and O. Scholten, *Phys. Rev. Lett.* **43**, 679 (1979).
22. V.C. Kar, *Functional Analysis Appl.* **9**, 91 (1975).
23. A.B. Balantekin, I. Bars and F. Iachello, *Phys. Rev. Lett.* **47**, 19 (1981).
24. A. B. Balantekin, I. Bars, R. Bijker and F. Iachello, *Phys. Rev. C* **27**, 2430 (1983).
25. A. Metz, J. Jolie, G. Craw, R. Ilertenberger, J. Groger, Ch. Günther, N. Warr and Y. Eisermann, *Phys. Rev. Lett.* **83**, 1542 (1999).
26. A. Metz, Y. Eisermann, A. Gollwitzer et al., *Phys. Rev. C* **61**, 064313 (2000).
27. J. Groger, J. Jolie, R. Krucken, et al., *Phys. Rev. C* **62**, 064304 (2000).
28. G. Parisi and N. Sourlas, *Phys. Rev. Lett.* **43**, 744 (1979).
29. Y. Nambu, in *Supersymmetry in Physics*, edited by V.A. Kostelecky and D.K. Campbell, *Physica D* **15**, 147 (1985).
30. F. Iachello, in preparation.

CHAIRMAN: F. IACHELLO

Scientific Secretaries: I. Malamos, T. Sykora

DISCUSSION

- *D'Enterria:*

You have presented the case that nuclei show supersymmetry. What do we learn from this fact regarding an effective nuclear interaction between nucleons?

- *Iachello:*

What we have discussed this morning was possible symmetries of systems consisting of bosons and fermions. In order to have SUSY, the Hamiltonian for this system must be such that when we apply a SUSY transformation to the bosonic piece, we obtain the fermionic piece. The occurrence of SUSY depends very much on the interactions.

What are the interactions in this case? They are the following: The boson-boson interaction has a direct term in which the fermions that form the boson pair interact and an exchange term, that takes into account for us the Pauli principle. The fermions instead will interact among themselves only directly.

In addition, we have interactions between bosons and fermions, again direct and exchange. So what we have learned from the fact that we observe SUSY in nuclei is that all these complicated interactions arrange themselves to produce a SUSY Hamiltonian.

Why is it so? The reason is that the same interaction that produces the bound states, produces also the boson-boson, boson-fermion and fermion-fermion interaction. The main question is whether, quantitatively, we can have SUSY or not.

I will give you an example. The ratio between coupling constants for SUSY is 1:1:2. If one does microscopic studies of the origin of SUSY, one does not obtain 1:1:2 precisely, but rather 1:0.9:1.8.

- *D'Enterria:*

If a supersymmetry is a valid symmetry of this nuclear effective Lagrangian, what is/are the associated supersymmetric conserved charge(s)?

- *Iachello:*

The types of SUSY we are considering here, as I mentioned this morning, are different from space-time SUSY. They are associated with superalgebras, which are compact superalgebras. But they are not only compact, they are also semisimple. An example of this situation is the superalgebra $U(n|m)$.

You are concerned with non semisimple superalgebras in which the commutation relations close back, as in the Poincaré case, to the momenta. Here this is not the case.

The commutation relations among the elements of the algebra show that they stay within $U(n|m)$.

If you wish, you can associate some of the conserved quantities with N , which is the total number of bosons plus fermions, $N = N_B + N_F$. That number is conserved within a given supermultiplet. One can exchange bosons into fermions but in such a way that the total number N is conserved. They must belong to some definite representation of this superalgebra $U(n|m)$.

Another example is provided by orthosymplectic algebras, $OSp(n|m)$ (i.e. superalgebras which are orthogonal in the bosonic sector and symplectic in the fermionic sector). In several studies they have been used. At the present time the only superalgebras that have some applications are unitary superalgebras.

- *Cerri:*

You basically presented two theories. The standard nuclear physics approach and nuclear physics in a SUSY approach. I understand that both have systematic issues but could you be clearer on the compatibility of the two models with experimental data?

Could you give me some comparison of the goodness of these two approaches? Is one of them better than the other one?

- *Iachello:*

Yes, this question has been addressed extensively. This morning I presented to you the pair of nuclei: osmium (even) and iridium (odd).

First of all we can try to do a calculation with the standard method. Unfortunately, for these nuclei it is not possible to do it. The reason is that the number of particles is so large that we cannot do a straightforward numerical diagonalization. Eventually, with further development of computers we will be able to do it.

There are some attempts to calculate nuclear structure ab initio. So far we are not there. Therefore, for this pair of nuclei, models based on SUSY are the only way to do calculations.

One may also extend the concept of SUSY Hamiltonians that I presented this morning in the special case of bosons with dynamic symmetry to more general cases. In such a case, the validity of the SUSY description will become larger.

Typically for supersymmetry, the breaking (in the energies) is of the order of 20 percent, and of the same order of magnitude as the el.-mg. transitions rates. This is a test of the bosonic sector of SUSY. The test of the fermionic sector, i.e. that operator changing bosons into fermions, is good within 40 percent. For standard nuclear physics calculations, we can achieve an accuracy of 5-10 percent. Of course, we are not interested only in the ground state energy, but in the entire excitation spectrum.

- *Skinner:*

Is there a superfield formalism for this type of SUSY?

- *Iachello:*

No, so far we have done everything in terms of a non-relativistic approach. Eventually, we would like to apply this formalism to condensed matter systems, like high T_c superconductors. Here, it would be very appropriate to construct it directly from fields. We hope to be able to do this in the future.

- *Skinner:*

Do you see any prospect for extending SUSY in condensed matter or nuclear physics?

- *Iachello:*

It could be. Right now our main concern is to see whether this type of SUSY can be applied to some other physical systems. In particular, high T_c superconductors. This is our first priority. There are some other systems where SUSY can play a role. There is something called the Jahn-Teller effect in molecules. It could be that SUSY plays a role in the Jahn-Teller effect.

- *Ludlam:*

How satisfactory is the experimental situation? Will the availability of radioactive beam facilities, which should greatly expand the range of nuclei available for study, have an important impact?

- *Iachello:*

Present data focus on clusters of nuclei in the periodic table. Studies with unstable nuclei, particularly neutron-rich nuclei, could provide important confirmation or expose problems with theory.

- *Markov:*

Did you apply your technique to the hadronic spectrum?

- *Iachello:*

Yes. There was an idea several years ago, which many of you might know. Instead of keeping the baryon as a state of three quarks, you consider it as a state made of a diquark Q and a quark q . The mesons are made of $q\bar{q}$ pair. A result is: if you look at the Regge trajectory for baryons and mesons, which is a plot of the square of masses as a function of angular momentum L , they have the same slope. In fact, this is a good approximation.

One can try to push this idea further. As a consequence of SUSY, there can be not only $q\bar{q}$ but also $Q\bar{Q}$ bound state. We made a speculation based on SUSY and since the masses are related to the SUSY scale, this object should be about 1 GeV. We suggested also that some of these particles, which are seen around 1 GeV, would be SUSY partners of the baryons.

- *Markov:*

As far as I know this diquark model is excluded because there are a lot of missing states...

- *Iachello:*

The situation is not simple. You may know that, if you look at the baryonic spectrum, many resonances are expected from the simple quark model (i.e. made of three quarks) but not observed experimentally. In the Thomas Jefferson Laboratory there is a program searching for these missing states. So far, none has been found. Instead, all of the states that the diquark model predicts, are there.

- *Bei:*

You told us about the possible application of this theory to high T_c superconductivity, but in the limit in which N goes to infinity, an interacting theory is not unitary equivalent to free bosons. Moreover the same problem should concern the application to subnuclear physics due to the same limit of quark gluon plasma. Maybe the solution is not gauge independent and N goes to infinity limit. (Unless you must break the supersymmetry).

- *Iachello:*

The first thing we are trying to do is to develop a model at zero temperature and study what happens there. The next step is to try and see what happens with growing temperature.

- *Casalderrey-Solana:*

What is responsible for the appearance of SUSY in systems where a fundamental force is different? (QCD in nuclei, QED in solid state.)

- *Iachello:*

To trace it back to the fundamental interactions of QCD is going to be more complicated. A few years ago, Ne'eman and Sawicki tried to do it. My present feeling is that this is an effective theory, not related to the fundamental theory.

The situation in superconductors is similar. The fundamental QED interaction is repulsive but, due to interactions with lattice vibrations, the effective interaction becomes attractive.

- *Gripaios:*

You mentioned using SUSY to relate BEC to fermionic condensates. Are we talking about coexisting condensates or does the SUSY relate two distinct physical systems? One with BEC and one with fermion condensate?

- *Iachello:*

I have not investigated this case in great depth. Recently, I was told that it has been possible to form systems where, inside traps, there are condensates of bosons and fermions. I am planning to investigate this situation in the future.

To have SUSY, you must have coexisting interactions between bosons and fermions. In this case bosons are composite objects as well, because the bosons in BEC are atoms.

- *Gripaios:*

Could I use the Wess-Zumino model to describe this?

- *Iachello:*

Maybe you can do that. But the number of particles involved in this condensate is not very large (from hundreds a thousand atoms).

- *Baldini:*

You said you have good chances to understand high T_c superconductivity in the SUSY frame. Does it mean that you think that, looking for supersymmetric partners, you can predict new high T_c superconductors?

- *Iachello:*

The first task is whether or not we can understand the present materials. If we really do, we may be able, eventually, to predict new ones. I will give you an example. We start with a material which has no superconductive properties, and we will dope it with some other material. Then the material becomes superconductive. If we find the mechanism by means of which doping induces superconductivity, we could, eventually, understand what atoms produce this. But we are far away from this understanding.

- *Kuperstein:*

Answering the first question today you said that some of the bosonic and fermionic degrees of freedom play the role of the conserved SUSY charge. What about the difference between these two numbers? Why we do not have equal number of bosonic and fermionic states?

- *Iachello:*

Here, the total sum is preserved. The separate numbers N_B and N_F are not the same, neither are the dimensions of bosonic and fermionic spaces. In other words, $N_B \neq N_F$, and in $U(n|m)$, $n \neq m$.

- *Casalderrey-Solana*

Are there some examples of systems where bosonisation occurs and there is not SUSY? Are they related?

- *Iachello:*

The answer to the first question is yes. The answer to the second question is no. The bosonization is not related to SUSY. There are systems with bosonization but without SUSY. In nuclei, bosonization is just a technique where we replace two fermions with one boson. We have usual bosonization in which the resulting angular momentum is zero but also we have bosonization with angular momenta equal to 2.

So it is a generalized form of bosonization. There is a general technique to construct the boson Hamiltonian from the Hamiltonian of the original fermion system.

- *Sykora:*

To which scale I can use your technique?

- *Iachello:*

There are two points. One is a temperature (or excitation energy) scale. There is of course the point at which the SUSY will be broken due to temperature effects. Typical temperature scale in nuclei is a few MeV. Another is a space scale. We have applied SUSY to nuclei (space scale a few fm). We also tried for molecules, but it does not work because the scale of the bosonic excitations and the scale of fermionic excitations are very different. Electron excitations in molecules are a scale of 10 times larger than the vibronic excitation (which are bosons).

Inflation, Dark Matter, Dark Energy

Edward W. Kolb

Fermilab Astrophysics Center, Fermi National Accelerator Laboratory, Batavia, Illinois, 60510-0500, USA,
and Department of Astronomy and Astrophysics, Enrico Fermi Institute,
University of Chicago, Chicago, Illinois 60637-1438, USA

Remarkable 20th-century cosmological discoveries and theoretical ideas led to the development of the present cosmological "standard model." In this lecture I will focus on one of the more recent ideas that may now be regarded as part of the framework of the standard big-bang model: namely, that structure in the universe results from the growth of small seed density fluctuations produced during the inflationary universe. In order to complete this picture, I will also discuss the idea that the present mass density is dominated by dark matter and that there is now a preponderance of dark energy.

I. THE EMERGENCE OF THE STANDARD HOT BIG BANG MODEL

At the beginning of the 20th century, the popular view of the universe was the so-called Kapteyn Universe, named after the Dutch astronomer J. C. Kapteyn. In this cosmology, the entire universe was contained within our Milky Way galaxy, with the solar system "at or very near" the center of the universe. The Kapteyn universe was a universe of stars. While at that time the origin of the universe was often considered to be outside the realm of scientific investigation, a popular scientific view at the beginning of the 20th century was that the universe was static and possibly infinitely old.

This view of the universe was drastically changed and enlarged in the first three decades of the 20th century. Harlow Shapley changed our belief that the solar system occupied a position of prominence at the center of the galaxy, and Edwin Hubble enlarged our conception of the vastness of the universe by demonstrating that spiral nebulae are outside of the Milky Way. Hubble's 1929 publication of the linear distance-redshift relation was one of the two great 20th century cosmological discoveries. The second great cosmological discovery was that of the cosmic microwave background radiation by Penzias and Wilson in 1965.

After the discovery of the microwave background radiation, the big-bang model emerged as the "standard model" of cosmology. In this standard model, the universe is described by a homogeneous and isotropic Robertson-Walker metric. The expansion age of the universe, H_0^{-1} , is $9.8 \times 10^9 h^{-1}$ years, where h is Hubble's constant in units of $100 \text{ km s}^{-1} \text{ Mpc}^{-1}$. In the middle of the 1960s, the density parameter Ω was known to be between $0.1 \leq \Omega \leq 1$, where Ω is the average mass density of the universe in units of the critical density: $\Omega \equiv \rho/\rho_C$, with $\rho_C = 3H_0^2/8\pi G = 1.88 \times 10^{-29} h^2 \text{ g cm}^{-3}$.

Although this standard cosmology seemed to give an adequate description of the universe, it gave no clue "why" the universe is approximately homogeneous and isotropic and why the density is anywhere close to critical (equivalently, why the spatial curvature scale of the universe is so large).

II. THE BIG BANG AUGMENTED BY INFLATION

We live in a very large, very old, and very nearly (perhaps exactly) spatially flat universe. The universe we observe is, at least on large scales, remarkably homogeneous and isotropic. These attributes of our universe can be accounted for as the result of a period of very rapid expansion, or inflation, at some time during the very early history of the universe (Guth 1981).

A sufficiently long epoch of primordial inflation leads to a homogeneous and isotropic universe that is old and flat. The really good news is that the idea of inflation seems compatible with what we think we know about high-energy physics. Very many reasonable particle-physics models have been proposed for inflation.¹ In some ways, inflation is generic. That is also the really bad news, since we would like to use the early universe to learn something about physics at energy scales we can't produce in terrestrial laboratories. We want to know more than just that inflation occurred, we want to learn something of the dynamics of the expansion of the universe during inflation. That may tell us something about physics at very high energies. It would also allow us to restrict the number of inflation models. If we can differentiate between various inflation models, then inflation can be used as a phenomenological guide for understanding physics at very high energies.

That fact that inflation leads to oldness, flatness, and homogeneity/isotropy only tells us about the minimum length of the inflationary era. Those attributes are not very useful discriminants to probe the dynamics of inflation. If knowledge of the dynamics of inflation is our goal, we must exploit another aspect of inflation. Luckily, there are two things associated with inflation that allow us to probe the dynamics of inflation: perturbations and preheating/reheating.

While the universe is homogeneous and isotropic on

¹ Perhaps a better statement is that there are many models that seemed reasonable to the people who proposed them at the time they were proposed.

large scales, it is inhomogeneous on small scales. The inhomogeneity in the distribution of galaxies, clusters, and other luminous objects is believed to result from the growth of small seed primordial perturbations in the density field that were produced during inflation. The seed perturbations also contribute to the observed anisotropy in the temperature of the cosmic microwave background radiation. If the primordial seeds were produced by inflation, there ought to be a background of primordial gravitational waves that also were produced during inflation. While the background gravitational waves do not provide the seeds or influence the development of structure, gravitational waves may lead to observable temperature variations in the cosmic microwave background radiation.

If we can extract knowledge of the primordial density perturbations from observations of large-scale structure and cosmic microwave background radiation temperature fluctuations, then we can learn something about the dynamics of inflation. If we can discover evidence of a gravitational wave background, then we will know even more about the dynamics of the expansion rate during inflation.

A simple thing we may be able to learn about inflation is the expansion rate of the universe during inflation. This would also tell us about the timescale associated with inflation. We do not yet know when inflation occurred, but the best guess for how inflation fits into the different epochs in the history of the universe is given in Table 1. It is useful to spend a few minutes discussing the movements of the Cosmic Symphony listed in Table 1.

The first movement of the Cosmic Symphony may be dominated by the string section if on the smallest scales there is a fundamental stringiness to elementary particles. If this is true, then the first movement in the Cosmic Symphony would have been a pizzicato movement of vibrating strings about 10^{-43} s after the bang. There is basically nothing known about the stringy phase, if indeed there was one. We do not yet know enough about this era to predict relics, or even the equation of state.

The earliest movement we can "hear" is the echo of the inflationary phase. The inflationary movement probably followed the string movement, and lasted approximately 10^{-30} seconds. During inflation the energy density of the universe was dominated by vacuum energy, with equation of state $p_V \simeq -\rho_V$. As we shall see, the best information we have of the inflationary phase is from the quantum fluctuations during inflation, which were imprinted upon the metric and can be observed as cosmic background radiation (CBR) fluctuations and the departures from homogeneity and isotropy in the matter distribution, e.g., the power spectrum. Inflation also produces a background of gravitational radiation, which can be detected by its effect on the CBR, or if inflation was sufficiently exotic, by direct detection of the relic background by experiments such as LIGO or LISA.

Inflation was wonderful, but all good things must end. A lot of effort has gone into studying the end of inflation

(for a review, see Kofman *et al.* 1997). It was likely that there was a brief period during which the energy density of the universe was dominated by coherent oscillations of the inflaton field. During coherent oscillations the inflaton energy density scales as a^{-3} where a is the scale factor, so the expansion rate of the universe decreased as in a matter-dominated universe with $p \sim 0$. Very little is known about this period immediately after inflation, but there is hope that one day we will discover a relic. Noteworthy events that might have occurred during this phase include baryogenesis, phase transitions, and the generation of dark matter.

We do know that the universe was radiation dominated for almost all of the first 10,000 years.² The best preserved relics of the radiation-dominated era are the light elements. The light elements were produced in the radiation-dominated universe one second to three minutes after the bang. If the baryon asymmetry is associated with the electroweak transition, then the asymmetry was generated during the radiation-dominated era. The radiation era is also a likely epoch for the origin of dark matter such as wimp or axions. If one day we can detect the 1.9 K neutrino background, it would be a direct relic of the radiation era. The equation of state during the radiation era is $p_R = \rho_R/3$.

The earliest picture of the matter-dominated era is the CBR. Recombination and matter-radiation decoupling occurred while the universe was matter dominated. Structure developed from small primordial seeds during the matter-dominated era. The pressure is negligible during the matter-dominated era.

Finally, if recent determinations of the Hubble diagram from observations of distant high-redshift Type-I supernovae are correctly interpreted, the expansion of the universe is increasing today ($\dot{a} > 0$). This would mean that the universe has recently embarked on another inflationary era, but with the Hubble expansion rate much less than the rate during the first inflationary era.

A. Simple dynamics of inflation: the inflaton

In building inflation models it is necessary to find a mechanism by which a universe dominated by vacuum energy can make a transition from the inflationary universe to a matter-dominated or radiation-dominated universe. There is some unknown dynamics causing the expansion rate to change with time. There may be several degrees of freedom involved in determining the expansion rate during inflation, but the simplest assumption is that

² Although I may speak of time after the bang, I will not address the issue of whether the universe had a beginning or not, which in the modern context is the question of whether inflation is eternal. For the purpose of this discussion, time zero of the bang can be taken as some time before the end of inflation in the region of the universe we observe.

tempo	epoch	age	ρ	p	$\rho + 3p$	relic
pizzicato	string dominated	$\lesssim 10^{-43}$ s	?	?	?	?
prestissimo	vacuum dominated (inflation)	$\sim 10^{-38}$ s	ρ_V	$-p_V$	-	density perturbations gravitational waves dark matter?
presto	matter dominated	$\sim 10^{-36}$ s	ρ_ϕ	0	+	phase transitions? dark matter? baryogenesis?
allegro	radiation dominated	$\lesssim 10^4$ yr	T^4	$T^4/3$	+	dark matter? baryogenesis? neutrino decoupling nucleosynthesis
andante	matter dominated	$\gtrsim 10^4$ yr	ρ_M	0	+	recombination radiation decoupling growth of structure
largo	vacuum dominated (inflation) <i>da capo?</i>	recent	ρ_V	$-p_V$	-	acceleration of the universe

TABLE I: Different epochs in the history of the universe and the associated tempos of the ever decreasing expansion rate H , along with the equation of state and some of the relics produced during the various eras.

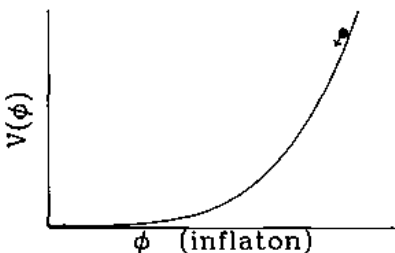


FIG. 1: A schematic illustration of the inflaton potential.

there is only one dynamical degree of freedom responsible for the evolution of the expansion rate.

The cosmological dynamics is traced by following the expansion rate, which in the usual inflation picture, is determined by the inflaton.

If there is a single degree of freedom at work during inflation, then the evolution from the inflationary phase

may be modeled by the action of a scalar field ϕ evolving under the influence of a potential $V(\phi)$. Let's imagine the scalar field is displaced from the minimum of its potential as illustrated in Fig. 1. If the energy density of the universe is dominated by the potential energy of the scalar field ϕ , known as the *inflaton*, then $\rho + 3p$ will be negative. The vacuum energy disappears when the scalar field evolves to its minimum. The amount of time required for the scalar field to evolve to its minimum and inflation to end (or even more useful, the number of e-folds of growth of the scale factor) can be found by solving the classical field equation for the evolution of the inflaton field.

This approach of modeling the dynamics of the expansion rate in terms of the dynamics of a single scalar field whose vacuum energy dominated the universe may seem clumsy, not to mention unimaginative. However, the dynamics of many other models of inflation can be expressed in terms of an equivalent inflaton field. The inflaton field need not be a fundamental scalar field; it may be associated with a flat direction in moduli space, the inverse of the radius of an extra dimension, or some such exotic creature.

B. Quantum fluctuations

In addition to the classical motion of the inflaton field, during inflation there are quantum fluctuations.³ Since the total energy density of the universe is dominated by the inflaton potential energy density, fluctuations in the inflaton field lead to fluctuations in the energy density. Because of the rapid expansion of the universe during inflation, these fluctuations in the energy density are frozen into super-Hubble-radius-size perturbations. Later, in the radiation or matter-dominated era they will come within the Hubble radius and appear as if they were *non-causal* perturbations. The character of the perturbations depends on the inflaton potential, so a careful study of the perturbations in the microwave background temperatures or the power spectrum for structure formation, may reveal something about the inflaton potential.

The generation of perturbations during inflation is an example of particle creation in a changing gravitational field caused by the expansion of the universe. This idea traces back at least as far as the work of Erwin Schrödinger in the late 1930s. In the mid-1930s, influenced by Eddington and Lemaître, Schrödinger became interested in cosmological issues. As the political situation in Austria caused Schrödinger to flee Gratz in 1938, he traveled to the Vatican and Belgium before finally settling in Ireland in 1939. During this period he wrote a remarkable paper, titled "The Proper Vibrations of the Expanding Universe" (Schrödinger 1939). In that paper he studied how the expansion of the universe would affect the quantum vacuum. In the introduction to his 1939 paper, he wrote,

... proper vibrations [particles and antiparticles] cannot be rigorously separated in the expanding universe. ... this is a phenomenon of outstanding importance. With particles it would mean production or annihilation of matter, merely by expansion, ... Alarmed by these prospects I have examined the matter in more detail.

Schrödinger went on to demonstrate that the effect of the changing gravitational field on vacuum fluctuations would lead to particle creation. In his 1939 paper he concluded,

There will be a mutual adulteration of positive and negative frequency terms in the course of time, giving rise to ... the 'alarming phenomenon' ...

If one considers the potential energy as the energy of a condensate of the zero-momentum (infinite-wavelength)

field quanta, then the expansion of the universe will adulterate the homogeneous arrangement of the universe and create nonzero momentum particles (i.e., particles with finite wavelength). These nonzero momentum quanta are perturbations to the perfectly smooth background. In a very real sense, the observation of CBR fluctuations is a picture of the quantum vacuum.

When we first learned of the quantum vacuum in the 6th grade, we were told that we could not observe the quantum vacuum because it was sub-microscopic. But the expansion of the universe froze a pattern of sub-microscopic quantum fluctuations, and through the expansion, stretched the sub-microscopic pattern to astronomical sizes.

C. Defrosting, preheating, and reheating

If the inflaton is completely decoupled, then once inflation ends the inflaton will oscillate about the minimum of the potential, with the cycle-average of the energy density decreasing as a^{-3} , i.e., as in a matter-dominated universe. But at the end of inflation the universe is cold and frozen in a low-entropy state: to a very good approximation the only degree of freedom is the zero-momentum mode of the inflaton field. It is necessary to "defrost" the universe and turn it into a "hot" high-entropy universe with many degrees of freedom in the radiation. Exactly how this is accomplished is still unclear. It probably requires the inflaton field to be coupled to other degrees of freedom, and as it oscillates, its energy is converted to radiation either through incoherent decay, or through a coherent process involving very complicated dynamics of coupled oscillators with time-varying masses. In either case, it is necessary to extract the energy from the inflaton and convert it into radiation.

I will now turn to a discussion of how defrosting might occur. It may be a complicated several-step process. I will refer to nonlinear effects in defrosting as "preheating" (for a review, see Kofman *et al.* 1997) and refer to linear processes as "reheating" (for a review, see Kolb & Turner 1990).

The possible role of nonlinear dynamics leading to explosive particle production has recently received a lot of attention. This process, known as "preheating," may convert a fair fraction of the inflaton energy density into other degrees of freedom, with extremely interesting cosmological effects such as symmetry restoration, baryogenesis, or production of dark matter. But the efficiency of preheating is very sensitive to the inflation model and the inflation model parameters.

Another possibility for defrosting is reheating. In reheating it is assumed that the comoving energy density in the inflaton field decays exponentially. This can be visualized as a linear, incoherent process involving the condensate of the inflaton field.

Perhaps some relic of defrosting, such as symmetry restoration, baryogenesis, or dark matter may one day

³ Here I will continue to assume there is only one dynamical degree of freedom.

provide a clue of the exact mechanism of defrosting, and perhaps even shed light on the dynamics of inflation itself.

D. Inflation conclusions

It might be said that we know everything we need to know about inflation. But we don't know how it began, how it proceeded, and how it ended. Knowledge about the beginning of inflation may be impossible to obtain. The issue may be intertwined with the issue of whether inflation is eternal or not, and the evidence may forever be outside of our horizon. The primordial background fluctuations and a gravitational wave background could shed light on the dynamics of inflation once it was well underway. The end of inflation and the defrosting of the frozen universe could involve interesting and complicated dynamics. It is too early to judge the prospects of learning about the end of inflation.

III. DARK MATTER

There is conclusive evidence that the dominant component of the matter density in the universe is dark (for a review, see Trimble 1987). The most striking indication of the existence of dark matter is the dynamical motions of astronomical objects. Observations of flat rotation curves for spiral galaxies indicate that the mass of the dark component of galactic halos is about ten times the mass of luminous component. Dynamical evidence for dark matter in galaxy clusters from the velocity dispersion of individual galaxies, as well as from the large x-ray temperatures of clusters, is also compelling. Bulk flows, as well as the peculiar motion of our own local group, also implies that the matter density is dominated by dark matter.

The masses of galaxy clusters inferred by their gravitational lensing of background images is consistent with the large dark-to-visible mass ratios determined by dynamical methods (Wittman, *et al.* 2000).

There is also compelling evidence that the bulk of the dark component must be nonbaryonic. The present baryonic density is restricted by big-bang nucleosynthesis to be less than that inferred by the methods discussed above (Burles, *et al.* 2001). The theory of structure formation from the gravitational instability of small initial seed inhomogeneities requires a significant nonbaryonic component to the mass density.

The dark-matter density inferred from dynamics is $\Omega_{DM} \equiv \rho_{DM}/\rho_c \gtrsim 0.3$. In addition, the most natural inflation models predict a flat universe, *i.e.*, $\Omega_0 = 1$, while standard big-bang nucleosynthesis implies that ordinary baryonic matter can contribute at most 10% to Ω_0 . This means that the bulk of the matter in our universe must be dark.

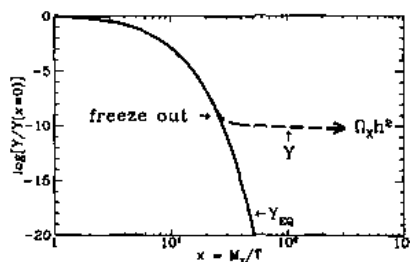


FIG. 2: A thermal relic starts in LTE at $T \gg M_X$. When the interaction rates keeping the relic in chemical equilibrium become smaller than the expansion rate, the density of the relic relative to the entropy density freezes out.

A. Thermal relics

It is usually assumed that the dark matter consists of a species of a new, yet to be discovered, massive particle, traditionally denoted by X . It is also often assumed that the dark matter is a thermal relic, *i.e.*, it was in chemical equilibrium in the early universe.

A thermal relic is assumed to be in local thermodynamic equilibrium (LTE) at early times. The equilibrium abundance of a particle, say relative to the entropy density, depends upon the ratio of the mass of the particle to the temperature. Define the variable $Y \equiv n_X/s$, where n_X is the number density of winsup X with mass M_X , and $s \sim T^3$ is the entropy density. The equilibrium value of Y , Y_{EQ} , is proportional to $\exp(-x)$ for $x \gg 1$, while $Y_{EQ} \sim \text{constant}$ for $x \ll 1$, where $x = M_X/T$.

A particle will track its equilibrium abundance as long as reactions which keep the particle in chemical equilibrium can proceed rapidly enough. Here, rapidly enough means on a timescale more rapid than the expansion rate of the universe, H . When the reaction rate becomes smaller than the expansion rate, then the particle can no longer track its equilibrium value, and thereafter Y is constant. When this occurs the particle is said to be "frozen out." A schematic illustration of this is given in Fig. 2.

The more strongly interacting the particle, the longer it stays in LTE, and the smaller its eventual freeze-out abundance. Conversely, the more weakly interacting the particle, the larger its present abundance. The freeze-out value of Y is related to the mass of the particle and its annihilation cross section (here characterized by σ_0) by (Kolb & Turner 1990)

$$Y \propto \frac{1}{M_X m_P \sigma_0}. \quad (1)$$

Since the contribution to Ω is proportional to the product $M_X \cdot n_X$, which in turn is proportional to $M_X Y$, the

present contribution to Ω from a thermal relic roughly is *independent* of its mass,⁴ and depends only upon the annihilation cross section. The cross section that results in $\Omega_X h^2 \sim 1$ is of the order 10^{-37} cm^2 , which is of the order of the weak scale. This is one of the attractions of thermal relics. The scale of the annihilation cross section is related to a known mass scale.

The simple assumption that dark matter is a thermal relic is surprisingly restrictive. The largest the annihilation cross section can be is roughly M_X^{-2} . This implies that large-mass wimps would have such a small annihilation cross section that their present abundance would be too large. Thus one expects a maximum mass for a thermal wimp, which turns out to be a few hundred TeV.

The standard lore is that the hunt for dark matter should concentrate on particles with mass of the order of the weak scale and with interactions with ordinary matter on the scale of the weak force. This has been the driving force behind the vast effort in dark matter direct detection.

If the wimp is a thermal relic, it must have a non-negligible annihilation cross section. So long as the annihilation products include quarks or electrons, the wimp must have a nonzero scattering cross section with matter. Thus, direct detection of a thermal relic is possible, at least in principle. Direct detection of nonthermal relics, on the other hand, may be impossible in principle because they may have only gravitational interactions.

B. Nonthermal relics

While a thermal origin for wimps is the most common assumption, it is not the simplest possibility. It has been recently pointed out that dark particles might have never experienced local chemical equilibrium during the evolution of the universe, and that their mass may be in the range 10^{12} to 10^{16} GeV, much larger than the mass of thermal wimps (for a review, see Chung *et al.* 1999). Since these wimps would be much more massive than thermal wimps, such superheavy dark particles have been called wimpzillas.

Since wimpzillas are extremely massive, the challenge lies in creating very few of them. Several wimpzilla scenarios have been developed involving production during different stages of the evolution of the universe.

Wimpzillas may be created during bubble collisions if inflation is completed through a first-order phase transition; at the preheating stage after the end of inflation with masses easily up to the Grand Unified scale of 10^{15} GeV or even up to the Planck scale; or during the reheating stage after inflation with masses which may be

as large as 2×10^3 times the reheat temperature.

Wimpzillas may also be generated in the transition between an inflationary and a matter-dominated (or radiation-dominated) universe due to the "nonadiabatic" expansion of the background spacetime acting on the vacuum quantum fluctuations. This mechanism has been studied in detail. The distinguishing feature of this mechanism is the capability of generating particles with mass of the order of the inflaton mass (usually much larger than the reheat temperature) even when the particles only interact extremely weakly (or not at all) with other particles, and do not couple to the inflaton.

Wimpzillas are an example of a nonthermal relic whose interactions with normal matter need only be gravitational. Although it may be endowed with other interactions (strong, weak, electromagnetic, etc.), it need only have gravitational interactions. If it is sterile in interactions with normal matter, direct laboratory detection of dark matter may never occur.

IV. DARK ENERGY

While the picture of a flat universe dominated by dark matter is compelling, it seems to be observationally challenged. Several pieces of evidence point to the possibility that the universe today is dominated by some non-clustering component of the mass-energy density, which has an equation of state that causes an acceleration of the expansion rate of the universe.

First, consider the "non-clustering" feature. The best efforts of our astronomer friends can only find a fraction of the critical density in the form of matter (for a review, see Bahcall 2000), while observations of the first acoustic peak of the angular correlation function of the cosmic background radiation strongly suggests that the universe is flat (as predicted by inflation), which implies a critical density. A simple explanation of this discrepancy is that the bulk of the mass-energy density is in the form of a smooth, non-clustering component. The simplest examples of such a component is either relativistic particles (radiation) or a cosmological constant.

The possibility that we live today in a radiation-dominated universe faces an age crisis since the age of a flat, radiation-dominated universe is $H_0^{-1}/2$ (even smaller than the age of a flat, matter-dominated universe: $2H_0^{-1}/3$). A radiation-dominated universe also has the problem that gravitational instability turns off when the universe is radiation dominated.

The age of a universe dominated by vacuum energy, or a cosmological constant (Λ), is larger than H_0^{-1} . While structure does not develop in a Λ -dominated universe, the transition from a matter-dominated to a Λ -dominated universe could have been quite recent, and sufficient time from matter-domination to Λ -domination for structure to develop would have occurred.

Determination of the statistics of clustering (the power spectrum) seems to be quite well understood by the pre-

⁴ To first approximation the relic dependence depends upon the mass only indirectly through the dependence of the annihilation cross section on the mass.

dictions of a Λ -dominated model universe, and not by a matter-dominated universe model. So observations of large-scale structure seems to suggest a model universe of critical density where about 30% is in the form of matter and 70% is in the form of a cosmological constant (or vacuum energy).

A universe dominated by vacuum energy would have an equation of state $p = -\rho$. This has important implications for the expansion of the universe. While the Friedmann equation describing the expansion rate of the universe depends only upon the matter-energy density ρ :

$$\frac{\dot{a}}{a} \equiv H = \sqrt{\frac{8\pi G}{3}\rho}, \quad (2)$$

the second-derivative of the scale factor depends on ρ and p :

$$\frac{\ddot{a}}{a} = -\frac{4\pi G}{3}(\rho + 3p). \quad (3)$$

For a matter-dominated or radiation-dominated universe $\rho + 3p$ is positive resulting in a negative value for \ddot{a} (deceleration), but for a Λ -dominated universe $\rho + 3p$ is negative, resulting in a *positive* value of \ddot{a} , or an *acceleration* of the scale factor.

Recent independent observations of high-redshift Type-I supernovae by two groups (Perlmutter *et al.* 1999, Riess *et al.* 1998) find that the supernovae are systematically dimmer than they would be if the expansion rate of the universe was decelerating today. So if the observations are correct, then either the expansion of the universe is accelerating today, there is some unknown systematic effect causing high-redshift supernovae to appear dimmer than expected, or the expansion rate of the universe is not given by the Friedmann equations.

V. CONCLUSIONS

The good news in cosmology today is that there is a standard model that seems able to describe the universe in unprecedented detail.

The bad news is that the cosmological standard model seems unnecessarily complicated.

In the cosmological standard model there are many contributions to the present mass-energy density. In terms of the fraction of the critical density, the contributions of the various components are given in Table 2.

A glance at the table brings to mind the remark of Alfonse the Wise when looking over the shoulders of his astronomers as they updated the cosmological standard model of the 13th century, the Ptolemaic model. Upon seeing the collection of epicycles, Alfonse reportedly said, "If I had been present at creation, I would have suggested a simpler arrangement."

One may make the same statement today. Why are there so many contributions to Ω today with roughly equal contributions? Where is the elegance? Where is

component	approximate contribution to Ω
radiation (photons)	0.00007
relativistic neutrinos	0.00003
nonrelativistic neutrinos	0.001
visible baryons	0.001
dark baryons	0.05
dark matter	0.25
dark energy	0.7
total	1.0

TABLE II: Approximate contributions to the total density (constrained to be $\Omega = 1$) from the various components.

the simplicity? It appears to be a universe designed by committee. It does not seem to be the sort of universe one would expect to see listed proudly on the resume of a supreme being. Is the table the modern version of epicycles?

Before abandoning the standard model, let us recall the true story of the demise of epicycles. It is often said that the Copernican model, with all its simplicity, did away with the need for epicycles and the complexity of the Ptolemaic model. Anyone who believes the *original* Copernican model was simpler than the Ptolemaic model should take a look at Book III of *De Revolutionibus*. Copernicus had epicycles in his model; in fact, by some accounts Copernicus had more epicycles than Ptolemy! Copernicus was forced to resort to epicycles because he assumed that planets executed uniform circular motion. Since planets orbit in ellipses with varying velocity (Kepler's first two laws), Copernicus could not account for the observed planetary motions without epicycles. Only after Kepler "corrected" the Copernican model did the heliocentric model become simpler.

Perhaps the central question about the present cosmological standard model is whether Table II resembles the epicycles of Ptolemy or the epicycles of Copernicus. Are the fundamental underpinnings of the model fatally flawed like the Ptolemaic model, or are the basics correct and we now await the 21st century version of Kepler to straighten it out. Time will tell.

Acknowledgments

I would like to thank the organizers of the conference for the opportunity to present this paper. This work was supported by the Department of Energy and NASA (NAG5-10842).

-
- [1] Bahcall, N. A. 2000, Phys. Scripta T85 32.
 - [2] Burles, S., Nollett, K. M., Turner, M. S. 2001, Phys. Rev. D 63, 063512.
 - [3] Chung, D.-H., Kolb, E. W., & Riotto, A. 1999, Phys. Rev. D 59, 023501.
 - [4] Guth, A. H. 1981, Phys. Rev. D 23, 347.
 - [5] Kofman, L., Linde, A. D., and Starobinsky, A. A. 1997, Phys. Rev. D 55, 3258.
 - [6] Kolb, E. W. and Turner, M. S. Turner 1990, *The Early Universe*, (Addison-Wesley, Menlo Park, Ca.).
 - [7] Perlmutter, S. et al. 1999, Ap. J. 517, 565.
 - [8] Schrödinger, E. 1939, Physica 6, 899.
 - [9] Riess, A. G. et al. 1998, Astron. J. 116, 1009.
 - [10] Trimble, V 1987, Ann. Rev. Astron. Astrophys 25, 425.
 - [11] Wittman, D. M., Tyson, J. A., Kirkman, D., Dell'Antonio, J., Bernstein, G. 2000, Nature 405, 143.

CHAIRMAN: E. KOLB

Scientific Secretaries: A. Tronconi, C. Zampolli

DISCUSSION

- *Skinner:*

The WMAP CMB power spectrum seems to indicate very little power on the largest scales, even accounting for cosmic variance. Do you think this is a sign of interesting new physics or just a statistical peculiarity?

- *Kolb:*

Thank you; it is a very interesting question. In agreement with COBE, WMAP sees anomalously low quadrupole and sextupole moments. There is a lack of correlations in CMB fluctuations on very large scales. So, for some reasons, on angles larger than 60 degrees in the sky there seems to be a lack of power in the correlation function. Now, some people have taken this to imply, in fact, that there is no power there and that is something fundamental. One thing that comes to mind is that we might be looking at the fundamental size for the universe and that this just hides correlations on larger sizes because the universe is smaller than we imagine. So it could be that it is a profound effect. Now, here is the problem: we will not in the future have observations that will come out to be better than this, and we may have to live with this statistical fluctuation that is down there unless we decide to go ten billion light years away and make the observation from another location. That would be something very interesting to do, but the funding agencies have not approved it yet. So it is very difficult to know what to make of this. People are now playing different statistical tricks to access the significance of this low point and that low point. You seem to get different readings on whether it is significant depending on whether you take a frequentist approach or a Bayesian approach. Now we know that all reasonable people are Bayesians, and if you take the Bayesian approach then the probability is one part in a couple of hundred. Perhaps you put your thumb on something that maybe a little chinch in the standard picture we may have something profound there. We just do not know.

- *Bozza:*

Could you say something about the tuning of the parameters of inflation models to reproduce physical observations?

- *Kolb:*

The question has to do with tuning parameters in the inflaton potential during inflation. Now one of the hallmarks for the inflaton potential is that it must be an extraordinarily flat potential. You can express this in two ways: one is that you just imagine that the potential is $\lambda\phi^4$ then λ has to be something as 10^{-13} to 10^{-14} . Another

way of studying the extraordinarily unusual feature of the potential is just to imagine that M , the mass of the inflaton, is 10^{13} GeV, but the displacement of the field from the origin is Planckian, 10^{19} GeV, so you are sampling a very flat potential. When new inflation was first proposed, people thought the flatness was very unusual and a very unattractive feature. Now it may remain to be an unattractive feature, but it is a feature we are used to seeing. We do not have a compelling explanation for it; however there are flat directions like moduli fields in supersymmetry. Maybe it is telling us something, that not every normal potential that you would draw qualifies as an inflaton potential. Maybe it is not a bug, but a feature.

- *Oswald*

If one looks at the universe at small scales, then it is not homogeneous; there are galaxies, clusters, etc. To account for that, one should assume initial fluctuations in the energy spectrum. Such fluctuations are, however, not stable: an excess of mass will produce a gravitational field, which can attract more mass. If one now interpolates back to very early times, then these fluctuations must have been "unnaturally" small. Does inflation explain this?

- *Kolb*:

One of the reasons to have a flat potential is in order to have those fluctuations be small. So, at the time of recombination, the density perturbations in some dimensionless unit, $\delta\rho/\rho$, is 10^{-5} . Now you are sitting there with a density fluctuation of 10^{30} compared to the average today. As you say, in a matter-dominated era, perturbations grow by gravitational instability. If you have a flat enough inflaton potential, if you swallow that, you can naturally generate fluctuations that are of the order of 10^{-5} . There are literally hundreds of models of inflation that are either completely disconnected or connected very strongly to well motivated particle physics models that can accomplish this.

- *Gripaios*:

Experiment, if it is to be believed, tells us that there was a period of cosmic acceleration some time after $z=1$. Can this experiment, or will future experiments, tell us anything else about the pattern of acceleration, such as when it began or ended or anything else?

- *Kolb*:

What we hope to do is to take the classical Hubble diagram out to redshifts larger than one, but not too much larger than one (perhaps to redshifts of order 2, maybe, 2.5). If the effect is a cosmological constant, by the time you look at redshift 2, you should see the Universe matter-dominated and not dominated by the effect of acceleration. So if you trace back to large enough z , you should see the decelerating phase and see a Universe that is matter-dominated. That is one of the goals of the next generation of Supernovae experiments. This may culminate in the launch of a satellite to observe high-redshift supernovae.

- *Balbinot:*

You mentioned today the issues of inflation transplanckian physics: are you referring to the problem of modes that had once transplanckian frequencies?

- *Kolb:*

Thanks for the question. The idea of transplanckian physics goes back to the work of several people maybe about 10 years ago. I mentioned that in order to calculate the perturbations, you have to solve a mode equation for a field which is a combination of the inflaton field and scalar perturbations. In order to solve the Klein-Gordon equation for this field, you have to impose boundary conditions, and the boundary conditions are conveniently imposed at infinite wave number. So at infinite wave number, you assume that it is something known as the adiabatic vacuum that essentially is just plain waves ($\exp(\pm i \omega t)$). But if you go to infinite momentum, you are looking at modes smaller than the Planck length scale. The final result is sensitive to the choice of boundary conditions. However I think it is an issue and not a problem. It is reasonable to assume that by the time you get the scales that are slightly larger than the Planck length, you are in the adiabatic vacuum, because if you would not be in the adiabatic vacuum there would be so much energy density around in these excited modes that you would remove the possibility of inflation. So there is a self-consistency argument that suggests that the only reasonable initial state to pick is related to the adiabatic vacuum. Now this is an issue that comes up in inflation and is also an issue that arose a long time ago in the study of black holes, and it is an issue that to my mind has not had a clear resolution. One of the things that may help us with inflation is there seems to be a hierarchy in scales between the Planck energy (10^{19} GeV) and the expansion rate of the universe during inflation which seems to be similar to 10^{12} - 10^{13} GeV. So most people believe that any transplanckian effects are suppressed by something like $(10^{12}/10^{19}$ GeV) 2 . It would be really wonderful if we could do observations with enough accuracy to start seeing those transplanckian effects. So the final answer is that it is an issue we should not close our eyes to. I do not take the point of view that this is a real problem for the standard model of inflation.

- *Krotov:*

You had a lot of candidates for the dark non-baryonic matter like axions, gravitinos, neutralinos... Why do we not see these particles in the Universe? Are there any consequences of their existence?

- *Kolb:*

That is a very good question. We are attempting to observe dark matter in the present universe; for instance, a cosmic background of axions and that is being searched for. There are also other ways to search for axions, axions from the sun, axions decaying around us to make optical photons or infrared or something like that. There is also a huge amount of effort that is going into detecting Dark Matter

neutralinos. Right in front of your nose there is Dark Matter. The challenge is to find it. It is very weakly interacting.

- *Raggi:*

What is the impact of recent ϵ'/ϵ measurements on cosmology? What other CP violation measurements are interesting for cosmologists?

- *Kolb:*

First of all, understanding the origin, in nature, of CP violation is an important issue for baryogenesis, for our understanding the origin of baryon asymmetry. That does not mean that every single parameter you measure in the laboratory associated with CP violation will be plugged into a formula that will give you the baryon asymmetry today. So, I do not believe that result for ϵ'/ϵ will get plugged in the same formula, saying the present baryon asymmetry is ϵ'/ϵ times this or whatever. However, knowing whether CP violation only comes from CKM, or whether it also arises from something different is important. A standard model of CP violation would be extraordinarily useful. In terms of what parameters I would like to see measured, this week I am working on leptogenesis, so I would like to see CP violation in the neutrino sector completely mapped out. I will have other opinions next week.

- *D'Enterria:*

This morning it was announced online that British Astronomers had discovered 3 elliptical galaxies whose rotational speed can be perfectly explained by classical Kepler dynamics. This result will appear in "Science" this week. Do you think that the fact that certain types of galaxies appear to be rich in Dark Matter while others seem to be deficient, constrains your list of Dark Matter candidates?

- *Kolb:*

One of the hopes of cosmologists is that some combination of astronomical observations will give us some information about the nature of dark matter, other than it is there with a certain density. Observations may tell us something about the interaction properties of Dark Matter; whether Dark Matter can be segregated from luminous matter or not. One of the things we do not know, for instance, is whether there are Dark Matter clumps that have no light associated with them. That is something we can look for in weak lensing experiments. The general idea of the segregation or not of dark matter and luminous matter is something that may shed light on the interaction properties of Dark Matter. So in that regard, it is observations like that that have the potential of being useful.

- *D'Enterria:*

We have heard of many cosmological effects being directly related to the phase transitions of the very early Universe (at the Planck scale, GUT or the Electroweak

phase transition). Is there any observational cosmological consequence of the quark-hadron phase transition that occurred a few seconds after the Big Bang?

- *Kolb:*

People have discussed the possibility that the quark-hadron phase transition was strongly first order and made inhomogeneities, which then could collapse into black holes. The holes would have solar mass or Jupiter mass. They could be the Dark Matter. That possibility is disfavoured because everyone believes that quark-hadron transition is not strongly first order, and probably not first order at all. Other possibilities of observable effects in the quark-hadron transition might be that inhomogeneities in the baryon density feed into inhomogeneities during big bang nucleosynthesis. I think much of the motivations for doing that have disappeared. The quark-hadron transition does not seem to have left behind any stable topological remnant that we can look for today.

- *Dainese:*

To what extent do you think heavy ion experiments can contribute to improving the knowledge of this stage of the Universe evolution? What is the intention of the cosmology community for heavy ion experiments?

- *Kolb:*

Honestly, the cosmological community is not paying very much attention to what is going on heavy ion physics. I think this is probably a bad thing and we should pay more attention to it. I am confident that you will figure it out and tell us how it works, give us the phase diagrams and things like that, and then we can ask questions like what would be the remnants of what went before. Remember the big bang was an experiment was done 14 billion years ago, so not only do you have to know how it happened, but what it left behind: something we can go out and study today. Much of what we learn from early universe cosmology involves a departure from equilibrium. Insofar as the universe was always in equilibrium, there is nothing we can learn, there is just no information there. Things like big bang nucleosynthesis are a departure from nuclear statistical equilibrium. Inflation is certainly a departure from equilibrium. Production of Dark Matter seems to be a departure from equilibrium. So what we learn about the universe is by looking at its imperfections, its departures from equilibrium. Phase transitions are a physical phenomenon that may be a departure from equilibrium, so any phase transition around would be very important for us to study and understand.

- *Cerri:*

Back to dynamical evidence of Dark Matter: you hinted to the possibility of a Dark Matter halo “flattening” due to angular momentum effects. Is there evidence of this or was that just speculative?

- *Kolb:*

There is some weak evidence for a flattening of the Dark Matter halo in several galaxy clusters by looking at x-ray gas around the clusters. This evidence is very interesting; something that people will study with CHANDRA and the next generation of x-ray telescopes, and maybe there are other ways we can confirm the flattening of the halo. Something else that is interesting about Dark Matter is whether Dark Matter has substructures or not. In the usual picture, Dark Matter is considered to be a uniform distribution in the galaxy. But what we expect, in fact, is that maybe Dark Matter clumps in our galaxy.

- *Cerri:*

Interpretation of the dynamic evidence for Dark Matter in spiral galaxies, pioneered by Van Alsdad and Sancisi, always was in the direction of minimizing the Dark Matter contribution (the so-called “Maximum disk ansatz”). What do we know nowadays on the $M_{\text{vis}}/M_{\text{dark}}$ in those systems?

- *Kolb:*

Vera Rubin and collaborators have compiled the rotation curves of a couple of hundred spiral galaxies. Almost all of them show a flat rotation curve and no sign of going down, but a couple of them show a fall-off. It is said that there is no such thing as a normal galaxy: if you've seen one galaxy you have seen one galaxy. The distribution of DM in galaxies is complicated by the fact that galaxies form from something we call mergers and acquisitions. So the big things eat the little things. It is sort of a cannibalistic process.

- *Pinfold:*

If we do observe a primordial tensor spectrum, then we can deduce the energy scale at which inflation occurred and maybe more. Is there any chance, in your opinion, that future experiments will be able to measure this tensor contribution?

- *Kolb:*

Inflation has made maybe 8 independent predictions; all, in principle, falsifiable. Six of the eight are consistent with observations today. Inflation also predicts the background of tensor perturbations, i.e., gravitational waves, which have not been detected. Now there are two ways to look for gravitational waves: one is just looking at the effects of gravitational waves on the C_l 's, the angular power spectrum of the microwave background. That is probably not the way gravitational waves will be detected. They will probably be detected by their effect on the polarization pattern of the microwave background. People are now talking about a dedicated satellite looking for polarization. The other approach is to look at it directly for the background gravitational waves that were produced during inflation. We just do not yet know the energy scale of inflation, so we cannot predict whether we will ever detect gravitational waves from inflation.

- *Sykora:*

Suppose the microwave background is isotropic only in one preferred system. Does it means that the Lorentz invariance is broken? And is it observed?

- *Kolb:*

The CMB is in fact isotropic in only one reference frame, i.e. the reference frame of homogeneity and isotropy of an expanding universe. It does not mean a fundamental breaking of Lorentz symmetry; you can choose to do a calculation in any frame that you wish. So when you have a thermal background, it is always isotropic in one reference frame.

- *Sykora:*

On one of your sheets you have mentioned a possible violation of Lorentz invariance. At which scale can it take place?

- *Kolb:*

Well, if you have branes and bulk and the bulk is warped, you can have violation of Lorentz invariance essentially in the infrared, and you can have strange things like a different propagation speed for gravitational waves signals that can go through the bulk while light will be stuck on the brane. This could be on astronomical scales.

- *Sykora:*

Can I imagine something like phase-transition of space-time, like gas-liquid transition?

- *Kolb:*

I do not know...

How many dimensions are really compactified?

I. Antoniadis¹

Department of Physics, CERN
Theory Division
CH-1211 Geneva 23, Switzerland

Abstract

The recent understanding of string theory opens the possibility that the string scale can be as low as a few TeV. The apparent weakness of gravitational interactions can then be accounted for by the existence of large internal dimensions, in the submillimeter region. Furthermore, our world must be confined to live on a brane transverse to these large dimensions, with which it interacts only gravitationally. In my lecture, I describe briefly this scenario which gives a new theoretical framework for solving the gauge hierarchy problem and the unification of all interactions. I also discuss its main properties and implications for observations at both future particle colliders, and in non-accelerator gravity experiments. Such effects are for instance the production of Kaluza-Klein resonances, graviton emission in the bulk of extra dimensions, and a radical change of gravitational forces in the submillimeter range.

¹On leave from Centre de Physique Théorique (UMR 7644 of CNRS), Ecole Polytechnique, F-91128 Palaiseau.

1 Introduction

In all physical theories, the number of dimensions is a free parameter fixed to three by observation, with one exception: string theory, which predicts the existence of six new spatial dimensions. This is the only known theory today that unifies the two great discoveries of the 20th century: quantum mechanics, describing the behavior of elementary particles, and Einstein's General Relativity, describing gravitational phenomena in our Universe.

String theory replaces all elementary point-particles that form matter and its interactions with a single extended object of vanishing width: a tiny string. Thus, every known elementary particle, such as the electron, quark, photon or neutrino, corresponds to a particular vibration mode of the string (see Fig. 1). The diversity of these particles is due to the different properties

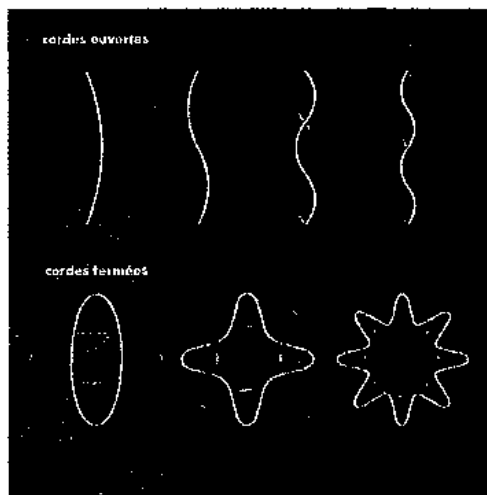


Figure 1: In string theory, the elementary constituent of matter is a minuscule string, having vanishing width but finite size. It can be open with free ends (upper part), or closed (lower part). Its vibration modes, like the ones shown above in two dimensions, correspond to various elementary particles.

of the corresponding string vibrations.

How can it be tested? If our universe has really six additional dimensions, we should observe new phenomena related to the existence of these dimensions. Why has nobody detected them until now? String theorists had an answer for a long time: because the size of the new dimensions is very small, in contrast to the size of the other three that we know, which is infinitely large.

An infinite and narrow cylinder for example is a two-dimensional space, with one dimension

forming a very small cycle: one can move infinitely far away along the axis, while one returns back at the same point when moving along the orthogonal direction (see Fig. 2). If one of the

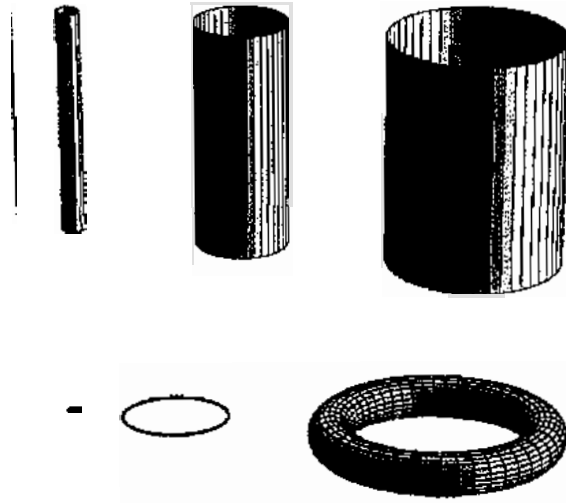


Figure 2: Possible forms of small extra dimensions of space. Far away they are unobservable, but at distances comparable to their size we start feeling their existence and exploring their shapes.

three known dimensions of space was small, say of millimeter size, we would be flat and, while we could move freely towards left or right, forward or backward, it would be impossible to do more than a few millimeters up or down where space ends.

For a long time, string physicists thought that the six extra dimensions were extremely small, having the smallest possible size of physics, associated to the Planck length $\sim 10^{-35}$ meters. In fact, strings were introduced to describe gravitation whose strength becomes important and comparable to the strength of the other three fundamental interactions (electromagnetic, nuclear strong and weak) at very short distances, of the order of the Planck length. It was then natural to assume that the size of the extra dimensions should be of the same order. In this case, the manifestation of new phenomena associated to the extra dimensions are by far out of experimental reach, at least in particle accelerators. Indeed, the Large Hadron Collider (LHC) which is the biggest accelerator under construction at CERN will explore short distances, only up to 10^{-19} meters.

The situation changed drastically recently. During the last three years, more and more theorists examine the possibility that the new dimensions of string theory may be much larger than we thought in the past [1, 2]. These ideas lead in particular to experimental tests of string theory that can be performed at TEVATRON and LHC, or at future colliders.

2 The universe as a braneworld

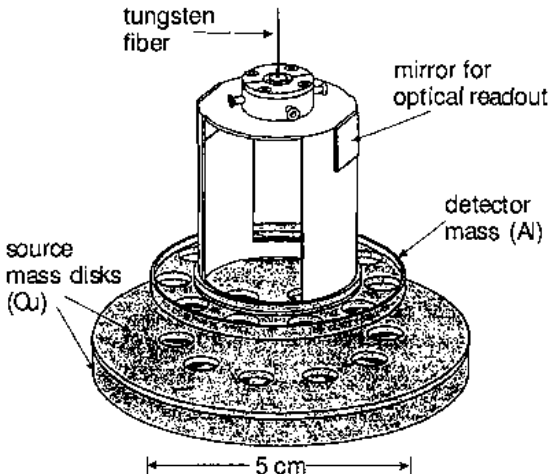


Figure 3: The Eöt-Wash short-range torsion pendulum experiment has tested the validity of Newton's law down to 0.2 millimeters [3]. Thus, the size of gravitational extra dimensions is constrained by this value. By improving the sensitivity of measure, one could see violations of Newtonian gravity at shorter distances. The weakness of gravity complicates considerably the experiments: there are several sources of background noise due to other forces that should be eliminated using appropriate devices. At very short distances, one should consider even the Casimir attraction due to vacuum fluctuations.

A particularly attractive scenario is when the string scale is in the TeV region, which stabilizes the mass hierarchy problem without need of supersymmetry [2]. A possible realization of this idea without experimental conflict is in models possessing large extra dimensions along which only gravity propagates: gravity appears to us very weak at macroscopic scales because its intensity is spread in the "hidden" extra dimensions. On the other hand, at TeV energies, it becomes comparable in strength with the other interactions, i.e. 10^{32} times stronger than what we believed in the past. In order to increase the gravitational force without contradicting

present observations, one has to introduce at least two such extra dimensions of size that can be as large as a fraction of a millimeter. At these distances, gravity should start to deviate from Newton's law, which may be possible to explore in laboratory experiments [3] (see Fig. 3).

A convenient perturbative framework realizing this idea is one of the five string theories, called type I, that contains simultaneously closed and open strings [2]. Our universe should be localized on a hypersurface, i.e. a membrane extended in p spatial dimensions with $p < 7$, called p -brane (see Fig. 4). Closed strings describe gravity and propagate in all nine dimensions of space: in those extended along the p -brane, as well as in the transverse ones. On the contrary, the endpoints of open strings describing the other (gauge) interactions are confined on the p -brane.

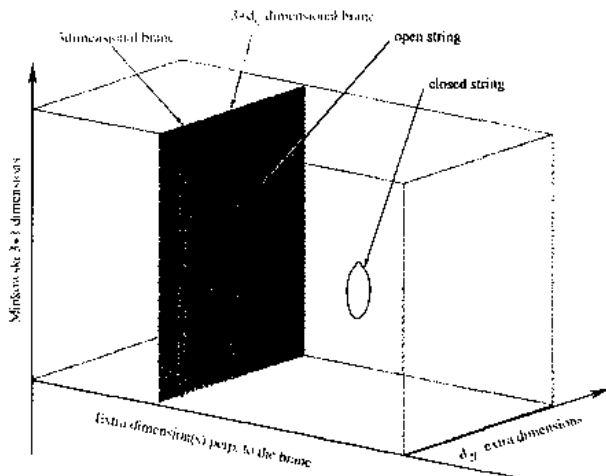


Figure 4: In the type I string framework, our Universe contains, besides the three known spatial dimensions (shown by a vertical line (denoted 3-dimensional brane)), some extra dimensions ($d_{\parallel} = p - 3$) parallel to our world p -brane (middle plane) along which the light described by open strings propagates, as well as some transverse dimensions (rest of the space) where only gravity described by closed strings can propagate. The longitudinal extra dimensions have the string size of the order of 10^{-18} meters, while the size of the transverse dimensions varies in the range of 10^{-24} meters to a fraction of a millimeter.

Obviously, our p -braneworld must have at least the three known dimensions of space. But it may contain more as opposed to the transverse dimensions that interact with us only gravitationally, the "longitudinal" to the brane extra dimensions can be "seen" by the light at sufficiently high energies, giving rise to the production of massive Kaluza-Klein particles in accelerators [4].

On the other hand, the existence of the extra large (sub)millimeter dimensions, transverse to our p -brane universe, guarantee that gravitational interactions appear to us very weak at macroscopic distances, larger than a millimeter. The size of these transverse dimensions varies from a fraction of millimeter (in the case of two) to a Fermi (10^{-14} meters, in the case of six). Their characteristic signal in particle colliders is graviton emission into the bulk, leading to missing energy that escapes detection [2, 5].

3 Limits on the size of extra dimensions and the string scale

3.1 Compactification of extra dimensions

Suppose that space-time has D extra dimensions compactified on a D -dimensional torus of volume $(2\pi)^D R_1 R_2 \cdots R_D$. The states propagating in this $(4+D)$ -dimensional space are seen from the four-dimensional point of view as having a (squared) mass (assuming periodicity of the wave functions along each compact direction):

$$M_{KK}^2 \equiv M_n^2 = m_0^2 + \frac{n_1^2}{R_1^2} + \frac{n_2^2}{R_2^2} + \cdots + \frac{n_D^2}{R_D^2}, \quad (1)$$

with m_0 the four-dimensional mass and n_i non-negative integers. The states with $\sum_i n_i \neq 0$ are called Kaluza-Klein (KK) states. An important remark is that not all states can propagate in the whole space. Some might be confined in subspaces with no KK excitations in the transverse directions. The simplest example of such a situation appears in compactification on S^1/Z_2 orbifolds obtained by gauging the Z_2 parity: $y \rightarrow -y \bmod 2\pi R$, where $y \in [-\pi R, \pi R]$ span the fifth coordinate. The spectrum of states has some interesting properties: (i) only states invariant under this Z_2 (which acts also on the gauge quantum numbers) are kept while the others are projected out; (ii) new ("twisted") states, localized at the end points have to be included. They have quantum numbers and interactions that were not present in the unorbifolded original 5-dimensional model. As they can not propagate in the extra-dimension, they have no KK excitations; (iii) The even states can have non-derivative renormalizable couplings to localized states. For instance, the couplings of massive KK excitations of even gauge bosons to localized fermions are given by:

$$g_n = \sqrt{2} \sum_i e^{-\ln \delta \sum_i \frac{n_i^2 l_s^2}{2 R_i^2}} g_0 \quad (2)$$

where $l_s \equiv M_s^{-1}$ is the string length and $\delta = 16$ in this case of Z_2 orbifolding. The $\sqrt{2}$ comes from the relative normalization of $\cos(\frac{n_i y}{R_i})$ wave function with respect to the zero mode while the exponential damping is a result of tree-level string computations [6].

Another example is obtained with intersecting branes (see Figs. 5 and 6). When the angle between the intersecting branes is $\pi/2$, the localized strings behave exactly as the Z_2 twisted

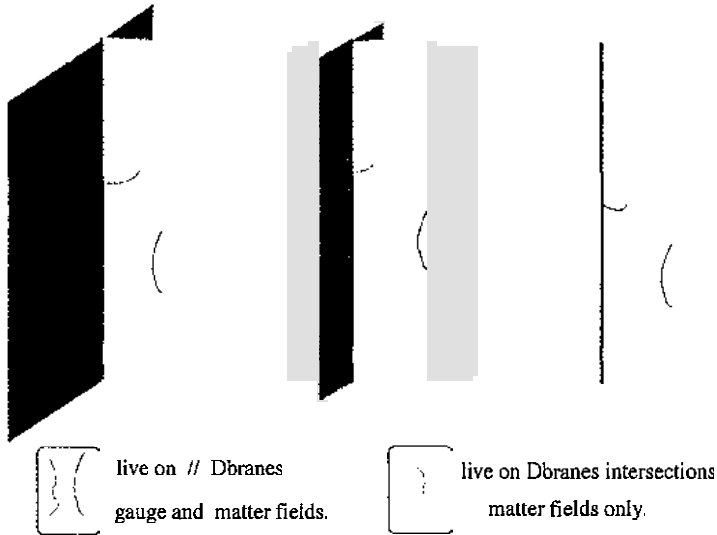


Figure 5: Zero modes of open strings stretched between two branes give rise to matter localized at their intersection. One of the branes is shown “losing” one of its longitudinal dimensions as the size of the latter shrinks. The final result is a small brane inside a bigger one.

states described above. The exponential form factor of the coupling of KK excitations can be viewed as the fact that the branes intersection has a finite thickness. In fact the interaction of the KK excitations of the gauge fields (on the big branes) $A^\mu(x, \vec{y}) = \sum_{\vec{n}} A_{\vec{n}}^\mu \exp i \frac{n_i y_i}{R_i}$ with the charge density $j_\mu(x)$ associated to massless localized fermions is described by the effective Lagrangian [7]:

$$\int d^4x \sum_{\vec{n}} e^{-\ln \delta \sum_i \frac{n_i^2 l_s^2}{2 R_i^2}} j_\mu(x) A_{\vec{n}}^\mu(x), \quad (3)$$

which can be written after Fourier transform as

$$\int d^4y \int d^4x \left(\frac{1}{l_s^2 2\pi \ln \delta} \right)^2 e^{-\frac{\vec{x}^2}{2l_s^2 \ln \delta}} j_\mu(x) A^\mu(x, \vec{y}), \quad (4)$$

from which we read that the localized fermions are felt as forming a Gaussian distribution of charge $e^{-\frac{\vec{x}^2}{2\sigma^2}} j_\mu(x)$ with a width $\sigma = \sqrt{\ln \delta} l_s \sim 1.66 l_s$.

3.2 Scattering of four localized fermions

The total amplitudes for the scattering of four fermions depend on the string coupling $g_s = g_{YM}^2$, the string scale $M_s \equiv 1/l_s$, the compactification radii R_i and on kinematical invariants that can be expressed in terms of the Mandelstam variables $s = -(k_1 + k_2)^2$, $t = -(k_2 + k_3)^2$ and $u = -(k_1 + k_3)^2$. The result can be decomposed as:

$$\mathcal{A} = \mathcal{A}^{(0)} + \mathcal{A}^{(KK)} + \mathcal{A}_w^{cont} + \mathcal{A}_{osc}^{cont}, \quad (5)$$

where $\mathcal{A}^{(0)}$ is the contribution of the lightest states (for example from standard model fields), $\mathcal{A}^{(KK)}$ the one from KK states of the form:

$$-\left[\bar{\psi}^{(1)}\gamma_M\psi^{(2)}\bar{\psi}^{(4)}\gamma^M\psi^{(3)}\right]\frac{g_s}{l_s^{-4}\prod_{i=1}^4 R_i}\sum_{m_i \in \mathbf{Z}-\{0\}}\frac{\delta^{-\sum_{i=1}^4 \frac{m_i^2 l_s^2}{R_i^2}}}{s - \sum_{i=1}^4 \frac{m_i^2}{R_i^2}}, \quad (6)$$

where $\delta = \delta(\theta)$ varies between $\delta = 16$ for $\theta = \pi/2$ to $\delta \rightarrow \infty$ when $\theta \rightarrow 0$. Note that the latter limit corresponds to the conservation of KK momenta in the absence of localization as seen in Fig. 6. The terms \mathcal{A}_w^{cont} and \mathcal{A}_{osc}^{cont} contain the contribution of long strings stretched between the intersections while winding around the compact dimension and the ones from heavy string oscillation modes, respectively. In the large compactification radius limit \mathcal{A}_w^{cont} is exponentially suppressed and we are left with²:

$$\mathcal{A}_{osc}^{cont} = -\left[\bar{\psi}^{(1)}\gamma_M\psi^{(2)}\bar{\psi}^{(4)}\gamma^M\psi^{(3)}\right](\frac{g_s}{M_s})^2 \int_0^1 \frac{dx}{x} \left(\frac{1}{[F_\theta(x)]^2} - 1\right)$$

where θ is the angle between the branes. For $\theta \rightarrow \frac{\pi}{2}$ we have $\int_0^1 \frac{dx}{x} \left(\frac{1}{[F_\theta(x)]^2} - 1\right) \rightarrow 0.59$. For $\theta \rightarrow 0$, $F_\theta(x) \rightarrow 1$ and this contact term vanishes. There is no tree level dimension six effective operator in the case of open strings ending on parallel branes but the final amplitude can be written as:

$$\mathcal{A}(s, t) = \mathcal{A}_{point}(s, t) \cdot \frac{\Gamma(1 - l_s^2 s) \Gamma(1 - l_s^2 t)}{\Gamma(1 - l_s^2 s - l_s^2 t)} = \mathcal{A}_{point}(s, t) \cdot \left[1 - \frac{\pi^2}{6} \frac{st}{M_S^4} + \dots\right] \quad (7)$$

where \mathcal{A}_{point} is the result usually derived from the (up-to-two-derivatives) low energy effective Lagrangian, while the dimension-eight operator here proportional to $\frac{st}{M_S^4}$ represents the tree-level lowest order correction and originates from the form factor due to the string-like structure.

3.3 The scenario

In order to pursue further, we need to provide the quantum numbers and couplings of the relevant light states. We consider (see Fig. 4):

²The generic cases with finite radii can be found in [7]

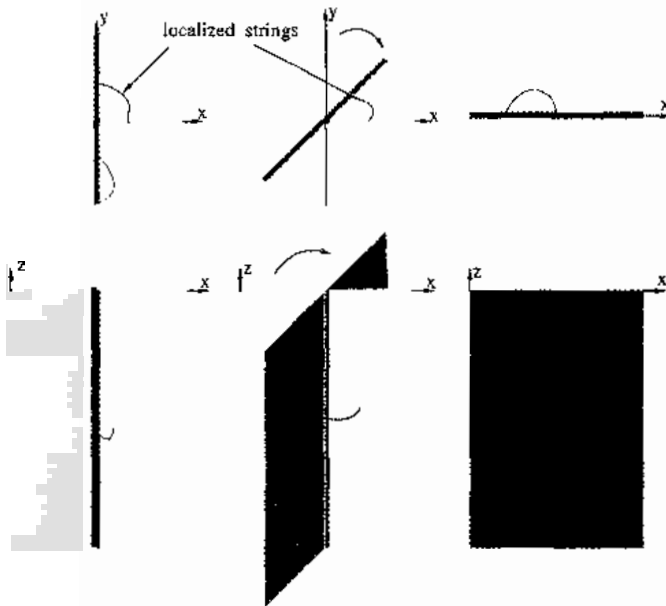


Figure 6: Rotating two branes from orthogonal position $\theta = \pi/2$ to parallel one $\theta = 0$.

- Closed strings correspond to gravitons which describe fluctuations of the metric propagating in the whole space.
- The gauge bosons propagate on a $(3+d)$ -branes. They correspond on Fig. 4 to the open strings with both ends on the big brane.
- The matter fermions, quarks and leptons, are localized on 3-branes (the small branes inside the bigger one on Fig. 4) and have no KK excitations. Our results strongly depend on this assumption. Instead, the possible localization of the Higgs scalar, as well as the possible existence of supersymmetric partners, do not lead to major modifications for most of the obtained bounds.

3.4 Extra-dimensions along the world brane: KK excitations of gauge bosons

The experimental signatures of extra-dimensions are of two types:

- Observation of resonances due to KK excitations. This needs a collider energy $\sqrt{s} \gtrsim 1/R_{\parallel}$ at LHC (see Fig. 7) [4]. The discovery limits in the case of one extra-dimension are given

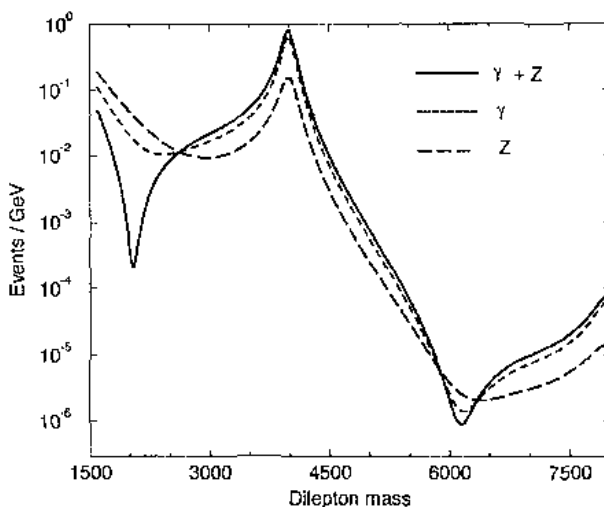


Figure 7: If there is an extra dimension of size 10^{-18} meters, felt by the electroweak interactions, LHC should produce the first Kaluza-Klein states of the photon and of the Z boson. We can then detect the electron-positron pairs produced by the disintegration of these states. The number of the expected events is computed as a function of the energy of the pair in GeV. From highest to lowest: excitation of photon+ Z , photon and Z boson.

in Table 1.

- Virtual exchange of the KK excitations which lead to measurable deviations in cross-sections compared to the standard model prediction. The exchange of KK states gives rise to an effective operator discussed above in section 3. For $d > 1$ the result depends then on both parameters $R_{||}$ and M_s . Example of analysis for $d = 2$ can be found in Ref. [4]. The simpler case of $d = 1$ has been studied in detail. Possible reaches of colliders experiments [4] are summarized in Table 1.

Provided with good statistics, there are some ways to help distinguish the corresponding signals from other possible origin of new physics, such as models with new gauge bosons: (i) the observation of resonances located practically at the same mass value; (ii) the heights and widths of the resonances are directly related to those of standard model gauge bosons in the corresponding channels; (iii) the size of virtual effects do not reproduce a tail of Bright-Wigner resonance and a dip is expected just before the resonance of the photon+ Z , due to the interference between the two.

Table 1: Limits on $R_{||}^{-1}$ in TeV at present and future colliders. The luminosity is given in fb^{-1} .

Collider	Luminosity	Gluons	W^\pm	$\gamma + Z$
Discovery of Resonances				
LHC	100	5	6	6
Observation of Deviation				
LEP 200	4×0.2	-	-	1.9
TevatronI	0.11	-	-	0.9
TevatronII	2	-	-	1.2
TevatronII	20	4	-	1.3
LHC	10	15	8.2	6.7
LHC	100	20	14	12
NLC500	75	-	-	8
NLC1000	200	-	-	13

3.5 Extra-dimensions transverse to the brane world: KK excitations of gravitons

During a collision of center of mass energy \sqrt{s} , there are $(\sqrt{s}R_{||})^{d_{\perp}}$ KK excitations of gravitons with mass $m_{KK\perp} < \sqrt{s} < M_s$, which can be emitted to the bulk [2, 5] (see Fig. 8). Each of these states looks from the four-dimensional point of view as a massive, quasi-stable, extremely weakly coupled (s/M_{pl}^2 suppressed) particle that escapes from the detector. The total effect is a missing-energy cross section roughly of order $\frac{(\sqrt{s}R_{||})^n}{M_{pl}^2} \sim \frac{1}{s} (\frac{\sqrt{s}}{M_s})^{n+2}$. Explicit computation of these effects leads to the bounds given in Table 2 [5] while astrophysical bounds [8, 9] arise from the requirement that the radiation of gravitons should not carry on too much of the gravitational binding energy released during core collapse of supernovae. The best cosmological bound [10] is obtained from requiring that decay of bulk gravitons to photons does not generate a spike in the energy spectrum of the photon background measured by the COMPTEL instrument. The bulk gravitons are themselves expected to be produced just before nucleosynthesis due to thermal radiation from the brane. The limits assume that the temperature was at most 1 MeV as nucleosynthesis begins, and become stronger if this temperature is increased. While the obtained bounds for $R_{||}^{-1}$ are smaller than those that could be checked in table-top experiments probing macroscopic gravity at small distances, one should keep in mind that larger radii are allowed if one relaxes the assumption of isotropy, by taking for instance two large dimensions with different radii.

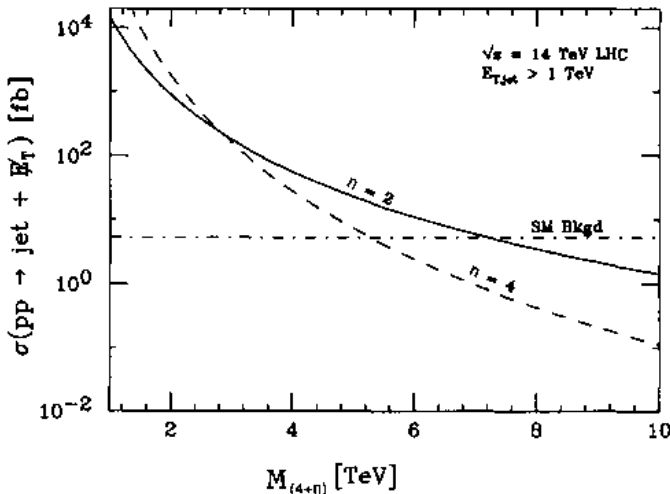


Figure 8: Missing energy due to graviton emission in the LHC experiment, as a function of the fundamental scale $M_{(4+n)}$ of quantum gravity that propagates in n large transverse dimensions. It is produced together with a hadronic jet that one detects in the collision of the two proton beams. The figure shows the expected cross-section for $n = 2$ and $n = 4$ extra dimensions, together with the background (horizontal dotted-dashed line) coming from other known sources.

3.6 Dimension-six effective operators

The dimension-six effective operators are generically parametrized as [11]:

$$\Lambda_{eff} = \frac{4\pi}{(1+\varepsilon)\Lambda^2} \sum_{a,b=L,R} \eta_{ab} \bar{\psi}_a \gamma^\mu \psi_a \bar{\psi}'_b \gamma_\mu \psi'_b \quad (8)$$

with $\varepsilon = 1$ (0) for $\psi = \psi'$ ($\psi \neq \psi'$), where ψ_a and ψ'_b are left (L) or right (R) handed spinors. Λ is the scale of contact interactions and η_{ab} parametrizes the relative strengths of various helicity combinations. The generic analysis of these operators can be found in [7]. We summarize here some of the results.

For $\psi \neq \psi'$ the contributions only from the exchange of the massive open string states on the small brane lead to parameters in eq. (8) as:

$$\eta_{LL} = \eta_{RR} = \eta_{LR} = \eta_{RL} = 1, \quad \Lambda \simeq \sqrt{\frac{4\pi}{0.59g_s}} M_s \quad (9)$$

The signs and relative ratios of the different terms in (8) correspond to what is usually referred to as Λ_{VV}^+ . The present bounds from LEP [12] are of the order of $\Lambda_{VV}^+ \gtrsim 16$ TeV which for

Table 2: Limits on R_\perp in mm from missing-energy processes.

Experiment	$R_\perp(n=2)$	$R_\perp(n=4)$	$R_\perp(n=6)$
Collider bounds			
LEP 2	4.8×10^{-1}	1.9×10^{-8}	6.8×10^{-11}
Tevatron	5.5×10^{-1}	1.4×10^{-8}	4.1×10^{-11}
LHC	4.5×10^{-3}	5.6×10^{-10}	2.7×10^{-12}
NLC	1.2×10^{-2}	1.2×10^{-9}	6.5×10^{-12}
Present non-collider bounds			
SN1987A	3×10^{-4}	1×10^{-8}	6×10^{-10}
COMPTEL	5×10^{-5}	-	-

$g_s = g_{YM}^2 \sim 1/2$, with g_{YM} the gauge coupling, leads to $M_s \gtrsim 2.5$ TeV. A stronger bound can be obtained from the analysis of high precision low energy data in the presence of effective four-fermion operators that modify the μ -decay amplitude. Using the results of Ref. [13], we obtain $M_s \gtrsim 3.1$ TeV.

In the case $\psi = \psi'$ as for Bhabha scattering in e^+e^- there is an additional contribution to the effective operator coming from the operators that are associated with the exchange of other massive oscillation modes leading instead to $0.75\eta_{LL} = 0.75\eta_{RR} \simeq \eta_{LR} = \eta_{RL} = 1$.

On the other hand, the contact interactions due to exchange of KK excitations give rise (for $d_\parallel = 1$ to Ref. [6]):

$$\Lambda_{eff}^{KK} \simeq -\frac{\pi^2}{3(1+\epsilon)} R^2 g_s \sum_{a,b=L,R} \eta_{ab} \bar{\psi}_a \gamma^\mu \psi_a \bar{\psi}_b' \gamma_\mu \psi_b' \quad (10)$$

Experimental constraints on such operators translate into lower bounds on the scale of compactification. For instance exchanges of KK excitations of photon corresponds to $\eta_{ab} = 1$ and $g_s/4\pi = 1/128$ from which we obtain a bound $R^{-1} \gtrsim 2.2$ TeV, using LEP bounds [12] $\Lambda_{VV}^- \gtrsim 14$ TeV. Low energy precision electroweak data lead instead to $R^{-1} \gtrsim 3.5$ TeV [14].

3.7 Dimension-eight effective operators

We consider two generic sources for dimension-eight operators: (i) form factors due to the extended nature of strings eq. (7) (ii) exchange of virtual KK excitations of bulk fields (gravitons, etc).

The limit obtained from dimension-eight operators (i) is of order $M_s \gtrsim 0.63$ TeV [15, 16]. Instead (ii) can not provide reliable model dependent results. The exchange of virtual KK

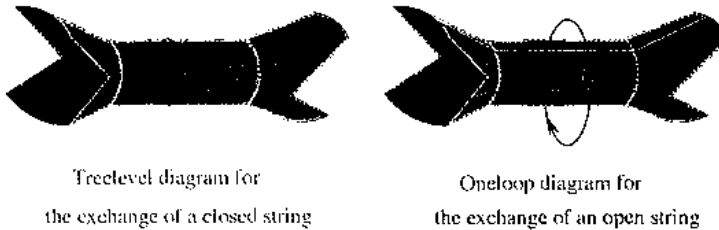


Figure 9: The exchange of virtual gravitons.

excitations of bulk gravitons is described in the effective field theory by an amplitude involving the sum $\frac{1}{M_p^2} \sum_n \frac{1}{s - \frac{n^2}{R^2_1}}$. For $n > 1$, this sum diverges. This means it is sensitive to the UV cut-off physics, thus cannot be computed reliably in field theory. In string models it reflects the ultraviolet behavior of open string one-loop diagrams which are compactification dependent.

In order to understand better this issue, it is important to remember that gravitons and other bulk particles correspond to excitations of closed strings. Their tree-level exchange of order g_s^2 is described by a cylinder which can also be seen as an annulus corresponding to an open string describing a loop (see Fig. 9). First, the result of such one-loop diagrams is compactification dependent. Second, they correspond to box diagrams in a gauge theory which are of order g_{YM}^4 thus smaller by a factor $g_s = g_{YM}^2$ compared to the ones in (i).

4 Gravity modification and sub-millimeter forces

Besides the spectacular experimental predictions in particle accelerators, string theories with large volume compactifications and/or low string scale predict also possible modifications of gravitation in the sub-millimeter range, which can be tested in “table-top” experiments that measure gravity at short distances. There are three categories of such predictions:

- (i) Deviations from the Newton’s law $1/r^2$ behavior to $1/r^{2+n}$, for n extra large transverse dimensions, which can be observable for $n = 2$ dimensions of (sub)-millimeter size. This case is particularly attractive on theoretical grounds because of the logarithmic sensitivity of Standard Model couplings on the size of transverse space [17], which allows to determine the desired hierarchy [18], but also for phenomenological reasons since the effects in particle colliders are maximally enhanced [5]. Notice also the coincidence of this scale with the possible value of the cosmological constant in the universe that recent observations seem to support.
- (ii) New scalar forces in the sub-millimeter range, motivated by the problem of supersymmetry

breaking, and mediated by light scalar fields φ with masses [19, 20, 2, 21]:

$$m_\varphi \simeq \frac{m_{susy}^2}{M_P} \simeq 10^{-4} - 10^{-6} \text{ eV}, \quad (11)$$

for a supersymmetry breaking scale $m_{susy} \simeq 1 - 10 \text{ TeV}$. These correspond to Compton wavelengths in the range of 1 mm to 10 μm . m_{susy} can be either the KK scale $1/R$ if supersymmetry is broken by compactification [20, 19], or the string scale if it is broken “maximally” on our world-brane [2, 21]. A model independent and universal attractive scalar force is mediated by the radius modulus (in Planck units)

$$\varphi \equiv \ln R, \quad (12)$$

with R the radius of the longitudinal (\parallel) or transverse (\perp) dimension(s), respectively. In the former case, the result (11) follows from the behavior of the vacuum energy density $\Lambda \sim 1/R_\parallel^4$ for large R_\parallel (up to logarithmic corrections). In the latter case, supersymmetry is broken primarily on the brane only, and thus its transmission to the bulk is gravitationally suppressed, leading to masses (11). Note that in the case of two-dimensional bulk, there may be an enhancement factor of the radion mass by $\ln R_\perp M_s \simeq 30$ which decreases its wavelength by roughly an order of magnitude [18].

The coupling of the radius modulus (12) to matter relative to gravity can be easily computed and is given by:

$$\sqrt{\alpha_\varphi} = \frac{1}{m} \frac{\partial m}{\partial \varphi} \quad ; \quad \alpha_\varphi = \begin{cases} \frac{\partial \ln \Lambda_{QCD}}{\partial \ln R} \simeq \frac{1}{3} & \text{for } R_\parallel \\ \frac{2n}{n+2} = 1 - 1.5 & \text{for } R_\perp \end{cases}, \quad (13)$$

where m denotes a generic physical mass. In the upper case of a longitudinal radius, the coupling arises dominantly through the radius dependence of the QCD gauge coupling [20], while in the lower case of transverse radius, it can be deduced from the rescaling of the metric which changes the string to the Einstein frame and depends on the dimensionality of the bulk n (varying from $\alpha = 1$ for $n = 2$ to $\alpha = 1.5$ for $n = 6$) [18]. Moreover, in the case of $n = 2$, there may be again model dependent logarithmic corrections of the order of $(g_s/4\pi) \ln RM_s \simeq \mathcal{O}(1)$. Such a force can be tested in microgravity experiments and should be contrasted with the change of Newton’s law due the presence of extra dimensions that is observable only for $n = 2$ [3]. In principle there can be other light moduli which couple with even larger strengths. For example the dilaton, whose VEV determines the (logarithm of the) string coupling constant, if it does not acquire large mass from some dynamical supersymmetric mechanism, can lead to a force of strength 2000 times bigger than gravity [22].

(iii) Non universal repulsive forces much stronger than gravity, mediated by possible abelian gauge fields in the bulk [8, 23]. Such gauge fields may acquire tiny masses of the order of M_s^2/M_P , as in (11), due to brane localized anomalies [23]. Although the corresponding gauge coupling is infinitesimally small, $g_A \sim M_s/M_P \simeq 10^{-16}$, it is still bigger than the gravitational

coupling $\sim E/M_P$ for typical energies E of the order of the proton mass, and the strength of the new force would be $10^6 - 10^8$ stronger than gravity. This is an interesting region which will be soon explored in micro-gravity experiments (see Fig. 10). Note that in this case the supernova

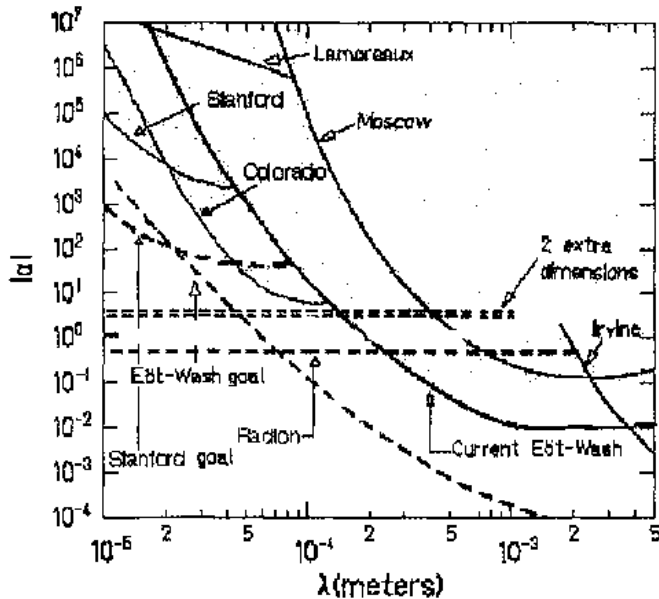


Figure 10: Present limits on non-Newtonian forces at short distances (grey regions), as a function of their range λ (horizontal axis) and their strength relative to gravity α (vertical axis). The limits are compared to new forces mediated by the graviton in the case of two large extra dimensions, and by the radion.

constraints impose that there should be at least four large extra dimensions in the bulk [8].

In Fig. 10 we depict the actual information from previous, present and upcoming experiments [18]. The solid lines indicate the present limits from the experiments indicated. The excluded regions lie above these solid lines. Measuring gravitational strength forces at such short distances is quite challenging. The most important background is the Van der Walls force which becomes equal to the gravitational force between two atoms when they are about 100 microns apart. Since the Van der Walls force falls off as the 7th power of the distance, it rapidly becomes negligible compared to gravity at distances exceeding 100 μm . The dashed thick lines give the expected sensitivity of the present and upcoming experiments, which will improve the

actual limits by roughly two orders of magnitude, while the horizontal dashed lines correspond to the theoretical predictions for the graviton in the case of two large extra dimensions and for the radion in the case of transverse radius. These limits are compared to those obtained from particle accelerator experiments in Table 2.

5 D-brane Standard Model

One of the main questions with such a low string scale is to understand the observed values of the low energy gauge couplings. One possibility is to have the three gauge group factors of the Standard Model (SM) arising from different collections of coinciding branes. This is unattractive since the three gauge couplings correspond in this case to different arbitrary parameters of the model. A second possibility is to maintain unification by imposing all the SM gauge bosons to arise from the same collection of D-branes. The large difference in the actual values of gauge couplings could then be explained either by introducing power-law running from a few TeV to the weak scale [24], or by an effective logarithmic evolution in the transverse space in the special case of two large dimensions [17]. However, no satisfactory model built along these lines has so far been presented.

Here, we will discuss a third possibility [25], which is alternative to unification but nevertheless maintains the prediction of the weak angle at low energies. Specifically, we consider the strong and electroweak interactions to arise from two different collections of coinciding branes, leading to two different gauge couplings [26]. Assuming that the low energy spectrum of the (non-supersymmetric) SM can be derived by a type I string vacuum, the normalization of the hypercharge is determined in terms of the two gauge couplings and leads naturally to the right value of $\sin^2 \theta_W$ for a string scale of the order of a few TeV. The electroweak gauge symmetry is broken by the vacuum expectation values of two Higgs doublets, which are both necessary in the present context to give masses to all quarks and leptons.

Another issue of this class of models with TeV string scale is to understand proton stability. In the model presented here, this is achieved by the conservation of the baryon number which turns out to be a perturbatively exact global symmetry, remnant of an anomalous $U(1)$ gauge symmetry broken by the Green-Schwarz mechanism. Specifically, the anomaly is canceled by shifting a corresponding axion field that gives mass to the $U(1)$ gauge boson. Moreover, the two extra $U(1)$ gauge groups are anomalous and the associated gauge bosons become massive with masses of the order of the string scale. Their couplings to the standard model fields up to dimension five are fixed by charges and anomalies.

5.1 Hypercharge embedding and the weak angle

The gauge group closest to the Standard Model one can hope to derive from type I string theory in the above context is $U(3) \times U(2) \times U(1)$. The first factor arises from three coincident

"color" D-branes. An open string with one end on them is a triplet under $SU(3)$ and carries the same $U(1)$ charge for all three components. Thus, the $U(1)$ factor of $U(3)$ has to be identified with *gauged* baryon number. Similarly, $U(2)$ arises from two coincident "weak" D-branes and the corresponding abelian factor is identified with *gauged* weak-doublet number. A priori, one might expect that $U(3) \times U(2)$ would be the minimal choice. However it turns out that one cannot give masses to both up and down quarks in that case. Therefore, at least one additional $U(1)$ factor corresponding to an extra " $U(1)$ " D-brane is necessary in order to accommodate the Standard Model. In principle this $U(1)$ brane can be chosen to be independent of the other two collections with its own gauge coupling. To improve the predictability of the model, here we choose to put it on top of either the color or the weak D-branes. In either case, the model has two independent gauge couplings g_3 and g_2 corresponding, respectively, to the gauge groups $U(3)$ and $U(2)$. The $U(1)$ gauge coupling g_1 is equal to either g_3 or g_2 .

Let us denote by Q_3 , Q_2 and Q_1 the three $U(1)$ charges of $U(3) \times U(2) \times U(1)$, in a self explanatory notation. Under $SU(3) \times SU(2) \times U(1)_3 \times U(1)_2 \times U(1)_1$, the members of a family of quarks and leptons have the following quantum numbers:

$$\begin{aligned} Q &= (\mathbf{3}, \mathbf{2}; 1, w, 0)_{1/6} \\ u^c &= (\bar{\mathbf{3}}, \mathbf{1}; -1, 0, x)_{-2/3} \\ d^c &= (\bar{\mathbf{3}}, \mathbf{1}; -1, 0, y)_{1/3} \\ L &= (\mathbf{1}, \mathbf{2}; 0, 1, z)_{-1/2} \\ l^c &= (\mathbf{1}, \mathbf{1}; 0, 0, 1)_1 \end{aligned} \quad (14)$$

Here, we normalize all $U(N)$ generators according to $\text{Tr}T^a T^b = \delta^{ab}/2$, and measure the corresponding $U(1)_N$ charges with respect to the coupling $g_N/\sqrt{2N}$, with g_N the $SU(N)$ coupling constant. Thus, the fundamental representation of $SU(N)$ has $U(1)_N$ charge unity. The values of the $U(1)$ charges x, y, z, w will be fixed below so that they lead to the right hypercharges, shown for completeness as subscripts.

The quark doublet Q corresponds necessarily to a massless excitation of an open string with its two ends on the two different collections of branes. The Q_2 charge w can be either +1 or -1 depending on whether Q transforms as a $\mathbf{2}$ or a $\bar{\mathbf{2}}$ under $U(2)$. The antiquark u^c corresponds to fluctuations of an open string with one end on the color branes and the other on the $U(1)$ brane for $x = \pm 1$, or on other branes in the bulk for $x = 0$. Ditto for d^c . Similarly, the lepton doublet L arises from an open string with one end on the weak branes and the other on the $U(1)$ brane for $z = \pm 1$, or in the bulk for $z = 0$. Finally, l^c corresponds necessarily to an open string with one end on the $U(1)$ brane and the other in the bulk.

The weak hypercharge Y is a linear combination of the three $U(1)$'s [27]:

$$Y = c_1 Q_1 + c_2 Q_2 + c_3 Q_3. \quad (15)$$

$c_1 = 1$ is fixed by the charges of l^c in eq. (14), while for the remaining two coefficients and the

unknown charges x, y, z, w , we obtain four possibilities:

$$\begin{aligned} c_2 &= \mp \frac{1}{2}, \quad c_3 = -\frac{1}{3}; \quad x = -1, \quad y = 0, \quad z = 0/-1, \quad w = \mp 1 \\ c_2 &= \mp \frac{1}{2}, \quad c_3 = \frac{2}{3}; \quad x = 0, \quad y = 1, \quad z = 0/-1, \quad w = \mp 1 \end{aligned} \quad (16)$$

To compute the weak angle $\sin^2 \theta_W$, we use eq. (15) to find:

$$\sin^2 \theta_W \equiv \frac{g_Y^2}{g_2^2 + g_Y^2} = \frac{1}{1 + 4c_2^2 + 2g_2^2/g_1^2 + 6c_3^2g_2^2/g_3^2}, \quad (17)$$

with $g_1 = g_2$ or $g_1 = g_3$ at the string scale.

We now show that the above prediction agrees with the experimental value for $\sin^2 \theta_W$ for a string scale in the region of a few TeV. For this comparison, we use the evolution of gauge couplings from the weak scale M_Z as determined by the one-loop beta-functions of the SM with three families of quarks and leptons and one Higgs doublet. In order to compare the theoretical relations for $g_1 = g_2$ and $g_1 = g_3$ with the experimental value of $\sin^2 \theta_W$ at M_s , we plot in Fig. 11 the corresponding curves as functions of M_s . The solid line is the experimental

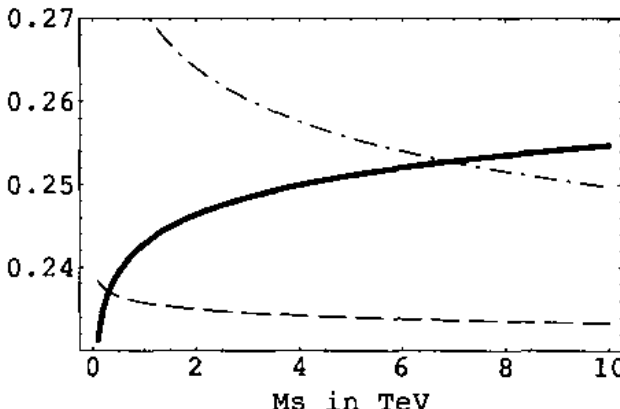


Figure 11: The experimental value of $\sin^2 \theta_W$ (thick curve), and the theoretical predictions.

curve. The dashed line is the plot of the function (17) for $g_1 = g_2$ with $c_3 = -1/3$ while the dotted-dashed line corresponds to $g_1 = g_3$ with $c_3 = 2/3$. The other two possibilities are not shown because they lead to a value of M_s , which is too high to protect the hierarchy. Thus, the second case, where the $U(1)$ brane is on top of the color branes, is compatible with low

energy data for $M_s \sim 6 - 8$ TeV and $g_s \simeq 0.9$. This selects the last two possibilities of charge assignments in Eq. (16).

From the general solution (16) and the requirement that the Higgs doublet has hypercharge 1/2, one finds the following possible assignments:

$$c_2 = \mp \frac{1}{2} : \quad H \ (1, 2; 0, \pm 1, 1)_{1/2} \quad H' \ (1, 2; 0, \mp 1, 0)_{1/2} \quad (18)$$

It is straightforward to check that the allowed (trilinear) Yukawa terms are:

$$\begin{aligned} c_2 = -\frac{1}{2} &: \quad H' Qu^c, \ H^\dagger L l^c, \ H^\dagger Q d^c ; \\ c_2 = \frac{1}{2} &: \quad H' Qu^c, \ H^\dagger L l^c, \ H^\dagger Q d^c \end{aligned} \quad (19)$$

Thus, two Higgs doublets are in each case necessary and sufficient to give masses to all quarks and leptons. The presence of the second Higgs doublet changes very little the curves of Fig. 11 and consequently our previous conclusions about M_s . Two important comments are in order: (i) The spectrum we assumed in Eq. (14) does not contain right-handed neutrinos on the branes. They could in principle arise from open strings in the bulk. Their interactions with the particles on the branes would then be suppressed by the large volume of the transverse space. More specifically, conservation of the three U(1) charges allow for the following Yukawa couplings involving the right-handed neutrino ν_R :

$$c_2 = -\frac{1}{2} : \quad H' L \nu_L \quad ; \quad c_2 = \frac{1}{2} : \quad H L \nu_R \quad (20)$$

These couplings lead to Dirac type neutrino masses between ν_L from L and the zero mode of ν_R , which is naturally suppressed by the volume of the bulk.

(ii) From Eq. (17) and Fig. 11, we find the ratio of the $SU(2)$ and $SU(3)$ gauge couplings at the string scale to be $\alpha_2/\alpha_3 \sim 0.4$. This ratio can be arranged by an appropriate choice of the relevant moduli. For instance, one may choose the color and U(1) branes to be D3 branes while the weak branes to be D7 branes. Then the ratio of couplings above can be explained by choosing the volume of the four compact dimensions of the seven branes to be $V_4 = 2.5$ in string units. This predicts an interesting spectrum of KK states, different from the naive choices that have appeared hitherto: the only SM particles that have KK descendants are the W bosons as well as the hypercharge gauge boson. However since the hypercharge is a linear combination of the three U(1)'s, the massive U(1) gauge bosons do not couple to hypercharge but to doublet number.

5.2 The fate of $U(1)$'s, proton stability and neutrino masses

The model under discussion has three $U(1)$ gauge interactions corresponding to the generators Q_1, Q_2, Q_3 . From the previous analysis, the hypercharge was shown to be either one of the

two linear combinations: $Y = Q_1 \mp \frac{1}{2}Q_2 + \frac{2}{3}Q_3$. It is easy to see that the remaining two $U(1)$ combinations orthogonal to Y are anomalous. In particular there are mixed anomalies with the $SU(2)$ and $SU(3)$ gauge groups of the Standard Model. These anomalies are canceled by two axions coming from the closed string sector, via the standard Green-Schwarz mechanism [28]. The mixed anomalies with the non-anomalous hypercharge are also canceled by dimension five Chern-Simmons type of interactions [25]. The presence of such interactions has so far escaped attention in the context of string theory.

An important property of the above Green-Schwarz anomaly cancellation mechanism is that the two $U(1)$ gauge bosons A and A' acquire masses leaving behind the corresponding global symmetries. This is in contrast to what would have happened in the case of an ordinary Higgs mechanism. These global symmetries remain exact to all orders in type I string perturbation theory around the orientifold vacuum. This follows from the topological nature of Chan-Paton charges in all string amplitudes. On the other hand, one expects non-perturbative violation of global symmetries and consequently exponentially small in the string coupling, as long as the vacuum stays at the orientifold point. Once we move sufficiently far away from it, we expect the violation to become of order unity. So, as long as we stay at the orientifold point, all three charges Q_1, Q_2, Q_3 are conserved and since Q_3 is the baryon number, proton stability is guaranteed.

To break the electroweak symmetry, the Higgs doublets in Eq. (18) should acquire non-zero VEV's. Since the model is non-supersymmetric, this may be achieved radiatively [29]. From Eq. (19), to generate masses for all quarks and leptons, it is necessary for both higgses to get non-zero VEV's. The baryon number conservation remains intact because both Higgses have vanishing Q_3 . However, the linear combination which does not contain Q_3 , will be broken spontaneously, as follows from their quantum numbers in Eq. (18). This leads to an unwanted massless Goldstone boson of the Peccei-Quinn type. The way out is to break this global symmetry explicitly, by moving away from the orientifold point along the direction of the associated modulus so that baryon number remains conserved. Instanton effects in that case will generate the appropriate symmetry breaking couplings in the potential.

A generic feature of the above models is that some of the Standard Model states should correspond to open strings with one end in the bulk, implying the existence of some extra branes, in addition to the ones used above. One can then introduce an extra brane in the bulk with a corresponding $U(1)_b$ bulk gauge group. This group is broken by anomalies, leaving behind an additional global symmetry that can be identified with the lepton number [30]. Lepton number conservation is important in particular for the extra dimensional neutrino mass suppression mechanism described above, that can be destabilized by the presence of a large Majorana neutrino mass term. Such a term can be generated by the lepton-number violating dimension five effective operator $LLHH$ that leads, in the case of TeV string scale models, to a Majorana mass of the order of a few GeV. Even if we manage to eliminate this operator in some particular model, higher order operators would also give unacceptably large contributions, as

we focus on models in which the ratio between the Higgs vacuum expectation value and the string scale is just of order $\mathcal{O}(1/10)$. The best way to protect tiny neutrino masses from such contributions is to impose lepton number conservation. The corresponding D-brane models are shown pictorially in Fig. 12.

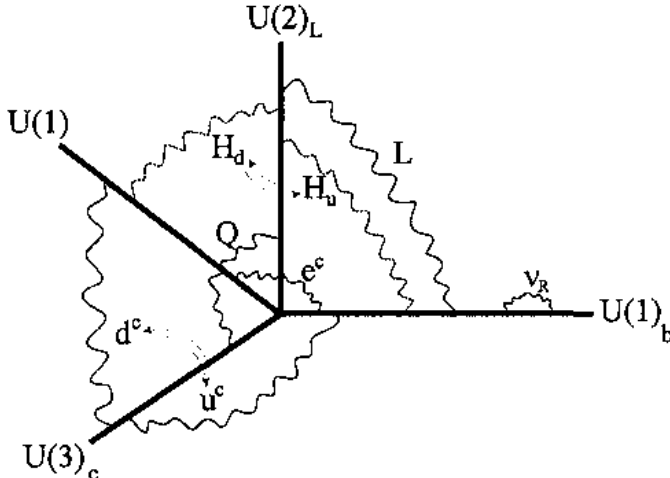


Figure 12: Pictorial representation of the D-brane models presented above. The $U(3)_c$ color, $U(2)_L$ weak and $U(1)_b$ bulk branes point in three orthogonal (complex) directions of the six-dimensional internal space. On the other hand, the $U(1)$ brane is on top of the color or the weak branes, leading to a prediction for $\sin^2 \theta_W$ analyzed above.

6 Conclusions

Clearly, today, these theories exist only in our imagination. However, we look forward to the next generation of high energy experiments and in particular to the most powerful machine, the LHC at CERN. In fact, it is designed since last decade to explore the origin of mass of elementary particles and to test, in particular, the idea of supersymmetry, looking for the production of superparticles. We now hope that this accelerator may discover more spectacular and "exotic" phenomena, such as the existence of large extra dimensions of space and of fundamental strings.

Acknowledgments

This work was partly supported by the European Commission under RTN contract HPRN-CT-2000-00148.

References

- [1] I. Antoniadis, *Phys. Lett. B* **246** (1990) 377.
- [2] N. Arkani-Hamed, S. Dimopoulos and G. Dvali, *Phys. Lett. B* **429** (1998) 263; I. Antoniadis, N. Arkani-Hamed, S. Dimopoulos and G. Dvali, *Phys. Lett. B* **436** (1998) 263.
- [3] C. D. Hoyle, U. Schmidt, B. R. Heckel, E. C. Adelberger, J. H. Gundlach, D. J. Kapner and H. E. Swanson, *Phys. Rev. Lett.* **86** (2001) 1418; J. Chiaverini, S. J. Smullin, A. A. Geraci, D. M. Weld and A. Kapitulnik, hep-ph/0209325; J. C. Long, H. W. Chan, A. B. Churnside, E. A. Gulbis, M. C. Varney and J. C. Price, hep-ph/0210004; D. E. Krause, E. Fischbach, *Lect. Notes Phys.* **562** (2001) 292 [hep-ph/9912276]; H. Abele, S. Haesler and A. Westphal, in 271st WE-Heraeus-Seminar, Bad Honnef, 25.2.-1.3.2002.
- [4] I. Antoniadis, K. Benakli and M. Quirós, *Phys. Lett. B* **331** (1994) 313 and *Phys. Lett. B* **460** (1999) 176; P. Nath, Y. Yamada and M. Yamaguchi, *Phys. Lett. B* **466** (1999) 100; T. G. Rizzo and J. D. Wells, *Phys. Rev. D* **61** (2000) 016007; T. G. Rizzo, *Phys. Rev. D* **61** (2000) 055005; A. De Rujula, A. Donini, M. B. Gavela and S. Rigolin, *Phys. Lett. B* **482** (2000) 195; E. Accomando, I. Antoniadis and K. Benakli, *Nucl. Phys. B* **579** (2000) 3.
- [5] G. F. Giudice, R. Rattazzi and J. D. Wells, *Nucl. Phys. B* **544** (1999) 3; E. A. Mirabelli, M. Perelstein and M. E. Peskin, *Phys. Rev. Lett.* **82** (1999) 2236; T. Han, J. D. Lykken and R. Zhang, *Phys. Rev. D* **59** (1999) 105006; K. Cheung and W.-Y. Keung, *Phys. Rev. D* **60** (1999) 112003; C. Balázs et al., *Phys. Rev. Lett.* **83** (1999) 2112; L3 Collaboration (M. Acciarri et al.), *Phys. Lett. B* **464** (1999) 135, *Phys. Lett. B* **470** (1999) 281; J. L. Hewett, *Phys. Rev. Lett.* **82** (1999) 4765; D. Atwood, C. P. Burgess, E. Filotas, F. Leblond, D. London and I. Maksymyk, *Phys. Rev. D* **63** (2001) 025007.
- [6] I. Antoniadis and K. Benakli, *Phys. Lett. B* **326** (1994) 69.
- [7] I. Antoniadis, K. Benakli and A. Laugier, *JHEP* **0105** (2001) 044.
- [8] N. Arkani-Hamed, S. Dimopoulos and G. R. Dvali, *Phys. Rev. D* **59** (1999) 086004.
- [9] S. Cullen and M. Perelstein, *Phys. Rev. Lett.* **83** (1999) 268; V. Barger, T. Han, C. Kao and R. J. Zhang, *Phys. Lett. B* **461** (1999) 34.

- [10] K. Benakli and S. Davidson, *Phys. Rev. D* **60** (1999) 025004; L. J. Hall and D. Smith, *Phys. Rev. D* **60** (1999) 085008.
- [11] E. Eichten, K. Lane and M. E. Peskin, *Phys. Rev. Lett.* **50** (811) 1983.
- [12] LEP and SLD experiments, preprint CERN-EP-2000-016.
- [13] R. Barbieri and A. Strumia, *Phys. Lett. B* **462** (144) 1999.
- [14] P. Nath and M. Yamaguchi, *Phys. Rev. D* **60** 1999116004; *Phys. Rev. D* **60** (116006) 1999; M. Masip and A. Pomarol, *Phys. Rev. D* **60** (096005) 1999; W.J. Marciano, *Phys. Rev. D* **60** (093006) 1999; A. Strumia, *Phys. Lett. B* **466** (107) 1999; T. G. Rizzo and J. D. Wells, *Phys. Rev. D* **61** (016007) 2000; R. Casalbuoni, S. De Curtis, D. Dominici and R. Gatto, *Phys. Lett. B* **462** (48) 1999; C. D. Carone, *Phys. Rev. D* **61** (015008) 2000; A. Delgado, A. Pomarol and M. Quirós, *JHEP* **1** (2000) 30; M. Masip, *Phys. Rev. D* **62** (105012) 2000.
- [15] S. Cullen, M. Perelstein and M. E. Peskin, *Phys. Rev. D* **62** (055012) 2000.
- [16] D. Bourilkov, *Phys. Rev. D* **62** (076005) 2000; L3 Collaboration (M. Acciarri et al.), *Phys. Lett. B* **489** (81) 2000.
- [17] C. Bachas, *JHEP* **9811** (1998) 23; I. Antoniadis and C. Bachas, *Phys. Lett. B* **450** (1999) 83; N. Arkani-Hamed, S. Dimopoulos and J. March-Russell, hep-th/9908146; I. Antoniadis, C. Bachas and E. Dudas, *Nucl. Phys. B* **560** (1999) 93.
- [18] I. Antoniadis, K. Benakli, A. Laugier and T. Maillard, *Nucl. Phys. B* **662** (2003) 40.
- [19] S. Ferrara, C. Kounnas and F. Zwirner, *Nucl. Phys. B* **429** (1994) 589.
- [20] I. Antoniadis, S. Dimopoulos and G. Dvali, *Nucl. Phys. B* **516** (1998) 70.
- [21] I. Antoniadis, E. Dudas and A. Sagnotti, *Phys. Lett. B* **464** (1999) 38; G. Aldazabal and A. M. Uranga, *JHEP* **9910** (1999) 024; C. Angelantonj, I. Antoniadis, G. D'Appollonio, E. Dudas and A. Sagnotti, *Nucl. Phys. B* **572** (2000) 36.
- [22] T. R. Taylor and G. Veneziano, *Phys. Lett. B* **213** (1988) 450.
- [23] I. Antoniadis, E. Kiritsis and J. Rizos, *Nucl. Phys. B* **637** (2002) 92.
- [24] K. R. Dienes, E. Dudas and T. Gherghetta, *Phys. Lett. B* **436** (1998) 55; *Nucl. Phys. B* **537** (1999) 47.
- [25] I. Antoniadis, E. Kiritsis and T. N. Tomaras, *Phys. Lett. B* **486** (2000) 186.

- [26] G. Shiu and S.-H. H. Tye, *Phys. Rev. D* **58** (1998) 106007; Z. Kakushadze and S.-H. H. Tye, *Nucl. Phys. B* **548** (1999) 180; L. E. Ibáñez, C. Muñoz and S. Rigolin, *Nucl. Phys. B* **553** (1999) 43.
- [27] N. D. Lambert and P. C. West, *JHEP* **9909** (1999) 021; G. Aldazabal, L. E. Ibáñez and F. Quevedo, *JHEP* **0001** (2000) 031 and **0002** (2000) 015.
- [28] A. Sagnotti, *Phys. Lett. B* **294** (1992) 196; L. E. Ibáñez, R. Rabadán and A. M. Uranga, *Nucl. Phys. B* **542** (1999) 112; E. Poppitz, *Nucl. Phys. B* **542** (1999) 31.
- [29] I. Antoniadis, K. Benakli and M. Quirós, *Nucl. Phys. B* **583** (2000) 35.
- [30] I. Antoniadis, E. Kiritsis, J. Rizos and T. N. Tomaras, *Nucl. Phys. B* **660** (2003) 81.

CHAIRMAN: I. ANTONIADIS

Scientific secretaries: F. Scardigli, E. Trincherini

DISCUSSION

- *Bozza:*

One of the problems of the Standard Model is the number of parameters. Does the scenario you showed lead to a reduction or to an increase in the number of parameters?

- *Antoniadis:*

The main motivation of this scenario was not to reduce the number of parameters; this is a different question. Actually you can ask the same question about supersymmetry.

The main motivation here is hierarchy, the big hierarchy between the electro-weak scale and the Planck scale, which plays the role of the ultraviolet cut-off. To stabilize hierarchy, you can either introduce new symmetries, like supersymmetry, or, in this scenario, you can lower the fundamental scale. Once you want to go further, and you want to use the fundamental theory to obtain the Standard Model, then certainly you will have to address all these questions about the number of parameters.

- *Bozza:*

Are you estimating the background for processes from Standard Model physics? What about the energy and momentum resolution of LHC experiments to disentangle the new physics from Standard Model physics?

- *Antoniadis:*

Consider the background, for example, in one of the picture I showed. This is the missing energy due to graviton emission, and you can compare it with the Standard Model background.

- *Bozza:*

This is only the physical background. It is not taking any detector into account.

- *Antoniadis:*

Of course, this is a theoretical work.

- *Krotov:*

How can I obtain the experimental restriction on the size of extra dimensions, 10^{-16} cm?

- *Antoniadis:*

Initially, when I talked about this, I wanted to give you just an idea, without making a precise analysis: to introduce the concept of compactification and to give an idea of what

are the bounds on the compactification scale, or the size of the extra dimensions.

If you have an extra dimension where the light can propagate, then the size of the extra dimension must be much smaller than a characteristic length which corresponds to the higher energy you can achieve in a laboratory. That is how the TeV scale, or 10^{-16} cm, came out. If you want to be more precise, then you have to do an accurate analysis and this is what I discussed later on, where I mentioned the bound of 3 TeV. But these bounds now depend on how the fermions are localized. This 3 TeV bound applies for extra dimensions where photons can propagate but quarks and leptons are localized. If quarks and leptons also see the extra dimension, then the bound is much weaker, around 500 GeV.

- *Cerri:*

Two questions, in some sense related. You mentioned bounds on the size of extra dimensions from supernovae observations. Can you give us an idea on how to get these limits? Is there any hope of getting limits on extra dimensions from large-scale (astronomical) dynamics of gravitational systems?

- *Antoniadis:*

Concerning the first question, I can show you this transparency. The bounds for supernovae came from the cooling that you have due to graviton production, so you compare the production of gravitons with the production of neutrinos and that is how you obtain the bounds. For the graviton emission, you have just to compute the number of gravitons, which is the temperature of the supernova to the power n (which is the number of extra dimensions) times the compactification volume. This is just dimensional analysis for temperatures which are bigger than the compactification scale. And then the production rate is the number of gravitons times the inverse mass Planck squared. You obtain this rate and you compare it with the production rate of neutrinos. In the case of two extra dimensions, you obtain a lower bound for the higher dimensional scale, which is 6-dimensional in this case, of 50 TeV, which still gives, if you put the factor of the gauge coupling, a string scale bigger than about 10 TeV.

There are also bounds that have been discussed in cosmology, like from the diffused photons, but these are more model-dependent. I am not aware of other type of bounds.

- *Skinner:*

It is perhaps a little disappointing that the fundamental scale of large extra dimensions can always be pushed out of reach of experiments. Can we think of an experiment that would in principle disfavour large extra dimensions up to a very high scale (10^{16} GeV)? In particular, perhaps you could talk about sensitivity of running of gauge coupling to threshold effects, and also gravitational wave experiments from the early universe.

- *Antoniadis:*

Theoretically there are no bounds for the string scale, which can be anywhere from a TeV up to the Planck scale. The main reason here why I considered the possibility of

being of the order of the TeV is because I wanted to replace supersymmetry in order to stabilize the hierarchy problem. Like in SUSY, if you do not find superpartners, you can push up the scale but then, at some point, you will start having problems with the fine-tuning. By itself, of course, this argument is theoretical but this is part of our logic.

The unification of coupling constants is a different issue. People have proposed alternatives in this framework but there is no concrete and appealing model that can replace the standard picture of the unification of couplings. So, if this framework is correct, at least at this moment I would say that the apparent unification of couplings should be considered as an accident.

- *Kuperstein:*

What is the connection, if any, between the scenario you have described this morning and the deconstruction theory by Arkani-Hamed three years ago?

- *Antoniadis:*

The idea of deconstruction came from the consideration of the effective field theory of the Kaluza-Klein modes. In other words, consider a higher dimensional theory compactified and you want to study the effective theory which includes some of the KK states. Then you can mimic the properties of the higher dimensional theory at low energy by some other effective field theory which is 4-dimensional. This brought the idea of deconstruction and then you forget about the higher dimensional theory.

- *Kuperstein:*

So there are no relations between these two scenarios?

- *Antoniadis:*

No.

- *Lendermann:*

The Standard Model fields are confined within 4-dimensional space-time. How is this confinement introduced in the theory? Is the boundary just a number put by hand or can it be deduced from some fundamental mathematical property of the model?

- *Antoniadis:*

There are some field theoretical methods to localize fields, but in the context of this string theory I have mentioned, the localization is built in. In other words, the theory has D-branes and these branes, which are classical solutions of the theory, necessarily have localized modes which are described by open strings.

The only input is that you have 10 dimensions; 6 of them must be compact. Out of these 6, some of them can be longitudinal, some others transverse. Ultimately if you are able to obtain a complete minimization of the theory, you could hope to determine the number of the compact extra dimensions and their size.

- *Menges:*

You mentioned that some theories have a new scalar field, called radion. What are the properties of it and can we see it?

- *Antoniadis:*

The radion is universal. When you have a bulk, the metric is higher dimensional so the volume of the bulk corresponds to the determinant of the internal metric along these extra dimensions. From the four-dimensional point of view, this looks like a scalar field, which is the radion. If the bulk is supersymmetric, this field would acquire a small mass and could generate an extra force. In general, of course, for any internal component of the metric, you have different scalar fields which are however model-dependent, they depend on the compactification you do. The radion which determines the total volume is model-independent.

- *Durin:*

Why can the string scale (at 1 TeV) be so different from the Planck mass (10^{19} GeV)?

- *Antoniadis:*

The logic is different; what I consider a fundamental scale of the theory is the string scale, which is 1 TeV. However, the Planck mass which determines the observed force of gravity is not fundamental, is an output of the theory and the reason why it is different is because you have some extra dimensions which have a size much bigger than the string length. I consider models where the string size is 10^{-16} cm, so this is the fundamental length of the theory. However, there could be some extra dimensions which are much bigger (1 mm). The question one should answer is how is it possible to have such different scales. There are two aspects of this hierarchy; one is the aspect of stability. In the same way, in Supersymmetry you introduce a SUSY breaking scale at the TeV to protect the hierarchy. SUSY guarantees that the radiative corrections do not destabilize this choice, but you need some dynamical mechanism behind this to derive the scale of supersymmetry breaking. For instance, by introducing a gaugino condensate due to some other strong interaction.

Similarly here, this classical choice is stable but you can ask what is the dynamical mechanism behind this, that would determine such a hierarchy. There are some ideas: for instance, in the case of 2 extra dimensions, you have logarithmic corrections, so you can obtain a potential that depends logarithmically on the size of the bulk and, by minimizing this potential, you could in principle find vacua where the size of the 2 extra dimensions is much different than the fundamental scale. In string theory, the whole minimization process becomes much more difficult and there are more theoretical problems.

- *Lipatov:*

Several years ago, there was a paper by Shifman and Dvali that suggested a new mechanism for understanding the existence of 3 generations of fermions on the base of the brane physics. What is the status of this hypothesis now?

- *Antoniadis:*

I am not aware of this paper that can explain the number 3 of generations.

- *Casalberry Solana:*

Can a compactified extra dimension be interpreted as a thermalized extra time dimension?

- *Antoniadis:*

In a Euclidean version of the theory, the answer is yes. You use the Euclidean version as a tool for computation but then you must always do the Wick rotation and interpret the real time. In the case of space dimensions, you do not do it.

- *Papadimitriou:*

Can you say a few more words about the set-up of the brane world scenario in the context of string theory? In particular, how you get chiral fermions in four dimensions?

- *Antoniadis:*

There are several ways to generate chiral fermions. One way is to do an orbifold compactification and then you place the branes at the orbifold singularities. Another way is to break supersymmetry by the brane intersections and then the number of generations corresponds to the number of intersections.

- *Papadimitriou:*

My question is, in this particular model do you do it in a particular way or your work fits in both ways?

- *Antoniadis:*

It fits in both ways. At least the properties I discussed this morning do not rely on the particular model building. I planned to discuss a bit more some particular embedding of the Standard Model with branes but I did not have time.

- *'t Hooft:*

We heard M. Duff talk about having more than one time-like extra dimension. Of course, that would be more exotic and with serious difficulties. But are such possibilities being seriously considered? There is for instance the difficulty of the tachyon modes.

- *Antoniadis:*

I guess there is the problem with unitarity and I do not see how you can get around it. One idea that has been proposed was to impose a constraint in such a theory which makes all particles propagate effectively with one time. The tachyon modes are then eliminated.

- *Scardigli:*

What are the theoretical principles, if any, which predict how many dimensions should be compactified? In other words, why is space-time four-dimensional?

- Antoniadis:

I do not know. I do not have an answer to this question. The only theory which fixes the number of dimensions is string theory, but it predicts more than four! So, some of them should be compactified. It could be useful since, for instance, otherwise we would not be able to lower the string scale. There have been some ideas to fix the number of dimensions, but I do not think there is any serious explanation. Ultimately, what you should do is to take all dimensions to be compact and then to compute the effective potential. If you are able to control the dynamics of the underlying theory, in principle you should be able to determine that some of them must be compact and determine their size.

ITP-UU-04/01
SPIN-04/01
gr-qc/yymmnnn

Horizons

Gerard 't Hooft

Institute for Theoretical Physics
Utrecht University, Leuvenlaan 4
3584 CC Utrecht, the Netherlands

and

Spinoza Institute
Postbox 80.195
3508 TD Utrecht, the Netherlands
e-mail: g.thooft@phys.uu.nl
internet: <http://www.phys.uu.nl/~thooft/>

Abstract

The gravitational force harbours a fundamental instability against collapse. In standard General Relativity without Quantum Mechanics, this implies the existence of black holes as natural, stable solutions of Einstein's equations. If one attempts to quantize the gravitational force, one should also consider the question how Quantum Mechanics affects the behaviour of black holes. In this lecture, we concentrate on the horizon. One would have expected that its properties could be derived from general coordinate transformations out of a vacuum state. In contrast, it appears that much new physics is needed. Much of that is still poorly understood, but one may speculate on the way information is organized at a horizon, and how refined versions of Quantum Theory may lead to answers.

1. Introduction: Black Holes as Inevitable Features of General Relativity

The fact that the gravitational force acts directly upon the inertial mass of an object, makes this force unique in Nature, and allows for an unambiguous description of the classical (*i.e.* unquantized) case, called "General Relativity". However, unlike the situation in electromagnetism, the gravitational force produces attraction rather than repulsion between like charges. An inevitable consequence of this is a fundamental instability: masses attract to form bigger masses, which attract one another even more strongly. Eventually, gigantic implosions of large accumulated quantities of mass may result. There is no obvious limit here, so one cannot avoid that the gravitational potential might cross an important threshold, where the escape velocity exceeds that of light.

Indeed, as soon as one is ready to accept the validity of General Relativity for classical systems, one can easily calculate what will happen. The final state that one then reaches is called a "black hole". In astronomy, the formation of a black hole out of one or several stars depends on the circumstances, among which is the equation of state of the material that the stars are made of. Because of this, the physics of black hole formation is sometimes challenged, and conjectures are uttered that black holes "are probably nothing else but commercially viable figments of the imagination" [1].

It is however easy to see that such a position is untenable. To demonstrate this, let me here show how to construct a black hole out of ordinary objects, obeying non-exotic equations of state. These objects could, for example, be television sets, acting on batteries. During the process of black hole formation, these objects will each continue to be in perfect working order. We begin with placing these in the following configuration: let them form a shell of matter, of thickness d and radius R . If d is kept modest, say a few kilometers, then R has to be taken very large, say a million light years. The television sets may stay at convenient distances away from each other, say a meter. The initial velocities are taken to be small; certainly objects close to each other must have very small relative velocities so that collisions have no harmful effects.

The objects attract one another. They don't feel it because, locally, they are under weightless conditions, but they do start to accelerate. So, the sphere shrinks. After thousands of years, the configuration is still spherical, the relative velocities for close-by objects are still small, the density is still low, the televisions are still in working order, but they pass the magical surface called "horizon". What happens is, that light emitted by the objects can no longer reach the outside world. The calculation is straightforward and robust, which means that small perturbations will not affect the main result: no light can be seen from these objects; they form a black hole.

What happens next, is that the sphere of objects continue to contract, and at some point, long after the horizon has been passed, the objects crush, television sets will cease to function, for a while the Standard model still applies to them, but eventually the matter density will

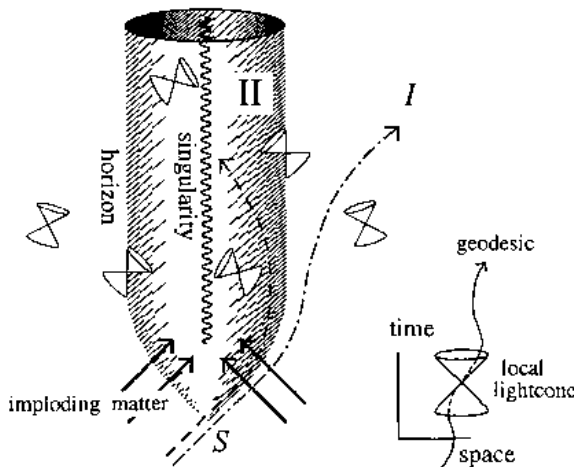


Figure 1: The space-time of a black hole

exceed all bounds, and a true singularity is encountered¹. It is here, at this singularity, where the laws of physics as we know them no longer apply, but whatever happens there is totally irrelevant for the phenomenology of a black hole; whatever an outside observer sees is determined by known laws of physics. The horizon acts as a "cosmic sensor", preventing us from observing the singularity. Whether all singularities in all solutions to the equations are always screened by this cosmic sensor is still being debated, but we do see this happen in all practical solutions known.

In Fig. 1, it is sketched what happens to space-time. The solution to Einstein's equations in General Relativity dictates that, locally, the light cones are tilted. The shaded surface, the horizon, is formed by constructing the tangent of these local light cones. Inside this surface, all local lightcones are pointed inwards, towards the central singularity. The radius of this horizon is found to be

$$R = 2G_N M/c^2 , \quad (1.1)$$

where M is the total mass-energy of the system.

Note that all signals seen by an outside observer in region I , when observing a black hole, originate at the point S . If only a finite amount of light is emitted from there, this light is spread over an infinite amount of time, and therefore infinitely red-shifted. Hence, one expects no signal at all; the black hole is black. It can be formed out of ordinary matter.

¹Small perturbations from spherical symmetry do affect the singularity in a complicated way, but this is not relevant for the nature of the horizon.

2. Black holes in particle physics

In elementary particle physics, the gravitational force is extremely weak, and can normally be ignored. It is, however, understood that there must be regions of particle physics where this force *must* play a decisive role. This is when the energy per particle tends to exceed the Planck scale. The Planck scale is set by considering the three fundamental constants of nature:

$$\begin{aligned} \text{The velocity of light, } & c = 2.9979 \times 10^8 \text{ m/sec,} \\ \text{Planck's constant, } & h/2\pi = \hbar = 1.0546 \times 10^{-34} \text{ kg m}^2/\text{sec,} \\ \text{Newton's constant, } & G_N = 6.672 \times 10^{-11} \text{ m}^3 \text{ kg}^{-1} \text{ sec}^{-2}. \end{aligned} \quad (2.1)$$

Out of these, one finds the following fundamental units:

$$\begin{aligned} L^{\text{Planck}} &= \sqrt{\hbar G_N/c^3} = 1.616 \times 10^{-33} \text{ cm,} \\ T^{\text{Planck}} &= \sqrt{\hbar G_N/c^5} = 5.39 \times 10^{-44} \text{ sec,} \\ M^{\text{Planck}} &= \sqrt{\hbar c/G_N} = 21.8 \mu\text{g}. \end{aligned} \quad (2.2)$$

If particles collide with the enormous c.o.m. energy of $M^{\text{Planck}}c^2$, gravitational effects must be important. If many particles with such energies accumulate in a region of size L^{Planck} , gravitational implosion must take place. Black holes must play an important role there.

It was S. Hawking's fundamental discovery [2], that, when applying the laws of Quantum Field Theory (QFT), black holes are no longer truly black. Particles are emitted at a fundamental temperature, given by

$$kT^{\text{Hawking}} = \frac{\hbar c^3}{8\pi G_N M_{\text{BH}}} = \frac{\hbar c}{4\pi R_{\text{BH}}}. \quad (2.3)$$

For astronomical black holes, this temperature is far too low to give observable effects, but in particle physics the Hawking effect is essential. For a further discussion of this phenomenon by the present author, see [3].

One might suspect now that black holes therefore behave a bit more like ordinary matter. Not only can they be formed by high-energy collisions, but they can also decay. Apparently, QFT restores (some) time-reversal symmetry in processes involving black holes. Are black holes elementary particles? Are elementary particles black holes? Probably, particles and black holes become indistinguishable at the Planck scale. It is instructive to consider the entire formation and decay of a black hole as if described by quantum mechanical amplitudes.

3. Information in a black hole

The absorption cross section σ is roughly given by

$$\sigma = 2\pi R_{\text{BH}}^2 = 8\pi M_{\text{BH}}^2, \quad (3.1)$$

and the emission probability *for a single particle in a given quantum state*:

$$W dt = \frac{\sigma(k) v}{V} e^{-E/kT} dt , \quad (3.2)$$

where k is the wave number characterizing the quantum state of the particle emitted, and T is the Hawking temperature. E is the energy of the emitted particle. Now, *assume* that the process is also governed by a Schrödinger equation. This means that there are quantum mechanical transition amplitudes,

$$T_{\text{in}} = {}_{\text{BH}}\langle M + E/c^2 | |M\rangle_{\text{BH}} |E\rangle_{\text{in}} , \quad (3.3)$$

$$T_{\text{out}} = {}_{\text{BH}}\langle M |_{\text{out}} \langle E | |M + E/c^2\rangle_{\text{BH}} , \quad (3.4)$$

where $|M\rangle_{\text{BH}}$ is the black hole state without the absorbed particle, having mass M , and $|M+E/c^2\rangle$ is the slightly heavier black hole with the extra particle absorbed. The absorption cross section is then

$$\sigma = |T_{\text{in}}|^2 \rho(M+E/c^2)/v , \quad (3.5)$$

where $\rho(M+E/c^2)$ is the level density of the black hole in the final state. This is what we get when applying Fermi's Golden Rule. The same Golden Rule gives us for the emission process *for each quantum state of the emitted particle*:

$$W = |T_{\text{out}}|^2 \rho(M) \frac{1}{V} . \quad (3.6)$$

Here, as before, v is the velocity of the emitted particle, and V is the volume, to be included as a consequence of the normalization of the quantum state.

We can now divide Eq. (3.1) by Eq. (3.2), and compare that with what we get when (3.5) is divided by (3.6). One finds:

$$\frac{\rho(M+E/c^2)}{\rho(M)} = e^{E/kT} = e^{8\pi G_N M E/\hbar c^3} . \quad (3.7)$$

One concludes that

$$\begin{aligned} \frac{\rho(M)}{\rho(M+dM)} &= e^{S(M)} , \\ S(M+dM) - S(M) &= 8\pi G_N M dM / \hbar c ; \end{aligned} \quad (3.8)$$

$$S(M) = \frac{4\pi G_N}{\hbar c} M^2 + C^m . \quad (3.9)$$

Thus, apart from an overall multiplicative constant, e^{C^m} , we find the *density of states* $\rho(M) = e^{S(M)}$ for a black hole with mass M . It can also be written as

$$\rho(M) = 2^{A/A_0} , \quad (3.10)$$

where A is the area $4\pi R^2$ of the black hole, and A_0 is a fundamental unit of area,

$$A_0 = 0.724 \times 10^{-65} \text{ cm}^2. \quad (3.11)$$

Apparently, the states of a black hole are counted by the number of bits one can put on its horizon, one bit on every A_0 .

This result is quite general. It also holds for black holes that carry electric charge or angular momentum or both. Usually, one expects the constant C^{nt} in Eq. (3.9) to be small, although its value is not known.

4. The Brick Wall

This result[4], obtained in the 1970's, is astounding. Black holes come in a denumerable set of states. These states seem to be situated on the horizon, and, as was stated in the Introduction, the physical properties of the horizon follow from simple coordinate transformation rules applied on the physical vacuum. We seem to have hit upon a novel property of the vacuum itself.

Naturally, we wish to learn more about these quantum states. It should be possible now to derive all their properties from General Relativity combined with Quantum Field Theory. However, when one tries to do these calculations, a deep and fundamental mystery emerges: direct application of QFT leads to an infinity of states, described by much more parameters than one bit of information per quantity A_0 of area. Writing the radial coordinate r and the external time coordinate t as

$$r = 2M + e^{2\sigma}; \quad t = 4M\tau, \quad (4.1)$$

in units where all Planckian quantities of Eq. (2.2) were put equal to one, it is quickly found that, at the horizon, in-going and out-going waves are plane waves in terms of σ and τ :

$$\psi(\sigma, \tau) \rightarrow \psi_{\text{in}}(\sigma + \tau, \Omega) + \psi_{\text{out}}(\sigma - \tau, \Omega), \quad (4.2)$$

where Ω stands short for the angular coordinates θ and φ on the horizon. Since σ runs to $-\infty$, an infinite amount of information can be stored in these waves.

By way of exercise, one can now compute how much information will be stored in these waves if

- the particle contents will be as dictated by the Boltzmann distribution corresponding to the Hawking temperature (2.3), and
- a *brick wall* is placed at some position $r_m = 2M + h$, where some boundary condition is imposed on the fields. One could impose a Neumann or Dirichlet boundary condition for the fields there, or something more sophisticated².

²Since one expects *all* continuous symmetries to be broken by the black hole, a *random* boundary condition could be preferred, but in practice the details of the boundary condition are not very important.

In a theory with N scalar fields, in the limit of small h one finds[3, 5] for the total energy of the particles:

$$U = \frac{2\pi^3}{15h} \left(\frac{2M}{\beta} \right)^4 N , \quad (4.3)$$

and for the total entropy:

$$S = \frac{16\pi^3 M}{45h} \left(\frac{2M}{\beta} \right)^3 N . \quad (4.4)$$

We can place the wall in such a way that the entropy matches Eq. (3.9):

$$h = \frac{N}{720\pi M} . \quad (4.5)$$

The total energy of the particles then makes up for $\frac{3}{8}$ of the black hole mass.

Only with this brick wall in place, a black hole would exactly live up to our intuitive expectations. Infalling waves would bounce back, so that an unambiguous S -matrix can be derived, and the entropy S would correspond to the total number of physical states. Although the wall position may seem to depend on the total mass M of the black hole, one finds that the *covariant* distance between wall and horizon is M independent:

$$\int_{r=2M}^{r=2M+h} ds = \sqrt{\frac{N}{90\pi}} . \quad (4.6)$$

But what would be the physical interpretation of this result? Surely, an infalling observer would not notice the presence of such a wall. For some reason, a quantum field cannot have physical degrees of freedom between the wall and the horizon, but why?

One obvious observation is that this is a region comparable to the Planck size (or even somewhat smaller). Surely, one is not allowed to ignore the intense gravitational self interactions of particles confined to such a small region, so that perturbative quantum field theory probably does not apply there. However, one could concentrate *only* on either the in-going or the out-going particles. They are just Lorentz transforms of regular states. Why should their degrees of freedom no longer count?

A more subtle suggestion is that, although we do have fields between the wall and the horizon, which do carry degrees of freedom, these degrees of freedom are not physical. They could emerge as a kind of *local gauge degrees of freedom*, undetectable by any observer. Such a suggestion ties in with what will be discussed later (Section 7).

5. The black hole caustic

One can do a bit more than speculate. In Ref. [3], it is described how to take into account that in-going and out-going particles interact gravitationally. We know now that such interactions

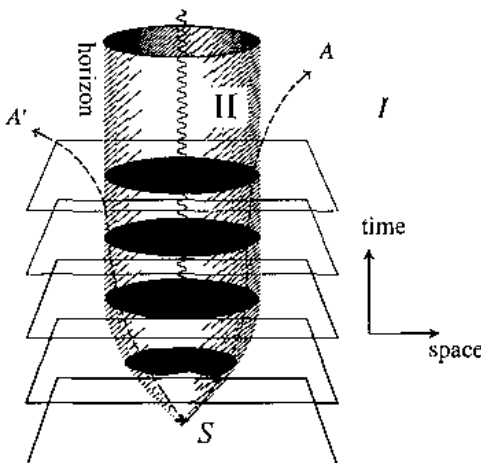


Figure 2: The black hole caustic

may not be ignored. What is found is that the position of the horizon depends on the mass distribution of matter falling in. In turn, this affects the quantum states of the particles moving out, so, unlike what one finds from linearized quantum field theory, there is a relation between in-going and out-going particles, and this relation can indeed be cast in the form of an *S*-matrix. The problem with this derivation is that one still does not find the correct density of distinct quantum states - there are too many states. It turns out that the quantum state of out-going matter appears to be described completely by the *geometry of the dynamic horizon*.

This can be understood in the following way. We define the horizon as the boundary between the region *I* of space-time from where signals can escape to infinity, and the region *II* from which no signals can be received. This means that the exact location of the horizon is obtained by following all light rays all the way to time $t \rightarrow +\infty$. If we have obtained the horizon at some (large) value of time t , we can integrate the equations to locate the horizon at earlier times. The procedure is sketched in Fig. 2. If, finally, we reach the instant when the black hole is formed, the horizon shrinks, until the region *II* ends. The horizon opens up at the point *S*, but, from its definition, we see that, there, it is a caustic. The details of this caustic can be quite complex, in principle. Indeed, the quantum state of the out going particles depends on where on this caustic these particles originated. One might conclude that the quantum state of the out-going particles might be determined completely by the geometric features of this caustic.

As yet, however, it has not been possible to distill a Hilbert space of out-going particles from such an assumption. In Fig. 2, we see that a signal observed by observer *A*, may

meet the signal seen by an observer A' at the caustic. A and A' need not be opposite to one another; there is a duality mapping from points A to points A' on the horizon. This mapping may be the one that determines the black hole's quantum state.

A particle seen by A and a particle seen by A' meet at S with tremendous c.o.m. energy. Let us consider their scattering in a time-reversed setting. Gravitational interactions cause both particles to undergo a large coordinate shift[6]. These shifts turn both particles into showers (backward in time). The quantum states of A and A' are determined by overlapping these showers with the vacuum fluctuations in the region below S .

6. Strings from black holes; white holes

How gravitational interactions lead to string-like amplitudes for the entire process of black hole formation and evaporation, has been described in refs. [3] and [7]. It is not exactly string theory what one gets, but rather a string with a purely imaginary string constant. Since the horizon itself acts as the string world sheet, this string may be some dual of the conventional string approach to black holes[8]. One can picture the scattering events as follows. The black hole is formed by a large number of particles contracting. Each of these particles is pictured as a closed string. Since the horizon acts as the string world sheet, our closed strings widen as they approach the horizon, and they scan the entire horizon as they do so. The strings recombine to form new closed strings, which then separate from the horizon acting as Hawking particles. A regular space-time with an expanding cloud of tiny closed strings forms the final state.

A peculiar by-product of this analysis is the resolution of an old problem in black hole physics: what is the time-reverse of a black hole? In the literature it is sometimes known as the "white hole": a shrinking black hole emitting classical objects and eventually disappearing. It may have been formed by a cloud of "time-reversed Hawking particles".

In our analysis the answer is as follows. By assuming that the out-state is controlled by the in-state through gravitational interactions, it is found that the amplitude automatically respects time-reversal invariance, basically because the gravitational forces respect Newton's law: action = reaction. It is found that the *positions* of the out-going particles are determined by the *momenta* of the in-going ones, and *vice-versa*. Quantum mechanically, the particles in the momentum representation are superpositions of the particles in the position representation. Therefore, one finds that *white holes are quantum superpositions of all possible black hole states* (in the same mass region), *and vice-versa*.

7. Information loss

Much of the investigations described above pertains to an apparent incongruity in any quantum picture of black holes. Classically, one sees that objects falling in cannot imprint all

information contained in them on the out-going states. They are described by quantum waves that require an infinite amount of time to enter the black hole. In contrast, the out-going particles were there already at the very beginning, waiting close to the horizon, at σ in the far negative region, until it is their turn to leave. Our quantum picture requires that these objects are nevertheless closely related. The analysis sketched in the previous sections might suggest that we have come close to resolving this problem: all one has to do is switch on the gravitational forces between in-going and out-going objects. String theory[8] also suggests that this problem can be cured.

However, it should be possible to identify these quantum states in terms of features of the vacuum in relation to general coordinate transformations. In particular, this should be possible for the horizon in the large mass limit. The space-time one then describes is known as Rindler space-time[9]. What seems to be missing is the identification of the quantum states in Rindler space-time and their relation to the quantum states characterizing the vacuum in a flat world. This flat world appears to allow for an unlimited amount of information to disappear across the horizon. To see this, all one has to do is subject ordinary particles to unlimited Lorentz boost transformations. In spite of all that has been said, this problem has not been solved in a satisfactory manner.

Since we are dealing here with quantum phenomena in an extremely alien world of highly curved coordinate frames, it is natural to ask the following question: *Why should these issues not be related to the question of the foundation of quantum mechanics?* There are more than just instinctive reasons to ask this question. As soon as one allows space and time to be curved, one has to confront the possibility that they form a closed, finite universe. Of course, quantum cosmology must be a legitimate domain of quantum gravity. But the formulation of the quantum axioms for closed universes leads to new difficulties. One of these is the fact that there is no external time coordinate, which means that one will not have transition amplitudes or S -matrices. One then encounters the difficulty of interpretation: if the universe is finite, one cannot repeat an experiment infinitely many times at far separated places, so, if a quantum calculation leads to the evaluation of a “probability”, how then can one verify this? In this universe, something happens or it does not, but probabilistic predictions then amount to imprecise predictions. Must we accept an imprecise theory? This difficulty shows up quite sharply in simple “model universes”, such as the one formed by gravitating particles in 2 space-, 1 time dimension. This is a beautiful model with only a finite number of physical degrees of freedom[10], so quantization should be straightforward; unfortunately, it is not, and the fore-mentioned difficulties are the reason.

Should we return to the old attempts at constructing “hidden variable theories” for quantum mechanics?[11] Usually, such endeavor is greeted with skepticism, for very good reasons. Under quite general assumptions, it has been demonstrated that: “hidden variables cannot be reconciled with locality and causality”.

This would indeed be a good reason to abandon such attempts. But, how general is this result? In Ref. [12], some very simple models are constructed that could be viewed as counter examples of the general theorem. We hasten to add that these models are not at all

free from problems. One might suspect, however, that the well-known no-go theorems for hidden variables do rely on some assumptions, which seem to be so natural that one tends to forget about them. Here, we list some of the small-print that may have gone into the derivation of the argument:

- It was assumed that an observer at all times is free to choose from a set of non-commuting operators, which of these (s)he wishes to measure.
- Rotations and other continuous symmetry operations can be performed locally, without disturbing any of the quantum states elsewhere.
- The vacuum is a single, unique state.

Assumptions of this kind may actually not be valid at the Planck scale. Indeed, in Ref. [12] it is assumed that only one class of operators can truly be observed at the Planck scale, and they all commute. They were called ‘beables’ there.

The most important problem of the ones just alluded to is that deterministic evolution seems to be difficult to reconcile with a Hamiltonian that is *bounded from below*. It is absolutely essential for Quantum mechanics to have a lowest energy state, i.e., a vacuum state. Now the most likely way this problem can perhaps be addressed is to assume not only deterministic evolution, but also *local information loss*. As stated, information loss is difficult to avoid in black holes, in particular when they are classical. It now seems that this indeed may turn up to be an essential ingredient for understanding the quantum nature of this world.

Simple examples of universes with information loss can be modeled on a computer as cellular automata[13]. An example is ‘Conway’s game of life’[14].

Information loss may indeed already play a role in the Standard Model! Here, *local gauge degrees of freedom* are pieces of information that do play a role in formulating the dynamical rules, but they are physically unobservable. An unorthodox interpretation of this situation is that these degrees of freedom are unobservable *because* their information contents get lost, much like information drained by a black hole.

We stated earlier that the fields between the horizon and the brick wall could be local gauge degrees of freedom. Now we can add to that that probably they represent lost information.

8. Freezing the horizon

String theory has produced some intriguing insights in the nature of the black hole microstates. Unfortunately, the results reported apply to exotic versions of black holes, and the ordinary Schwarzschild black hole is conspicuously absent. Yet it is the Schwarzschild black hole that we hold here as the prototype. What went wrong?

The black holes handled in string theory are all *extreme black holes* or close-to-extreme black holes. What is an extreme black hole?

The prototype of that can be obtained from the Reissner-Nordström black hole, a black hole with a residual electric charge. Due to the stress-energy tensor of the electric field, the metric is modified into

$$ds^2 = - \left(1 - \frac{2M}{r} + \frac{Q^2}{r^2} \right) dt^2 + \frac{dr^2}{1 - \frac{2M}{r} + \frac{Q^2}{r^2}} + r^2 d\Omega^2 , \quad (8.1)$$

where M is the mass, as before, and now Q is the electric charge (in Planck units). As long as $Q < M$, the quantity $1 - \frac{2M}{r} + \frac{Q^2}{r^2}$ has two zeros,

$$r_{\pm} = M \pm \sqrt{M^2 - Q^2} . \quad (8.2)$$

The largest of these is the location of the horizon. The smaller value represents a second horizon, which is hidden behind the first. The physical interpretation of these horizons is nicely exhibited in Ref. [15], but does not concern us here very much. The *extreme case* is when Q approaches M . Then, the quadratic expression becomes $(1 - \frac{M}{r})^2$, and it has two coinciding horizons at $r = r_+ = r_- = M$. It is this kind of horizon that can be addressed by string theories.

Actually, the situation is a little bit deceptive. One could argue that, in the extreme limit (which can probably be approached physically, but never be reached exactly), the two horizons do not coincide at all. This is because, if we follow a $t = \text{constant}$ path from r_+ to r_- , the metric distance between the horizons becomes

$$\int_{r_-}^{r_+} \sqrt{-g_{11}} dr \rightarrow M\pi , \quad (8.3)$$

and this does not tend to zero in the limit (and it is a time-like distance, not space-like). Moreover, the distance between the r_+ horizon and any point in the regular region I of the surrounding universe (say the point $r = 2M$), tends to infinity:

$$\int_{r_+}^{2M} \sqrt{g_{11}} dr \rightarrow \infty . \quad (8.4)$$

In the extreme limit, the horizon is also infinitely red-shifted, the gravitational field κ there tends to zero, and so does the Hawking temperature. In all respects, the extreme horizon is a *frozen horizon*. Its surface area is still $4\pi r_-^2 = 4\pi M^2 \neq 0$. Accordingly, the entropy $S = \pi M^2 \neq 0$. However, sometimes it is argued that extreme black holes should have vanishing entropy. What happened?

The entropy for the Reissner-Nordström black hole is

$$S = \pi r_+^2 = \pi \left(M + \sqrt{M^2 + Q^2} \right)^2 . \quad (8.5)$$

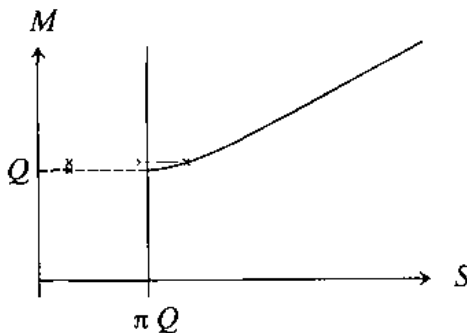


Figure 3: The energy plotted against entropy at fixed Q . The dotted horizontal line does not follow from Eq. (8.6), but from physical considerations.

Inverting this gives the mass-energy M as a function of Q and S :

$$M = \frac{Q}{2} \left(\sqrt{\frac{\pi Q}{S}} + \sqrt{\frac{S}{\pi Q}} \right) , \quad T = \frac{\partial M}{\partial S} \Big|_Q . \quad (8.6)$$

This curve, at a fixed value for Q , is sketched in Fig. 3. It begins at $S = \pi Q$ since, as we see from (8.5), $S \geq \pi Q$. At the extreme point, the temperature T is zero.

Our physical intuition, however, tells us that perhaps states with more order in them also exist, so that one can indeed lower S . The temperature will not become less than zero, so one simply expects a straight horizontal line from $S = 0$ to $S = \pi Q$ (dotted line in Fig. 3). One might suspect that, in a superior quantum theory, tiny deviations from the straight line may occur.

Now what happens if we take one of these ordered states, with $S \ll \pi Q$ (lowest cross in Fig. 3), and cause a minor disturbance, for instance by throwing in a light neutrino? The energy rises slightly (cross top left), and the hole will no longer be extreme. However, the correct solution is now the position on the curve at the right. Complete disorder must take place (arrow). Apparently, the slight perturbation from the neutrino now caused complete disorder. This can be understood in simple models. Since the horizon is no longer extreme, it is also no longer frozen. Dynamical evolution sets in, and this causes disorder. The situation can again be modeled in simple cellular automata.

9. Conclusion

With some physical intuition, one can view the horizon of a black hole as an intriguing physical object. Its microstates as yet cannot be linked to local properties of the vacuum

configuration out of which the horizon is transformed, but string theory has made progress in picturing frozen or slowly evolving horizons. In principle, what has been discussed here should also apply to horizons in different settings, such as cosmological horizons. Considerable caution is then asked for, however, since quantum mechanics might not apply to an entire cosmos.

References

- [1] M. Veltman, *Acta Phys. Polon.* **B25** 1399 (1994), hep-ph/9404358.
- [2] S.W. Hawking, *Commun. Math. Phys.* **43** (1975) 199;
J.B. Hartle and S.W. Hawking, *Phys. Rev.* **D13** (1976) 2188.
- [3] G. 't Hooft, *J. Mod. Phys.* **A11** (1996) 4623; gr-qc/9607022.
- [4] J.D. Bekenstein, *Nuovo Cim. Lett.* **4** (1972) 737; *Phys. Rev.* **D7** (1973) 2333; **D9** (1974) 3292.
- [5] G. 't Hooft, *Nucl. Phys.* **B256** (1985) 727.
- [6] T. Dray and G. 't Hooft, *Nucl. Phys.* **B253** (1985) 173.
- [7] G. 't Hooft, *Phys. Scripta* **T15** (1987) 143.
- [8] M. Perry, *Black holes and string theory*, in *The Future of Theoretical Physics and Cosmology, Celebrating Stephen Hawking's 60th Birthday*, eds. G.W. Gibbons et al, Cambridge University Press 2003, p. 291, and references therein.
- [9] W. Rindler, *Am.J. Phys.* **34** (1966) 1174.
- [10] G. 't Hooft, *Class. Quantum Grav.* **10** (1993) S79; *Nucl. Phys.* **B30** (Proc. Suppl.) (1993) 200.
- [11] D. Bohm, *Phys. Rev.* **85** (1952) 166, 180.
- [12] G. 't Hooft, *Class. Quant. Grav.* **16** (1999) 3263, gr-qc/9903084; also published in: Fundamental Interactions: from symmetries to black holes (Conference held on the occasion of the "Eméritat" of François Englert, 24-27 March 1999, ed. by J.-M. Frère et al, Univ. Libre de Bruxelles, Belgium, p. 221; see also G. 't Hooft, hep-th/0104080, hep-th/0104219.
- [13] S. Wolfram, *A New Kind of Science*, Wolfram Media, Inc., Canada, ISBN 1-57955-008-8.
- [14] M. Gardner, *Scientific American* 223 (October 1970) 120.
- [15] S. W. Hawking and G. F. R. Ellis, *The Large Scale Structure of Space-time*, Cambridge: Cambridge Univ. Press, 1973.

NEUTRINO OSCILLATIONS PHYSICS

GIANLUIGI FOGLI

*Dipartimento di Fisica and Sezione INFN, Via Amendola 173, I-70126 Bari
E-mail: gianluigi.fogli@ba.infn.it*

We review the status of the neutrino oscillations physics, with a particular emphasis on the present knowledge of the neutrino mass-mixing parameters. We consider first the $\nu_\mu \rightarrow \nu_\tau$ flavor transitions of atmospheric neutrinos. It is found that standard oscillations provide the best description of the SK+K2K data, and that the associated mass-mixing parameters are determined at $\pm 1\sigma$ (and $N_{DF} = 1$) as: $\Delta m^2 = (2.6 \pm 0.4) \times 10^{-3}$ eV 2 and $\sin^2 2\theta = 1.00^{+0.00}_{-0.05}$. Such indications, presently dominated by SK, could be strengthened by further K2K data. Then we point out that the recent data from the Sudbury Neutrino Observatory, together with other relevant measurements from solar and reactor neutrino experiments, in particular the KamLAND data, convincingly show that the flavor transitions of solar neutrinos are affected by Mikheyev-Smirnov-Wolfenstein (MSW) effects. Finally, we perform an updated analysis of two-family active oscillations of solar and reactor neutrinos in the standard MSW case.

1. Introduction

In its first phase of operation (years 1996–2001), the Super-Kamiokande (SK) experiment has provided, among other important results, compelling evidence for atmospheric ν_μ disappearance ^{1,2}. This evidence, now firmly based on a high-statistics 92 kton-year exposure ³, has not only been corroborated by consistent indications in the MACRO ⁴ and Soudan 2 ⁵ atmospheric neutrino experiments, but has also been independently checked by the first long-baseline KEK-to-Kamioka (K2K) accelerator experiment ^{6,7}, using SK as a target for ν_μ 's produced 250 km away with $\langle E_\nu \rangle \sim 1.3$ GeV. Neutrino flavor oscillations, interpreted in terms of nonzero mass-mixing parameters ($\Delta m^2, \sin^2 2\theta$) in the $\nu_\mu \rightarrow \nu_\tau$ channel, provide by far the best and most natural explanation for the observed ν_μ disappearance ^{1,2}.

In Section 2 we review the phenomenological status of the standard oscillations in the $\nu_\mu \rightarrow \nu_\tau$ channel, in the light of the latest SK atmospheric zenith distributions ³ and of the first spectral results from the K2K experiment ⁷.

On the solar neutrino front, the Sudbury Neutrino Observatory (SNO) experiment has recently released new data ⁸ with enhanced sensitivity to neutral-current (NC) interactions of solar neutrinos in deuterium. Charged current (CC) and elastic scattering (ES) events have also been statistically separated from NC events in a model-independent way, i.e., without using priors on the ${}^8\text{B}$ neutrino energy spectrum shape ⁸. These data corroborate the explanation of the solar neutrino deficit

in terms of (dominant) two-family $\nu_e \rightarrow \nu_a$ flavor transitions ($\nu_a = \nu_{\mu,\tau}$), which have convincingly emerged from the combined data of previous solar neutrino experiments (Chlorine ⁹, Gallium ^{10,11,12}, Super-Kamiokande (SK) ^{13,14}, and SNO ^{15,16,17}) and of long-baseline reactor oscillation searches at KamLAND ¹⁸. Moreover, the new SNO data appear to forbid relatively high values of the neutrino mixing angle θ_{12} (close to maximal mixing) and of the squared mass difference δm^2 (close to the CHOOZ ¹⁹ upper bound), which were marginally allowed prior to ⁸ (see, e.g., ^{20,21}). In the current global fit ⁸, the mass-mixing parameters appear to be tightly confined in the so-called large mixing angle (LMA) region, and especially in a subregion often denoted as LMA-I ²⁰.

In the LMA parameter range, flavor transitions between ν_e and ν_a should be significantly affected by the neutrino interaction energy difference $V = V_e - V_a$ arising in solar (and possibly Earth) background matter ^{22,23},

$$V(x) = \sqrt{2}G_F N_e(x) , \quad (1)$$

where N_e is the electron number density at the point x . The associated flavor change, known as Mikheyev-Smirnov-Wolfenstein (MSW) effect ²², should occur adiabatically ²⁴ in the solar matter, for LMA parameters. In the context of Hamiltonian (\mathcal{H}) evolution of 2ν active flavors, the MSW effect enters through a dynamical term \mathcal{H}_{dyn} in matter, in addition to the kinetic term \mathcal{H}_{kin} in vacuum:

$$i \frac{d}{dx} \begin{pmatrix} \nu_e \\ \nu_a \end{pmatrix} = (\mathcal{H}_{\text{dyn}} + \mathcal{H}_{\text{kin}}) \begin{pmatrix} \nu_e \\ \nu_a \end{pmatrix} , \quad (2)$$

where

$$\mathcal{H}_{\text{dyn}} = \frac{V(x)}{2} \begin{pmatrix} 1 & 0 \\ 0 & -1 \end{pmatrix} \quad (3)$$

and

$$\mathcal{H}_{\text{kin}} = \frac{\delta m^2}{4E} \begin{pmatrix} -\cos 2\theta_{12} & \sin 2\theta_{12} \\ \sin 2\theta_{12} & \cos 2\theta_{12} \end{pmatrix} , \quad (4)$$

E being the neutrino energy.

In a previous recent work ²⁵ we pointed out that, while the evidence for $\mathcal{H}_{\text{kin}} \neq 0$ was overwhelming, the phenomenological indications in favor of $\mathcal{H}_{\text{dyn}} \neq 0$ (and thus of MSW effects) were not as compelling. In particular, we introduced in ²⁵ a free parameter a_{MSW} modulating the overall amplitude of the dynamical term \mathcal{H}_{dyn} through the substitution

$$V \rightarrow a_{\text{MSW}} \cdot V , \quad (5)$$

both in the Sun and in the Earth. We showed that a_{MSW} was poorly constrained, despite an intriguing preference for the standard MSW expectation $a_{\text{MSW}} \sim 1$ ²⁵. The null hypothesis $a_{\text{MSW}} = 0$ was not clearly disproved by any single experiment, and could be rejected at a relevant confidence level ($\Delta\chi^2 \simeq 13$, formally

equivalent to $\sqrt{\Delta\chi^2} \simeq 3.5\sigma$) only in the global fit. We concluded that the available phenomenological data clearly favored MSW effects in solar neutrinos, but did not prove unequivocally their occurrence. We deemed it necessary to wait for new KamLAND or SNO data, in order to clarify the situation and to probe MSW effects with higher statistical significance²⁵.

In this work, we point out that the recent SNO data⁸ contribute significantly to disprove the null hypothesis of no MSW oscillations. In the global combination of solar and reactor data, we find that, with respect to the (preferred) standard case $a_{\text{MSW}} \sim 1$, the null hypothesis $a_{\text{MSW}} = 0$ can be safely rejected at the level of $\sim 5.6\sigma$, despite the fact the allowed range of a_{MSW} is still rather large. In other words, the evidence in favor of MSW effects is now very strong, although precision tests of the MSW physics cannot be performed until new, high statistics KamLAND data become available (as we show later).

In Section 3, we analyze the current solar and reactor neutrino phenomenology with an increasing degree of dependence on assumptions about the MSW effect.^a In Subsec. 3.1 we do not make any hypothesis about MSW effects, and show that SNO data alone, as well as a model-independent SNO+SK combination, constrain the energy-averaged ν_e survival probability $\langle P_{ee} \rangle$ to be significantly smaller than 1/2. This fact, by itself, excludes the vacuum case $a_{\text{MSW}} = 0$ (which would predict $\langle P_{ee} \rangle \geq 1/2$ in the LMA region selected by KamLAND), and proves that dynamical effects *must* occur in solar neutrino propagation with unspecified amplitude $a_{\text{MSW}} > 0$. In Subsec. 3.2 we fit all the available solar and reactor data with $(\delta m^2, \theta_{12}, a_{\text{MSW}})$ taken as free parameters. We find that MSW effects with standard amplitude ($a_{\text{MSW}} = 1$) are favored, while the null hypothesis ($a_{\text{MSW}} = 0$) can be safely rejected at the $\sim 5.6\sigma$ level. However, we show that the allowed range of a_{MSW} is still very large, and can be significantly narrowed only by future KamLAND data. Assuming standard MSW effects ($a_{\text{MSW}} = 1$), we perform in Subsec. 3.3 an updated analysis of the 2ν kinematical parameters $(\delta m^2, \sin^2 \theta_{12})$. We briefly discuss the impact of 3ν mixing in Sec. 4, and conclude our work in Sec. 5.

2. "Atmospheric" neutrinos

A careful analysis of the SK and K2K data sets used in the following can be found in²⁶. Concerning SK atmospheric neutrino data (92 kton-year³), we use the usual zenith angle (θ_z) distributions of leptons: sub-GeV e -like and μ -like events, divided in 10+10 bins; multi-GeV e -like and μ -like events, divided in 10+10 bins; upward stopping and through-going μ events, divided in 5+10 bins. The calculation of the theoretical events rates R_n^{theo} in each of the 55 bins is done as in^{27,28,29}. The SK statistical analysis is considerably improved with respect to^{27,29}. Now the set of systematic errors has been enlarged to 11 entries, leading to a more complex structure of correlated errors affecting the R_n^{theo} 's. As emphasized in³⁰, systematic

^aIn any case, we assume active flavor oscillations only, and discard hypothetical sterile neutrinos.

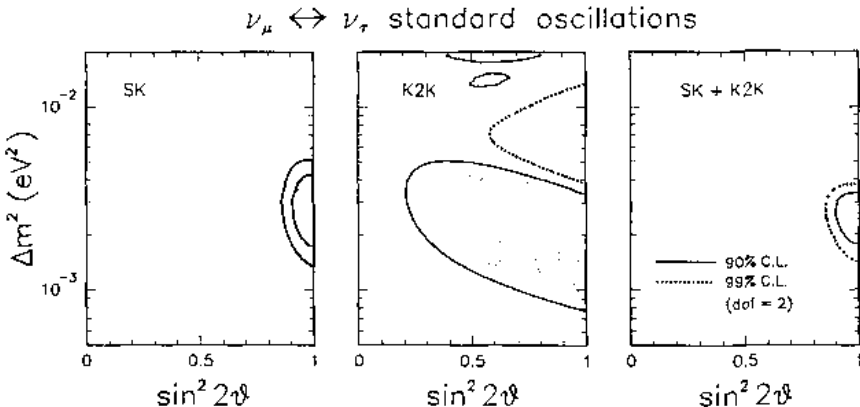


Figure 1. Standard oscillations in the $\nu_\mu \rightarrow \nu_\tau$ channel: bounds on the parameters (Δm^2 , $\sin^2 2\theta$) from SK atmospheric data (left panel), K2K spectral data (middle panel), and their combination (right panel).

uncertainties can be implemented in the χ^2 statistics through two equivalent methods, the “covariance method” or the “pull method”. The latter approach, adopted in this work, allows to study how systematic errors alter the theoretical predictions from the central values R_n^{theo} to “shifted” values \bar{R}_n^{theo} , in order to match the data. The difference $\bar{R}_n^{\text{theo}} - R_n^{\text{theo}}$ is thus useful to gauge the size and the direction of systematic effects.

Concerning the K2K data, we use the absolute spectrum of muon events in terms of the reconstructed neutrino energy E ⁷, which provides a total of 29 events (here divided in 6 bins). In this sample, the parent neutrino interactions are dominantly quasi-elastic (QE), and the reconstructed energy E is thus closely correlated with the true neutrino energy E_ν .

Let us now discuss the updated bounds on the parameters (Δm^2 , $\sin^2 2\theta$), governing the scenario of standard oscillations.

Figure 1 shows the joint bounds on the (Δm^2 , $\sin^2 2\theta$) parameters from our analysis of SK, K2K, and SK+K2K data. The bounds in the left panel are very close to the official SK ones, as presented in³. The bounds in the middle panel are instead slightly weaker than the official K2K ones⁷, especially in terms of $\sin^2 2\theta$. In particular, we do not find a lower bound on $\sin^2 2\theta$ at 99% C.L. (for $N_{\text{DF}} = 2$). The reason is that we cannot use the additional (dominantly) non-QE event sample of K2K (27 events), which would help to constrain the overall rate normalization and thus $\sin^2 2\theta$. This fact might also explain why we find the K2K best fit at $\sin^2 2\theta = 0.82$ rather than at 1.00 as in⁷. By comparing left and right panels of Fig. 1, the main effect of K2K appears to be the strengthening of the upper bound on Δm^2 , consistently with the trend of the first K2K data (rate only⁶, no spectrum)²⁹. The main reason is that, for $\Delta m^2 \sim (4-6) \times 10^{-3} \text{ eV}^2$, the first oscillation minimum would be located at—or just above—the K2K energy spectrum peak, implying a strong local and overall suppression of the expected events.

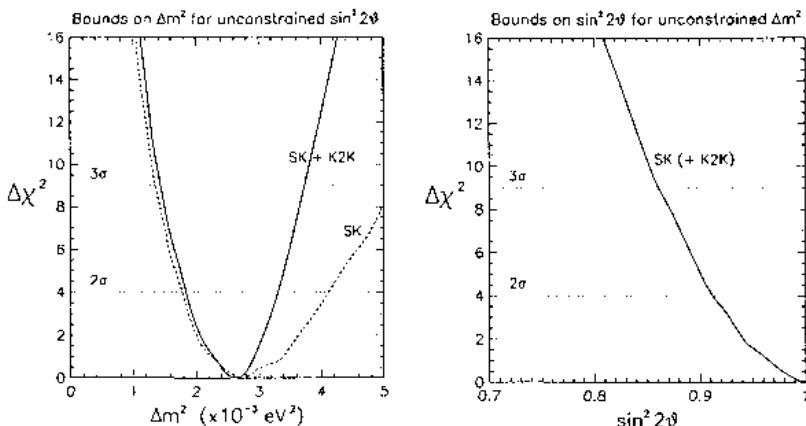


Figure 2. Standard oscillations in the $\nu_\mu \rightarrow \nu_\tau$ channel. On the left: bounds on Δm^2 for unconstrained $\sin^2 2\theta$ from SK (dashed curve) and SK+K2K (solid curve). On the right: bounds on $\sin^2 2\theta$ for unconstrained Δm^2 from SK data. The inclusion of K2K data induces here negligible changes (not shown).

Figure 2 shows on the left the SK and SK+K2K bounds on Δm^2 , when the $\sin^2 2\theta$ parameter is projected (minimized) away. The linear scale in Δm^2 makes the K2K impact on the upper limit more evident. Notice that, up to $\sim 3\sigma$, the global (SK+K2K) χ^2 function is approximately parabolic in the *linear* variable Δm^2 , so that one can define a one-standard-deviation error for this parameter. This feature, here confirmed through a full analysis, was already argued on the basis of a graphical reduction of the official SK and K2K likelihood functions³¹. By keeping only the first significant figure in the error estimate, a parabolic fit provides the $\pm 1\sigma$ range,

$$\Delta m^2 = (2.6 \pm 0.4) \times 10^{-3} \text{ eV}^2. \quad (6)$$

The bounds on $\sin^2 2\theta$ are instead entirely dominated by SK. This is shown on the right of Fig. 2, where the $\Delta\chi^2$ function in terms of $\sin^2 2\theta$ is reported, for Δm^2 projected (minimized) away in the SK fit. Here the addition of K2K data would insignificantly change the bounds (not shown), which thus hold for both the SK and the SK+K2K fit. Also in this case, the nearly parabolic behavior of $\Delta\chi^2$ allows to properly define a 1σ range,

$$\sin^2 2\theta = 1.00^{+0.00}_{-0.05}, \quad (7)$$

with the lower $N\sigma$ error scaling linearly with N (up to $N \simeq 3$). Equations (6) and (7) concisely review the current fit to the standard oscillation parameters, as anticipated in the Introduction.

Figure 3 shows the comparison between observations and best-fit predictions for the SK zenith distributions. Since the very good agreement between data and theory is no longer a surprise, in the following we comment on the “fine structure” of the SK data fit. This requires, however, that the reader can grasp the difference

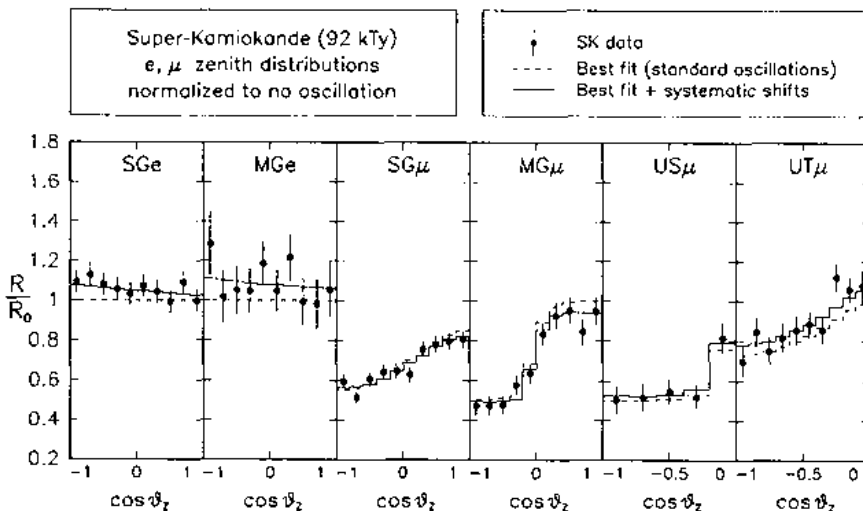


Figure 3. SK experimental zenith distributions ($\pm 1\sigma_{\text{stat}}$), compared with the corresponding theoretical ones at the global (SK+K2K) best-fit point. All distributions are normalized to the unoscillated predictions in each bin. For the theoretical event rates, we show both the central values R_n^{theo} (dashed histograms) and the “shifted” values \bar{R}_n^{theo} (solid histograms), which embed the effect of systematic pulls. The difference between \bar{R}_n^{theo} and R_n^{theo} shows how much (and in which direction) the correlated systematic errors tend to stretch the predictions in order to match the data.

between theoretical predictions with and without the shifts induced by correlated systematics (solid and dashed histograms in Fig. 3, respectively).

In particular, the comparison between solid and dashed histograms in Fig. 3 shows that systematic shifts are often comparable in size to statistical errors, implying that just increasing the SK atmospheric ν statistics will hardly bring decisive new information on the standard oscillation scenario. In the SG and MG samples, the fit clearly exploits the systematic uncertainties to increase the e -like event normalization, especially in the upward direction, so as to reduce the “electron excess” possibly indicated by SK data.

Concerning μ -like events in the SG and MG samples, the fit shows an opposite tendency to slightly decrease the normalization of (especially down-going) events. The tendency appears to be reversed in the high-energy UT sample. Taken together, these opposite shifts of e -like and μ -like expectations in the SG and MG samples seem to suggest some systematic deviation from the predicted μ/e flavor ratio which, although not statistically alarming, should be kept in mind: deviations of similar size might have their origin in neutrino physics beyond 2ν oscillations. Unfortunately, since such effects are typically not larger than the systematic shifts in Fig. 3, they are likely (if any) to remain hidden in higher-statistics SK data, unless a significant reduction of the current systematics can be accomplished. The happy side of the story is that, for the same reasons, typical subleading effects beyond standard 2ν

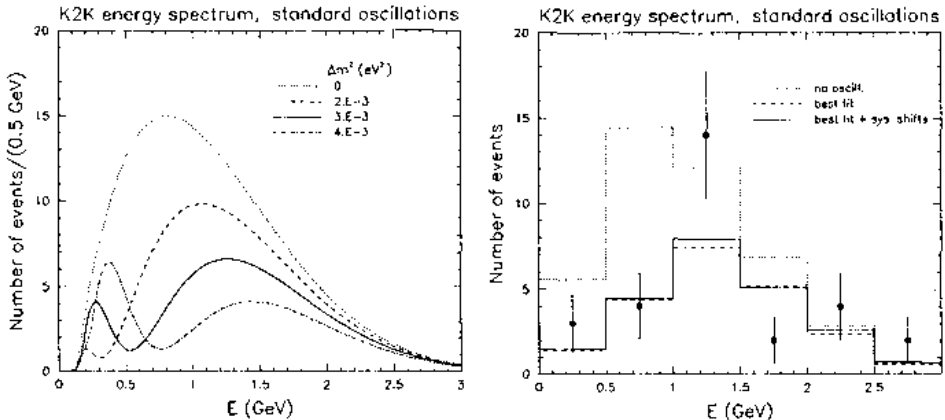


Figure 4. Comparison between the unbinned K2K theoretical spectrum at maximal mixing for three representative values of Δm^2 and the absolute spectrum of the events in K2K, as a function of the reconstructed neutrino energy E . The data points (29 events total) are shown as dots with $\pm 1\sigma_{\text{stat}}$ in each of the six bins. The dotted histogram represents our calculations for no oscillation. The solid and dashed histograms represent the theoretical predictions N_n^{theo} and N_n^{theo} at the global (SK+K2K) best-fit point, with and without systematic shifts, respectively.

oscillations do not significantly alter the fit results in Eqs. (6) and (7).

Finally, Figure 4 shows the comparison between theory and data for the K2K energy spectrum, for the same oscillation best-fit point as in Fig. 3. In this case, the amount of systematic deviations preferred by the fit is much smaller than the current statistical error: there is then a great potential for improvements with higher K2K statistics.

3. Solar neutrinos (a 2ν analysis)

3.1. Model-independent constraints

It has been shown in ³² (see also ³⁰) that the SK and SNO experiments probe the same energy-averaged ν_e survival probability $\langle P_{ee} \rangle$ to a good accuracy, provided that the detector thresholds are appropriately chosen. For the kinetic energy threshold ($T_{\text{SNO}} = 5.5$ MeV) and energy resolution characterizing the latest SNO data ⁸, we find that the equivalent SK threshold is $E_{\text{SK}} \simeq 7.8$ MeV in total energy. For equalized thresholds, the SK ES flux and the SNO NC and CC fluxes are linked by the exact relations ³²

$$\Phi_{\text{ES}}^{\text{SK}} = \Phi_B [\langle P_{ee} \rangle + r(1 - \langle P_{ee} \rangle)] , \quad (8)$$

$$\Phi_{\text{CC}}^{\text{SNO}} = \Phi_B \langle P_{ee} \rangle , \quad (9)$$

$$\Phi_{\text{NC}}^{\text{SNO}} = \Phi_B , \quad (10)$$

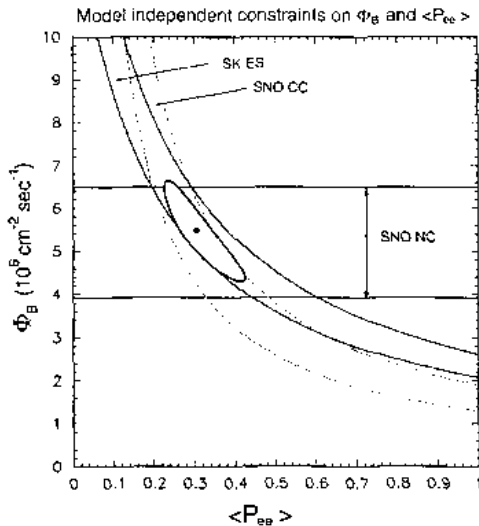


Figure 5. Results of the model-independent analysis of SNO (CC and NC) and SK (ES) neutrino fluxes. The projections of the ellipse provide 3σ bounds on the ${}^8\text{B}$ neutrino flux Φ_B and on the energy-averaged ν_e survival probability $\langle P_{ee} \rangle$.

where $r = 0.154$ is the ratio of (properly averaged) $\nu_{\mu,\tau}$ and ν_e CC cross sections, and Φ_B is the true ${}^8\text{B}$ flux from the Sun. From the above equations, one can (over)constrain both Φ_B and $\langle P_{ee} \rangle$ in a truly model-independent way, namely, without any prior assumption about the energy profile of P_{ee} or about Φ_B predictions in standard solar models (SSM).

Figure 5 shows the current constraints on Φ_B and on $\langle P_{ee} \rangle$ as derived from the final SK ES data¹³ and from the latest SNO CC and NC fluxes⁸ (correlations included³³). The constraints are shown both by individual bands and by their combination at the 3σ level ($\Delta\chi^2 = 9$). The projections of the SNO+SK combination (solid ellipse in Fig. 5) provide the range

$$\Phi_B = (5.5 \pm 1.2) \times 10^6 \text{ cm}^{-2}\text{s}^{-1} (3\sigma), \quad (11)$$

in good agreement with SSM predictions³⁴, and

$$\langle P_{ee} \rangle = 0.31^{+0.12}_{-0.08} (3\sigma). \quad (12)$$

The above 3σ limits on $\langle P_{ee} \rangle$ are in very good agreement with the “ 3σ range” obtained by naively triplicating the errors of the SNO CC/NC flux ratio, which is a direct measurement of $\langle P_{ee} \rangle$: $\Phi_{\text{CC}}^{\text{SNO}}/\Phi_{\text{NC}}^{\text{SNO}} = 0.306 \pm 0.105(3\sigma)$ ⁸. However, as emphasized in³³, the errors of the CC/NC ratio are not normally distributed, and should not be used in fits. Conversely, our bounds in Eq. (12) are statistically safe and well-defined, and will be used in the following discussion.

The above SK+SNO constraints appear to be currently dominated by the SNO

data. In particular, the upper bound on the ν_e survival probability,

$$\langle P_{ee} \rangle < 0.43 \text{ (3}\sigma\text{)} , \quad (13)$$

can be basically derived from the SNO (CC+NC) data ⁸ alone. The upper limit in Eq. (13) is significantly stronger than the one derived in³⁰, prior to the latest SNO data ⁸. In particular, we have now robust, model-independent evidence that P_{ee} is definitely smaller than 1/2 at $> 3\sigma$ level. This inequality has important consequences for both the dynamical and the kinematical term in Eq. (2). First, in the δm^2 range accessible to KamLAND and below the CHOOZ bound ($\delta m^2 \sim O(10^{-4 \pm 1}) \text{ eV}^2$), the absence of the dynamical MSW term \mathcal{H}_{dyn} (i.e., the case $a_{\text{MSW}} = 0$) would imply $\langle P_{ee} \rangle \geq 1/2$ (see, e.g.,²⁵), contrary to Eq. (13). Second, assuming standard MSW dynamics ($a_{\text{MSW}} = 1$), the inequality in Eq. (13) allows to place upper limits on the kinematical parameters δm^2 and $\sin^2 \theta_{12}$ (see, e.g., the discussions in^{25,35,36}).

Summarizing, the latest SNO CC and NC data ⁸, either by themselves or in combination with the SK ES data ¹⁴, provide the strong, model-independent upper bound $\langle P_{ee} \rangle < 0.43$ at 3σ . In the context of 2ν mixing, and within the mass-mixing region probed by KamLAND, this bound allows to reject the null hypothesis ($a_{\text{MSW}} = 0$), and provides upper limits on the mass-mixing parameters in the standard MSW case ($a_{\text{MSW}} = 1$). In the next Section, we examine the more general case of variable a_{MSW} , in order to test whether current and future data can significantly constrain, by themselves, the size of matter effects.

3.2. Constraints on the MSW dynamical term

In this subsection we present the results of a global analysis of solar and reactor (KamLAND + CHOOZ) data with $(\delta m^2, \sin^2 \theta_{12}, a_{\text{MSW}})$ unconstrained. The latest SNO data ⁸ are incorporated according to the recommendations in³³. The reader is referred to²⁵ for other details of the analysis.

Figure 6 shows the results of the global χ^2 fit, in terms of the function $\Delta\chi^2(a_{\text{MSW}})$ after $(\delta m^2, \sin^2 \theta_{12})$ marginalization. Such marginalization is appropriate to test the size of \mathcal{H}_{dyn} independently of \mathcal{H}_{kin} . It can be seen that the best fit is intriguingly close to the standard case ($a_{\text{MSW}} = 1$), although there are other acceptable local minima over about three decades in a_{MSW} . As discussed in²⁵ for the case of variable a_{MSW} , the δm^2 range allowed by solar neutrino data sweeps through the tower of LMA- n solutions allowed by KamLAND, leading to a series of “bumps” in the $\Delta\chi^2$ function (solid line). Such features are unavoidable, as far as KamLAND allows multiple solutions in the mass-mixing parameter space. However, the situation should improve with higher KamLAND statistics. Assuming that KamLAND will confirm the current best-fit solution in the $(\delta m^2, \sin^2 \theta_{12}, a_{\text{MSW}})$ space, and simulating the corresponding KamLAND data, we obtain the prospective dotted and dashed curves in Fig. 6, which refer to a fivefold and tenfold increase of the present statistics (54 events¹⁸), respectively. It appears that, with the help

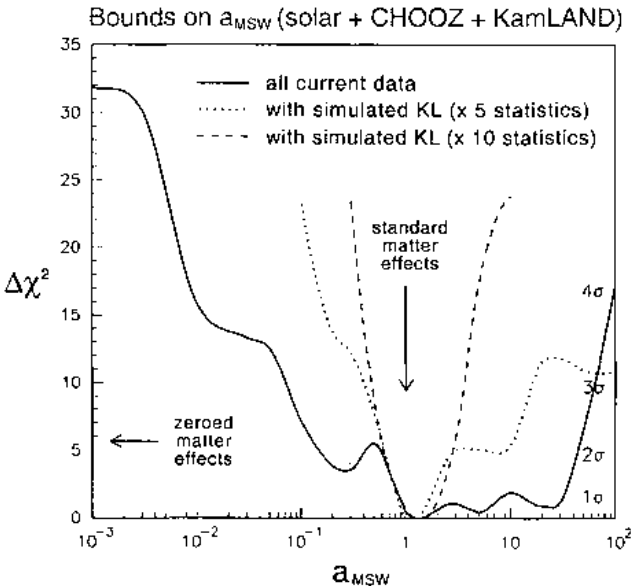


Figure 6. Bounds on a_{MSW} (considered as a continuous free parameter), including all current solar, CHOOZ, and KamLAND data (solid curve). Prospective KamLAND data with higher statistics are used to draw the dotted and dashed curves. See the text for details.

of a few hundreds KamLAND events, the global fit of solar and reactor data can pinpoint the predicted size of MSW effects within a factor of ~ 2 , allowing future “precision tests” of these effects (e.g., to probe additional nonstandard interactions).

Although the current bounds on a_{MSW} appear to be rather weak, the rejection of the null hypothesis $a_{\text{MSW}} = 0$ is quite strong, and corresponds to a significance level of $\Delta\chi^2 \simeq 32$, i.e., $\sim 5.6\sigma$. Summarizing the results of this and the previous section, we can state that current solar and reactor data reject the hypothesis of no MSW effect at $> 5\sigma$ level, with a $> 3\sigma$ contribution from the recent SNO data⁸. Therefore, in our opinion, the phenomenological indications in favor of MSW effects can now be promoted to the level of evidence.

3.3. Constraints on kinematical mass-mixing term

In this subsection, assuming standard MSW dynamics, we update our previous bounds²⁰ on the mass-mixing parameters ($\delta m^2, \sin^2 \theta_{12}$) which govern the kinematical term \mathcal{H}_{kin} . The reader is referred to^{20,30} for technical details. Here we just add that the statistical correlations of recent SNO data³³ are incorporated through a straightforward generalization of the pull approach³⁰, as explicitly described in³⁷. We have checked that our analysis “SNO data only” reproduces the results of²⁰ with very good accuracy. Finally, we have updated the total rate and winter-summer asymmetry from Gallium experiments³⁸. In total, we have 84 solar neutrino observables, plus 13 KamLAND bins.

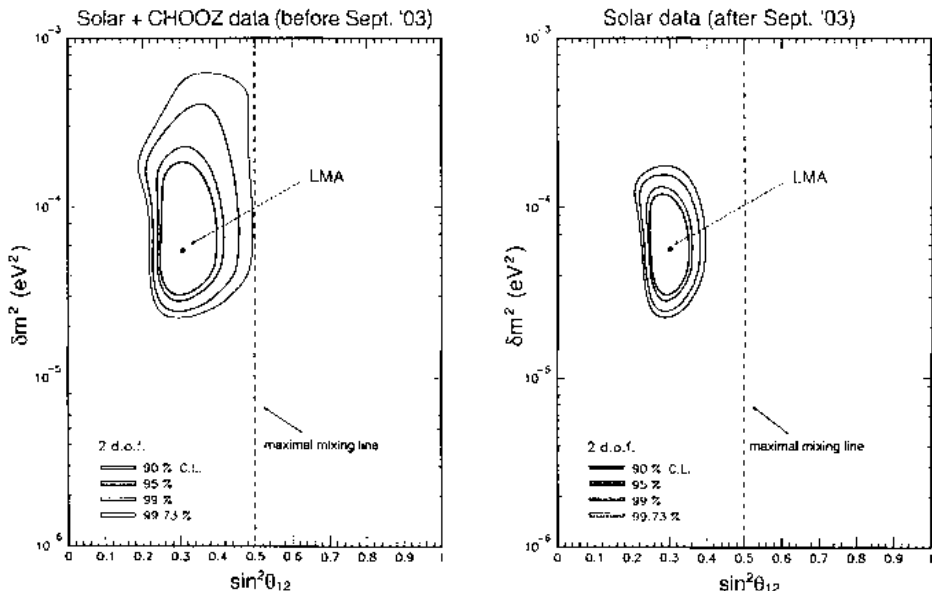


Figure 7. Two-flavor active neutrino oscillations, for standard MSW effects. On the left, global analysis of solar and CHOOZ neutrino data in the $(\delta m^2, \sin^2 \theta_{12})$ parameter space, restricted to the LMA region, without including the last data from SNO. On the right, the global analysis including all the present solar neutrino data, in particular the last SNO results. The best fit is indicated by a black dot.

Figure 7 shows the results of our fit to all solar neutrino data, with a comparison with the fit before the inclusion of the last SNO data⁸. In the analysis on the right, also the CHOOZ data are added, in order to strengthen the upper bound on δm^2 . Conversely, current solar neutrino data make this addition no longer necessary in the context of 2ν mixing with standard MSW effects. The best fit on the left side ($\chi^2_{\min} = 72.9$) is reached at $\delta m^2 = 5.7 \times 10^{-5}$ and $\sin^2 \theta_{12} = 0.29$. The upper and lower bounds on the mass-mixing parameters are in good agreement with the results in⁸, and confirm that the solar neutrino parameter space is steadily narrowing.

Figure 8 incorporates the analysis of KamLAND data¹⁸ as in²⁰. The best fit ($\chi^2_{\min} = 79.7$) is reached at $\delta m^2 = 7.2 \times 10^{-5}$ and $\sin^2 \theta_{12} = 0.29$ (LMA-I solution), while the second best fit (LMA-II solution) is only marginally allowed at the $\Delta \chi^2 = 9.4$ level ($\sim 99\%$ C.L. for $N_{DF} = 2$). Also in this case, we find good agreement with the results in⁸, modulo the obvious transformation from our linear abscissa $\sin^2 \theta_{12}$ to their logarithmic abscissa $\tan^2 \theta_{12}$.

In conclusion, the kinematical 2ν mass-mixing parameters appear to be strongly constrained in a basically unique region (LMA-I), with only a marginal possibility left for the LMA-II region. The decrease of the previous LMA-II likelihood²⁰ is an important contribution of the latest SNO data⁸.

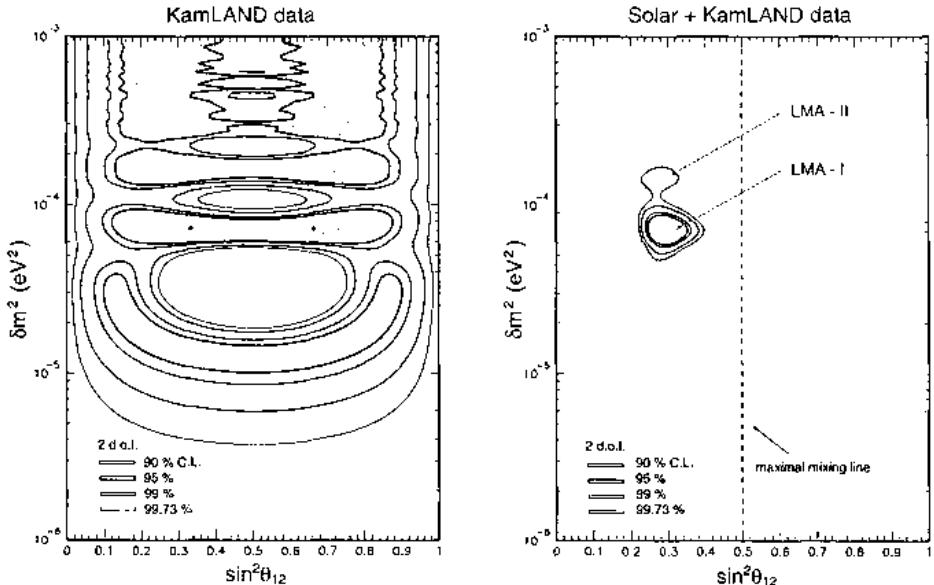


Figure 8. Two-flavor active neutrino oscillations, for standard MSW effects. On the left, global analysis of KamLAND data in the $(\delta m^2, \sin^2 \theta_{12})$ parameter space. On the right, global analysis of solar and KamLAND neutrino data. As an effect of the last SNO data, the LMA region is significantly restricted and, of the two subregions (LMA-I and LMA-II), LMA-II is only marginally allowed. The best fits are indicated by a black dot.

4. Comments on three-family mixing

So far, we have assumed flavor oscillations in the active 2ν channel $\nu_e \rightarrow \nu_a$ (ν_a being a linear combination of ν_μ and ν_τ) driven by the $(\delta m^2, \theta_{12})$ parameters. The (ν_μ, ν_τ) combination orthogonal to ν_a is probed by atmospheric $\nu_\mu \rightarrow \nu_\tau$ oscillations, with different parameters $(\Delta m^2, \theta_{23})$ ³⁹. As far as the third mixing angle θ_{13} is zero (and $\delta m^2 / \Delta m^2 \ll 1$), the two oscillation channels are practically decoupled, and all our previous considerations hold without changes. However, for small but nonzero θ_{13} , the 3ν survival probability deviates from the 2ν case for both solar and KamLAND ν_e oscillations:

$$P_{ee}^{3\nu} \simeq (1 - 2 \sin^2 \theta_{13}) P_{ee}^{2\nu}. \quad (14)$$

Concerning θ_{13} , until very recently the upper bound on θ_{13} (dominated by CHOOZ and atmospheric data) could be quoted as $\sin^2 \theta_{13} < 0.05$ (3σ)²⁰, leading to $P_{ee}^{3\nu}(a_{\text{MSW}} = 0) > 0.45$. A new SK atmospheric data analysis⁴⁰, however, appears to imply the weaker bound $\sin^2 \theta_{13} < 0.067$ (3σ)⁴¹, leading to $P_{ee}^{3\nu}(a_{\text{MSW}} = 0) > 0.43$. In both cases, there is no overlap with the experimental upper bound of Eq. (13). Therefore, the null hypothesis $a_{\text{MSW}} = 0$ can be rejected at the 3σ level also in the 3ν mixing case, using only SNO(+SK) data.

In the more general case of variable a_{MSW} , we have not performed the 3ν gen-

eralization of the analysis in Subsec. 3.2. Our educated guess is that an allowance for small values of θ_{13} should only slightly weaken—but should not spoil—the main results discussed therein.

5. Conclusions

We have analyzed in detail the current SK atmospheric neutrino data and the first K2K spectral data, in order to review the status of standard $\nu_\mu \rightarrow \nu_\tau$ oscillations. We have then provided updated bounds for the standard oscillation parameters. In particular, the statistical analysis of the uncertainties reveals that K2K will lead further progress in this field, especially through higher-statistics tests of the low-energy spectrum bins.

Going to solar neutrinos, we have pointed out that recent SNO data⁸ strongly favor the occurrence of MSW effects in the solar matter and, together with world solar and reactor data, provide a many-sigma rejection of the null hypothesis. We have also performed an analysis where the MSW interaction energy is freely rescaled, and found poor constraints on the scaling parameter. These constraints can be potentially improved by higher-statistics KamLAND data, which will then allow more precise tests of the MSW dynamics. In the standard MSW case, we have also performed an updated analysis of two-family active oscillations of solar and reactor neutrinos.

We conclude by observing that, although MSW effects are an unavoidable consequence of the standard theory of electroweak interactions, their basic confirmation in the current neutrino phenomenology represents an important and reassuring experimental accomplishment, which strengthen our confidence in the emerging picture of neutrino masses and mixings.

6. Acknowledgments

The author thanks the organizer of the School, prof. Antonino Zichichi, for the kind hospitality. This work is supported in part by the Istituto Nazionale di Fisica Nucleare (INFN) and by the Italian Ministry of Education (MIUR) through the “Astroparticle Physics” project.

References

1. SK Collaboration, Y. Fukuda *et al.*, Phys. Rev. Lett. **81**, 1562 (1998) [hep-ex/9807003].
2. T. Kajita and Y. Totsuka, Rev. Mod. Phys. **73**, 85 (2001).
3. SK Collaboration, M. Shiozawa *et al.*, in *Neutrino 2002*, Proceedings of the 20th International Conference on Neutrino Physics and Astrophysics (Munich, Germany, 2002), to appear.
4. MACRO Collaboration, M. Ambrosio *et al.*, Phys. Lett. B **517**, 59 (2001).
5. Soudan 2 Collaboration, W.W. Allison *et al.*, Phys. Lett. B **449**, 137 (1999).
6. K2K Collaboration, S.H. Ahn *et al.*, Phys. Lett. B **511**, 178 (2001).

7. K2K Collaboration, M.H. Ahn *et al.*, Phys. Rev. Lett. **90**, 041801 (2003).
8. SNO Collaboration, S.N. Ahmed *et al.*, nucl-ex/0309004, submitted to Phys. Rev. Lett.
9. Homestake Collaboration, B.T. Cleveland, T. Daily, R. Davis Jr., J.R. Distel, K. Lande, C.K. Lee, P.S. Wildenhain, and J. Ullman, Astrophys. J. **496**, 505 (1998).
10. SAGE Collaboration, J.N. Abdurashitov *et al.*, J. Exp. Theor. Phys. **95**, 181 (2002) [Zh. Eksp. Teor. Fiz. **95**, 211 (2002)].
11. GALLEX Collaboration, W. Hampel *et al.*, Phys. Lett. B **447**, 127 (1999).
12. T. Kirsten for the GNO Collaboration, in *Neutrino 2002*, 20th International Conference on Neutrino Physics and Astrophysics (Munich, Germany, 2002).
13. SK Collaboration, S. Fukuda *et al.*, Phys. Rev. Lett. **86**, 5651 (2001); *ibidem*, 5656 (2001).
14. SK Collaboration, S. Fukuda *et al.*, Phys. Lett. B **539**, 179 (2002).
15. SNO Collaboration, Q.R. Ahmad *et al.*, Phys. Rev. Lett. **87**, 071301 (2001).
16. SNO Collaboration, Q.R. Ahmad *et al.*, Phys. Rev. Lett. **89**, 011301 (2002).
17. SNO Collaboration, Q.R. Ahmad *et al.*, Phys. Rev. Lett. **89**, 011302 (2002).
18. KamLAND Collaboration, K. Eguchi *et al.*, Phys. Rev. Lett. **90**, 021802 (2003).
19. CHOOZ Collaboration, M. Apollonio *et al.*, Phys. Lett. B **466**, 415 (1999); M. Apollonio *et al.*, Eur. Phys. J. C. **27**, 331 (2003).
20. G.L. Fogli, E. Lisi, A. Marrone, D. Montanino, A. Palazzo, and A. Rotunno, Phys. Rev. D **67**, 073002 (2003).
21. J. N. Bahcall, M. C. Gonzalez-Garcia, and C. Peña-Garay, JHEP **0302**, 009 (2003).
22. L. Wolfenstein, Phys. Rev. D **17**, 2369 (1978); S.P. Mikheev and A.Yu. Smirnov, Yad. Fiz. **42**, 1441 (1985) [Sov. J. Nucl. Phys. **42**, 913 (1985)].
23. V.D. Barger, K. Whisnant, S. Pakvasa, and R.J.N. Phillips, Phys. Rev. D **22**, 2718 (1980).
24. L. Wolfenstein, in *Neutrino '78*, 8th International Conference on Neutrino Physics and Astrophysics (Purdue U., West Lafayette, Indiana, 1978), ed. by E.C. Fowler (Purdue U. Press, 1978), p. C3.
25. G.L. Fogli, E. Lisi, A. Palazzo, and A.M. Rotunno, Phys. Rev. D **67**, 073001 (2003).
26. G.L. Fogli, E. Lisi, A. Marrone and D. Montanino, Phys. Rev. D **67**, 093006 (2003).
27. G.L. Fogli, E. Lisi, A. Marrone, and G. Scioscia, Phys. Rev. D **59**, 033001 (1999).
28. G.L. Fogli, E. Lisi, and A. Marrone, Phys. Rev. D **64**, 093005 (2001).
29. G.L. Fogli, E. Lisi, and A. Marrone, Phys. Rev. D **65**, 073028 (2002).
30. G.L. Fogli, E. Lisi, A. Marrone, D. Montanino and A. Palazzo, Phys. Rev. D **66**, 053010 (2002).
31. G.L. Fogli, G. Lettera, E. Lisi, A. Marrone, A. Palazzo, and A. Rotunno, Phys. Rev. D **66**, 093008 (2002).
32. F.L. Villante, G. Fiorentini, and E. Lisi, Phys. Rev. D **59**, 013006 (1999).
33. SNO Collaboration, "How to use the SNO Salt flux results", available at www.sno.phy.queensu.ca
34. J.N. Bahcall, M.H. Pinsonneault, and S. Basu, Astrophys. J. **555**, 990 (2001).
35. M. Maris and S.T. Petcov, Phys. Lett. B **534**, 17 (2002).
36. P.C. de Holanda and A. Yu. Smirnov, JCAP **0302**, 001 (2003).
37. A.B. Balantekin and H. Yuksel, JCAP **0302**, 001 (2003).
38. E. Bellotti and V. Gavrin, talks at LowNu 2003 (Paris, France, 2003), available at cdfinfo.in2p3.fr/LowNu2003
39. See, e.g., the reviews: S.M. Bilenky, C. Giunti, and W. Grimus, Prog. Part. Nucl. Phys. **43**, 1 (1999); P. Langacker, in *NOW 2000*, Proceedings of the Neutrino Oscillation Workshop 2000 (Conca Specchiolla, Italy, 2000), ed. by G.I. Fogli, Nucl. Phys. Proc.

- Suppl. **100**, 383 (2001); M. C. Gonzalez-Garcia and Y. Nir, Rev. Mod. Phys. **75**, 345 (2003).
- 40. Y. Hayato, "*Status of the Super-Kamiokande, the K2K and the J-Park ν project*", talk at *HEP 2003*, International Europhysics Conference on High Energy Physics (Aachen, Germany, 2003).// Website: eps2003.physik.rwth-aachen.de
 - 41. G.L. Fogli, E. Lisi, A. Marrone, D. Montanino, A. Palazzo, and A. Rotunno, hep-ph/0308055.

CHAIRMAN: G. L. FOGLI*Scientific Secretaries: C. Bozza, A. Mirizzi***DISCUSSION**

- *Gripaios:*

Are there plausible theoretical explanations for the neutrino mass hierarchy?

- *Fogli:*

There are several hypotheses based on the GUT groups that can justify some pattern: there are theoretical approaches that try to justify, starting from several hypotheses on first quantities in the mass matrix, why we find small values of some mixing angles and large values of the other ones. I think the question deserves a comment: from the theoretical point of view, we cannot expect very important new information because essentially the values of the parameters are known and the errors are not so big. So, if you are able, you can try to understand the origin for the experimental values we have determined. An open question is the θ_{13} problem. This is a very small parameter but we do not have any plausible reason to take it equal to zero. We do not have a symmetry that gives a reason to take it equal to zero. So we hope that it is small but different from zero: in this case you can go further, and you can try to measure, in the future, the CP violation for the neutrino sector and so on.

- *Bettini:*

The Spergel et al. (2003) analysis does not only introduce new data (Lyman α forest) but also allows for a dependence of the spectral index from k (this gives an effect similar to neutrino mass). This is the reason why the limit on neutrino mass weakens a bit.

- *Fogli:*

Maybe. It is difficult to follow the exact approach they make in their papers. In any case, with the addition of new data the limit increases.

- *Sykora:*

There is nothing strange in having different limits if the technique to handle the data changes. So there is no surprise that the limit changes.

- *Fogli:*

I agree. They add new data, but maybe they also add the running spectral index. The point is that we have two limits and we do not know which is the more reliable of the two. There are other papers on this subject, which introduce other kinds of analysis and new limits also, so there is some uncertainty in this problem. A more conservative approach is the one followed by Hannestad: care must be taken in the fit of cosmological parameters. The upper bound on $\Omega_0 h^2$ depends on the "priors" on some of them. Adding

new data, Hannestad finds a better limit but in any case this analysis does not reproduce the limit obtained by the WMAP Collaboration. The final considerations by Hannestad are the following: the upper limit from WMAP and 2dFGRS is weak, the addition of small scale data breaks the degeneracy and tightens the limit, and adding "priors" on both H_0 and Ω_m further strengthens the limit.

- *Balbinot:*

How can you be sure that this dark matter is made of neutrinos and not of some sort of exotic matter?

- *Fogli:*

The idea is that there are only neutrinos and that the neutrino families are three, and that you are in the standard electroweak sector, and so on. This is an assumption. Of course, you can have also other particles, such as axions and so on, which can contribute. In the literature you can find other considerations and estimates.

- *Krotov:*

How can the mass of neutrino be reconstructed from the anisotropy of relic radiation? How does the standard cosmological restriction for m_ν relate to the presented restrictions?

- *Fogli:*

The small-scale part of the power spectrum is sensitive to the neutrino mass because the neutrino has a free-streaming behaviour and so, too large neutrino masses would destroy the small-scale structures. If you are able to reproduce very well the spectrum, in principle you can estimate the neutrino mass. However, the WMAP data do not explore the small scales but instead the large ones and you have to add other data to complete the spectrum. There is also the problem of the linear behaviour, which is not exact in the case of the small scales. So these estimates are essentially correct, but cannot be taken as a precise measurement. They are only an estimate with some uncertainty, which is essentially related to the way you take all these data into account and the cosmological model in which you use them.

- *Menges:*

Normally the LSND data is not used in ν oscillation. Can you give reasons why it is not used?

- *Fogli:*

In conclusion, in order to accommodate LSND with solar and atmospheric neutrino results, it is necessary to introduce a fourth sterile neutrino. Then there are two possible mass spectra: the 3 + 1 (with the sterile neutrino mass well separated from the others) and the 2 + 2 (with two pairs of masses). However, in the 3 + 1, accelerator and reactor data fail to agree simultaneously with LSND data. In the 2 + 2, solar and atmospheric data fail to agree with each other. Maybe it is too early for a definitive "no-go theorem" but life is certainly hard for the sterile neutrino.

FUNDAMENTAL CONSTANTS AND THEIR POSSIBLE TIME DEPENDENCE

Harald Fritzsch

Ludwig-Maximilians-University Munich, Sektion Physik

March 16, 2004

Abstract

Astrophysical indications that the fine-structure constant has undergone a small time variation during the cosmological evolution are considered within the framework of the standard model of the electroweak and strong interactions and of grand unification. A variation of the electromagnetic coupling constant could either be generated by a corresponding time variation of the unified coupling constant or by a time variation of the unification scale. The various possibilities, differing greatly in their implications for the variation of low energy physics parameters like the nuclear mass scale, are discussed. The case in which the variation is caused by a time variation of the unification scale is of special interest.

Usually in particle physics, we deal with the local laws of nature, say the field equations of the gauge theory. But when it comes to the fundamental constants, like the fine-structure constant α , we must keep in mind that questions about also the boundary conditions of the universe come up. We do not know where these constants, like α or α_s , or the lepton and quark masses, come from, but it could well be that at least a few of them are products of the Big Bang, and if the Big Bang would be repeated, these constants would assume different values. But if things would be like that, it is clear that the constants could never be calculated.

So in connection to the fundamental constants the question comes up, whether they are really cosmic accidents, or whether they are determined by the dynamics, whether they are changing in time or in space, or whether they are indeed calculable in a hypothetical theory going far above the present Standard Model. Also considerations, related to the Anthropic Principle, should be made. Life in our universe can exist only if the values of the fundamental constants take on certain values. In a universe in which, for example, the u -quark is heavier than the d -quark, the proton would decay in a neutron, and life would not exist, at least not in a form known to us. Also a substantial change of the fine-structure constant α would make normal life impossible.

One can take the attitude, taken e. g. by Einstein, who believed that the constants of nature are all calculable, i. e. fixed by the dynamics. In a letter written in 1950 to Ilse Rosenthal-Schneider he wrote: "Dimensionless constants in the laws of nature, which from the purely logical point of view can just as well have different values, shall not exist. To me, with my "trust in God" this appears to be evident, but there will be few who are of the same opinion."

One aspect which needs to be stressed is the fact that fundamental constants do not exist *a priori*, but are depending on the specific theory. Only the underlying theory decides which parameters are the fundamental ones.

An example is the fine-structure constant α , introduced by Sommerfeld in 1916. The inverse of α is, of course, close to the integer number 137. The number excited many physicists. Heisenberg speculated about it. He even published a formula: $\alpha = 2^{-4}3^{-3}\pi$. W. Pauli, who was very sick, was able to fix the number of the room in the Zuerich clinic, in which he died, to be 137.

On one of the occasions I had lunch with D. Feynman, he told me that every theoretician should have written on the blackboard in his office: 137 – how little we know. When we came back from lunch, I checked Feynman's office, and nothing was written on his blackboard. So I took a piece of chalk and wrote in big letters: 137 – how little we know. One hour later Feynman came to me and thanked me for the remark.

In superstring-theory people might find a way to fix or calculate the fine-structure constant. In the connection I like to draw attention again to a formula which was derived in the seventies by A. Wyler:

$$\alpha = \frac{9}{8\pi^4} \left(\frac{\pi^5}{2^4 5!} \right)^{1/4}. \quad (1)$$

This formula works very well and was derived by considering ratios of certain topological spaces – perhaps in string theory something similar can happen.

Of course, today α is just the interaction constant, describing e. g. electron-scattering

at low energies:

$$\alpha^{-1} = 137.03599976 . \quad (2)$$

But it is remarkable. Based on this number, one can calculate all effects in QED to an accuracy of about 1 : 10.000.000, e. g. the magnetic moment of the electron. Of course, QED is only a part of the Standard Model of today, based on a superposition of QCD and the $SU(2) \times U(1)$ - electroweak theory, and α is just one of at least 18 parameters, entering the Standard Model.

One of the fundamental quantities is the proton mass. I should like to stress that the proton mass is a rather complicated object in the Standard Model. The coupling constant of QCD follows in leading order the equation:

$$\alpha_s(Q^2) = \frac{2\pi}{b_0 \ln(Q/\Lambda)}, \quad b_0 = 11 - \frac{2}{3}n_f . \quad (3)$$

Here the scale parameter Λ enters, which has been determined to be:

$$\Lambda = 214^{+38}_{-35} \text{ MeV} . \quad (4)$$

Λ is a free parameter of QCD, and all numbers of QCD scale with Λ , at least in the limit where the masses of the quarks are set to zero. But Λ can be expressed in terms of MeV, i. e. it is given in reference to the electron mass, which is outside QCD. The physical parameters like the proton mass are simply proportional to Λ . The scale of confinement of the quarks is inversely proportional to Λ . The proportionality constant has been calculated in lattice QCD and seems to be in agreement with the observation.

Let me mention one remarkable success of lattice QCD. The pion decay constant has been calculated:

$$F_\pi/\Lambda = 0.56 \pm 0.05 . \quad (5)$$

The experimental value is 0.62 ± 0.10 , i. e. in good agreement with the theoretical value.

The experimental value of the nucleon mass is 938.272 MeV. However, in the theory there is a contribution, given by the proton expectation value of $m_u \bar{u}u + m_d \bar{d}d$, the σ -term, which is about 45 MeV, but it is not known to be better than about 10%.

Also s -quarks contribute. If we say, in accordance with experiment, that the $\bar{s}s$ -pairs should contribute about 10% as much as the $\bar{u}u$ and $\bar{d}d$ -pairs, the proton expectation value for $m_s \bar{s}s$ is about 40 MeV, i. e. about as large as the $\bar{u}u/\bar{d}d$ -contribution. This implies that the nucleon in a world without s -quarks would have a mass of about 900 MeV. The same is true for charmed quarks. There are, of course, much less charmed quarks in the nucleon than strange quarks, but when it comes to the expectation value of $m_c \bar{c}c$, one finds: $\langle pm_c \bar{c}cp \rangle \sim 30$ MeV, with a large uncertainty.

We can write down the nucleon mass:

$$M = c_0 \Lambda + c_u m_u + c_d m_d + c_s m_s + c_c m_c + c_{\text{em}} A_u , \quad (6)$$

where the numbers c_u, c_n, \dots eventually can be calculated with high precision in the future. Today not very much is known.

If we say, the physical proton mass is 100%, then about 87% are due to Λ , about 2,3 % due to the u - and d quarks, about 4,6% due to the s -quarks, 3,5% due to the c -quarks, and

about 0.2% due to electromagnetic effects. Something similar can be said about the magnetic moments of the nucleon. It will be dominated by a term given by Λ , while the quark mass terms contribute not much.

I should also remind you that Grand Unification imposes that the parameters α_s , α and α_w are not independent, but are related to each other, and related to the unified coupling constant, describing the interaction at the unification scale Λ_{un} . It is also known that the group $SU(5)$ does not describe the observations, since the three coupling constants do not converge precisely. If supersymmetric particles are added at an energy scale of about 1 TeV, a convergence takes place, however [1]. In $SO(10)$ [2] the situation is different, since in this group the unification is a two-step process, where another mass scale, the mass scale for the righthanded W -boson, enters. If this mass scale is chosen in the right way, the unification can be achieved without supersymmetry.

After these preparations let me come to the question of time dependence. A group of physicists from Australia, England and the US has recently published their evidence that the fine-structure constant had a different value billions of years ago [3]. They were investigating the light from about 150 quasars, being on its way for up to 11 billion years. They used the so-called "many multiplet method". They were looking at the fine-structure of atomic lines, originating from elements like Fe, Ni, Mg, Sn, Ag etc. .

One particular aspect is that the fine-structure is a rather complex phenomenon, causing in particular also sign changes in the fine-structure effects. These sign changes have been observed and used in fixing the experimental values of α . The result is:

$$\frac{\Delta\alpha}{\alpha} = (-0.72 \pm 0.18) \cdot 10^{-5}. \quad (7)$$

Thus α was slightly larger in the past. If one takes a linear approximation and uses a cosmic lifetime of 14 billion years, the effect is $\dot{\alpha}/\alpha \approx 1.2 \cdot 10^{-15}$ per year.

I should mention that considerations related to a time-dependence of fundamental parameters have a long history. In the thirties Dirac [4] considered a time-variation of G , and independently also Milne [5]. P. Jordan [6] looked at the time-dependence of other parameters, e. g. nuclear parameters. L. Landau speculated in the fifties about a time-variation of α [7].

If α depends on time, the question arises, how this time-variation is generated. Since $\alpha = e^2/\hbar c$, a time variation could come from a time variation of \hbar or c . Both cases are, I think, not very likely. If c depends on time, it would mean that we have a serious problem with relativity. If \hbar would depend on time, atomic physics runs into a problem. So I think that a time dependence of α simply means that e is becoming time-dependent.

Let me also mention that according to the results of Dyson and Damour [8] there is a rather strong constraint on a time-variation of α . If no other parameters change as well, the relative change $(\dot{\alpha}/\alpha)$ per year cannot be more than 10^{-17} , i. e. there is a problem with the astrophysical measurements, unless the rate of change for α has become less during the last 2 billion years. The constraint is derived by looking at the position of a nuclear resonance in Samarium, which cannot have changed much during the last 2 billion years. However, I tend not to take this constraint very seriously. According to the Grand Unification α_s and Λ should have changed as well, and the two effects (change of α and of Λ) might partially cancel each other.

The idea of Grand Unification implies that the gauge group $SU(3)_c$ of the strong interactions and the gauge group $SU(2) \times U(1)$ of the electroweak sector are subgroups of a simple group, which leads to the unification of the interactions.

Both the groups $SU(5)$ and $SO(10)$ are considered in this way. I like to emphasize that the group $SO(10)$ has the nice property that all leptons and quarks of one generation are described by one representation, the 16-representation. It includes a righthanded neutrino, which does not contribute to the normal weak interaction, but it is essential for the appearance of a mass of the neutrino, which is expected in the $SO(10)$ -Theory. In $SU(5)$ two representations of the group are needed to describe the leptons and quarks of one generation, a 10- and a $(\bar{5})$ -representation.

I should also like to emphasize that the gauge couplings α_s , α_w and α meet in the $SU(5)$ -theory only, if one assumes that above about 1 TeV supersymmetry is realized. In the $SO(10)$ -theory this is not needed. A convergence of the coupling constants can be achieved, since at high energies another energy scale enters, which has to be chosen in a suitable manner.

A change in time of α can be obtained in two different ways. Either the coupling constant α_{un} stays invariant, or the unification scale changes. I consider both effects in the $SU(5)$ -model with supersymmetry. In this model the relative changes are related:

$$\frac{1}{\alpha} \frac{\dot{\alpha}}{\alpha} = \frac{8}{3} \frac{1}{\alpha_s} - \frac{10}{\pi} \frac{\dot{\Lambda}_{un}}{\Lambda_{un}} \quad (8)$$

One may consider the following scenarios:

- 1) Λ_G invariant, $\alpha_u = \alpha_u(t)$. This is the case considered in (R) (R), and one finds

$$\frac{1}{\alpha} \frac{\dot{\alpha}}{\alpha} = \frac{8}{3} \frac{1}{\alpha_s} \frac{\dot{\alpha}_s}{\alpha_s} \quad (9)$$

and

$$\frac{\dot{\Lambda}}{\Lambda} = -\frac{3}{8} \frac{2\pi}{b_3^{SM}} \frac{1}{\alpha} \frac{\dot{\alpha}}{\alpha}. \quad (10)$$

- 2) α_u invariant, $\Lambda_G = \Lambda_G(t)$. One finds

$$\frac{1}{\alpha} \frac{\dot{\alpha}}{\alpha} = -\frac{1}{2\pi} \left(b_2^S + \frac{5}{3} b_1^S \right) \frac{\dot{\Lambda}_G}{\Lambda_G}, \quad (11)$$

$$\frac{\dot{\Lambda}}{\Lambda} = \left(\frac{b_3^S}{b_3^{SM}} \frac{1}{\alpha} \frac{\dot{\alpha}}{\alpha} \right) \approx -30.8 \frac{\dot{\alpha}}{\alpha} \quad (12)$$

- 3) $\alpha_u = \alpha_u(t)$ and $\Lambda_G = \Lambda_G(t)$. One has

$$\begin{aligned} \frac{\dot{\Lambda}}{\Lambda} &= -\frac{2\pi}{b_3^{SM}} \frac{1}{\alpha_u} \frac{\dot{\alpha}_u}{\alpha_u} + \frac{b_3^S}{b_3^{SM}} \frac{\dot{\Lambda}_G}{\Lambda_G} \\ &= -\frac{3}{8} \frac{2\pi}{b_3^{SM}} \frac{1}{\alpha} \frac{\dot{\alpha}}{\alpha} - \frac{3}{8} \frac{1}{b_3^{SM}} \left(b_2^S + \frac{5}{3} b_1^S - \frac{8}{3} b_3^S \right) \frac{\dot{\Lambda}_G}{\Lambda_G} \\ &= 46 \frac{\dot{\alpha}}{\alpha} + 1.07 \frac{\dot{\Lambda}_G}{\Lambda_G} \end{aligned} \quad (13)$$

where theoretical uncertainties in the factor $R = (\dot{\Lambda}/\Lambda)/(\dot{\alpha}/\alpha) \approx 46$ have been discussed in [9]. The actual value of this factor is sensitive to the inclusion of the quark masses and the associated thresholds, just like in the determination of Λ . Furthermore higher order terms in the QCD evolution of α_s will play a role. In ref. [9] it was estimated: $R = 38 \pm 6$.

The case in which the time variation of α is not related to a time variation of the unified coupling constant, but rather to a time variation of the unification scale, is of particular interest. Unified theories, in which the Standard Model arises as a low energy approximation, might well provide a numerical value for the unified coupling constant, but allow for a smooth time variation of the unification scale, related in specific models to vacuum expectation values of scalar fields. Since the universe expands, one might expect a decrease of the unification scale due to a dilution of the scalar field. A lowering of Λ_G implies according to (11)

$$\frac{\dot{\alpha}}{\alpha} = -\frac{1}{2\pi}\alpha \left(b_2^S + \frac{5}{3}b_1^S \right) \frac{\dot{\Lambda}_G}{\Lambda_G} = -0.014 \frac{\dot{\Lambda}_G}{\Lambda_G}. \quad (14)$$

If $\dot{\Lambda}_G/\Lambda_G$ is negative, $\dot{\alpha}/\alpha$ increases in time, consistent with the experimental observation. Taking $\Delta\alpha/\alpha = -0.72 \times 10^{-5}$, we would conclude $\Delta\Lambda_G/\Lambda_G = 5.1 \times 10^{-4}$, i.e. the scale of grand unification about 8 billion years ago was about 8.3×10^{12} GeV higher than today. If the rate of change is extrapolated linearly, Λ_G is decreasing at a rate $\frac{\dot{\Lambda}_G}{\Lambda_G} = -7 \times 10^{-14}/\text{yr}$.

According to (12) the relative changes of Λ and α are opposite in sign. While α is increasing with a rate of $1.0 \times 10^{-15}/\text{yr}$, Λ and the nucleon mass are decreasing, Λ e.g. with a rate of $1.9 \times 10^{-14}/\text{yr}$. The magnetic moments of the proton μ_p as well of nuclei would increase according to

$$\frac{\dot{\mu}_p}{\mu_p} = 30.8 \frac{\dot{\alpha}}{\alpha} \approx 3.1 \times 10^{-14}/\text{yr}. \quad (15)$$

The time variation of the ratio M_p/m_e and α discussed here are such that they could be discovered by precise measurements in quantum optics. The wave length of the light emitted in hyperfine transitions, e.g. the ones used in the cesium clocks being proportional to $\alpha^4 m_e/\Lambda$, will vary in time like

$$\frac{\dot{\lambda}_{hf}}{\lambda_{hf}} = 4 \frac{\dot{\alpha}}{\alpha} - \frac{\dot{\Lambda}}{\Lambda} \approx 3.5 \times 10^{-14}/\text{yr} \quad (16)$$

taking $\dot{\alpha}/\alpha \approx 1.0 \times 10^{-15}/\text{yr}$ [3]. The wavelength of the light emitted in atomic transitions varies like α^{-2} :

$$\frac{\dot{\lambda}_{at}}{\lambda_{at}} = -2 \frac{\dot{\alpha}}{\alpha}. \quad (17)$$

One has $\dot{\lambda}_{at}/\lambda_{at} \approx -2.0 \times 10^{-15}/\text{yr}$. A comparison gives:

$$\frac{\dot{\lambda}_{hf}/\lambda_{hf}}{\dot{\lambda}_{at}/\lambda_{at}} = -\frac{4\dot{\alpha}/\alpha - \dot{\Lambda}/\Lambda}{2\dot{\alpha}/\alpha} \approx -17.4. \quad (18)$$

At present the time unit second is defined as the duration of 6.192.631.770 cycles of microwave light emitted or absorbed by the hyperfine transition of cesium-133 atoms. If Λ indeed changes, as described above, it would imply that the time flow measured by the cesium clocks does not fully correspond with the time flow defined by atomic transitions.

Recently a high precision experiment was done at the MPQ in Munich, using the precise cesium clock PHARAO from Paris [11]. The preliminary result is consistent with no change of the frequencies - one measures for the transition in hydrogen a frequency of 2466 061 413 187 127 (18) Hz. This gives a change of $2.8(5.7) \cdot 10^{-15}$ per year.

According to eq. (18) the effect should be about ten times larger. Although this result is still preliminary, one is supposed to think what might be the reason for the small effect.

One possibility is, of course, that the astrophysical measurements of the change of α are not correct. Another interesting possibility, however, needs to be studied. It might be that both α_{aa} and Λ_G change such that the result of λ_{hf} is essentially zero - both effects cancel each other in leading order. Nevertheless on the level of 10^{-15} an effect should be seen. More refined experiments are needed to search for a time dependence of Λ .

References

- [1] U. Amaldi, W. de Boer and H. Furtenau, Phys. Lett. **260**, 447 (1991)
- [2] H. Fritzsch and P. Minkowski, Annals of Physics **93**, 193 (1975)
- [3] J. K. Webb *et al.*, Phys. Rev. Lett. **87** 091301 (2001) [[arXiv:astro-ph/0012539](#)].
- [4] P. M. Dirac, Nature **192**, 235 (1937).
- [5] E. A. Milne, Relativity, Gravitation and World Structure, Clarendon press, Oxford, (1935), Proc. Roy. Soc. A, **3**, 242 (1937).
- [6] P. Jordan, Naturwiss., **25**, 513 (1937), Z. Physik, **113**, 660 (1939).
- [7] L. D. Landau, in W. Pauli, ed., Niels Bohr and the Development of Physics, McGraw-Hill, NY, p.52, (1955).
- [8] T. Damour and F. Dyson, Nucl. Phys. B **480**, 37 (1996) [[arXiv:hep-ph/9606486](#)].
- [9] X. Calmet and H. Fritzsch, [arXiv:hep-ph/0112110](#), to appear in Eur. Phys. J. C.
- [10] P. Langacker, G. Segre and M. J. Strassler, Phys. Lett. B **528**, 121 (2002) [[arXiv:hep-ph/0112233](#)];
- [11] T. W. Haensch, "Laser Frequency Combs and Ultraprecise Spectroscopy," Proc. of the Inst. Conf. on Laser Spectroscopy (JCOALS 2003), Palm Cove (Australia).

CHAIRMAN: H. FRITZSCH

Scientific Secretaries: D. Galletly, Y.F. Zhou

DISCUSSION

- *Skinner:*

What limits does nucleosynthesis place on the variation of α ?

- *Fritzscher:*

The constraints for the variation of α from nucleosynthesis are rather poor. We are not talking about a huge variation in α - an effect of the order of 10^{-5} which is large for laboratory purposes, but is small compared to nucleosynthesis. Nucleosynthesis gives a limit of the order of 1%, which is not enough to get reasonably precise information unless you talk about cosmological models, where in the Big Bang huge variations may take place. There you can place limits.

- *Skinner:*

If the astrophysics result is correct and the time variation of α is not zero, what do we learn, if anything about the underlying theory?

- *Fritzscher:*

That is a good question. For that reason we did other experiments, like those in quantum optics, to learn other constraints on other parameters. However what you reveal from the theory is still unclear. There are models in String theory but we are far from being able to trust any model yet. I think it is more important to first confirm our current experimental results, and find other constraints on other parameters, including the weak interactions. Weak interactions are very difficult. Again nucleosynthesis can place a limit on these, but it is a very poor limit. It seems to be very hard to get further information about weak interactions. I do not see any reasonable way now.

- *Alberici:*

Does there exist an astrophysical observation that suggests that in the past the structure constant α , or some other constant, had a different value?

- *Fritzscher:*

Well yes, I was just mentioning the results by Webb and Wolfe and others. There were earlier indications before that there was an effect of that order, and people had seriously discussed it, but nobody took it seriously. Then all of a sudden it became more serious because of these experiments. There were no serious experimental results prior to this, however this is not surprising as this is a very difficult experiment to carry out. A new experiment is being prepared right now. The first result may be obtained in about two years.

- *Cerri:*

You discussed mostly the possibility of a time dependence on α . What about other variables and/or other dependencies? What would be your next candidate for detecting some variation?

- *Fritzscher:*

I discussed α because there is this experiment which indicated a time dependence of α . For other parameters I mostly don't know. Most of the other parameters are not so well known as α , so their time dependence is harder to get. For example, the gravitational constant is much less well known. Dirac had suggested a time dependence of G of the order of 1 on the lifetime of the universe. So in 14 billion years you need an accuracy for G of around 10^{-12} which only now is being approached. With α we are five orders of magnitude better at 10^{-15} . There is no point in talking about parameters related to unstable particles, like the b quark mass. Even for stable masses such as the electron mass, proton mass, the $n-p$ mass difference, etc, getting good limits seem to be impossible right now. If there is a time dependence, then probably all the parameters in the standard model will be time dependent. The question then is where will we get the best handle on the time dependence. α seems to be a good candidate.

- *Gripaios:*

Let us consider the situation where the unit of electric charge e depends on time. Then considering just QED, the action is no longer gauge invariant. What are the consequences of this? Firstly we lose renormalizability. Secondly we lose electric charge conservation. Why has this not been seen in particle accelerators?

- *Fritzscher:*

I do not think this is really a problem. You just have to redefine slightly what you mean by charge. Conservation of charge means that no charged particles are created freely out of space, and this still holds if α depends on time.

- *Skinner:*

This does not break gauge invariance.

- *Fritzscher:*

Yes, I think so too. Of course if we want a theory where α depends on time, we must go beyond QED, as QED states that α is time independent. What the form of this theory would be, we do not know just now. We need more information from experiment.

- *Kuperstein:*

Do we have any field theory toy model with a time dependent coupling constant or cut-off?

- *Fritzscher:*

I do not know of any, but this not something I am worried about at the moment. I would first like to find out from experiment whether or not we have time dependence.

- *Haidt:*

The test of time dependent constants should be discussed in the context of the "region of validity" of the theory under consideration. How do you know the theory is valid?

- *Fritzscher:*

That is a difficult philosophical question. I think it is a matter of taste. People believe the theory is right, but nobody knows for sure.

- *Haidt:*

Okay, for a gauge theory the situation is relatively clear. You formulate it and you leave a certain number of quantities free. These numbers are determined by experiment and if we get consistency, you say the theory is confirmed, but that does not mean very much. It is just consistency.

- *Fritzscher:*

No, it's more than that. You can fix α , say, in QED.

- *Haidt:*

Sure, but if you say α changes?

- *Fritzscher:*

Yes, but you have a basic parameter which eventually changes in time, but this is a cosmological time evolution. We are not talking about big effects.

- *Haidt:*

But at the level of 10^{-15} : how can you ever tell the theory is valid?

- *Fritzscher:*

Yes, because we have other tests up to the same precision. Haensch is doing experiments up to 10^{-17} , and QED works fine. If the total time dependence can be placed into a small time dependence of α , it would be important to know. Of course if the time dependence is more complex and could not be absorbed in α , then the whole theory breaks down. That could happen but I hope not. However we are talking about a very small effect, around 10^{-15} each year, which we should be able to tolerate.

- *Sjkora:*

It is not such an important question. You mentioned that in the change of α you would like to keep \hbar and c to be constant and e is changed, but \hbar and c can be related

to the geometric properties of our universe. So, why do you believe in the change of e and not \hbar or c ?

- *Fritsch:*

No, it is a matter of taste; I still believe in general relativity and special relativity. If \hbar and c depend on time, this is going to be a problem. If \hbar depends on time, there will be problems in atomic physics. If atoms keep fluctuating, it becomes a mess, and for me the best thing is just to have the time dependence of e . But it is a matter of taste. As a particle physicist, I am used to having c and \hbar equal to 1.

- *Sjkora:*

You are playing a game today, you are discussing two possible reasons for changing α , you have two different terms, then you discuss the first and the second, then you discuss the cancellation. I think for example for \hbar , there will be reasons to think about a change of it.

- *Fritsch:*

I do not think so, but it is a matter of taste. I hate these papers coming right now, every week I get papers with time dependence of c , let's forget about it. But that is really a matter of taste, and the time dependence of e seems to me most reasonable, because it is the quantity we do not know.

- *Haline:*

I was wondering, we are quite used to the concept of the coupling constant running with scale, how sure are we that in the back of time, the quantum field theory is exactly the same? You know, we are talking about very small effects, maybe the coupling was renormalized to the slightly different constant.

- *Fritsch:*

Yes, but I do not see any problem.

- *Haline:*

No.

- *Fritsch:*

Just have a different value, but when you come very close to the Big Bang, then the big question comes.

- *Haline:*

Yes, maybe it is just a measurement which is not properly interpreted, in terms of comparing the constant at the same scale.

- *Fritzscher:*

I doubt it, I do not think so. Look at these atomic fine structures within the quasars, nothing wrong with it. If you look at the data, it is rather convincing.

- *Haline:*

Yes, but what I mean is that maybe in fact the variation of time should be replaced by the variation of scale.

- *Fritzscher:*

No, but what scale? These are atoms, and atoms have no scales, there is no particular scale.

- *Wolf:*

In order to study the time dependence of the fine structure constant, one should start to search for discrete lines in the cosmic ray microwave background. This would bring us to close to the Big Bang with $t=0$.

- *Fritzscher:*

But how can you see these lines in the background?

- *Wolf:*

People have to start looking.

- *Fritzscher:*

You see any chance in time?

- *Wolf:*

I do not know.

- *Fritzscher:*

I doubt it.

- *Wolf:*

I mean, you will doubt it until somebody looks into it.

- *Fritzscher:*

I doubt it, but one thing could really happen. The change of α could be much larger at the beginning, at the Big Bang; I mean at the time of nucleosynthesis, or less.

- *Rotaev:*

Let us assume that the constant α is a function of time. Then this function should contain some parameters. How many parameters should there be?

- *Fritzscher:*

I do not really fully understand this question. We just have a rather small of time dependence of α , that's it. And we have no way to calculate it from a basic theory.

- *Krotov:*

Every object has its own α , depending on the distance. Is there any program, to study each quasar in space, depending on the distance?

- *Fritzscher:*

Well, in principle you could talk about it, but it is expensive, because measuring the fine structure is not such a trivial thing. But what has been done by Webb et al. is that you look at about 240 quasars, all together, and that is, I think, enough. You do not have to look into all the quasars in the world.

- *Bozza:*

Maybe it is possible to decouple the effect of explicit dependence of α and some implicit dependence of α , maybe on some other values.

- *Fritzscher:*

Yes, maybe, but also it would be interesting to look at the quasars in different directions to see not only time dependence, but also space dependence. But so far, it does not seem to be. We do not see any space dependence so far. Somehow the space dependence is less, but we have to check this in detail.

Highlights from BNL New Phenomena at RHIC

T. Ludlam
Brookhaven National Laboratory

Introduction

Since its commissioning in the summer of 2000, Brookhaven's Relativistic Heavy Ion Collider, RHIC, has been producing collisions of heavy nuclei at the highest energies ever achieved. The primary mission for RHIC, which is now the U.S. Department of Energy's largest facility for nuclear physics research, is to create and study, under laboratory conditions, the quark-gluon plasma – the deconfined phase of strongly interacting matter that is a central prediction of quantum chromodynamics (QCD). The early experiments at RHIC have shown in dramatic fashion that the predicted conditions for realizing the transition from ordinary matter to “quark matter” can be reached, and provide evidence that a new form of matter is being observed. This lecture describes the data and the nature of the experiments that are being carried out, and discusses the scientific implications of the results so far.

What are we trying to learn?

The quest to understand the nature and origins of matter at its most basic level is as old as civilization. Some 30 years ago experiments with high-energy collisions of subatomic particles demonstrated that the basic building blocks of atomic nuclei, the protons and neutrons, are not “elementary” particles, but structures made up of quarks, inextricably bound together by forces carried by gluons. The theory of Quantum Chromodynamics (QCD) has since evolved to describe the fundamental interactions among quarks and gluons and, in particular, the forces that confine small multiplets of quarks into hadrons. QCD predicts that at extraordinarily high temperatures and densities – conditions that have not prevailed in the natural universe since a few microseconds after the Big Bang – matter takes a different form, consisting not of neutrons and protons, but an extended volume of interacting quarks, anti-quarks, and gluons. This is the Quark Gluon Plasma [1], the state now thought to have been the precursor for all of the observable matter in the present universe. It is believed that the conditions to create this extreme form of matter can be reproduced in very high energy collisions of heavy nuclei [2]. The first, and most compelling question is whether experiment can confirm the existence of the quark gluon plasma state, and compare its detailed properties with the predictions of QCD.

The ability to reproduce the transition between hadronic matter and quark matter under relatively controlled conditions in the laboratory promises to answer fundamental questions about the origin and properties of strongly-interacting matter, and opens up important new avenues of research for nuclear and particle interactions, as well as for astrophysics and condensed matter physics. The ability to make specific comparisons

between experiment and QCD (through lattice gauge calculations) makes it possible to address such questions as:

- How do particles get their mass through spontaneous breaking of chiral symmetry?
- What is the nature (order) of the transition from confined to deconfined matter? Are confinement and chiral symmetry related?
- What is the equation of state of the quark gluon plasma?

The RHIC facility at Brookhaven is now addressing these questions with colliding beams of gold ions with c.m. collision energies up to 200 GeV/nucleon. The machine is capable of colliding lighter species of nuclei, including spin-polarized protons up to 500 GeV, and can also provide collisions of very light ions (deuterons) in one beam with very heavy ions (gold) in the other. This flexibility has proved to be critically important in providing control data for comparison with the gold-gold results. The experiments at RHIC are being carried out with four collider detectors (BRAHMS, PHENIX, PHOBOS, STAR), each operated by an international collaboration of scientists [3].

The Results so Far

The first important results from RHIC became apparent in a matter of weeks after the first collisions were observed, in June 2000. The very earliest data established that at the top RHIC energy the multiplicity density of particles produced in the most central Au+Au collisions shows a steady increase with collision energy [4]. This multiplicity density can be directly related to estimates for the energy density of the expanding volume from which the observed hadrons emerged. The estimated energy densities are >5 GeV/fm³. This is well beyond the expected threshold for the deconfining phase transition.

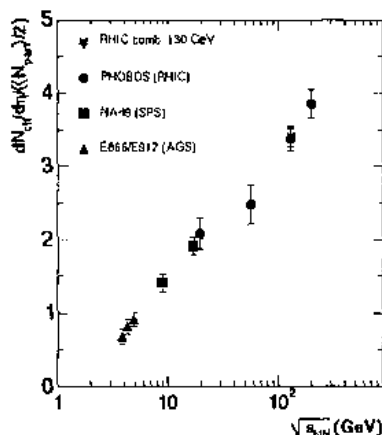


Figure 1: Charged particle multiplicity density per interacting nucleon pair vs. c.m. collision energy, for central Au+Au interactions.

Data from Ref. 4

The relative abundance of observed particle types in these central collisions is very well described by statistical calculations for a macroscopic system in thermal and chemical equilibrium [5]. The equilibrium temperature at chemical freeze-out is determined from these analyses to be ~ 170 MeV, corresponding accurately to the most recent QCD lattice calculations of the critical temperature for the deconfining phase transition [6]. The ratio of antibaryons to baryons at the top RHIC energy is very nearly 1, closely approximating the “baryon-free” condition of the early universe. Thus, the early RHIC data clearly showed that the aftermath of central Au+Au collisions appears to be both dense enough and hot enough to spark the production of the predicted plasma.

A key further result provided evidence that the medium produced under these conditions is actually collectively-interacting “matter”. This indication comes from the measurement of anisotropic (“elliptic”) flow. The effect referred to as elliptic flow results from the asymmetric shape of the overlap volume that results when two nuclei collide with non-zero impact parameter. As the hot matter in this volume expands, pressure gradients due to thermal interactions give rise to a measurable anisotropy in the momentum distribution with respect to the reaction plane. This anisotropy, which has no analog in proton-proton collisions, has been measured in the RHIC experiments as a function of transverse momentum, and found to be consistent with the behavior of an ideal hydrodynamic fluid [7-9]. This aspect is quite different from the behavior seen in lower-energy collisions (at the CERN SPS), and is a significant indicator that the RHIC collisions result in a significant volume of self-interacting matter at high temperature and density.

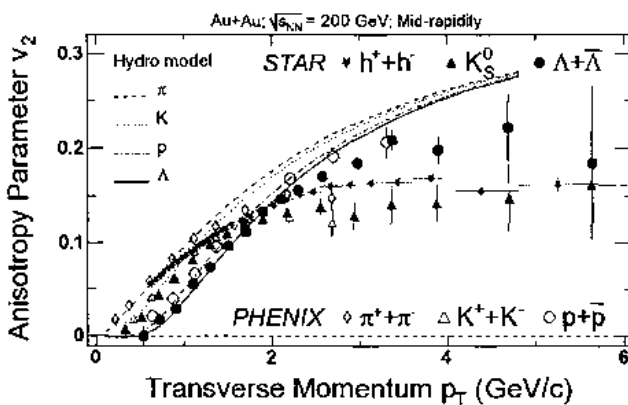


Figure 2: Measured effects of elliptic flow, compared with the predicted behavior of an expanding hydrodynamic fluid. The data are from Ref.s 8 and 9. The hydro calculations are from Huovinen et al., Phys. Lett. B 503 58 (2001).

One of the most dramatic of the observations so far at RHIC is the phenomenon called “jet quenching”, which provides a powerful new probe of the hot, dense matter

created in the collisions. The collision energy is high enough to produce the hard-scattering of partons that produces the well-known jets seen at large transverse momenta in high-energy proton-proton and proton-antiproton collisions. The cross sections for hard-scattering in nucleon-nucleon collisions, and the subsequent fragmentation of the scattered partons into hadrons, is well described by perturbative QCD. In the RHIC experiments, hard parton-parton scattering is seen in nuclear collisions for the first time [10,11]. These observations provide a direct signal of high-energy quarks or gluons emerging from the initial collision stage. Significantly, the RHIC data show a deficit of high- p_T particles in central Au+Au collisions [10-13].

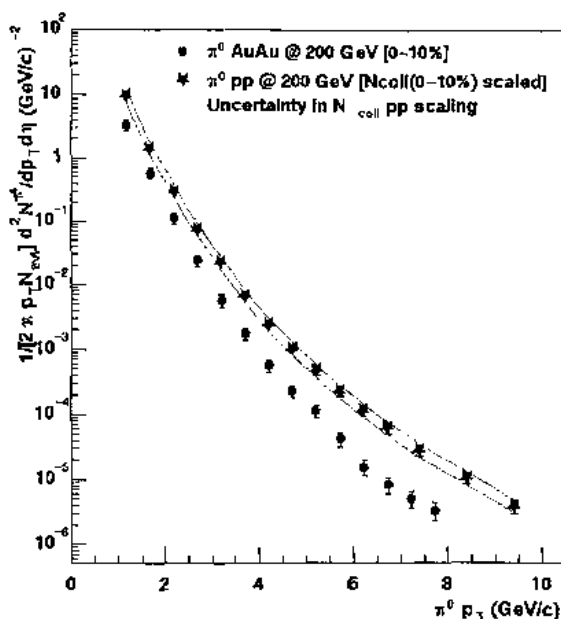


Figure 3: The measured rate, per interacting nucleon, of neutral pion production, as a function of the pion transverse momentum for proton-proton collisions and central Au+Au collisions at c.m. energy of 200 GeV/nucleon. The suppression in Au+Au collisions at high p_T is clearly seen. The data are from the PHENIX experiment, Ref. 12.

These data provide striking support for theoretical predictions that in collisions of heavy nuclei such a deficit is the result of a slowing down, or quenching, of the most energetic quarks as they propagate through a dense volume of quark gluon plasma. In the presence of a color-deconfined medium the partons are predicted to lose much of their energy via gluon bremsstrahlung, with a strong and calculable dependence of ΔE on the gluon density [14].

While the jet quenching results appear to provide compelling evidence for a dense, strongly-interacting medium created in the final state of the central collision

events, recent theoretical conjectures offer a possible alternative explanation. This work suggests that, in very high-energy nuclear interactions, the initial-state density of gluons becomes so high that the effective number of interacting particles in the collision saturates, thus limiting the number of hard-scattering events. Thus, another possible reason for the apparent suppression of jets might simply be that the wavefunction of a nucleus during a high-energy collision differs significantly from a simple superposition of nucleon wavefunctions [15]. The notion of gluon saturation at very small values of Feynman x is motivated by recent results on deep inelastic electron-proton scattering at HERA. The theoretical predictions suggest a universal form of matter called the "Color Glass Condensate". As described by QCD, this condensate is present in all strongly interacting particles, but shows itself only in very high-energy collisions. It is a very dense superposition of gluons, similar to a Bose condensate. It has properties similar to glasses; i.e., very slow evolution compared to the natural time scales of constituent interactions.

The color glass condensate is thought to provide the initial conditions for the quark gluon plasma produced in high-energy heavy nuclei. Indeed, the quantitative dependence of multiplicity density with collision energy, shown in Fig. 1, is consistent with this conjecture. Whether or not its effects are manifested in the jet-quenching results observed at RHIC is a question that can be addressed directly by experiment. One can test the color-glass conjecture by bombarding heavy nuclei with very light nuclei (or free nucleons) and seeing if the results differ from a straightforward superposition of nucleon-nucleon collisions. This test was carried out by the RHIC experiments in 2003, by accelerating deuterons in one ring and gold nuclei in the other, colliding them at an energy of 100 GeV/nucleon in each beam.

The results from that run show no evidence of jet suppression at high p_T in the d+Au data, even when the most central collision events are selected [16]. Thus, the suppression observed in central Au+Au collisions is most likely due to jet energy loss in the hot extended medium. This is illustrated in Figure 4. Data from PHENIX (Fig. 4a) show that the production rate of high- p_T pions, scaled to account for the number of participating nucleons in the collision, is significantly suppressed in central Au+Au collisions as compared to proton-proton or d+Au collisions. Fig. 4b shows data from STAR in which two-particle angular correlations clearly show back-to-back jet structure at high p_T in the proton-proton and d+Au data, while the recoil jet peak is clearly absent in central Au+Au collisions.

Figure 4: Evidence for jet quenching in high-energy Au+Au collisions.

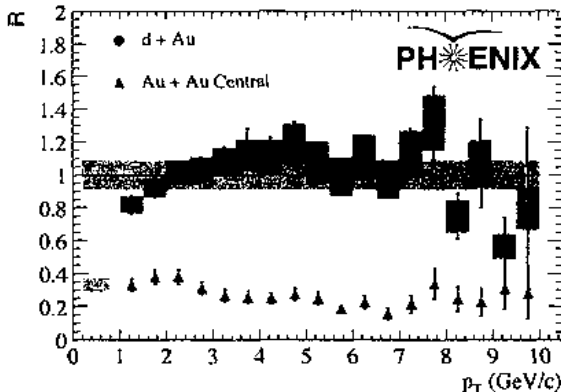


Fig. 4a. The ratio, R , of the rate of particle production (in this case, π^0 mesons) at mid-rapidity in nuclear collisions to that seen in proton-proton collisions, plotted as a function of the π^0 transverse momentum. This ratio scales the observed production rates in nuclear collisions by the number of nucleon-nucleon collisions, and is 1.0 if there are no effects other than this scaling. At lower collision energies, the nuclear effect is to enhance the rate of particle production at large transverse momenta, due to multiple-scattering of nucleons in the colliding nuclei. By contrast, in the RHIC data, seen here from the PHENIX experiment, high- p_T particle production is clearly suppressed in central gold-gold collisions. This suppression is not seen in the deuteron-gold collision data. [Reference 16]

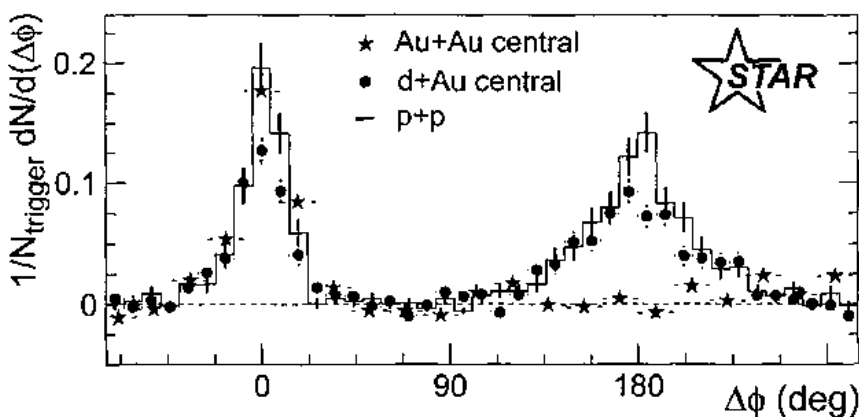


Fig. 4b. Data from the STAR experiment show angular correlations between pairs of high transverse-momentum charged particles, referenced to a "trigger" particle that is required to have p_T greater than 4 GeV/c. The proton-proton and deuteron-gold collision data indicate back-to-back pairs of jets (a peak associated with the trigger particle at $\Delta\phi = 0$ degrees, and a somewhat broadened recoil peak at 180 degrees). The central gold-gold data, shown in the lower panel, indicate the characteristic jet peak around the trigger particle, at 0 radians, but the recoil jet is absent. [Reference 16]

What have we learned to date?

The RHIC data have given convincing evidence that high-energy collisions of heavy nuclei produce, in the final state, a hot and dense medium characterized by strong collective interactions. There is clear evidence that in the earliest stages of the collision process the temperature and energy density far exceed the theoretical requirements for the creation of the quark gluon plasma. Furthermore, the data may be providing us with a window on yet another elemental form of matter predicted by QCD: the color glass condensate. Although the data illustrated in Fig. 4 show that the high- p_T effects seen at mid-rapidity are not the result of initial-state gluon saturation, subsequent results, looking at high- p_T effects at large rapidity, where smaller values of Feynman- x are sampled, may be showing the first indications of this phenomenon [17].

Figure 5 shows a theoretical interpretation of the picture emerging from the experimental data in terms of the evolution of the energy density with time: At a maximum energy density about 100 times that of cold nuclear matter, the initial condensate of color glass gives rise to a thermalized quark gluon plasma, which then expands and cools, condensing into the observed final-state hadrons after a time of about 10 fm/c.

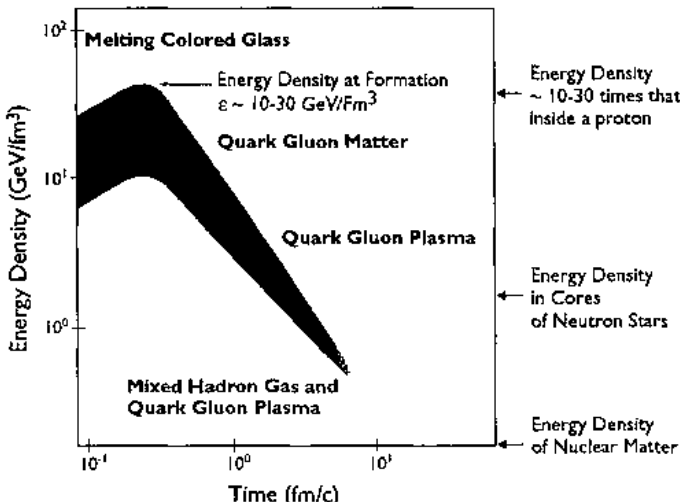


Figure 5: Estimates of energy density vs. time during the evolution of a collision, based on the RHIC data, and the corresponding predicted sequence of states of QCD matter. (L. McLerran).

Among the most important results from this program so far is the demonstration that direct and detailed comparisons can be made between experiment and theory, despite the enormous complexity of these interactions. Thus, continuing measurements at RHIC promise to open new chapters in nuclear and particle physics, as well as the physics of condensed matter.

References

1. See lectures at this School by F. Karsch, "Quark Gluon Plasma Physics"
2. A brief summary of accelerator experiments aimed at producing the quark gluon plasma can be found in T. Ludlam and L. McLerran, Phys. Today, Oct. 2003, p. 48.
3. M.H. Harrison et al., eds., Nucl. Instrum. Meth. **499**, Nos. 2-3 (special volume on the RHIC machine and detectors), 2003.
4. PHOBOS, B. Back et al., PRL **88**, 022302 (2002), and references therein.
5. P. Braun-Munzinger et al., Phys. Lett. **B518**, 41 (2001), and references therein
6. F. Karsch, Nucl. Phys. **A698**, 199c (2002).
7. STAR, C. Adler et al., Phys. Rev. **C66**, 034904 (2002) [contains references to earlier STAR, SPS, and AGS flow data]
8. PHENIX, S. Adler et al., PRL **91**, 172301 (2003)
Scaling properties of proton and anti-proton production in $\sqrt{s_{nn}} = 200 \text{ GeV}$ Au+Au collisions
9. STAR, J. Adams et al., PRL **92**, 052302 (2004)
Particle-type dependence of azimuthal anisotropy and nuclear modification of particle production in Au+Au collisions at $\sqrt{s_{nn}} = 200 \text{ GeV}$
10. STAR, C. Adler et al., PRL **90**, 082302 (2003)
Disappearance of back-to-back high-pT hadron correlations in central Au+Au collisions at $\sqrt{s_{nn}} = 200 \text{ GeV}$
11. PHENIX, PRL **88**, 022301 (2002)
Suppression of hadrons with large transverse momentum in central Au+Au collisions at $\sqrt{s_{nn}} = 130 \text{ GeV}$
12. PHENIX, S. Adler et al., PRL **91**, 072301 (2003)
Suppressed π^0 production at large transverse momentum in central Au+Au collisions at $\sqrt{s_{nn}} = 200 \text{ GeV}$
13. STAR PRL **91**, 172302 (2003)
Transverse-momentum and collision-energy dependence of high-pT hadron suppression in Au+Au collisions at ultrarelativistic energies
14. M. Gyulassy et al., "Jet Quenching and Radiative Energy Loss in Dense Matter", published in *Quark Gluon Plasma 3*, R.C. Hwa and X. N. Wang, eds., World Scientific, Singapore (2003).

15. For a recent review, see E. Iancu, Nucl. Phys. **A715**, 219c (2003).
16. Simultaneously published d+Au suppression results:
 - PHOBOS, B. Back et al., PRL **91**, 072302 (2003)
 - PHENIX, S. Adler et al., PRL **91**, 072303 (2003)
 - STAR, J. Adams et al., PRL **91**, 072304 (2003)
 - BRAHMS, I. Arsene et al., PRL **91**, 072305 (2003)
17. BRAHMS, I. Arsene et al., nucl-ex/0403005 (Mar. 2004), to be published in Physical Review Letters. *On the evolution of the nuclear modification factors with rapidity and centrality in d+Au collisions at $\sqrt{s_{NN}} = 200 \text{ GeV}$.*

Highlights from BABAR

Marcello A. Giorgi

Stanford Linear Accelerator Center
2575 Sand Hill Rd, Menlo Park, CA 94025, USA

Università di Pisa (Italy) Dipartimento di Fisica "E. Fermi"
and INFN Sezione di Pisa
Edificio C Polo Fibonacci, Via F. Buonarroti, 2
Pisa 56127, Italy

ABSTRACT

The scientific program of the Experiment BABAR that is taking data at PEP-II e^+e^- asymmetric B-Factory of SLAC is presented together with the most relevant results achieved since the start-up of the operations in 1999. The total sample of data collected contains a number of $B\bar{B}$ events in excess of 130 millions. Beyond CP violation results, new charm state discovery is also presented.

Introduction

Since its discovery in the K sector in 1964 in the famous Brookhaven experiment¹ of Christensen, Cronin and Fitch, the CP symmetry violation has been one of the most intriguing arguments of modern physics. The still very vital interest in this field and in the interaction responsible for such effect observed initially in K sector has been raised by the A. Sakharov suggestion² that CP violation is one of the ingredients necessary to explain the excess of matter over antimatter and the ratio between photons and baryons in the universe.

The standard model with the three families of elementary fermions quarks and leptons allows through the Cabibbo³ Kobayashi Maskawa⁴ flavour mixing matrix (hereinafter referred to as CKM matrix) for CP violation.

The flavour changing weak decays observed since a long time (kaon decay into pions) and firstly described in a two quark family environment by means of the Cabibbo angle, has been extended to the three quark families and it is represented by a 3x3 matrix (the CKM matrix), whose unitarity is required by the observed suppression of the flavour changing neutral current processes (FCNC).

As well known, while the 2x2 matrix in the 2 family picture is a real rotation matrix containing only one parameter, the rotation Cabibbo angle, the CKM matrix contains 4 independent parameters left after the application of the unitarity condition of the Kobayashi and Maskawa matrix and the removal of arbitrary phases in the definition of the quark fields. Within the Standard Model framework, the flavour mixing mechanism between the left handed quarks in processes induced by charged currents (mediated by W's) and the simultaneous parameters, one of which is an off diagonal complex phase. Such a term allows for CP violation in a natural way.

The Standard Model and CKM predict indirect CP Violation in neutral K decays at the level observed and ϵ'/ϵ (direct CP violation parameter in decay of K_L) recently measured; they also predict large CP violating asymmetries in B meson decays.

But let us quickly introduce the mixing formalism and some phenomenological elements relative to the b quark decay in the Standard Model.

1 Mixing Formalism

Let us take a system of a neutral meson and its antiparticle partner and let us call X^0 and \bar{X}^0 . It can be in actual fact K^0 and \bar{K}^0 or B^0 and \bar{B}^0 ; its closest and easiest to build analogy in classical mechanics is the system made of 2 penduli coupled by a spring and constrained to a plane motion.

B^0 and \bar{B}^0 are distinguished by the flavour, by having b or anti-b quark as constituent, as well as K^0 is distinguished from \bar{K}^0 because of strangeness anti-strangeness content.

The formalism that I report here can be found in many review papers as in textbooks⁵ and let us use in what follows without losing generality B^0 and \bar{B}^0 .

The Schrödinger equation that describes the time evolution of the system is:

$$i \frac{d}{dt} |\Psi(t)\rangle = H |\Psi(t)\rangle$$

Since the status represents particles decaying weakly it can be represented at $t=t_0 \gg \tau_{\text{strong.e.m.}}$ time of creation, it must contain all the states of the decay products:

$$|\Psi(t)\rangle = a(t)|B^0\rangle + b(t)|\bar{B}^0\rangle + c(t)|X_c l\nu\rangle + d(t)|\pi\pi\rangle + \dots$$

At t_0 , the initial instant of the creation of $B^0 \bar{B}^0$ is of course

$$|\Psi(t_0)\rangle = a|B^0\rangle + b|\bar{B}^0\rangle$$

for $t_0 \rightarrow -\infty$.

The Hamiltonian $H=H_0+H_w$ is an Hermitian matrix in the representation of the infinite dimension Hilbert space containing the B mesons states and all the states describing the decay products. H_0 is here the free Hamiltonian plus the H_Y and H_{St} describing electromagnetic and strong interactions that do not contribute to the decay, only the weak interaction H_w contributes to the decay and it induces the change of flavour by one unit $|\Delta b|=1$.

We are only interested in the time evolution of B mesons and we limit therefore to the study of $a(t)$ and $b(t)$ at a time $t >$ typical time of strong and e.m. interactions. Then with the above assumptions⁶ we rewrite the Schrödinger equation making use of an effective Hamiltonian H_e

$$i \frac{d}{dt} |\psi(t)\rangle = H_e |\psi(t)\rangle \quad \psi(t) = \begin{pmatrix} a(t) \\ b(t) \end{pmatrix}$$

represented by a complex 2x2 matrix in the sub space limited to B^0 and \bar{B}^0 .

Of course a complex Matrix H_e can be always decomposed in the following way with matrices M and Γ Hermitian. M is called the mass matrix and Γ the decay matrix:

$$H_e = M - \frac{i}{2}\Gamma$$

It can easily be verified that decay rate can be obtained as:

$$\frac{d}{dt} \langle \psi(t) | \psi(t) \rangle = \left\langle \dot{\psi}(t) \middle| \psi(t) \right\rangle + \left\langle \psi(t) \middle| \dot{\psi}(t) \right\rangle = \left\langle \psi(t) \middle| -iM - \frac{\Gamma}{2} \right\rangle + \left\langle \psi(t) \middle| iM - \frac{\Gamma}{2} \right\rangle = -\langle \psi(t) | \Gamma | \psi(t) \rangle$$

In order to evaluate the matrix elements in terms of the H_w and H_0 let us use the interaction representation and remind some useful relations including those relative to the in and out states, after some calculation as in Appendix A:

$$\begin{aligned} M_{11} &= m + \sum_f P \left(\frac{\langle B^0 | H_w | f \rangle \langle f | H_w | B^0 \rangle}{m - m_f} \right) \\ M_{22} &= m + \sum_f P \left(\frac{\langle \bar{B}^0 | H_w | f \rangle \langle f | H_w | \bar{B}^0 \rangle}{m - m_f} \right) \\ M_{12} &= m + \sum_f P \left(\frac{\langle B^0 | H_w | f \rangle \langle f | H_w | \bar{B}^0 \rangle}{m - m_f} \right) \end{aligned}$$

And for the elements of Γ matrix we have:

$$\begin{aligned} \Gamma_{11} &= 2\pi \sum_f \delta(m - m_f) \langle B^0 | H_w | f \rangle \langle f | H_w | B^0 \rangle \\ \Gamma_{22} &= 2\pi \sum_f \delta(m - m_f) \langle \bar{B}^0 | H_w | f \rangle \langle f | H_w | \bar{B}^0 \rangle \\ \Gamma_{12} &= 2\pi \sum_f \delta(m - m_f) \langle B^0 | H_w | f \rangle \langle f | H_w | \bar{B}^0 \rangle \end{aligned}$$

M_{11} and Γ_{11} , M_{22} and Γ_{22} are real. We are then left with 8 independent quantities: M_{11} , M_{22} , Γ_{11} , Γ_{22} , ReM_{12} , ImM_{12} , $Re\Gamma_{12}$ and $Im\Gamma_{12}$.

Conservation of T, CP and CPT imposes some clear conditions on the matrix elements of H_e .

CPT invariance of the Hamiltonian, namely of the weak interactions implies on $\langle f | H_w | B^0 \rangle = \langle f | (CPT)^{-1} H_w CPT | B^0 \rangle = \langle \bar{f} | H_w | \bar{B}^0 \rangle$ the antiunitary character of T implies the complex conjugate of the matrix element and \bar{f}' is the charge conjugate of the final state with the spin reversed. Since we are considering the summation over the final states that form a complete system, the results are independent of the spin direction and $\langle \bar{f}' | H_w | \bar{B}^0 \rangle^*$ is equivalent to $\langle \bar{B}^0 | H_w | f \rangle$ when it is part of summation in the matrix elements giving M and Γ . A consequence is then M_{11} is equal to M_{22} and Γ_{11} equal to Γ_{22} .

In addition T invariance of H_w implies $\langle \bar{B}^0 | T^{-1} H_w T | f \rangle = \langle \bar{B}^0 | H_w | f' \rangle^*$ the summation on final states makes the result independent of spin reversal then $\Gamma_{12} = \Gamma_{12}^* = \Gamma_{21}$ and $M_{12} = M_{12}^* = M_{21}$.

Let us focus our attention on CP symmetry; CP changes the electric charge as well as the other flavour charge and leptonic and baryonic numbers of a particle to those of its antiparticle so:

$$CP |B^0\rangle = e^{i\alpha} |\bar{B}^0\rangle \text{ in which a phase factor appears to multiply the antiparticle state.}$$

$$\text{In analogous way } CP |\bar{B}^0\rangle = e^{-i\alpha} |B^0\rangle$$

$$\text{so that } \langle B^0 | B^0 \rangle = \langle B^0 | CPCP | B^0 \rangle = \langle \bar{B}^0 | CPCP | \bar{B}^0 \rangle = \langle \bar{B}^0 | \bar{B}^0 \rangle = 1.$$

Of course $\langle B^0 | CP = e^{-i\alpha} \langle \bar{B}^0 |$ and $\langle \bar{B}^0 | CP = e^{i\alpha} \langle B^0 |$; if we take for example Γ_{12} and assume CP invariance of the weak interaction we have:

$$\Gamma_{12} = 2\pi \sum_f \delta(m - m_f) \langle B^0 | H_w | f \rangle \langle f | H_w | \bar{B}^0 \rangle = 2\pi \sum_f \delta(m - m_f) \langle B^0 | CPH_w CP | f \rangle \langle f | CPH_w CP | \bar{B}^0 \rangle$$

making use of the above relations and considering that since the summation on $|f\rangle$ is extended to all possible decay channels $\sum_f CP |f\rangle \langle f| CP = \sum_f |f\rangle \langle f|$ and $\Gamma_{12} = \Gamma_{12} = e^{i\xi} \Gamma_{21} = e^{i\xi} \Gamma_{21}^*$ and

$$\text{similarly } M_{12} = e^{i\xi} M_{21} = e^{i\xi} M_{21}^* \text{ and } \frac{\Gamma_{12}}{M_{12}} = \frac{\Gamma_{12}^*}{M_{12}^*}$$

Γ_{12} and M_{12} ARE RELATIVELY REAL!

With some direct calculation as in Appendix B we can find now the eigenstates and the eigenvalues of H_e as linear combinations of $|B^0\rangle$ and $|\bar{B}^0\rangle$:

$$|B_+\rangle = \frac{1}{\sqrt{|p_+|^2 + |q_+|^2}} (p_+ |B^0\rangle + q_+ |\bar{B}^0\rangle)$$

$$\text{and } |B_-\rangle = \frac{1}{\sqrt{|p_-|^2 + |q_-|^2}} (p_- |B^0\rangle - q_- |\bar{B}^0\rangle) \text{ that must satisfy the eigenvalue equations:}$$

$$H_e |B_\pm\rangle = \alpha_\pm |B_\pm\rangle.$$

If CPT holds or CP holds independently of CPT: $H_{11}=H_{22}$, $\delta M=\delta\Gamma=0$

$$\text{and } \frac{q}{p} = \frac{q_+}{p_+} = \frac{q_-}{p_-} = \sqrt{\frac{(M_{12}^* - i\frac{\Gamma_{12}}{2})}{(M_{12} + i\frac{\Gamma_{12}}{2})}}$$

Of course the masses and decay widths of the B_+ and B_- states are $m_\pm = \text{Re}(a_\pm)$

and $\Gamma_\pm = -2\text{Im}(a_\pm)$ we can also define $\Delta m = (m_+ - m_-) = \text{Re}(\Delta a)$

and $\Delta\Gamma = (\Gamma_+ - \Gamma_-) = -2\text{Im}(\Delta a)$

If CPT holds and in addition CP (and of course T) holds:

$$M_{12} \text{ and } \Gamma_{12} \text{ are relatively real and } \left| \frac{q}{p} \right| = 1.$$

If instead CPT is not conserved but T is conserved and not CP then: $\left| \frac{q}{p} \right| = 1$

if CP is conserved and not T then: $H_{11}=H_{22}$, $\delta M=\delta\Gamma=0$ and $\left| \frac{q}{p} \right| = 1$.

But if the T violation effect is small then $\left| \frac{q}{p} \right| \approx 1 - \text{Im}\left(\frac{\Gamma_{12}}{M_{12}}\right)$

In the case of B decays, since the number of channels accessible to both B^0 and \bar{B}^0 is small, we also expect a small deviation from 1 smaller than in K sector ($\varepsilon_k = O(10^{-3})$).

The Standard Model predicted value is: $\left| \frac{q}{p} \right| - 1 = 4\pi \frac{m_c^2}{m_t^2} \sin\beta = 5 \times 10^{-4}$

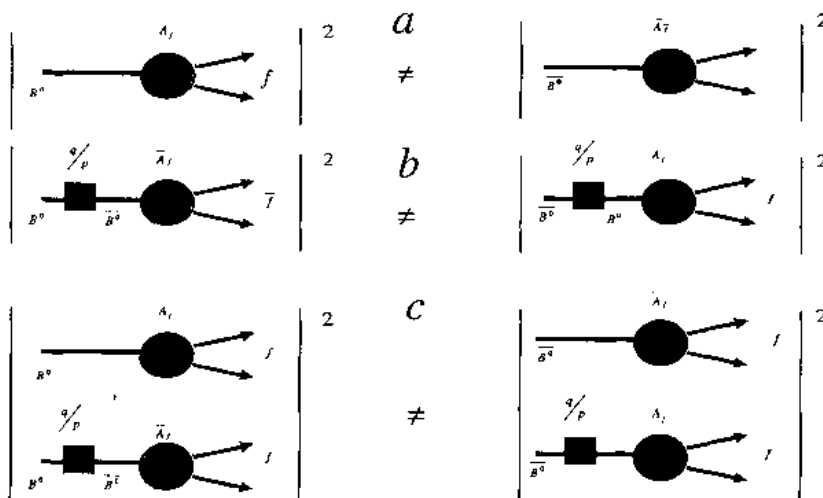


Fig. 1-1: The three CP Violation mechanisms

In all the discussion about CP in B sector some "usual" assumptions are made:

1) CPT holds

$$2) \left| \frac{q}{p} \right| = 1$$

We also use them for simplicity, but in our most recent analysis we fit data with free parameters to look for joint and/or separate CP,T and CPT violations.

In principle there are three ways of establishing CP violation:

The figure 1.1 shows clearly the three violation ways:

a) Direct violation in decay, when the probability of the state B^0 going into a final state f is different from the probability that the CP conjugate state \bar{B}^0 goes into the CP conjugate state \bar{f}

$$\text{then } \left| \frac{A_f}{\bar{A}_{\bar{f}}} \right| \neq 1 \quad (\text{Charged \& neutral states are involved})$$

b) Violation in the mixing $\left| \frac{q}{p} \right| \neq 1$ it can be seen for example measuring the dilepton asymmetry:

$$A_{CP,T} = \frac{N(l^+l^+) - N(l^-l^-)}{N(l^+l^+) + N(l^-l^-)} \approx \frac{1 - |q/p|^4}{1 + |q/p|^4}$$

c) Violation from the interference between mixing and decay amplitudes when both B^0 and \bar{B}^0 decay into the same final CP eigenstate (asymmetries are measured by comparing the decay times of B^0 and \bar{B}^0 (In this case only neutral states involved)

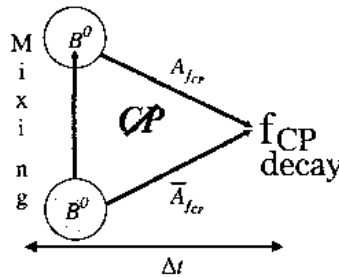


Fig. 1-2: CP Violation from the interference between mixing and decay amplitudes

We will focus our attention on this third mode of CP violation to describe the time dependent asymmetry in the B system produced in pair ($B^0 \bar{B}^0$) in an Asymmetric $e^+ e^-$ Bfactory.

Decay rates of $|B_0(t)\rangle_{phys} = e^{-imt} e^{-\frac{\Gamma}{2}t} (\cos \Delta m t |B^0\rangle - i \frac{q}{p} \sin \Delta m t |\bar{B}^0\rangle)$ and

$$|\bar{B}_0(t)\rangle_{phys} = e^{-imt} e^{-\frac{\Gamma}{2}t} (\cos \Delta m t |\bar{B}^0\rangle - i \frac{p}{q} \sin \Delta m t |B^0\rangle)$$

are obtained by taking $\langle f_{CP} | H_w | B_0(t) \rangle_{phys}^2$ and $\langle f_{CP} | H_w | \bar{B}_0(t) \rangle_{phys}^2$ and after defining

$$A_f = \langle f_{CP} | H_w | B_0 \rangle \text{ and } \bar{A}_f = \langle f_{CP} | H_w | \bar{B}_0 \rangle \text{ we define } \lambda_{CP} = \eta_{CP} \frac{q}{p} \frac{\bar{A}_f}{A_f}$$

Then the CP Asymmetry results:

$$A_{f,cr}(t) = \frac{\Gamma(\bar{B}_0^0(t) \rightarrow f_{CP}) - \Gamma(B_0^0(t) \rightarrow f_{CP})}{\Gamma(B_0^0(t) \rightarrow f_{CP}) + \Gamma(\bar{B}_0^0(t) \rightarrow f_{CP})}$$

$$A_{CP} = -C_{f_{cr}} \cos(\Delta m t) + S_{f_{cr}} \sin(\Delta m t) \quad \text{with}$$

$$C_{f_{cr}} = \frac{1 - |\lambda_{f_{cr}}|^2}{1 + |\lambda_{f_{cr}}|^2} \quad \text{and} \quad S_{f_{cr}} = \frac{2 \operatorname{Im} \lambda_{f_{cr}}}{1 + |\lambda_{f_{cr}}|^2}$$

It is evident that $C_{f_{cr}} \neq 0$ implies DIRECT CP VIOLATION

$$|\lambda_{f_{cr}}| \neq 1 \Rightarrow \operatorname{Prob}(\bar{B}_{phys}^0(t) \rightarrow f_{CP}) \neq \operatorname{Prob}(B_{phys}^0(t) \rightarrow f_{CP})$$

Since the 2 neutral B produced at the machine centre of mass energy of the Y(4s) are pseudoscalar bosons, produced almost at threshold from the decay of the pseudovector bottomium, during their time evolution (including mixing), they conserve their initial orthogonality (they mix in a coherent way). If one meson at the instant t is B^0 then the other must be \bar{B}^0 .

To build the asymmetry

a) we must know the flavour of the meson decayed in the final CP eigenstate f_{CP}

b) we need to measure the decay time or at least the elapsed time between the two B mesons.

To satisfy the requirement a) we make use of the information about the orthogonal character of the two mesons, therefore the flavour of the particle decayed into f_{CP} at time t_0 is correlated to the flavour of the other B that decays at time t_1 . Of course the flavour of the latter is identified only if it decays semileptonic (by the sign of the lepton) or into charm that decays into a final state containing K (by the sign of the kaon).

To satisfy the requirement b) two ingredients of the same level of relevance are needed: a very precise vertex detector in order to measure the interaction point and to separate the decay vertices of B^0 and \bar{B}^0 . Actually decay vertices need to be physically separated in the laboratory system and they are not in the c.m.s. of Y(4s), therefore a Lorentz boost to the system is necessary to allow a separation compatible with the best Vertex Detector capability. This boost is provided by the asymmetry of the e+ e- collider (PEPII). The following figure is presenting in a pictorial way the principal ingredients of the time dependent approach to the measurement of CP violation in the interference between mixing and decay amplitudes

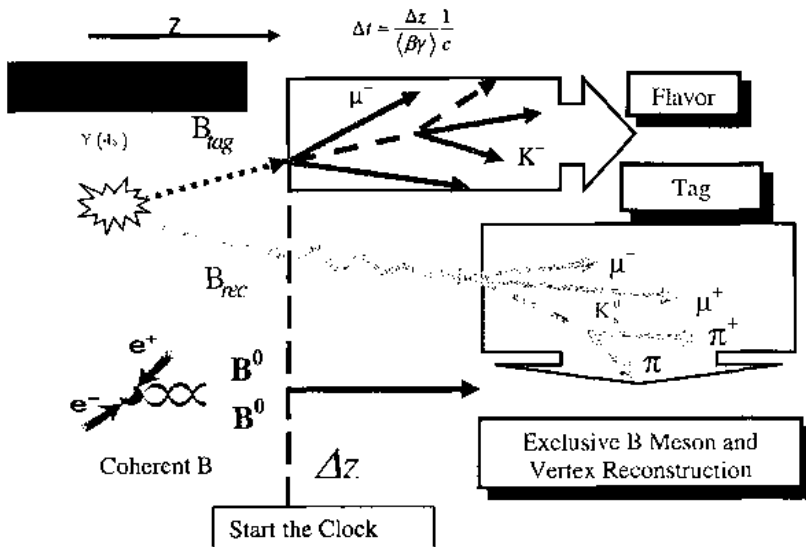


Fig. 1-3: Schematic view of the time dependent approach to the measurement of CP violation in the interference between mixing and decay amplitudes.

2 B decays in Standard Model

The Standard Model of the Unified Electromagnetic and Weak Interactions allows a very elegant and successful description of the decay mechanism of heavy quarks mediated by the gauge bosons.

The charge current taking part to the interaction can therefore be described in terms of quark states as

$$J_{ch}^\mu = (\bar{u} \quad \bar{c} \quad \bar{s}) \gamma^\mu (1 - \gamma_5) \begin{pmatrix} d' \\ s' \\ b' \end{pmatrix} \text{ where the } q' \text{ are here the eigenstates of the weak interaction in}$$

principle different from the mass eigenstates. As originally described by Nicola Cabibbo³ for the 2 family system the q' can be expressed in terms of q the mass eigenstates by means of a transformation (Unitary).

$$V = \begin{pmatrix} V_{ud} & V_{us} & V_{ub} \\ V_{cd} & V_{cs} & V_{cb} \\ V_{td} & V_{ts} & V_{tb} \end{pmatrix} = \begin{pmatrix} 1 - \frac{1}{2}\lambda^2 & \lambda & A\lambda^2(\rho - i\eta) \\ -\lambda & 1 - \frac{1}{2}\lambda^2 & A\lambda^2 \\ A\lambda^2(1 - \rho - i\eta) & -A\lambda^2 & 1 \end{pmatrix} + O(\lambda^4) \quad \begin{pmatrix} d' \\ s' \\ b' \end{pmatrix}_L = V \begin{pmatrix} d \\ s \\ b \end{pmatrix}_L$$

In the 2 family case V is a 2×2 rotation matrix and the rotation angle θ_c is the Cabibbo angle. The 3×3 V matrix has been introduced by Kobayashi and Maskawa and is usually referred as Cabibbo Kobayashi Maskawa matrix or CKM. Phase redefinition and unitarity condition leave in the matrix 4 real parameters, whose values are related to experimental measurements.

The above parametrization is due to Wolfenstein⁷ and λ is the $\sin \theta_c$, the presence of η allows for CP violation.

The Unitarity condition for V : $V^\dagger V = V V^\dagger = I$ gives 6 relations involving the V matrix elements as for example $V_{ud} V_{ub}^* + V_{cd} V_{cb}^* + V_{td} V_{tb}^* = 0$

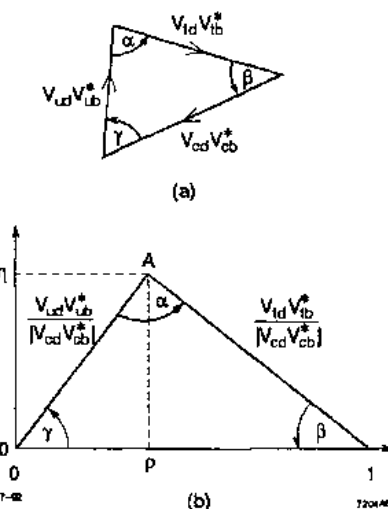
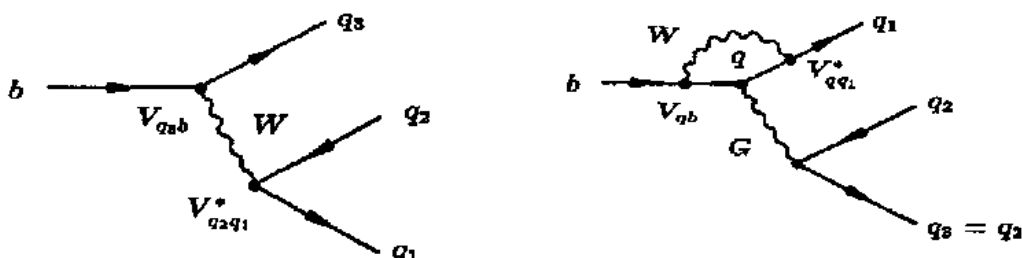


Fig. 2-1: Graphical representation of the Unitarity relation $V_{ud} V_{ub}^* + V_{cd} V_{cb}^* + V_{td} V_{tb}^* = 0$ in the ρ, η plane. In b) the triangle is presented in the ρ, η plane making use of the Wolfenstein parameterization.

The 3 terms are of the same order of magnitude $O(\lambda^3)$ and in a complex plane this relation can be represented as one triangle where the length of the three sides are of the same order, other relations contain terms with different order of magnitude as for example:

$V_{ub} V_{cb}^* + V_{cb} V_{ub}^* + V_{ub} V_{tb}^* = 0$, where the first term is $O(\lambda^4)$ and the other two are instead $O(\lambda^2)$. The graphical representation as a triangle of the second example is not particularly useful, being the triangle collapsed as a degenerate superposition of two sides. The first example allows a very useful graphical representation, where angles and sides can be associated to CP asymmetries and b branching fractions in various decay modes.

The decaying amplitudes of b in Standard Model can proceed through so called Tree or Penguin processes represented by the following diagrams:



TREE

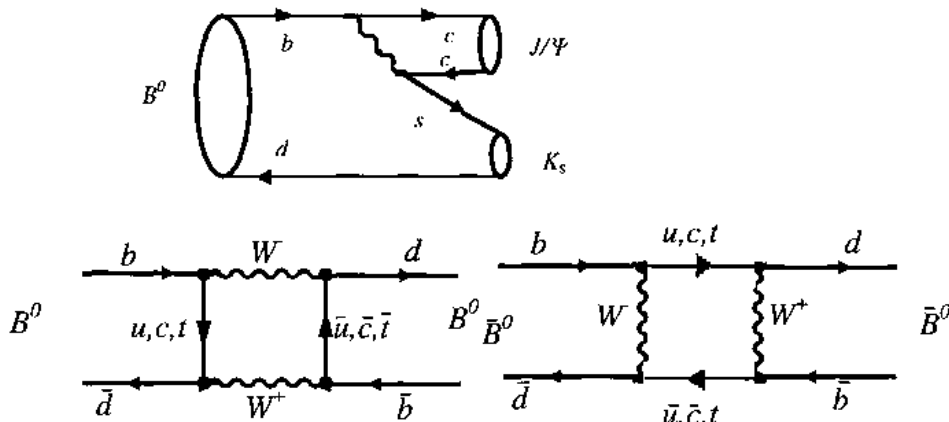
PENGUIN

In the following table are reported as example the contributions to some b decay channels within the Standard Model, is interesting to notice that the β angle can be extracted by a time dependent asymmetry either in charmonium decay (big Tree contribution in $J/\Psi K_s$) and in $b \rightarrow s \bar{s} s \bar{s}$ (pure Penguin in ΦK_s)

Quarks	Leading Term	Secondary	Decay channel B_d	Angle
ccs	$V_{cb} V_{cs}^* = A\lambda^2$ T+P(c-t)	$V_{ub} V_{us}^* = A\lambda^4(\rho-i\eta)$ P(u-t)	$J/\Psi K_s$	β
sss	$V_{cb} V_{cs}^* = A\lambda^2$ P(c-t)	$V_{ub} V_{us}^* = A\lambda^4(\rho-i\eta)$ P(u-t)	ΦK_s	β
ccd	$V_{cb} V_{cd}^* = A\lambda^2$ T+P(c-u)	$V_{ub} V_{ud}^* = -A\lambda^3(1-\rho+i\eta)$ P(t-u)	$D^+ D^-$	$\beta(LT)$
uud/ddd	$V_{ub} V_{ud}^* = A\lambda^3(\rho-i\eta)$ T+P(u-c)	$V_{ub} V_{ud}^* = -A\lambda^3(1-\rho+i\eta)$ P(t-c)	$\pi\pi, \rho\pi, a_1\pi$	$\alpha(LT)$

Table 2-1: Leading and secondary contributions to some B decays

Let us take now the "golden" decay channel $J/\Psi K_s$ and consider the time dependent asymmetry coming out of the interference between the tree diagram and the mixing diagrams.



Mixing diagram contribute to $\frac{q}{p}$ term in $\lambda_{J/\psi K_s} = \eta_{J/\psi K_s} \left(\frac{q}{p} \right)_b \frac{\bar{A}_f}{A_f} \left(\frac{q}{p} \right)_s$, where b-mixing and s-mixing are present. In SM the main contribution to box diagram of mixing are expected to come from the internal quark line of top for b-mixing and of charm for s-mixing.

So in terms of the CKM elements λ_{CP} appears as:

$$\lambda_{CP} = \eta_{CP} \left(\frac{V_{tb}^* V_{cd}}{V_{cb} V_{td}^*} \right) \left(\frac{V_{cs}^* V_{cb}}{V_{cs} V_{cb}^*} \right) \left(\frac{V_{cd}^* V_{cs}}{V_{cd} V_{cs}^*} \right) \approx \eta_{CP} \left(\frac{V_{cd}^* V_{cb}}{V_{cb} V_{tb}^*} \right)$$

And assuming for CP=-1 for s and looking at the unitarity triangle previously drawn it appears that $Im \lambda_{J/\psi K_s} = \sin 2\beta$.

So that in the Time Dependent Asymmetry (TDA): $A_{CP} = -C_{f_{CP}} \cos(\Delta m t) + S_{f_{CP}} \sin(\Delta m t)$ is $S_{f_{CP}} = \sin 2\beta$.

If only one amplitude contributes to the decay ($A_{CP}^* = \overline{A_f}$) from B to $\pi^+ \pi^-$ the TDA would allow the measurement of $S_{f_{CP}} = \sin 2\alpha$. In actual fact the presence of a penguin amplitude contribution to the decay introduces another parameter, a strong phase hard to be determined experimentally that allows in a simple way only the measurement of the sine of an effective angle $\sin 2\alpha_{eff} = \sin 2(\alpha + \delta)$.

3 Analyses Tools

Here I will focus schematically the attention on the most relevant tools necessary for the extraction of the CP asymmetries from the time dependent analyses.

They are: Vertexing and Δt ; Probability Distribution Function (PDF), Flavour Tagging, Full reconstruction of the CP eigenstate.

3.1 Vertexing

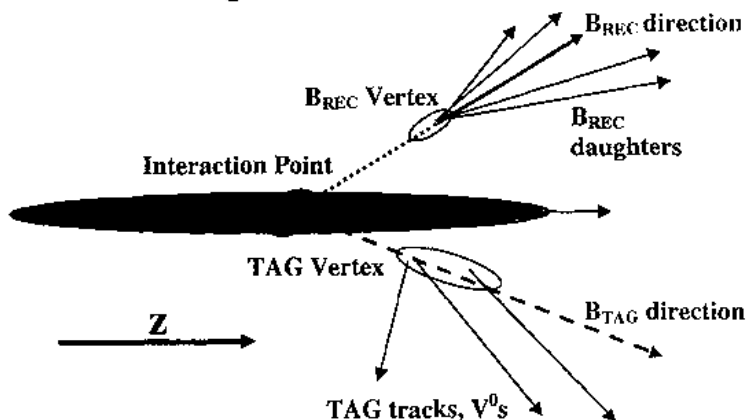


Fig. 3-1: Schematic view of a typical decay of B mesons in BaBar

The recipe for the Vertex tool is:

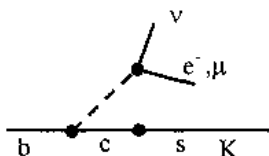
- Reconstruct B_{rec} vertex from charged B_{rec} daughters ($\sigma_z(B_{\text{rec}}) = 65 \mu\text{m}$)
- Determine B_{tag} vertex from
 - charged tracks not belonging to B_{rec}
 - B_{rec} vertex and momentum
 - beam spt and $Y(4S)$ momentum
- High efficiency (93%) through inclusion of t-prong tags
- Average resolution in Δz is $180 \mu\text{m}$ ($<|\Delta z|> = \beta\gamma ct = 260 \mu\text{m}$) corresponding to time instrumental resolution of $\Delta z/c = 0.6 \text{ ps}$.
- Δt resolution function measured from data (B_{flav} sample)

3.2 Tagging Tool

The tagging of the flavour is based on the identification of the most frequent decay modes : semileptonic and $b \rightarrow c$ as can be seen in the following diagram:

Therefore we can hierarchically define the following tagging categories:

- Lepton – charge of lepton
- Kaon – net charge of kaon
- NT1 and NT2 are neural networks that exploit information from momentum spectrum of charged particles, soft π from D^* , unidentified leptons and K.



Large B sample provide the measurement of the tagging performance as reported in the following table containing the tagging efficiencies of BABAR:

Tagging category	Efficiency ϵ (%)	Mistag fraction w (%)	B^0/B^0 diff. Δw (%)	$Q = \epsilon(1-w)^2$ (%)
Lepton	11.1 ± 0.2	8.6 ± 0.9	0.6 ± 1.5	7.6 ± 0.4
Kaon	34.7 ± 0.4	18.1 ± 0.7	0.9 ± 1.1	14.1 ± 0.6
NT1	7.7 ± 0.2	22.0 ± 1.5	1.4 ± 2.3	2.4 ± 0.3
NT2	14.0 ± 0.3	37.3 ± 1.3	-4.7 ± 1.9	0.9 ± 0.2
ALL	67.5 ± 0.5			25.1 ± 0.8

3.3 Full reconstruction of the CP state

Two Kinematical variables are used in BABAR analyses to reconstruct the B meson

- 1) The energy substituted mass : $m_{es} = \sqrt{s/4 - p_B^2}$
The resolution in m_{es} depends on the beam energy uncertainty and it is 2.5 MeV
- 2) The energy difference $\Delta E = E_B - \sqrt{s}/2$. Its resolution depends on the decay channel (mass of products) and on momentum and angle resolution.

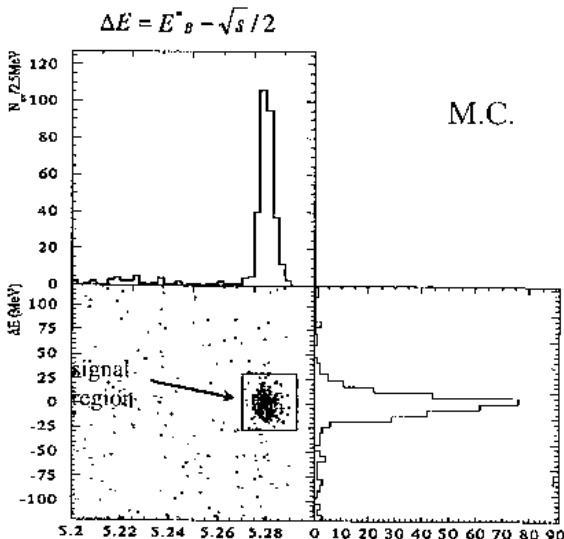


Fig. 3-2: Example of distribution of energy substituted mass and energy difference

4 The PEP-II Storage Rings

PEP-II is an e^+e^- storage ring system designed to operate at a centre of mass energy of 10.58 GeV, corresponding to the mass of the $\Upsilon(4S)$ resonance. The $\Upsilon(4S)$ decays almost exclusively to $B\bar{B}$ and $B+B-$ pairs, providing an ideal laboratory for the study of B mesons⁸.

The electron beam of 9.0 GeV collides head-on with the positron beam of 3.1 GeV resulting in a boost of the $\Upsilon(4S)$ resonance in the laboratory frame of $\beta\gamma = 0.56$. This boost produces an average separation of $\beta\gamma c t = 250 \mu\text{m}$ between the decay vertices of the two B mesons and makes it possible to measure the time dependence of their decay rates and hence to perform a time-dependent CP asymmetry measurement.

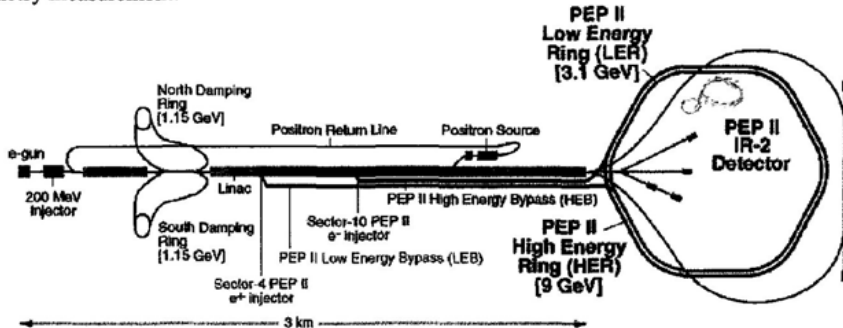


Fig. 4-1: PEPII Layout.

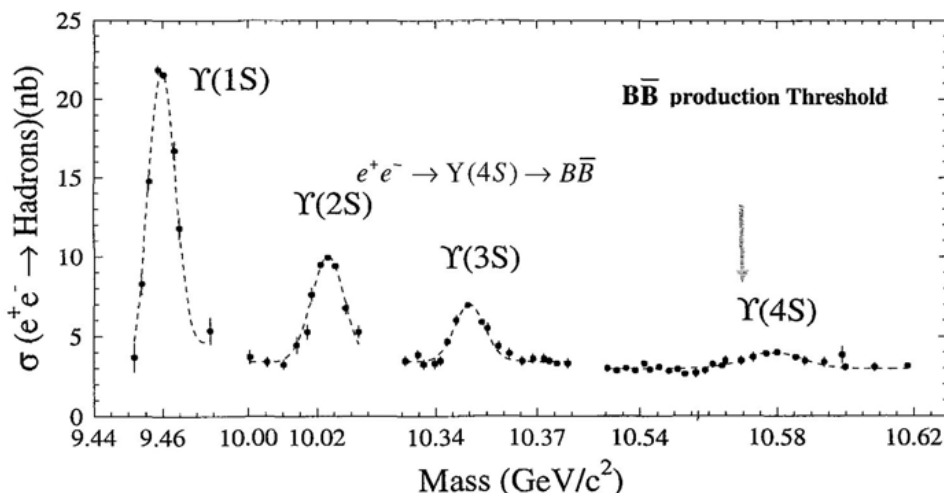


Fig. 4-2: Production cross section for hadrons in e^+e^- collisions as a function of the centre of mass energy.

The interaction region is enclosed by a water-cooled beam pipe of 27.9 mm outer radius which is composed of two layers of beryllium with a water channel between them. To attenuate synchrotron radiation, the inner surface of the pipe is coated with a 4 μm thin layer of gold. The total thickness of the central beam pipe section at normal incidence corresponds to 1.06% of a radiation length.

The bunches collide head-on and are separated magnetically in the horizontal plane by a pair of dipole magnets located at 21 cm on either side of the IP, followed by a series of quadrupoles.

The collision axis is off-set from the z -axis of the BABAR detector by about 20 mrad in the horizontal plane to minimize the perturbation of the beams by the solenoid field.

The beam pipe, the permanent magnets and the inner tracker system of the BABAR detector (SVT), after being assembled and aligned, were enclosed in a 4.5 m long support tube. The central section of the support tube is made of a carbon-fibre epoxy composite with a 0.79% radiation length.

Design Parameters for PEP II

	9.0/3.1	channel	nb
Energy HER/LER (GeV)	9.0/3.1		
Current HER/LER (A)	1.15/1.45	bb	1.10
Number of bunches	1034	cc	1.30
Bunch spacing (m)	1.89	ss	0.35
(μm)	110	uu	1.39
σ^*_{y} (μm)	4.5	dd	0.35
σ^*_{z} (cm)	9	$\tau^+\tau^-$	0.94
β^*_{y} (cm)	1.2	$\mu^+\mu^-$	1.16
β^*_{x} (cm)	28	e $^+$ e $^-$	~40
Instantaneous luminosity ($10^{33} \text{ cm}^{-2}\text{s}^{-1}$)	7		
Daily Integrated luminosity (pb^{-1}/d)	480		
Instantaneous Design Luminosity ($10^{33} \text{ cm}^{-2}\text{s}^{-1}$)	3		
Daily Integrated Design Luminosity (pb^{-1}/d)	135		

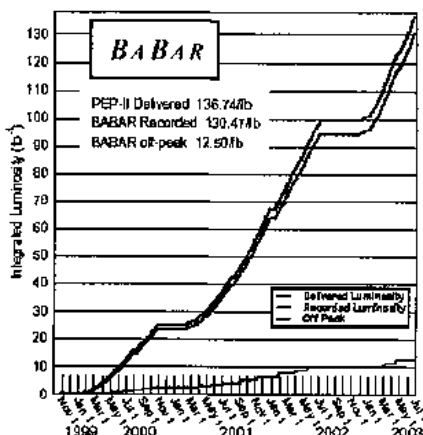
Table 4-1: Production cross-section¹ at $\sqrt{s} = M_{\gamma(4S)}$

Table 4-2: Design parameters for PEP-II

2003/06/28 06:26

The Table 4.2 lists the main parameters of the PEP-II energy asymmetric storage rings. PEP-II has surpassed its design goals, both in terms of the instantaneous and the integrated daily luminosity. Radiative Bhabha scattering measurement provides a fast monitor of the relative luminosity for operations, absolute luminosity comes from e $^+$ e $^-$ and muon pair events.

Fig. 4-3: Integrated Luminosity from 1999 until July 2003



5 Experimental Apparatus

The Babar detector⁹ is a multipurpose detector similar to all the hermetic detectors of the colliding experiments, but with some relevant differences due to the fundamental beam energy asymmetry. It consists of course of a tracker made of a Vertex detector (SVT) + a central tracking Drift Chamber (DCH), a Cherenkov detector (DIRC) an electromagnetic calorimeter (EMC).

These detection systems are surrounded by a superconducting solenoid that generates a field of 1.5 T. The iron for the flux return of the magnetic field is instrumented for muon and neutral hadron detection (IFR).

The polar angle coverage extends to 350 mrad in the forward direction and to 400 mrad in the backward direction, defined relative to the high energy beam.

The BABAR right-handed coordinate system is shown in the detector schematic drawing in Fig. 2-1. The z -axis coincides with the principal axis of the drift chamber, the positive y-axis points upward and the positive x -axis points away from the center of the PEP-II storage rings.

Simulation of the BABAR detector response is realized with a GEANT4-based application.

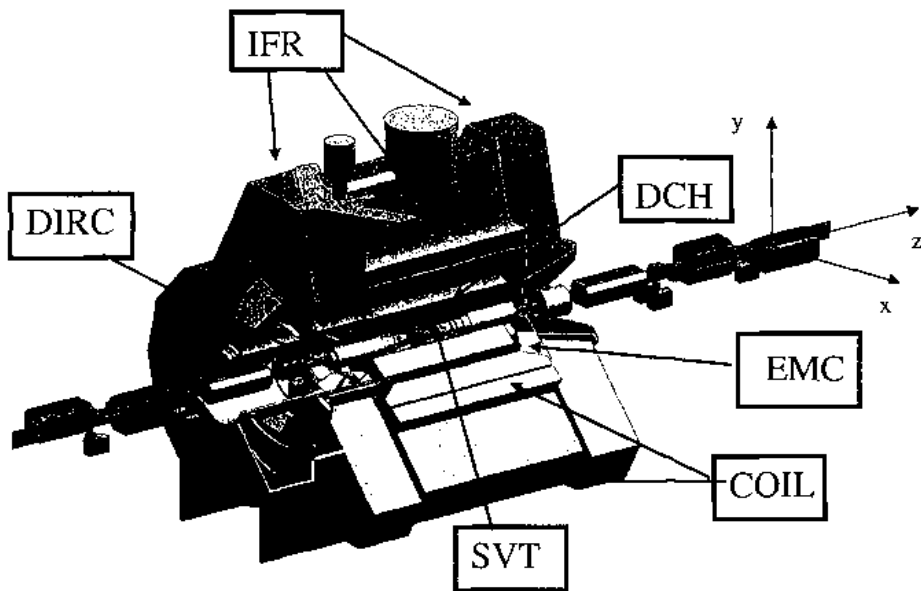


Fig. 5-1: BABAR Detector

5.1 The Silicon Vertex Tracker

The BABAR Silicon Vertex Tracker is composed of five layers of double-sided silicon strip detectors. The SVT has been designed to provide precise reconstruction of charged particle trajectories and decay vertices near the interaction region. The design choices were driven primarily by direct requirements from physics measurements and from constraints imposed by the PEP-II interaction region.

The SVT is critical for the measurement of the time-dependent CP asymmetry. To provide a vertex resolution compatible with the measurement of the time CP asymmetry, the mean vertex resolution along the beam axis should be better than 80 μm .

The required resolution in the x-y plane is about 100 μm to detect charm and τ decays.

The SVT must provide standalone tracking for particles with transverse momentum less than 120 MeV, which cannot be measured reliably in the DCH alone.

The SVT can supply particle ID information both for low and high momentum tracks. For low momentum tracks the SVT dE/dx measurements is the only PID information available, for high momentum tracks the SVT provides the best measurements of tracks angles, which is required to achieve the design resolution for the Cerenkov angle measured in the DIRC.



Fig. 5-2: View of the Silicon Vertex Tracker

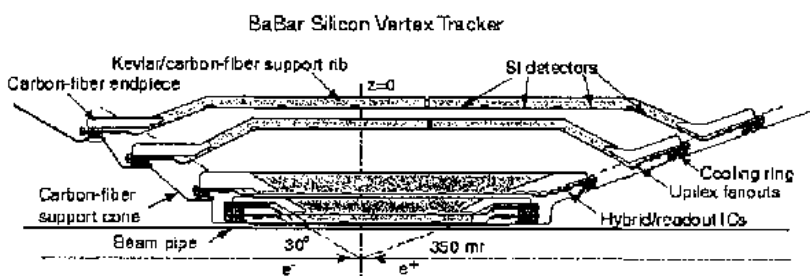


Fig. 5-3: Silicon Vertex Tracker longitudinal section

5.1.1 SVT Performance

The BABAR Silicon Vertex Tracker has satisfied the original design goals regarding the efficiency, hit resolution and reconstruction of low transverse momentum tracks.

The SVT hit reconstruction efficiency is calculated for each half-module as the ratio of the number of hits associated to a reconstructed track over the total number of tracks crossing the half-module. The combined hardware and software efficiency is about 97 %.

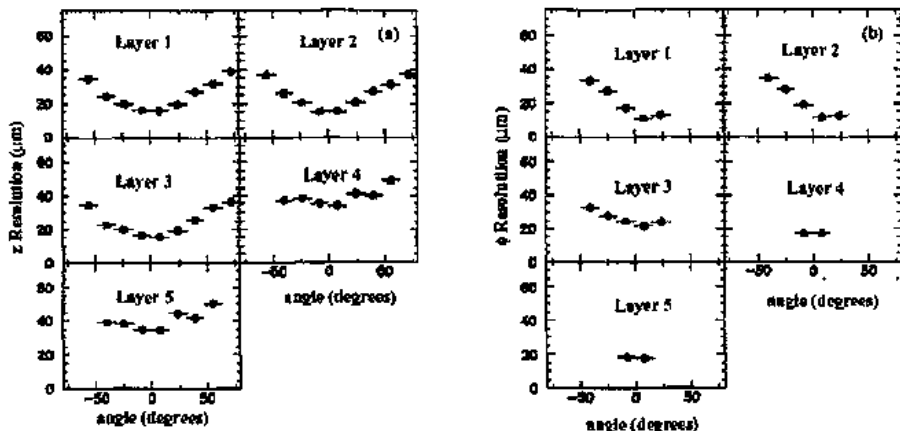


Fig. 5-4: SVT hit resolution in the z (left) and $r\phi$ (right) coordinates, signals from at least four silicon sensors.

5.2 The Drift Chamber

The principal purpose of the Drift Chamber (DCH) is the momentum measurement of charged particles. It complements the measurement of the impact parameter and the direction of charged tracks provided by the SVT near the IP. Moreover, as the reconstruction of the decay vertices outside the SVT volume, such as part of the K_S decays, relies entirely on the DCH, it is required to measure the longitudinal position of a track with a resolution of about 1 mm.

The DCH is the main tool for the particle identification of charged particles with transverse momentum lower than 700 MeV/c. It provides a dE/dx measurement with a resolution of about 7% and represents the only device discriminating particles in the extreme forward and backward direction, out of the geometric acceptance of the DIRC.

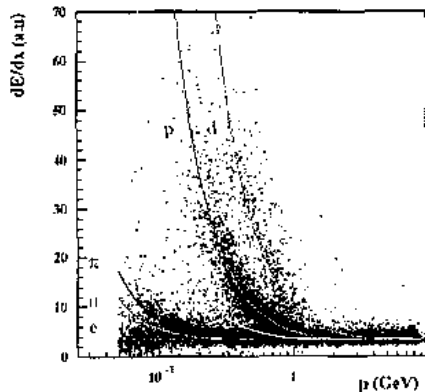


Fig. 5-5: the measured dE/dx for selected particles. The resolution is approximately 14 % for Minimum Ionizing Particles and a 2σ separation between kaons and pions can be achieved up to momenta of 500 MeV.

The Drift Chamber consists of 7104 drift cells arranged in 40 concentric layers, providing up to 40 spatial and ionization loss measurements for charged particles with transverse momentum greater than 180 MeV/c. It is asymmetrically located with respect to the interaction point so that particles with polar angles between 17.2° and 152.6° traverse at least half of the layers.

Longitudinal position information is obtained by placing the wires in 24 of the 40 layers at small angles with respect to the z-axis. Each cell consists of one sense wire surrounded by six field wires. The field wires are grounded, while a positive high-voltage is applied to the sense wires. An avalanche gain of approximately 5×10^4 is obtained at the typical operating voltage of 1960 V and with a 80:20 helium:isobutane gas mixture.

The DCH tracking efficiency is measured by combining the information coming from SVT and DCH. It is determined as the ratio of the number of tracks reconstructed both in the SVT and in the DCH, and the total number of tracks detected in the SVT which fall within the acceptance of the DCH. At the operating voltage of 1960 V, the efficiency averages $98 \pm 1\%$ for track momenta above 200 MeV/c and polar angle > 500 mrad.

5.3 The Detector of Internally Reflected Cherenkov Light

The ability to identify the nature of the charged particles detected by the tracking system has a fundamental role in many aspects of the physics studied in BABAR. The study of the time dependent CP violation requires the tagging of one of the two decaying B mesons through the positive identification of a charged lepton or a kaon. The selection of many important B decay modes is possible if very good pion/kaon discrimination is achievable.

Particle identification (PID) at momenta below 700 MeV/c relies primarily on the dE/dx measurements in the DCH and SVT. Above that threshold the separation between leptons, pions and kaons is provided by a ring-imaging Cherenkov detector which is sensitive to the velocity of the particle through the measurement of the angle of the cone of the emitted light.

The DIRC is placed before the calorimeter. To minimize the energy resolution degradation of the calorimeter and its cost, the DIRC was required to be thin and uniform in terms of radiation lengths and small in the radial dimension. A fast signal response and a high background tolerance were also required for operation at high luminosity.

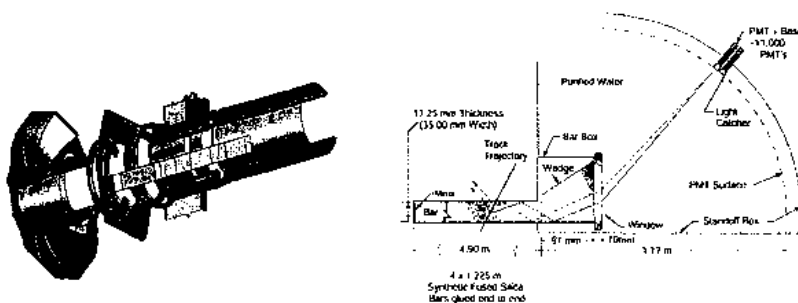


Fig. 5-6: on the left an expanded view of the DIRC, on the right is schematically illustrated the working principle.

The Cherenkov light produced in a quartz bar is transferred by total internal reflection, while preserving the angle, to a large water tank outside the backward end of the magnet. The light is detected by an array of photomultipliers. The expected Cherenkov light pattern is essentially a

conic section, where the cone opening-angle is the Cherenkov-effect angle depending on the refractive index and the velocity of the charged particle.

A total of 144 quartz bars ($n = 1.473$), where Cherenkov light is produced and propagated, are distributed into 12 hermetically sealed containers each one containing 12 bars, for a total of 144.

A mirror placed at extremity of each bar on the side opposite to the readout reflects back the Cherenkov radiation to the instrumented backward end.

Once the photons arrive at the instrumented end, most of them emerge into a water-filled expansion region ($n = 1.346$). A fused silica wedge at the exit of the bar reflects photons at large angles relative to the bar axis.

5.3.1 DJRC Performance

A relevant observable to distinguish between signal and background photons is the difference between the measured and expected photon arrival time. Timing information allows suppressing background hits from the beam induced background, excluding tracks in the same event as the source of the photon and resolving the ambiguities in the hit-to track association.

The time of a photomultiplier hit is measured to a precision of 17 ns.

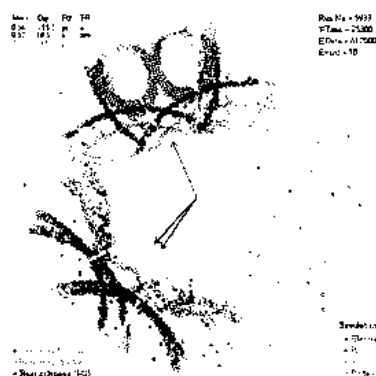


Fig. 5-7: patterns due to particles as reconstructed by using DIRC informations after background suppression.

In normal data-taking conditions the Cherenkov photons from signal events come with hundreds of random photons from background events within the trigger acceptance window (≈ 300 ns). The plot in figure XX shows the signal from all DIRC PMTs as detected within 8 ns of the expected Cherenkov photon arrival time.

In the absence of correlated systematic errors, the resolution on the track Cherenkov angle should scale as $\sigma_{\text{track}} = \frac{\sigma_r}{\sqrt{N_{pe}}}$ where σ_r is the single photon Cherenkov angle resolution and N_{pe}

is the number of photons detected. The angular resolution for the single photon is about 10.2 mrad. With an average of 30 photons per track, the "per track" Cherenkov resolution is about 2.8 mrad, corresponding to a separation of approximately two standard deviations between charged kaons and pions of 4 GeV/c momentum.

5.4 The Electromagnetic Calorimeter

The electromagnetic calorimeter (EMC) is designed to detect and measure the electromagnetic showers with high efficiency and very good energy and angular resolution over an energy range from 20 MeV to 9 GeV. Electromagnetic showers, not associated to charged tracks, are identified as photons. These can be grouped in pairs to reconstruct the π^0 's. Below energies of 2 GeV the π^0 mass resolution is dominated by the energy resolution. The most stringent requirement for energy resolution comes from the measurement of extremely rare decays of B containing π^0 's. Above 2 GeV the angular resolution becomes dominant and it is required to be of the order of a few mrad. To answer all these needs, stable operating conditions have to be maintained. This requires close monitoring of temperature and radiation exposure and frequent and precise calibration of electronics and energy response.

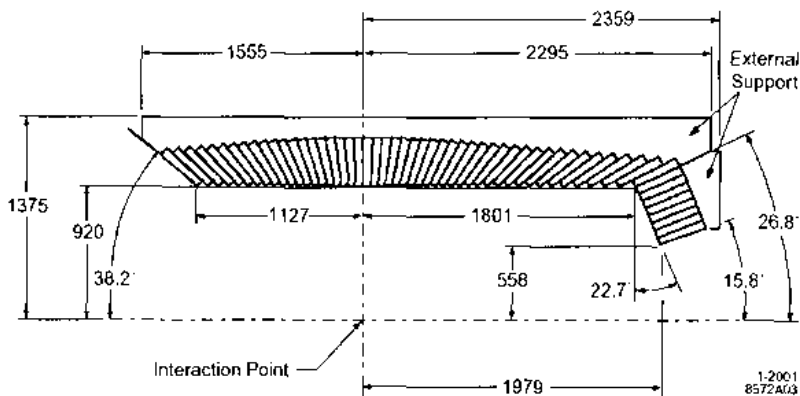


Fig. 5-8: Longitudinal section of the EMC

The BABAR calorimeter is a total absorption calorimeter composed of a segmented array of thallium-doped cesium iodide ($\text{CsI}(\text{Tl})$) crystals. It is constituted by a cylindrical barrel and a conical forward end-cap, providing a full azimuthal coverage and extending in polar angle from 15.8° to 141.8° .

The barrel consists of 5,760 crystals arranged in 48 distinct rings, containing 120 identical crystals each. The end-cap consists of 820 crystals arranged in eight rings. The crystals have trapezoidal cross section and their length increases from 29.6 cm ($16.0\chi_0$) in the backward to 32.4 cm ($17.5\chi_0$) in the forward direction, in order to limit the effects of shower leakage from the increasingly higher energy particles. The crystals are arranged to be slightly non projective in θ with respect to the interaction point, in order to minimize the loss of tracks that traverse the inactive material between crystals. The scintillation light generated inside each crystal is detected by two $2 \times 1 \text{ cm}^2$ silicon PIN diodes placed in the center of the rear face of the crystal.

5.4.1 EMC performance

The energy resolution as a function of energy is extracted from real data through a variety of processes, characterized by the presence of photons in different energy ranges. A fit to the resolution dependence on the energy gives the result:
$$\frac{\sigma_E}{E} = \frac{(2.32 \pm 0.30)\%}{E(\text{GeV})^{1/4}} \otimes (1.85 \pm 0.12)\%$$

where E and σ_E are the photon energy and its r.m.s. error. The first term, decreasing with the increase of the photon energy, arises primarily from the statistical photons fluctuation, but

depends also on the electronic noise of the photon detector and electronics, and on the presence of beam-generated background. The other term is constant in energy and arises from non-uniformity of light collection, leakage or absorption in the material between and in front of the crystals, and uncertainties in the calibrations.

The angular resolution is primarily measured using γ from π^0 decays, and it varies between 3 mrad at high energies and 12 mrad at low energies. A fit to the resolution dependence on the energy gives the result: $\sigma_\theta = \sigma_\phi = \frac{(3.87 \pm 0.007)}{\sqrt{E(\text{GeV})}} \oplus (0.00 \pm 0.004) \text{ mrad}$. The resolution is determined by the transverse crystal size and the distance from the interaction point.

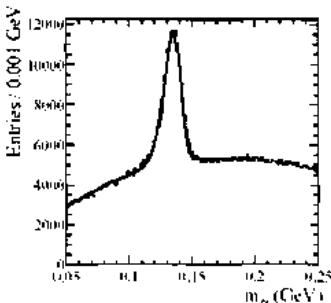


Fig. 5.9: Invariant mass of two photons selected in B events by requiring $E(\gamma) > 30$ MeV and $E(\gamma\gamma) > 300$ MeV. The fit result is superimposed. The reconstructed π^0 invariant mass is 135.1 MeV/ c^2 with a width of approximately 6.9 MeV/ c^2 .

5.5 The Instrumented Flux Return

The Instrumented Flux Return (IFR) was designed to detect muons with good efficiency and purity and identify neutral hadrons such as K_L and neutrons. Muons are used in the identification of the B_d flavor via its semileptonic decay, in the reconstruction of the vector mesons like J/Ψ and in the selection of semileptonic B, D and τ decays. The K_L reconstruction is important for the selection of the CP eigenstates B decays, such as B_d into $J/\Psi K_L$.

The IFR detector is composed by the iron flux return of the magnet, which is used as a muon filter and hadron absorber, and by the Resistive Plate Chambers (RPCs), which are the active part of the detector. The steel is segmented into 18 plates with a variable thickness from 2 cm (inner layers) and 10 cm (outer layers). The steel segmentation has compromise between the subsystem cost (proportional to the volume) and the need of a good efficiency for low momentum (> 700 MeV/c) muon detection, minimizing at the same time the fraction of K_L that do not interact inside the

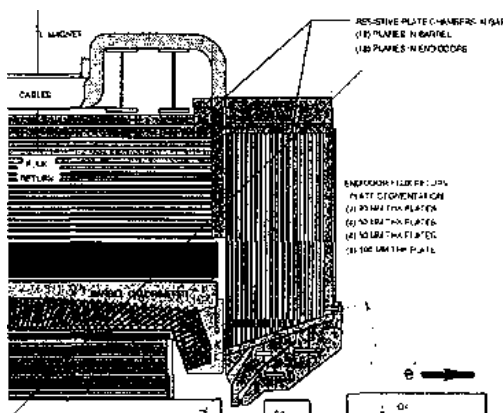


Fig. 5.10: IFR schematic

IFR. The gaps between the steel plates have a width varying from 3.5 cm for the inner layers to 3.2 cm elsewhere, and house the RPCs.

There are 19 RPC layers in the barrel and 18 in the end-caps. In addition, two layers of cylindrical RPCs are installed between the EMC and the magnet cryostat to detect particles exiting the EMC.

The resistive plate chambers detect the streamers generated by ionizing particles crossing the chambers. This kind of detector is characterized by a large signal and a fast response.

The gas inside the chamber is a mixture of Argon (56.7%), Freon-134a (38.8%) and Isobutane (4.5%). The RPCs consist of two bakelite sheets 2 mm-thick and separated by a gap of 2 mm. The external surfaces are coated with graphite, one connected to high voltage (about 8 kV) and the other to ground. The bakelite surface, facing the gap, is treated with linseed oil.

The signals are read out by external capacitive coupled electrodes made of aluminium strips and placed orthogonally on both sides of the gap. The cylindrical RPCs have resistive electrodes made of special plastic and no linseed oil or any other surface treatments have been applied.

5.5.1 IFR Performance

After the installation in 1999, all RPC modules were tested with cosmic rays and an average efficiency of $\approx 92\%$ was measured. The average chamber efficiencies during the 2000 run were $\approx 78\%$ in the barrel and $\approx 87\%$ in the forward end-cap. The RPC chambers of the forward end-cap have been completely replaced with new ones in the summer 2002. The barrel efficiencies are still decreasing and are at the level of 40%, while the average efficiency in the new forward end-cap is greater than 90%.

The dependence of the reconstruction efficiency on the transverse momentum and the polar angle are reported in Fig. 5-11 for one of the muon selectors used in BABAR.

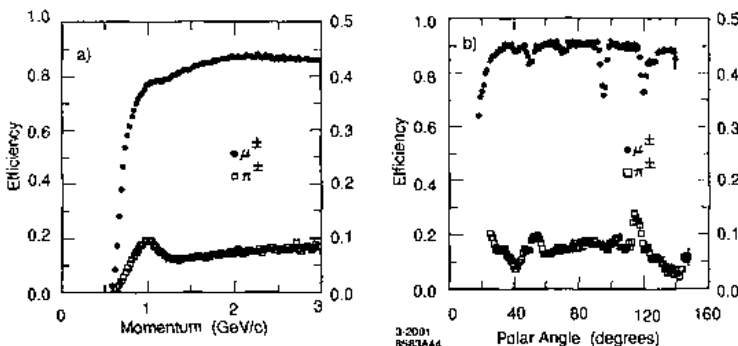


Fig. 5-11: IFR muon efficiency and misidentification fraction as a function of momentum in the laboratory frame and the polar angle.

The K_L detection efficiency of BABAR using the combined information of EMC and IFR increases almost linearly with momentum; ranging between 20 and 40% for a Kaon momentum between 1 and 4 GeV/c .

6 Experimental results

In 2001 BABAR discovered the CP violation in the b sector and measured $\sin 2\beta$. Since then many new results have come out of the experiment. In what follows I will present only some results, representing significant examples of the wide spectrum covered by the BABAR

experiment. The first relevant result came out of a very clean and straightforward time dependent analysis of the decay of neutral B^0 in $J/\Psi K_s$.

A very important issue in this analysis is the validation of the results and the control of the systematic uncertainties related to the time measurement, the method used is based on the measurement of the lifetime and on the flavour mixing as a function of the time. Let us remind the m_{ES} and ΔE definitions $m_{ES} = \sqrt{(E_{beam}^{CM})^2 - (p_B^{CM})^2}$, $\Delta E = E_{J/\Psi} + E_K - E_{beam}^{CM}$. Once the fully reconstructed sample is extracted by means of the kinematical variable m_{ES} and ΔE as shown in the following figure for a restricted data sample containing about half of the present statistics collected, the selected events are fitted using an unbinned maximum likelihood method.

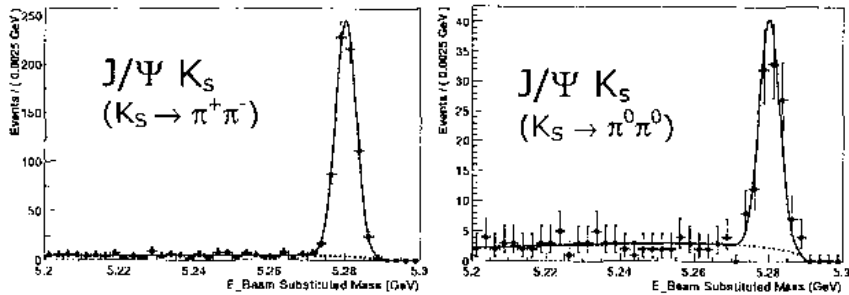


Fig. 6-1: Energy substituted mass for the $J/\Psi K_s$ decay channel

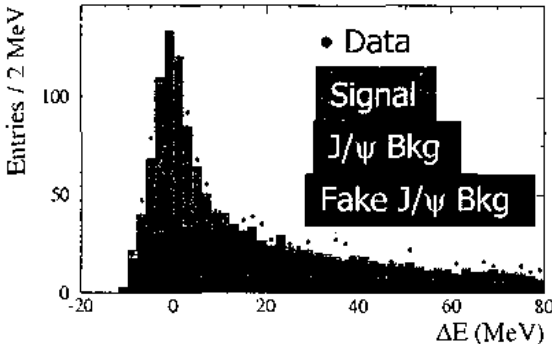


Fig. 6-2: ΔE distribution for the $J/\Psi K_s$ decay channel. The background is determined from m_{ES} fit (flat contribution) or MC (for the peaking component). The mistag rates w and Δt resolution both for signal and for background are extracted from data using the flavour data sample. A total of 34 parameters enter in the Likelihood

In the expression of the time dependent asymmetry previously discussed, the simplified probability function containing only the sine coefficient (i.e. $\sin 2\beta$) is folded with the time measurement resolution R coming from vertexing. As can easily be seen, this expression is different from the experimental distribution of the mixing that still contains w the wrong tag rate and the resolution R . In the fit for the extraction of $\sin 2\beta$ Δm_d and τ_b are fixed to the measured values :

$$f_{mixing,\pm(\Delta t)} = \left\{ e^{-\frac{i\omega}{\tau_{B_d}} \times (1 \pm (1 - 2w)\cos(\Delta m_d \Delta t))} \right\} \otimes R$$

$$f_{cp,\pm}(\Delta t) = \left\{ e^{-\frac{i\omega}{\tau_{B_d}} \times (1 \pm \eta_f \sin 2\beta (1 - 2w)\sin(\Delta m_d \Delta t))} \right\} \otimes R$$

$\tau_B = 1.548 \text{ ps}$
 $\Delta m_d = 0.472$

The validation of the method is coming from the measurement of the lifetime and the mixing parameter. In Fig. 6-3 is shown the time evolution describing the mixing $B^0 \leftrightarrow \bar{B}^0$ in a self-tagging decay mode as $B \rightarrow K \pi$, the sign of K identify unambiguously the flavour of the neutral B.

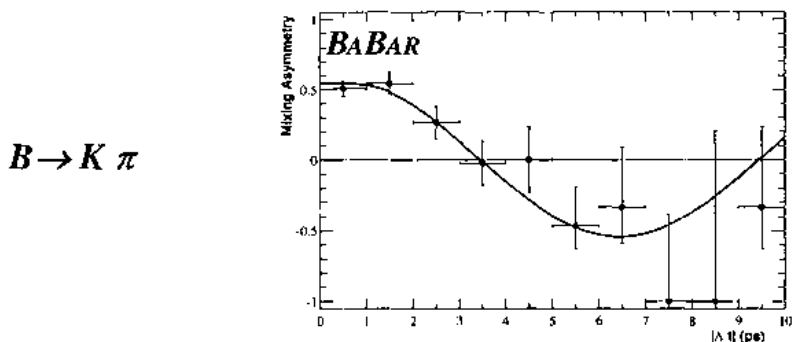


Fig. 6-3: Time dependent mixing asymmetry

The parameter $S_{CP} = \sin 2\beta$ was extracted by using the unbinned maximum likelihood as previously described and for the various decay channels with charmonium we obtained with 81 fb^{-1} :

CHANNEL	$\sin 2\beta$ (BABAR)	BELLE
$J/\Psi K_S, \Psi(2S)K_S, \chi_1 K_S, \eta_c K_S$	$0.76 \pm 0.07_{\text{stat}}$	
$J/\Psi K_L$	$0.72 \pm 0.16_{\text{stat}}$	
$J/\Psi K^{*0} (K^{*0} \rightarrow K_S \pi^0)$	$0.22 \pm 0.52_{\text{stat}}$	
All charmonium	$0.741 \pm 0.067 \pm 0.034$	$0.733 \pm 0.057 \pm 0.028$

Table 6-1: $\sin 2\beta$ measurement in the decay charmonium modes

The averaged value for $\sin 2\beta$ from Charmonium for BABAR¹⁰ and BELLE¹¹ was calculated by the HFAG group and at 93% C.L. was obtained $\sin 2\beta = 0.736 \pm 0.049$.

The fit has also been made without the "usual assumptions" as previously discussed:

$$z = 2 \frac{\delta M - (i/2)\delta\Gamma}{\Delta m - (i/2)\Delta\Gamma} = 0, \quad \left| \frac{q}{p} \right| = 1, \quad |\lambda_{cp}| = 1 \quad \text{and} \quad \frac{\Delta\Gamma}{\Gamma} = 0.$$

The fit has instead been performed leaving these four parameters free to test CPT validity, CP violation in Mixing and Measurement or limit on $\frac{\Delta\Gamma}{\Gamma}$. The result¹², within the present statistics, is compatible with the "usual assumptions" as shown in the following table and presented in Fig. 6-4.

PARAMETER	Measured value	90% C.L. interval
$\text{sgn}(\text{Re } \lambda_{CP}) \Delta \Gamma / \Gamma$	$-0.008 \pm 0.037(\text{stat.}) \pm 0.018(\text{syst.})$	$[-0.084, 0.068]$
$ q/p $	$1.029 \pm 0.013(\text{stat.}) \pm 0.011(\text{syst.})$	$[1.001, 1.057]$
$(\text{Re } \lambda_{CP} / \lambda_{CP}) \text{Re } z$	$0.014 \pm 0.035(\text{stat.}) \pm 0.034(\text{syst.})$	$[-0.072, 0.101]$
$\text{Im } z$	$0.038 \pm 0.029(\text{stat.}) \pm 0.025(\text{syst.})$	$[-0.028, 0.104]$

Table 6-2: Time dependent CP violation from the CPT analysis

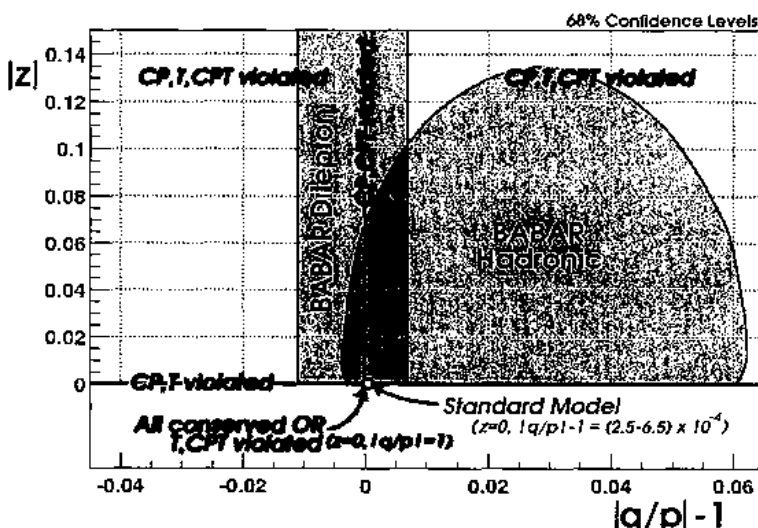
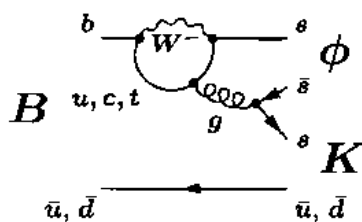


Fig. 6-4: CPT analysis results

But $\sin 2\beta$ can also be measured, according to CKM in SM, by looking at CP asymmetry in the decay $b \rightarrow s\bar{s}s$. This channel as discussed before is a pure penguin channel and in principle, if new heavy quanta (supersymmetric particles) exist they should contribute to the loop in the penguin, a difference could then show up between the S_{CP} measured in say $B^0 \rightarrow \Phi K_S$ and $\sin 2\beta$ measured from charmonium channels.

Fig. 6-5: Diagram of a $b \rightarrow s\bar{s}s$ penguin decay mode

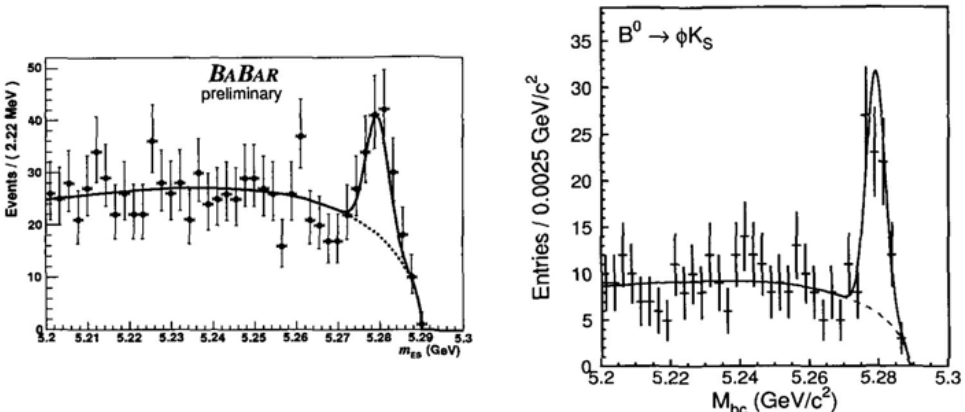


Fig. 6-6: Energy substituted mass distribution for the channel $B^0 \rightarrow \Phi K_S$ obtained from the BaBar experiment (left) and the Belle experiment (right)

BABAR and Belle have both shown a clear signal for this decay as presented in the above figures. The statistics of BABAR is 70 ± 9 events on 112 fb^{-1} collected and Belle has 68 ± 11 on an integrated luminosity of 140 fb^{-1} . Different analyses with different efficiencies explain the discrepancy for Signal / Luminosity between the two experiments.

The results for the measurements of S_{CP} and C_{CP} are:

BABAR finds $S_{CP} = 0.45 \pm 0.43 \pm 0.07$ and $C_{CP} = -0.38 \pm 0.37 \pm 0.12$

and Belle finds $S_{CP} = -0.96 \pm 0.50^{+0.09}_{-0.11}$ and $C_{CP} = 15 \pm 0.29 \pm 0.07$

where the world average value from charmonium is $\sin 2\beta = 0.736 \pm 0.049$. Also looking to all penguin modes, with the statistics so far accumulated at Bfactory experiments (BABAR and BELLE) the presence of New Physics cannot yet been established! The HEFAG group has made the average between BABAR¹³ and BELLE¹⁴ results for penguin modes reported in the following table.

$b \rightarrow s \bar{s} s$ mode	S_{CP} BABAR	S_{CP} BELLE	S_{CP} AVERAGE.
ΦK_S	$0.45 \pm 0.43 \pm 0.07$	$-0.96 \pm 0.50^{+0.09}_{-0.11}$	-0.14 ± 0.33 (only stat) CL=0
$\eta' K_S$	$0.02 \pm 0.34 \pm 0.03$	$0.43 \pm 0.27 \pm 0.05$	0.27 ± 0.21 (only stat) CL=0
$K^+ K^- K_S$	-	$0.51 \pm 0.26 \pm 0.05^{+0.18}_{-0.00}$	

Table 6-3: Heavy Flavor Averaging Group (HEFAG) averages of $b \rightarrow s \bar{s} s$ CP asymmetries measurements

With higher statistics (more than a factor of 2 in both experiments) after the summer 2004, something quite exciting could be found.

6.2 Beyond β , toward measuring the other angles

The important role in the measurement of α is played by the charmless decay modes, unfortunately Tree and Penguin amplitudes contribute to these decays.

The extraction of α and γ angles is possible only after a complex analysis which removes an unknown strong phase.

Experimental Observables:

-Time Integrated (Direct) CP asymmetries

$$A_{CP} = \frac{\Gamma(B \rightarrow f) - \Gamma(\bar{B} \rightarrow \bar{f})}{\Gamma(B \rightarrow f) + \Gamma(\bar{B} \rightarrow \bar{f})}$$

-Branching fractions for various non-charm B decays with Tree and Penguins both contributing

$$A = -(|T|e^{iy} + |P|e^{i\delta}) \quad \bar{A} = -(|\bar{T}|e^{-iy} + |\bar{P}|e^{i\delta})$$

$$Br \propto 1 + 2 \left| \frac{P}{T} \right| \cos(\delta \pm y) + \left| \frac{P}{T} \right|^2$$

$$A_{CP} = -2 \left| \frac{P}{T} \right| \sin \delta \sin y$$

The determination of $|P/T|$ ratio and the relative strong phase δ are required for a clean extraction of CKM angles. In absence of pollution the "usual assumptions" as in the β case hold and

$$\lambda = \eta \frac{V_{ub}^* V_{td} V_{ub} V_{td}^*}{V_{ub} V_{td}^* V_{ub}^* V_{td}} = e^{i2\alpha} \quad C = 0 \quad \text{and} \quad S = \sin(2\alpha)$$

But if we consider the presence of Penguin and Tree amplitudes

$$\lambda = e^{i2\alpha} \frac{1 + \left| \frac{P}{T} \right| e^{i\delta} e^{iy}}{1 + \left| \frac{P}{T} \right| e^{i\delta} e^{-iy}}$$

A few comments are needed on the already established pattern from the charmless 2-body decays as $K\pi$ and $\pi\pi$.

Assuming only Tree contributions one could expect

$$\frac{B \rightarrow K\pi}{B \rightarrow \pi\pi} \approx 5\%$$

Measurements show in fact

$$\frac{B \rightarrow K\pi}{B \rightarrow \pi\pi} \approx 4$$

That is an indication of large Penguin contribution.

On the other hand a method proposed by Gronau and London¹⁵ could allow the determination of δ through an isospin amplitude analysis that produces two relations:

$$0.5 \times A(B^0 \rightarrow \pi^+ \pi^-) + A(B^0 \rightarrow \pi^0 \pi^0) = A(B^+ \rightarrow \pi^+ \pi^0) \text{ and}$$

$0.5 \times \bar{A}(\bar{B}^0 \rightarrow \pi^+ \pi^-) + \bar{A}(\bar{B}^0 \rightarrow \pi^0 \pi^0) = \bar{A}(B^- \rightarrow \pi^- \pi^0)$ where it must be noticed that $A(B^0 \rightarrow \pi^+ \pi^-)$ and $A(B^0 \rightarrow \pi^0 \pi^0)$ take contribution from Tree and QCD Penguin diagrams (both $\Delta I=1/2$ and $\Delta I=3/2$ contributions), while in absence of EW Penguin (or in presence of very small EW effects) $A(B^+ \rightarrow \pi^+ \pi^0)$ receives contribution only from Tree diagram ($\Delta I=3/2$ contributions).

Therefore $|A(B^+ \rightarrow \pi^+ \pi^0)| = |\bar{A}(B^- \rightarrow \pi^- \pi^0)|$. This condition allows building two triangles with a common side as shown in the following figure:

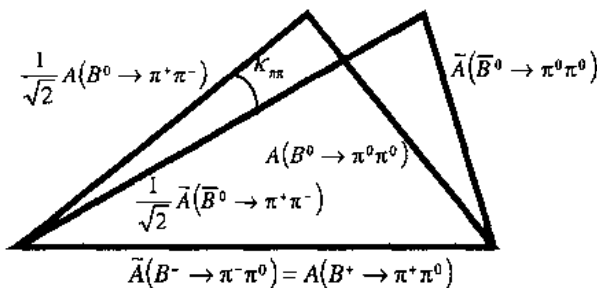


Fig. 6-7

Results from BABAR are based on full data sample 113 fb^{-1} , a total number of events $N_{\pi\pi} = 256.9 \pm 24$ was selected by means of the described Kinematical tools.

Belle analysis was based on 78 fb^{-1}

Data were fitted to the time dependent function to get $C_{\pi\pi}$ and $S_{\pi\pi}$.

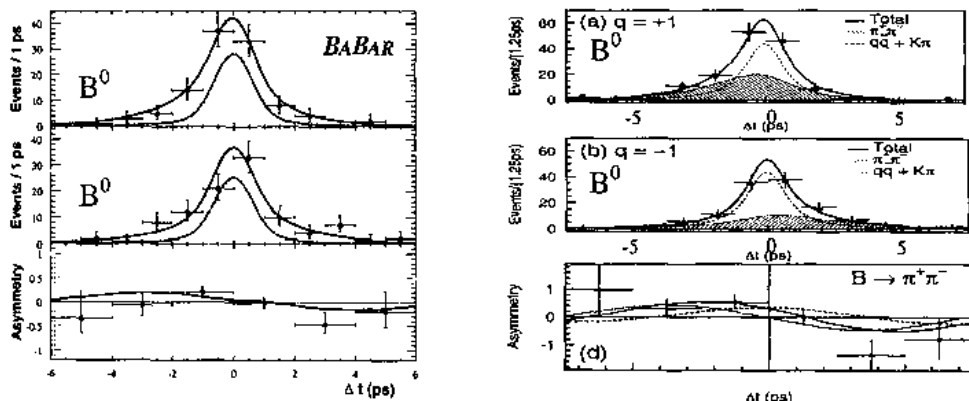


Fig. 6-8: Time dependent asymmetries in charmless two-body decays from BaBar (left) and Belle (right)

Time distributions for B^0 and \bar{B}^0 are shown together with the time dependent asymmetries. The BABAR results from fit are:

For BaBar¹⁶ $S_{\pi\pi} = -0.40 \pm 0.22 \pm 0.03$ and $C_{\pi\pi} = -0.19 \pm 0.19 \pm 0.05$

For Belle¹⁷ $S_{\pi\pi} = -1.23 \pm 0.41^{+0.08}_{-0.07}$ and $C_{\pi\pi} = -0.77 \pm 0.27 \pm 0.08$

A discrepancy appears between BaBar and Belle data, which are still statistically not incompatible. The extraction via isospin analysis of α from $S_{\pi\pi}$ implies the measurement of the $\pi^0 \pi^0$ branching fraction of the neutral B decay.

BaBar has made the first observation¹⁸ of the $B \rightarrow \pi^0 \pi^0$ decay, based on full data sample collected with 113 fb^{-1} . $N_{\pi^0 \pi^0} = 45.6^{+13.9}_{-12.5}$ events have been identified giving the value of the branching fraction of $Br(B^0 / \bar{B}^0 \rightarrow \pi^0 \pi^0) = 2.10 \pm 0.6 \pm 0.3 \times 10^{-6}$ with a significance of 4.2σ .

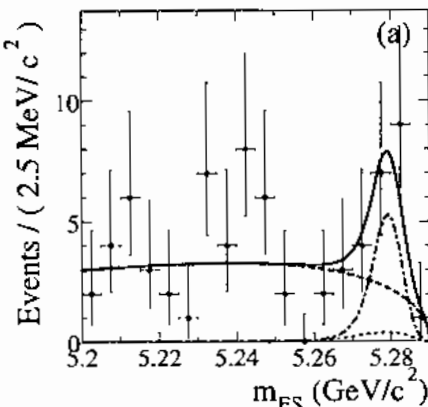


Fig. 6-9: $B \rightarrow \pi^0\pi^0$ invariant mass distribution from BaBar

Of course the full isospin analysis needs the separate measurements of $Br(B^0 \rightarrow \pi^0\pi^0)$ and $Br(\bar{B}^0 \rightarrow \pi^0\pi^0)$, however following the Grossman and Quinn method¹⁹, a limit can be set for $\delta = \alpha_{eff} - \alpha$ being $\sin(2\alpha_{eff}) = S_{\pi\pi}$

$$\cos 2(\alpha - \alpha_{eff}) \geq \frac{1 - 2B^{00}/B^{+-}}{\sqrt{1 - C_{\pi\pi}^2}} |\alpha - \alpha_{eff}| (48^\circ \text{ at 90% CL})$$

In addition to $\pi\pi$ also $\rho\pi$ and ρk have been studied for α extraction and preliminary results have been obtained. In what follows the attention will focussed on $\rho\rho$ analysis.

The decay $B^0 \rightarrow \rho^+\rho^-$ is analog of $B^0 \rightarrow \pi^+\pi^-$ in: both decays the contributions from tree and penguin diagrams can be present and a CP eigenstate can be isolated:

In general in the decay of B^0 into 2 vector particles as in $B^0 \rightarrow \rho^+\rho^-$, the final state is a mixture of angular states (S, P, D), therefore it is not a pure CP eigenstate, but an angular analysis allows to separate the various polarization states, different polarization correspond to different CP eigenvalues:

-A state with Transverse Polarization is CP odd.

-A state with Longitudinal Polarization is CP even

For a state with pure polarization a time dependent analysis can be carried out in a way similar to $\pi\pi$ and S and C coefficient measure $\text{Sin}2\alpha_{eff}$ and Direct CPV as in $\pi^+\pi^-$.

$$A_{\rho\rho}(B^0/B^0) \approx -C_{\rho\rho}^{Long} \cos(\Delta m \Delta t) + S_{\rho\rho}^{Long} \sin(\Delta m \Delta t)$$

The components of $B \rightarrow \rho\rho$ are studied $B^0 \rightarrow \rho^+\rho^-$, $B^+ \rightarrow \rho^+\rho^0$ and $B^0 \rightarrow \rho^0\rho^0$. In the final state the ρ 's result nearly 100% longitudinally polarized corresponding to an even CP eigenstate. Preliminary limit has also been set on $B^0 \rightarrow \rho^0\rho^0$ and by applying as in $\pi\pi$ the Quinn-Grossman bound to the longitudinally polarized component of the rates²⁰:

$$\sin^2(\alpha_{eff} - \alpha) \leq \frac{(f_L^{\rho^0\rho^0} \times B^{\rho^0\rho^0})}{(f_L^{\rho^0\rho^0} \times B^{\rho^0\rho^0})} (0.10 \text{ at 90% CL}) \text{ Therefore } |\alpha_{eff} - \alpha| \leq 19^\circ$$

6.3 Recoil Method

A very interesting method has been developed in the BABAR analyses, it allows in principle to work with an effective pure neutral or charged beam.

The figure describe synthetically what in fact happens to a BABAR event when one of the two B mesons is fully reconstructed, what remains in the event (the recoil part) are the decay products of the partner that is positively identified. It is quite evident that such a very powerful tool which is peculiar of the $B\bar{B}$ production at an e^+e^- factory running at the center of mass energy corresponding to the mass of the $Y(4s)$, would allow with High integrated luminosity the study of very rare decay modes that in principle could open windows on new physics beyond the standard model, as the channels with neutrinos in the final state.

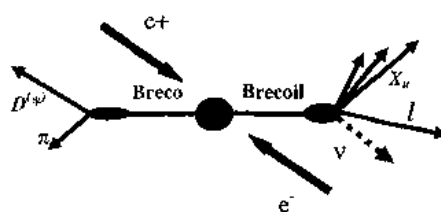


Fig. 6-10: Schematic view of the recoil method

6.4 But not only B Physics in BaBar

PEPII has been built as a B Factory to study CP violation and rare B decays its maximum peak luminosity has been so far $6.5 \cdot 10^{33} \text{ cm}^{-2} \text{ s}^{-1}$ and in fact due to its very high luminosity it is also behaving as a charm and τ factory.

BaBar has so far collected about 120 million of charm and τ pairs. In addition thanks to the high luminosity we can make use of the Initial State Radiation to explore down to quite low invariant mass states, it certainly allows for example a very interesting measurement of

$$R = \frac{\sigma(e^+e^- \rightarrow \text{hadrons})}{\sigma(e^+e^- \rightarrow \mu^+\mu^-)}.$$

The high statistics of charm events collected has allowed BaBar to give a relevant contribution to the charm spectroscopy. Just before the spring 2003 a new narrow charm state has been identified²² at a mass $m=2317 \text{ MeV}/c^2$. This new particle called $D_s^+(2317)$ has been measured in the decay $D_s^+(2317) \rightarrow D_s^+(1970)\pi^0$. Where the $D_s^+(1970)$ has been identified in both decays: $D_s^+(1970) \rightarrow K^+K^-\pi^+$ and $D_s^+(1970) \rightarrow K^+K^-\pi^+\pi^0$ as clearly shown in the following figures

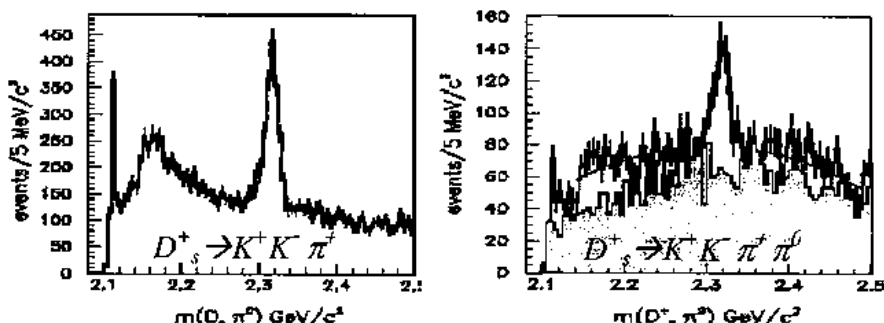


Fig. 6-11: Invariant mass distribution for $D_s^+(2317) \rightarrow D_s^+(1970)\pi^0$ where the D_s^+ 's is reconstructed in the modes $D_s^+(1970) \rightarrow K^+K^-\pi^+$ (left) and $D_s^+(1970) \rightarrow K^+K^-\pi^+\pi^0$ (right)

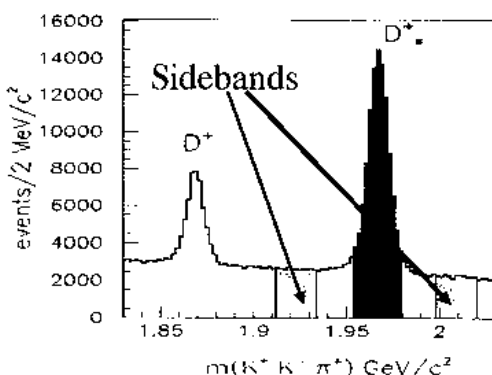


Fig. 6-12: D_s^* invariant mass distribution

Data were analyzed according to the following strategy used to suppress background:

- Select the samples of $K^+K^-\pi^+$ and $D_s^+ \rightarrow K^+K^-\pi^+\pi^0$.
- Ask for K^*K ($K \rightarrow K\pi$) or $\Phi\pi$ ($\Phi \rightarrow KK$) in the final state.
- Cut on decay angle $|\cos \theta| > 0.5$.

The signal of D_s^+ emerges clearly as can be seen in Fig. 6-11. Then, once the D_s^+ signal is identified, it is combined with a good π^0 and the result shows a clean peak at 2317 MeV/c², where instead background events from the D_s^+ plot sidebands (background) give only a non peaking contribution as shown in Fig. 6-13.

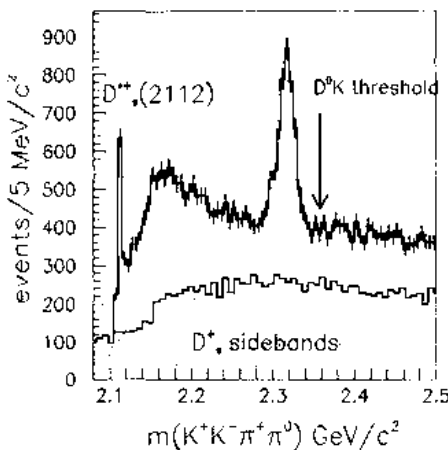


Fig. 6-13: Invariant mass distribution for the new charm state

A relevant question about the nature of the new state is: are 2γ (not a true π^0) giving any peaking contribution when combined with a D_s^+ , at a mass of $2317 \text{ MeV}/c^2$? The answer is no: peaking contribution from 2γ taken from sidebands outside peak from $\pi^0 \rightarrow \gamma\gamma$ plot, as shown in Fig. 6-14.

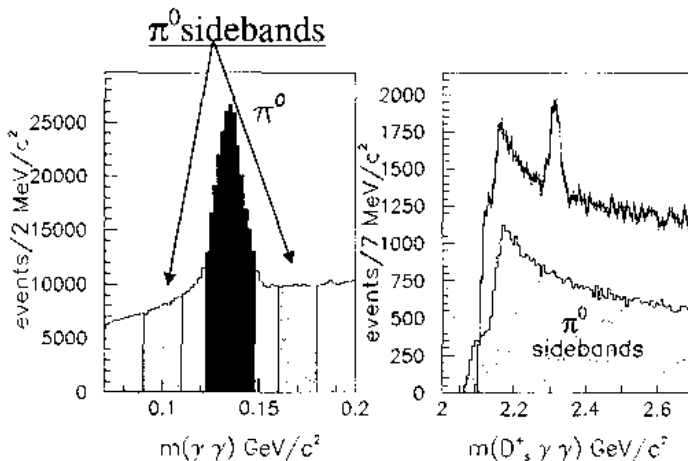


Fig. 6-14: Invariant mass distribution for the π^0 (left) and the new charm state (right). The shadowed areas are obtained using the π^0 sidebands.

The mass fit of the peak, using events with $D_s^+(1970) \rightarrow K^+K^-\pi^+$ gave $M = 2316.8 \pm 0.4 \text{ MeV}/c^2$ and a particle width $\sigma = 8.6 \pm 0.4 \text{ MeV}/c^2$. This result is consistent with what was

obtained in the fit for the events containing D_s^+ when $D_s^+(1970) \rightarrow K^+ K^- \pi^+ \pi^0$ $M = 2317.6 \pm 1.3 \text{ MeV}/c^2$ and $\sigma = 8.8 \pm 1.1 \text{ MeV}/c^2$ (only statistical errors are taken into account).

The angular distribution corrected for efficiency is compatible with a spin=0 particle or a higher spin unaligned state. The non observation of the decay mode $D_s^+ \gamma$ and the low mass of the particle if the decay is parity conserving suggests that this new particle has the natural spin-parity $0+$.

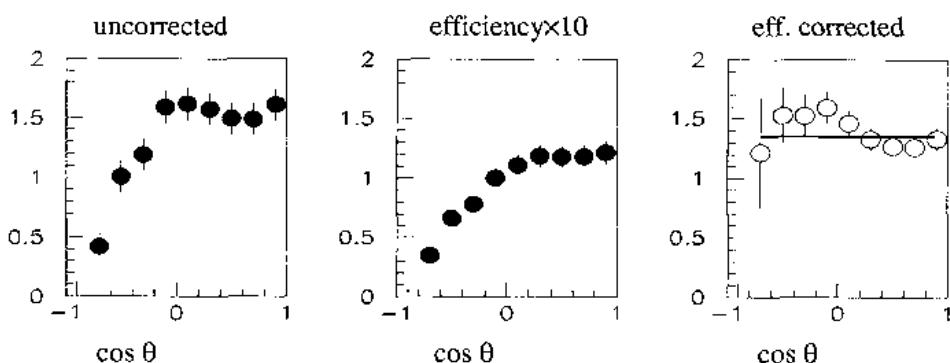
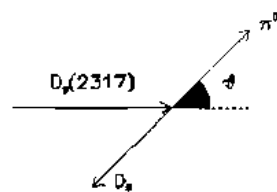
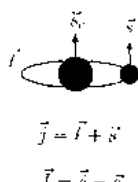


Fig. 6-15: Angular distribution of the π^0 candidates from the decay of the new charm state

$D_s^+ \pi^0$ state has: charm, strangeness, isospin, then if the initial state is $c\bar{s}$, we are in presence of a strong isospin-violating decay.

Some comments are also due related to the $c\bar{s}$ spectroscopy. The state can be treated as an hydrogenoid atom²¹ since it is an heavy quark-light quark bound state, in this sense the total light quark momentum $j=l+s$ is nearly conserved in the limit $m_c \rightarrow \infty$, $J=j+s_c$ is in fact really conserved.



The p wave states $l=1$ form a family of 12 states as shown in Fig. 6-16 where the splitting of the states is induced by the interactions.

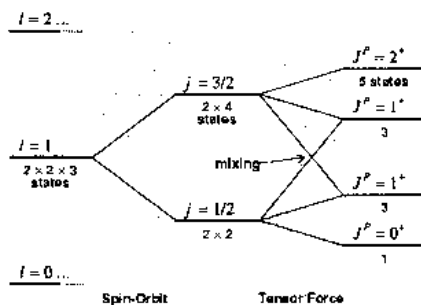


Fig. 6-16: cs spectroscopy

Where the S-wave states 1S_0 and 3S_1 are the well known $D_s(1970)^+$ and the $D_s^*(2112)^+$.

The only two $c\bar{s}$ states previously observed are $D_{s1}^*(2536)^+$ and $D_{s2}^*(2573)^+$, the first has been detected in D^*K mode and the angular analysis indicates 1^+ , the second has been seen in D^0K^+ , in this case although not yet established 2^+ is consistent with experimental results.

The theoretical estimates for these P-wave states, based on potential calculations assigned to all the states mass values higher than the BaBar measured $2317 \text{ MeV}/c^2$, that is $41 \text{ MeV}/c^2$ below the DK threshold, once the radiative decay has ruled out it can explain the decay with isospin violation, that also can explain the extreme narrowness of the discovered particle.

The discovery of the $D_{s1}^*(2317)^+$ ²² was then confirmed by Cleo²³ and Belle²⁴ experiments. After about 30 years since the discovery of J/ψ a new and very exciting season of hunting for new charm states has been started. Other states have been found since then and others are at hand, marking in a simple way the high discovery potential of a very high luminosity machine.

7 Acknowledgements

I would like to thank SLAC and all the agencies that made possible this marvelous BABAR adventure: DOE and NSF (USA), NSERC (Canada), IHEP (China), CEA and CNRS-IN2P3 (France), BMBF and DFG (Germany), INFN (Italy), FOM (Netherlands), NFR (Norway), MIST (Russia), PPARC (UK).

I also intend to warmly thank Antonino Zichichi for his kind invitation and for having given to me the pleasure and the privilege to attend the Subnuclear School and present there the results of my collaboration in the unique environment of Erice. I would like also thank Luisa Cifarelli for her always friendly and intelligent assistance.

Appendix A

Let us introduce the interaction representation and remind some useful relations including those relative to the *in* and *out* states

$$7-1 \quad |\psi(t)\rangle = e^{-iH_0 t} |\psi(0)\rangle,$$

And at the production time for $t_0 \rightarrow -\infty$ $|\psi(t_0)\rangle = a|B^0\rangle + b|\bar{B}^0\rangle$ and of course

$$|\psi(-\infty)\rangle = |\psi(-\infty)\rangle, \text{ since the interaction is not acting.}$$

And with the definition of $U(t, t_0) = e^{iH_0 t} e^{-iH(t-t_0)} e^{-iH_0 t_0}$ of course is

$$|\psi(t)\rangle_i = U(t, t_0) |\psi(t_0)\rangle, \text{ and for } t_0 \rightarrow -\infty \quad |\psi(t_0)\rangle_i = |\psi(t_0)\rangle$$

From the definition of $U(t, t_0)$ following a standard method we have $U(0, -\infty) = \lim_{\epsilon \rightarrow 0+} \frac{i\epsilon}{H_0 - H + i\epsilon}$

$$\lim_{t_0 \rightarrow -\infty} U(t, t_0) = U(t, 0) \lim_{t_0 \rightarrow -\infty} U(0, t_0) = e^{iH_0 t} e^{-iHt} \lim_{\epsilon \rightarrow 0+} \frac{i\epsilon}{H_0 - H + i\epsilon}$$

Let us define $|\psi in\rangle = U(0, -\infty) |\psi(-\infty)\rangle$ and of course $|\psi in\rangle = |\psi(0)\rangle$, and

$$|\psi in\rangle = a|B^0 in\rangle + b|\bar{B}^0 in\rangle.$$

$|B^0 in\rangle = U(0, -\infty) |B^0\rangle$ and $|\bar{B}^0 in\rangle = U(0, -\infty) |\bar{B}^0\rangle$ in addition from the definition follows that

$H|B^0 in\rangle = HU(0, -\infty) |B^0\rangle = mU(0, -\infty) |B^0\rangle$ and $H_0|B^0\rangle = m|B^0\rangle$ and the Shroedinger equation in the interaction representation is:

$$7-2 \quad i \frac{d}{dt} |\psi(t)\rangle_i = e^{iH_0 t} H_w e^{-iH_0 t} |\psi(t)\rangle_i = H_i |\psi(t)\rangle_i$$

In addition:

$$7-3 \quad |\psi(t)\rangle_i = U(t, -\infty) |\psi(-\infty)\rangle = e^{iH_0 t} e^{-iHt} U(0, -\infty) |\psi(-\infty)\rangle = e^{iH_0 t} e^{-iHt} |\psi in\rangle$$

Using equation 7-1, we have that $e^{-iHt} |\psi in\rangle = |\psi(t)\rangle = a(t)|B^0\rangle + b(t)|\bar{B}^0\rangle$

Then from equations 7-2 and 7-3 follows:

$$ie^{iH_0 t} \frac{d}{dt} |\psi(t)\rangle_i = H_0 |\psi(t)\rangle_i + H_i |\psi(t)\rangle_i = H_0 e^{iH_0 t} e^{-iHt} |\psi in\rangle + H_i e^{iH_0 t} e^{-iHt} |\psi in\rangle$$

$$ie^{iH_0 t} \frac{d}{dt} |\psi(t)\rangle_i = H_0 e^{iH_0 t} e^{-iHt} |\psi in\rangle + e^{iH_0 t} H_w e^{-iHt} |\psi in\rangle = H_0 e^{iH_0 t} e^{-iHt} |\psi in\rangle + e^{iH_0 t} H_w e^{-iHt} |\psi in\rangle$$

and

$$\langle B^0 | \frac{d}{dt} |\psi(t)\rangle = m \langle B^0 | e^{-iHt} |\psi in\rangle + \langle B^0 | H_w e^{-iHt} |\psi in\rangle$$

$$\text{Where } \langle B^0 | e^{-iHt} |\psi in\rangle = \langle B^0 | \psi(t)\rangle = \left\langle B^0 \left(a(t)|B^0\rangle + b(t)|\bar{B}^0\rangle \right) \right\rangle = a(t)$$

$$\text{and } \langle B^0 | H_w e^{-iHt} |\psi in\rangle = \left\langle B^0 \left(H_w \left(a(t)e^{-iHt}|B^0 in\rangle + b(t)e^{-iHt}|\bar{B}^0 in\rangle \right) \right) \right\rangle$$

$$\text{but } \langle B^0 | H_w |B^0 in\rangle = \langle B^0 | H_w |B^0\rangle + \lim_{\epsilon \rightarrow 0+} \sum_f \frac{\langle B^0 | H_w |f\rangle \langle f | H_w |B^0 in\rangle}{m - H_0 + i\epsilon}$$

$$\text{and } \langle B^0 | H_w | \bar{B}^0 in \rangle = \langle B^0 | H_w | \bar{B}^0 \rangle + \lim_{\epsilon \rightarrow 0+} \sum_f \frac{\langle B^0 | H_w | f \rangle \langle f | H_w | \bar{B}^0 in \rangle}{m - H_0 + i\epsilon}$$

obviously $\langle B^0 | H_w | B^0 \rangle = 0$ $\langle B^0 | H_w | \bar{B}^0 \rangle = 0$ because H_w allows only transitions with $|\Delta\text{flavour}|=1$.

$$i \frac{d}{dt} \langle B^0 | \psi(t) \rangle = i \frac{d}{dt} a(t) = m a(t) + \lim_{\epsilon \rightarrow 0+} \sum_f \frac{\langle B^0 | H_w | f \rangle \langle f | H_w e^{-imt} (a | B^0 in \rangle + b | \bar{B}^0 in \rangle)}{m - H_0 + i\epsilon}$$

$$i \frac{d}{dt} a(t) = m a(t) + \lim_{\epsilon \rightarrow 0+} \sum_f \frac{\langle B^0 | H_w | f \rangle \langle f | H_w (a(t) | B^0 \rangle + b(t) | \bar{B}^0 \rangle)}{m - H_0 + i\epsilon}$$

and making use of:

$$\lim_{\epsilon \rightarrow 0+} \sum_f \frac{\langle B^0 | H_w | f \rangle \langle f | H_w | B^0 in \rangle}{m - m_f + i\epsilon} = \sum_f P \left(\frac{\langle B^0 | H_w | f \rangle \langle f | H_w | B^0 in \rangle}{m - m_f} \right) - i\pi \sum_f \delta(m - m_f) \langle B^0 | H_w | f \rangle \langle f | H_w | B^0 in \rangle$$

we can now identify the matrix elements of H_e , keeping in mind that Hermiticity of M and Γ implies $M_{11}=M_{12}^\dagger$ and $G_{21}=G_{12}^\dagger$

$$M_{11} = m + \sum_f P \left(\frac{\langle B^0 | H_w | f \rangle \langle f | H_w | B^0 \rangle}{m - m_f} \right)$$

$$M_{22} = m + \sum_f P \left(\frac{\langle \bar{B}^0 | H_w | f \rangle \langle f | H_w | \bar{B}^0 \rangle}{m - m_f} \right)$$

$$M_{12} = m + \sum_f P \left(\frac{\langle B^0 | H_w | f \rangle \langle f | H_w | \bar{B}^0 \rangle}{m - m_f} \right)$$

And for the elements of Γ matrix we have:

$$\Gamma_{11} = 2\pi \sum_f \delta(m - m_f) \langle B^0 | H_w | f \rangle \langle f | H_w | B^0 \rangle$$

$$\Gamma_{22} = 2\pi \sum_f \delta(m - m_f) \langle \bar{B}^0 | H_w | f \rangle \langle f | H_w | \bar{B}^0 \rangle$$

$$\Gamma_{12} = 2\pi \sum_f \delta(m - m_f) \langle B^0 | H_w | f \rangle \langle f | H_w | \bar{B}^0 \rangle$$

M_{11} and Γ_{11} , M_{22} and Γ_{22} are real. We are then left with 8 independent quantities: M_{11} , M_{22} , Γ_{11} , Γ_{22} , $\text{Re}M_{12}$, $\text{Im}M_{12}$, $\text{Re}\Gamma_{12}$ and $\text{Im}\Gamma_{12}$.

Appendix B

Derivation of the eigenstates and the eigenvalues of H_e as linear combinations of $|B^0\rangle$ and $|\bar{B}^0\rangle$:

$$|B_+\rangle = \frac{1}{\sqrt{|p_+|^2 + |q_+|^2}} (p_+ |B^0\rangle + q_+ |\bar{B}^0\rangle)$$

and $|B_-\rangle = \frac{1}{\sqrt{|p_-|^2 + |q_-|^2}} (p_- |B^0\rangle - q_- |\bar{B}^0\rangle)$ that must satisfy the eigenvalue equations:

$H_e |B_\pm\rangle = a_\pm |B_\pm\rangle$. By solving the equations one obtains:

$$a_\pm = \frac{(H_{11} + H_{22}) \pm \sqrt{(H_{11} - H_{22})^2 + 4H_{12}H_{21}}}{2}$$

$$\frac{(H_{11} + H_{22})}{2} = \frac{M_{11} + M_{22}}{2} - i \frac{\Gamma_{11} + \Gamma_{22}}{2} \equiv M - i \frac{\Gamma}{2} \quad \text{and}$$

$$\frac{(H_{11} - H_{22})}{2} = \frac{M_{11} - M_{22}}{2} - i \frac{\Gamma_{11} - \Gamma_{22}}{2} \equiv \delta M - i \frac{\delta \Gamma}{2}$$

$$\text{Then : } a_\pm = (M - i \frac{\Gamma}{2}) \pm \sqrt{(\delta M - i \frac{\delta \Gamma}{2}) + (M_{12} - i \frac{\Gamma_{12}}{2})(M_{12}^* - i \frac{\Gamma_{12}^*}{2})}$$

$$\text{Or } a_\pm = (M - i \frac{\Gamma}{2}) \pm \Delta a$$

$$\text{And } p_\pm = \pm (\delta M - i \frac{\delta \Gamma}{2}) + \sqrt{(\delta M - i \frac{\delta \Gamma}{2}) + (M_{12} - i \frac{\Gamma_{12}}{2})(M_{12}^* - i \frac{\Gamma_{12}^*}{2})}$$

$$\text{and } q_\pm = (M_{12}^* - i \frac{\Gamma_{12}^*}{2})$$

References

1. J. H. Christenson, J. W. Cronin, V. L. Fitch and R. Turlay, *Evidence For The 2 Pi Decay Of The K(2)0 Meson*, Phys. Rev. Lett. **13**, 138 (1964).
2. A. D. Sakharov, Violation Of CP Invariance, C Asymmetry, And Baryon Asymmetry Of The Universe, Pisma Zh. Eksp. Teor. Fiz. **5** (1967) 32
3. N. Cabibbo, *Unitary Symmetry And Leptonic Decays*, Phys. Rev. Lett. **10**, 531 (1963).
4. M. Kobayashi and T. Maskawa, *CP Violation In The Renormalizable Theory Of Weak Interaction*, Prog. Theor. Phys. **49** (1973) 652.
5. I. I. Y. Bigi and A. I. Sanda, *CP Violation*, Cambridge Monogr. Part. Phys. Nucl. Phys. Cosmol. **9** (2000) 1.
6. P. K. Kabir, *The CP Puzzle*, Academic Press, 1968
7. L. Wolfenstein, *Parametrization Of The Kobayashi-Maskawa Matrix*, Phys. Rev. Lett. **51**, 1945 (1983).
8. D. Boutigny et al., *Techincal Design Report for the BaBar Detector*, SLAC-R-95-457, March 1995
9. B.Aubert et al. , *The BaBar detector*, Nucl. Instrum. Meth. **A479**, 1 (2002)
10. B. Aubert et al. [BABAR Collaboration], *Measurement of the CP-violating asymmetry amplitude sin 2beta*, Phys. Rev. Lett. **89**, 201802 (2002)

-
- ¹¹ K. Abe *et al.* [Belle Collaboration], *An improved measurement of mixing-induced CP violation in the neutral B meson system*, Phys. Rev. **D66**, 071102 (2002)
- ¹² B.-Aubert *et al.* [BABAR Collaboration], Limits on the decay rate difference of neutral-B mesons and on CP, T, and CPT violation in B^0 anti- B^0 oscillations, arXiv:hep-ex/0403002
- ¹³ B. Aubert *et al.* [BABAR Collaboration], Measurements of branching fractions in $B \rightarrow \Phi K$ and $B \rightarrow \Phi \pi$ and search for direct CP violation in $B^{+} \rightarrow \Phi K^{+}$, Phys. Rev. **D69**, 011102 (2004); B. Aubert *et al.* [BABAR Collaboration], *Measurement of the time-dependent CP asymmetry in the $B^0 \rightarrow \Phi K^0$ decay*, arXiv:hep-ex/0403026; B. Aubert *et al.* [BABAR Collaboration], *Measurements of CP-violating asymmetries and branching fractions in B meson decays to eta' K*, Phys. Rev. Lett. **91**, 161801 (2003)
- ¹⁴ K. Abe *et al.* [Belle Collaboration], *Measurement of time-dependent CP-violating asymmetries in $B^0 \rightarrow \Phi K^0(S)$, $K^+ K^- K^0(S)$, and eta' $K^0(S)$ decays*, Phys. Rev. Lett. **91**, 261602 (2003)
- ¹⁵ M. Gronau and D. London, Phys. Rev. Lett. **65**, 3381 (1990)
- ¹⁶ H. Jawahery, Proceedings of the XXI International Symposium Lepton and Photon Interactions
- ¹⁷ K. Abe *et al.* [Belle Collaboration], Evidence for CP-violating asymmetries $B^0 \pi^+ \pi^-$ decays and constraints on the CKM angle phi(2), Phys. Rev. **D68**, 012001 (2003)
- ¹⁸ B. Aubert *et al.* [BABAR Collaboration], *Observation of the decay $B^0 \rightarrow \rho^0 \pi^0$* , Phys. Rev. Lett. **91**, 241801 (2003)
- ¹⁹ Y. Grossman and H. R. Quinn Phys. Rev. **D58**, 017504 (1998)
- ²⁰ B. Aubert *et al.* [BABAR Collaboration], Observation of the decay $B^0 \rightarrow \rho^0 \rho^0$ and measurement of the branching fraction and polarization, Phys. Rev. **D69**, 031102 (2004)
- ²¹ A. DeRujula, H. Georgi, S. L. Glashow P.R.L. **37**, 785 (1976),
- ²² B. Aubert *et al.* [BABAR Collaboration], *Observation of a narrow meson decaying to $D/s + \pi^0$ at a mass of 2.32-GeV/c**2*, Phys. Rev. Lett. **90**, 242001 (2003)
- ²³ D. Besson *et al.* [CLEO Collaboration], *Observation of a narrow resonance of mass 2.46-GeV/c**2 decaying to $D/s^* + \pi^0$ and confirmation of the $D/sJ^*(2317)$ state*, Phys. Rev. **D68**, 032002 (2003)
- ²⁴ P. Krokovny *et al.* [Belle Collaboration], *Observation of the $D/sJ(2317)$ and $D/sJ(2457)$ in B decays*, Phys. Rev. Lett. **91**, 262002 (2003)

CHAIRMAN: M. GIORGI

Scientific Secretaries: R. Capra, P. Laycock

DISCUSSION

- *Laycock:*

Could you please show the $B \rightarrow \pi_0 \pi_0$ m_{ES} "peak"? My question is, how do you get a peak from that?

- *Giorgi:*

To separate signal from background, we make use of a Fischer discriminant. As you know, the Fischer discriminant is a linear discriminant between two different populations by means of several parameters. When you have two populations that are separated in some multidimensional space you can build a hyperplane and separate them. This is a well-known technique that was introduced by Fischer in 1935. I showed the particular channel in the transparency.

- *Laycock:*

OK, you have convinced me. My second question is, for these very interesting rare decays you suffer from statistics. What is the likelihood that you will produce significant results from these channels, from this channel and several other results that you showed?

- *Giorgi:*

This is a general fit and in general the confidence level that you have is very high, sometimes it is much more than 90% or even 99%, it depends of course on the quantity that we extract and on the cleanliness of the channel.

- *Laycock:*

I meant that when you are extracting $\sin 2\beta$ or whichever...

- *Giorgi:*

$\sin 2\beta$ has been extracted by means of a general unbinned maximum likelihood fit and, as I presented, in the particular case without the "usual assumptions" we have left free 35 parameters. We give as input probability distribution functions (PDF). Some of the most relevant inputs are of course the PDF of Δt as you can expect. Another important input is the tag information and the likelihood, which is strongly related to the identification of the channel, and then other parameters including in general the probability of particle identification, including neutrals such as π_0 . This is a very complicated analysis and if you simply want to approach this sort of CP analysis with a method à la "Cut and count", which was one traditional way, it would be more difficult to end up with something reasonable. Not only can you reduce statistics, but you can also hide correlations and systematics.

- *Laycock:*

My real point was that, for example, with the ϕ measurements, when you get to the final measurements of $\sin 2\beta$, the statistical significance of the result is not so great, without putting too fine a point on it.

- *Giorgi:*

Yes, in fact the study of ϕK_s comes from 70 ± 9 events in the peak and Belle has 68 ± 11 . So I agree with you. This is reflected in the fact that the error, the uncertainty on the extracted “ $\sin 2\beta$ effective”, which is not $\sin 2\beta$, is quite large. In fact Belle has -0.96 ± 0.50 and we have 0.45 ± 0.43 , which is the origin of the controversy. I pointed out in my lecture this morning this channel because, in my view, this is the typical channel from which we can expect in the future to open up the possibility for new physics in precision measurements. This channel is theoretically clean; it is a pure penguin, so if in the loop you have new quanta they should produce an effect. We could see a difference between $\sin 2\beta$ that we measure in the charmonium channel (tree diagram contribution) and $\sin 2\beta$ effective that we measure with this channel. In principle this is one of the most sensitive channels to new physics and for this reason it is very important. At the moment I am convinced that our measurement is correct and that the measurement of Belle is compatible with ours and I think that we have to accumulate more statistics. Next year we will have doubled the statistics so, if you now combine our data with their data, you end up with an error which is 0.33. If you divide this by 1.4, you end up with something about 0.2, therefore we could have already something that can allow comparisons.

- *Menges:*

A very important quantity in the reconstruction of CP violating events is the beam-constrained mass. How do you measure the beam energy?

- *Giorgi:*

The beam energy is known from the machine directly and if you want to know how we calibrate the energy of the machine I can tell you. We calibrate precisely resulting in a total error on the beam energies at the level of several MeV. The calibration is made by looking at the $Y(3S)$ resonance, which is a very narrow peak; we scan on that. It is quite a precise calibration and so you calibrate the energy of the machine and then you move and also measure accurately the $Y(4S)$ resonance parameters. We have made it public.

- *Cerri:*

I want to clarify something that probably would not be needed in a B physics audience but that is probably useful here. You mentioned several ways of measuring the top right side of the CKM triangle and of course you mentioned those that are relevant for B factories.

- *Giorgi:*

I didn't mention Δm_S , which is very important. Although, by discussing in my final transparencies the comparison between B factories and hadron machines, I mentioned that the hadron machines can measure B_S very well.

- *Cerri:*

Yes, but you forgot another experiment that is running right now, CDF, which is still hoping to measure B_S at some point. I am just kidding.

- *Giorgi:*

Yes, you are. Certainly you know that CDF is an experiment that is very close to my heart: I was the director of Pisa for such a long time that CDF is an experiment where the role of my institution is fundamental.

- *Cerri:*

Ok now the question. On the ϕK signal I was wondering how come Belle have a much better S/B, first of all? And why, even with that, do they have a statistical error that is worse than BaBar?

- *Giorgi:*

What do you mean? The analysis of Belle is a completely different analysis from ours. They use a "Cut and count" analysis to extract signals from background. For this reason they are in a sense less efficient than we are. We are not simply removing the background by fitting a line once you have reduced it after several cuts in sequence. This explains why we have the same statistics despite the difference in the integrated luminosity. It is a completely different way to extract the data. I explained before the method we use. Are you then asking why the final result is different? Are you saying that they have an error that is much worse than ours? Well, as a percentage it is not much worse.

- *Cerri:*

No, the statistical error on the Belle result is larger and given that S over S+B is better than in the case of BaBar, I would expect it to be the other way around.

- *Giorgi:*

No, actually they have an equivalent number of events but in the fit to extract the asymmetry it is not only the number of events that matters: to make an example the tagging is very important, as is the Δt resolution etc...

- *Cerri:*

Yes, but you basically use the same tagger ...

- *Giorgi:*

No.

- *Cerri:*

I mean, you basically have the same performance...

- *Giorgi:*

No.

- *Cerri:*

...order of magnitude...

- *Giorgi:*

Order of magnitude! We are not different by orders of magnitude. But our apparatuses are not identical. Our Cherenkov is performing very well and our vertex detector is very good. This means that we have very good resolution functions. Among the differences between the apparatus it is worth quoting that we have a better angular coverage with the vertex detector, we have 5 layers and a nice, funny shape in our vertex detector, we cover more of the forward region.

- *Cerri:*

So these two effects balance each other.

- *Giorgi:*

Yes.

- *Shekhovtsova:*

You mentioned about initial state radiation in BaBar. If I am not wrong, there are not enough data for the hadronic cross section in the region from 1 to 3 GeV. Is it possible to scan this region at BaBar? And also, can you measure the contribution from exclusive channels to the hadronic cross section?

- *Giorgi:*

First of all the answer is yes. Of course, there is a problem with the statistics we can accumulate, but the answer is yes. Of course, your statistics will become lower and lower as you move away from the Y(4S) resonance. We have an analysis group that is based in Novosibirsk and other people in the collaboration in other countries involved. They are examining the data and expect soon some final result, the statistics so far is not too rich in some mass regions, but we are confident that in the future we will extract important results. In principle you can go down to threshold. However, this is just in principle because eventually you do not have statistics, but you can do it.

- *Shekhovtsova:*

In BaBar, are photons registered or not?

- *Giorgi:*

Yes.

- *Shekhovtsova:*

What kind of kinematics do you use: a collinear photon or emission at a wide angle?

- *Giorgi:*

You can take the emitted photon, you measure it, in principle you could measure both sides, you could take photons on the positron and/or on the electron side for this measurement. You can then use this information to understand that you are taking ISR events.

- *Shekhovtsova:*

Yes, I understand, but I asked what kind of photons you really use: a collinear photon or emission at a wide angle?

- *Giorgi:*

Photons are of course mainly collinear; we take them in the EMC endcap (we have only one endcap in the direction of the high energy beam).

- *Otiougova:*

What kind of resistive plate chamber (RPC) were you using in the experiment? Why did you decide to replace them with other detectors?

- *Giorgi:*

I expected a question of this kind. I mentioned the fact that we are going to replace the RPC. We installed in 1999 RPCs made with bakelite and linseed oil and quite some time afterwards we discovered that the efficiency in some regions was decreasing. Then we set up a careful investigation and we discovered that somehow there was a change in the resistivity of the surface due to a change in the linseed oil properties. If linseed oil is not polymerised then it is a quite unstable mixture of different compounds. The polymerisation of linseed oil is related to chemical and physical conditions including the presence of oxygen, the temperature and the presence of ultraviolet light. Two years ago we decided to replace the forward endcap, to replace the RPCs with new RPCs and to add brass absorber. In the post mortem analysis of the extracted chambers we discovered many problems. We have seen that in many cases the linseed oil was not polymerised, we have seen drops, stalagmites and it was quite evident that there were places where the electric field was discharging. After replacement the forward endcap has behaved better. However in the forward endcap it is still possible to intervene and change chambers if they show problems. The situation is more serious as far as the barrel is concerned. The barrel is not accessible in an easy way and to replace detectors we need to stop data taking for a quite long period of something between 5 and 8 months. On the other hand, the efficiency for muon detection was going down and down and without any intervention we could expect something of 20% in 2005. We have therefore decided to replace the RPCs with something more robust. So the decision was to move to

plastic streamer tubes. Plastic streamer tube production has been started and the main responsibility lies on several Italian and US institutions. We will start the replacement in 2004 for 2 months and we will complete it in 2005.

- *Rotaev:*

There are quite a few experimental questions that suffer from a lack of statistics. For example, when you compare some results from Belle with the same from BaBar, the statistical error is comparable with the effect. How much time do we need to gain sufficient statistics?

- *Giorgi:*

I think that this is a very appropriate question. I think that in the profile that I presented this morning, about the possible increase of luminosity, both BaBar and Belle will go to an upgrade in the machine luminosity. So according to the upgrade plans of the machine groups, both in PEP and KEK, we can think of achieving a factor 4 more statistics by the end of 2005 and a factor 8 in statistics by the end of 2008. With an integrated luminosity of about 1 ab^{-1} the error in a channel such as ϕK_S and in the other rare channels, mainly taking contributions from penguin diagrams which are the most sensitive to the new physics, will be substantially reduced by almost a factor 3. At the moment altogether we have a statistical error on the $B \rightarrow \phi K_S$ channel that is 0.33. If you can reduce that to 0.1 then we could have something that can be really compared to $\sin 2\beta$ from golden channels. So I think the scale can be fixed at about 5 years.

- *Lysov:*

Could you explain the way you have checked CPT?

- *Giorgi:*

It is a general fit and it is very ambitious. As you can see, there are some parameters that normally, using the usual assumptions, are set by default to some values. So for example, $|q/p|$ is set to 1 and z is set equal to 0 by default. In fact this is one of the sensitive channels to CPT violation. If you leave all these parameters free and you make a general fit, then you end up with a check of all the quantities. So far, the result you find is in general agreement with the usual assumptions. So for example, we measure $|q/p|$ in several independent ways, by looking at the violation in the mixing; so far we have found no discrepancies from 1. So far we find total agreement, within the errors, with the values expected for CPT conservation. And again, to check more precisely we need higher statistics, because at this level the errors are still quite large with respect to the effect that we intend to look for.

- *Dainese:*

The B oscillation amplitude depends on the top mass. Can you say something on m_t from your data?

- *Giorgi:*

No, I don't think so. Well, actually in the general fit that I presented for the CKM triangle there are some broad regions with different colours. The boundaries of these regions have been evaluated using all the information available.

- *Ting:*

I just wanted to take a look at the best fit of the Standard Model with your data.

- *Giorgi:*

OK, this was the best fit made by the CKM averaging group. It uses the new 2003 world average that is 0.736 ± 0.049 and actually this will determine the allowed region very precisely. This is the best fit that we have at the moment; this includes all of the statistics of Belle and BaBar.

- *Ting:*

Basically, Marcello, you do not see a deviation from the Standard Model here.

- *Giorgi:*

No, we do not see so far any deviation from the Standard Model. It will not be easy to find a deviation. We are working hard, but it will be very tough. I indicated in my talk that we expect deviations coming from some particular channel involving loops sensitive to new quanta, more than from a general fit. This was in fact the kind of message that I wanted to convey this morning in the lecture.

HIGHLIGHTS FROM FERMILAB

STEPHEN PARKE

*Theoretical Physics Department
Fermi National Accelerator Laboratory
P.O.Box 500, Batavia, IL 60510, U.S.A.
E-mail: parke@fnal.gov*

The Fermilab High Energy Physics program is a very diverse program with many different types of experiments being performed. In this talk I covered recent results from the collider program as well as the neutrino program. I also discussed future experiments.

1 Fermilab

Currently Fermilab operates the highest energy particle accelerator in the world: a 2 TeV proton-antiproton collider, the Tevatron, with two detector CDF and D0. This complex of machines is exploring nature at the smallest possible distance scale with the hopes of discovering physics beyond the Standard Model, e.g. super-symmetry. Many precision measurements of Standard Model physics are also being made: properties of the top quark, W and Z bosons, B mesons and baryons, QCD jets. As well as searching for the SM Higgs boson.

Fermilab also has an extensive neutrino program with the recent completion of DONUT, which observed the first τ -neutrinos. Mini-BOONE is currently running with the goal of confirming or refuting the LSND $\nu_\mu \rightarrow \nu_e$ signal and MINOS whose primary goal is to measure the δm^2 associated with atmospheric neutrinos with about 10% precision by sending a beam of neutrinos from Fermilab to Soudan, Minnesota.

Future project at Fermilab are BTeV which will study B-mesons produced in the hadronic environment and NuMI-Off-Axis which will explore CP-violation in the neutrino sector.

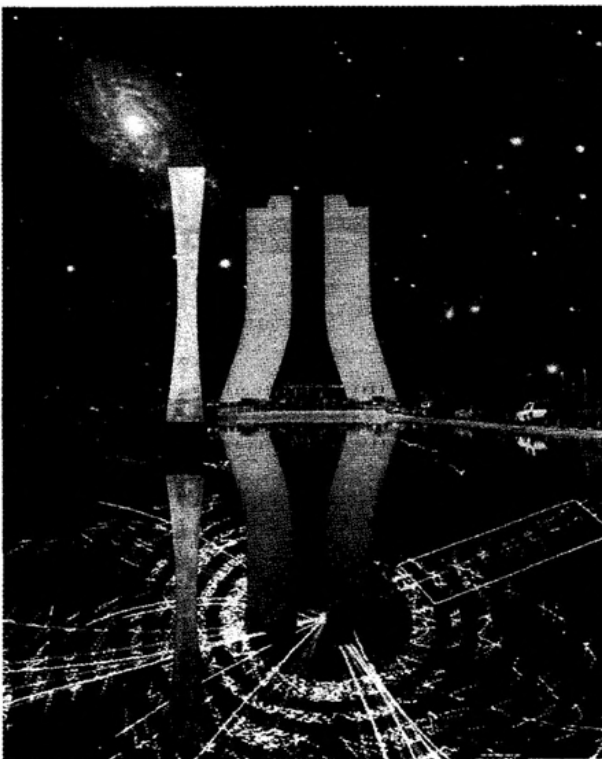
The author has decided not to condense his talk into little more than sound bites of the various topics mentioned above which are already dated but to provide a reference web page which contains a full copy of the talk presented at this summer school¹.

Acknowledgments

The author would like to thank all of the organizers of this school for the opportunity and hospitality provided to him while in beautiful Erice.

References

1. http://theory.fnal.gov/people/parke/TALKS/2003/030830_crice.pdf



**HIGHLIGHTS
from
FERMILAB**

**Stephen Parke
Fermilab**

**Erice Summer School
September 1, 2003**



Contributions from...



- Lepton-Photon Speakers:
 - Patrizia Azzi (Padova), Terry Wyatt (Manchester)
 - Michael Schmitt (NorthWestern), Robert Hirosky (Virginia)
 - Koichiro Nishikawa (Kyoto)
- Fermilab JET Seminar Speakers:
 - Aaron Dominguez (LBNL), Robert Kehoe (MSU).
- Many Fermilab Colleagues including
 - Peter Cooper, Stephen Kent, John Beacom, Adam Para,
 - Heidi Schellman, Rajendran Raja,



Outline:



- **Vernon Hughes:**
 - E061 and E665
- **Tevatron Collider:**
 - Machine, Detectors and Physics
- **Hadronic Fixed Target:**
- **Theory:**
- **Astrophysics:**
- **Neutrinos:**
- **Summary:**



Vernon Hughes at Fermilab



- E61 Proposed March 1977
- Proposal to Measure
Polarization in $p\bar{p}$, π^-p and
 π^+p Elastic Scattering at 50,
100 and 150 GeV/c at FNAL.
- First pub May 1977
- Completed Oct 1977
- 3 papers: 2 in PRL, 1 PRD

Volume 31, Number 6

PHYSICAL REVIEW LETTERS

8 August 1977

Measurement of the $\pi^+\mu$ and $\pi^-\mu$ Polarization Parameters at 100 GeV/cS. P. Adler, D. Hill, R. Sandter,^{1a} and A. Yokosawa
Argonne National Laboratory, Argonne, Illinois 60529

and

W. Drechsler, G. Chapman, R. Stettler, and G. Shapiro
Lawrence Berkeley Laboratory, Berkeley, California 94720

and

A. Jacobsberg and D. F. M. Koschier
Fermilab National Accelerator Laboratory, Batavia, Illinois 60510

and

R. V. Ellis, M. E. Law, and T. M. Pipkin
Massachusetts Institute of Technology, Cambridge, Massachusetts 02139

and

W. Johnson
Syracuse University, Syracuse, New York 13244

and

J. Snyder and M. E. Zeller
Fermilab National Accelerator Laboratory, Batavia, Illinois 60510
(Received 24 May 1977)

We report measurements of the polarization parameters in $\pi^+\mu$ and $\pi^-\mu$ elastic scattering at an incident momentum of 100 GeV/c. The results cover the range $0.18 \leq |\cos\theta| \leq 1.4$ GeV/c and are in agreement with various Regge-model predictions.

In the first experiment of its kind at Fermilab we have measured the polarization parameters $P(\theta)$ in the elastic scattering of mesons and protons from polarized protons. We present here the results for $\pi^+\mu$ and $\pi^-\mu$ scattering which were obtained by averaging over the range over the range of the square of the four-momentum transfer $Q^2 = 0.18 \leq -t \leq 1.4$ GeV².

Up to recent measurements of elastic differential cross sections in this kinematic region¹⁻⁴ have confirmed phenomenological predictions of the π and ρ dependence of the dominant transverse amplitude. In particular, measurements presented here strengthen these predictions because they are sensitive to the difference between amplitudes. For example, a model in which ρ -meson and π -meson exchange are proportional to each other, $P(\theta)$ in πp scattering would be proportional to ϵ^2 with $\epsilon = \alpha_F/(1-\alpha_F)$, where ϵ is the square of the total energy of the system, and $\alpha_F \approx 0.50$ for $\pi^+\mu$ scattering and ≈ 0.40 for $\pi^-\mu$ scattering, respectively. This ϵ dependence is approximately $\epsilon^{-1/3}$ at small $|\theta|$.

This model also predicts that the mirror symmetry $P(\theta) = P(-\theta)$ is violated at large $|\theta|$. In the range $0.8 \leq |\cos\theta| \leq 1.5$ GeV/c the dominant amplitudes are strongly affected by absorption and absorption results in small polarization values at high energies.

The experiment was performed in the 2.5-meter beam (MD) in the Meson Laboratory which had a size of 2.72 cm^2 and a divergence of 0.2° around the beam axis. The beam had a momentum limit of ≈ 100 GeV/c. The small divergence was necessary for kinematic separation of elastic from quasielastic events. In order to determine polarizations of $\pi^+\mu$ and $\pi^-\mu$ scattering, we placed polarimeters in the beam, enabling the separation to better than 0.05° . The beam was focused by a sequence of lenses to a width of $\approx 100 \mu\text{m}$.

The detector system was located automatically in Fig. 2. It consisted of a double-arm spectrometer capable of detecting both final-state particles with uniform acceptance over the angular range $0 < |\theta| < 1.4$ GeV/c. The two detectors were instrumented with eight planes of multiwire proportional chambers (PMWC's) in

315



Vernon Hughes (cont)



- E665
 - Proposed Oct 1980,
 - Began 1987
- VH also on CERN's EMC
- Muon Scattering with Hadron Detection at the Tevatron.
- First Results Pub. Aug 1991
- Completed Jan 1992
- 26 papers: 6 in PRL

VOLUME 68, NUMBER 22

PHYSICAL REVIEW LETTERS

15 NOV 1992

Saturation of Shadowing at Very Low Bjorken x

M. R. Adams,^{1,2} G. Alt,³ F. J. Andreotti,⁴ M. D. Bishai,⁵ J. Bravar,⁶ A. J. Busza,^{7,8} S. C. Chanowitz,⁹ W. Denner,¹⁰ J. M. Gaunt,¹¹ D. G. Gettleman,¹² B. G. Green,¹³ J. D. Guss,¹⁴ K. Grzadkowski,¹⁵ V. Ekelman,¹⁶ U. Dohrmann,¹⁷ A. Etkin,¹⁸ J. Flauger,¹⁹ H. J. Geissel,²⁰ D. K. Glazier,²¹ R. Gilman,²² M. C. Gonzalez-Garcia,²³ J. G. Gordon,²⁴ J. G. Hardy,²⁵ J. H. Hart,²⁶ J. Heisler,²⁷ D. H. Hoyle,²⁸ D. E. Ioffe,²⁹ G. Jones,³⁰ D. M. Jones,³¹ S. Kaedinger,³² B. R. Kelly,³³ G. E. Koepke,³⁴ S. Korytowski,³⁵ E. Krauss,³⁶ J. J. Lang,³⁷ H. J. Lubatti,³⁸ D. McLeod,³⁹ S. Magill,⁴⁰ P. Mielicki,⁴¹ A. Mian,⁴² J. C. Molesky,⁴³ D. G. Michael,⁴⁴ P. W. Maki,⁴⁵ P. Mandrigan,⁴⁶ J. G. McGhee,⁴⁷ J. G. McGhee,⁴⁸ J. G. McGhee,⁴⁹ K. Okuniewicz,⁵⁰ D. Pashen,⁵¹ P. Pavlak,⁵² J. Pava,⁵³ N. Phillips,⁵⁴ V. M. Pugach,⁵⁵ E. J. Ramirez,⁵⁶ J. J. Rybczynski,⁵⁷ R. J. Rybczynski,⁵⁸ G. A. Shaw,⁵⁹ S. Soldner-Rembold,⁶⁰ P. H. Stoeberl,⁶¹ H. L. Stone,⁶² P. Stepp,⁶³ R. A. Stevens,⁶⁴ R. Tufay,⁶⁵ S. Trivedi-Repeta,⁶⁶ H.-J. Tho,⁶⁷ H. Venkatesan,⁶⁸ M. Vidal,⁶⁹ J. Wilkens,⁷⁰ J. Williams,⁷¹ B. Wenz,⁷² R. A. Witten,⁷³ and T. Zhou⁷⁴

Erratum: E665 Collaboration

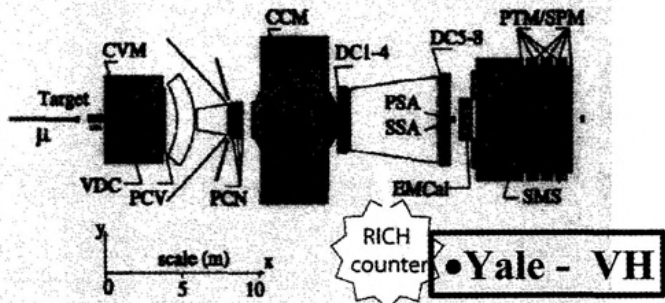
¹Albert-Ludwig-Universität, D-7800 Freiburg im Breisgau, Germany²University of California, Berkeley, California 94720³Fermilab National Accelerator Laboratory, Batavia, Illinois 60510⁴University of Colorado, Boulder, Colorado 80309⁵University of Illinois, Urbana 61801⁶University of Michigan, Ann Arbor, Michigan 48106⁷Institute for Nuclear Physics, Krakow, Poland⁸Institute for Nuclear Physics, Krakow, Poland, Poland⁹University of Maryland, College Park, Maryland 20742¹⁰Massachusetts Institute of Technology, Cambridge, Massachusetts 02139¹¹University of Michigan, Ann Arbor, Michigan 48106¹²University of Minnesota, Minneapolis, Minnesota 55455¹³University of Washington, Seattle, Washington 98195¹⁴Yale University, New Haven, Connecticut 06511¹⁵Yale University, New Haven, Connecticut 06511¹⁶Yale University, New Haven, Connecticut 06511¹⁷Yale University, New Haven, Connecticut 06511¹⁸Yale University, New Haven, Connecticut 06511¹⁹Yale University, New Haven, Connecticut 06511²⁰Yale University, New Haven, Connecticut 06511²¹Yale University, New Haven, Connecticut 06511²²Yale University, New Haven, Connecticut 06511²³Yale University, New Haven, Connecticut 06511²⁴Yale University, New Haven, Connecticut 06511²⁵Yale University, New Haven, Connecticut 06511²⁶Yale University, New Haven, Connecticut 06511²⁷Yale University, New Haven, Connecticut 06511²⁸Yale University, New Haven, Connecticut 06511²⁹Yale University, New Haven, Connecticut 06511³⁰Yale University, New Haven, Connecticut 06511³¹Yale University, New Haven, Connecticut 06511³²Yale University, New Haven, Connecticut 06511³³Yale University, New Haven, Connecticut 06511³⁴Yale University, New Haven, Connecticut 06511³⁵Yale University, New Haven, Connecticut 06511³⁶Yale University, New Haven, Connecticut 06511³⁷Yale University, New Haven, Connecticut 06511³⁸Yale University, New Haven, Connecticut 06511³⁹Yale University, New Haven, Connecticut 06511⁴⁰Yale University, New Haven, Connecticut 06511⁴¹Yale University, New Haven, Connecticut 06511⁴²Yale University, New Haven, Connecticut 06511⁴³Yale University, New Haven, Connecticut 06511⁴⁴Yale University, New Haven, Connecticut 06511⁴⁵Yale University, New Haven, Connecticut 06511⁴⁶Yale University, New Haven, Connecticut 06511⁴⁷Yale University, New Haven, Connecticut 06511⁴⁸Yale University, New Haven, Connecticut 06511⁴⁹Yale University, New Haven, Connecticut 06511⁵⁰Yale University, New Haven, Connecticut 06511⁵¹Yale University, New Haven, Connecticut 06511⁵²Yale University, New Haven, Connecticut 06511⁵³Yale University, New Haven, Connecticut 06511⁵⁴Yale University, New Haven, Connecticut 06511⁵⁵Yale University, New Haven, Connecticut 06511⁵⁶Yale University, New Haven, Connecticut 06511⁵⁷Yale University, New Haven, Connecticut 06511⁵⁸Yale University, New Haven, Connecticut 06511⁵⁹Yale University, New Haven, Connecticut 06511⁶⁰Yale University, New Haven, Connecticut 06511⁶¹Yale University, New Haven, Connecticut 06511⁶²Yale University, New Haven, Connecticut 06511⁶³Yale University, New Haven, Connecticut 06511⁶⁴Yale University, New Haven, Connecticut 06511⁶⁵Yale University, New Haven, Connecticut 06511⁶⁶Yale University, New Haven, Connecticut 06511⁶⁷Yale University, New Haven, Connecticut 06511⁶⁸Yale University, New Haven, Connecticut 06511⁶⁹Yale University, New Haven, Connecticut 06511⁷⁰Yale University, New Haven, Connecticut 06511⁷¹Yale University, New Haven, Connecticut 06511⁷²Yale University, New Haven, Connecticut 06511⁷³Yale University, New Haven, Connecticut 06511⁷⁴Yale University, New Haven, Connecticut 06511⁷⁵Yale University, New Haven, Connecticut 06511⁷⁶Yale University, New Haven, Connecticut 06511⁷⁷Yale University, New Haven, Connecticut 06511⁷⁸Yale University, New Haven, Connecticut 06511⁷⁹Yale University, New Haven, Connecticut 06511⁸⁰Yale University, New Haven, Connecticut 06511⁸¹Yale University, New Haven, Connecticut 06511⁸²Yale University, New Haven, Connecticut 06511⁸³Yale University, New Haven, Connecticut 06511⁸⁴Yale University, New Haven, Connecticut 06511⁸⁵Yale University, New Haven, Connecticut 06511⁸⁶Yale University, New Haven, Connecticut 06511⁸⁷Yale University, New Haven, Connecticut 06511⁸⁸Yale University, New Haven, Connecticut 06511⁸⁹Yale University, New Haven, Connecticut 06511⁹⁰Yale University, New Haven, Connecticut 06511⁹¹Yale University, New Haven, Connecticut 06511⁹²Yale University, New Haven, Connecticut 06511⁹³Yale University, New Haven, Connecticut 06511⁹⁴Yale University, New Haven, Connecticut 06511⁹⁵Yale University, New Haven, Connecticut 06511⁹⁶Yale University, New Haven, Connecticut 06511⁹⁷Yale University, New Haven, Connecticut 06511⁹⁸Yale University, New Haven, Connecticut 06511⁹⁹Yale University, New Haven, Connecticut 06511¹⁰⁰Yale University, New Haven, Connecticut 06511¹⁰¹Yale University, New Haven, Connecticut 06511¹⁰²Yale University, New Haven, Connecticut 06511¹⁰³Yale University, New Haven, Connecticut 06511¹⁰⁴Yale University, New Haven, Connecticut 06511¹⁰⁵Yale University, New Haven, Connecticut 06511¹⁰⁶Yale University, New Haven, Connecticut 06511¹⁰⁷Yale University, New Haven, Connecticut 06511¹⁰⁸Yale University, New Haven, Connecticut 06511¹⁰⁹Yale University, New Haven, Connecticut 06511¹¹⁰Yale University, New Haven, Connecticut 06511¹¹¹Yale University, New Haven, Connecticut 06511¹¹²Yale University, New Haven, Connecticut 06511¹¹³Yale University, New Haven, Connecticut 06511¹¹⁴Yale University, New Haven, Connecticut 06511¹¹⁵Yale University, New Haven, Connecticut 06511¹¹⁶Yale University, New Haven, Connecticut 06511¹¹⁷Yale University, New Haven, Connecticut 06511¹¹⁸Yale University, New Haven, Connecticut 06511¹¹⁹Yale University, New Haven, Connecticut 06511¹²⁰Yale University, New Haven, Connecticut 06511¹²¹Yale University, New Haven, Connecticut 06511¹²²Yale University, New Haven, Connecticut 06511¹²³Yale University, New Haven, Connecticut 06511¹²⁴Yale University, New Haven, Connecticut 06511¹²⁵Yale University, New Haven, Connecticut 06511¹²⁶Yale University, New Haven, Connecticut 06511¹²⁷Yale University, New Haven, Connecticut 06511¹²⁸Yale University, New Haven, Connecticut 06511¹²⁹Yale University, New Haven, Connecticut 06511¹³⁰Yale University, New Haven, Connecticut 06511¹³¹Yale University, New Haven, Connecticut 06511¹³²Yale University, New Haven, Connecticut 06511¹³³Yale University, New Haven, Connecticut 06511¹³⁴Yale University, New Haven, Connecticut 06511¹³⁵Yale University, New Haven, Connecticut 06511¹³⁶Yale University, New Haven, Connecticut 06511¹³⁷Yale University, New Haven, Connecticut 06511¹³⁸Yale University, New Haven, Connecticut 06511¹³⁹Yale University, New Haven, Connecticut 06511¹⁴⁰Yale University, New Haven, Connecticut 06511¹⁴¹Yale University, New Haven, Connecticut 06511¹⁴²Yale University, New Haven, Connecticut 06511¹⁴³Yale University, New Haven, Connecticut 06511¹⁴⁴Yale University, New Haven, Connecticut 06511¹⁴⁵Yale University, New Haven, Connecticut 06511¹⁴⁶Yale University, New Haven, Connecticut 06511¹⁴⁷Yale University, New Haven, Connecticut 06511¹⁴⁸Yale University, New Haven, Connecticut 06511¹⁴⁹Yale University, New Haven, Connecticut 06511¹⁵⁰Yale University, New Haven, Connecticut 06511¹⁵¹Yale University, New Haven, Connecticut 06511¹⁵²Yale University, New Haven, Connecticut 06511¹⁵³Yale University, New Haven, Connecticut 06511¹⁵⁴Yale University, New Haven, Connecticut 06511¹⁵⁵Yale University, New Haven, Connecticut 06511¹⁵⁶Yale University, New Haven, Connecticut 06511¹⁵⁷Yale University, New Haven, Connecticut 06511¹⁵⁸Yale University, New Haven, Connecticut 06511¹⁵⁹Yale University, New Haven, Connecticut 06511¹⁶⁰Yale University, New Haven, Connecticut 06511¹⁶¹Yale University, New Haven, Connecticut 06511¹⁶²Yale University, New Haven, Connecticut 06511¹⁶³Yale University, New Haven, Connecticut 06511¹⁶⁴Yale University, New Haven, Connecticut 06511¹⁶⁵Yale University, New Haven, Connecticut 06511¹⁶⁶Yale University, New Haven, Connecticut 06511¹⁶⁷Yale University, New Haven, Connecticut 06511¹⁶⁸Yale University, New Haven, Connecticut 06511¹⁶⁹Yale University, New Haven, Connecticut 06511¹⁷⁰Yale University, New Haven, Connecticut 06511¹⁷¹Yale University, New Haven, Connecticut 06511¹⁷²Yale University, New Haven, Connecticut 06511¹⁷³Yale University, New Haven, Connecticut 06511¹⁷⁴Yale University, New Haven, Connecticut 06511¹⁷⁵Yale University, New Haven, Connecticut 06511¹⁷⁶Yale University, New Haven, Connecticut 06511¹⁷⁷Yale University, New Haven, Connecticut 06511¹⁷⁸Yale University, New Haven, Connecticut 06511¹⁷⁹Yale University, New Haven, Connecticut 06511¹⁸⁰Yale University, New Haven, Connecticut 06511¹⁸¹Yale University, New Haven, Connecticut 06511¹⁸²Yale University, New Haven, Connecticut 06511¹⁸³Yale University, New Haven, Connecticut 06511¹⁸⁴Yale University, New Haven, Connecticut 06511¹⁸⁵Yale University, New Haven, Connecticut 06511¹⁸⁶Yale University, New Haven, Connecticut 06511¹⁸⁷Yale University, New Haven, Connecticut 06511¹⁸⁸Yale University, New Haven, Connecticut 06511¹⁸⁹Yale University, New Haven, Connecticut 06511¹⁹⁰Yale University, New Haven, Connecticut 06511¹⁹¹Yale University, New Haven, Connecticut 06511¹⁹²Yale University, New Haven, Connecticut 06511¹⁹³Yale University, New Haven, Connecticut 06511¹⁹⁴Yale University, New Haven, Connecticut 06511¹⁹⁵Yale University, New Haven, Connecticut 06511¹⁹⁶Yale University, New Haven, Connecticut 06511¹⁹⁷Yale University, New Haven, Connecticut 06511¹⁹⁸Yale University, New Haven, Connecticut 06511¹⁹⁹Yale University, New Haven, Connecticut 06511²⁰⁰Yale University, New Haven, Connecticut 06511²⁰¹Yale University, New Haven, Connecticut 06511²⁰²Yale University, New Haven, Connecticut 06511²⁰³Yale University, New Haven, Connecticut 06511²⁰⁴Yale University, New Haven, Connecticut 06511²⁰⁵Yale University, New Haven, Connecticut 06511²⁰⁶Yale University, New Haven, Connecticut 06511²⁰⁷Yale University, New Haven, Connecticut 06511²⁰⁸Yale University, New Haven, Connecticut 06511²⁰⁹Yale University, New Haven, Connecticut 06511



E665 unpolarized muon scattering at 500 GeV



Fermilab Experiment E665 Muon-Nucleon Scattering



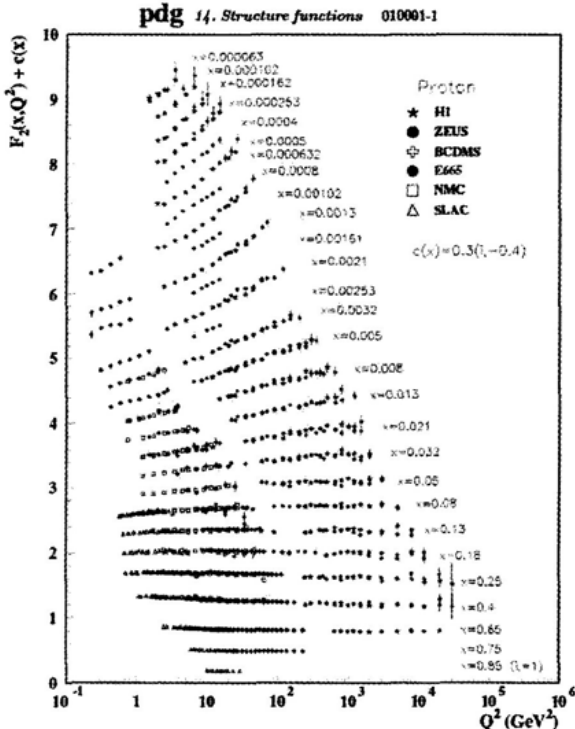
500 GeV Muons
1m Liquid H₂ and D₂ Targets ■■■
~150 Layers of Tracking ■■■■■
2 Open Dipole Magnets ■■■■
Electromagnetic Calorimeter ■■■■
Hadron Absorber/Muon Tagger ■■■■



E665 Fame



Structure Functions at Low x and Q squared



Structure functions at low X and Q²

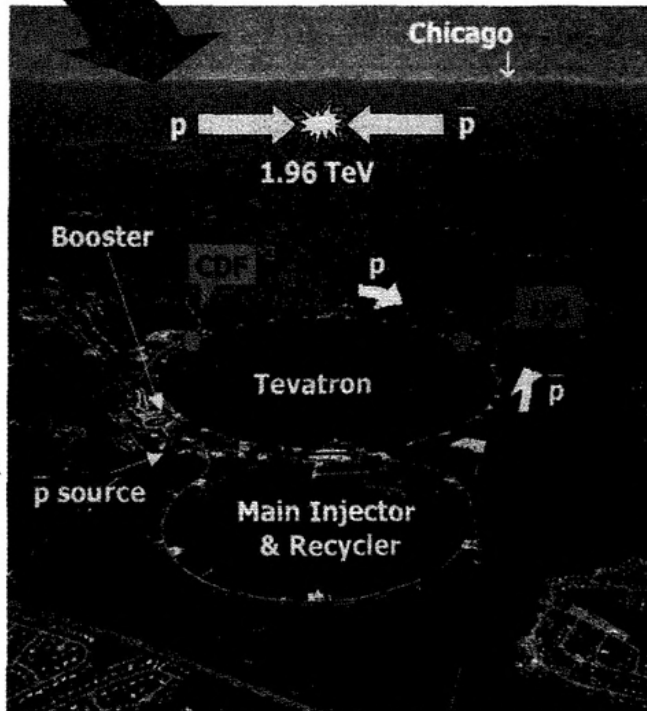
Stephen Parke, Fermilab



Tevatron Collider in Run II

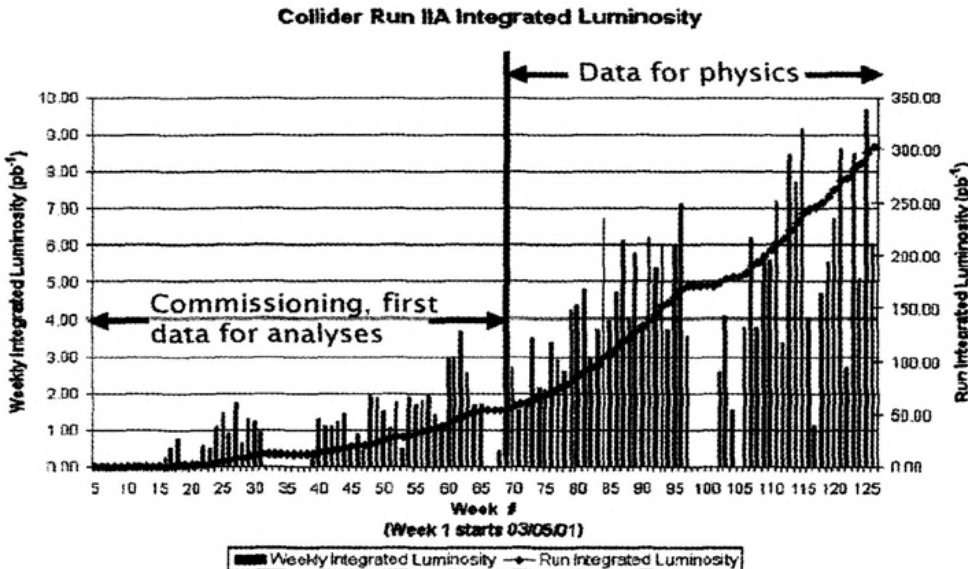


- The Tevatron is a proton-antiproton collider with 980 GeV/beam. 10% increase over Run I
- Main Ring → Main Injector
- 36 p and pbar bunches → 396 ns between bunch crossing
 - Increased from 6x6 bunches with 3.5 μ s in Run I
- Increased instantaneous luminosity:
 - Run II goal $30 \times 10^{31} \text{ cm}^{-2} \text{ s}^{-1}$
 - Current: $3 \text{ to } 5 \times 10^{31} \text{ cm}^{-2} \text{ s}^{-1}$





Run II Data Taking Status



- $L_{int} \sim 300 \text{ pb}^{-1}$ delivered
- Good quality data since Spring 2002
- Data collection efficiency 85÷90%
- Best $L_{peak} \sim 5 \times 10^{31} \text{ cm}^{-2} \text{ s}^{-1}$
- Best Week $\sim 10 \text{ pb}^{-1}$
- Steady Improvement.

Stephen Parke, Fermilab



Integrated Luminosity Projections



- **Original Goals:**

- Run II-a 2 fb^{-1}
- Run II-b 15 fb^{-1}

- **Current Goals:**

- FY 2003 $\sim 225 \text{ pb}^{-1}$ ***ACHIEVED
- FY 2004 $200 - 300 \text{ pb}^{-1}$ ***Recycler Studies will limit this number
- FY 2005 $390 - 670 \text{ pb}^{-1}$
- Giving a Total of 1 fb^{-1} sometime in 2005

- **By End of FY 2009:**

“Base” 4.4 fb^{-1} “Design” 8.6 fb^{-1}

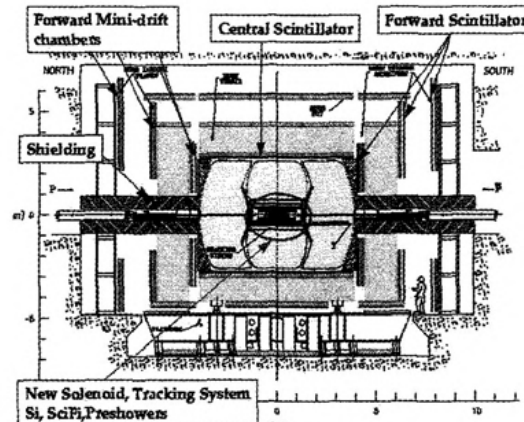
- **Lab is revisiting the questions?**

- Detector upgrades - silicon
- Roll of Recycler
- Electron cooling of anti-protons



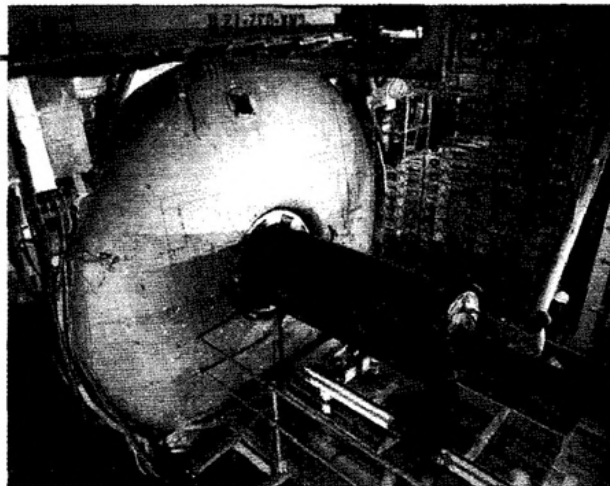
D0 Detector

D0



- Both detectors
 - silicon microvertex detectors
 - axial solenoid
 - central tracking
 - high rate trigger/DAQ system
 - calorimeter & muon systems

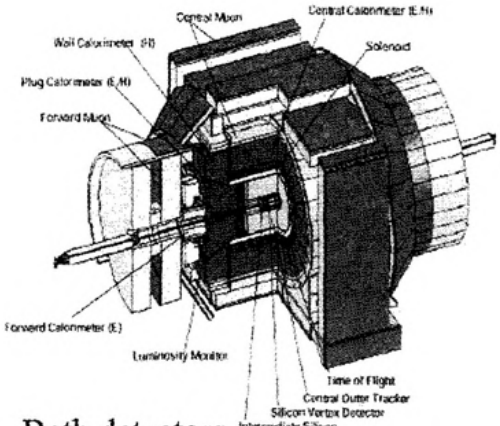
DØ fiber tracker installation



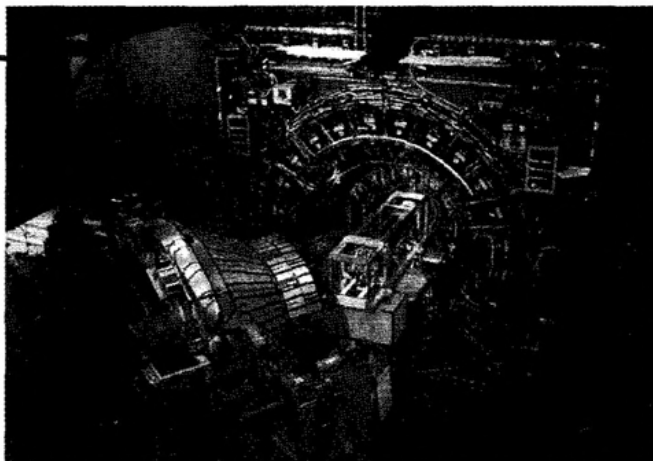
- New tracking: silicon and fibers in magnetic field
- Upgraded muon system
- Upgraded DAQ/trigger
(displaced track soon)
- **Excellent tracking acceptance**
- **Excellent electron & muon ID**



CDF Detector



CDF silicon detector installation



- Both detectors
 - silicon microvertex detectors
 - axial solenoid
 - central tracking
 - high rate trigger/DAQ system
 - calorimeter & muon systems

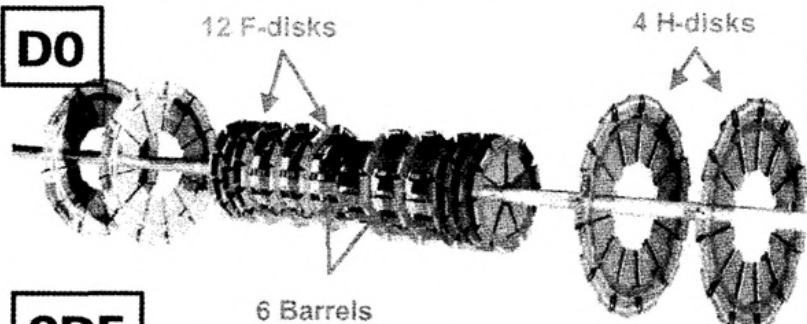
- New bigger silicon,
new drift chamber
- Upgraded calorimeter, μ
- Upgraded DAQ/trigger,
esp. displaced-track trigger
- Particle ID (TOF and dE/dx)
- Excellent mass resolution



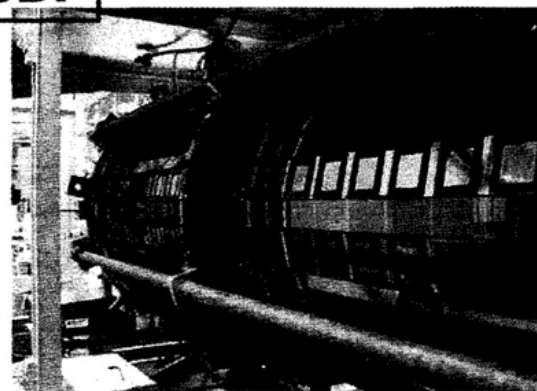
New Silicon Detectors:



D0

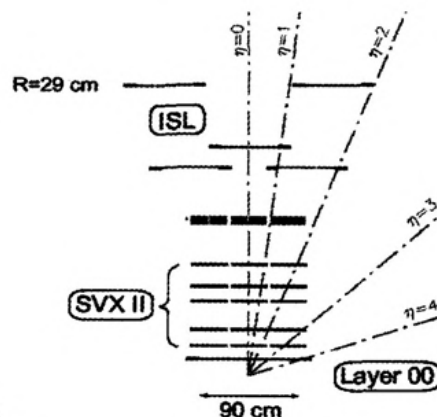


CDF



Common features:

- Coverage of the luminous regions
- Extended acceptance at large pseudo-rapidity
- 3D Tracking capability
- Excellent I.P. resolution



Stephen Parke,

13



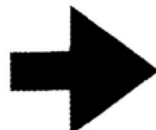
The Tevatron Collider Program



- The **Accelerator complex** and the **CDF** and **D0** experiments have been rebuilt for Run-II, to initially collect 2000 pb^{-1} per experiment..

Physics of the Weak Energy Scale

- Supersymmetry
- Precise t, W mass measurements
- Low mass Higgs with more luminosity
- Search for effects of large hidden dimensions or other new physics.



Today's Physics Topics:

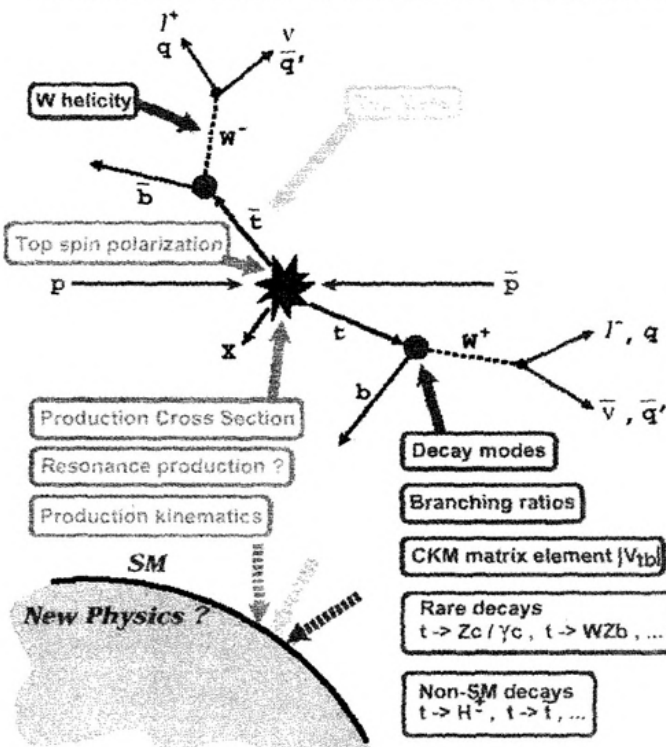
- Top Quark
- QCD Jets
- Electro-Weak
- Heavy (b,c) Flavors

CP Violation

- Use B_s mixing to determine V_{ts}
- Measure CP-violating asymmetries

TOP

TOP QUARK PHYSICS:



Program

• Top production & decay

• Tools

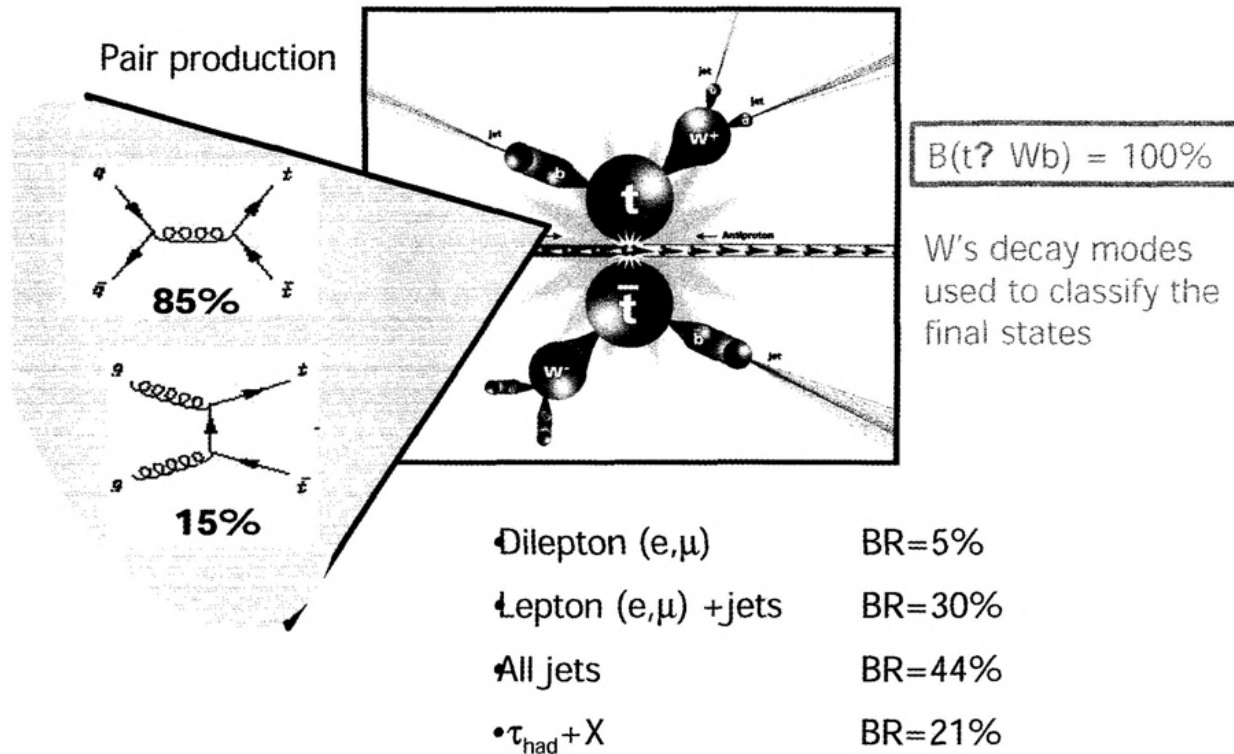
• Cross section

• Single top

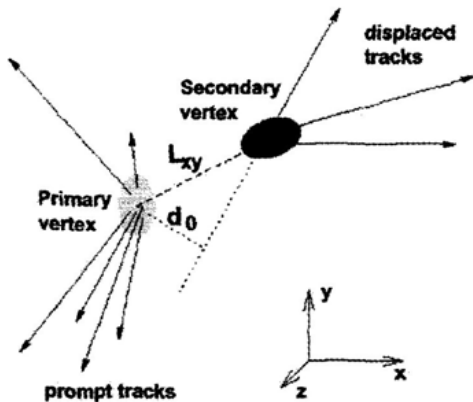
• W helicity

• Mass

•Top Quarks at the Tevatron

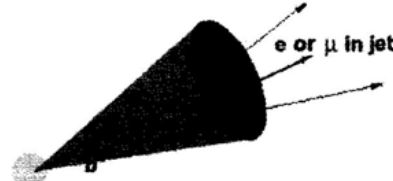


How to tag a high p_T B-jet



Silicon Vertex Tag

- Signature of a b decay is a displaced vertex:
 - Long lifetime of b hadrons ($c\tau \sim 450 \mu\text{m}$) + boost
 - B hadrons travel $L_{xy} \sim 3\text{mm}$ before decay with large charged track multiplicity



- $b \rightarrow \ell\nu c$ ($\text{BR} \sim 20\%$)
- $b \rightarrow c \rightarrow \ell\nu s$ ($\text{BR} \sim 20\%$)

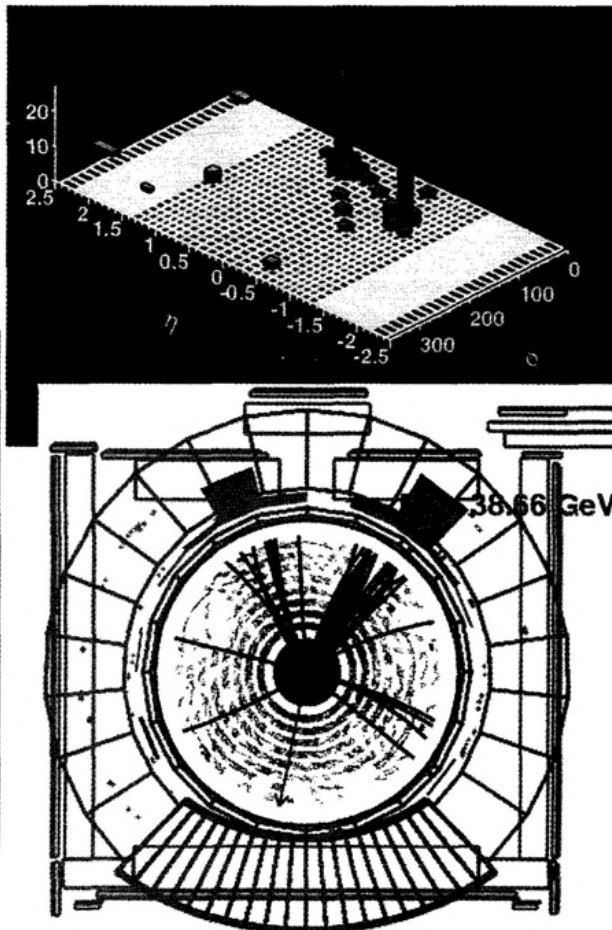
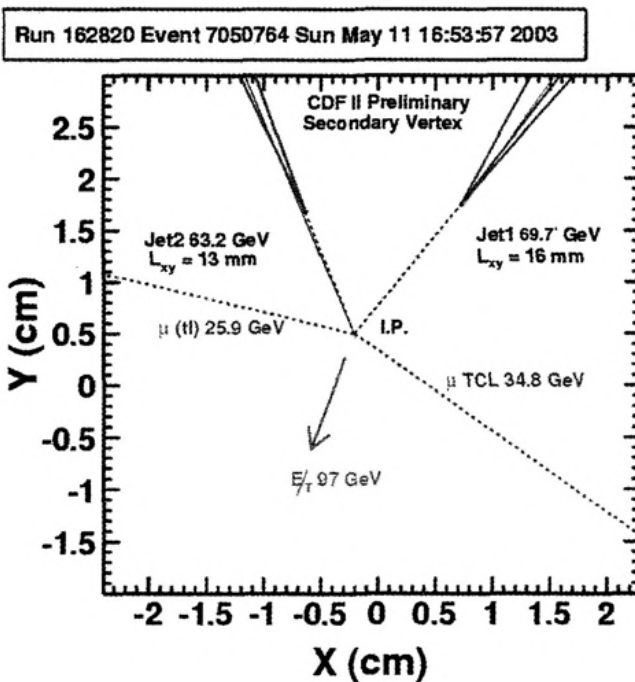
Soft Lepton Tag

- Exploits the b quarks semi-leptonic decays
 - ⇒ These leptons have a softer p_T spectrum than W/Z leptons
 - ⇒ They are less isolated

B-tagging at hadron machines established:
crucial for top discovery in RunI
essential for RunII physics program

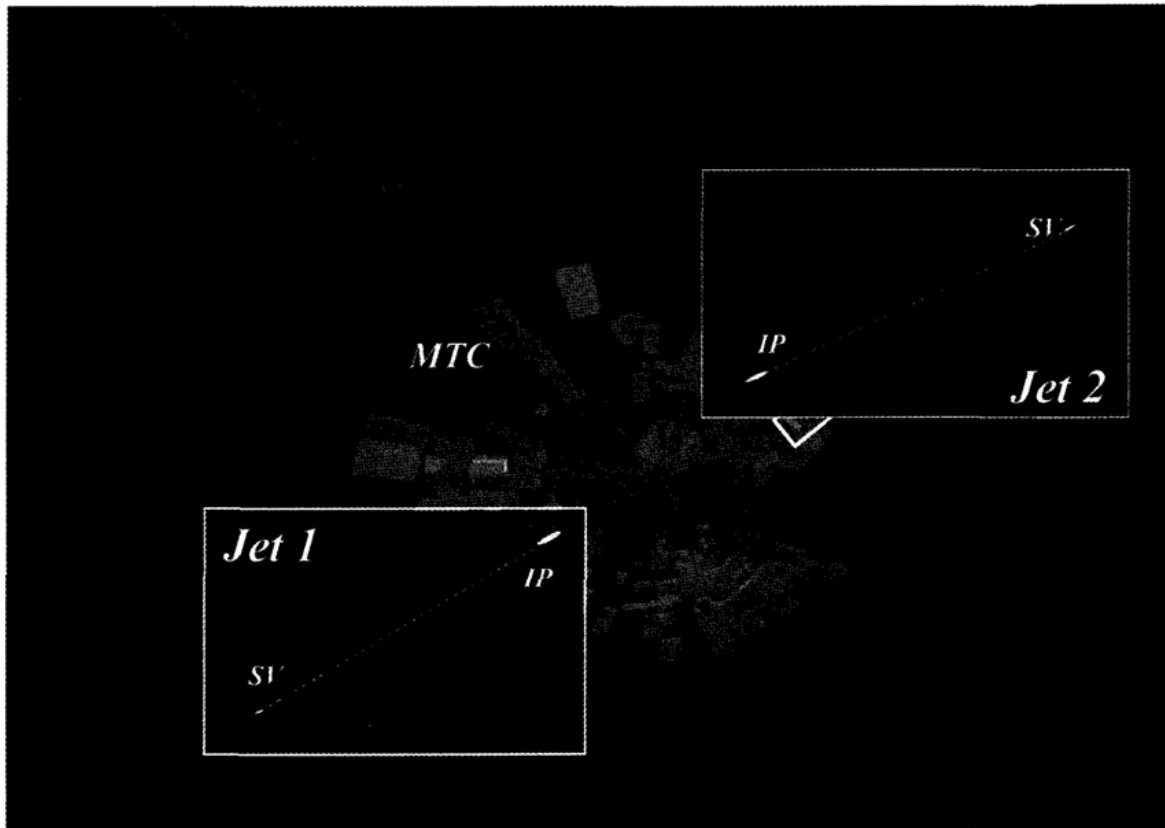


Double b-tagged dilepton event @ CDF





$\mu + \text{jets}$ double tagged event @D0

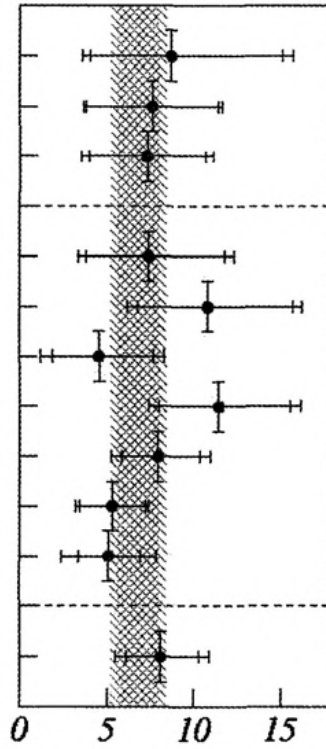




Run II cross section summary



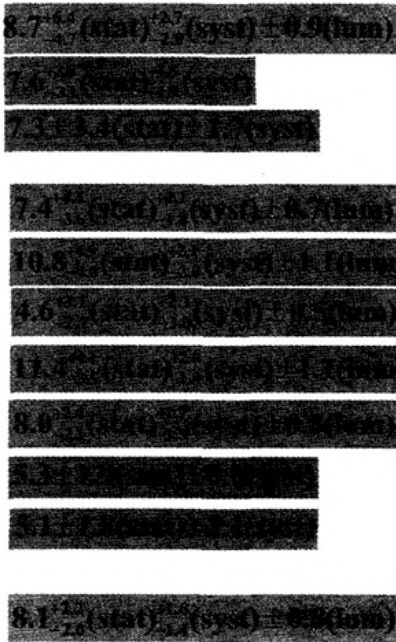
CDF and DØ Run II Preliminary



$D\bar{\phi}$ Dileptons $90-107 \text{ pb}^{-1}$
 CDF Dileptons 126 pb^{-1}
 CDF L+Track 126 pb^{-1}

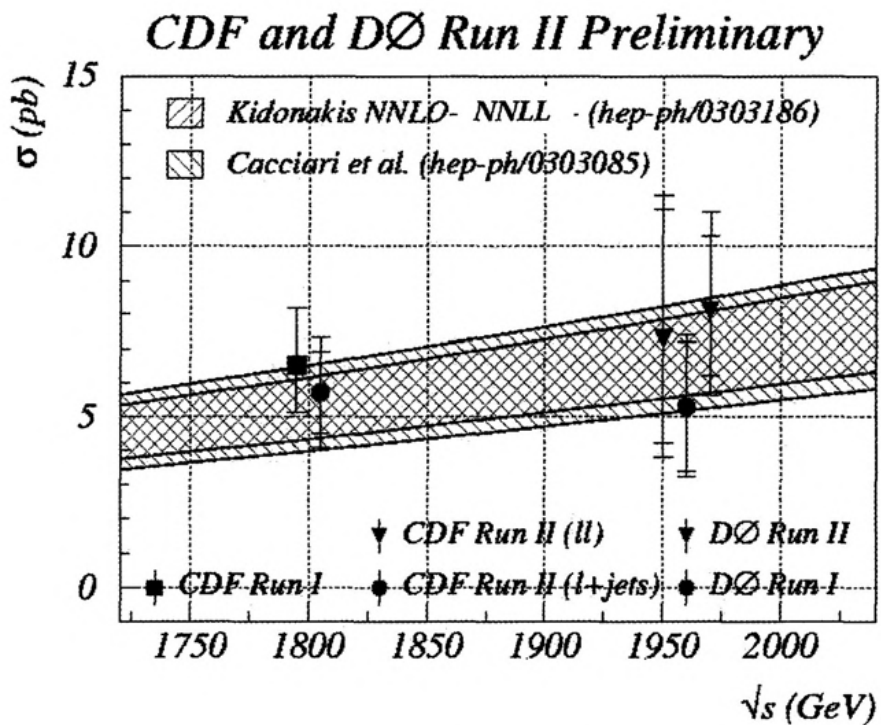
 $D\bar{\phi}$ L+jets/CSIP 45 pb^{-1}
 $D\bar{\phi}$ L+jets/SVT 45 pb^{-1}
 $D\bar{\phi}$ L+jets/topo 92 pb^{-1}
 $D\bar{\phi}$ L+jets/soft muon 92 pb^{-1}
 $D\bar{\phi}$ L+jets combined 92 pb^{-1}
 CDF L+jets/SVX 57 pb^{-1}
 CDF L+jets/HT 126 pb^{-1}

 $D\bar{\phi}$ Combined $90-107 \text{ pb}^{-1}$



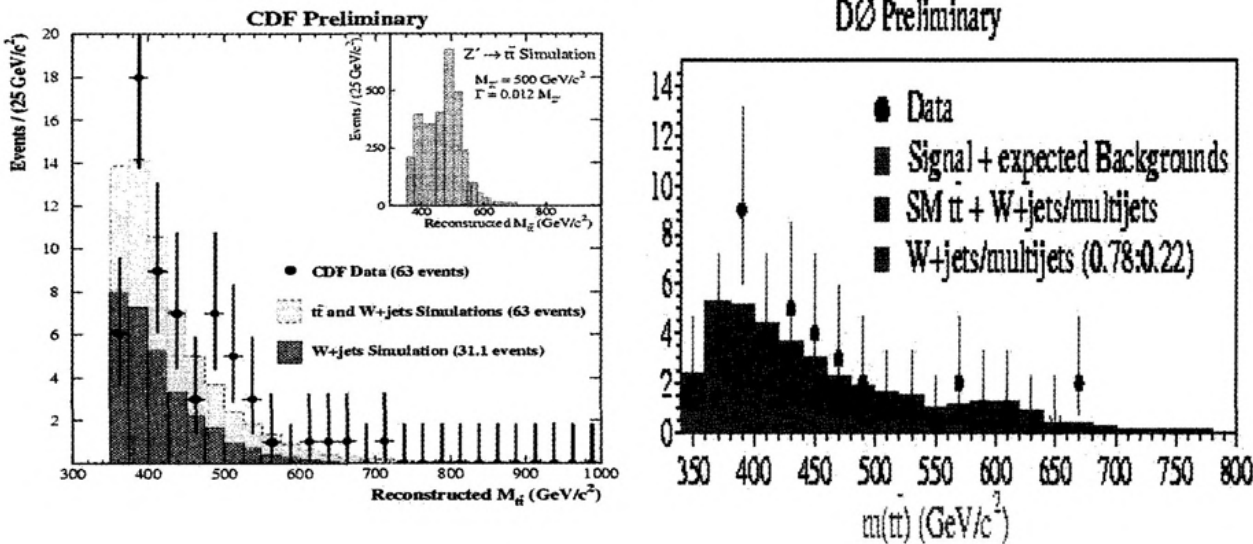


Cross section \sqrt{s} dependence





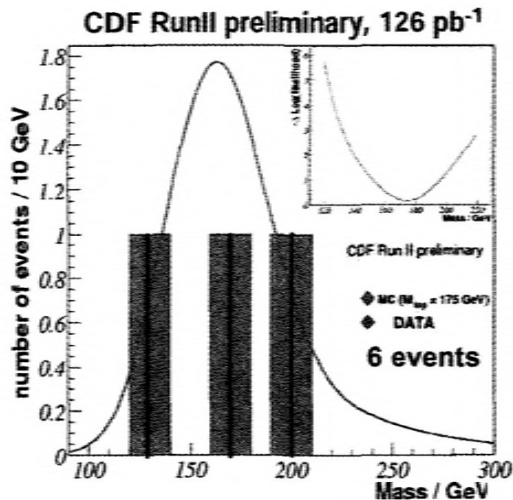
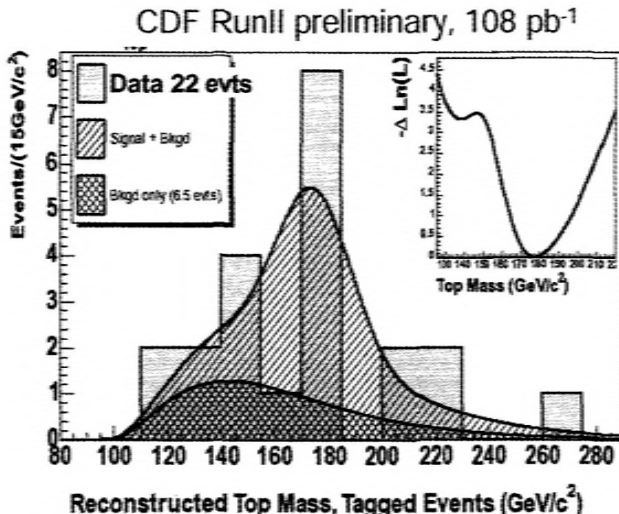
Test for new physics in ttbar production



Model independent search for a narrow resonance
 $X \rightarrow t\bar{t}$ exclude a narrow, leptophobic X boson with
 $m_X < 560$ GeV/c² (CDF) and $m_X < 585$ GeV/c² (D0)



First look at top mass in Run II



Mass in lepton+jets channel
with a b-tagged jet

$177.5^{+12.7}_{-9.4}(\text{stat}) \pm 7.1(\text{syst}) \text{ GeV}/c^2$

Mass in dilepton channel

$175.0^{+17.4}_{-16.9}(\text{stat}) \pm 7.9(\text{syst}) \text{ GeV}/c^2$



Top Conclusions



- Top quark existence established at the Tevatron in 1995
- Several top properties studied using Run I data
 - limited statistic
- The Tevatron is the top quark factory until LHC:
 - Run II ~50 times Run I statistics → precision measurements
 - Constraints on the SM Higgs boson mass and SM consistency
 - ...or surprises?
 - First Run II results cover a variety of channels and topics
 - CDF and D0 are exploiting their upgraded detector features

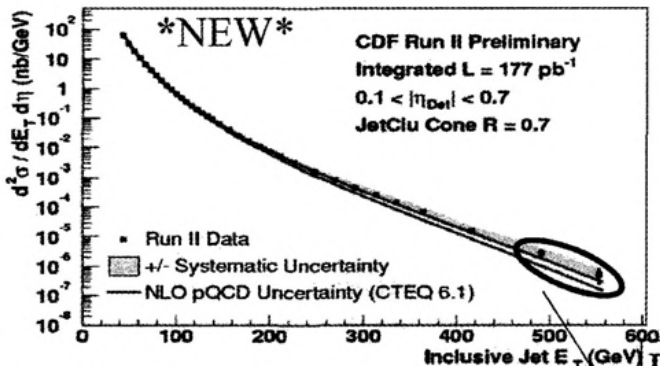
A very rich top physics program is underway:

let's see what the top quark can do for us!

JETS - QCD



Inclusive Jets



Central $0.1 < |h| < 0.7$ inclusive jets
 $R=0.7$ Run I cone algorithm
 $L = 177 \text{ pb}^{-1}$

Overall Escalate normalized to Run 1
(w/ $5 \pm 3\%$ [*NEW*] correction
factor)

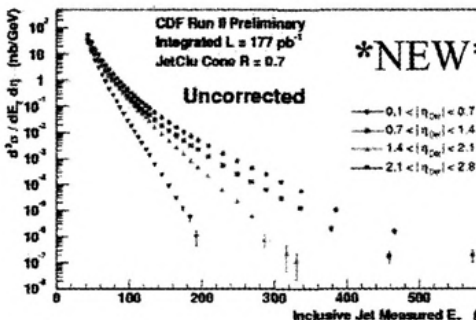
Reapply PT-dependent systematics
from Run I

Extended wrt Run I by 150 GeV!

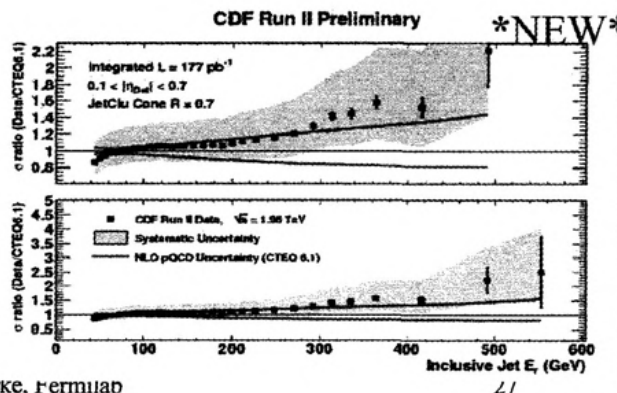
Scale dominates systematics

$\pm \sim 6\%$ normalization

Preliminary distributions for $|\eta| < 2.8$



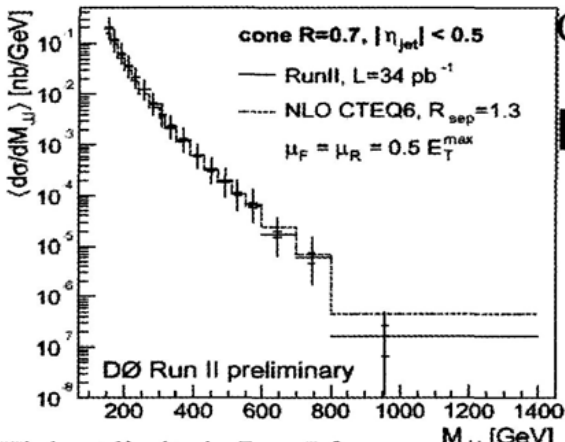
uncorrected



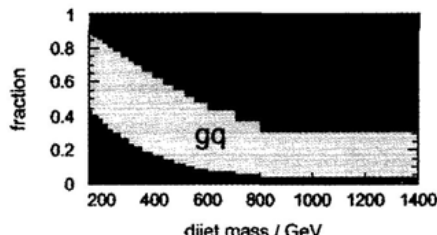
Stephen Parke, Fermilab



Dijet mass spectrum



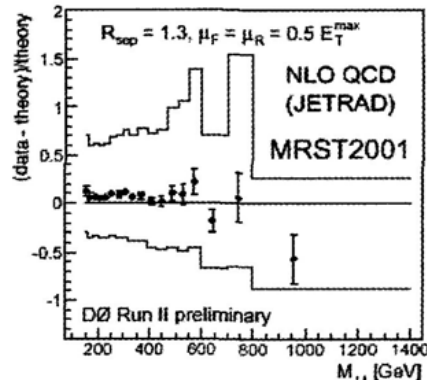
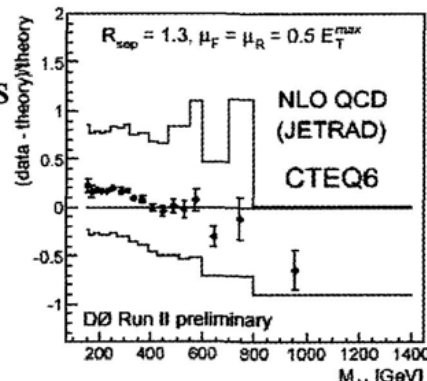
Highest limits in Run I for
Compositeness from this analysis



Also good sensitivity
to gluons at large-x

Stephen Parke, Fermilab

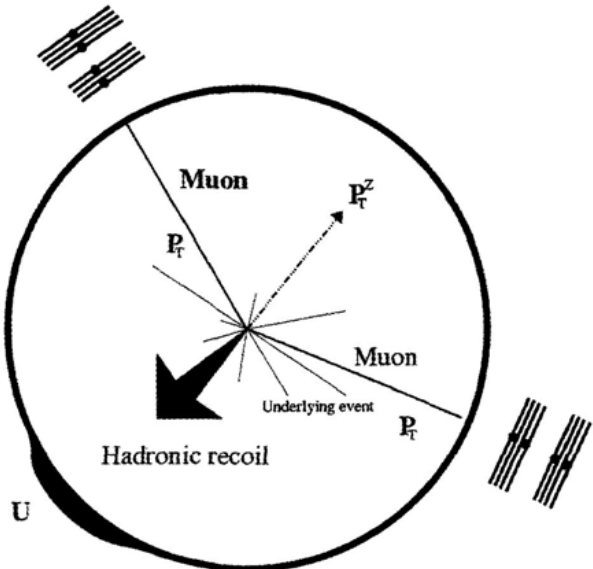
Central
 $|\eta| < 0.5$ jets
 $L = 34 \text{ pb}^{-1}$



W and Z



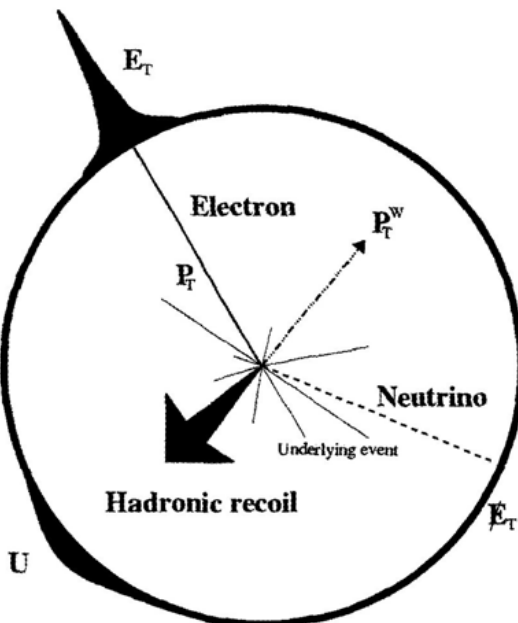
Experimental Signature: Z? 1⁺¹⁻



- pair of charged leptons:
 - high p_T
 - isolated
 - opposite-charge
- redundancy in trigger and offline selection
- low backgrounds
- control of systematics



Experimental Signature: W? lν



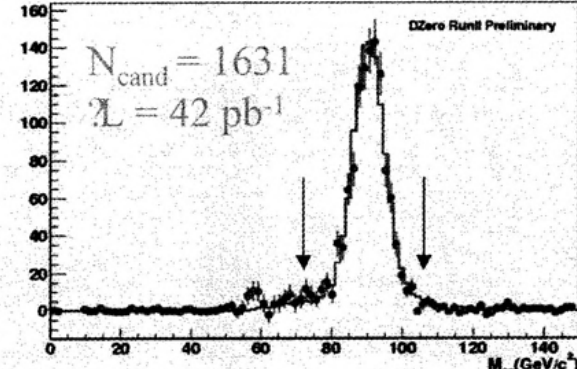
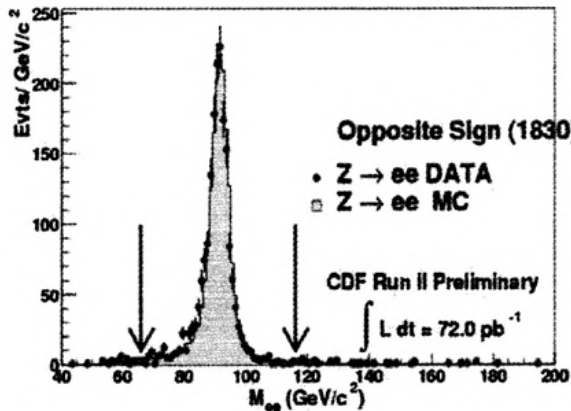
- single charged lepton:
 - high p_T
 - isolated
- E_T^{miss} (from neutrino)
- less redundancy in trigger and offline selection
- more difficult to control backgrounds and systematics
- need to understand hadronic recoil
- but more ‘interesting’ than Z! (post-LEP)
- $s \cdot Br$ 10 times larger than Z



CDF and DØ Z? e⁺e⁻



Two isolated electrons, $E_T > 25$ GeV, $|?| < 1.1$



$$\text{CDF: } s_Z \cdot \text{Br}(Z? e^+e^-) = 267.0 \pm 6.3 \pm 15.2 \pm 16.0 \text{ pb}$$

$$\text{DØ: } s_Z \cdot \text{Br}(Z? e^+e^-) = 275 \pm 9 \pm 9 \pm 28 \text{ pb}$$

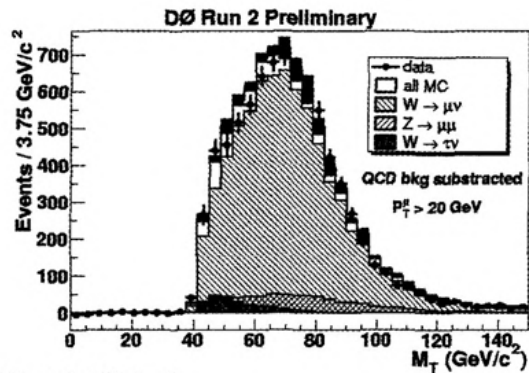
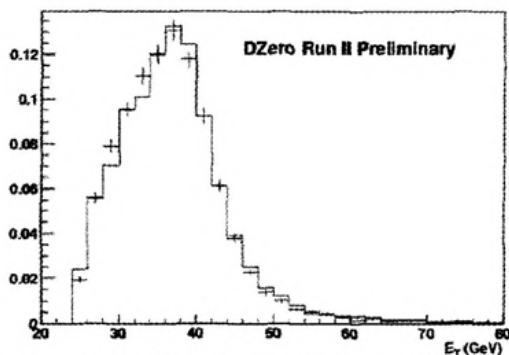
stat. syst. lumi.



DØ: W? ev and W? μν



- $p_T(e) > 25 \text{ GeV}$
- $E_T^{\text{miss}} > 25 \text{ GeV}$
- $N_{\text{cand}} = 27370$
- $\mathcal{L} = 42 \text{ pb}^{-1}$
- $p_T(\mu) > 20 \text{ GeV}$
- $E_T^{\text{miss}} > 20 \text{ GeV}$
- $N_{\text{cand}} = 8302$
- $\mathcal{L} = 17 \text{ pb}^{-1}$



$$s_W \cdot \text{Br}(W? \text{ ev}) = 2.884 \pm 0.021 \pm 0.128 \pm 0.284 \text{ nb}$$

$$s_W \cdot \text{Br}(W? \mu\nu) = 3.226 \pm 0.128 \pm 0.100 \pm 0.322 \text{ nb}$$

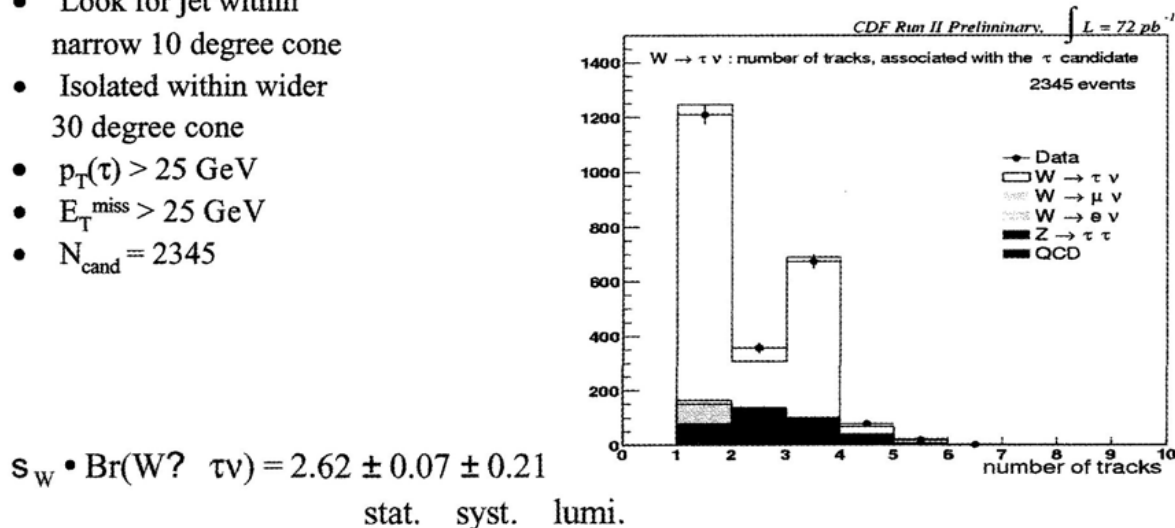
stat. syst. lumi.



CDF: W? τv



- Look for jet within narrow 10 degree cone
- Isolated within wider 30 degree cone
- $p_T(\tau) > 25 \text{ GeV}$
- $E_T^{\text{miss}} > 25 \text{ GeV}$
- $N_{\text{cand}} = 2345$



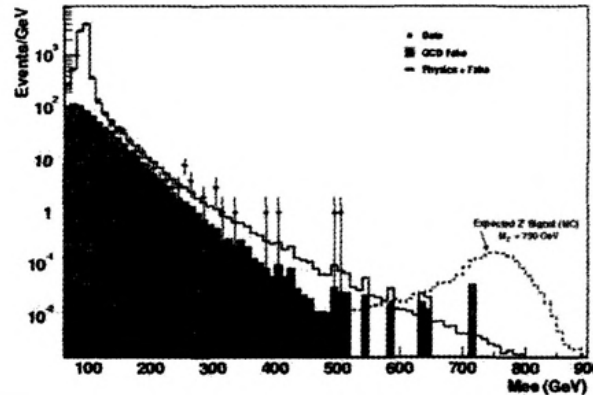
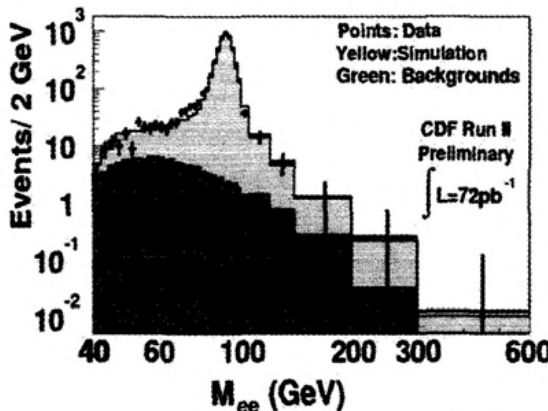


Other measurements with W, Z events

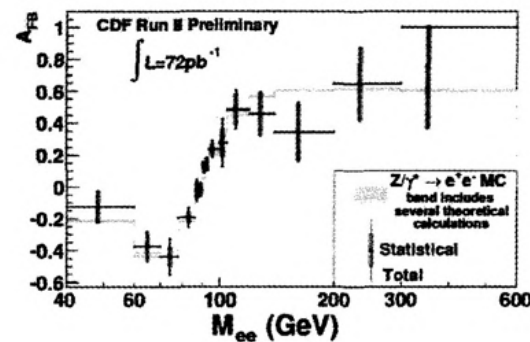


- High mass tail of Z

DØ Run II Preliminary

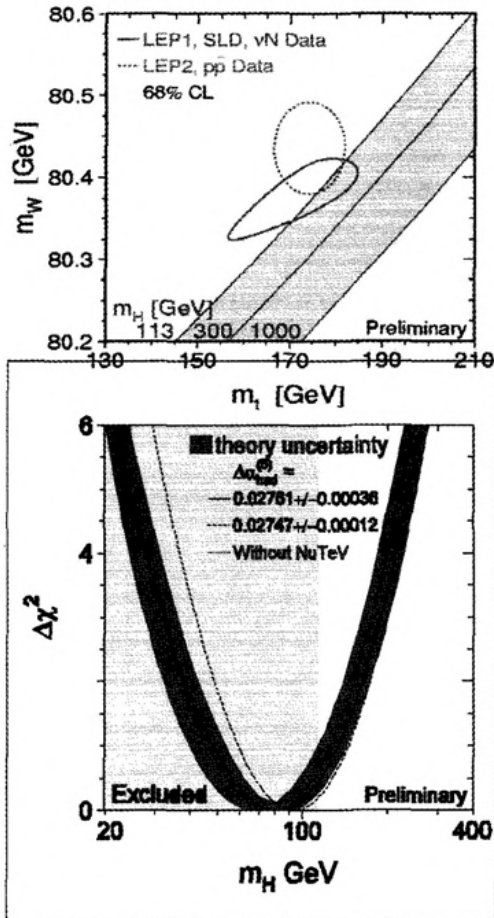


- Forward-backward asymmetry





Higgs Search



- Report at LP03 the Results of New Study:
(W B Bbar channel)

- 4 to 5 fb^{-1} CDF + D0 can exclude SM Higgs up to 130 GeV.
(range dictated by MSSM).
- 8 to 10 fb^{-1} might find 3 sigma evidence.

B physics



B Physics at the Tevatron



- Heavy flavor production
 - charm cross section
- Lifetimes
- B hadron masses
- Branching ratios
 - $B_s \rightarrow K^+ K^-$, $\Lambda_b \rightarrow \Lambda_c \pi$, $B_s \rightarrow D_s \pi^+$
- Mixing
 - B_d, B_s

Notation:

$$B_d = B^0 = |\bar{b}d\rangle$$

$$B_u = B^+ = |\bar{b}u\rangle$$

$$B_s = |\bar{b}s\rangle$$

$$B_c = |\bar{b}c\rangle$$

$$\Lambda_b = |udb\rangle$$

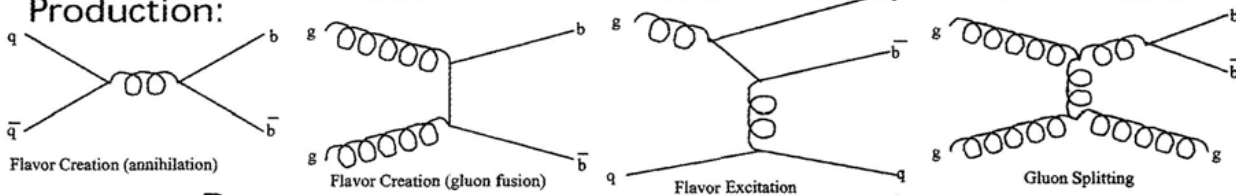


B Physics at Hadron Machines



b's produced by strong interaction, decay by weak interaction

Production:



Pros

- Enormous cross-section
 - $\sim 100 \text{ }\mu\text{barn}$ total
 - $\sim 3\text{-}5 \text{ }\mu\text{barn}$ "reconstructable"
 - **At $4 \times 10^{31} \text{ cm}^{-2}\text{s}^{-1} \Rightarrow \sim 150 \text{ Hz of reconstructable } B\bar{B}!!$**
- All B species produced
 - $B_u, B_d, B_s, B_c, \Lambda_b, \dots$
- Production is incoherent
 - Measure of B and B ~~not~~ required

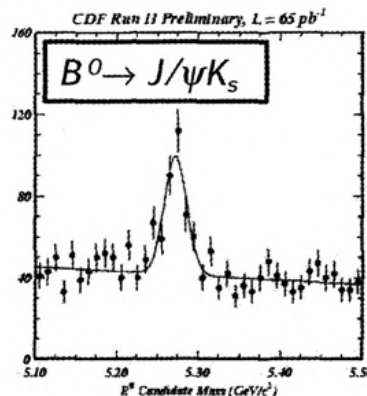
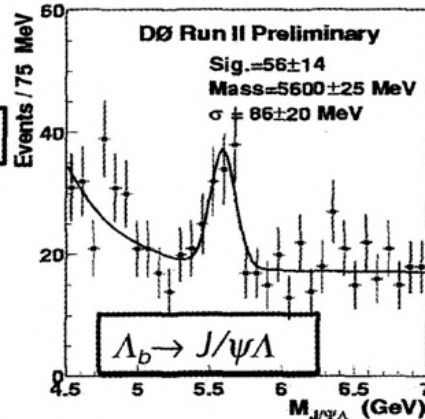
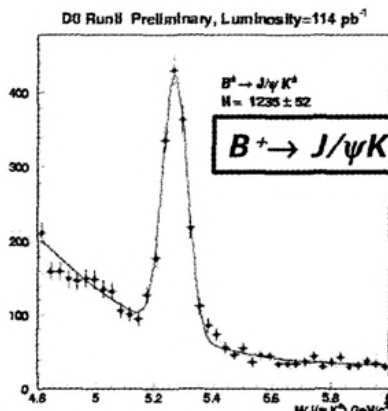
Cons

- Large inelastic background
 - Triggering and reconstruction are challenging
- Reconstruct a B hadron, $\sim 20\text{-}40\%$ chance 2nd B is within detector acceptance
- p_T spectrum relatively soft
 - **Typical $p_T(B) \sim 10\text{-}15 \text{ GeV}$ for trigger+reconstructed B 's ...softer than B 's at LEP!**

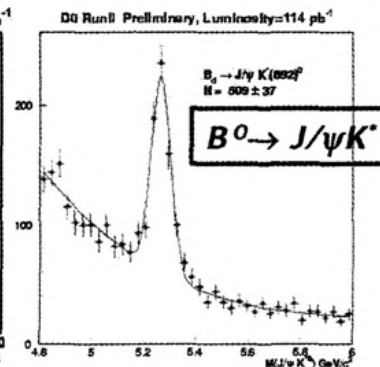
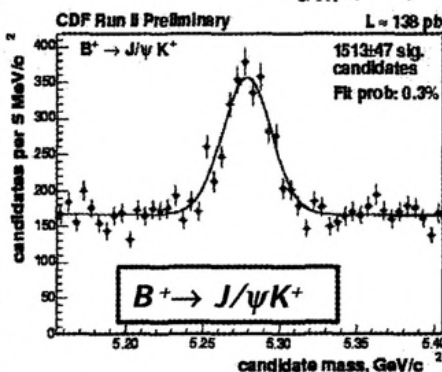
Disclaimer: acceptance comments relevant to "central" detectors like DØ and CDF



Yields in $B \rightarrow J/\psi X$ Modes



- Trigger on low p_T dimuons (1.5-2GeV/ μ)
- Fully reconstruct
 - ✓ $J/\psi, \psi(2s) \rightarrow \mu^+ \mu^-$
 - ✓ $B^+ \rightarrow J/\psi K^+$
 - ✓ $B^0 \rightarrow J/\psi K^*, J/\psi K_s$
 - ✓ $B_s \rightarrow J/\psi \phi$
 - ✓ $\Lambda_b \rightarrow J/\psi \Lambda$





B_s Lifetime

$B_s \rightarrow J/\psi \phi$, with $J/\psi \rightarrow \mu^+ \mu^-$ and $\phi \rightarrow K^+ K^-$

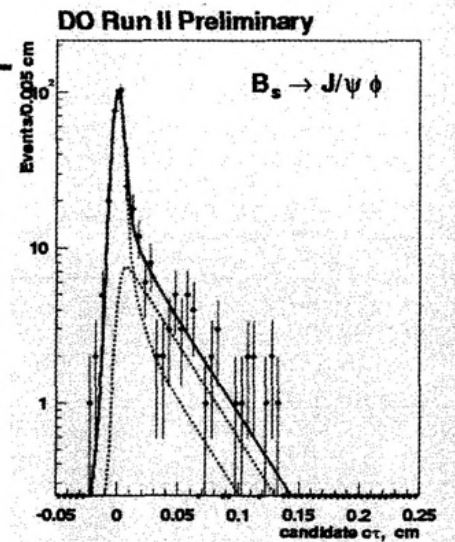
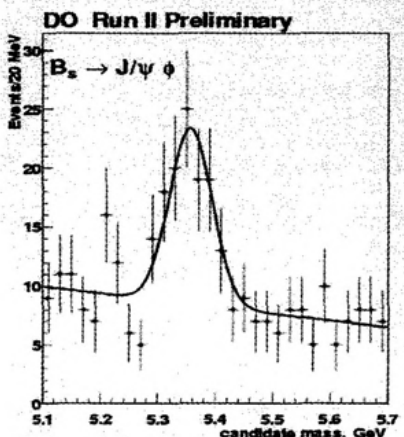
DØ (115 pb⁻¹): (shown here)

$$\tau(B_s) = 1.19^{+0.19}_{-0.16} \text{ (stat.)} \pm 0.14 \text{ (syst.) ps}$$

$$\tau(B_s)/\tau(B^0) = 0.79 \pm 0.14 \text{ (uncorrected for CP composition)}$$

CDF (138 pb⁻¹):

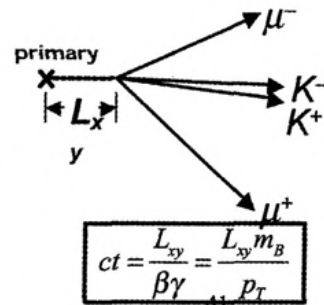
$$\tau(B_s) = 1.33 \pm 0.14 \text{ (stat.)} \pm 0.02 \text{ (syst.) ps}$$



Interesting B_s physics:

- Search for CPV in $B_s \rightarrow J/\psi \phi$... sensitive to new physics
- Width difference $\Delta\Gamma$
- B_s mixing

Stephen Parke, Fermilab

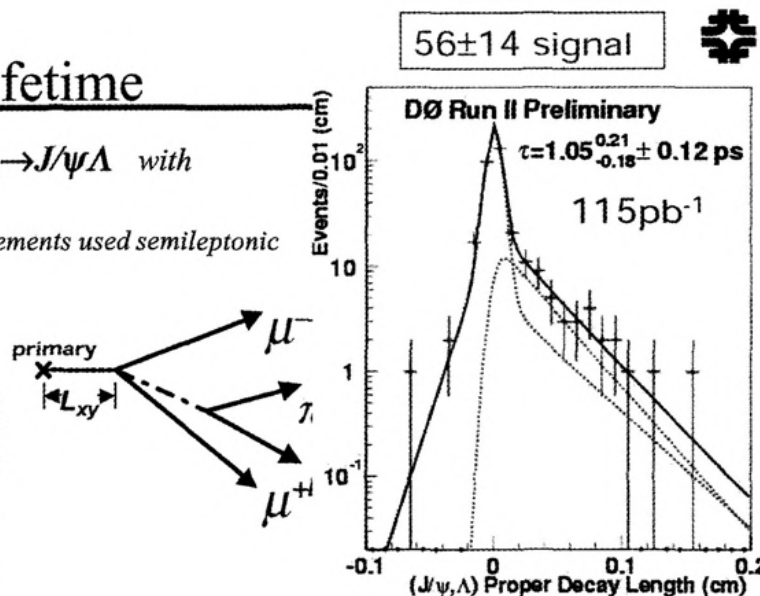
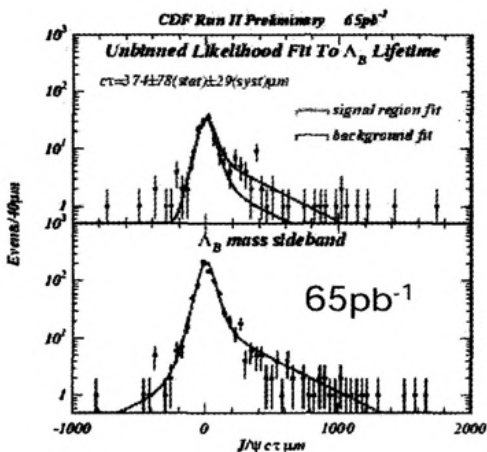




Λ_b Lifetime

- Use fully reconstructed $\Lambda_b \rightarrow J/\psi \Lambda$ with $J/\psi \rightarrow \mu^+ \mu^-$ and $\Lambda \rightarrow p \pi$
 - Previous LEP/CDF measurements used semileptonic $\Lambda_b \rightarrow \Lambda c \bar{v}$
 - Systematics different

CDF 46±9 signal



CDF

$$\tau(\Lambda_b) = 1.25 \pm 0.26 (\text{stat.}) \pm 0.10 (\text{syst.}) \text{ ps}$$

D0

$$\tau(\Lambda_b) = 1.05^{+0.21}_{-0.18} (\text{stat.}) \pm 0.12 (\text{syst.}) \text{ ps}$$

Stephen Parke, Fermilab

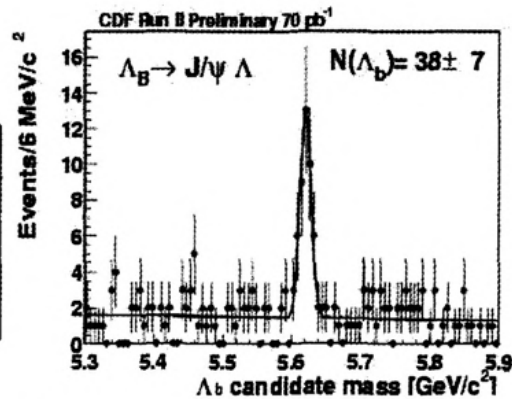
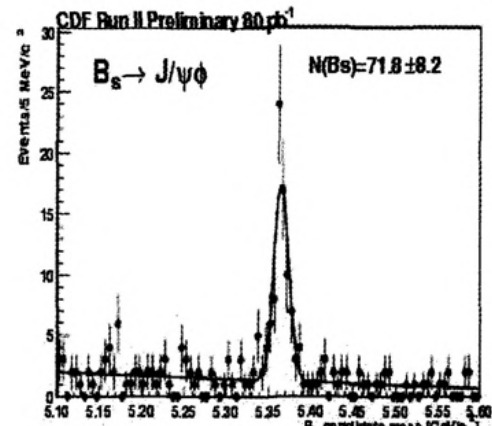


B Hadron Masses

- Measure masses using fully reconstructed $B \rightarrow J/\psi X$ modes
- High statistics $J/\psi \rightarrow \mu^+ \mu^-$ and $\psi(2s) \rightarrow J/\psi \pi^+ \pi^-$ for calibration.
- Systematic uncertainty from tracking momentum scale
 - Magnetic field
 - Material (energy loss)
- B^+ and B^0 consistent with world average.
- B_s and Λ_b measurements are world's best.

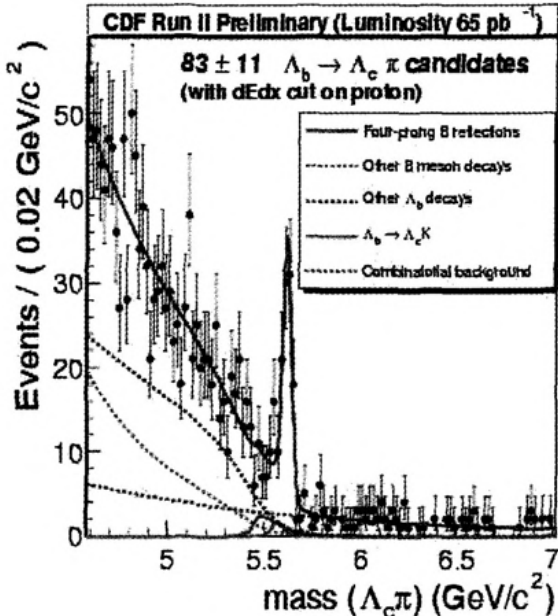
CDF result: $M(B_s) = 5365.50 \pm 1.60$ MeV
 World average: $M(B_s) = 5369.6 \pm 2.4$ MeV

CDF result: $M(\Lambda_b) = 5620.4 \pm 2.0$ MeV
 World average: $M(\Lambda_b) = 5624 \pm 9$ MeV





CDF $\Lambda_b \rightarrow \Lambda_c \pi$ with $\Lambda_c \rightarrow p K \pi$



Backgrounds: real B decays
Reconstruct π as p : $B_d \rightarrow D^- \pi^+ \rightarrow K^+ \pi^- \pi^- \pi^+$

- Use MC to parametrize the shape.
- Data to normalize the amplitude
- Dominant backgrounds are real heavy flavor
- proton particle ID (dE/dx) improves S/B

Fitted signal:

$$N_{\Lambda_b} = 96 \pm 13(\text{stat.})^{+6}_{-7}(\text{syst.})$$

Measure:
$$\frac{\sigma_b \times f_{baryon} \times BR(\Lambda_b \rightarrow \Lambda_c^+ \pi^-)}{\sigma_b \times f_d \times BR(B^0 \rightarrow D^- \pi^+)}$$

New Result!

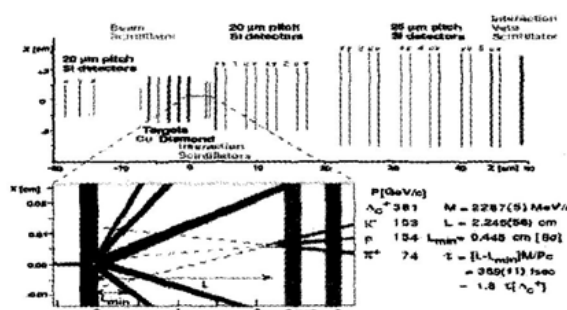
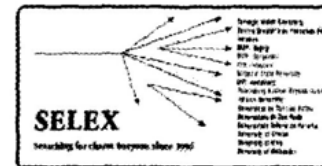
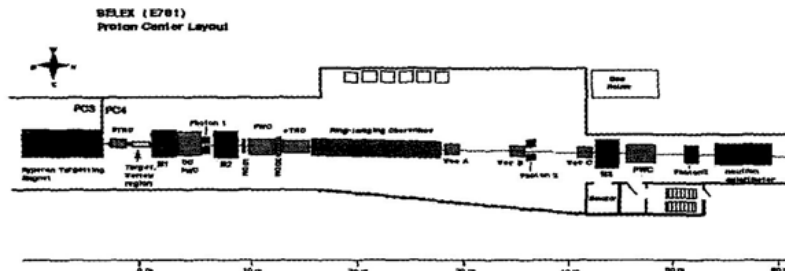
$$BR(\Lambda_b \rightarrow \Lambda_c \pi^\pm) = (6.0 \pm 1.0(\text{stat}) \pm 0.8(\text{sys}) \pm 2.1(\text{BR})) \cdot 10^{-3}$$

Fixed Target



Selex Experiment at Fermilab

Charmed Hadroproduction with π^- , p and Σ^- beams



SELEX Experiment

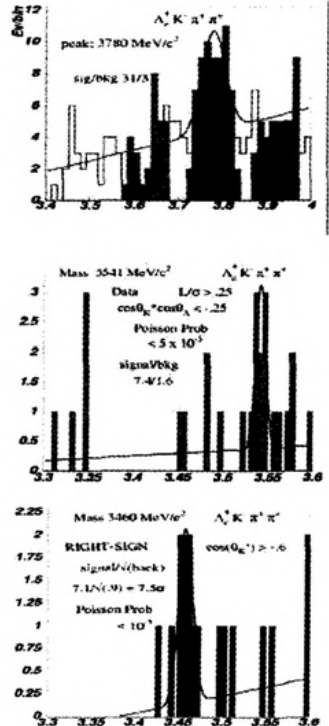
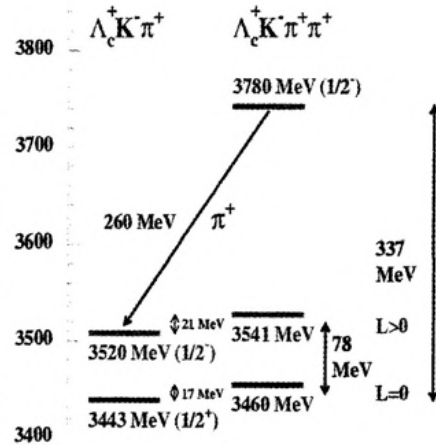
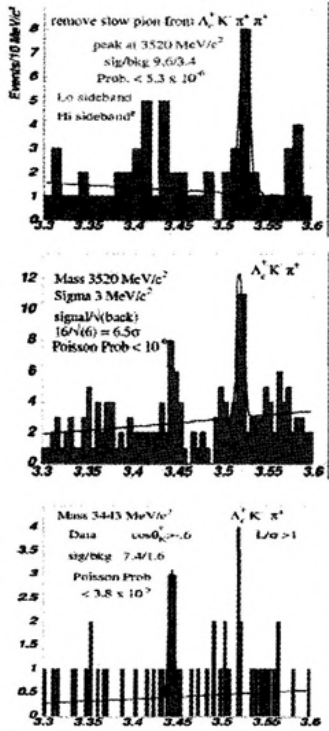
- Forward charm production $x_F > 1$
- π^- , p and Σ^- beams @ 600 GeV/c
- Typical boost ~ 100
- RICH PID above 22 GeV/c
- 20 plane – 4 view SVX $\sigma > 4 \mu\text{m}$
- data taken in 1996-7

Stephen Parke, Fermilab

46

SELEX Doubly Charmed Baryon States

An excited state and pair of isodoublets?



Stephen Parke, Fermilab

NEUTRINOS



The Neutrino Program



- **DONUT**
 - Observe Tau Neutrinos
- **MiniBooNE**
 - will make possible a decisive check of the Oscillation hypothesis of the LSND anomaly; if confirmed we need more than 3 neutrinos, $\Delta m^2 \sim 1 \text{ eV}^2$.
 - Running now!!!
 - 1 GeV v, 500 m distance
- **MINOS**
 - will observe and measure the atmospheric neutrino oscillation with high statistics and a controlled source;
 - will start operating in FY05.
 - 3-20 GeV v, 740 km distance



DONUT Status



FNAL E872 Beam dump beam

Status :

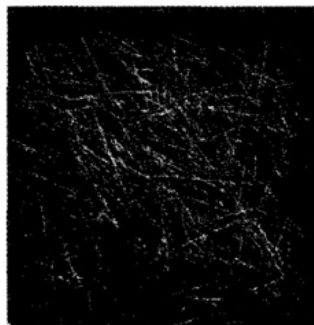
406 neutrino interaction analyzed.

7 ν_τ CC event detected

On-going :

Component analysis of the prompt
neutrino beam

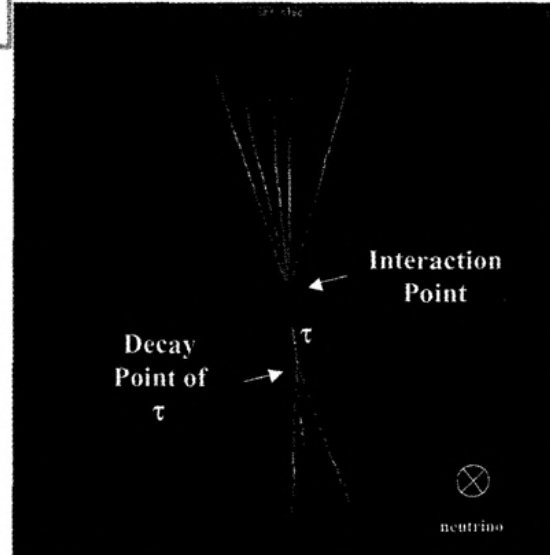
?_e : ? _{μ} : ? _{τ}



All tracks in the Scanning region
(4179 tracks)



Reject Low
momentum tracks
(114 tracks remained)
Reject passing
through tracks
(420 tracks remained)



Vertex detection :

Neutrino interaction and decay
of short lived particles

Detection of ν_τ CC in DONUT

Stephen Parke, Fermilab

50



A Little Neutrino Phenomenology



— very —

If neutrinos have mass then they may oscillate between flavors with the following probability

$$P = \sin^2 2\theta \sin^2(1.27\Delta m^2 L / E)$$

L is the distance that the neutrino travels (the baseline) - km

E is the neutrino energy - GeV

$\sin^2 2\theta$ is the oscillation mixing angle

Δm^2 is the mass difference squared between neutrino mass eigenstates – eV²

MiniBooNE Goal: Investigate LSND

Taking atmospheric, solar, reactor, and LSND results together ... either ...

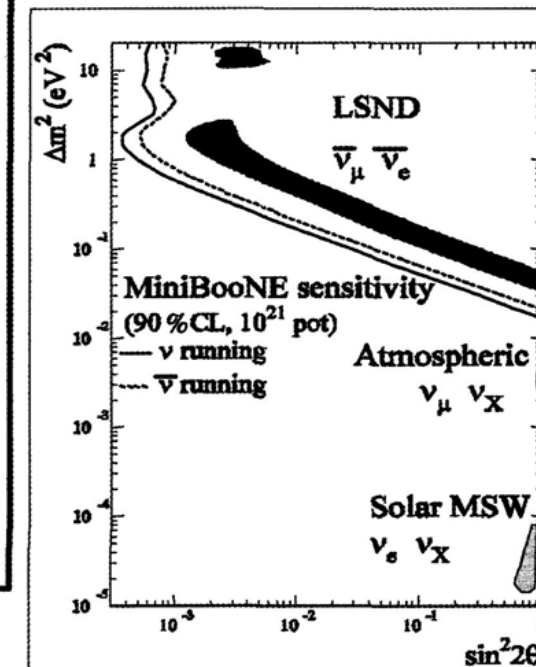
- One or more of the experiments are not seeing oscillations
- or there are >3 neutrinos (gives you 3 independent Δm^2 scales)
- or CPT is not a good symmetry (gives you different mass scales for $\nu, \bar{\nu}$)

Barenboim, Borissov, Lykken, hep-ph/0212116

- or ???

To check LSND want:

- similar L/E
- different systematics
- higher statistics



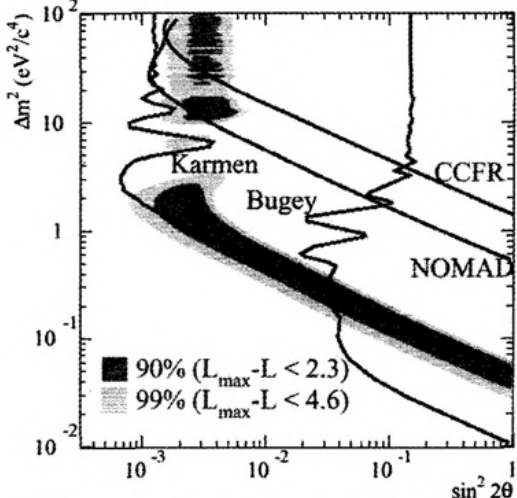
→ MiniBooNE!



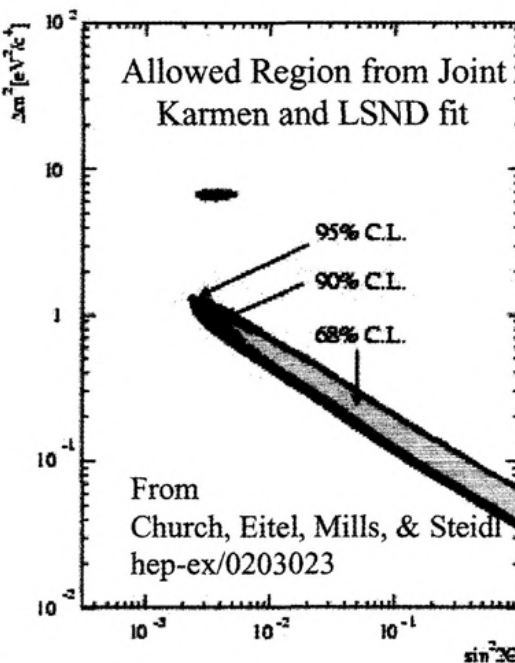
The Other Experiments



Several other experiments have looked for oscillations in this region.

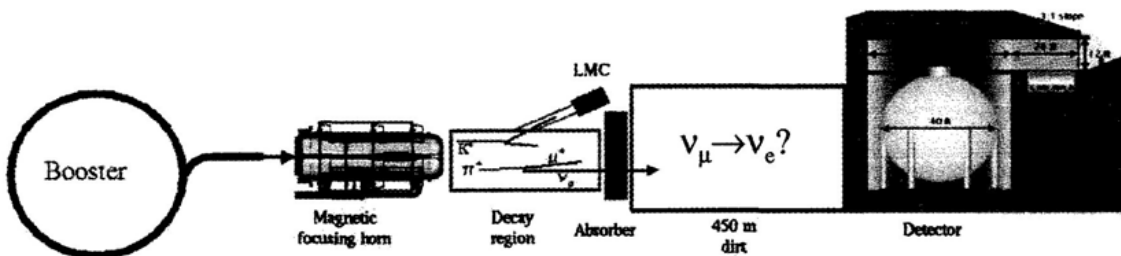


The most restrictive limits come from the Karmen Experiment.





The MiniBooNE Neutrino Beam



Start with a very intense 8 GeV proton beam from the Booster.

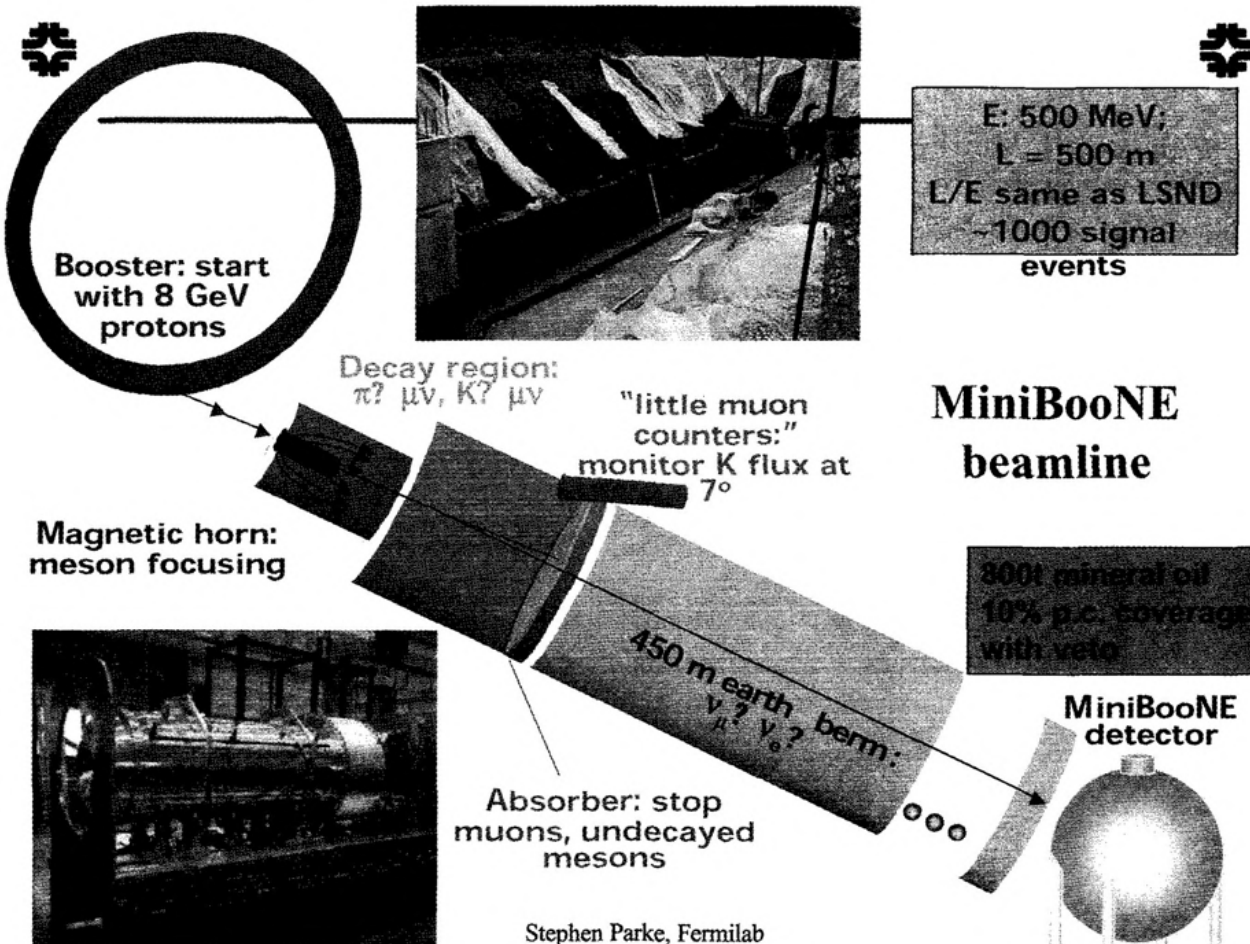
The beam is delivered to a 71 cm long Be target.

In the target primarily pions are produced, but also some kaons.

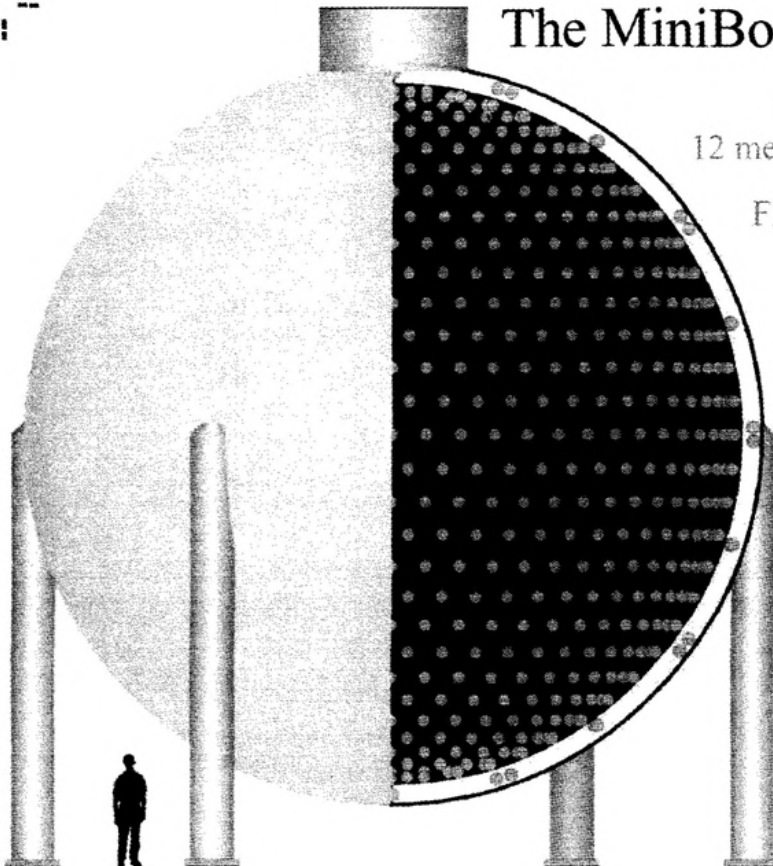
Charged pions decay almost exclusively as $\pi^\pm \rightarrow \mu^\pm \nu_\mu$.

The decays $K^\pm \rightarrow \pi^0 e^\pm \nu_e$ and $K_L \rightarrow \pi^\pm e^\mp \nu_e$ contribute to background.

There are also ν_e 's from muon decay.



The MiniBooNE Detector



12 meter diameter sphere

Filled with 950,000 liters of
pure mineral oil — 20+ meter
attenuation length

Light tight inner region with
1280 photomultiplier tubes

Outer veto region with 240
PMTs.

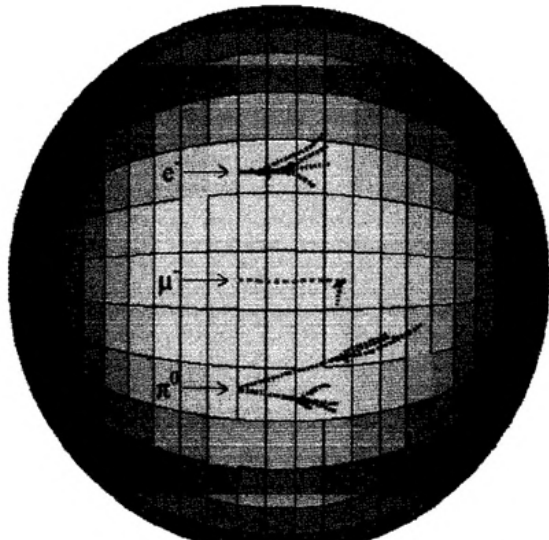
Neutrino interactions in oil
produce:

- Prompt Cerenkov light
- Delayed scintillation light

Cerenkov:scintillation \sim 5:1

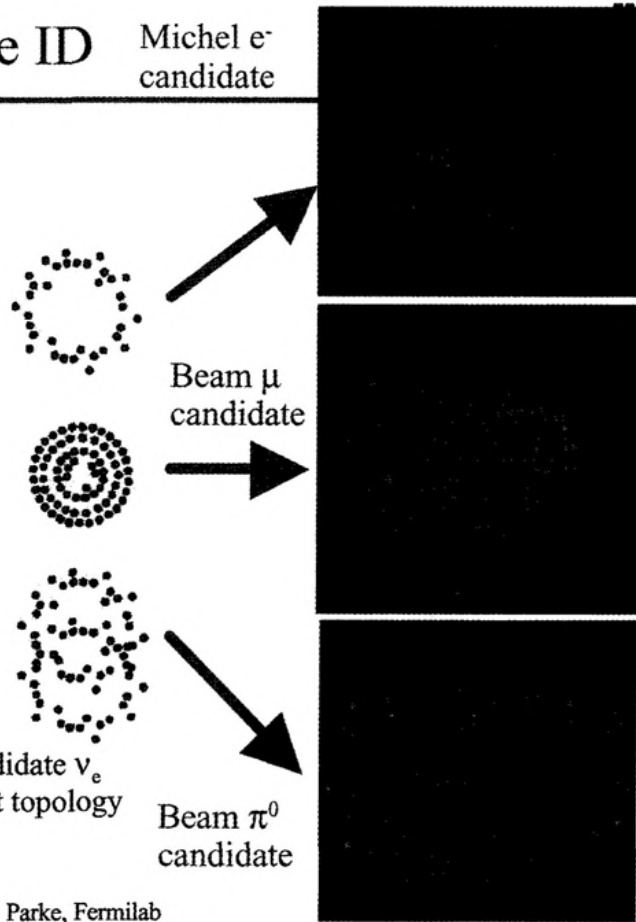


MiniBooNE Particle ID



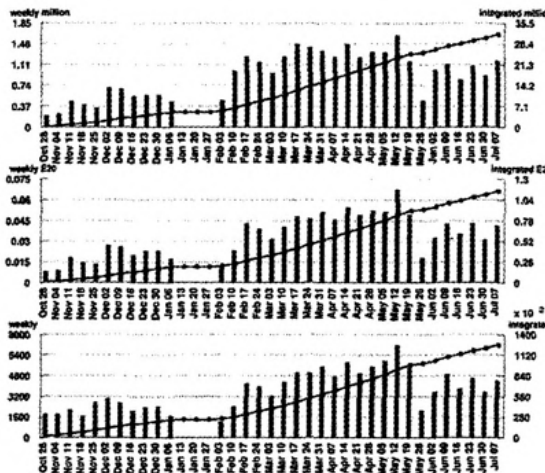
Identify electrons (and thus candidate ν_e events) from characteristic hit topology of mineral oil Cherenkov light

Stephen Parke, Fermilab





Overall MiniBooNE Status



Number of Horn Pulses

To date: 31.58 million
Largest week: 1.63 million
Latest week: 1.18 million

Number of Protons on Target

To date: 1.149 E20
Largest week: 0.0671 E20
Latest week: 0.0413 E20

Number of Neutrino Events

To date: 125616
Largest week: 7192
Latest week: 4364

Steadily taking data

- Currently at ~10% of 1×10^{21} POT goal
- Have collected >125,000 v events
- Detector performing well
- Still need more beam!

- Proton rate delivered by Booster has dramatically improved over time

- Further Booster upgrades in the works to reach intended rate
- Detector works beautifully!
- Expect first physics results in the Fall – WIN'03 October

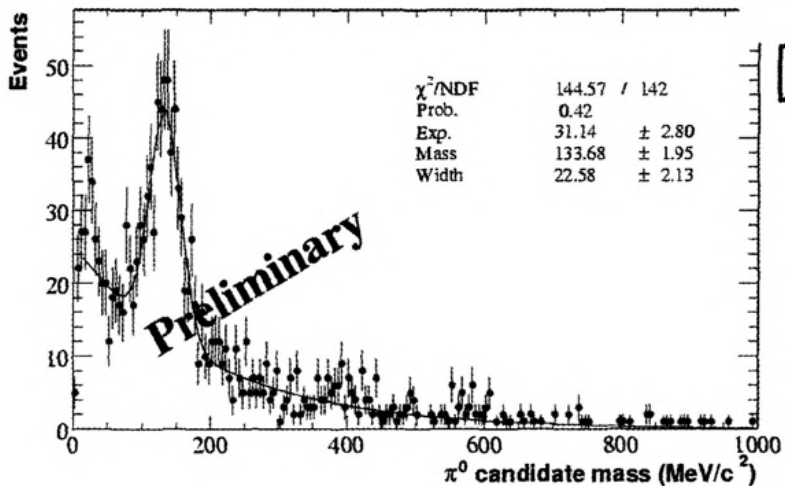


π^0 Background

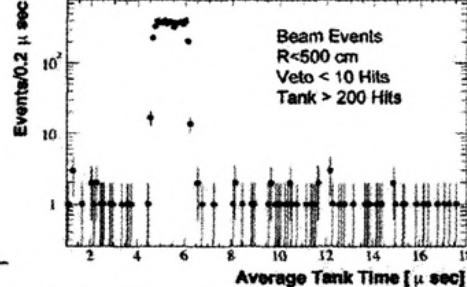
π^0 background to $\nu_\mu \rightarrow \nu_e$ search

$\pi^0 \rightarrow \gamma\gamma$ can mimic an electron

- escaping γ
- asymmetric decays
- ring overlap



Stephen Parke, Fermilab



non-beam background to $\sim 10^{-3}$

π^0 events are a useful calibration source



59



MINOS Physics Goals



- Demonstrate & Confirm the presence of oscillations.
 - A number of detection channels are available. Best is comparison of near and far Charged Current energy spectrum. The beamline and detectors are designed to do this with a total systematic error of $< 2\%$ per 2 GeV bin.
- Provide precision measurements of oscillation parameters.
- Provide determination of flavor participation to 2%.
- Comparison of oscillation parameters for atmospheric neutrinos and antineutrinos.



The MINOS Experiment



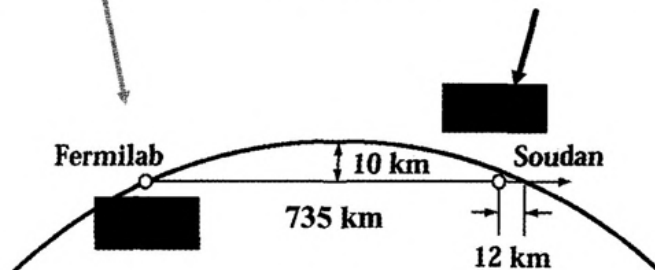
Status

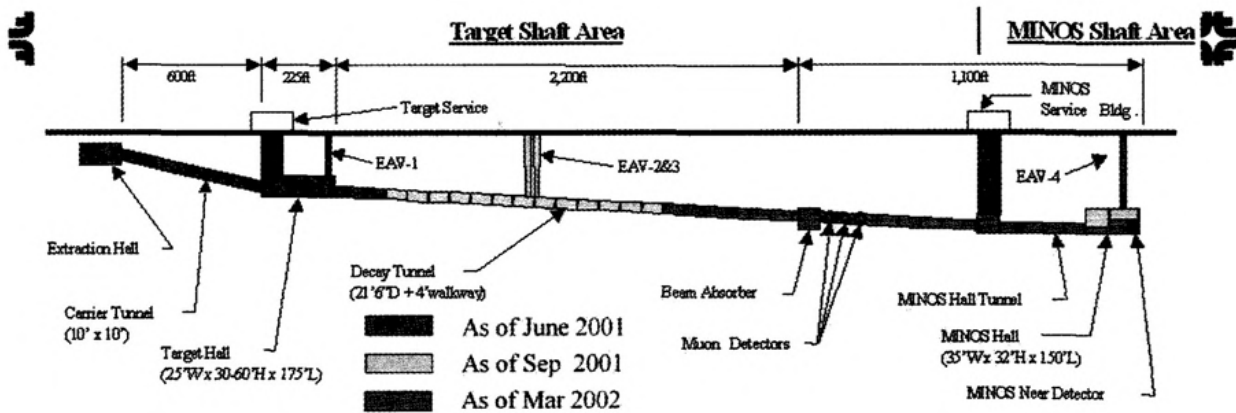
- The installation in the Target Hall will start in September 2002
- The installation in the Near Detector Hall in December 2002
- The first beam on target in December '04.
- The Far Detector is now complete, with both coils energized and veto shield also finished.
- Taking good atmospheric $\nu\mu$ and $\bar{\nu}\mu$ data.



Near Detector: 980 tons

Far Detector: 5400 tons

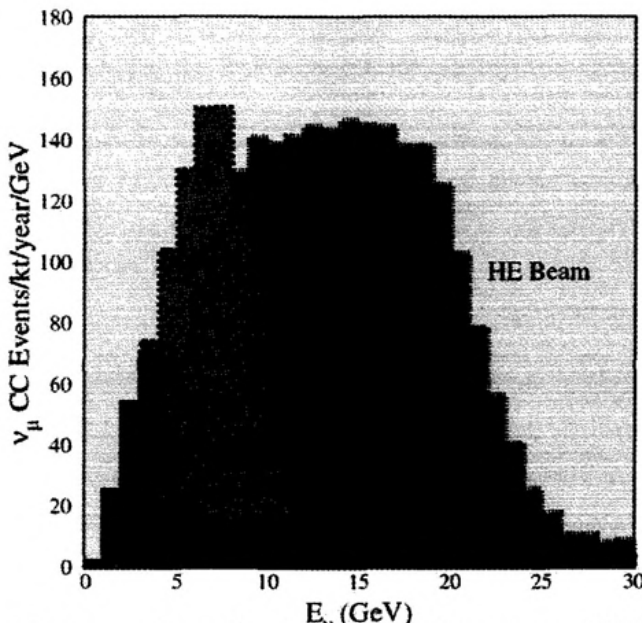




First piece of decay pipe



The NuMI Neutrino Energy Spectra



ν_μ CC Events/kt/year

Low	Medium	High
470	1270	2740

ν_μ CC Events/MINOS/2 year

Low	Medium	High
5080	13800	29600

4×10^{20} protons on target/year

4×10^{13} protons/2.0 seconds

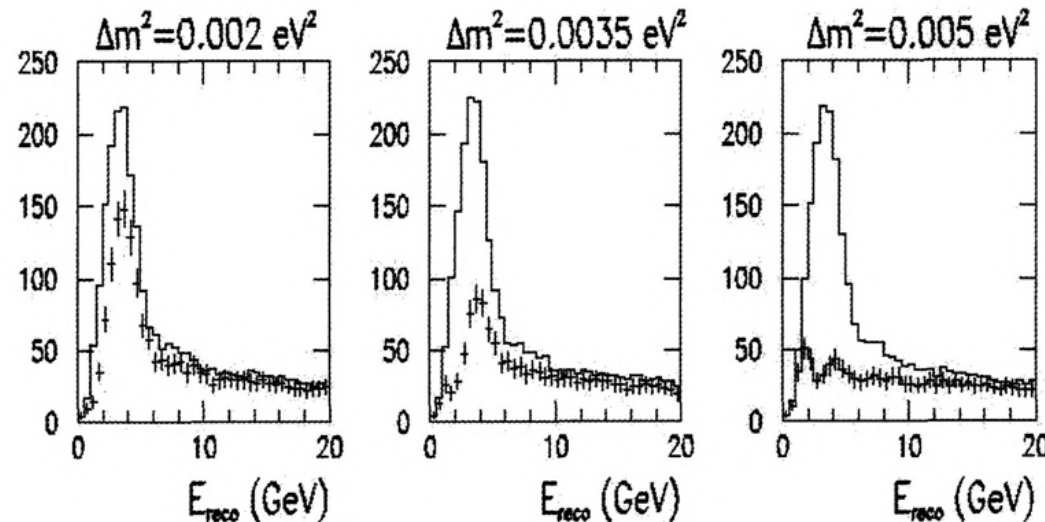
By moving the horns and target, different energy spectra are available using the NuMI beamline. The energy can be tuned depending on the specific oscillation parameters expected/observed.



Charge Current Energy Distributions

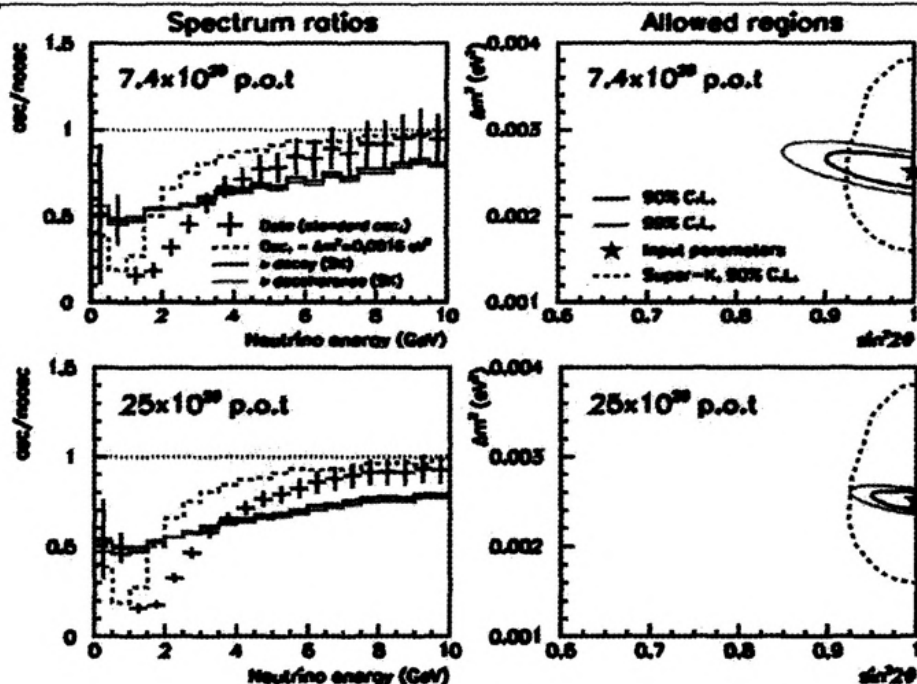


CC energy distributions – Ph2le, 10 kt.yr., $\sin^2(2\theta)=0.9$



Note: 10 kt. Yr. = ~ 2 live years of running. Results still statistics limited at that time.

Measurement of Oscillations in MINOS



For $\Delta m^2 = 0.0025 \text{ eV}^2$, $\sin^2 2\theta = 1.0$

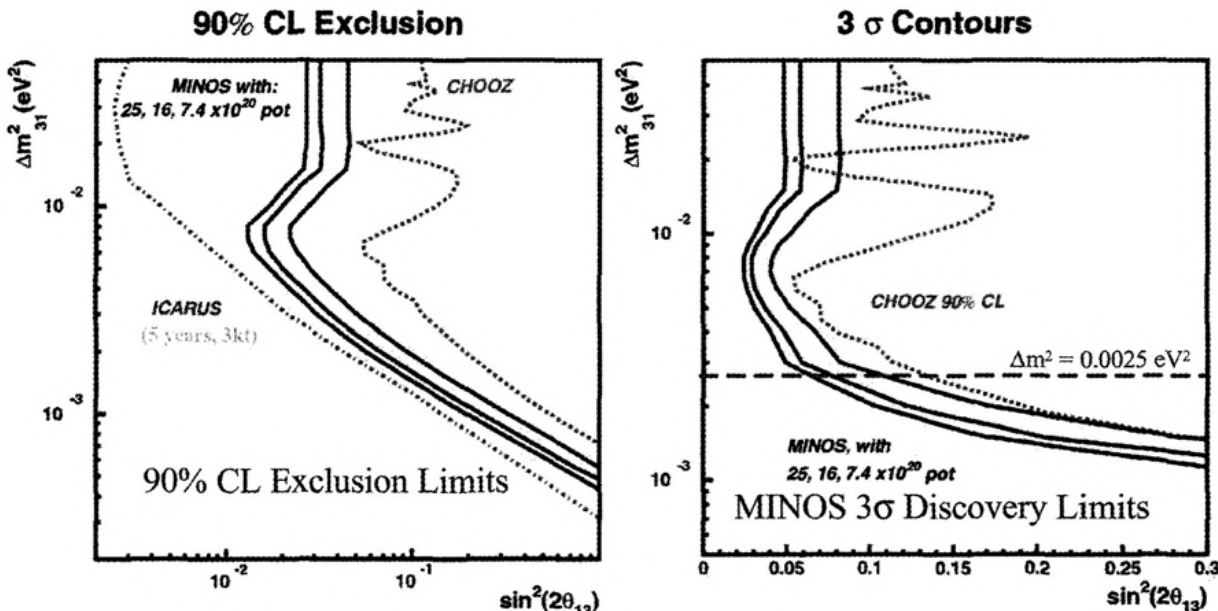
Oscillated/unoscillated ratio of number
of ν_μ CC events in the far detector

Stephan Panksepp, Fermilab

MINOS 90% and 99% CL allowed
oscillation parameter space. 65

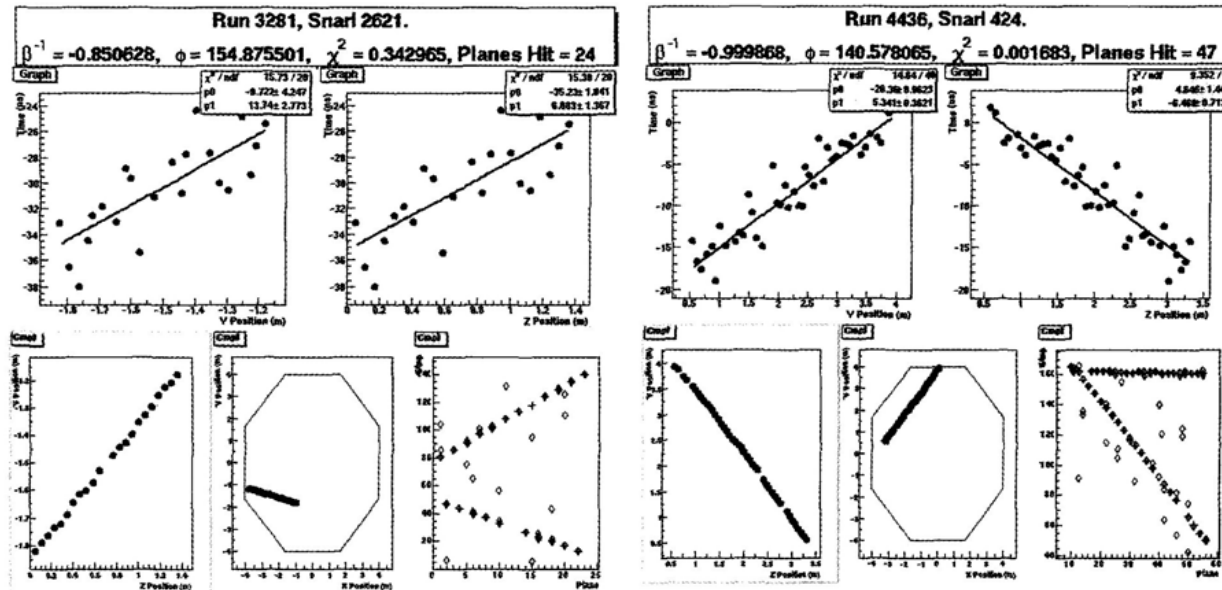


Appearance of Electrons



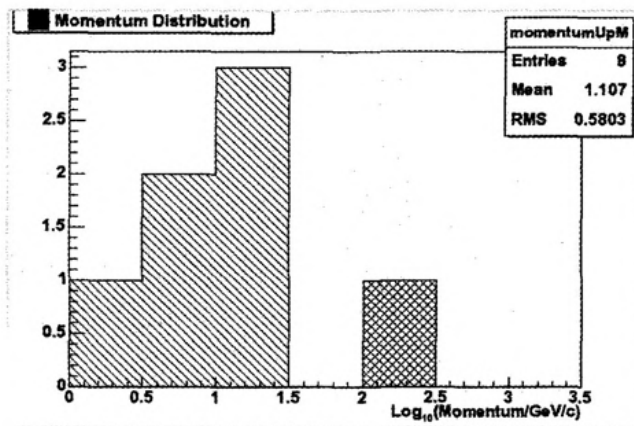
- MINOS sensitivities based on varying numbers of protons on target

1st and 2nd Neutrino Events at Far Detector

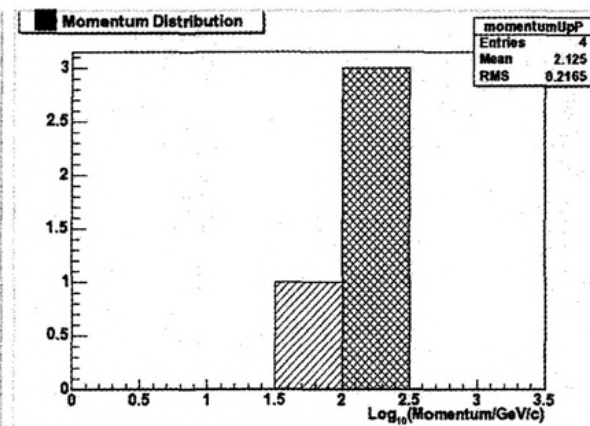




Charge and Momentum of Upgoing Muons



•One Sign



•Other Sign

THEORY



Theoretical Physics



- **Particle Theory Group: Topics**

- Beyond Standard Model
 - Supersymmetry, Extra Dimension, Model building
 - Neutrinos
- Phenomenology
 - Collider Physics, Heavy Flavors
 - QCD Perturbative, Lattice

- **Astrophysics Theory Group: Topics**

- Dark Matter, Dark Energy, inflation, Large-Scale Structure, Cosmic Microwave Background, Gravitational Lensing, Cosmic Rays, Neutrinos

Astro-Physics



The Experimental Particle Astrophysics Program



- Fermilab has an important role in astrophysics experiments, as a partner with NSF, U.S. university groups (DOE and NSF), and foreign institutions:
 - The **Cryogenic Dark Matter Search** (CDMS-II) is going to extend its search for direct detection of cold dark matter with a new facility in the Soudan mine.
 - The **Auger Cosmic Ray Observatory** will study cosmic rays with energy $10^{19} - 10^{21}$ ev at Los Leones, Argentina.
 - The **Sloan Digital Sky Survey** is now operating at Apache Point Observatory, NM and many results are attracting great attention.

1. Image $\frac{1}{4}$ of sky in 5 bands
 2. Obtain redshifts of 1 million galaxies and quasars

2.5 m Telescope
 Apache Point NM



Mosaic Imaging Camera



640 Fiber Spectrograph



Measure large scale structure of universe
 a) galaxies in 0.2% of the visible universe
 b) quasars in 100% of the visible universe

Address fundamental question in cosmology

Status (Aug 2003)

- Percent Complete
- Baseline

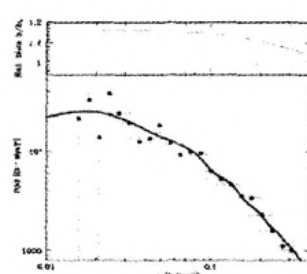
IMAGING	8452 sq. deg.
	78% as of Aug 6, 2003

SPECTROSCOPY 1688 tiles

- 48% as of Aug 6, 2003



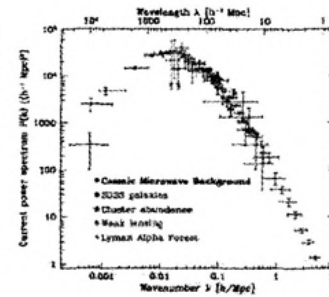
Distribution of Galaxies around Sun to $z=0.15$
(Blanton 2003)



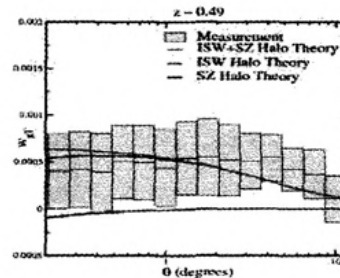
? CDM
adjusted to
 L^* galaxy

$O_M h = 0.213 \pm .023$
 $s_8 (\text{gal}) = 0.96 \pm .02$
 $n = 0.995$

Three-dimensional Power Spectrum
(Tegmark et al 2003)



SDSS vs WMAP: Correlation of
temp. fluctuations with galaxy counts
(Scranton et al. 2003)



Strong evidence for dark energy
dominated universe (?CDM)

FUTURE PROJECTS



Future Projects: CP Violation



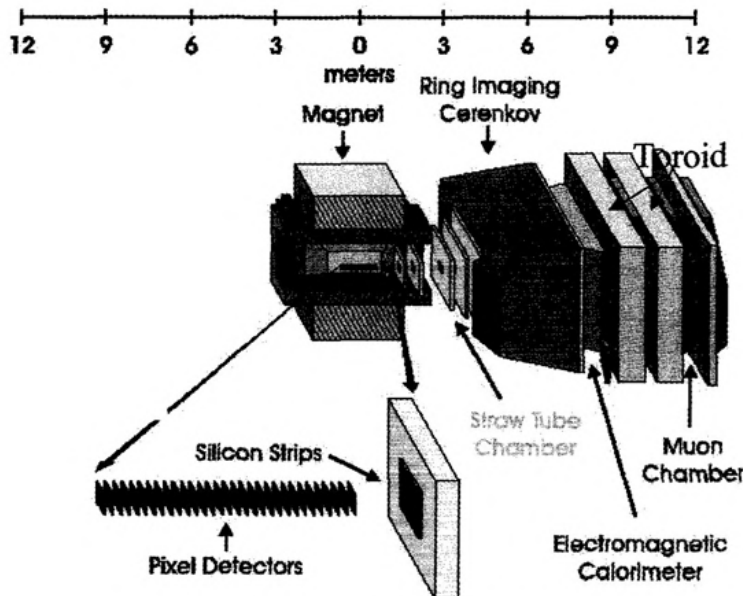
- BTeV
 - Dedicated B-physics Detector at Tevatron Collider
 - The BTeV experiment will exploit the large B meson cross section at the Tevatron to make *precision* measurements of B decays, particularly B_s decays, that have very robust theoretical predictions.
- CKM
 - Precision Measurement of $K^+ \rightarrow \pi^+ \nu \bar{\nu}$
 - The CKM experiment (Charged Kaons at the Main injector) will exploit the large flux of charged kaons produced by the Main Injector proton driver to make a *precision* measurement the ultra-rare $K^+ \rightarrow \pi^+ \nu \bar{\nu}$ process. ($BR \sim 1 \times 10^{-10}$).
- NuMI Off-Axis
 - $\nu_\mu \rightarrow \nu_e$
 - Measure Θ_{13} , mass hierarchy and CP violating phase, δ .



Reduced Scope BTeV Spectrometer



BTeV Detector Layout



Since B's are produced by gluon-gluon fusion, both B's are boosted in the direction of the more energetic gluon, and go into the same arm. If this were not so, tagging would not be efficient with one Arm.

The Re-scoped Version of BTeV 's Stage I approval was recently reconfirmed, unanimously, by the FNAL PAC.

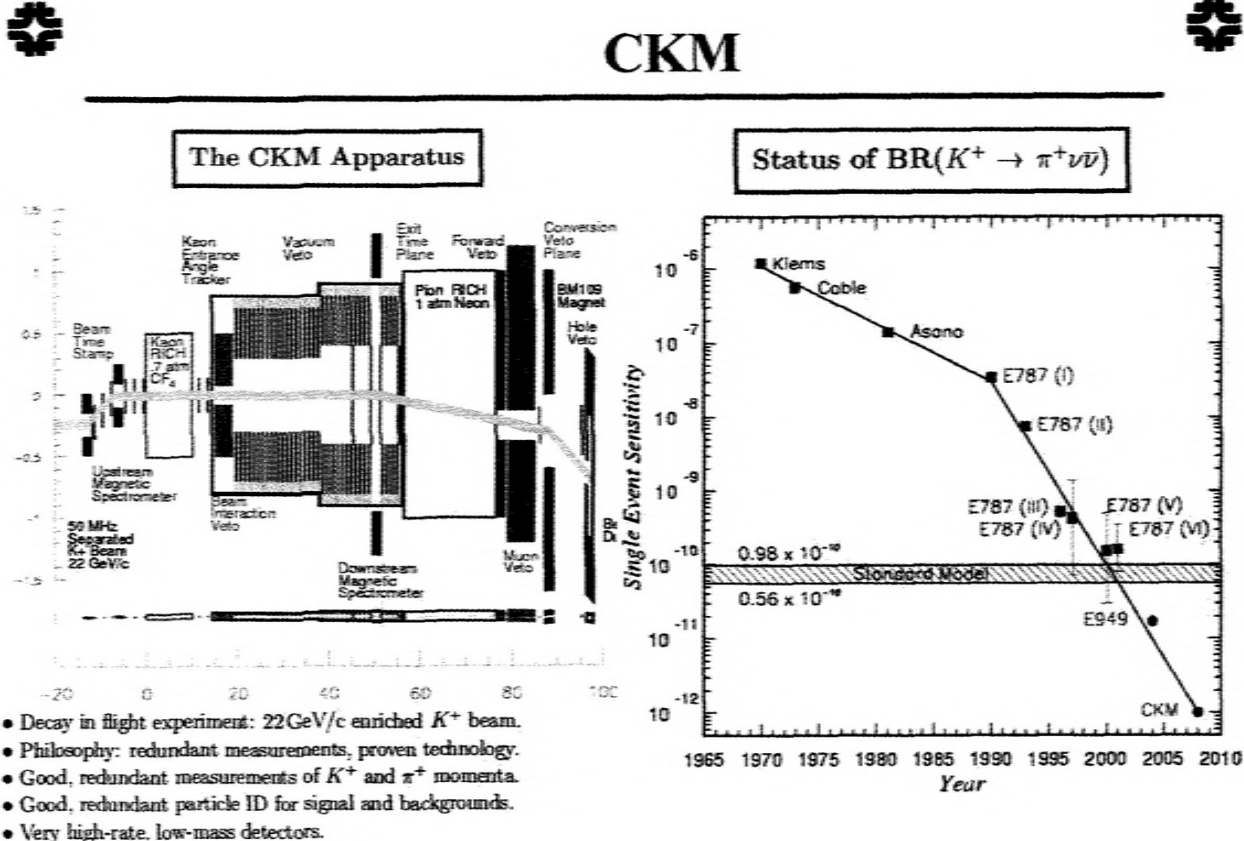


BTeV Physics Reach - 1 Year



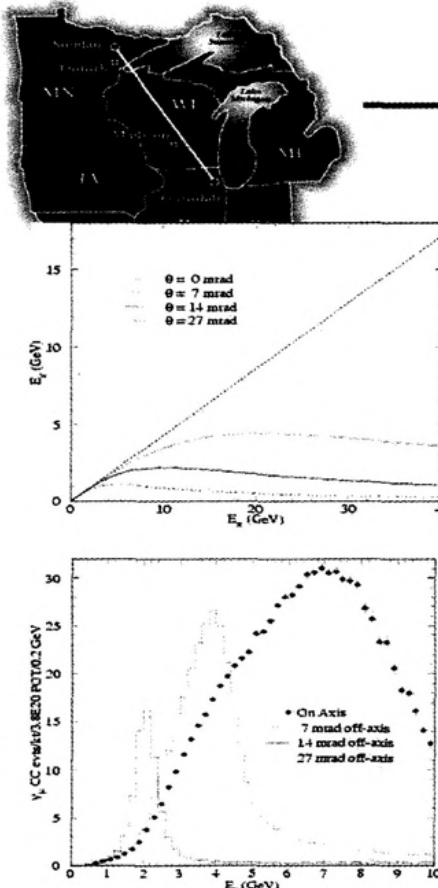
Quantity	Uncertainty (σ) 2×10^{-32} 1 year
$\delta \sin 2\beta$	0.018
α	
$B \rightarrow \rho \pi$	$\pm 4.3^{\circ}$
γ	
$B_s^- \rightarrow D_s^- K^-$	$\pm 10^{\circ}$
$B^- \rightarrow D^0 K^-$	$\pm 14^{\circ}$
$B^0 \rightarrow K \pi$	$\pm 7^{\circ}$ (plus theory)
$\text{Sin}(2\chi)$	
$B_s^- \rightarrow J/\psi \eta^{(\prime)}$	0.03
$\pi\pi$ asym	0.034
$x_s (D_s \pi)$	up to 60

CKM

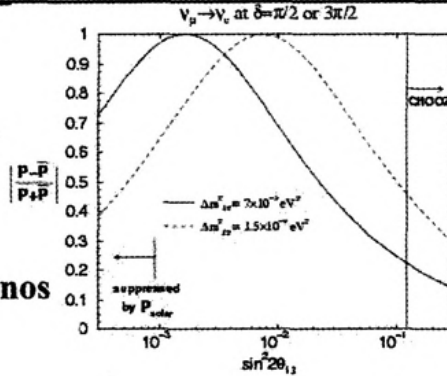




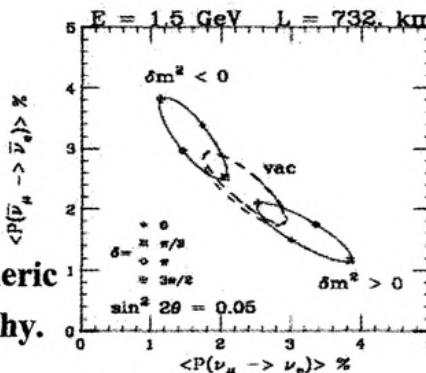
NuMI Off-Axis: $\nu_\mu \rightarrow \nu_e$



Large
Asymmetry
Neutrinos
Verse
Anti-Neutrinos



Matter
Effects give
NuMI
sensitive to
The Atmospheric
Mass Hierarchy.





OUTLOOK



- **The Fundamental Scales of Mass and Energy**
 - What breaks the electroweak symmetry and sets the electroweak scale of 246 GeV? Top, EW and Higgs.
 - Is there a supersymmetry that is broken at this scale?
- **Neutrinos**
 - What is the pattern of neutrino masses and mixing? CP violation
- **Quarks and CP violation**
 - Are all CP violations consistent with a single source?
- **Cosmological Dark Matter & Dark Energy.**
 - Do new particles make up a significant component of dark matter?
- **Radically New Physics**
 - Eg Are there observable effects of large hidden dimensions?

The Fermilab program will address all of these questions this decade.



Summary



- We have great opportunities for discoveries at Fermilab.
 - An excellent program in the fast-moving area of neutrinos – MiniBOONE, MINOS, NuMI-Off-Axis
 - Exploring a new mass region at the Tevatron
 - Unique experiments in particle astrophysics
 - A big leap in energy scale at the LHC
 - BTeV and CKM which will explore CP violation precisely
- We are also doing R&D on the accelerators needed to advance the field.

CHAIRMAN: S. PARKE*Scientific Secretaries: A. Cerri, A. Hamilton***DISCUSSION***- Haidt:*

Is the quoted top mass a new measurement or is it including old Run I data?

- Parke:

It is a brand new determination. CDF and D0 underwent major changes between Run I and Run II and decided not to include the old data, up to now. The error bars on the new measurements are larger than the ones on the old measurements and therefore merging the old and the new data would yield basically the same result as the old measurements.

- Haidt:

How many events are included in these new measurements, roughly?

- Parke:

For the di-lepton channel, CDF has about 6 events, and for the lepton+jets CDF has of the order of 40 or so. It is actually a smaller number than in Run I at this point.

- Haidt:

When will you be able to make a scatter plot where on one side is the top mass and on the other side is the W mass?

- Parke:

I suspect within one year we will have that. And the reason why you are interested in that is that you want to know what the Higgs mass is? In the SM there is correlation between the t, W and H masses and, as we all know, the data up to now is hinting to an H mass which has already been excluded by LEP.

- Haidt:

I have a more mundane reason: figuring out what the background is, because I am still worried that a lot of background events are included in this analysis and therefore the absolute value of the [top quark] mass could be modified.

- Parke:

I think that in the di-lepton measurements we have very little background; the lepton+jet where you have two b-tags probably has little background also, but I think you are worried about the one with only one b-tag. As you get more data, you can tighten the cuts and with 2 fb^{-1} the claim is that we should get a top quark mass with an uncertainty of about 2-3 GeV.

- *Haidt:*

In the very first analysis of the di-lepton events there was for some time a very low top mass. Is it understood?

- *Parke:*

Is this in the new events or the old events?

- *Haidt:*

In the old events there was one analysis giving a mass of 145 GeV. The error of course was ± 20 GeV so there was really no reason to worry, but as you increase the energy perhaps you have a better understanding.

- *Parke:*

I do not think so at this point in time. The di-lepton events, at least in Run I, were few; of the order of 5-6 per experiment. A number of those events were quite anomalous and we do not understand them: there is one di-lepton event with the two leptons going in approximately the same direction, which is very unexpected. Either it hints to new physics, which is going to be a lot of fun; we need more data.

- *Baldini:*

Do you know if there is a specific reason why the Tevatron did not yet reach the expected luminosity?

- *Parke:*

The non-answer is that there was not enough preparation done for this run.

- *Galletly:*

Over the last 30 years, the pattern of the high energy laboratories was to use hadron machines to push the energy scales being investigated, and after use lepton machines to get precision measurements of the new physics that you found. With the LHC coming on, do you see the next machine built at Fermilab being a lepton machine or rather another hadron machine?

- *Parke:*

The US high energy community has determined that a lepton machine is the next machine that will be built in the US. It is not clear whether it will be built in Fermilab or not. The trouble I see with building a high energy lepton machine of the order of 500 GeV is that we could be left in the situation where the LHC sees nothing but the SM Higgs at 160 GeV. This is not such an interesting mass value because $H \rightarrow W+W-$ would be the dominant decay mode with other decay modes very rare. The SM could work up to a very high mass scale. If the Tevatron or LHC discovers supersymmetry then we will know what mass scale to aim at to build a precision machine.

- *Galletly:*

So there are no plans at the moment to build a large hadron machine in the US?

- *Parke:*

People at Fermilab are thinking about how to build a Very Large Hadron Collider, of the order of 100-200 Km in circumference. The question is how cheaply you can do it.

- *Cifarelli:*

I was delighted to see this morning the $\Lambda_b \rightarrow \Lambda_c \pi$ signal which was observed a long time ago for the first time at CERN. It is good to see such statistics. My question is: do you also see anything in the $\Lambda_b \rightarrow \Lambda_c \pi \pi \pi$ channel?

- *Parke:*

Not officially.

- *Cifarelli:*

Maybe you would be favoured by the branching ratio. But I guess we have to wait for that.

- *Parke:*

B physics people are one of the few people who do not have to wait for a large integrated luminosity, except for B_s mixing.

- *Menges:*

I thought that many of the measurements that you have shown from the Tevatron are dominated by the luminosity uncertainty. Can you give some details on how they do it and if it will be improved?

- *Parke:*

One of the biggest uncertainties is that D0 and CDF use a different value of the total $p\bar{p}$ elastic cross section at 2 TeV. People are working on fixing this but it is not the highest priority. That error will definitely go down dramatically.

There are a couple of slides that I did not show which stress this discrepancy between CDF and D0, but it will just go away. If you normalize the measurement to some other cross section, that could help tremendously.

- *Zichichi:*

Inconsistencies are very interesting!

- *Parke*

It is inconsistent because they use a different total cross section for the elastic scattering. If they were to use the same cross section this inconsistency would go away. So that is pretty boring: it is not the kind of inconsistency you would like.

- *'t Hooft:*

You gave the impression that Fermilab measurements will cease to have any importance as soon as the LHC is switched on, but the LHC will need some years to reach the designed luminosity and it is a different machine. Do you expect a few years of peaceful coexistence checking each other's results?

- *Parke:*

Of course, I was referring to the moment LHC begins producing substantially new physics. The projections of the luminosity I gave go up to October 2009 while the LHC is supposed to turn on sometime in 2007. There are a number of years where the two machines will overlap.

For physics for which there is a common mass reach, like the top quark, the Tevatron can be seen as a $q\bar{q}$ collider, while the LHC is a gg collider. Both production mechanisms and backgrounds are very different, which makes a good way of checking real physics. However for LHC, the top cross section is more than a 100 times larger than the Tevatron. If you see something new you can check whether it is a by-product of the method you use for the measurement or if it really is physics. Very much like the way MiniBoone is checking LSND: with very different experiments.

- *Zichichi:*

As you correctly pointed out, the top has only been seen, for obvious reasons, at Fermilab. Do you have a data summary where we can deduce the statistical significance of this effect? To what extent can you evaluate the risk that the top is not there? For example if the mass is even higher (200 GeV): there is reason to believe that the top is even heavier than measured. In order to understand why SUSY has not been discovered yet. To what extent are you really sure that the top is so light?

- *Parke:*

If you look at lepton+jets and you plot the number of events versus the number of jets which are b-tagged, you will see an excess at 3 and 4 jets, which is considered the top evidence since QCD predicts a constant ratio between what you see in 1 jet/2 jets, 2 jets/3 jets etc.

Something has been found that has been interpreted as the top quark. Is it really the top quark? That question I think is still not really quite determined. What we know is that it predominantly decays into W and b , but do we know that it is spin 1/2? There are several questions we have to settle to figure out if this is really the top quark. We do know that it has approximately the right cross section to be a top quark of that mass, but I do not think this is conclusive evidence at this point. Fermilab Run I gave a sort of a 0th order pass over whether this particle is the top or not. Run II will eventually do higher precision measurements; one that I would like to see is the W polarization for $t(Wb)$. This is expected to be about 70% longitudinal and 30% transverse (that is just $m_t^2 : 2m_W^2$). Whether the W is longitudinal or transverse can be measured from how hard the lepton P_t is. This is something that CDF and D0 will measure quite precisely in this run and will be fairly strong evidence that this really is the top quark. But there are people out there who think that what we have found is the SUSY partner of the top quark.

- *Zichichi:*

When you say 70/30, to what extent can you exclude 50/50?

- *Parke:*

At this point you cannot: this is the measurement of this ratio from Run I parametrized as this "F" quantity which is the ratio of the longitudinal polarization to the total, which therefore should be close to 70% for the top quark. The lepton Pt fit shows the combination of everything and in green the component coming from the longitudinally polarized W (which gives very low Pt leptons). In Run I they measured (56(31)% which I do not think excludes anything at this point. But that will improve with the increased statistics of top quarks from Run II.

In Run I, the total number of top events which was observed was about 100, in Run II it will be 50 times that, with a factor 20 coming from the increased luminosity, and another factor 2.5 coming from the combination of the increase in the detector efficiency and the growth of the $t\bar{t}$ production cross section between 1.8 and 1.96 TeV.

The top quark has not been completely nailed down yet, but if this is the top quark, these measurements will prove it.

- *Zichichi:*

Can you exclude the possibility that this is the SUSY partner of the top?

- *Parke:*

The cross section for stop is 1/6th of the top one at the energy of the Tevatron. This value is probably excluded by SUSY at this point unless you start doing some funny things.

- *Zichichi:*

Can you exclude higher mass states from the data you have so far?

- *Parke:*

Up to some cross section, yes. I showed earlier today a plot of the invariant mass distribution of the $t\bar{t}$ pairs, so in some sense these events have been selected but they do not show any evidence of a resonance. This is the distribution of $t\bar{t}$ pairs. What you expect from the top is this yellow distribution, and the data fits it. The data however is so low statistics that there is no conclusive evidence of resonant structures. There is no evidence for a higher mass state.

- *Zichichi:*

Could you make a statement on how many standard deviations you associate with the existence of the top as it is now?

- *Parke:*

I would say 5-6 standard deviations, but I am not an experimentalist and I am merely speculating. The existence of a 175 GeV state that decays primarily into Wb is well established.

Diffracti \circ n studied with a Hard Scale at HERA

Günter Wolf

Deutsches Elektronen Synchrotron DESY

E-mail: Guenter.Wolf@desy.de

Abstract

New HERA data are discussed on diffraction in deep inelastic scattering which span a wide range in Q^2 and W . Diffraction is found to account for a large fraction of inclusive scattering. Analysis of the diffractive structure function of the proton suggests a pQCD-like evolution of diffraction with x_p , β and Q^2 .

1 Introduction

The large body of data on inclusive deep inelastic scattering (DIS), $ep \rightarrow e + \text{anything}$, see Fig. 1, led to a precise description of the nucleon structure functions by QCD in terms of the perturbative DGLAP expansion of the quark and gluon densities of the proton. It has been shown that diffraction, where the target proton or a low-mass nucleonic system together with a low mass hadronic system X emerge from the interaction, $ep \rightarrow eXN$, contributes a substantial part of the DIS cross section [1]. Efforts are underway to understand the diffractive subcomponent of DIS in terms of conditional parton distribution functions. According to the QCD factorisation theorem [2], these distribution functions will also undergo QCD evolution.

For hadron-hadron collisions, the data on total and elastic cross sections have been successfully parametrised in Regge theory by the exchange of the Pomeron trajectory [3]. In Ref. [4] it has been suggested to describe diffraction in DIS in terms of the Pomeron flux and the diffractive structure function of the proton. Such a model depends on the validity of Regge factorisation which requires that the Pomeron flux be independent of Q^2 .

For scattering of on-shell particles, like $\gamma p \rightarrow \gamma p$, the optical theorem ties the imaginary part of the forward elastic amplitude to the total γp cross section. This suggests,

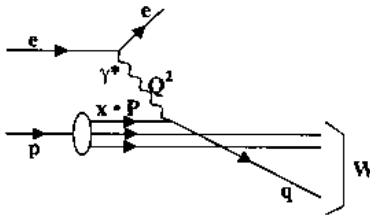


Figure 1: Diagram for deep inelastic nondiffractive scattering.

that also diffractive scattering of *virtual* photons leading to low-mass hadron production is closely related to the total virtual photon cross section e.g. in terms of their dependences on the total c.m. energy W . A - maybe naive - expectation is that if the total cross section has a W dependence of the type $\sigma^{\text{tot}} \propto W^\alpha$ then the diffractive cross section behaves as $\sigma^{\text{diff}} \propto W^{2\alpha}$.

In this report, preliminary high statistics results from the H1 [5] and ZEUS experiments [6], [7] at HERA are presented on total and diffractive deep inelastic scattering, see Figs. 1 and 2. The data have been obtained by colliding $E_e = 920$ (820) GeV protons head-on with $E_e = 27.5$ GeV electrons or positrons. At the Q^2 values of the diffractive analyses presented below, the reaction $e^-(k) p(P) \rightarrow e^-(k') + \text{anything}$ at fixed squared centre-of-mass energy, $s = (k + P)^2$, proceeds entirely by scattering of a virtual photon $q = k - k'$ on the proton, $\gamma^* p \rightarrow XN$. The reaction is described in terms of

$$Q^2 \equiv -q^2 = -(k - k')^2 \quad (1)$$

$$x = Q^2/(2P \cdot q) \quad (2)$$

For $E_e = 27.5$ GeV, $E_p = 920$ GeV the total c.m. energy is $\sqrt{s} = 318$ GeV. The fractional energy transferred to the proton in its rest system is $y = Q^2/(sx)$. The c.m. energy of the total hadronic system, W , is given by

$$W^2 = [p + (k - k')]^2 = m_p^2 + Q^2(1/x - 1) \approx Q^2/x = ys, \quad (3)$$

where m_p is the mass of the proton. The cross section for diffractive scattering, see Fig. 2, was studied in terms of Q^2 , W and M_X , the mass of the hadronic system X . The diffractive structure function was analyzed in terms of the momentum fraction of the proton carried by the Pomeron,

$$x_P = [(P - N) \cdot q]/(P \cdot q) \approx (M_X^2 + Q^2)/(W^2 + Q^2), \quad (4)$$

and the fraction of the Pomeron momentum carried by the struck quark,

$$\beta = Q^2 / [2(P - N) \cdot q] \approx Q^2 / (M_X^2 + Q^2). \quad (5)$$

The variables x_{ν} and β are related to the Bjorken scaling variable x via $x = \beta \cdot x_{\nu}$.

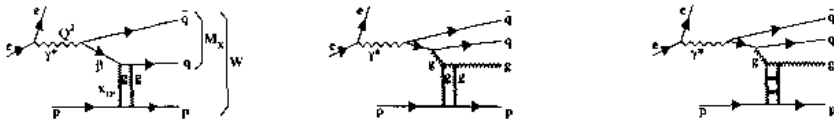


Figure 2: Diagrams for deep inelastic diffractive scattering via $ep \rightarrow eXN$.

2 Details of the analyses

The H1 analysis is based on information from the central detector combined with that from the PLUG calorimeter, the Forward Muon Detector and the Proton Remnant Tagger. The reaction analysed is of the type $ep \rightarrow eXY$, where X is the hadronic system observed in the central detector and Y is either a proton or a nucleonic system with mass $M_Y < 1.6$ GeV, separated by a large rapidity gap from the system X . The measured cross sections include diffractive and Reggeon exchange contributions.

The ZEUS results were obtained by two different techniques. In the LPS analysis, the leading proton spectrometer (LPS) combined with the central detector are used to isolate the reaction $\gamma^* p \rightarrow pX$. The LPS measures the four-momentum transfer squared t between incoming and outgoing proton. The FPC analysis, measuring $\gamma^* p \rightarrow XN$, $M_N < 2.3$ GeV, exploits the newly installed Forward Plug Calorimeter (FPC) to increase the kinematic range for diffraction. The diffractive component is identified with the $\ln M_X$ method [1] which rejects contributions from nonperipheral scattering and from Reggeon exchange.

3 Structure function F_2 and the total $\gamma^* p$ cross section

The structure function $F_2(x, Q^2)$ of the proton is shown in Fig. 3 as a function of x . The $F_2(x, Q^2)$ values measured by the FPC analysis (labelled ZEUS 98-99) are

in good agreement with previous results. Starting from $x = 1$ the structure function shows a rapid rise in the valence region ($x > 0.1$) which is followed by a plateau. At small $x < 0.01$ (sea region), $F_2(x, Q^2)$ rises rapidly as $x \rightarrow 0$; the rise is accelerated as Q^2 increases.

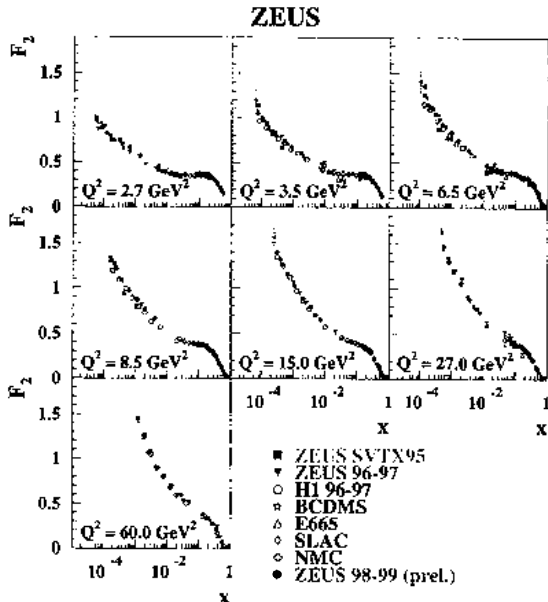


Figure 3: The proton structure function F_2 determined by the FPC analysis and compared with previous determinations.

From the measurements of F_2 the total cross section for virtual photon proton scattering,

$$\sigma_{\gamma^* p}^{\text{tot}} \equiv \sigma_T(x, Q^2) + \sigma_L(x, Q^2) \quad (6)$$

was extracted using

$$\sigma_{\gamma^* p}^{\text{tot}} = \frac{4\pi^2\alpha}{Q^2(1-x)} F_2(x, Q^2). \quad (7)$$

The total cross section multiplied by Q^2 , shown in Fig. 4, exhibits a strong rise with W , becoming steeper as Q^2 increases. This behaviour of σ_{tot} with W reflects the x -dependence of F_2 as $x \rightarrow 0$. Under the assumption that $\sigma_{\gamma^* p}^{\text{tot}}$ can be described by the exchange of a single Pomeron with trajectory $\alpha_P(t)$, the data yield $\sigma_{\gamma^* p}^{\text{tot}} \propto$

$W^{2(\alpha_P(0)-1)} = W^{0.32 \pm 0.05}$ for $Q^2 = 2.7 \text{ GeV}^2$ increasing to $\sigma_{\gamma^* p}^{\text{tot}} \propto W^{0.54 \pm 0.03}$ at $Q^2 = 55 \text{ GeV}^2$. The values of $\alpha_P(0) = 1.16 \pm 0.025$ ($Q^2 = 2.7 \text{ GeV}^2$) and 1.27 ± 0.015 ($Q^2 = 55 \text{ GeV}^2$) are much larger than observed for hadron-hadron scattering where $\alpha_P(0) = 1.096^{+0.012}_{-0.009}$ [8]. The strong rise of $\sigma_{\gamma^* p}^{\text{tot}}$ with W, Q^2 finds a natural explanation in pQCD [9] where the parton distribution functions of the proton evolve with x and Q^2 .

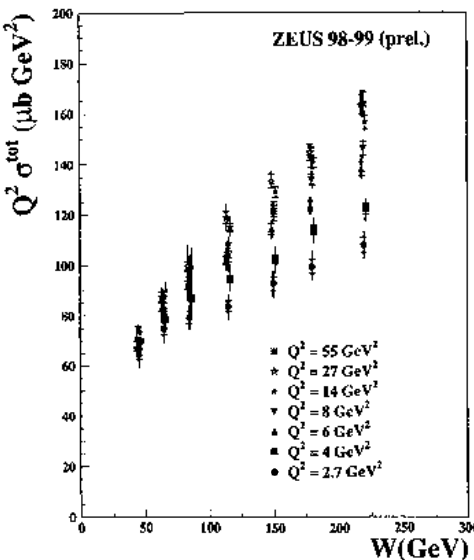


Figure 4: The total virtual photon proton cross section, $\sigma_{\text{tot}}(\gamma^* p)$, multiplied by Q^2 , as a function of the c.m. energy of the hadron system W , for the Q^2 intervals indicated. For better visibility, the points for successive values of Q^2 have been shifted in W by zero, $+1.5 \text{ GeV}$, -1.5 GeV .

In Regge theory, assuming the exchange of a single Pomeron, the cross section factorizes into the vertex functions for the $(\gamma^* IP\gamma^*)$ and $(pIPp)$ vertices, and a term which depends on W and on the intercept $\alpha_P(0)$ of the Regge trajectory, but not on Q^2 . The strong rise of $\alpha_P(0)$ with increasing Q^2 implies that in the case of single Pomeron exchange, Regge factorisation is broken.

It has been conjectured [10] that the dominant contributions to the total $\gamma^* p$ cross section arise from Pomeron plus multi-Pomeron (Regge cut) exchanges. The cut contribution is expected to be important only at low Q^2 while for Q^2 above 5-10 GeV^2 the bare pomeron should be dominant. Recently, it has been conceded that the continuing rise of $\alpha_P(0)$ with Q^2 observed beyond $Q^2 = 10 \text{ GeV}^2$ may have to be attributed to QCD evolution [11].

4 Diffractive cross section

The LPS analysis determined the diffractive cross section as a function of t . Parametrization of the diffractive cross section as

$$d\sigma_{\gamma^* p \rightarrow Xp}^{diff}/dt \propto e^{-bt}, \quad (8)$$

led to the values of the slope b shown in Fig. 5 as a function of x_p . Taking an average over $2 < Q^2 < 100 \text{ GeV}^2$, $M_X > 1.5 \text{ GeV}$ and $0.075 < |t| < 0.35 \text{ GeV}^2$ yielded $b = 7.9 \pm 0.5(\text{stat.})^{+0.8}_{-0.5}(\text{syst.}) \text{ GeV}^{-2}$. The value for b is similar to values measured for elastic πp scattering at high energy. Assuming b to be independent of t , the

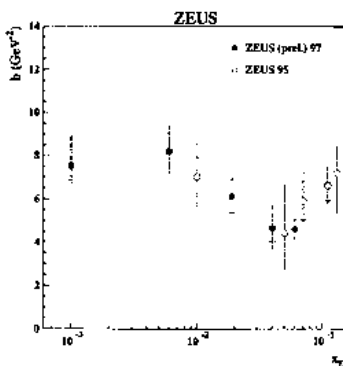


Figure 5: The slope b of the diffractive cross section (ZEUS-LPS).

measured LPS diffractive cross sections were extrapolated to the full kinematically allowed t -range. Figure 6 presents the differential cross section, $d\sigma_{\gamma^* p \rightarrow Xp}/dM_X$ for diffractive scattering plus Reggeon exchange, as a function of Q^2 for different M_X and W bins. For $x_p \geq 0.01$ substantial contributions from Reggeon exchange are expected in these data. At low Q^2 , the cross section drops slowly with increasing Q^2 . For $Q^2 > 10 \text{ GeV}^2$ the cross section is falling rapidly with Q^2 . If parametrized in terms of $d\sigma_{\gamma^* p \rightarrow Xp}^{diff}/dM_X \propto (1/Q^2)^n$ one finds for $M_X \leq 5 \text{ GeV}$, n to be larger than unity, which shows the presence of a substantial higher twist component. For $M_X > 22 \text{ GeV}$ the power n is about unity, compatible with a dominant leading twist behaviour.

In the FPC analysis, the diffractive cross section is determined with the $\ln M_X$ method which rejects Reggeon contributions. The diffractive cross section $d\sigma_{\gamma^* p \rightarrow XN}^{diff}/dM_N$, $M_N < 2.3 \text{ GeV}$, measured in the FPC analysis is shown in Fig. 7 as a function of W for different Q^2 and M_X . Comparison with the LPS data from $x_p < 0.01$ shows that about 30% of the FPC cross section is due to nucleon dissociation with $M_N < 2.3 \text{ GeV}$.

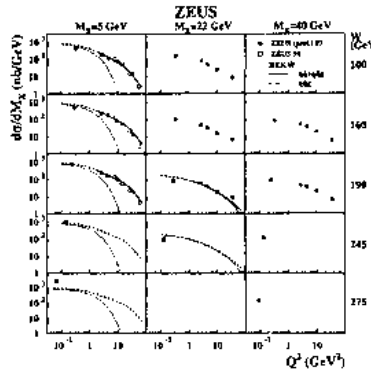


Figure 6: The cross section for diffractive scattering plus Reggeon exchange as a function of Q^2 for different bins in M_X and W (ZEUS-LPS). Reggeon contributions can be neglected for $(Q^2 + M_X^2)/(Q^2 + W^2) < 0.01$.

In the lowest M_X bin, $0.28 < M_X < 2$ GeV, the diffractive cross section is rather constant with W , while at higher M_X , a strong rise with W is observed. Fits of $d\sigma^{diff}/dM_X$ to the form

$$d\sigma^{diff}/dM_X = h \cdot W^{a^{diff}} \quad (9)$$

resulted in the a^{diff} values shown in Fig. 8(left) as a function of Q^2 . For $M_X > 2$ GeV, there is a clear tendency for a^{diff} to rise for $Q^2 \geq 20$ GeV 2 .

Assuming single Pomeron exchange, a^{diff} is related to the intercept of the Pomeron trajectory, $\overline{\alpha_p} = 1 + a^{diff}/4$, where $\overline{\alpha_p}$ is the Pomeron trajectory averaged over the t -distribution, $\overline{\alpha_p} \approx \alpha_p^{diff}(0) - 0.02$. Hadron-hadron scattering leads to $\alpha_p(0) = 1.096_{-0.009}^{+0.012}$ (see above) and to a t -averaged value of $a^{soft} = 0.302_{-0.036}^{+0.048}$ shown by the band in Fig. 8(left), which is in agreement with the data at $Q^2 < 10$ GeV 2 . For $Q^2 > 20$ GeV 2 , however, a^{diff} lies above a^{soft} : the data give evidence for a^{diff} rising with Q^2 which indicates breaking of Regge factorisation under the assumption that a single Regge pole contributes.

In Fig. 8(right) the Q^2 -dependence of $\alpha_p^{tot}(0)$ obtained from the W dependence of the total $\gamma^* p$ -cross section is compared with $\alpha_p^{diff}(0)$ measured for the diffractive cross section for $4 < M_X < 8$ GeV. The diffractive result lies approximately half-way in between the soft Pomeron value and the result for $\alpha_p^{tot}(0)$ obtained from $\sigma_{\gamma^* p}^{tot}$. The diffractive data are well described by the shaded band which represents 'half' of the W rise of the total cross section, $\alpha_{p,1/2} = 1 + (\alpha_p^{tot}(0) - 1)/2$. In other words, for $M_X > 2$ GeV, the diffractive and total cross sections have approximately the same W dependence.

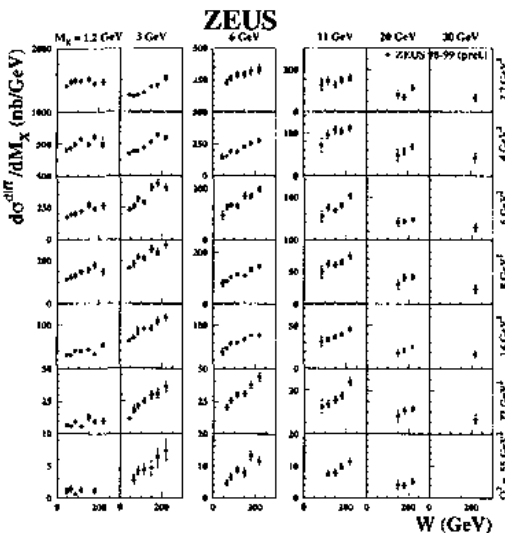


Figure 7: The diffractive cross section as a function of W for different bins in M_X and Q^2 (ZEUS-FPC).

4.1 M_X - dependence of the diffractive cross section

The M_X - dependence of the diffractive cross section, multiplied by Q^2 , is shown in Fig. 9 at $W = 220$ GeV for different values of Q^2 . The cross section was multiplied by a factor of Q^2 since a leading twist behaviour will lead to approximate constancy for $Q^2 \cdot d\sigma^{diff}/dM_X$ as a function of Q^2 . The region of M_X below about 6 GeV shows a rapid decrease with Q^2 which is evidence for a predominantly higher twist behaviour. Above $M_X = 11$ GeV, only little dependence on Q^2 is observed; the diffractive cross section is here of leading twist.

4.2 Diffractive contribution to the total cross section

Under certain assumptions, the (W, Q^2) dependences of the total and diffractive cross sections are related to each other. One may expect, for instance, that the imaginary part of the amplitude for elastic scattering, $A_{\gamma^* p \rightarrow \gamma^* p}(t, W, Q^2)$, at $t = 0$ is linked to the total cross section by a generalisation of the optical theorem to virtual photon scattering. Assume now $\sigma_{\gamma^* p}^{tot} \propto W^{2(\alpha_P(0)-1)}$. The additional assumption that elastic and inclusive diffractive amplitudes at $t = 0$ are purely imaginary and have the same (W, Q^2) dependences then leads to $A_{\gamma^* p \rightarrow \gamma^* p}(t = 0, W, Q^2) \propto W^{2(\alpha_P(0)-1)}$. Provided, that the real part of the scattering amplitudes can be neglected the rise of

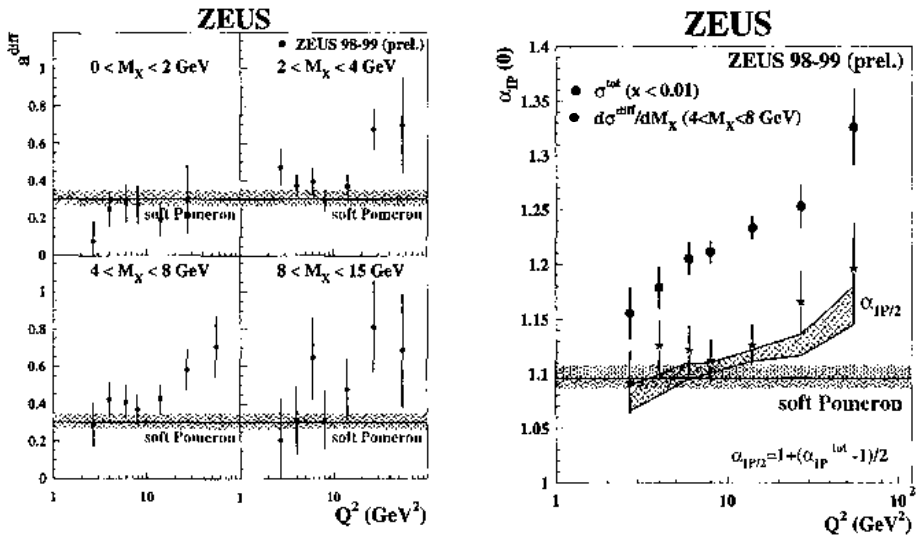


Figure 8: Left: The power a^{diff} obtained from fitting the diffractive cross section, $d\sigma_{\gamma^* p \rightarrow XN}^{\text{diff}}(M_X, W, Q^2)/dM_X = h \cdot W^{a^{\text{diff}}}$, as a function of Q^2 for different M_X -bins. The shaded band shows the expectation for a^{diff} in the case of a soft Pomeron. Right: The intercept of the Pomeron trajectory, $\alpha_p(0)$, as a function of Q^2 , obtained from the W -dependences of the total $\gamma^* p$ cross section and from the diffractive cross section for $M_X = 4 - 8 \text{ GeV}$. The shaded band shows the expectation for a soft Pomeron. The cross hatched band represents "half" of the W -rise of the total cross section, $\alpha_{p,1/2} = 1 + (\alpha_p^{\text{tot}}(0) - 1)/2$ (ZEUS-FPC).

the diffractive cross section with W should then be proportional to $W^{4(\alpha_p(0)-1)}$, in contradiction with the data shown above.

The ratio $r_{\text{tot}}^{\text{diff}}$ of the diffractive cross section (integrated over the measured M_X -range) to the total cross section,

$$r_{\text{tot}}^{\text{diff}} \equiv \frac{\sigma^{\text{diff}}}{\sigma^{\text{tot}}} = \frac{\int_{M_a}^{M_b} dM_X d\sigma_{\gamma^* p \rightarrow XN, M_N < 2.3 \text{ GeV}}^{\text{diff}} / dM_X}{\sigma_{\gamma^* p}^{\text{tot}}} \quad (10)$$

was evaluated as a function of W in bins of Q^2 . The low M_X bins show a strong decrease of $r_{\text{tot}}^{\text{diff}}$ with increasing Q^2 , while for $M_X > 4 \text{ GeV}$ this decrease becomes less dramatic, and for $M_X > 8 \text{ GeV}$ almost no Q^2 dependence is observed. Here, the diffractive cross section has approximately the same W and Q^2 -dependences as the total cross section. The observed near constancy of $r_{\text{tot}}^{\text{diff}}$ is explained by the dipole

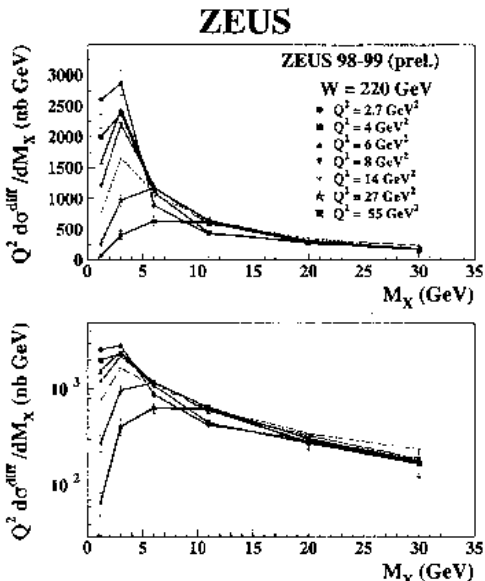


Figure 9: The diffractive cross section multiplied by Q^2 , $Q^2 \cdot d\sigma_{\gamma^* p \rightarrow X N}^{\text{diff}} / dM_X$, $M_N < 2.3$ GeV, for $W = 220$ GeV as a function of M_X for the Q^2 intervals indicated. Top: on a linear scale; Bottom: on a logarithmic scale. The lines connect the points measured for the same value of Q^2 (ZEUS-FPC).

saturation model [12]. The term “dipole” refers to the $(q\bar{q})$ state resulting from the $\gamma^* \rightarrow q\bar{q}$ splitting, see Fig. 2.

The ratio of the total observed diffractive cross section to the total cross section was evaluated as a function of Q^2 for the highest W bin, 200 -245 GeV, which provides the highest reach in the diffractive mass, $0.28 < M_X < 35$ GeV. At $Q^2 = 2.7 \text{ GeV}^2$, $\sigma_{\text{obs}}^{\text{diff}} / \sigma^{\text{tot}}$ reaches $19.8^{+1.5\%}_{-1.4\%}$, decreasing slowly with Q^2 to $10.1^{+0.6\%}_{-0.7\%}$ at $Q^2 = 27 \text{ GeV}^2$. Hence, diffractive processes account for a substantial part of the total deep inelastic cross section. The range in $M_X^2/W^2 \leq 0.024$ reached in this analysis has to be compared with the limit $M_X^2/W^2 = 0.05 - 0.1$ up to which diffractive contributions have been observed in hadronic interactions. It is conceivable, therefore, that the *total* diffractive contribution to DIS is considerably larger than obtained here by integration over a limited range in M_X^2/W^2 .

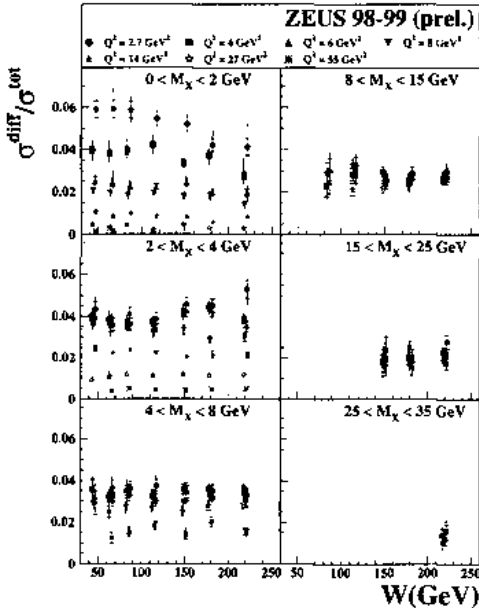


Figure 10: The ratio of the diffractive cross section, integrated over the M_X intervals indicated, $\int_{M_a}^{M_b} dM_X d\sigma_{\gamma^* p \rightarrow X N, M_N < 2.3 \text{ GeV}}^{\text{diff}} / dM_X$, to the total $\gamma^* p$ cross section, $r_{\text{tot}}^{\text{diff}} = \sigma^{\text{diff}} / \sigma_{\gamma^* p}^{\text{tot}}$, as a function of W for the M_X and Q^2 intervals indicated (ZEUS-FPC).

5 Diffractive structure function of the proton

The diffractive structure function of the proton, $F_2^{D(3)}(\beta, x_p, Q^2)$, can be related to the diffractive cross section for $W^2 \gg Q^2$ as follows:

$$\frac{1}{2M_X} \frac{d\sigma_{\gamma^* p \rightarrow X N}(M_X, W, Q^2)}{dM_X} = \frac{4\pi^2 \alpha}{Q^2(Q^2 + M_X^2)} x_p F_2^{D(3)}(\beta, x_p, Q^2). \quad (11)$$

If $F_2^{D(3)}$ is interpreted in terms of quark densities, it specifies the probability to find, in a diffractive process, a quark carrying a fraction $x = \beta x_p$ of the proton momentum.

5.1 Data from H1

The diffractive structure function multiplied by x_p is shown in Fig. 11 as a function of x_p for different β and Q^2 values. New data were added in the regions of very small

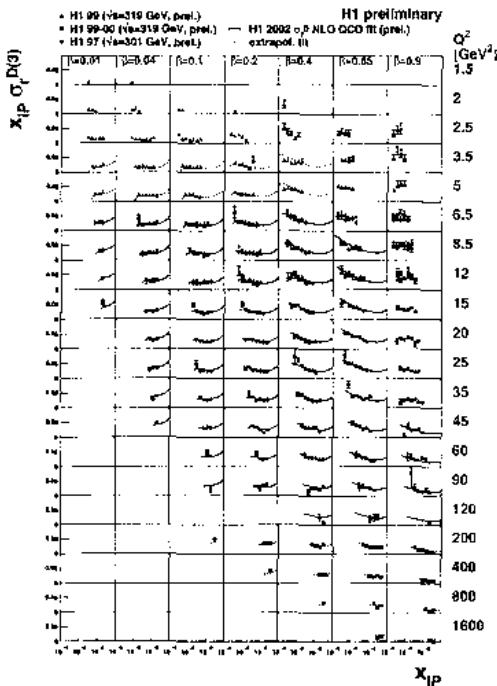


Figure 11: The diffractive structure function of the proton as a function of x_{IP} for different β and Q^2 values (H1).

and very large Q^2 . Note, that for $x_{IP} > 0.01$, also Reggeon contributions might be present. The data now span the Q^2 -range from 1.5 to 1600 GeV 2 . At small x_{IP} and $Q^2 < 60$ GeV 2 , the diffractive structure function is seen to rise as $x_{IP} \rightarrow 0$.

The curves represent a QCD fit to the data with $6 < Q^2 < 120$ GeV 2 , see below. The Pomeron was modelled in terms of a light quark flavour singlet:

$$\sum(z) = u(z) + d(z) + s(z) + \bar{u}(z) + \dots \quad (12)$$

plus a gluon density $g(z)$. By factorising the diffractive structure function of the proton into the probability for finding a Pomeron with a fraction x_{IP} of the proton momentum times the structure function of the Pomeron,

$$F_2^{D(3)}(x_{IP}, \beta, Q^2) \equiv \sigma_r^{D(3)} = f_{IP}(x_{IP}) \cdot F_2^{D(2)}(\beta, Q^2) \quad (13)$$

one can study the structure function of the Pomeron, denoted by H1 as the reduced cross section divided by the Pomeron flux, $\sigma_r^{D(3)}/f_{IP}(x_{IP})$, which is shown in

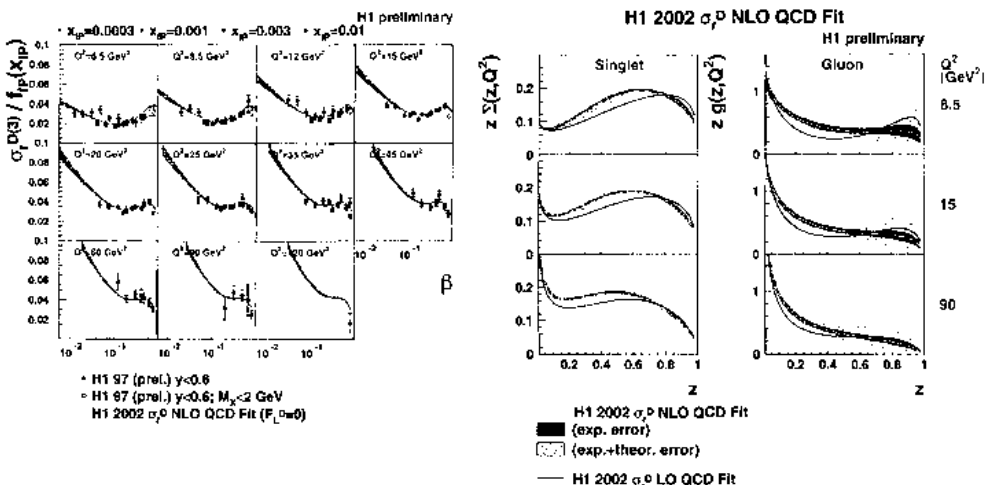


Figure 12: Left: The reduced cross section $\sigma_r^{D(3)}/f_{IP}(x_p)$ as a function of β for different x_p and Q^2 values. Right: Diffractive parton densities obtained from the QCD fit, normalized such that the pomeron flux is unity at $x_p = 0.003$. Right: quark singlet distributions under the assumption $u = d = s = \bar{u} = \bar{d} = \bar{s}$, plus the gluon density. The inner error bands show the experimental uncertainties; the outer error bands include the experimental and theoretical uncertainties (H1).

Fig. 12(left) as a function of β . The NLO QCD fit shown by the curves gives a good description of the data.

The diffractive quark and gluon densities resulting from the fit are displayed in Fig. 12(right). The inner (outer) error bands show the experimental errors (theoretical uncertainties). According to H1, $75 \pm 15\%$ of the Pomeron momentum with $0.01 < z < 1$ is carried by gluons, the rest by quarks.

5.2 Data from ZEUS

Figure 13 shows the diffractive structure function of the proton, multiplied by x_p , measured by ZEUS-LPS as a function of x_p for different values of β and Q^2 . The data show $x_p F_2^{D(3)}$ rising as $x_p \rightarrow 0$. Some bins of β, Q^2 show $x_p F_2^{D(3)}$ also rising as $x_p \rightarrow 1$: this rise is attributed to Reggeon exchange in the t -channel.

The measurements of $x_p F_2^{D(3)}$ from ZEUS-FPC are displayed in Fig. 14. For the lowest M_X region, which corresponds to high β , little dependence on x_p is observed, in contrast to the lower β region where $x_p F_2^{D(3)}$ rises strongly as $x_p \rightarrow 0$, reflecting

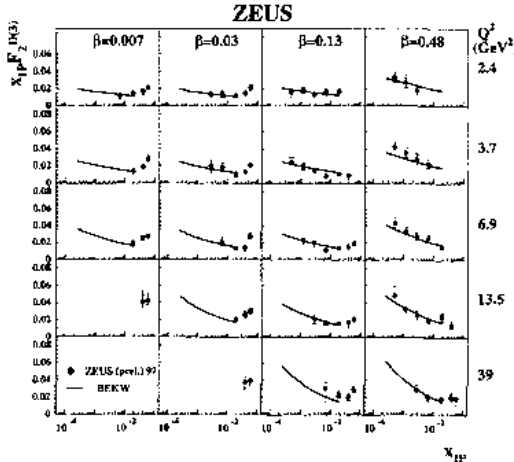


Figure 13: The diffractive structure function of the proton as a function of x_P for different β and Q^2 values. For $x_P > 0.01$, the data include some Reggeon contributions. The curves show the BEKW(mod) fit performed to the ZEUS-FPC data (ZEUS-LPS).

the rapid increase of the diffractive cross section with rising W . The strong increase of $x_P F_2^{D(3)}$ as $x_P \rightarrow 0$ is reminiscent of the rise of the proton structure function $F_2(x, Q^2)$ as $x \rightarrow 0$ which in pQCD is attributed to the rapid increase of the gluon density in the proton as $x \rightarrow 0$.

In determining the structure function of the Pomeron, ZEUS allowed the flux of Pomerons from the proton to depend on x_P and on Q^2 :

$$F_2^{D(3)}(x_P, \beta, Q^2) = f_P(x_P, Q^2) \cdot F_2^P(\beta, Q^2) \quad (14)$$

where $f_P(x_P, Q^2)$ is generically called the Pomeron flux factor. In this model, the flux factor is assumed to be of the form

$$f_P(x_P, Q^2) = (C/x_P) \cdot (x_0/x_P)^{n(Q^2)}. \quad (15)$$

Taking for the arbitrary normalization constant: $C = 1$, leads to

$$F_2^P(\beta, Q^2) = x_0 \cdot F_2^{D(3)}(x_0, \beta, Q^2). \quad (16)$$

For a given (Q^2, β) combination, those $x_P F_2^{D(3)}$ measurements with $0.5 \cdot x_0 < x_P < 1.5 \cdot x_0$ were selected. The resulting measurements of $F_2^P(\beta, Q^2)$ are presented in Fig. 15. The structure function of the Pomeron shows several remarkable properties. For $\beta > 0.1$, it exhibits a maximum near $\beta = 0.5$, consistent with a $\beta(1 - \beta)$ variation expected in the dipole model [13] where the lowest order term arises from photon splitting into a $q\bar{q}$ dipole. In the region of small $\beta < 0.1$, F_2^P is rising as $\beta \rightarrow 0$, and

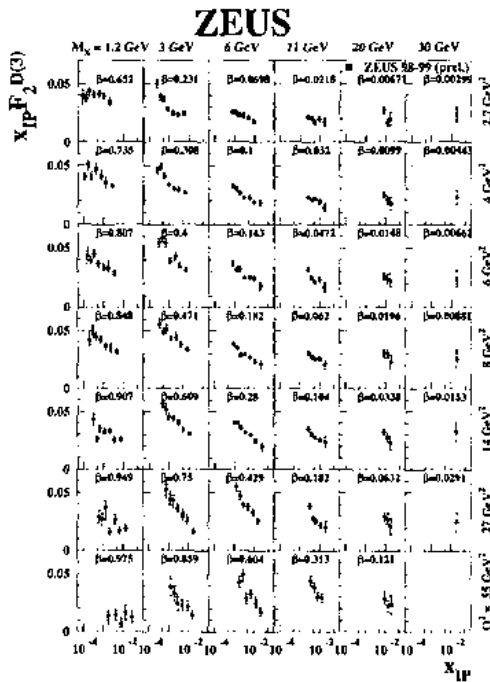


Figure 14: The diffractive structure function of the proton multiplied by x_p , $x_p F_2^{D(3)}$, as a function of x_p , for different regions of Q^2 and β . Also indicated are the values of M_X (ZEUS-FPC).

is rising as Q^2 increases. This is consistent with photon splitting into $q\bar{q}g$ plus higher order configurations. These features strongly suggest a pQCD-like evolution with β and Q^2 of diffraction in DIS.

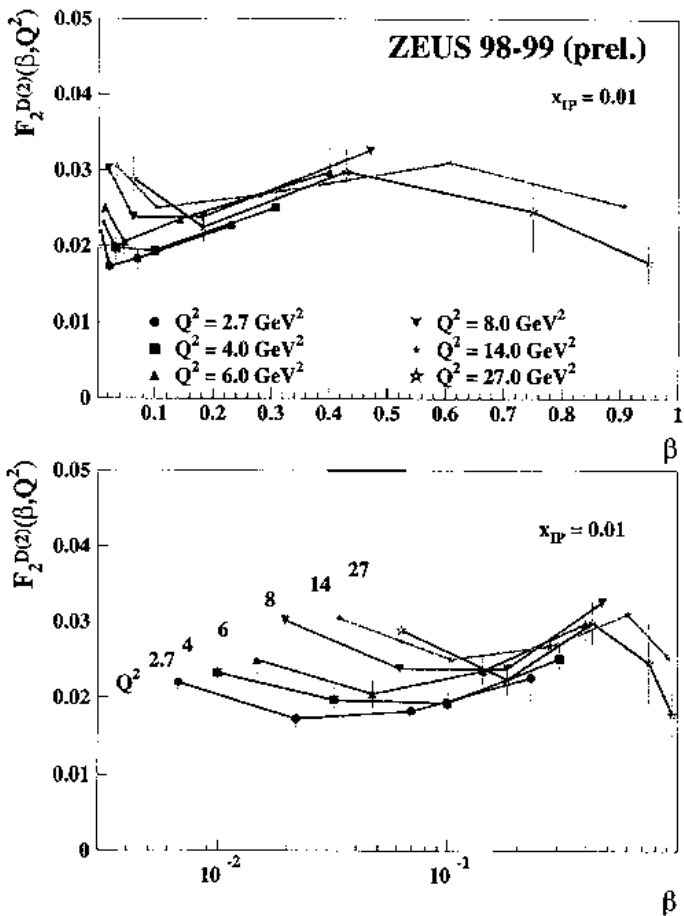


Figure 15: The structure function $F_2^{D(2)}(\beta, Q^2)$ for $\gamma^* p \rightarrow XN, M_N < 2.3 \text{ GeV}$, as a function of β , for the Q^2 values indicated, as extracted from the $x_p F_2^{D(3)}$ values measured near $x_p = 0.01$, see text. The straight lines connect measurements at the same value of Q^2 (ZUS-FPC).

6 Summary

The total $\gamma^* p$ cross section is strongly rising with c.m. energy W . Parametrising $\sigma_{\gamma^* p}^{tot} \propto W^{2(\alpha_P - 1)}$, shows that the power α_P is rising with Q^2 . Under the assumption of a single Pomeron exchange, this result implies that Regge factorisation is broken in DIS. The diffractive cross section shows a similar W dependence while naive expectation would lead to a much steeper rise: $d\sigma_{\gamma^* p \rightarrow XN}^{diff}/dM_X \propto W^{4(\alpha_P - 1)}$. Under the assumption of a single Pomeron exchange, also the diffractive data give evidence for breaking of Regge factorisation with Q^2 . Inspection of the Q^2 dependence of the diffractive cross section shows that in the region of low M_X , $Q^2 \cdot d\sigma_{\gamma^* p \rightarrow XN}^{diff}/dM_X$ decreases fast with Q^2 , while for $M_X \geq 10$ GeV, the diffractive cross section is of leading twist, $Q^2 \cdot d\sigma_{\gamma^* p \rightarrow XN}^{diff}/dM_X$ being approximately constant with Q^2 . Comparison of diffractive and total cross sections shows that diffraction accounts for a substantial part of inclusive deep inelastic scattering.

The diffractive structure function of the proton, $x_p F_2^{D(3)}(x_p, \beta, Q^2)$, for $M_X > 2$ GeV is strongly rising as $x_p \rightarrow 0$. This is reminiscent of the rise of the proton structure function $F_2(x, Q^2)$ as $x \rightarrow 0$, which in pQCD is attributed to the rapid increase of the gluon density in the proton as x becomes small.

The diffractive structure function of the proton has been factorised into the probability for finding a Pomeron in the proton and the structure function of the Pomeron, $F_2^P(\beta, Q^2)$. The data from H1 on $x_p F_2^{D(3)}$ can be described by pQCD, assuming the flux of Pomerons to be independent of Q^2 and making an ansatz for the quark and gluon densities. About three quarters of the Pomeron momentum was found to be carried by gluons.

The ZEUS data for the structure function of the Pomeron show several remarkable properties. There is an indication that $F_2^P(\beta, Q^2)$ decreases at high β with increasing Q^2 . For $0.9 > \beta > 0.1$, F_2^P is consistent with a $\beta(1 - \beta)$ variation as expected by the dipole model. In the region $\beta < 0.1$, F_2^P is rising as $\beta \rightarrow 0$, and is also rising as Q^2 increases. These features observed at high and low β strongly suggest a pQCD-like evolution of F_2^P with β and Q^2 . Taken together with the observed (x_p, Q^2) dependence of $x_p F_2^{D(3)}(x_p, \beta, Q^2)$, the data suggest the diffractive structure function of the proton to evolve in all three variables: Q^2 , β and x_p .

In conclusion, we are beginning to understand diffraction in deep inelastic scattering in terms of QCD evolution of diffractive parton distribution functions of the proton. A further extension of the kinematic regime for DIS diffraction and an increase of the event statistics by an order of magnitude will help to reach eventually a similar precision for diffractive as for inclusive parton densities. Finally, since the rapidity space for QCD evolution is smaller for diffraction than for nonperipheral inclusive scattering, a combined analysis of both processes should lead to a modification of the inclusive parton densities which had been extracted so far for the nucleon.

References

- [1] ZEUS Coll., J. Breitweg et al., Eur. Phys. J. C6, 43 (1999).
- [2] J.C. Collins, Phys. Rev. D57, 3051(1998); Erratum Phys. Rev. D61, 019902 (1998).
- [3] K. Goulianatos, Nucl. Phys. B, Proc. Suppl. 12, 110 (1990).
- [4] G. Ingelman and P.E. Schlein, Phys. Lett. B152, 256 (1985).
- [5] H1 Collaboration, Contribution submitted to Int. Europhysics Conf. on High Energy Physics,2003, Aachen, Germany, Abstract 089.
- [6] ZEUS Collaboration, Contribution submitted to Int. Europhysics Conf. on High Energy Physics,2003, Aachen, Germany, Abstract 538.
- [7] ZEUS Collaboration, Contribution submitted to Int. Europhysics Conf. on High Energy Physics,2003, Aachen, Germany, Abstract 540.
- [8] A. Donnachie and P.V. Landshoff, Nucl. Phys. B244, 322 (1984); Phys. Lett. B296, 227 (1992). J.R. Cudell, K. Kang and S.K. Kim, Phys. Lett. B395, 311 (1997).
- [9] V.N. Gribov and L. N. Lipatov, Sov. J. Nucl. Phys. 15, 438 (1972); ibid. 675. L.N. Lipatov, Sov. J. Nucl. Phys. 20, 95 (1975). Yu. L. Dokshitzer, Sov. Phys. JETP 46, 641 (1977). G. Altarelli and G. Parisi, Nucl. Phys. B126, 298 (1977).
- [10] A. Capella, A. Kaidalov, C. Merino and J. Tran Tanh Van, Phys. Lett. B337, 358 (1994)
- [11] A. Kaidalov, C. Merino and D. Peterman, hep-ph/9911331 (1999).
- [12] K. Golec-Biernat and M. Wüsthoff, Phys. Rev. D59,014017 (1999); Phys. Rev. D60, 114023 (1999).
- [13] J.D. Bjorken, J.B. Kogut and D.E. Soper, Phys. Rev. D3, 1382 (1970). N.N. Nikolaev and B.G Zakharov, Z. Phys. C49, 607 (1991); Z. Phys. C53, 331 (1992). A.H Mueller, Nucl. Phys. B415, 373 (1994). J. Bartels, K. Golec-Biernat and H. Kowalski, Phys. Rev. D66, 014001 (2002).

CHAIRMAN: G. WOLF

Scientific Secretaries: F. Noferini, R. Preghenella

DISCUSSION

- *D'Enterria:*

This morning we have seen many comparisons of HERA data to QCD predictions based on standard DGLAP evolution. How do models based on the idea of gluon saturation (e.g. the Golec-Biernat and Wüstof approach) compare to the new data on diffractive photoproduction?

- *Wolf:*

As far as the data go which were previous to this year, the model of Golec-Biernat and Wüstoff does a very good job, up to Q^2 , if I remember correctly, of about 30 or 50 GeV². The new data on inclusive diffraction have not yet been compared with this model. There is also an extension of this model by Kowalski and Teaney based on the impact parameter distribution of the partons in the proton, which should be compared with the new data.

- *Cerri:*

How do you see the short and long term role of HERA in the High Energy Physics community? What are you planning next?

- *Wolf:*

HERA had been closed at the end of 2000, followed by a complete remodelling of the interaction regions for H1 and ZEUS in order to increase the luminosity by a factor 3-5 and to equip both interaction regions with spin rotators to allow left-handed / right-handed electron and positron proton scattering. The remodelling has been tested during 2002 and beginning of 2003 with the following results: the specific luminosity has increased by a factor 3 to 5 and the polarization achieved within 2 weeks was 50%, in agreement with expectation. However, the experiments were hampered by a very large background of synchrotron radiation and stray particles, due in part to the superconducting quadrupoles installed inside the detector. So HERA operation was interrupted in March of this year to redo the masking in the interaction regions of H1 and ZEUS. This work is finished and HERA is now being run in with beams. A first data run of about 6 weeks is scheduled for October to December. HERA can be expected to reach next year high luminosity with acceptable background so that the foreseen program of 100 pb to 150 pb for each of the four types of beams: right-handed electrons, left-handed electrons, right-handed positrons, left-handed positrons, can be completed by 2007. PETRA, the electron/positron and proton injector for HERA will then be revamped for exclusive production of

synchrotron radiation. At that time, particle physics will stop at DESY and the HEP sector expects to concentrate on the planned electron-positron collider TESLA.

- *Cifarelli:*

As far as I remember, the Pomeron was defined as a more complicated object than qq. Could you please comment?

- *Wolf:*

What is traditionally called a Pomeron is a colour neutral state which leads to cross sections that are constant or rising with c.m. energy independent of Q^2 . A colour neutral state can be made of quark-antiquark or gluon-gluon pairs or of more involved configurations. What we see now in the data I have presented is that the energy dependence of the diffractive cross section depends also on the resolution Q^2 . In order to describe these data, one needs now an infinite numbers Pomerons as considered e.g. by Lipatov and co-workers in the BFKL approach.

- *Laycock:*

The experimental data above Q^2 of 10 are consistent with being flat!

- *Wolf:*

No, look for example at the total cross section and its behaviour with W. The W slope is rising continuously for Q^2 between 2 and 100 GeV 2 . Also, the ZEUS data on diffraction indicate that the W-slope is rising with Q^2 for $Q^2 > 10$ GeV 2 . For a single Pomeron, the slope should be independent of Q^2 . If a process with Pomeron + cut is added, as advocated for example by Kaidalov and others, one expects the slope to increase at low Q^2 , e.g. for $Q^2 < 10$ GeV 2 , and then reach a constant value, in contradistinction to the data.

- *Lendermann:*

How universal is diffraction? What conclusion can we draw from comparing ep and pp results on diffraction?

- *Wolf:*

In contrast to original expectations, a large fraction (10 – 40 %) of deep-inelastic electron proton scattering (DIS) proceeds via diffraction in much the same way as observed for proton-proton scattering. However, in distinction to proton-proton scattering, DIS depends on a further variable, the spatial resolution Q^2 , and the new data show that in DIS diffraction depends also on Q^2 .

- *Shekovtsova:*

In your analysis, $F_L = 0$. Are you going to take it into account in the future experiment?

- *Wolf:*

No, this is not true: only an extra term involving F_L was assumed to be 0. The contribution from this term is negligible for $W < 200$ GeV. For certain subclasses of DIS diffraction, like vector-meson production, the production and decay distributions tell one the fraction produced by longitudinal photons. Assuming the low mass bin ($MX < 2$ GeV) to be completely dominated by the production of vector-mesons, the highest W points from ZEUS would have to be increased by about 5%.

- *Schäfzel:*

How do you deduce from $F_2^{D(2)}$ (the structure function of the Pomeron) that the Pomeron is quark dominated?

- *Wolf:*

Sorry, I was careful to say that the high beta region – i.e. beta above 0.1 – looks like being quark dominated. The region beta < 0.1 looks gluon dominated (see also comparison with the BEKW fit). Note also that the ZEUS data indicate a dip around beta = 0.1 which speaks against having a predominant gluon contribution all the way from beta = 0.01 up to beta = 0.9 as stipulated by the H1 QCD analysis.

- *Schäfzel:*

Shouldn't you be aiming to do some sort of QCD analysis to extract the structure function with the parton density?

- *Wolf:*

Yes.

- *Laycock:*

H1 extracts F_L from their NLO QCD fit?

- *Wolf:*

I think so.

- *Lipatov:*

You did not mention the alternative description of the existing experimental data by the BFKL approach, where the number of Pomerons is infinite, which is a consequence of perturbative QCD. What do you think about this approach?

- *Wolf:*

The BFKL approach is certainly viable.

- *Laycock:*

QCD hard scattering factorization for diffractive DIS ($\gamma^* p \rightarrow X p$) has been proven now for several years: how do we at HERA make experimental progress?

- *Wolf:*

We (ZEUS) have still something like 20 times more data for this subject than we have analysed up to now. This will give us precise data up to Q^2 of a few hundred GeV^2 . Secondly, we have to perform a DGLAP-type analysis of diffraction like H1 has already done. Thirdly, those groups performing DGLAP type QCD analyses using the proton structure function F_2 and others as input in order to extract the parton densities of the proton, must include diffraction as a separate process. Diffraction has a smaller rapidity space available for QCD evolution.

- *Abramowicz:*

I have a comment: the factorization theorem was proven for the inclusive case of structure function evolution.

- *Wolf:*

No. What I meant was: one has to allow for two components in the QCD evolution: the inclusive one and the diffractive one. They have different evolution space in rapidity for the quark, gluon cascade.

- *Abramowicz:*

No, because for whatever we know, the Pomeron could be simply a soft particle which is there in the initial conditions and therefore the evolution for the inclusive part is the same for the diffractive part. This implies that one cannot take out diffraction from the evolution.

- *Wolf:*

I did not mean to exclude diffraction from QCD evolution. What I mean, is that diffraction has a smaller space in rapidity for QCD evolution than the inclusive process and this has to be taken into account.

THE LARGE HADRON COLLIDER: A STATUS REPORT

Luciano Maiani

CERN

1211 Geneva 23

SUMMARY

1. Introduction
2. New Physics at High Energy
3. LHC Construction:
 - Civil Engineering
 - Machine components
 - Installation in the Tunnel
4. LHC Detectors
5. Computing
6. Conclusions

1. Introduction

The installation of a Large Hadron (proton-proton) Collider in the LEP tunnel, Fig. 1, was first considered at the beginning of the 80's and it was approved by the CERN Council in December 1996. The tunnel has a circumference of 27 km. The nominal beam energy was determined to be 7 TeV, corresponding to a nominal magnetic field in the cryogenic dipoles of 8.3 Tesla¹.

From the outset, it was decided that the LHC should accelerate both protons and heavy ions. The LHC energy range and luminosity will allow it to aim at several physics goals.

- i. the search for the Higgs boson in the whole mass region where it is predicted by the Standard Theory, from the LEP reach up to almost 1 TeV;
- ii. the search for new particles, such as those associated to Supersymmetry, indicated as the remedy to the "unnaturalness" of the Standard Theory itself;
- iii. high precision study of CP violation in B meson decays;
- iv. the study of the physical properties of the new phase of nuclear matter at high temperature (quark-gluon plasma) that supposedly is produced in relativistic heavy ion collisions.

In 1996, a cost was stated for the LHC proper (the hardware that goes in the LEP tunnel and the civil engineering works to adapt the tunnel and to build the experimental areas) assuming that all other expenses would be covered by the normal operational budget of the Laboratory.

During the years 2000 and 2001, the LHC programme underwent a full cost and schedule review, including the costs associated with the refurbishing of the injection line (which uses the existing PS and the SPS machines), the cost-to-completion of the four detectors, the cost of the computing infrastructure, as well as overall personnel costs and contingency. The result was approved by Council in December 2002 to form the basis of the present CERN planning and is as follows.

- **Machine:** 4.8 BCHF. This includes:
 - Materials and CERN Personnel expenses for the whole LHC;
 - 330 MCHF for residual contingency and for a reserve for the cost escalation of LHC contracts.
- **Detectors:** 1.2 BCHF, of which 20% is supported by the CERN budget.

The figures given above include special contributions that CERN has received from the Host States (Switzerland and France) and from several CERN non-Member States (US, Japan, Russia, Canada, India), the latter adding to about 0.75 BCHF. These contributions are mostly in-kind, with items provided by industry and by the main particle physics laboratories in these countries. The world-wide participation to the machine and detector construction makes the LHC the first really global particle physics project.

The construction of such a large machine is requiring an unprecedented effort from the Laboratory. The last approved Long Term Plan, which covers the period 2003-2010, indicates that around 80% of CERN resources (Personnel plus Materials) are allocated to the LHC programme of the total resources (directly \approx 50%, indirectly \approx 30%).

In this talk, I'd like to first review briefly the physics that can be expected from the LHC. For time reasons, I will restrict to the High Energy frontier, namely the physics with ATLAS and CMS.

Then I will give you a tour of the civil engineering of the detector caverns, the industrial production and installation of the LHC, machine and detectors. With the main contracts in place since last year, we are now assisting to a very exciting ramping up of the industrial production, due to reach the cruising speed during the next year.

Finally, I will say a few words on the financing of the LHC project. After the difficult discussions we had with the CERN Council over the last two years, and a drastic reformulation of CERN internal strategies, the financial set up is now considered to be on solid, if very tight, ground.

Given all these results, Management is in the position to confirm the LHC schedule already announced in March 2002, namely:

- completion of the LHC machine in the last quarter of 2006,
- first beams injected during the spring of 2007,
- first collisions in mid 2007.

2. New Physics at High Energy

At the LHC scale of exchanged momenta, valence quarks in the proton have lost much of their importance. Gluons and the sea of quark-antiquark pairs dominate. Unlike at lower energy, proton-proton and proton-antiproton collisions are much alike at these energies. This feature and the very high luminosity (target luminosity $10^{34} \text{ cm}^{-2}\text{s}^{-1}$) will make the LHC a real factory for any conceivable particle, from Higgs bosons, B mesons...to mini black holes, should they exist. Table I shows the yearly production of several kinds of particles, compared to the total statistics that will be collected at previous machines by 2007.

The LHC will be a very versatile machine indeed, with an expected lifetime spanning over two decades, possibly extended by a luminosity upgrade, which is being considered just in these days.

Let me review the main High Energy Physics targets in turn.

Process	Events/s	Events per year	Total statistics collected at previous machines by 2007
$W \rightarrow e\nu$	15	10^8	10^4 LEP / 10^7 Tevatron
$Z \rightarrow e^+e^-$	1.5	10^7	10^7 LEP
$t\bar{t}$	1	10^7	10^4 Tevatron
$b\bar{b}$	10^6	$10^{12} - 10^{13}$	10^9 Belle/BaBar ?
H, m=130 GeV	0.02	10^5	?
gluino pairs, m=1 TeV	0.001	10^4	...
Black holes, m > 3 TeV ($M_b=3$ TeV, n=4)	10^{-4}	10^3	---

Table 1. Expected event production rates in ATLAS or CMS for some (known and new) physics processes at the initial “low” luminosity of $L = 10^{33} \text{ cm}^{-2}\text{s}^{-1}$.

2.1 Searching for the Higgs Boson.

There are little doubts that the LHC and its planned detectors will be able to detect the Standard Theory Higgs boson over the whole mass range where it is predicted², from around 114 GeV (the LEP limit) up to about 1 TeV. Fig. 2 gives the confidence limit with which one can establish a signal in one year at low luminosity ($3 \cdot 10^{33} \text{ cm}^{-2}\text{s}^{-1}$, corresponding to an integrated luminosity of 10fb^{-1}) or in one year at the nominal luminosity (30fb^{-1}). The lowest mass region is particularly difficult, which shows the usefulness of the magnificent job done by the accelerator physicists and by the LEP collaborations to extend the lower bounds as much as possible. Of particular importance in this region is the recently studied W or Z fusion channel:

$$q\bar{q} \rightarrow q\bar{q}H \rightarrow q\bar{q}\tau^+\tau^-$$

with one of the quarks in the final state tagged as a forward jet.

The mass of the Higgs boson will be measured with very good precision, much the same as the W mass was measured at the Tevatron. At the end of the day, after ten years at nominal luminosity (i.e. an integrated luminosity of 300fb^{-1}) one may be able to attain errors of the order of per mill, in most of the low mass range, to order of per cent, in the higher mass range.

2.2 Higgs Boson couplings.

The real signature of spontaneous symmetry breaking is, of course, that the values of the Higgs boson couplings to the various particles should be in the ratio of the corresponding masses. The absolute values of the couplings are hard to measure in a

hadron collider, due to not well-known production cross sections and total Higgs boson width. However, a lot of uncertainties disappear in the ratios and coupling constant ratios would give anyway decisive evidence that the observed particle is indeed the long sought Higgs boson. Fig. 3 shows that 10-20% precisions can be obtained for a number of important channels. Increasing the LHC luminosity by a factor 10 (as considered at present for the LHC upgrading) could reduce errors by a factor of 2 and give some access to the triple Higgs coupling³. It is here that a low energy electron-positron linear collider (LC) could make significant progress, measuring absolute couplings down to few percent errors.

2.3 The Standard Theory becomes “unnatural” above the TeV region.

Scalar particle masses are not protected against becoming of the order of the largest mass of the theory, the cut-off, because of quantum corrections. As formulated by 't Hooft⁴, for this to happen, some new symmetry must appear when the mass vanishes. We know many instances where this occurs: fermions (at vanishing mass, chiral symmetry is achieved) spin one bosons (gauge symmetry) π -meson (spontaneously broken chiral symmetry).

Nothing like that happens in the Standard Theory for the Higgs boson. Thus the Higgs boson mass is not protected against quantum corrections to become of the order of $M_{\text{Planck}} = 10^{19}$ GeV, the largest physical mass in the Standard Theory. Only an unreasonable fine tuning between the bare mass and its quantum corrections could make $M_H \ll M_{\text{Planck}}$ as required by observation.

Three different solutions have been developed until present:

- The Higgs boson is not elementary but rather a fermion-antifermion state, bound by new strong forces at the TeV scale⁵ (dubbed by the generic name Technicolor); this solution is strongly disfavoured by the LEP/Tevatron data and I will not consider it;
- Supersymmetry in the TeV region⁶. In exact SUSY, a vanishing mass of the Higgs boson produces a vanishing mass for its fermionic partner, hence chiral symmetry. In softly broken SUSY⁷, the Higgs mass is determined by the scale of SUSY breaking. Minimal SUSY models are compatible with LEP and Tevatron data; a (quasi) stable neutral lightest supersymmetric particle seems today the best candidate for the cosmological cold dark matter indicated by astronomical observations;
- Additional space dimensions with a very large radius⁸, where gravity is characterized by a mass which is itself of the order of TeV: in this case the Planck mass has no fundamental meaning and even unprotected masses are of the order of a TeV.

The LHC will be able to shed decisive light on these alternatives.

2.4 Searching for SUSY

As for particle content, MSSM features:

- two Higgs doublets, with five physical scalar bosons, three neutral: h , H , A and two charged ones: H^\pm

- the SUSY partners of known particles:
 - spin 0: scalar quarks, scalar leptons;
 - spin 1/2: gluinos, gauginos, Higgsino.

The decay chains of the SUSY partners are likely to contain several neutral, invisible particles, giving rise to spectacular missing energy signal.

Minimal Supersymmetric Standard Models (MSSM) of the SUGRA type are characterized by two mass parameters: m_0 , $m_{1/2}$, and one sign, μ . The allowed region in parameter space is restricted by

- The non-observation of SUSY signals at LEP and Tevatron;
- The values of the cosmological observables reflecting cold dark mass distribution.

When the available experimental information is put together, one gets the presently allowed region in the mass parameter space reported⁹ in Fig. 4 for the two signs of μ . Note that there are “typical regions” where no conspiracies among constants are at work, and “fine tuned” regions, allowed by special cancellations of different parameters to form the observables. Fig. 5 shows the LHC reach for observing squarks and gluinos. Clearly, if the lightest supersymmetric particle provides the cosmological dark mass and parameters are in the “typical region”, SUSY can be discovered very quickly at the LHC. At full luminosity, LHC can discover squarks and gluinos up to about 3 TeV¹⁰. Masses can also be determined, in several instances with good precision (few to several percent) by the observation of end points in the mass distribution of different particle combinations (dileptons, jets etc).

2.5 MSSM benchmarking of colliders

“Filaments” in Fig. 4 correspond to regions allowed only because of somewhat special cancellations between different parameters. In these regions, the masses of the extra particles predicted by the MSSM can take large values. In some cases, they could even escape detection at the LHC. This has been studied in ref. 9 with the results shown in Fig. 6. A number of points in parameter space have been chosen (labelled A, B, ..., M, ...) and for each of them the authors have computed the number of SUSY particles that will be observed at the LHC and other colliders. In line with the previous considerations, the LHC will see squarks and sgluons in most cases, in some cases also sleptons. However, there are some “nasty” cases (cases M and K) where SUSY particles will be out of reach and only a Standard Theory Higgs boson will be seen.

The situation with a “low energy” electron-positron collider of 0.5 TeV is also shown. In generic cases, sleptons will be seen much more efficiently than with the LHC, as had to be expected, but the bad cases remain. A real resolution of the issue requires collider energies as high as 3 or 5 TeV, such as may be attainable with the double beam acceleration method (CLIC).

2.6 Extra Dimensions at mm scale?

The quest for a unified theory of General Relativity and Quantum Mechanics has led to a revival of the old idea, introduced by Kaluza and Klein in the thirties, that space time must have extra space dimensions, besides the familiar 3 space + 1 time dimensions.

Kaluza and Klein assumed that the extra dimensions are compact, with radius R , so that particles could not feel the extra space dimensions until their quantum wave length was smaller than R . But, what is R ? Recent ideas, ref. 8, combine Kaluza Klein extra dimensions with a new notion, namely that matter and gauge fields can be confined to a lower dimensional manifold (a D-brane), while gravity extends instead to all space. This opens up the revolutionary idea that R may be very large, on particle physics scale, and we would not detect the extra dimensions simply because the particles we are made are dynamically confined to a D-brane with 3+1 dimensions.

To understand the situation better, we need to recall that the gravitational potential at short distances feels the full $4+\delta$ space-time (δ is the number of extra dimensions) and it has the form:

$$r \ll R :$$

$$V = \frac{m_1 m_2}{(M_D)^{2+\delta}} \frac{1}{r^{1+\delta}}$$

The strength of the coupling is characterised by the constant M_D , with dimension of a mass.

At very large distances, the potential goes over to its familiar 3+1 dimensional form and an elementary calculation gives:

$$r \gg R :$$

$$V = \frac{m_1 m_2}{(M_D)^{2+\delta}} \frac{1}{R^\delta} \frac{1}{r}$$

If we compare with the Newtonian potential:

$$V_{\text{Newton}} = \frac{m_1 m_2}{(M_{\text{Planck}})^2} \frac{1}{r}$$

we can relate R , M_D , δ and M_{Planck} according to:

$$R = \frac{1}{M_D} \left(\frac{M_{\text{Planck}}}{M_D} \right)^{\frac{2}{\delta}}$$

The upshot of the exercise is that indeed M_D could be of the order of, say, 1 TeV – therefore no naturalness or hierarchy problem - provided R is rather large:

$$R \approx 1 \text{ mm}$$

$$(\delta = 2)$$

$$R \approx 10^{-2} \mu\text{m}$$

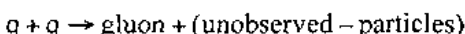
$$(\delta = 3)$$

Since normal matter is confined, we would not be in danger of losing pieces of our bodies in the extra dimension even for R as large as a millimetre.

There are two ways we can put this idea to a test.

First, at distances of order of R , gravitational forces should show deviations from the $1/r^2$ Newton law. Present results do exclude this down perhaps to a micron, which is still roughly compatible with the idea.

Second, in high energy collisions, at exchanged momenta $\gg 1/R$, gravitons and excited gravitons would be radiated with large cross sections (and leave the apparatus undetected), causing deviations from the expected, QCD or QED cross sections. The idea has been put to test already at LEP. Fig. 7 shows the limits on M_D one can obtain at the LHC¹¹, from the observation of the reaction:



Related to the same idea of a strong gravity in $4+\delta$ dimensions is the possibility of producing mini black holes in LHC collisions. Tiny black holes of $M_{BH} \sim \text{TeV}$ can be produced if partons ij with $\sqrt{s}_{ij} = M_{BH}$ pass at a distance smaller than their Schwarzschild radius, which would also be of the order of TeV^{-1} . One expects large partonic cross-sections. For $M_D \sim 3 \text{ TeV}$ and $\delta = 4$, one finds $\sigma(pp \rightarrow BH) \sim 100 \text{ fb}$, leading to 1000 (very spectacular) events in 1 year at low luminosity.

In conclusions:

- LHC will give a definite answer to the Higgs boson problem and will explore the TeV region with very good efficiency;
- A sub-TeV Linear Collider is needed for precision Higgs boson physics particularly in the case of a light Higgs boson;
- The LC would be also useful to distinguish SM from Minimal Supersymmetric SM;
- Multi TeV capability is needed to really understand Supersymmetry ... or to identify other alternatives.

Pursuing accelerator R&D on MultiTeV accelerators, CLIC and the Very Large Hadron Collider/Eloisatron is vital for the future of particle physics.

3. LHC construction

Decisive progress has been made during the last 12 months, in all sectors of the LHC project. Old concerns have been overcome, for example those due to the insolvencies of some crucial companies, new concerns are appearing but no potential show stopper is in sight. With the help of some pictures, I will make you a guided tour through the LHC works: civil engineering, production of machine hardware components and the new activity, started this year, namely LHC installation in the tunnel.

3.1 Civil engineering

The preparation of the experimental caverns and related structures is reaching its final phase, with more than 80% of the work completed.

The big ATLAS cavern has been inaugurated on June 4, 2003 and handed over to the experimental collaboration. The situation in July is shown in Fig. 8, with the 13 floors metallic structure by now installed on both sides. The big cranes have been transferred down the shaft (a good exercise for the future transfer of the ATLAS detector parts) and installed.

The CMS cavern is completely excavated. Both the main and service shafts have revealed some cracks and water leaks, due presumably to movements of the rock produced by the excavation of the main cavern below. The repair may entail some extra cost and some delay in CMS installation, which are at present under evaluation.

3.2 Machine components

With all main contracts assigned, the real problem is the follow-up of the industrial production, to make sure that companies respect the promised schedule. The situation is made more delicate by the fact that CERN, in many cases, has the double role of supplier and end customer (e.g. supplying the superconducting cables to the dipole cold mass assemblers). Adequate stocks must be built up at CERN, any delay in the intermediate steps will entail additional costs. The crux of the matter is (Fig. 9): vendors lie!

The LHC Dashboard. To monitor the progress in production, we have introduced the LHC Dashboard. For the main LHC components (superconducting cables, dipole assembly, etc.) the Dashboard shows:

- the contractual evolution, as defined in February 2002 when the present LHC schedule was agreed;
- the number of delivered components vs. time;
- the “just in time delivery curve”, going to the right of which implies a delay in the completion of magnet production at the agreed date (mid 2006).

The LHC Dashboard can be accessed from the LHC project home page¹² and is updated every month. This tool gives us objective early warning signals in case something is going wrong and actions have to be taken. The site has been very frequently visited in the last year and we hope it contributes to increase the transparency of the process.

Superconducting cables. Taken from the Dashboard, Fig. 10 shows the latest data concerning the production of the so-called inner cable (at the moment the less advanced one). Cable production was quite a concern in 2002, due to the difficult start up of the production in some companies and to the breaking of the cabling machine in Brugg. As the figure shows, the situation is considerably better now, with a reasonable production rate. As of August 31, about 42% of the inner cable billets and 51% of the outer cable billets have been manufactured and approved. This is enough to build magnets for more than 3 octants (462 dipoles).

Cryogenic dipoles assembly I. The next crucial item is the assembly of the cryogenic dipoles by three European companies. A summary is shown in Fig. 11, again from the LHC Dashboard. The ramping up of the slope in the production of collared coils is impressive: 23 collared coils have been received and approved in July, i.e. one per working day. This is not far from the expected cruising rate of 35 collared coils/month. The figure shows also the present bottleneck, which is in the cold testing of the full (cryostatted) magnet done at CERN. Delays in the delivery to CERN of the cold feed boxes made so that until summer we had available only 4 test stations, over the 12 foreseen. In July two other cold feed boxes had been commissioned and two new ones had arrived. We plan to reach the 12 units by the end of the year, which should enable us to eliminate the backlog.

Responding to various rumours to the contrary, I want to state explicitly that all dipoles will be cold tested before installation in the tunnel, in particular to make sure that short circuits are not created by spurious metallic fragments in the coils, under the enormous electromagnetic forces that develop when cold dipoles are fully powered at 12000 A.

Cryogenic dipoles assembly II. The companies that make the cold mass assembly had to ramp up in available space, tooling and personnel over the last year. They did it, remarkably well (see the assembly room in Ansaldo, Fig. 12). Recruitment of young, enthusiastic people has taken place in all three companies and technology transfer from CERN can be considered as completed. Fig. 13 shows the learning curve for coil winding at Nöll Nuclear. Upper (less efficient) peaks correspond to new recruits, lower (more efficient) peaks to senior people. All in all, the learning curve is approaching the expected asymptotic value, on which unit prices have been based in the contract! A similar learning curve applies to the very delicate soldering process of the two half shells that close the cold mass, as shown in Fig. 14 for Alstom. The theoretical 50 hours time is now being approached.

It is reassuring that the quality of the magnets we are receiving is quite good. Fig. 15 gives the histogram of the quenches to reach the nominal 8.33 Tesla field, for the 50 cold tested dipoles: 80% get to the nominal field with not more than one quench, 50% of them showing no quench at all. One case over 50 did not reach the nominal field because of a construction fault. We seem to have a robust and reliable design.

Quadrupoles subcomponents. Corrector magnets supply for the Short Straight Section quadrupoles is still a problem, due to failure of a subcontractor to comply with the agreed schedule. To compensate for the delay, the contract for the assembly of SSS quadrupoles has been extended for (up to) one more year, with no effect on the overall planning but some extra cost.

Installation. The LHC tunnel is being prepared to receive the LHC components. Sector 7-8, where the LHC-b cavern (previously DELPHI) is located, was ready on schedule. Installation of the cryogenic line has started on June 21, with some six week delay, which we hope to recuperate. Information on the general installation progress can be found by clicking on *General Coordination* (also updated monthly) in the LHC Dashboard.

To conclude:

- The insolvency cases occurred in 2002 have been dealt with without impacting on the overall project schedule (but some increase in the cost to completion).
- Superconducting cable production has about reached its nominal rate.
- Cryogenic-dipole production is ramping up in all 3 firms.
- Installation is proceeding with some initial delay.
- The LHC Dashboard address, with component production and master schedule, is given in ref. 12.

Present concerns are:

- Extra costs in civil engineering;
- Cracks at CMS shafts;
- Production of corrector magnets for the SSS quadrupoles;
- Late production of cold feed boxes is delaying dipole cold testing at CERN.

4. LHC Detectors

Unlike the LHC machine, the construction of detector parts has been going on in a diffused way, in the large network of the collaborating Institutions. The advancements made in civil engineering over the last two years have made it possible to start the assembly of the detectors at CERN and, in some cases, their integration with the machine. This is, of course, a formidable challenge that is putting extreme strain on the Laboratory infrastructure and manpower and is requiring special coordination and monitoring tools. The result, however, is that CERN now starts to be populated by gigantic, sophisticated, "toys" being assembled in different places.

Fig. 16 gives an artist's impression of how the ATLAS cavern should look like in about a year from now. A comparison with Fig. 9 gives a good idea of the enormous amount of work which is ahead of us. Figs. 17 to 20 give views of the ATLAS construction (integration of the barrel toroids in the CERN West Area), of CMS (the insertion test of the central solenoid in Point 5), of ALICE (the L3 magnet entirely refurbished in the experimental cavern) and LHC-b (magnet assembly in the former DELPHI pit).

Naturally, concerns abound, but it is encouraging to see, also here, that old concerns have mostly been overcome and progress is taking place.

The schedule remains very tight. The extra costs-to-completion of ATLAS, CMS and, to a lesser extent, ALICE, which have been declared in 2001, are at present covered by the Funding Agencies only up to some 70-80%. This will make it necessary to stage and de-scope the detectors, at least in the first go, leading to painful and risky choices. The more technical concerns have been summarised by R. Cashmore at the June Council:

ATLAS

- Barrel Toroid Schedule;
- TRT schedule;
- Production of DMILL electronics by ATMEL.

CMS

- ECAL production;
- Silicon tracker mass production.

ALICE

- TPC Production.

All in all, Collaborations are confident that they will provide properly working detectors at the start up of the machine.

5. LHC Computing

The enormous flux of information coming out of LHC collisions and the need to transfer all these data to a world-wide network of Institutions make the LHC the ideal testing ground of a new idea, developed at the end on the 90's, the GRID¹³.

By this, we mean an infrastructure, based on the existing high band telecommunication network, with imbedded nodes (Tiers) which can store data and applications and send them to a diffused population of users. The name GRID, in fact is coined after the Power GRID, whereby a user draws energy just by plugging in his electrical appliance, but he neither owns the source of the energy, nor even knows where the energy is coming from (see **Fig. 21**).

Over the last years, a wealth of projects to develop the GRID has started, in Europe and in the US. CERN has promoted the EU funded Data GRID project.

In 2001, CERN has launched a specific project for LHC computing, the LHC Computing GRID (LCG), which is now deploying a prototype service.

Data GRID has been followed by a wider scope project, with large European participation, called *Enabling Grid for E-science in Europe* (EGEE) and aimed at expanding GRID applications to other sciences and industry. EGEE is funded within the 6th Framework Programme by 32 MEuro over two years, an important sign of interest from the side of the European Community. LCG will use the middleware produced by the EGEE project and by the analogous US projects (Globus, Condor, PPDG and GriPhyN).

6. Conclusions: where are we?

In September 2001, a mid-project analysis of the whole LHC programme showed a sizeable extra cost to completion, above the cost stipulated in 1996. I can summarize the subsequent steps taken to remedy the situation as follows.

- **Sept. 2001:**
 - An extra cost-to-completion of the LHC programme was declared, of about 800 MCHF (machine, detectors, computing, missing extra contributions with respect to the 1996 plan).
- **Dec. 2001:**
 - The main remaining contracts were adjudicated (cold mass assembly, cryogenic line).
- **March 2002:**
 - LHC commissioning was rescheduled to April 2007, to comply with the industrial production rate of the main components (e.g. cables).
- **June 2002:**
 - Following internal reviews and the recommendations by an External Review Committee, Management proposed a “balanced package” of measures, *to absorb the extra cost in a constant CERN budget*. In round figures, the package was as follows:
 - 400 MCHF programme reduction, focusing of personnel on LHC; savings, extra external resources (e.g. for computing);
 - 100 MCHF rescheduling LHC to 2007;
 - 300 MCHF full repayment of the LHC reported from 2008 to 2010.
- **Dec. 2002:**
 - The Management’s Long Term Plan for the years 2003-2010 was approved by Council;
 - A long term loan (300 MEUROS) was obtained by the European Investment Bank, to cover the LHC cash-flow peak.

Thus, in December 2002 we could conclude that the LHC was back on track, with a sound, if very tight, financial plan, including the means to overcome the cash-flow we shall face in the coming years.

Today the progress of the LHC is gauged by *new, specific control tools* in addition to the classical peer committee reviews:

Today the progress of the LHC is gauged by *new, specific control tools* in addition to the classical peer committee reviews:

- Machine:
 - Earned Value Management for the materials budget;
 - Cost & Schedule Annual Review;
 - *LHC Dashboard* to report monthly on production and installation progress.
- Detectors:
 - Regular Integration reviews;
 - Periodic machine-detector meetings.

In addition:

- The LHC cost has remained stable over the last year;
- The production of machine and detector components, installation and integration are approaching the cruising speed;
- Several old concerns have been overcome; new concerns appear, but no show stopper.

In conclusion, I can say that CERN has profited from the cost-to-completion crisis in 2001 to enforce real changes: we have a much leaner programme, but have also succeeded in making CERN into a well-focused Laboratory, an indispensable condition to carry forward such a large project under tight constraints.

Drawing from the results I presented in this lecture, and with fewer reservations than last year, CERN Management can confirm the following LHC schedule:

- completion of the LHC machine in the last quarter of 2006,
- first beams injected during the spring of 2007,
- first collisions mid 2007.

Thinking about LHC upgrading has started!

Acknowledgements

I am greatly indebted to Fabiola Gianotti for providing much of the physics material presented here and to Lyn Evans, Roger Cashmore and Lucio Rossi for sharing with me their deep knowledge of the LHC. Of course any imprecision on both physics and LHC construction is exclusively my responsibility. I would like to thank Verónica Riquer for assistance in the preparation of this lecture and for the very efficient editing of the discussion session.

REFERENCES

- ¹ L.R. Evans "Beam Physics at LHC", Particle Accelerator Conference, PAC 2003. Portland USA, 2003, CERN-LHC-PROJECT-REPORT-635;
 L.R. Evans "The Large Hadron Collider - Present Status and Prospects", Presented at 18th International Conference on High Energy Accelerators HEACC 2201, Tsukuba, Japan 2001, CERN-OPEN-2001-027 and references therein;
 L.R. Evans "The Large Hadron Collider -Present Status and Prospects", *IEEE Transactions on Applied Superconductivity*: **10**, 44 (2002).
- ² See e.g. ATLAS Collaboration, "Detector and Physics Performance", Technical Design Report, CERN/LHCC/99-15;
 S. Asai et al., "Prospects for the Search of a Standard Model Higgs Boson in ATLAS Using Vector Boson Fusion", ATLAS Scientific Note, SN-ATLAS-2003-024;
 D. Denegri et al. "Summary of the CMS discovery potential for the MSSM SUSY Higgs bosons", CMS NOTE 2001/032, hep-ph/0112045;
 R. Kinnunen, for CMS Collaboration, "Higgs Physics at the LHC", presented at 10th International Conference on Supersymmetry and Unification of Fundamental Interactions (SUSY02), Hamburg, Germany 2002,
 Published in Hamburg 2002, Supersymmetry and Unification of Fundamental Interactions, vol.1 p. 26-42.
- ³ F. Gianotti, M. Mangano, T. Virdee et al. "Physics Potential and Experimental Challenges of the LHC Luminosity Upgrade", CERN-TH/2002-078, hep-ph/0204087.
- ⁴ G. 't Hooft in Recent Developments in Gauge Theories, Proceedings of the NATO Advanced Study Institute, Cargese, 1979, eds. G. 't Hooft et al., (Plenum Press NY, 1980).
- ⁵ E. Farhi, L. Susskind, "Technicolor", *Phys. Rept.* **74**: 277 (1981).
 For recent reviews see e.g. K. Lane, "Two Lectures in Technicolor", FERMILAB-PUB-02-040-T (February 2002), hep-ph/0202255;
 R.S. Chivukula, "Lectures on Technicolor and Compositeness", Lectures given at Theoretical Advanced Study Institute in Elementary Particle Physics (TASI 2000): Flavour Physics for the Millennium, Published in Boulder 2000, Flavour Physics for the Millennium, p. 731-772.
- ⁶ L. Maiani, "All You Need to Know About the Higgs Boson", Proceedings of the 1979 Gif-sur-Yvette Summer School on Particle Physics, eds. M. Davier et al.;
 E. Witten "Mass Hierarchies in Supersymmetric Theories", *Phys. Lett.* **B105**:267 (1981).
- ⁷ S. Dimopoulos, H. Georgi, "Softly Broken Supersymmetry and SU(5)", *Nucl. Phys.* **B193**:150 (1981).
 For a recent discussion, see e.g. M.E. Peskin, "Supersymmetry: The Next Spectroscopy", Presented at Werner Heisenberg Centennial Symposium Developments in Modern Physics, Munich, Germany 2001, SLAC-PUB-9613, hep-ph/0212204.

⁸ N. Arkani-Hamed, S. Dimopoulos, G. Dvali, "Phenomenology, Astrophysics and Cosmology of Theories with Sub-Millimeter Dimensions and TeV Scale Quantum Gravity", *Phys. Rev.* **D59**:086004 (1999);

G.F. Giudice, R. Rattazzi, J.D. Wells, "Quantum Gravity and Extra Dimensions at High Energy Colliders", *Nucl. Phys.* **B544**: 3 (1999);

E.A. Mirabelli, M. Perelstein, M.E. Peskin, "Collider Signatures of New Large Space Dimensions", *Phys. Rev. Lett.* **82**: 2236 (1999).

See also L.J. Hall, "Beyond the Standard Model", Proceedings of the 30th International Conference on High Energy Physics (ICHEP2000), Osaka, Japan, 2000, eds. C.S. Lim, Taku Yamanaka, (World Scientific, Singapore, 2001).

⁹ M. Battaglia, A. De Roeck, J. Ellis, F. Gianotti, K.A. Olive, L. Pape , "Updated Post-WMAP Benchmarks for Supersymmetry", CERN-TH-2003-138, UMN-TH-2005-03, FTPI-MINN-03-16, hep-ph/0306219.

¹⁰ S. Abdullin et al., *J.Phys.G:Nucl.Part.Phys.* **28**, 469 (2002);

S. Abdullin et al., "Search for SUSY at large $\tan \beta$ in CMS, the low luminosity case", CMS NOTE 1999/018.

For ATLAS, see the first paper under Ref. 2.

¹¹ L. Vacavant and I. Hinchliffe, "Model Independent Extra-dimension Signatures with ATLAS", ATLAS Internal Note ATL-PHYS-2000-016, hep-ex/0005033.

¹² <http://lhc-new-homepage.web.cern.ch/lhc-new-homepage/>

¹³ C. Kesselman and I. Foster (eds.), "The Grid: Blueprint for a New Computing Infrastructure", (Morgan Kauffman, San Francisco, CA, 1999), 677 p.

Figures Captions

Fig. 1. The Large Hadron Collider in the LEP tunnel (artist's impression).

Fig. 2. *Left figure.* Confidence level on Higgs bosons discovery as function of its mass to be reached by ATLAS in one year running at low luminosity (integrated luminosity 10fb^{-1}) or in one year at the nominal luminosity (30fb^{-1}). The discovery limit is at a value of five standard deviations. *Right figure.* Contributions to the confidence level from different decay channels.

Fig. 3. The error attainable on the ratios of the Higgs boson couplings to different particles. *Closed symbols:* nominal LHC (600fb^{-1}). *Open symbols:* luminosity upgraded LHC (6000fb^{-1}).

Fig. 4. The allowed parameter space for the Minimal Supersymmetric Standard Models (MSSM, see text). Points labelled A, B ... give a representative set of models to benchmark the discovery potential of different colliders.

Fig. 5. The discovery potential for supersymmetric particles of CMS.

Fig. 6. The number of supersymmetric particles that can be observed at different colliders in correspondence to the different MSSMs identified in Fig. 5.

Fig. 7. Lower bounds for the parameter M_{Pl} , characterizing the strength of gravity in $4+\delta$ dimensions, which can be obtained at the LHC as a function of δ .

Fig. 8. ATLAS cavern: inside

Fig. 9. Vendors lie. From the LHC magnets review, June 2003.

Fig. 10. Production of the superconducting inner cable (LHC Dashboard, August 31, 2003).

Fig. 11. Overview of the LHC main dipoles production (LHC Dashboard, August 31, 2003).

Fig. 12. ANSALDO Magnet: the assembly hall of the LHC main dipole cold masses.

Fig. 13. Nöll Nuclear: the learning curve for the winding of the LHC main dipoles coils.

Fig. 14. ALSTOM: the learning curve for the welding of the LHC main dipole cold mass.

Fig. 15. Histogram of the number of quenches to reach the nominal LHC field (8.33 Tesla) for the first 50 dipoles.

Fig. 16. The projected status of ATLAS on October 2004 (artist's view).

Fig. 17. ATLAS: assembly of the barrel toroids in the West Hall at CERN.

Fig. 18. CMS: the test for the insertion of the solenoid has been successfully completed at CERN.

Fig. 19. ALICE: the refurbishing of the former L3 magnet, to be re-used in this experiment, is now completed.

Fig. 20. LHC-b: assembly of the magnet's yoke in the former DELPHI pit.

Fig. 21. Conceptual scheme of the Data GRID.

FIGURES

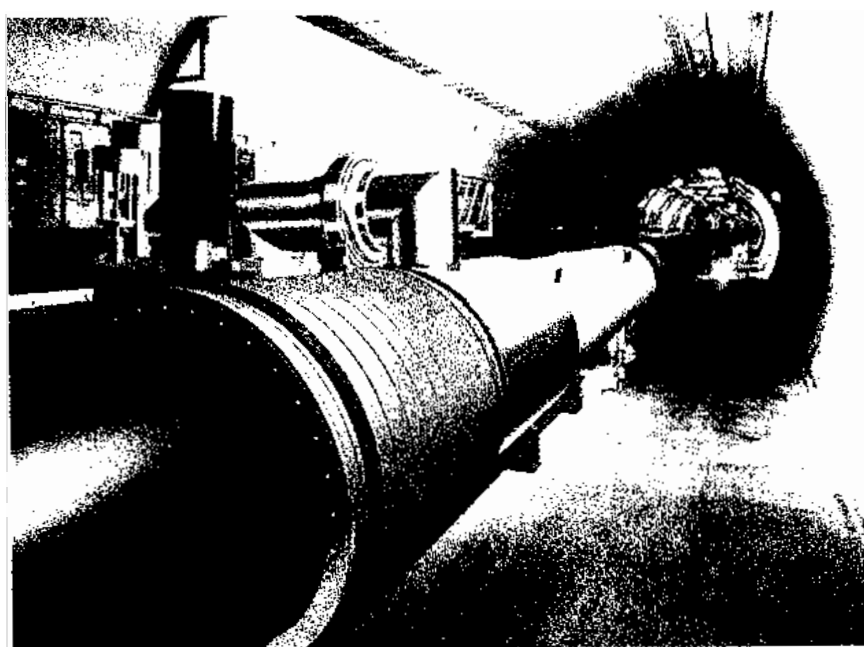


Fig 1.

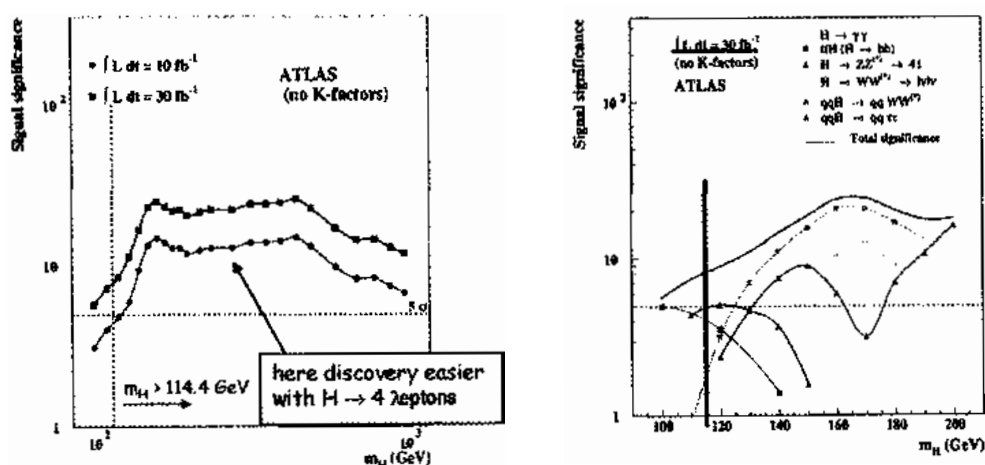


Fig. 2

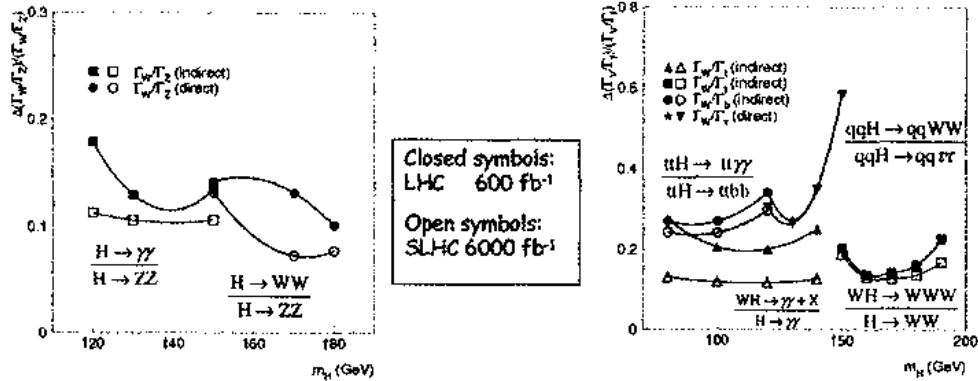


Fig. 3

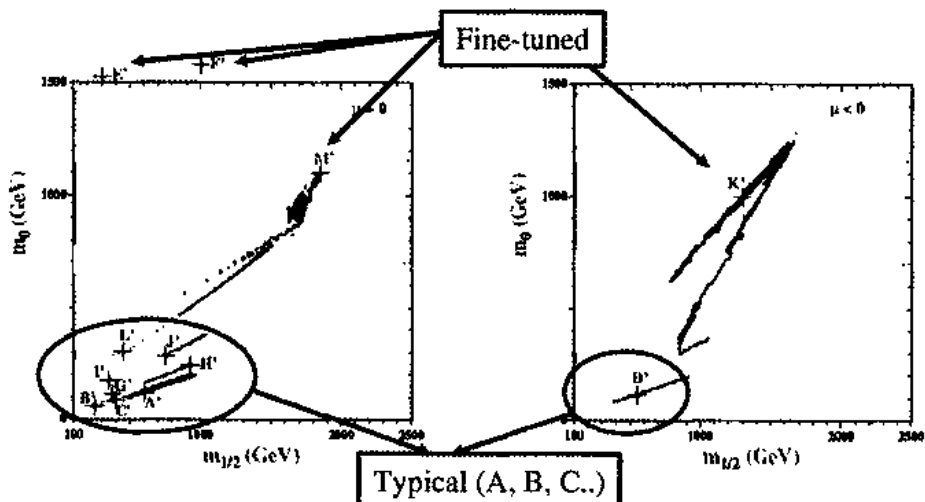


Fig. 4

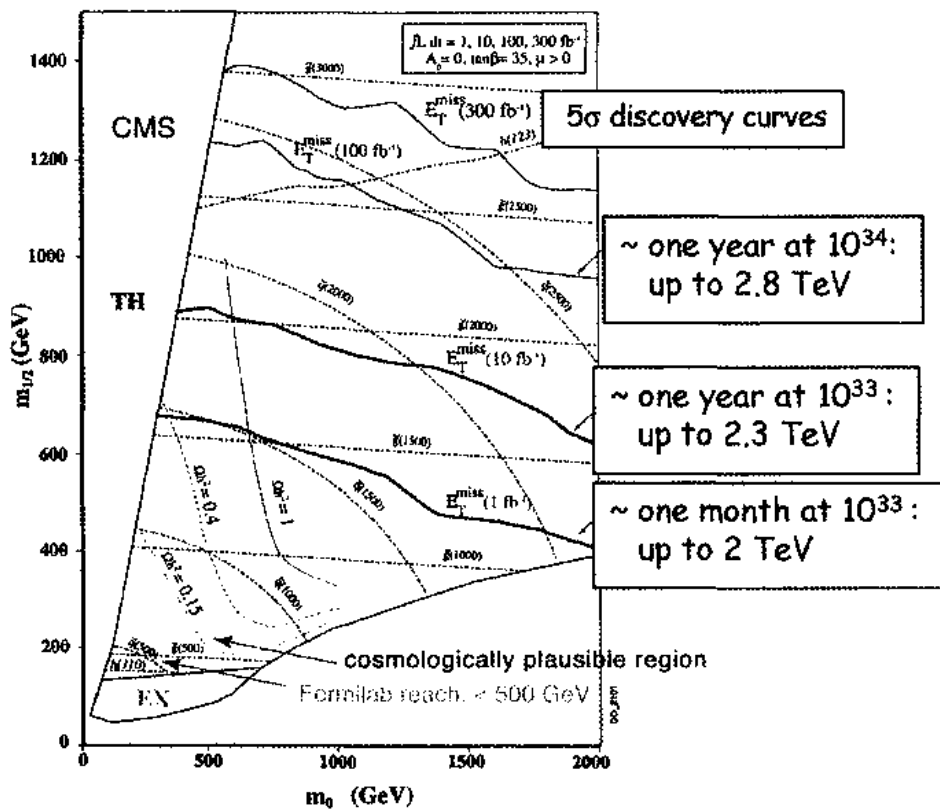


Fig. 5

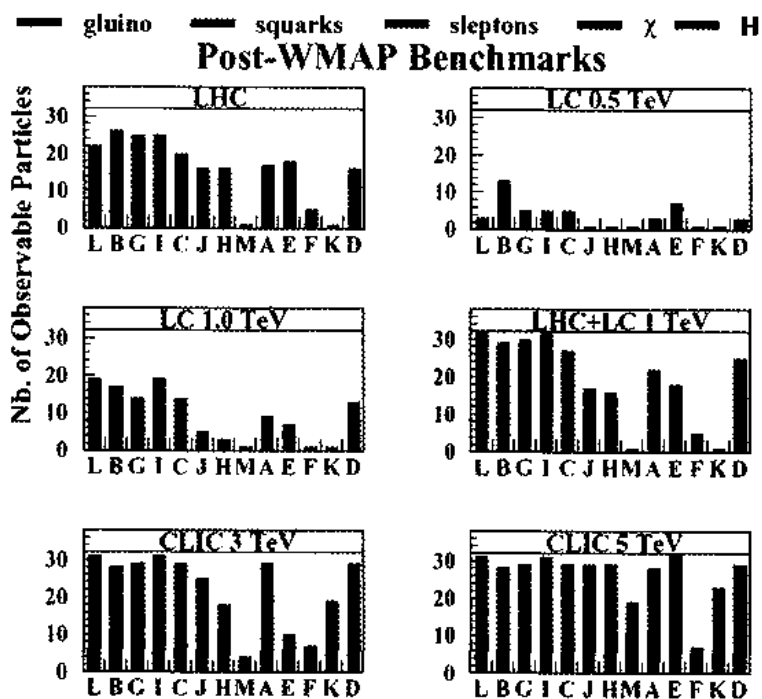


Fig. 6

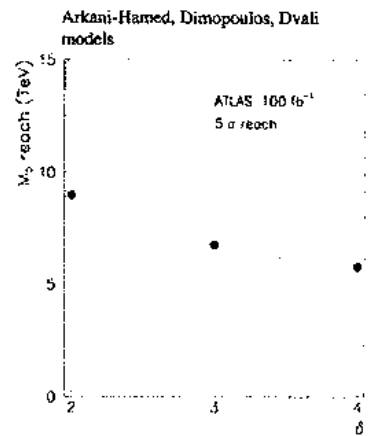


Fig. 7



Fig. 8

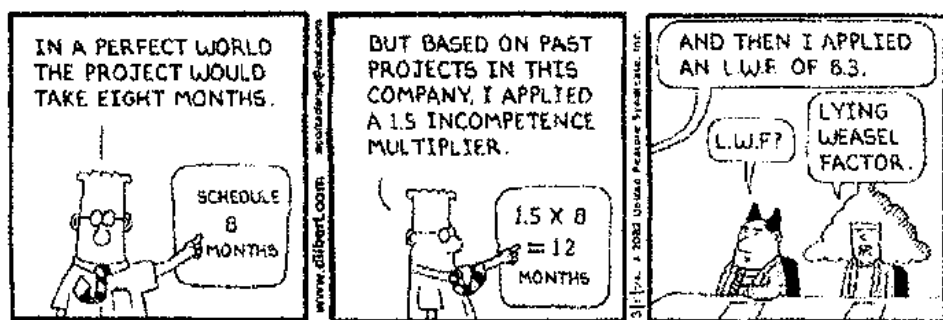


Fig. 9

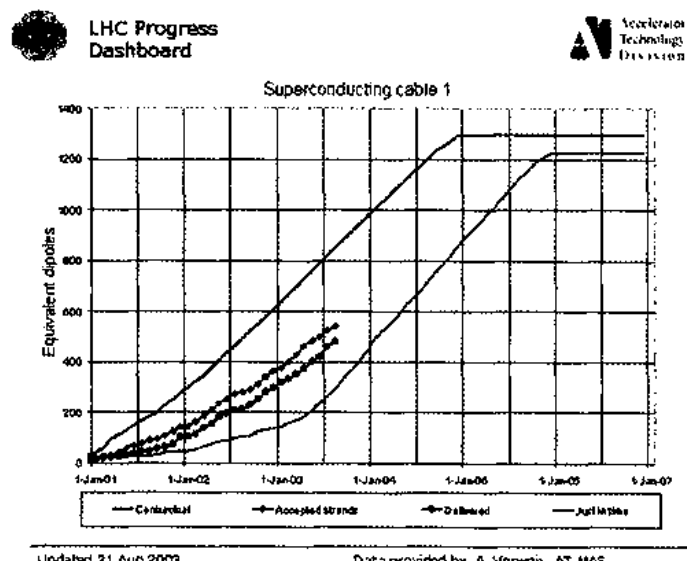


Fig. 10

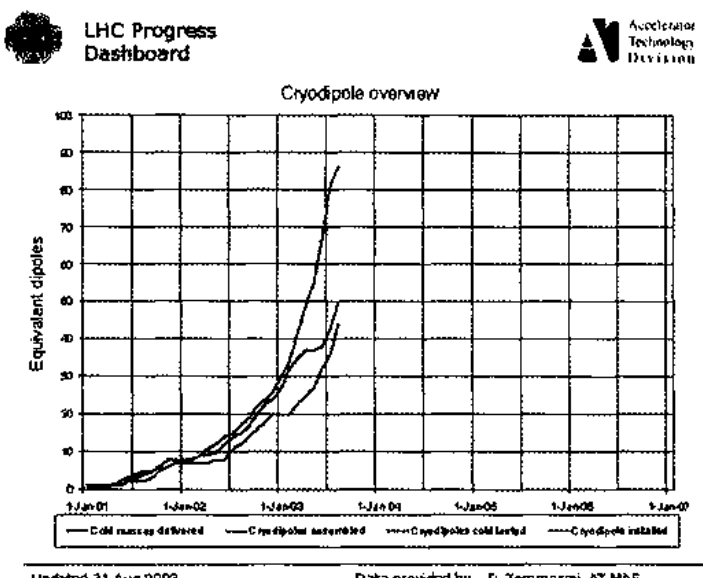


Fig. 11



Fig. 12

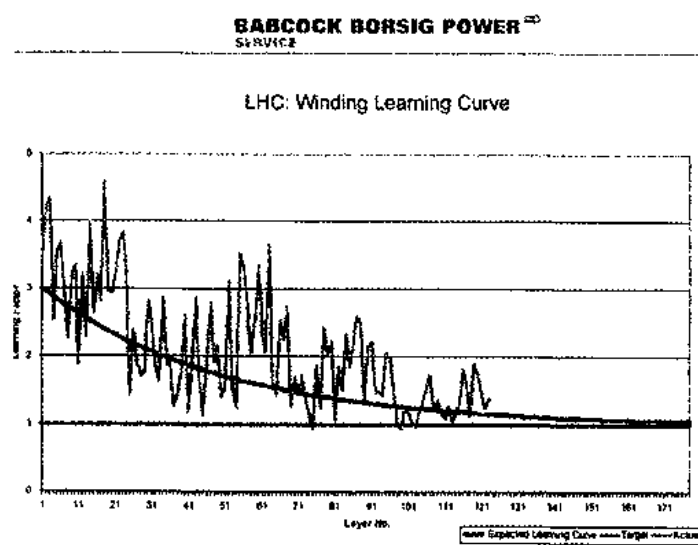


Fig. 13

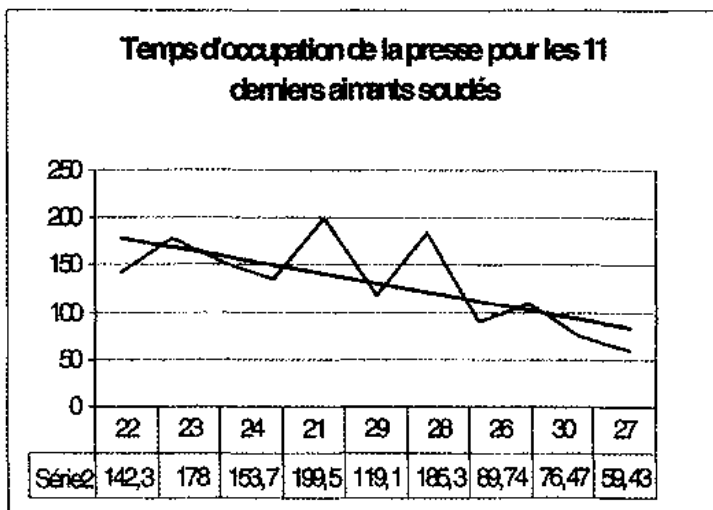


Fig. 14

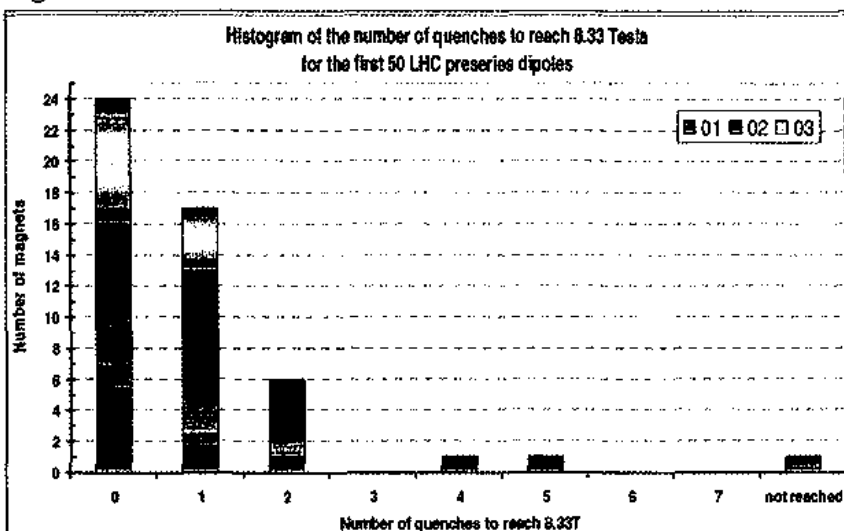


Fig. 15

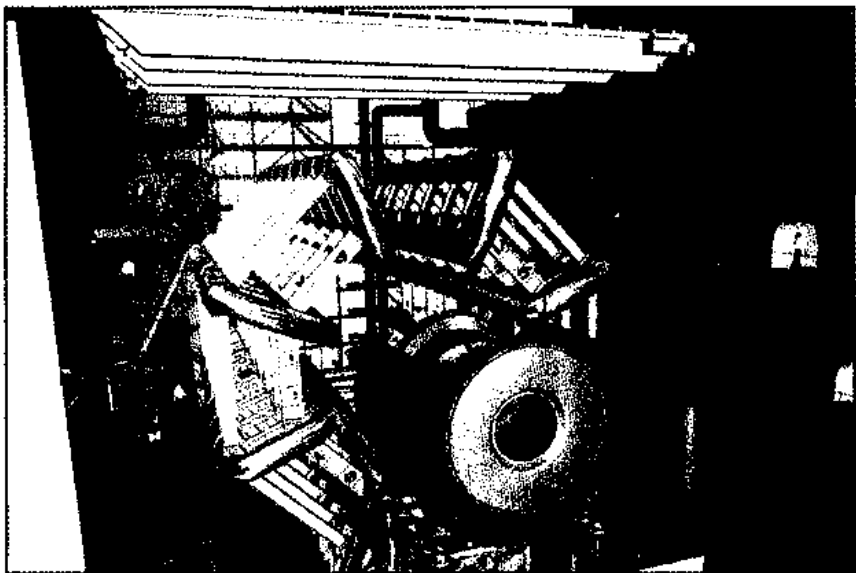


Fig. 16



Fig. 17

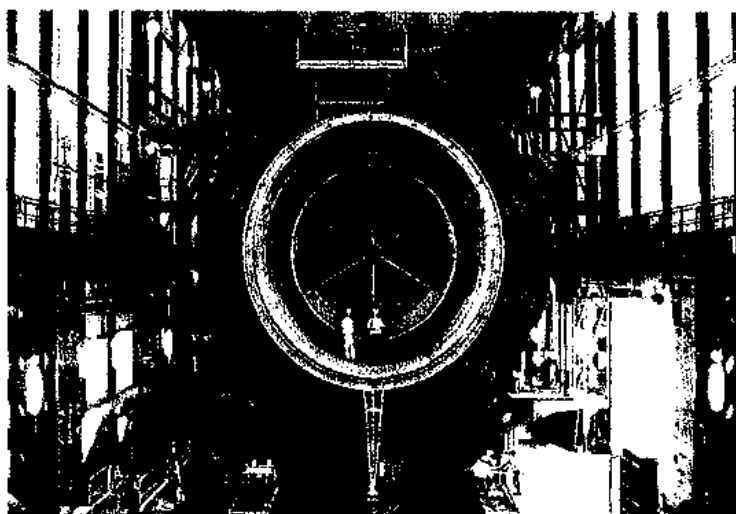


Fig. 18



Fig. 19

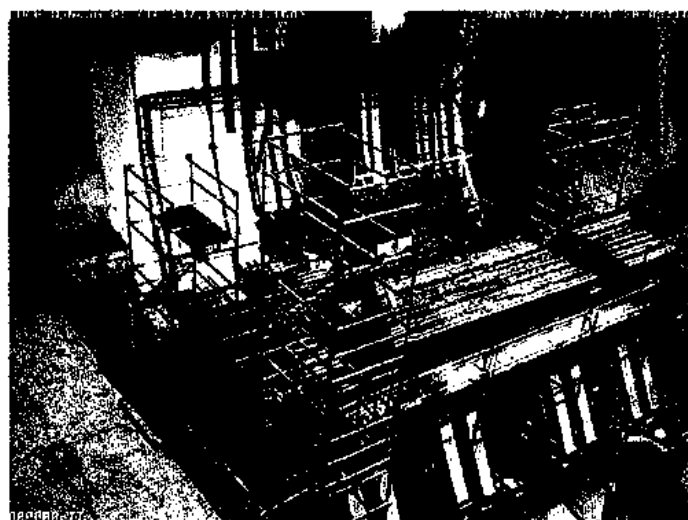


Fig. 20

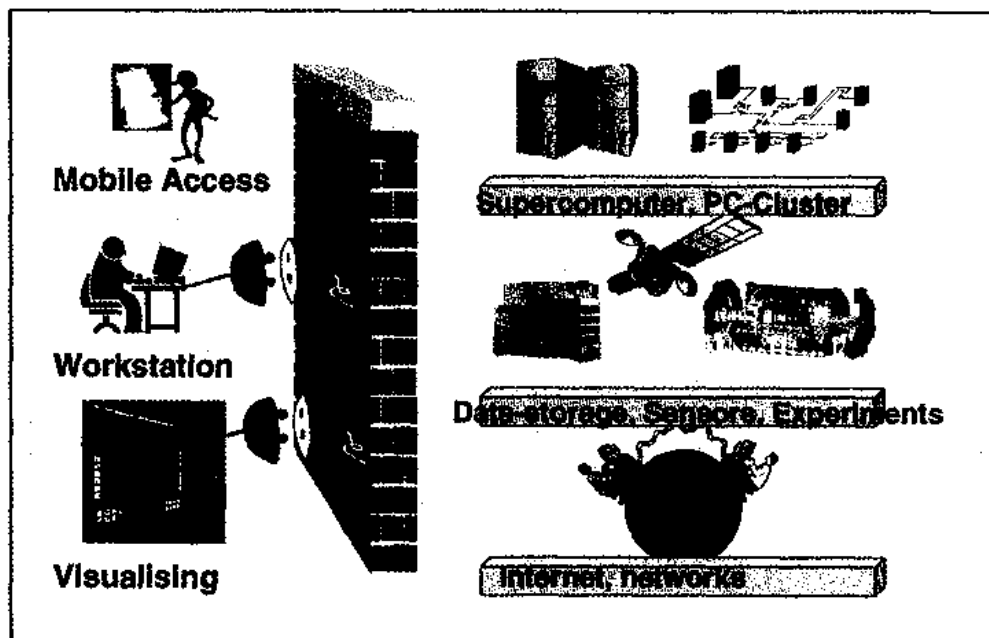


Fig. 21

CHAIRMAN: L. MAIANI*Scientific Secretary: V. Riquer***DISCUSSION**

- *Sykora:*

We saw that CERN is a really big company with an excellent management, pretty good infrastructure, good informatics, etc.. Are you, as any other big company, ready for failure? I mean do you have some team (rescue team) for the situation that on the scale up to 3 TeV there will be no new physics?

- *Maiani:*

Nobody can predict what a machine will find. However there are a number of benchmarks on which you will put your machine and we know for sure that if the Higgs boson is there, LHC is going to see it. Now if the Higgs boson is not there, then our chairman, Prof. 't Hooft, will have to say something and we will see certainly hints of what is the substitute. It is a fact that the symmetry breaking that we see in Nature must be produced by something and it cannot be simply obtained by giving a mass to the W as we used to do in the old times. So, the Higgs boson is one possibility and it is conceivable that we will see only the Higgs boson. I would consider that this would already justify such a big effort because the Standard Theory is not consistent without it. If you go back in time when the Bevatron was built in Berkeley, it was aimed at detecting the antiproton and you could ask exactly the same question. It is a fact that Bevatron found a lot of new things and we hope that this will be the case for the LHC. There are many indications, as I mentioned at the beginning, that 1 TeV is a region where, without doing anything, the Standard Theory starts becoming more and more unnatural, even with the Higgs boson. So the energy region of the LHC is just there and we will see what happens. In any case, we will take what comes. We are sure that the machine and the detector will be fitting to the task; it is like with telescopes: you build the telescope and then you look. That is Science. If we knew for sure what would come out, we would not build this machine, and we would not spend all this money. We do it because we do not know.

- *Parke:*

You showed a table of LHC events versus total observed events from other experiments for various physics channels. Do these LHC event rates have detector efficiencies folded in or are they just production rates? Can you estimate the detector efficiencies for some of these physics channels?

- *Maiani:*

These are only production rates. Of course, it is clear that they have to be extracted from the background. As for the Higgs boson in the case of the Tevatron, I do not know

what is the rate at the present luminosity. Well, of course you may make a lot of Higgs bosons but they cannot be seen out of the background. On the other hand, I showed you that, in the case of the LHC, they will be seen out of the background. As for the B mesons, it is clear that BaBar and Belle have very clean events. However the LHC gives the possibility of finding strange B's. Also the experience with the Tevatron shows that at the end, with a lot of ingenuity and hard work, you can well fight the background and luminosity is what matters.

- *Menges:*

You mentioned the SLHC option with 6000 fb^{-1} ! How many years do you need to collect this luminosity?

- *Maiani:*

With the LHC, 300 fb^{-1} would be 10 years at maximum luminosity. It is what is called the result "at the end of the day" like Tevatron today. 10 fb^{-1} is 1 year at the initial luminosity and 30 will be 1 year at the target luminosity. If we go to the Super LHC, I think it would not be so difficult to increase the luminosity by a factor of 10. So you can estimate the time needed for your integrated luminosity. I hope this answers your question. However at that point it is not much a matter of the machine, it is a matter of the detectors. In fact, I think that, at least in the first years, the luminosity of the machine will be limited by the detectors, not by the machine itself. As for 10^{35} luminosity, I am not an accelerator physicist, but I am convinced that it can be obtained and this would be certainly interesting.

- *Rotaev:*

It was said that you would expect the radius of extra dimension to be $R = 1\text{mm}$ if $\delta = 2$ or $R = 10^{-2} \mu\text{m}$ if $\delta = 3$. If it is so, then why have not we observed this yet?

- *Maiani:*

In fact, I think that 1 millimetre is essentially excluded because you can feel the extra dimension by the Cavendish experiments. Gravity goes everywhere, so the gravity potential would be modified when you go at distances which are of the order of radius of the extra dimension. And we know that the inverse square law of Newton holds certainly up to mm and the most recent experiments go rather to the micron. But of course this is a game in which you do not know how many extra dimensions are there, so you can play with that. To feel safe I would say that the limit that we have from direct test of the Newton law would say that the extra dimensions cannot be much larger than a micron. This corresponds to the last paper that I saw a couple of years ago. But this would be still extraordinarily large compared to particle physics dimensions and would still allow very spectacular phenomena to be seen, maybe not the LHC but perhaps at some higher energies.

- *Rotaev:*

But an object about millimetres we can see in a microscope.

- *Maiani:*

No, because the microscope will work only with light, and the light does not go there. That is the whole idea. The whole idea is this dynamic confinement which was first found for chiral fermions. The gauge fields and quarks are confined to within say 10^{-15} centimetres to our three-dimensional world, so the microscope will show you nothing, only gravity can go there.

- *Krotov:*

What is the experiment such as we can distinguish the radius of compactification $R = 1\text{mm}$ and for example $R = 1\text{\mu m}$?

- *Maiani:*

There are two lines, two possibilities. One: you do Cavendish experiments so you test the $1/r^2$ law to the smaller possible distance. I do not think you can go much further than 1 micron in this way. The other: you measure quark-quark or e^+e^- which go, say, to gluon or gamma plus invisible particles. Now, if you are at the energy which is of the order of the inverse of this radius, then you will produce not only one graviton but also all the excited states of the graviton and the cross-section becomes large. So you will see deviations from the QCD or QED cross-section. This has been tested already with LEP data. In another part of my computer I have the LEP picture. Any measurement of the cross-section quark-quark goes into gluon plus nothing compared with QCD will give a limit which will be a limit on M_D as a function of δ . If you instead find a deviation, you get the Nobel Prize.

- *Cerri:*

Do you agree that rather than "ingenuity", as you said before, the ability of collecting clean events at the Tevatron (i.e. Triggering ability) is rather the product of experience, hard work and commitment?

- *Maiani:*

Yes, I would say ingenuity plus experience, hard work and commitment.

- *Cerri:*

The Tevatron commissioning experience has been, in some aspects, painful. Has this kind of experience been treasured in building predictions for the beginning of the LHC era?

- *Maiani:*

The answer is "not really", because that is a completely different story. I mean we are not increasing the luminosity of an existing machine. I think that the real problem is to get the magnets in place at the appropriate time. If we get the magnets in place for

summer 2006, I think there are good chances that the schedule will work. In a way, cryogenic machines are different from the others. The experience of RHIC (the Relativistic Heavy Ion Collider) at Brookhaven is very clear. You go in steps, commissioning the machine first warm and then cold. In RHIC they did not find any particularly serious problem. As for the injectors, we are now testing the PS and the SPS and we know that we have already essentially the quality of the beam that would be needed for 10^{34} luminosity. So I think that the real point is to have, well you can never say that absolutely, but our main worry is to have all tested magnets in the tunnel by the end of 2006.

- *Casalderrey-Solana:*

Constructing LHC is already a multi-billion project. How long will the HEP community be able to convince society to support their projects and what are the alternatives?

- *Maiani:*

Well, the alternatives depend in a way from what we find. I mean, suppose that you really find a new world, as it was the case with the Bevatron. They started to see a rather simple thing: the antiproton, which everybody believed to exist, and they found a completely new realm of particles. Now, if anything like this happens, then I am sure that the resources for further explorations will be found. The scale of the expenses in absolute is not that big. I mean, it is maybe two or three days of the Iraq war, it is not this that makes the problem. The problem is whether we can find enough intellectual energy to mobilize governments and public opinion. Now if it happens, as your colleague said, that we do not find anything with the LHC, then I will tell you: we shall quit, because it will be very difficult to make another machine. But if we find the Higgs boson, and/or if we find hints of a new physics, then of course there will be enough momentum to push the world to go to higher energy. I think that we will have to do it globally. Do not forget that the LHC is constructed by one region, i.e. Europe. There are contributions from other regions, but they are only at the level of 15%. So, joining resources from all regions, one could go still further. What will happen after the next step it is something that will happen in 40 years from now, and my ability to predict the future is not that sharp.

- *Kolb:*

You remarked that a benefit of the 2001 Budget crisis was that the Laboratory "focused" on LHC. You also said that over 80% of the Laboratory is involved with LHC. Is the Laboratory over-focused now, is such a focusing healthy, and is it sustainable for the future?

- *Maiani:*

Well, certainly it cannot go on forever, if that is what you want to say. The present mix of activities is a sort of war economy, like: "You guys, everybody works on that" and that is very clear. Indeed one of the reasons of the overcost was that in fact there were

many parts of CERN that tried to follow other lines and therefore if you do not have enough manpower to do the LHC, you have to buy manpower. Now if you do not have the money, then you will take the other people and say: "Well, sorry you have to do the LHC". My feeling is that our plan goes until 2010 which will be, say, 3 years after the first exploitation of the LHC. I think that until then the Laboratory will be happy doing the LHC and doing other things at low cost like the neutrino to Gran Sasso, the nuclear physics neutron time-of-flight, etc. Small things, of course, on the LHC scale. We are continuing on a small scale, the R&D on CLIC preparing for a multi-TeV linear collider. It is clear that after 2007 or 2008, more money will have to be put into R&D if we really want to make an effort to prepare the Lab for the next step. Then, there are attempts to find extra resources by joining forces. There are many laboratories in Europe and particularly in Russia that will see their effort in the LHC decreasing in the coming years and if we could join resources with them, we could have some intermediate project like a neutrino super-beam, or something like that, which would fill the gap. This is the strategy that I would recommend. For the moment, as I said, since two years we have understood that we had to go into a war economy and that is where we are.

- *Cifarelli:*

Since you mentioned the RHIC Collider, what are your physics views on the heavy ion runs at LHC?

- *Maiani:*

The Heavy Ion program will start on day one. Let me be more precise. Even ALICE wants a proton run, so they will start with the proton run on day one, and the ion line will come later, in due time, as foreseen. I think that this is very interesting physics and it will require a lot of effort, so this is one example of physics that will last for a long time. For instance, to see the lepton radiation, measuring the temperature by appropriate probes etc. will need a lot of effort. I think that the SPS has done a wonderful job, we see now very good results from RHIC and LHC will bring us into another new region. So there are all possibilities to have a very good physics coming out of the LHC. And a lot of good theory also.

Status of non-LHC experiments at CERN
 Dieter Schlatter/CERN-PH
 Erice, September 2003

From the few non-LHC experiments still done at CERN, three experiments are presented. One experiment is completed (NA48 on direct CP violation in kaon decays), two others (NA48/1 on rare kaon decays and DIRAC on Pionium lifetime) have first physics results. The last chapter is a reminder of the SMC experiment in memory of Vernon Hughes (1921-2003), who was the spokesperson.

1) CP violation in $K^0 \rightarrow \pi\pi$ decay, the NA48 experiment 1996-2002

Direct CP violation in the decays of neutral kaons has been studied intensively since its discovery in 1964 [J.H. Christenson, et al., Phys. Rev. Lett. 13 (1964) 138]. At CERN the NA48 experiment has recently published its final result on direct CP violation in the decay of neutral kaons into two pions [J.R. Batley, et al., Phys. Lett. B 544,(2002),97].

Subtle differences between K_L and K_S decays to 2π due to different contributions from isospin $I=0$ and 2 lead to differences in particle and antiparticle decay rates.

The double ratio of decay widths

$$R = \frac{\Gamma(K_S \rightarrow \pi^+ \pi^-) \cdot \Gamma(K_L \rightarrow \pi^0 \pi^0)}{\Gamma(K_L \rightarrow \pi^+ \pi^-) \cdot \Gamma(K_S \rightarrow \pi^0 \pi^0)} = 1 - 6 \operatorname{Re}(\epsilon'/\epsilon)$$

is convenient to measure $\operatorname{Re}(\epsilon'/\epsilon)$ and thus determine the direct CP violation parameter ϵ' . The parameter ϵ is known from the indirect CP violation in K^0 mixing to be $(2.28 \pm 0.02) \times 10^{-3}$. The Standard Model predictions, based on the diagrams shown in Fig. 1.1, are not precise, the range for $\operatorname{Re}(\epsilon'/\epsilon)$ is from -10×10^{-4} to $+30 \times 10^{-4}$.

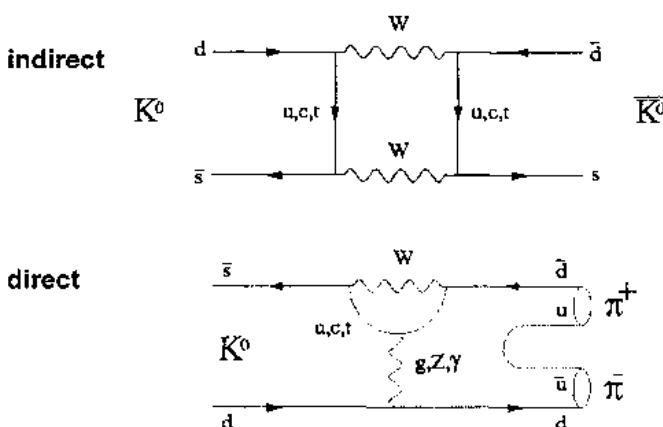


Fig. 1.1 Direct and indirect CP violating diagrams for K^0 in the Standard Model.

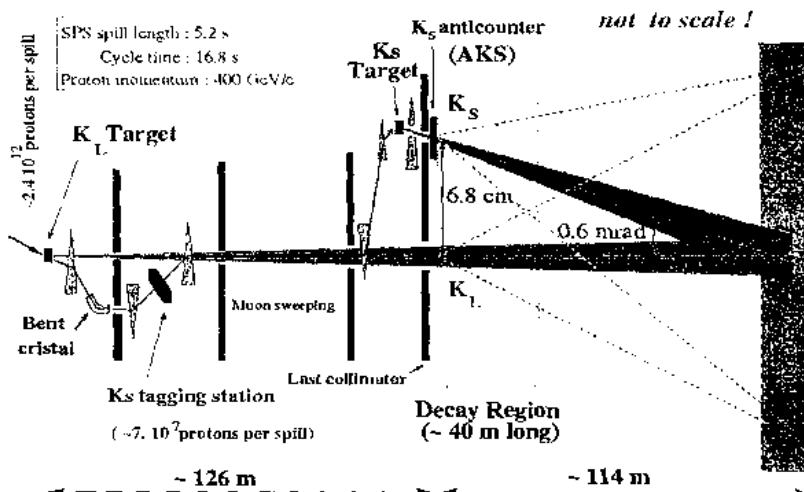


Fig 1.2. Layout of the NA48 neutral kaon beam at CERN.

The NA48 experiment at CERN is a second generation kaon experiment in a neutral kaon beam where K_L and K_S are produced simultaneously. The layout of this beam is shown in figure 1.2.

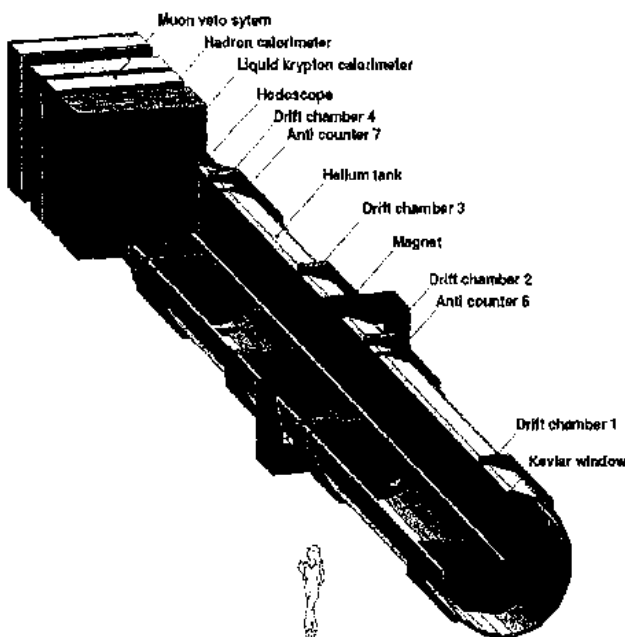


Fig 1.3 Schematic view of the NA48 spectrometer.

The main components of the detector are the magnetic tracking system, the high resolution liquid krypton calorimeter, used to reconstruct $K \rightarrow 2\pi^0$ decays, the hadron calorimeter and a muon veto system (see Fig. 1.3).

The experiment has measured all 4 decay modes of the double ratio simultaneously which lead to a cancellation of dead time and inefficiencies. K_L and K_S mesons come from the same decay region, which minimises the detector acceptance correction. Actually, this is done by weighting the K_L events to have the same decay distribution as K_S . The K_S and K_L mesons are identified by tagging the proton creating the K_S .

NA48 collected data during two periods, the result for the period 1998/1999 is $Re(\epsilon'/\epsilon) = (15.3 \pm 2.6) \times 10^{-4}$ and for 2001 $Re(\epsilon'/\epsilon) = (13.7 \pm 3.1) \times 10^{-4}$. The combined NA48 result is:

$$Re(\epsilon'/\epsilon) = (14.7 \pm 2.2) \times 10^{-4}$$

where the statistical and systematic errors contribute about equal to the combined value.

In Fig. 1.4 these results are compared to the previous measurements from NA31 at CERN [G. Barr, et al., Phys. Lett. B 317 (1993) 233] and from E731 [L.K. Gibbons, et al., Phys. Rev. Lett. 70 (1993) 1203] and KTeV [A. Alavi-Harati, et al., Phys. Rev. Lett. 83 (1999) 22] at FNAL.

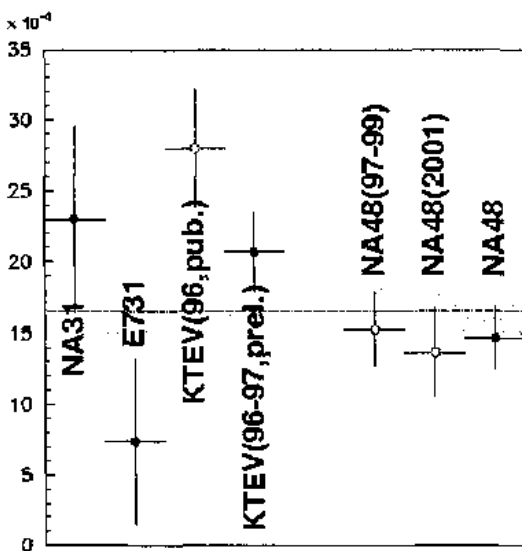


Fig. 1.4 Summary of results of $Re(\epsilon'/\epsilon)$ from CERN and FNAL.
The overall average, $\epsilon'/\epsilon = (16.6 \pm 1.6)$ is shown as band.

2) Rare neutral Kaon decays: CP violation in $K_L \rightarrow \pi^0 e^+ e^-$

After the successful completion of the direct CP violation measurement in the $K \rightarrow 2\pi^0$ decay the NA48 collaboration has started to look for CP violation effects in rare kaon decays.

The decay $K_L \rightarrow \pi^0 e^+ e^-$ has three components:

- a CP conserving from the process $K_L \rightarrow \pi^0 \gamma\gamma$ as shown in Fig. 2.1a.
- a direct CP violating term from loops sensitive to $V_{td} V_{ts}$ indicated by the diagram shown in Fig. 2.1b. Its strength is expected to be a few times 10^{-12} .
- an indirect CP violating term, which is linked to the branching ratio $\text{BR}(K_S \rightarrow \pi^0 e^+ e^-)$ and expressed by the equation $\text{BR}(K_L \rightarrow \pi^0 e^+ e^-)_{\text{ind}} = |\varepsilon|^2 (\tau_L/\tau_S) \text{BR}(K_S \rightarrow \pi^0 e^+ e^-)$.

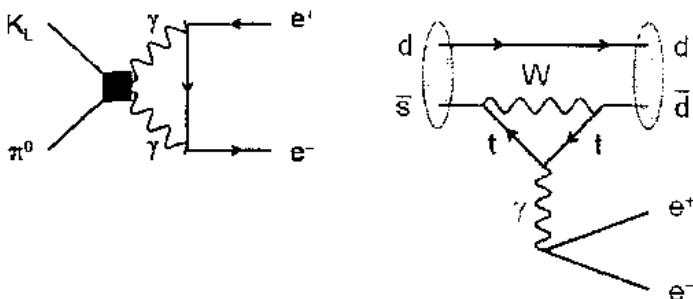


Fig. 2.1: Rare $K_L \rightarrow \pi^0 e^+ e^-$ decay, a) (left) CP conserving and b) (right) CP violation diagrams.

The direct and indirect CP violating components interfere:

$$\text{BR}(K_L \rightarrow \pi^0 e^+ e^-)_{\text{CPV}} = 1 \times 10^{-12} (15.3 a_s^2 \pm 6.8 \times 10^{-4} \text{Im}(\lambda_t) |a_s| + 2.8 \times 10^{-8} / m(\lambda_t)^2) \text{ and}$$

$$\text{BR}(K_S \rightarrow \pi^0 e^+ e^-) = 5 \times 10^{-9} |a_s|^2. \quad [\text{D'Ambrosio, et al., JHEP 9808:004, 1998}].$$

The measurements of the branching $\text{BR}(K_S \rightarrow \pi^0 e^+ e^-)$, fixing $|a_s|$, and $\text{BR}(K_L \rightarrow \pi^0 \gamma\gamma)$ determine whether it will be possible to measure the direct CP violation in $K_L \rightarrow \pi^0 e^+ e^-$. The current limit is $< 5.1 \times 10^{-10}$ coming from 2 events seen by KTeV with an expected background of 1.1 [A. Alavi-Harati et al., PRL 86 (2001) 397].

NA48 has measured the branching ratio $\text{BR}(K_L \rightarrow \pi^0 \gamma\gamma)$ and the vector coupling constant from which the CP-conserving component of the $K_L \rightarrow \pi^0 e^+ e^-$ decay

$$\text{BR}(K_L \rightarrow \pi^0 e^+ e^-)_{\text{CP conserving}} = 4.7^{+2.2}_{-1.8} \times 10^{-13} \quad [\text{A. Lai et al., Phys Lett B 536 (2002) 229}]$$

has been derived.

During 2002 NA48/I took data to search for the decay $K_S \rightarrow \pi^0 e^+ e^-$ which branching ratio is expected to be about $5 - 50 \times 10^{-10}$ [G. Ecker, A. Pich, E. de Rafael, Nucl.Phys. B291(1987) 692]. The signature is two photons in the electromagnetic calorimeter and an $e^+ e^-$ pair. A cut on the $e^+ e^-$ mass of 165 MeV is applied to suppress $K_S \rightarrow \pi^0 \pi^0$ with a missing photon. Seven events have been observed in a background free signal region. In a larger control region zero events have been found with an expected background of 0.15. The probability that all 7 events are background is 10^{-10} . The result for the branching ratio is

$$\text{BR}(K_S \rightarrow \pi^0 e^+ e^-, m_{ee} > 165 \text{ MeV}) = (3.0^{+1.5}_{-1.2}(\text{stat}) \pm 0.2(\text{sys})) \times 10^{-9}$$

[J.R. Batley et al., Phys.Lett. B576 (2003) 43].

Assuming a vector matrix element and a form factor equal to one the measurement gives:

$$\text{BR}(K_S \rightarrow \pi^0 e^+ e^-) = (5.8^{+2.9}_{-2.4}) \times 10^{-9}.$$

in remarkable agreement with the prediction 5.5×10^{-9} of L.M. Seghal [L.M. Seghal Nucl. Phys. B 19 (1970) 445]. In the notation of D'Ambrosio et al. $|a_S| = 1.08^{+0.26}_{-0.21}$ meaning that the direct CP violated component predicted from the Standard Model is small with respect to the indirect component.

A global fit for $\text{Im}(\lambda_t)$, using also b decay data, leads to $\text{Im}(\lambda_t) = (1.30 \pm 0.12) \times 10^{-4}$ [Kettell, Landsberg, Nguyen, hep-ph/0212321].

Fig. 2.4 shows the constraints on the direct CP violation in the $K_L \rightarrow \pi^0 e^+ e^-$ decay for the branching ratio as function of the two sign choices of a_S . The implication from this result and the global fit indicates that the CP-violation contribution to this decay is only a few times 10^{-11} .

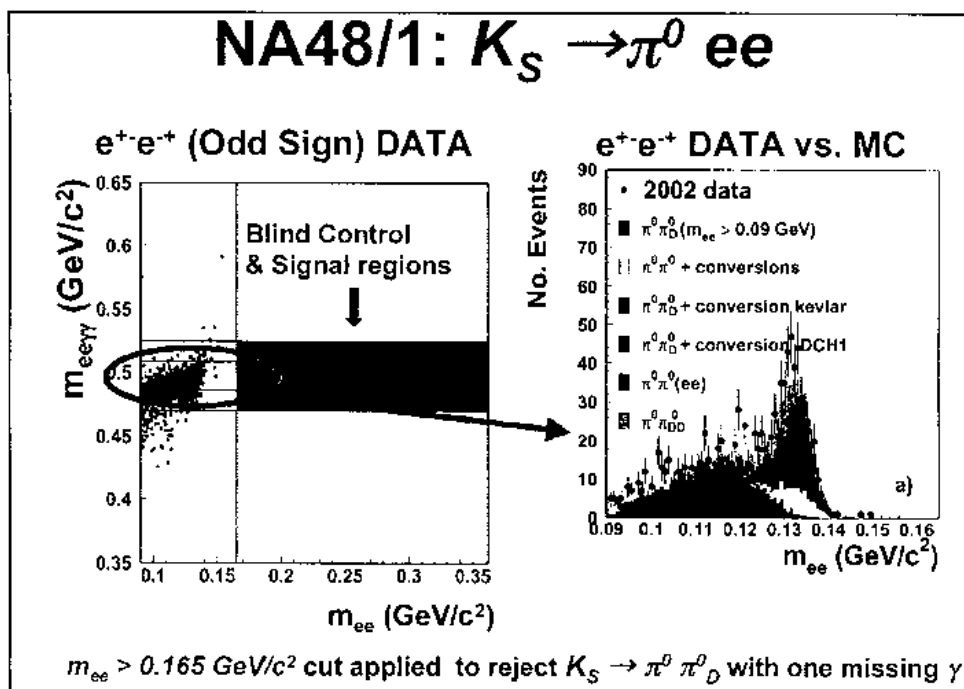


Fig. 2.2 Distribution of $m(ee\gamma\gamma)$ versus $m(ee)$ for the background to $K_S \rightarrow \pi^0 e^+ e^-$.

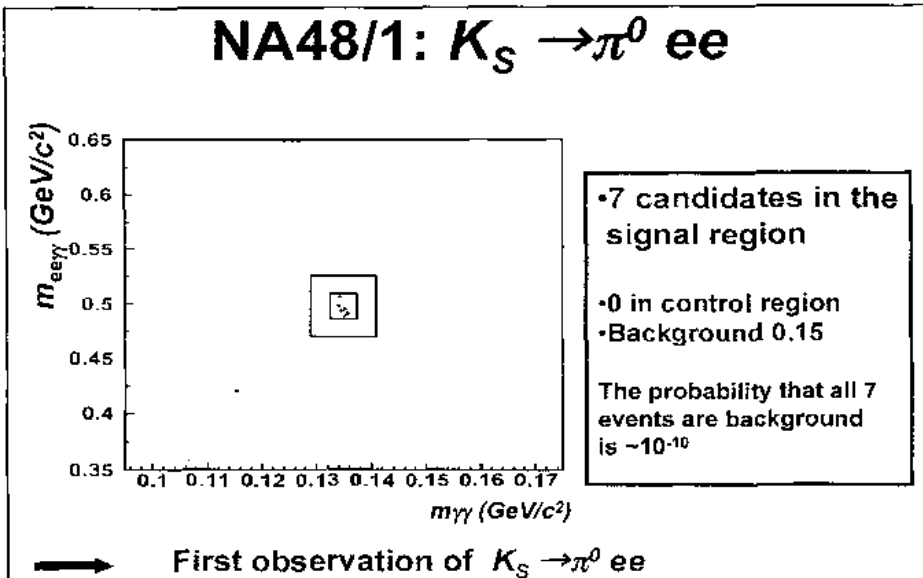


Fig. 2.3 Distribution of $m(ee\gamma\gamma)$ versus $m(\gamma\gamma)$ for the signal events. The smaller square is the signal region, the larger square is a control region.

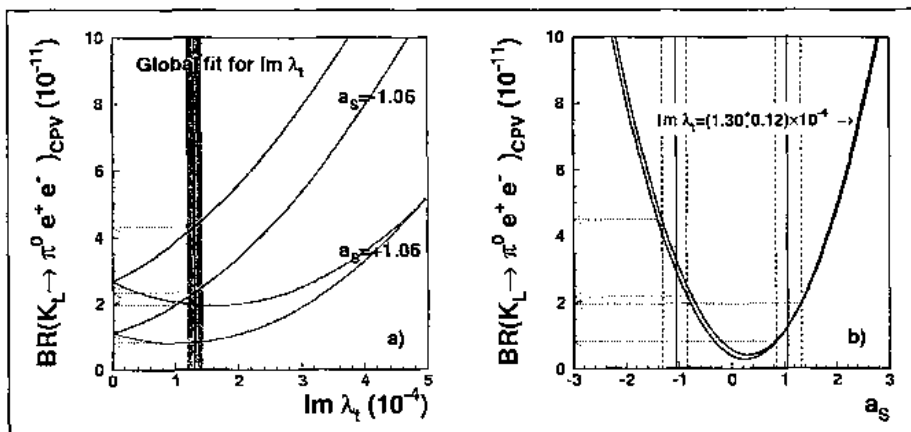


Fig. 2.4 CP violating branching ratio $\text{BR}()$: a) as a function of the $\text{Im}(\lambda_1)$ for two values of a_s , b) as a function of a_s using $\text{Im}(\lambda_1)$ from a global fit.

3) DIRAC experiment and the Lifetime of Pionium as test of low energy QCD

The DIRAC Experiment at the PS at CERN [B. Adeva et al., 1995 CERN/SPSLC 95-1, Geneva 1995] has the goal to measure the $\pi^+\pi^-$ atom lifetime with 10% precision, predicted by Chiral Perturbation Theory to be 2.9 ± 0.1 fs. This measurement will provide in a model-independent way the difference between the isoscalar and isotensor S-wave $\pi\pi$ scattering lengths $|a_0 - a_2|$ with 5 % precision. Low energy QCD - Chiral Perturbation Theory predicts this difference with very high accuracy ~ 2 % and hence the lifetime with ~ 3.3 % [G. Colangelo et al., Phys. Lett. B 488 (2000) 262]. Therefore, the measurement of the lifetime of the pionic atom will be a sensitive check of the understanding of chiral symmetry breaking of QCD.

Coulomb bound $\pi^+\pi^-$ states, so-called Pionium or $A_{2\pi}$, can be produced in the interaction of a proton beam with nuclear targets. These exotic atoms originate from Coulomb attraction in the final state, when the relative distance between 2 pions is of the order of some fm. Pionium will decay strongly into $2\pi^0$ with a lifetime of ≈ 3 fs.

The $\pi^+\pi^-$ pairs, originating from $A_{2\pi}$, break-up (ionization) in the nuclear target are characterized by a small opening angle (< 3 mrad) and a small relative momentum $Q < 3$ MeV/c.

The pionic atoms are produced by the Final State Coulomb interaction of a pion pair in proton-target collisions but also free Coulomb pairs are created in the proton-target collisions. The atom production is proportional to Coulomb pairs production at low relative momentum, $N_A = K_N N_C$. The pionic atoms evolve in the target and some of them (n_A) break up with a probability $P_{br} = n_A/N_A$. The dependence of the break-up probability on the lifetime is accurately known [C. Santamarina et al., J.Phys.B.At.Mol.Opt.Phys.36 (2003) 4273]. Examples of such calibration curves are shown in Fig. 3.2.

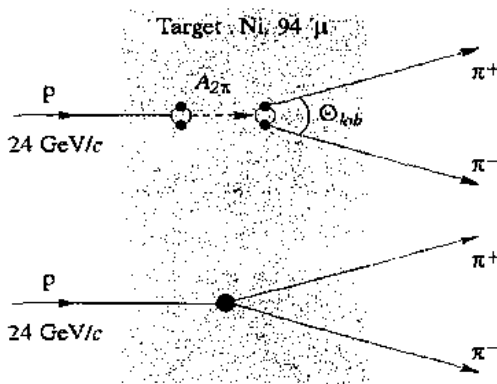


Fig. 3.1: $A_{2\pi}$ production in a nuclear target and Coulomb pair background.

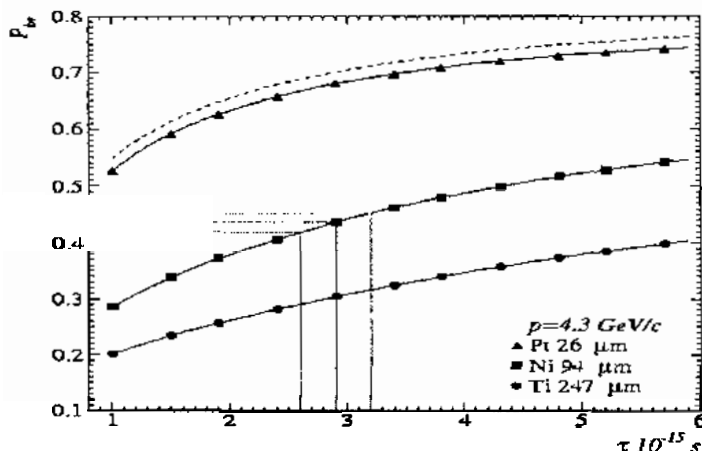


Fig. 3.2: Calibration function of the break-up probability as a function of the $A_{2\pi}$ lifetime.

Using the 24 GeV/c proton beam of the PS at CERN pionium can be produced in a nuclear target like Ni. The DIRAC experiment, a double arm magnetic spectrometer as show in Fig. 3.3, is analysing the low relative momentum spectrum of $\pi^+\pi^-$ pairs.

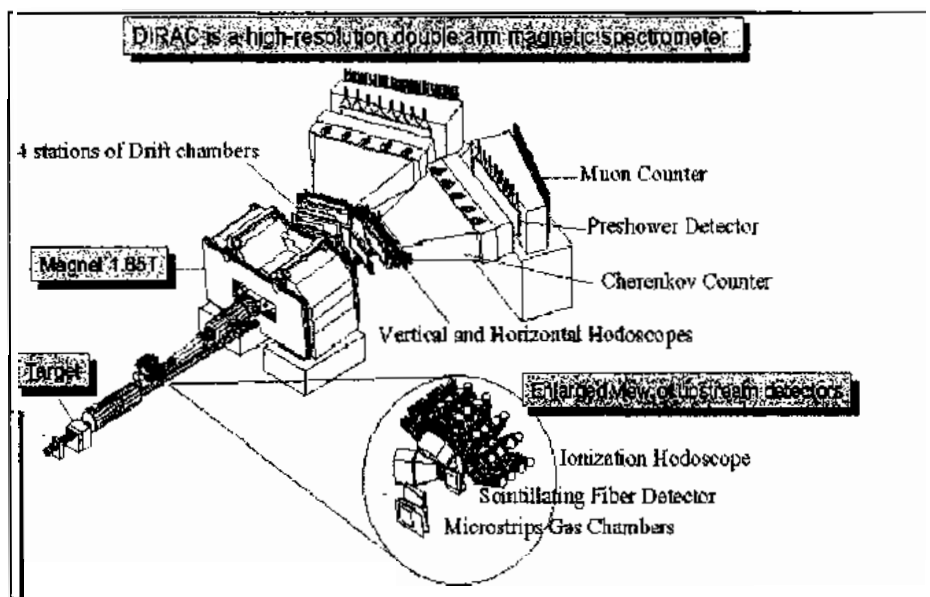


Fig. 3.3 Layout of the DIRAC double arm spectrometer

The two pion final state is identified with the spectrometer, the accidental (non correlated) pairs are suppressed using the timing of the tracking chambers. The relative momentum, Q , of $\pi^+\pi^-$ pairs and its longitudinal component Q_L , are analyzed. Distribution of Q and Q_L , after subtraction of the remaining accidental background, are shown in Fig. 3.4 demonstrating a signal at low values consistent with the expectations for Pionium production.

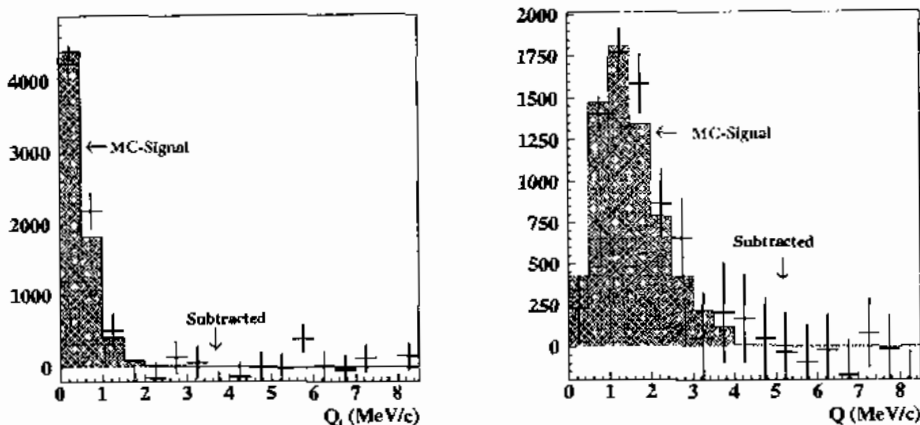


Fig. 3.4: Distribution of relative momentum of pion pairs after background subtraction, together with simulated atomic pair events.

A preliminary result has been achieved by analyzing data collected in 2001:

$$\tau = (3.1^{+0.9}_{-0.7}(\text{stat}) \pm 0.8(\text{syst})) \cdot 10^{-15} \text{s}$$

The statistical accuracy in the lifetime determination reaches 25% and the systematic one is 26%. Analysis of data collected in 2000 and 2003 together with the systematic error reduction will improve the accuracy up to the level of 14%. This error should decrease further with the data to be taken during 2004.

4. Vernon W. Hughes (1921–2003): Polarised muon scattering at CERN

The European Muon Collaboration, EMC, had performed muon scattering with polarised target and finished its programme at CERN during 1984/1985 with the observation of a quark spin deficit in the proton (“spin crisis”).

To study this puzzle, Vernon Hughes proposed to succeed the EMC experiment with a similar one but with a polarized muon beam. This experiment became known as the Spin Muon Collaboration, SMC [SMC, CERN/SPSC 88-47 (1988) P242], of which V. Hughes was the Spokesperson. The data taking reached from 1991 to 1996.

The goal was

- to study the spin-dependent structure functions of proton and neutron,
- to test the Bjorken sum rule and
- have a first estimate of the polarised gluon distribution in the nucleon.

The spin content of the proton can be formulated as:

$$\frac{1}{2} = \Delta_q + L_q + \Delta G + L_G$$

where Δq is the intrinsic quark contribution, L_q the quark angular momentum, ΔG the intrinsic gluon contribution and L_G the gluon angular momentum.

Polarised Deep Inelastic Scattering experiments with lepton on nucleon can measure Δq , ΔG . Isospin symmetry requires that the total quark spin contribution is identical for proton and neutron.

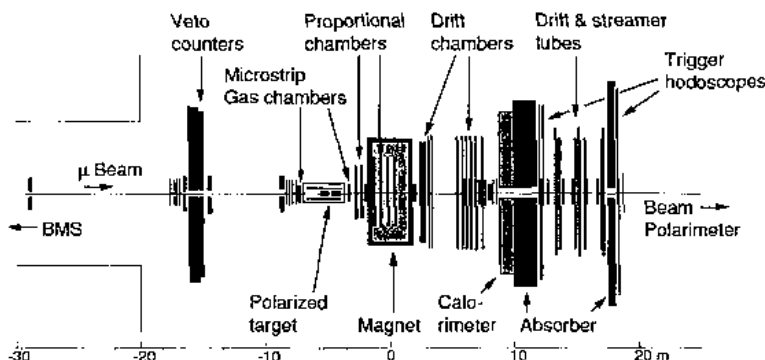


Fig. 4.1: Layout of the SMC experiment at the SPS at CERN.

The SMC used a 190 GeV muon beam with an average longitudinal polarisation of 80%. Two target cells, longitudinally polarized in opposite directions, allow a direct measurement of spin asymmetries: $P_B \approx 90\%$ and $P_D \approx 50\%$. A conventional magnetic spectrometer based on wide-aperture dipole magnet provides the reconstruction of the scattered muon and the hadron final states.

The differential cross section for polarised lepton-nucleon scattering has two components, the unpolarised cross section, σ_0 , and the polarised part $\Delta\sigma$:

$$\frac{d^3\sigma}{dx dy d\phi} = \frac{d^3\sigma_0}{dx dy d\phi} + \frac{d^3\Delta\sigma}{dx dy d\phi}$$

with

$$\frac{d^3\Delta\sigma}{dx dy d\phi} = \frac{2\alpha^2}{MExy} \left\{ \cos\beta \left[\left(1 - \frac{y}{2} - \frac{Mxy}{2E} \right) g_1(x, Q^2) - \frac{Mx}{2E} g_2(x, Q^2) \right] - \right. \\ \left. - \cos\phi \sin\beta \frac{\sqrt{Q^2}}{v} \sqrt{1 - y - \frac{Mxy}{2E} \left[\frac{y}{2} g_1(x, Q^2) + g_2(x, Q^2) \right]} \right\}$$

x is the fraction of nucleon's momentum carried by struck quark and y is the fraction of the lepton's energy lost measured in the laboratory system. The spin-dependent structure functions g_1 and g_2 can be disentangled by varying the angle β . The definition of the scattering angles β , θ and ϕ can be found in Fig. 4.2.

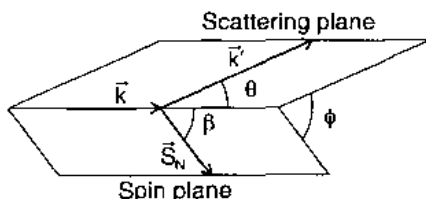


Fig. 4.2: Definition of the muon scattering angles θ and ϕ and the nucleon spin angle β .

Considering the simplest case of longitudinally polarised beam scattered on a longitudinally polarised spin 1/2-target gives rise to two asymmetries:

$$A_{\parallel} = \frac{\sigma^{\parallel\parallel} - \sigma^{\parallel\perp}}{\sigma^{\parallel\parallel} + \sigma^{\parallel\perp}} = DA_{\parallel}, \quad A_{\parallel}(x) = \frac{g_{\parallel}(x)}{F_{\parallel}(x)}$$

D is a kinematic factor, $F_{\parallel}(x)$ an unpolarised structure function. $g_{\parallel}(x)$ is a spin-dependent structure function which is interpreted in the Quark-Parton-Model as:

$$g_{\parallel}(x) = \frac{1}{2} \sum_i e_i^2 |q_i^+(x) - q_i^-(x)|$$

The functions $q_i^{(\parallel\perp)}$ are the distribution of quarks (flavour i) with spin parallel (antiparallel) to the nucleon spin.

The SMC experiment determined $g_{\parallel}(x)$ with proton and deuteron targets [B. Adeva et al., Phys. Lett. B 412 (1997) 414 and D. Adams et al., Phys. Lett. B 396 (1997) 338]. The results are compared to those from similar experiments at SLAC (E142/E143/E154) and DESY (HERMES). The neutron data has been obtained by analysing the deuteron – proton difference (SMC, E143, E154) or by a “direct” measurement with polarised ${}^3\text{He}$ target (E142, HERMES). All results are compiled in Fig. 4.3.

For certain moments of the structure function, QCD can make predictions which can be confronted to measurements. Consider moments of the spin-dependent structure functions:

$$\Gamma_{\parallel}(Q_0^2) = \int_0^1 g_{\parallel}(x, Q_0^2) dx$$

The Ellis–Jaffe sum rules

$$\Gamma_{\parallel}^{P(n)} = \frac{1}{12} \left[+(-) a_3 + \frac{1}{3} a_8 \right] + \frac{1}{9} a_0$$

relates the first moment of g_{\parallel} to the weak axial-vector couplings, a_n , defined as:

$$a_u = \Delta u + \Delta d + \Delta s = \Delta \Sigma, \quad a_3 = \Delta u - \Delta d = \frac{g_A}{g_V}, \quad a_8 = \Delta u + \Delta d - 2\Delta s$$

Δu etc: are moments of polarised parton distributions, a_0 is the total quark distribution to the nucleon spin. The “naïve” QPM prediction is $a_0 \approx 0.58$. The SMC results for a_0 are shown in Fig. 4.4 for different renormalisation schemes, confirming the disagreement with the naïve QPM prediction.

Another sum rule, known as the Bjorken sum rule, is about the difference of the proton – neutron moments:

$$\Gamma_{\parallel}^p - \Gamma_{\parallel}^n = \frac{1}{6} \left| \frac{g_A}{g_V} \right| \times \left[1 - \frac{\alpha_s(Q^2)}{\pi} - \dots \right]$$

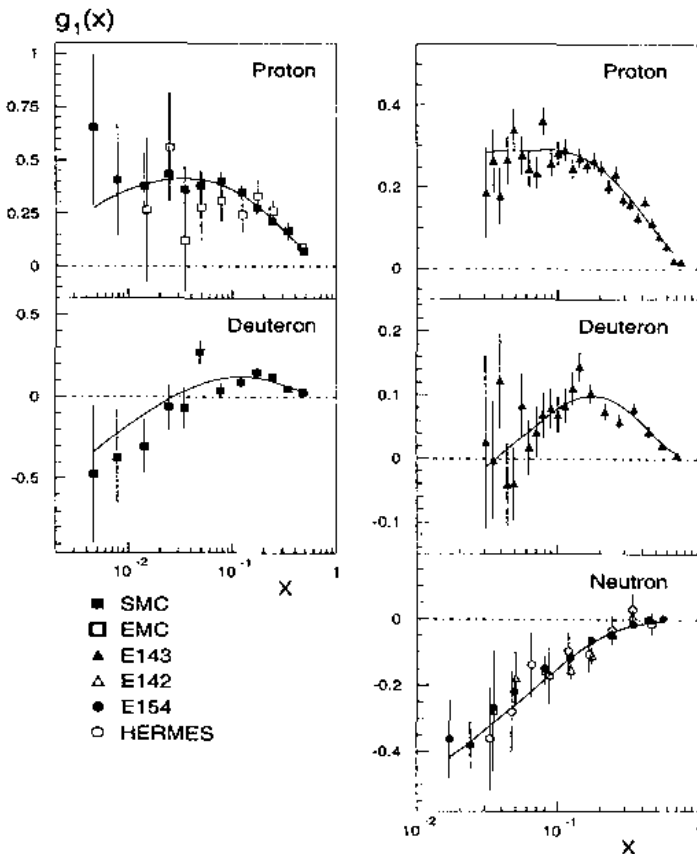


Fig.4.3: Nucleon spin structure function $g_1(x)$ from polarised lepton nucleon scattering experiments at CERN, SLAC and DESY for proton and deuteron targets.

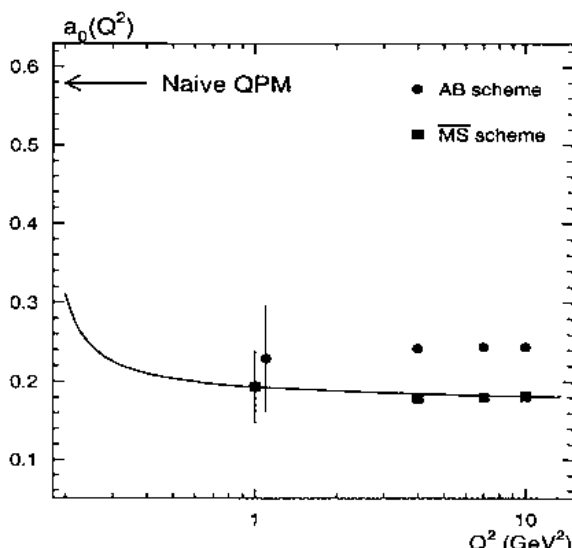


Fig. 4.4: Total quark contribution to proton spin from SMC data in different renormalisation schemes.

The quantities g_a , g_V are the axial-/vector weak couplings in neutron b decay.

Today this sum rule is understood as a fundamental QCD and known up to $\alpha_S^3(Q^2)$ and considered as a stringent experimental test of QCD. In Fig 4.5 all the measurements for Γ_1^n and Γ_1^p are shown. The Bjorken sum rule is well confirmed by all experiments, while the Ellis-Jaffe sum rule is strongly violated. The detailed composition of nucleon spin is still poorly known!

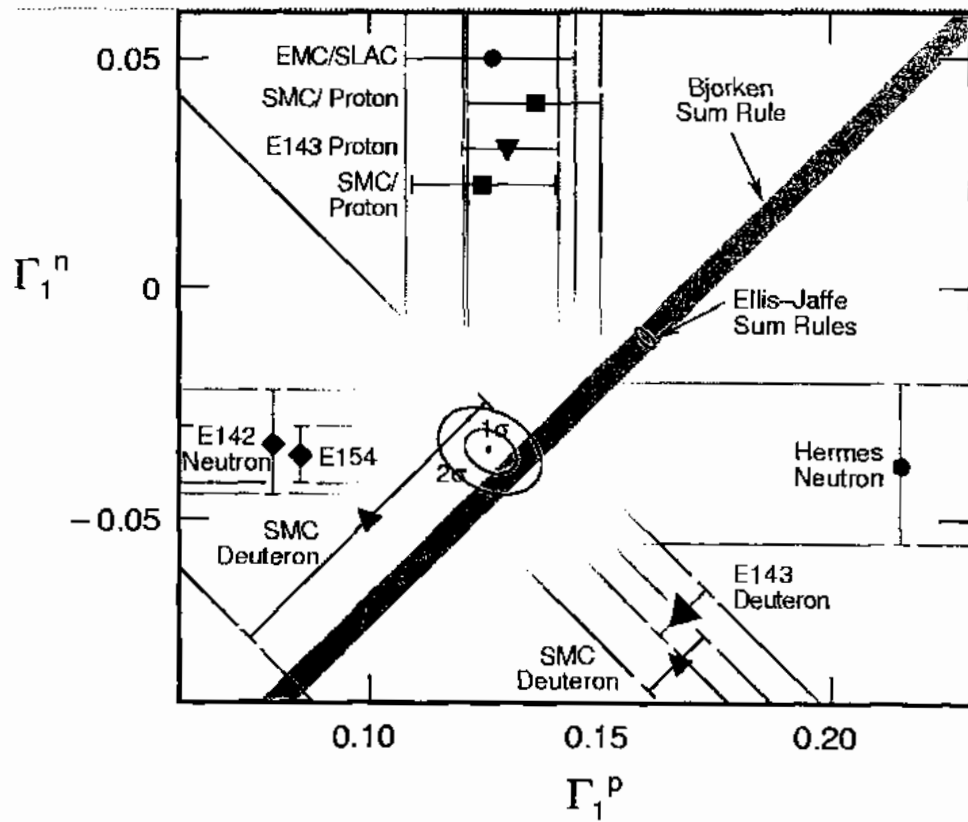


Fig. 4.5: Γ_1^n versus Γ_1^p for the CERN, SLAC and DESY measurements together with the Bjorken and Ellis-Jaffe Sum Rule predictions.

CHAIRMAN: D. SCHLATTER

Scientific Secretaries: A. Dainese, V. Lendermann

DISCUSSION

- *d'Enterria:*

What is the status of the heavy ion experiment NA60 at the CERN SPS?

- *Schlatter:*

NA60 is a fixed target experiment aiming at identifying open charm production in heavy ion collisions. The main difference with respect to previous experiments is the introduction of a silicon pixel detector that should allow the identification of charmed hadron decays. The assembly of the pixel detector is now being finalized. An Indium beam run is scheduled for October, while for the next year a proton-beam run is planned. This will complete the programme of NA60. During 2005, the current accelerator experiments will be stopped for one year in order to save resources for the Large Hadron Collider programme (LHC).

- *Cerri:*

In the discussion of the DIRAC results, you showed a distribution of the relative arrival time of the two pions. Can you comment on the asymmetry of the distribution around $\Delta t = 0$? Can you explain the sign convention being used?

- *Schlatter:*

I do not know the reason for this small asymmetry.

- *Cerri:*

ICARUS has commissioned prototypes of the final detector. What is their performance? Was it compliant to the design specifications? What are the perspectives for the final apparatus?

- *Schlatter:*

After a long but successful R&D phase, the ICARUS collaboration has operated successfully a 600 t liquid Argon TPC, T600. They plan to install it at the Gran Sasso Laboratory. According to my knowledge, after a recent incident with environment pollution, all activities involving toxic liquids in the Gran Sasso laboratory are suspended. Having provided the requested safety evaluations, the ICARUS Collaboration is waiting to get the permission to install the T600 module and start construction of the first of the two T1200 modules to be ready in time, i.e. by end 2006.

- *Cerri:*

This question is on the LHC physics. In case of low mass Higgs boson, what is the programme of ATLAS and CMS for the detection of $H \rightarrow b\bar{b}$?

- *Schlatter:*

This and other channels are being looked at by both the ATLAS and CMS collaborations and feasibility studies are in progress. Tagging of b-quarks is challenging in the LHC environment and the performance of the tracking systems is crucial for such measurements.

- *Menges:*

If OPERA and ICARUS record only 5-6 events after 5 years of running, what will be the possibilities to extend the running period by another 2 or 3 years?

- *Schlatter:*

Rather than on extending the running period, I would push for an improvement of the neutrino beam flux from CERN, with respect to the present design parameters. In the past, the CERN accelerator experts have been quite successful in upgrading beam performance. However, the overall performance depends also on the efficiency of the whole CERN accelerator complex. Some components, like the Proton Synchrotron (PS), are 40 years old and inefficiency due to ageing problems may occur.

- *Menges:*

What do you think about the future of CERN, after the LHC?

- *Schlatter:*

After 2010, financial resources will be available for a new project. At present, there is only one R&D accelerator project carried out at CERN: the linear e^+e^- collider project CLIC, aiming at a centre-of-mass energy of 3-5 TeV. By 2004-2005 at test facility CTF3 will test the technology necessary to achieve the required high gradients (~ 150 MV/m) with long pulses with the aim to demonstrate the technical feasibility of the CLIC two-beam scheme. In case these tests are successful and LHC physics results require experiments at a multi-TeV e^+e^- collider, CLIC may be an option.

- *Baldini:*

What is the status of the COMPASS experiment?

- *Schlatter:*

The COMPASS experimental programme foresees (a) the study of nucleon structure using a muon beam to improve the knowledge of the polarized structure functions and (b) hadron spectroscopy with charmed mesons and baryons and search for glueballs. They took data, mostly with the muon beam, and first physics results are expected soon.

- *Raggi:*

Is there any low energy programme foreseen at CERN during the LHC running period?

- *Schlatter:*

The PS proton beam is used to produce antiprotons with the Antiproton Deceleration facility (AD). There are currently three experiments using AD, one to study antiprotonic Helium and two in order to create and trap cold antihydrogen atoms. The latter two experiments have demonstrated the production and detection of ~ 1000 antiatoms. They will continue for some time, aiming at much higher antihydrogen production rates. After 2010, another laboratory, GSI (Darmstadt), plans to build an antiproton facility and may lead the field.

At the SPS, there is at the moment only one experiment, COMPASS, which may continue to take data over the next couple of years. In addition, it is not excluded that there will be some resources available for fixed target experiments exploiting the improved SPS which will be upgraded as LHC injector.

- *Rotaev:*

You were showing results on CP violation by the NA48 experiment. Is there any precision experiment testing the possibility of CPT violation?

- *Schlatter:*

New tests on the validity of the CPT theorem could in principle be tested by the antihydrogen experiments, but a very large statistics would be required. This is not possible for the currently running experiments at CERN but it is the aim of these experiments to study spectroscopy with antihydrogen to test CPT.

- *Zhou:*

Can one expect new results on ϵ'/ϵ and with what precision?

- *Schlatter:*

Precise measurements on ϵ'/ϵ are from NA48 at CERN, and KTeV at FNAL. At the moment there are no plans for further measurements. This is motivated by the fact that we have a 10σ evidence for a direct CP violation in neutral kaon decays. On the other hand, theoretical calculations are not at the same level of precision, so that we cannot fully profit from these experimental results. It is, therefore, preferable to get a better theoretical understanding before planning more precise measurements.

- *Krotov:*

Are the searches for extra dimensions included in the LHC experimental programme?

- *Schlatter:*

Yes, this is part of the physics programmes of ATLAS and CMS. The question is to what scale these searches can be extended. At LEP2, limits at a scale of ~ 1 mm were reached.

- *Wolf:*
Are there any plans for building a neutrino factory at CERN?
- *Schlatter:*
Certainly in the community there are discussions for a possible neutrino factory and there is an R&D project on muon cooling (MICE) in view of a neutrino factory. CERN is not able to commit resources to this effort; instead, the Rutherford Laboratory is actively supporting MICE.
- *Otiugova:*
Are there new results by the L3 Collaboration?
- *Schlatter:*
Although the LEP experiments have finished data taking and have now been dismantled, all LEP experiments, not just L3, have still a number of PhD theses that are in progress and will probably be concluded within one year. Beside results from a single experiment, there will still be results for which data have to be combined in order to improve the statistical precision, the most important being the measurement of the W mass. This result should be published soon, when the estimation of the systematic uncertainties in the hadronic decay channel will be completed.
- *Dainese:*
What are the prospects for a participation of ATLAS in the LHC heavy ion programme?
- *Schlatter:*
As far as I understand, there is a group in ATLAS interested in heavy ion physics and also CMS has established a programme to study heavy ion collisions.

Highlights from Gran Sasso

A. Bettini

Dipartimento di Fisica G. Galilei dell'Università di Padova
INFN Gran Sasso National Laboratory and Sezione di Padova

Abstract

After an introduction on the new neutrino physics and an overview of the experimental programme at the INFN Gran Sasso National Laboratory (LNGS), I'll concentrate on three activities: the Supernova neutrinos with LVD, the dark matter search with DAMA and CRESST and the nuclear astrophysics program of LUNA and LUNA2. I'll focus on how experiments at LNGS can give essential contributions to physics beyond the Standard Model.

1. Introduction

The Standard Model of subnuclear physics has been tested with great precision with experiments at particle accelerators and colliders, but this is far from being enough. The coupling constants of three fundamental forces, the strong, the electromagnetic and the weak, become closer to one another when energy increases, converging to a common value at about 10^{16} GeV. Clearly, to understand the nature of the forces we should make experiments at these energies. Of the remaining force, gravity, we do not even have a microscopic theory; to discover it we need data close to the Planck scale, 10^{19} GeV, extremely large just because the gravitational charge is so small. There are no possibilities to reach these energy scales with accelerators.

Astro Particle Physics is, albeit indirectly, the only way to have experimental, or at least observational, information of those scales. We try to understand elementary particles and their fundamental interactions from the observation of natural, but very rare, phenomena like proton decay, neutrino-less double beta decays, phenomena connected with the Majorana mass, etc. Or we can detect and study radiations from the Universe such as the cold dark matter, antimatter, topological defects, etc. In both cases, the searched phenomena are extremely rare and we must reduce all the interfering natural backgrounds, both in the environment and in the detector itself. The struggle against background is the way to push back the high-energy frontiers. Underground laboratories provide the necessary low radioactivity environment^[1].

2. The Gran Sasso Laboratory (LNGS)

The INFN LNGS is located besides a freeway tunnel under the Apennines, at about 6 km from the west entrance, 120 km from Rome.

The horizontal access allows easy transportation and installation of large pieces of apparatus and drive-in to the experiments. The underground facilities consist of three experimental halls and a set

of connecting tunnels and service areas, for a total surface of 18 000 m². The three halls are approximately 100x18x18 m³. An almost angle-independent 1400 m rock overburden provides a μ flux attenuation of 10⁻⁶. The neutron flux is $\text{flux} = 3.7 \pm 0.3 \cdot 10^{-2} \text{ m}^{-2}\text{s}^{-1}$

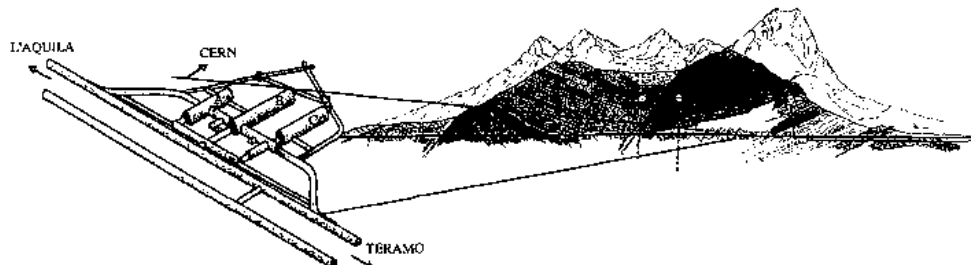


Fig. 1. The underground facilities and the Gran Sasso massif geology

The infrastructures of the laboratory are completed by a number of buildings on the surface, near the western entrance of the tunnel, hosting offices, laboratories, shops, library, canteen, etc. General services include the headquarters, the secretariats and user support offices, the administrative offices, the prevention, safety, security and environmental protection services, the general, electrical and safety plants services and, in direct support to the experiments, low activity techniques (including very low background facilities with Ge detectors underground), cryogenics, mechanics, chemistry, electronics, computing and networking. Last but not least, since many years now, the laboratory has an important activity in the outreach and in the diffusion of the scientific culture. The laboratory has 66 permanent position contracts. Presently, the users are 755 in number, from 25 different countries. After a more than ten-years operational life, several first generation experiments have been completed and decommissioned; other will finish in the next few years. A programme for the second phase has been studied and is now being implemented.

Neutrino physics will be the principal, but not the only chapter of this programme. Experiments both with naturally produced neutrinos (from the Sun, from the atmospheric and from Supernova explosion) and artificially produced ones are running, being built or planned. On solar neutrinos, GNO is taking data, BOREXINO is in its final phase of construction (even if presently halted by the spill accident), LENS in an advanced phase of R&D. On Supernova neutrinos LVD is taking data with an up-time larger than 99.5%. The joint with CERN CNGS project is optimised for tau neutrino appearance in the longer period oscillation phenomenon; of the two experiments, OPERA - based on emulsion techniques - is in the construction phase; for ICARUS - based on liquid argon TPC - a first 600 t module has been constructed and tested on the surface; safety issues are being studied and the modifications necessary for a safe operation and with the limitations of power consumption and dissipation inherent to underground environment are being implemented.

LNGS hosts the most sensitive experiments in $\beta\beta$ decay in each of two different isotopes, ^{76}Ge (H-M and GENIUS-TF now, GENIUS in perspective) and ^{130}Te (presently CUORICINO, in perspective

CUORE). The measurements of thermonuclear cross-sections at energies relevant for the stars and Sun combustion processes will be pursued with improved underground accelerator facilities, LUNA and LUNA2.

In the search for dark matter, DAMA is now a completed experiment, after seven years of observations. The observed annual modulation signal is a model-independent signature for WIMPs in the Galaxy, a result that must be independently checked. Unfortunately, the other experiments, which do not look for the modulation, cannot be compared in a model-independent way. At Gran Sasso, a set of complementary approaches is being pursued with LIBRA, the successor of DAMA, CRESST, and possibly with GENIUS-TF and CUORICINO.

Finally it must be mentioned that a number of experiments in different disciplines, mainly geology and biology, are profiting from the particular conditions of the laboratory.

Rather than over viewing the whole scientific programme of the laboratory, I'll concentrate, in order to obtain a deeper insight, on three experimental programs: Supernova neutrinos, search for cold dark matter and nuclear astrophysics. I'll start with a summary of the new neutrino physics referring to the lecture of Prof. Fogli^[2] for a more complete review.

3. The New Neutrino Physics. A summary

Experiments on electron neutrinos from the Sun (Homestake, GALLEX and GNO, SAGE, KamiokaNDE and SuperKamiokaNDE and SNO) and electron and muon neutrinos indirectly produced by cosmic rays in the atmosphere (SuperKamiokaNDE, MACRO and SOUDAN2) have shown that neutrinos oscillate amongst states of definite flavour. This discovery has been later confirmed by experiments on artificial neutrino beams from an accelerator (K2K) and from reactors (KamLAND). This phenomenon, forbidden in the Standard Model, implies that, contrary to its assumptions: 1. electron, muon, and tau neutrinos are not the mass eigenstates (we will call them ν_1 , ν_2 , and ν_3 , and m_1 , m_2 and m_3 their masses); 2. at least two of the masses are not zero; 3. flavour lepton numbers are not conserved, so that, for example, an originally pure muon neutrino beam can produce tauons and electrons, provided we wait long enough. While in the case of quarks, each mass eigenstate is dominated by a single flavour component, neutrino eigenstates are radically different from flavour states.

A particle and its antiparticle - the charge conjugated state - have opposite values of all, not only the electric, charges. The only charge of neutrino is the lepton number, so that neutrinos differ from antineutrinos by having opposite flavour and total lepton numbers. But we have seen that flavour lepton numbers are not conserved; muon flavour can change into tau flavour for example. If neither the total lepton number is conserved, neutrino and its charge conjugate antineutrino may be two states of the same particle. Neutrinos are then called Majorana particles. As we do not have any experimental evidence for neutrinos to be Dirac or Majorana particles, we must leave the issue open. Notice that neutrino and antineutrino states are anyway distinguishable: the first is a left particle

(meaning the $(1+\gamma_5)/2$ projection), and produces charged leptons, the second is right and produces antileptons.

As far as we know, in Nature, neutrino flavours are three. The flavour eigenstates are linear combinations of the mass eigenstates, $\nu_l = \sum_{i=1}^3 U_{li} \nu_i$, where $l = e, \mu, \tau$ and U is the mixing (unitary) matrix.

The elements of the mixing matrix can be expressed in terms of six independent real parameters: three mixing angles, θ_{12} , θ_{13} and θ_{23} , and three phase factors, which can give CP violation. Two phase factors, α and β , can be eliminated if neutrino and antineutrinos are different (Dirac) particles; they are relevant in double beta decay but are irrelevant for oscillations.

Having three neutrino species, the oscillation phenomenon is, in general, a superposition of oscillations involving all flavour states. In a monochromatic beam initially containing only one neutrino flavour, the probability to observe one of the other flavours oscillates as a function of the proper time or, to be closer to the experimental conditions, x/E , the ratio of the path x and the neutrino energy E . The oscillation is a superposition of harmonic functions with periods inversely proportional to the difference between the squares of the masses of the eigenstates and amplitudes, which are functions of the mixing angles dependent of the initial and final flavours.

In practice, one of the observed periods, the one corresponding to solar neutrinos oscillations, is an order of magnitude larger than the other, which corresponds to the atmospheric neutrinos phenomenon. These circumstances make the description much simpler.

First, atmospheric muon neutrinos disappear (oscillate to other flavours) with the shorter period, when the longer period oscillation is not yet started. The time evolution is, to a very good approximation, the same, simply periodic, as in the two-flavour case, but, unlike that case, muon neutrinos can "convert" in both tau and electron neutrinos, with probabilities dependent on the mixing angles. SuperKamiokaNDE data show also that the muon neutrinos disappearance is as large as it can be, implying that $\theta_{23} \approx \pi/4$. The square mass difference is $\Delta m^2 \approx 2000-2500$ meV 2 . Data suggest that the oscillation should be predominantly into ν_e , but we do not have direct evidence for that yet, this being the main target of the CNGS programme. Neither we have experimental evidence for the minority ν_μ oscillation into ν_e but only an upper limit on its amplitude $|U_{e\mu}|^2 = |\theta_{13}|^2 < 0.025$, the evidence coming from the CHOOZ electron antineutrinos disappearance experiment.

Second, the flight times relevant for the solar neutrinos phenomenon are much longer than the first period. As solar neutrinos are not monochromatic, observations average on several periods of the first oscillation, which becomes non-observable. Again, only one periodic oscillation phenomenon is relevant similarly to the two-flavour oscillation in a vacuum. Again, the similarity is not complete, because neutrinos, produced in the centre of the Sun, must travel into matter before leaving the Sun. If an electron neutrino (or antineutrino) beam propagates into matter (in the Sun, in the Earth or in a Supernova) another mechanism may cause flavour conversion, the so-called MSW effect^[3]. Electron neutrinos (and antineutrinos) interact with electrons via charged current weak interactions giving, in particular, coherent forward scattering, a phenomenon exactly similar to the forward scattering of

light in matter at the origin of the refractive index. Similarly to light, the electron neutrino wave acquires a refractive index different than in vacuum, or, equivalently a different effective mass. Notice that the effect is proportional to the forward scattering amplitude, hence to the Fermi constant, not to the cross section, which is proportional to its much smaller square. This explains its importance. Contrarily to a common belief, even neutrinos feel the presence of matter. The phenomenon is limited to electron neutrinos because the other neutrino flavours interact via neutral current only and the effects of negative electrons and positive nuclei compensate.

The conclusion is that electron neutrinos move under the action of an attractive potential, and anti electron neutrinos under an equal and opposite potential. The mass eigenstates in matter are not, as a consequence ν_1 , ν_2 , and ν_3 and must be found by diagonalizing the mass-matrix. The effect depends on the electron density (N_e) times the neutrino energy (E). In appropriate conditions a level crossing phenomenon takes place: at a critical $N_e E$ value the effective electron neutrino "mass" becomes equal to that of a different flavour. Electron neutrinos will convert into neutrinos of that flavour while crossing a variable density medium when they reach this critical value. Notice that what we have said holds also for Majorana neutrinos; even in this case neutrinos and antineutrinos are in fact distinguishable.

Coming back to the solar neutrinos phenomenon, we must say that an enormous progress has taken place in the last months. Referring to Prof. Fogli's lecture for the details, I'll only recall that we have now established that: 1. the phenomenon is mainly due to matter MSW effect, 2. of the several possible solutions in the parameters space we have established, the correct one: $\delta m^2 \approx 70$ meV 2 , $\sin^2 \theta_{12} \approx 0.3$. Notice, in particular that θ_{12} is large, but not equal to maximal mixing.

Summarising, we know that the neutrino mass spectrum consists of a doublet and a singlet. The singlet has a very small (if any) electron neutrino component (U_{e3} is small). We call m_1 , m_2 with $m_2 > m_1$ the masses of the doublet and $\delta m^2 = m_2^2 - m_1^2$. We call the mass of the singlet m_3 and $\Delta m^2 = m_3^2 - m_2^2$. The smaller mass difference δm^2 is responsible for the solar flavour conversion, the larger one Δm^2 of the atmospheric oscillation.

We do not know either the sign Δm^2 or the absolute value of the masses, because oscillations are not sensitive to these values. There are then three basic alternatives for the mass spectrum: almost degenerate, when the masses are much larger than the mass differences, "normal" ($\Delta m^2 > 0$) if the singlet is higher, or "inverted" if it is lower ($\Delta m^2 < 0$) than the doublet.

The absolute scale of neutrino masses is smallest in the hierachic case; for normal spectrum we have the lower limits $m_3 \geq \sqrt{\Delta m^2} \approx 50$ meV and $m_2 \geq \sqrt{\delta m^2} \approx 7.5$ meV. The unit for neutrino masses is the millielectronvolt.

Notice that in the seesaw mechanism, the natural one to generate neutrino masses, $m_i = v^2/M$, where M is a large mass, the energy scale of lepton number violation. With $v=M_m$ and m , a few meV, we have $M \approx 10^{15}\text{-}10^{16}$ GeV. The smallness of the neutrino masses, compared with quarks (or to the electroweak scale), gives a lepton number (and baryon number, perhaps) violation scale close to the

GUT scale. We see, in this example, how the search for rare phenomena can give information on the largest energies.

To complete our knowledge of the neutrino mass spectrum, we need one more experimental input. It can come from at least three different and complementary sets of experiments: cosmology, beta decay and double beta decay. Let us briefly describe these possibilities.

Cosmology has made a tremendous progress in the last years, both in measuring and in modelling the Universe. Large amounts of data are produced with unprecedented precision with different types of telescopes on the surface, on balloons and on satellites and with laboratory experiments. As the Universe is unique, the only possibility to compare a theory with Nature is through consistency checks and, indeed, the data that become available allow rather stringent tests over constraining the models. A Standard Cosmological Model has emerged based on a flat, accelerating universe, whose structures are seeded by initial quantum fluctuations and which has gone through an early period of inflation. Notice that the model is purely phenomenological, lacking the theoretical bases of the particle Standard Model, but its main parameters are rather well determined by independent observations. [see, http://lambda.gsfc.nasa.gov/product/map/pub_papers/firstyear/basic/wmap_params_table.pdf]

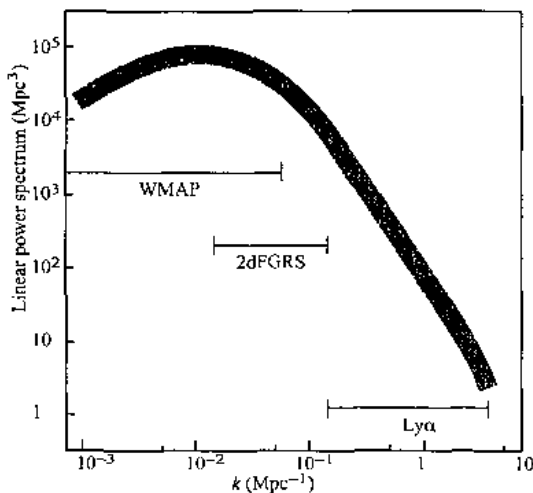


Fig. 2. Schematic representation of the Large-Scale Structures (LSS) in the Universe

Neutrino mass density is one of these parameters. As the number densities of the three neutrino states, ν_1 , ν_2 , and ν_3 , are independent on their masses, a limit on (or a value of) neutrino mass density gives a limit on (a value of) the sum of the masses of the three neutrinos. As the neutrino mass density parameter has an influence on the formation of the large structures in the Universe, it can be determined by the spectrum of these structures. Let us see how.

Fig. 2 shows schematically the relevant function, called power spectrum $P(k)$, which is, in simple words, the Fourier-transform of the distribution of the density fluctuations at large scales. The "wave number" k is the conjugate of the size of the structures. Three types (at least) of observations are relevant. At extremely high scales the structures are the temperature fluctuations in the CMB spectrum; the range is labelled in Fig. 2 as WMAP, which is the most accurate experiment. At intermediate scales the structures are the super clusters and clusters of galaxies, which are point-like at these scales; data come from the galaxies surveys, which only recently with 2dFGRS and with SDSS extend to distances (order of 1000 Mpc, $z = 0.3$) larger than the largest structures (200 Mpc). Finally, at still smaller scales, data are those of the so-called Lyman α forest.

Neutrinos moving at relativistic speeds tend to suppress smaller scale (say 10 Mpc) structures. The observed power spectrum at small and intermediate scales (large k) follows a power law, turning over at larger scales (say 100 Mpc). Its shape depends on neutrino density, which, in its turn, is linked to total neutrinos mass by

$$h^2 \Omega_\nu = \frac{\sum m_i}{94 \text{ eV}}$$

where h is the reduced Hubble constant. Using their own data, those of 2dFGRS and Lyman α forest data, the WMAP collaboration^[4] gave an upper limit on neutrino masses, $\sum_{i=1}^3 m_i < 700 \text{ meV}$. This is the best available limit on neutrino masses. Fig. 3 (thanks to Vissani) shows the three neutrino masses as functions of their sum and the limit.

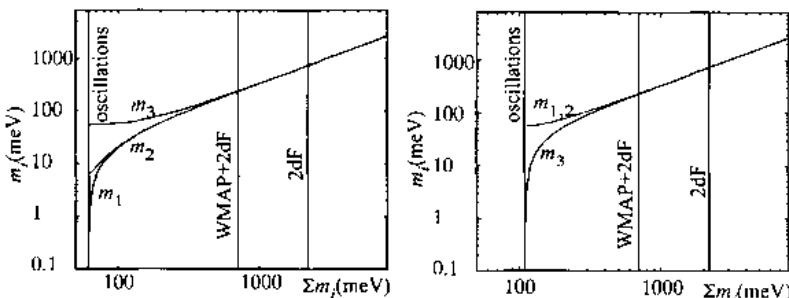


Fig. 3. The three neutrino masses as functions of their sum: left panel is for normal hierarchy, right one for inverse

Notice that the limit depends somewhat on the assumptions made in the analysis and on the data used. It worsens by almost a factor of two if, for example, the most uncertain, Lyman α forest data are not included. On the other hand, further progress is expected from the data of the Sloan Digital Sky Survey (SDSS), which is expected to measure the spectrum with 1% accuracy. We can expect to be in a few years sensitive to $\sum m_i = 300 \text{ meV}$ or even better. Optimistically, if systematic uncertainties will be also reduced, cosmology may become close to the lower limit of neutrino masses, $\sum m_i > \sqrt{\Delta m^2} = 50 \text{ meV}$ for normal, $\sum m_i > 2\sqrt{\Delta m^2} = 100 \text{ meV}$ for inverse hierarchy.

The measurement of the electron energy spectrum from the beta-decay of Tritium gives a lower limit (or a value) of the so-called "electron neutrino mass" $\langle m_{\nu_e} \rangle$. Near the end point the slope is zero, if neutrinos have no mass. If neutrinos are massive, the maximum electron energy is smaller and three steps of vertical slope should be present at the end of the spectrum, one for each of the masses. The individual steps are not resolvable and one measures a linear combination of the mass squared, namely $\langle m_{\nu_e}^2 \rangle = |U_{e1}|^2 m_1^2 + |U_{e2}|^2 m_2^2 + |U_{e3}|^2 m_3^2$. Knowing that $|U_{e3}|^2$ is very small and from our knowledge of the other two mixing parameters, $\langle m_{\nu_e}^2 \rangle = 0.67m_1^2 + 0.33m_2^2$

Presently two experiments, from the Mainz and Troitzk groups^[5] give upper limits of a few electronvolts, $\langle m_{\nu_e} \rangle < 2.2$ eV for the Mainz experiment. For the future, a new spectrometer, KATRIN, by the joint two groups, aims to be sensitive down to 350 meV. Fig. 4 gives the behaviour of $\langle m_{\nu_e} \rangle$ as a function of the sum of the neutrino masses, with the limits from beta decay, cosmology and double beta decay, which we will discuss now. Notice that the expected KATRIN limit will be comparable with the present one from cosmology, but it will be a direct model-independent experimental measurement.

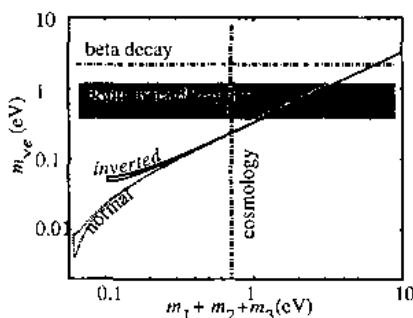


Fig. 4. Electron neutrino "mass" parameter as a function of the sum of the neutrino masses for normal and inverse hierarchies. Bands take into account the uncertainties on the mixing parameters. Present limits from beta decay, cosmology and – if neutrinos are Majorana particles – from double beta decay are shown (thanks to F. Vissani)

If neutrinos are massive Majorana particles, a very rare process, the neutrino-less double beta decay ($0\nu2\beta$) can happen in some nuclides, a process that violates the lepton number by two units.

The double beta active nuclides are stable against normal beta decay, i. e. $Z \rightarrow (Z+1) + e^- + \bar{\nu}_e$ is forbidden, but have the two-neutrino double beta decay ($2\nu2\beta$) channel open: $Z \rightarrow (Z+2) + 2e^- + 2\bar{\nu}_e$. This last is a very rare, but standard, second order weak process and happens if the ground level of the Z isotope is lower than that of $Z+1$ but higher than that of $Z+2$.

After measuring or limiting the ($0\nu2\beta$) lifetime of a nuclide, we can extract the "effective mass" $|M_{ee}^M| = |U_{e1}|^2 m_1 + |U_{e2}|^2 e^{2ia} m_2 + |U_{e3}|^2 e^{2ib} m_3|$. As double beta decays happen in nuclei, the relevant nuclear matrix elements must be known. The uncertainty on the (calculated) matrix elements induces uncertainties on M_{ee}^M typically of a factor two-three (that we'll call h).

Presently the best limit, $M_{ee}^M < 270 \text{ h meV}$ (90% c.l.), based on the half-life limit of 2.1×10^{25} years, is given by the Heidelberg-Moscow^[6] experiment at Gran Sasso, obtained with a 37.2 kg yr exposure of an enriched ^{76}Ge detector.

Notice that cancellations can take place in M_{ee}^M , due to the phase factors. Fig. 5, from ref. [7] shows M_{ee}^M as a function of the lightest neutrino mass. The widths of two bands, one for normal and one for inverse hierarchy, are determined by our complete ignorance on the Majorana phases. Two experiments now in the R&D phase at LNGS, CUORE^[8] and GENIUS^[9], aiming at 50 meV sensitivity, may well reach the discovery region.

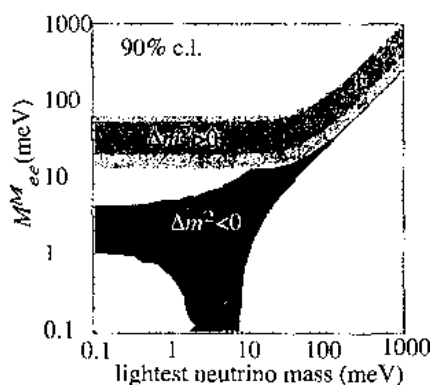


Fig. 5. Electron neutrino "Majorana mass" as a function of the smallest mass eigenvalue for normal and inverse hierarchy. The bands show the uncertainties due to the lack of knowledge of phase factors.

4. Neutrinos from Supernovae. LVD

The evolution of iron core massive stars may lead to the collapse of its core, a (particular type of) Supernova explosion. Most of the gravitational energy is emitted in neutrinos and antineutrinos. The total emitted energy is enormous, $3 \times 10^{46} \text{ J}$ at a rate that is larger than the luminosity of the entire Galaxy. The detection of the neutrinos and the measurement of their spectra and time evolution will provide important information on neutrino physics and on the implosion dynamics.

The burst can be observed, with sub-megaton mass detectors, only if the explosion is in the Galaxy or in the Magellanic Clouds. From observational data and SN morphology, Cappellaro and Turatto^[10] estimate 3-4 core collapse SNe per century. An independent estimate can be obtained from the fact that about 7 SNe have been observed in our Galaxy in the last 1000 years and that all of them have been in about 20% of the Galaxy volume, on our side of the galactic centre. This suggests that many SNe are dark and that we can expect 2-4 explosions per century, consistent with the previous estimate. These estimates are probably pessimistic, not taking into account possible surprises, as that of the SN 1987a, which exploded in the Magellanic Clouds, a region where such phenomena were not expected.

In the SN explosion, when it happens, neutrinos and antineutrinos of the three flavours are produced in the core in a burst lasting 20-50 s. Neutrinos then cross a medium of very high density and important matter induced flavour conversions take place. As a consequence, the flux of a given flavour reaching the Earth and measured by our detectors is different from that originally produced. [If neutrinos cross the Earth before interacting in the detector, MSW effect in the Earth matter takes place; we will not consider here this phenomenon, discussed in the literature.] From these differences we can extract information on neutrino mixing and mass hierarchy, as we will see. Notice, on the other hand, that there is no sense in the idea to measure the difference between, say, ν_μ and ν_e "masses" from a delay in the arrival of the ν_μ relative to the ν_e . It is the mass eigenstates and not the flavour states that propagate in the vacuum from the Supernova to us; the detected ν_μ and ν_e not necessarily left the Supernova as such.

There are two mechanisms that produce neutrinos in a Supernova: neutronisation and thermal emission. In the neutronisation process, electrons are captured by protons and nuclei; a ν_μ flux results, dominant in the first few milliseconds. Thermal emission follows, due to $e^+ e^-$ annihilation into neutrino-antineutrino pairs of all the flavours. Clearly for each flavour the neutrino and antineutrino fluxes are equal. Notice also that muon and tau neutrino fluxes are identical because both are due only to neutral currents. For the same reason, ν_μ and ν_τ are in equilibrium into a smaller sphere than ν_e 's, which have also charged current interactions. In this smaller neutrino-sphere, temperature is higher and, as a consequence, the spectrum of ν_μ and ν_τ (and of their antineutrinos) is harder (average energy approximately 20 MeV) than that of ν_e 's (average energy approximately 12 MeV). There are large uncertainties on these estimates.

At Gran Sasso, the LVD is a dedicated experiment with 1080 t sensitive mass of organic liquid scintillator in a modular structure consisting of 912 tanks, each seen by three photomultipliers. The tanks are read out independently, allowing a very high up time (99.5-99.8% in the last years). LVD is mainly sensitive to electron-antineutrinos through the process $\bar{\nu}_e + p \rightarrow n + e^+$ followed by the neutron capture $n + p \rightarrow d + \gamma + 2.2$ MeV, used as a tag with 60% efficiency. A few hundreds of events are expected for a SN explosion in the centre of the Galaxy (8.5 kpc). Their number and their energy spectrum can help in distinguishing amongst the different neutrino mass spectra.

LVD is sensitive to electron neutrinos and antineutrinos through the charged current process $\nu_e + {}^{12}C \rightarrow e^- + {}^{12}N$, followed by ${}^{12}N \rightarrow {}^{12}C + e^+ + \nu_e$ (energy threshold at 17.3 MeV) and $\bar{\nu}_e + {}^{12}C \rightarrow e^+ + {}^{12}B$ followed by ${}^{12}B \rightarrow {}^{12}C + e^- + \bar{\nu}_e$ (threshold at 14.4 MeV). For both, a handful of events are expected if no MSW conversion would take place in the SN because electron neutrinos and antineutrinos spectrum would be soft, below the thresholds for a large fraction. On the contrary, as we will see, MSW can make one of the two spectra harder, increasing the corresponding rate.

Finally, the experiment is sensitive to the neutral current process $\nu_x + {}^{12}C \rightarrow \nu_x + {}^{12}C^*$ followed by ${}^{12}C^* \rightarrow {}^{12}C + \gamma$ with threshold at 15.1 MeV). As due to all neutrino flavours, its rate is insensitive to flavour conversion.

The flavour conversion in the SN depends on the mass hierarchy of the neutrino spectrum (the sign of Δm^2) and the size of the mixing parameter $|U_{\alpha}|^2$; measurement of the rates of the above processes can give us information on these two parameters. Let us see how.

Consider first neutrinos (as opposed to antineutrinos). As recalled in chapter 3, in matter the mass matrix is not diagonal, because ν_e 's feel an attractive potential due to the charged currents weak interactions; as a consequence, ν_1 , ν_2 and ν_3 are no longer the eigenstates. The mass matrix contains non-diagonal elements given by the term $A=2G_F N_e E$, where G_F is the Fermi constant, N_e is the electron number density - depending on the distance from the centre - and E is the neutrino energy. In the SN core $A \gg \Delta m^2 \gg \delta m^2$, a condition that makes calculations simple; diagonalisation can be done by series expansion. One finds⁽¹¹⁾ that the mass eigenstates ν_1^m , ν_2^m and ν_3^m are the electron neutrino ν_e and suitable linear combinations of muon and tau neutrinos that we call ν_μ and ν_τ . Notice that ν_μ and ν_τ are indistinguishable in the SN because they have only charged current identical interactions.

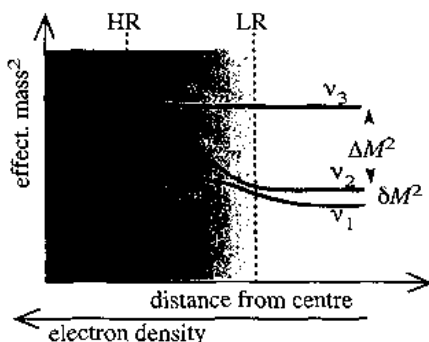


Fig. 6. Schematic representation of the MSW effect in a Supernova

Let us consider first the case of "normal" spectrum; the singlet eigenstate ν_3 is higher than the doublet. Fig. 6 shows schematically the situation; notice that there are two separate resonance conditions: one at higher density (HR) corresponding to Δm^2 and one at lower densities corresponding to δm^2 . Let us consider the electron neutrinos. They are produced in the core and then travel in a decreasing density medium; their effective mass (the eigenvalue of the mass matrix) decreases as a consequence. When the ν_e reach the first resonance stay on the upper level, finally leaving the Supernova as a pure ν_3 beam, provided that the adiabaticity conditions are satisfied. This happens if the relevant mixing angle is not too small; in the case under consideration, $\theta_{13}^2 \approx |U_{\alpha}|^2 > \text{a few } 10^{-4}$. If not, ($\theta_{13}^2 < \text{a few } 10^{-4}$) electron neutrinos continue on the lower curve and reach the LR; here they certainly stay on the upper level, because now the relevant mixing angle is θ_{12} , which is large. They leave the SN as a pure ν_2 beam.

In the case of "inverse" hierarchy, the highest vacuum eigenstate is ν_2 and the HR corresponds to δm^2 . The transition certainly happens, because the relevant angle is θ_{12} and electron neutrinos exit as ν_1 . This completes the discussion for neutrinos (for antineutrinos see the conclusions later).

As LVD detects electron neutrinos, we must consider the probabilities to observe this state in the three cases we have discussed. We call P_{ee} this probability that a neutrino born as ν_e is observed as ν_e (= leaves the SN as ν_e). Clearly $P_{ee} = |U_{e1}|^2$, hence very small, in the first case and $P_{ee} = |U_{e2}|^2 = \sin^2 \theta_{12} \cos^2 \theta_{13} \approx \sin^2 \theta_{12} \approx 0.3$ in the other two cases.

Call Φ_e the ν_e flux detected on Earth and Φ_e^{SN} that produced in the SN core; as $\Phi_e^{SN} = \Phi_e$ we call them Φ_e^{SN} . It is not difficult to show that $\Phi_e = \Phi_{\mu e}^{SN} + P_{ee}(\Phi_e^{SN} - \Phi_{\mu e}^{SN})$.

We see that in case of normal hierarchy, adiabatic HR, being P_{ee} very small, $\Phi_e \approx \Phi_{\mu e}^{SN}$. No original ν_e is detected as such, all the originally $\nu_{\mu e}$'s are detected as ν_e 's; the effect doubles the average electron neutrinos energy; the spectrum is, say, hard.

The other two cases are indistinguishable. For them $\Phi_e = 0.7 \Phi_{\mu e}^{SN} + 0.3 \Phi_e^{SN}$. The spectrum is harder than the original one, but not so much as in the first case (medium).

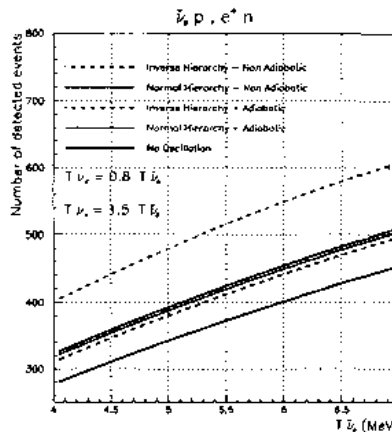


Fig. 7. Yield for $\bar{\nu}_e + p \rightarrow n + e^+$ expected in LVD for a Supernova explosion at 10 kpc as a function of the electron-neutrino temperature in different mixing hypotheses (Thanks to M. Selvi)

Coming now to the antineutrinos, the situation is similar, but with an opposite sign in the potential. Then anti- ν_e 's leave the SN as anti- ν_e for inverse hierarchy and $\theta_{13}^2 > \text{a few } 10^{-4}$. The anti- ν_e spectrum at the detector is hard. In the other two cases they leave as anti- ν_e , and the anti- ν_e spectrum at the detector is $\Phi_e = 0.3 \Phi_{\mu e}^{SN} + 0.7 \Phi_e^{SN}$, again, even not exactly the same as before, medium.

Notice, in particular, that if the HR is adiabatic (an information that may come from other measurements) the ν_e spectrum is hard and the anti- ν_e is soft if $\Delta m^2 > 0$, while if $\Delta m^2 < 0$, vice versa, the ν_e spectrum is soft and the anti- ν_e is hard. So that the ratio of the electron neutrino and antineutrino events may give a handle to establish the mass hierarchy.

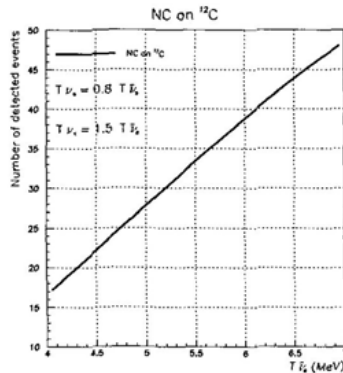


Fig. 8 Yield for $\nu_x + {}^{12}\text{C} \rightarrow \nu_x + {}^{12}\text{C}^*$ expected in LVD for a Supernova explosion at 8 kpc as a function of the electron-neutrino temperature in different mixing hypotheses (Thanks to M. Selvi)

Detailed calculations for LVD have been done by Marco Selvi of the Bologna group. I'll report the principal results. The yields are calculated for a SN explosion at 10 kpc.

Fig. 7 shows the yield for the principal process $\bar{\nu}_e + p \rightarrow n + e^+$ as a function of the neutrino temperature, a parameter that is not well known. As expected from the previous discussion, the case of inverse hierarchy, adiabatic HR can be distinguished from the other three, provided the neutrino temperature is known. Information on the temperature comes from the yield of the neutral current process $\nu_x + {}^{12}\text{C} \rightarrow \nu_x + {}^{12}\text{C}^*$, as seen in Fig. 8.

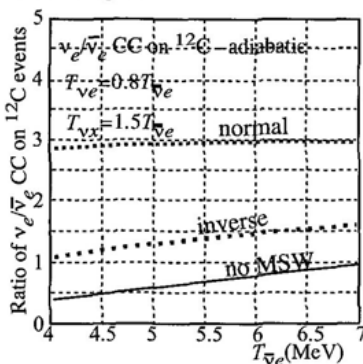


Fig. 9. Ratio of electron neutrinos and antineutrinos inverse beta decay on Carbon rates in LVD

LVD cannot distinguish between neutrino and antineutrino charged currents interactions on carbon on an event by event basis, but can separate statistically (especially if the SN is not too far) $\nu_e + {}^{12}\text{C} \rightarrow e^- + {}^{12}\text{N}$ from $\bar{\nu}_e + {}^{12}\text{C} \rightarrow e^+ + {}^{12}\text{B}$ because the β decay lifetime of ¹²B is 29.4 ms while that of ¹²N is 15.9 ms. Fig. 9 reports the ratio of the two yields, in the ideal case of perfect separation,

showing that normal and inverse hierarchies differ by a factor three, almost independently on the temperature (but depending on the temperature ratio of the neutrino species, a better known quantity).

5. The Search for Cold Dark Matter

We have already recalled in Section 3 that recently a Standard Model of Cosmology has been formulated, consistently explaining the available data. The budget of the Universe has become known from independent pieces of evidence. In particular, the density of matter divided by the critical density is $\Omega_m=0.27\pm0.04$, according to the WMAP⁴¹ fit. Of this, ordinary matter, made of atoms, nuclei and electrons and called baryonic by the cosmologists, is only a very small fraction, $\Omega_b=0.044\pm0.004$ (as a fraction of the critical density). We have also seen that the contribution of neutrinos is very small. In conclusion, we do not know the particles that constitute the largest fraction of the matter in the Universe. We know only that it does not produce light, and call it "dark".

Dark matter manifests itself through its gravitational effects. The first evidence came from the observation of Fritz Zwicky in 1933 that the thousands of galaxies of the Coma cluster move at speeds higher than the escape velocity from the cluster, as inferred from its visible matter. He concluded that the cluster had to contain much more, invisible, mass to keep the galaxies bound together. A conclusion confirmed by similar observations in other clusters of galaxies.

The masses of several spiral galaxies were determined, starting in the mid 1970s, by measuring the speeds and the radii of the clouds of hydrogen and helium that orbit around them: the total masses are about ten times larger than the luminous ones, extending at distances from the centre much larger than the luminous radius. The mass of the galaxies is predominantly dark.

The total mass of a galaxy or of a cluster of galaxies can be independently determined using an effect called "gravitational lensing". Consider an astronomical source sending us its light and a dark massive object in between. The gravitational field of this body bends the light rays and the image of the source is deformed. If the distance of the object is known, the magnitude and the shape of the distortions allow us to evaluate its mass. Again it is much larger than the expectations assuming only the contribution of the stars. Other consistent evidence comes from X-ray images of the clusters. Independent evidence for dark matter comes from the fine details in the cosmic microwave background (CMB), the primordial radiation that fills the Universe, a snapshot of when it was 380,000 years old and a thousand times smaller than today.

All data and more are consistent with the same value of the dark matter density, $\Omega_{dm}=0.23\pm0.05$. This value is also consistent, when added to the above-mentioned value of Ω_b , to the recalled value of Ω_m . It is mandatory for experimental physics to try to detect the dark matter particles and to understand what they are. Their flux is as high as about 10^{11} (GeV/M_w) m⁻²s⁻¹, but their detection is extremely difficult. Dark matter particles have neither electromagnetic nor strong interactions; otherwise we would have already seen them. If they do not have even weak charge, we do not have any hope to observe them. Assuming they do have weak charges, we call them WIMPs (Weakly Interacting

Massive Particles). The Standard Model has no space for WIMPs but its Supersymmetric extensions have clear candidates: the lightest particle of the supersymmetric zoo, presumably the neutralino, is stable, provided *R*-parity is conserved. As such, neutralinos produced very early in the history of the Universe, should be still present around us.

There are two basic approaches to WIMPs detection, indirect - searching for high-energy neutrinos from the Sun and the Earth or antiprotons and positrons in the Galaxy - and direct, performed in underground laboratories. We assume that our Galaxy contains cold dark matter in the form of WIMPs distributed smoothly as an enormous cloud with a density, near the Sun, of 0.3 GeV/cm³. The Sun moves in the Galaxy at 230 km/s crossing the WIMPs cloud.

In the direct detection of WIMPs, one measures the energy of the nuclear recoil produced by an elastic scattering. For masses from several tens of GeV (masses below 30 GeV have been excluded by LEP) to a few TeV, the recoil energies are very low, $E_r = 1\text{--}100$ keV. At these low energies, radioactive background is severe, due not only from the environment but also from the detector itself and its surroundings. The signal spectrum is a decreasing function of the energy, very similar to that of the background.

The signals from WIMPs are very rare too. The use of heavy nuclei as target is convenient, as neutralinos, in many coupling schemes, interact coherently with nuclei, with a probability proportional to A^2 . But even for coherent interactions the rates are small. For example, supersymmetric models predict rates between 10 and 10^{-6} events per day per kilogram of detecting mass. A low background environment is clearly mandatory. Detectors must have a very low energy threshold, large sensitive mass, good energy resolution, ultra high radio-purity and efficient background discrimination.

There are two main backgrounds: gamma rays and electrons on one side, nuclear recoils due to elastic scattering by neutrons on the other. The second is practically undistinguishable from the signal, because the energies of nuclei recoiling from a scattering with a neutron or a WIMP may be similar. The (dominant) electromagnetic background can be distinguished and largely reduced by measuring two quantities, energy deposit and ionisation (or light). CRESST at LNGS, for example, measures heat deposit and scintillation light. The experiments using these techniques compare the counting rate left after all the background suppression procedures with the expectations. If no statistically significant excess is found (this being always the case), a corresponding upper limit in the signal rate can be given. This limit must then be transferred into a limit in the physical parameter space, which is usually taken as WIMP-proton cross-section vs. WIMP mass; this is not possible without the assumption of a definite model framework, in which the WIMP density, velocity distribution, coupling with the nucleus, etc. are assumed. As a consequence, the exclusion curves shown in the parameter plane are model dependent.

The DAMA^[12] experiment at Gran Sasso, on the contrary, looks for WIMP specific signatures. The counting rate will depend on the average velocity of the WIMPs relative to the detector. That varies

periodically during the year because the orbital speed of the Earth, 30 km/s, adds in June, subtracts in December to the Sun 230 km/s. As a consequence, the flux of WIMPs impinging on the detector and the counting rate should be modulated with the following characteristics: 1. period = 1 year; phase: maximum at June 2nd; 3. amplitude of a few percent; 4. modulation present only in the lowest energy bins. 5. If enough statistics is collected, a further signature can be considered, namely the shape of the annual modulation, which would be sinusoidal, not only periodic. A further signature is obtained using a multi-counter array of adjacent crystals: 6. hits must be in one detector only. These features are not easily reproduced by the backgrounds and, if evidence is found, it is model-independent. But, in order to exploit the technique, one needs a large detector mass - at least 100 kg - made of super radio-clean materials and long term - several years - stability and control in all the running conditions.

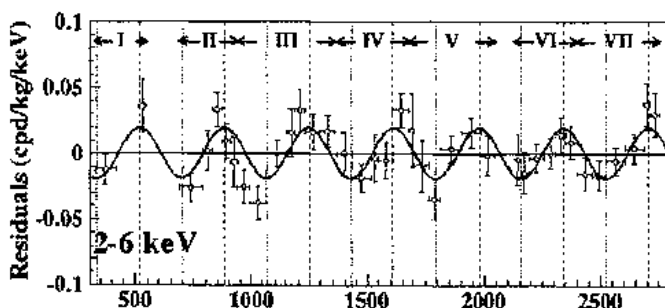


Fig. 10. The residuals of DAMA over seven years for recoils energy between 2 and 6 keV

DAMA, after several years of R&D of the techniques necessary to reach extremely high radio-purity levels, produced a set of 9 NaI (Tl) scintillator crystals, of 9.7 kg each, viewed by two low-background photomultipliers connected to each of the sides through 10 cm long light guides. Special care has been taken in the control of the stability of the experimental conditions. The background counting rate after noise removal in the relevant energy region of 2-3 keV is about 0.5-1 counts/(keV kg d). Notice that this rate must contain the time independent part of the WIMPs signal, which, if the below reported conclusions are correct, is very relevant, almost saturating the observed rate.

DAMA has recently published the results of the last three-year data taking period^[13] to be added to the previous four years, for a total exposure of 107 731 kg d. The main result shown in Fig. 10 is the difference R between the actual counting rate and its average value as a function of time. One can see evidence for the expected modulation, confirming the observations made with four years data. Fitting a sinusoidal behaviour to the data $R=A\cos[\omega(t-t_0)]$, the authors find $A=(2.00\pm 0.32)\times 10^{-2}$ counts/(kg keV d), $t_0=140\pm 22$ d (maximum expected on June 2nd = 153rd day), $A=1.00\pm 0.01$ y and

conclude that data favour the presence of a modulated behaviour with the proper features at 6.3σ confidence level.

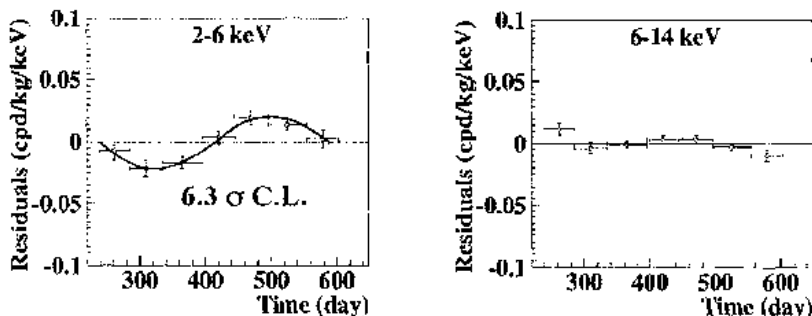


Fig. 11. a) The residuals as function of the time of the year starting on August 7th for recoil energy between 2 and 6 keV (curve added by me); b) same with recoil energy between 6 and 14 keV

Fig. 11, left panel, shows the residuals of the seven-year period as function of the time from August 7th (as if they were relative to a single year); as one can see, the behaviour is not only periodic but also consistent with a sinusoid. Finally Fig. 11, right panel, shows the residuals in an immediately higher energy band, between 6 and 14 keV; as expected, no modulation is observed.

DAMA has made the necessary investigations on possible alternative explanations of the observed effect, looking for possible instabilities faking the modulation in the temperature, the radon flux, the noise, the energy scale, the efficiencies, the backgrounds, and the possible effect of the μ flux modulation observed by MACRO (it is annual with maximum in summer). The upper limits on each of these possible alternatives have been found to be between several per mil and 1%.

One can now assume the WIMPs to be neutralinos and evaluate their mass. This is possible only after having chosen model framework; in one of these, for example, one finds the data to be compatible with a neutralino-WIMP mass of 50-60 GeV and a cross-section on protons of about 7×10^{-36} cm², values that are not unreasonable. More carefully, one finds a region of possible existence of a WIMP, whose extension and location depend on the variety of values of the parameters entering the calculation.

On theoretical grounds, the rates predicted for neutralino-WIMPs extend from 1-10 events/(kg day) down to $10^{-4} \times 10^{-5}$ events/(kg day) in typical detectors, as shown (dots) in Fig. 12. A small fraction of this window is testable by some of the leading experiments. In the same figure, a region corresponding to the DAMA observation is reported; it is calculated for the first four early periods only but it does not change substantially adding the last three, the relevant point being its model dependence. The figures report the upper limits of the leading experiments that are not sensitive to annual modulation and that exclude to a greater or lesser extent the DAMA region.

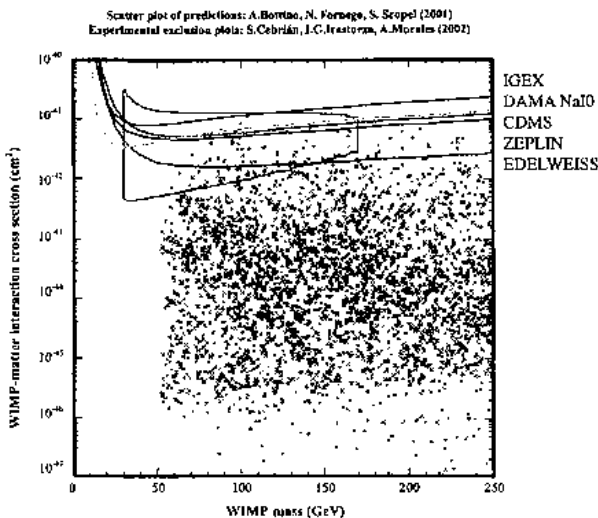


Fig. 12. Exclusion curves are from a compilation by S. Cebrian, Irastorza and A. Morales^[14]; theoretical expectations and contour of the DAMA region are from A. Bottino, N. Fornengo and S. Scopel.

The DAMA results are clearly extremely important, but they should be checked by an independent experiment. This, in my view, must be sensitive to the model-independent modulation signature. At LNGS, on this line, LIBRA a 250 kg NaI array, by the DAMA group, has been installed and is starting its run, CUORICINO, 40 kg TeO₂ array, meant primarily for double beta decay and presently taking data, is trying to reduce the background at low energies to become sensitive to the modulation and similarly GENIUS-TF, several kilograms of Ge.

Complementarily, the CRESST collaboration searches for WIMPs looking for an excess over background of the counting rate. The calorimeters, which are both targets and detectors, developed by the collaboration work at several millikelvin temperatures. Cryogenic detectors use much lower energy excitations, such as phonons, than more traditional devices. The basic unit is a crystal on a surface of which a superconducting film is evaporated. When the film is held at a temperature in the middle of the superconducting to normal transition, it becomes a very sensitive thermometer.

Background discrimination is achieved by CRESST^[15] simultaneously detecting phonons and light. As shown in Fig. 13, obtained with an exposure of a prototype detector to γ , electron and neutron sources, high discrimination efficiency against the dominant gamma background can achieve even at the low (15-20 keV) relevant energies. For the presently used CaWO₄ crystals, the measured rejection is 99.7% for $E > 15$ keV.

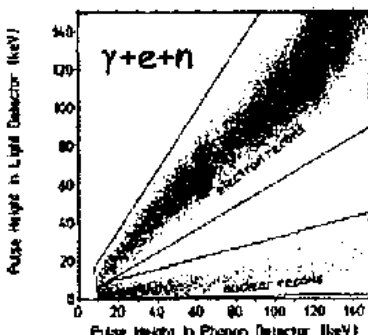


Fig. 13. Light yield vs. energy deposit as measured in a CaWO₃ CRESST2 crystal

CRESST2 plans to have a sensitive mass of 10 kg, based on 33 modules of 300 g each. The expected sensitivity with an exposure of 10 kg years, an energy threshold of 15 keV and a background at threshold of 1c/(kg keV d), is below 10^{-10} nb allowing exploring a relevant fraction of the parameter space.

7. Nuclear astrophysics. LUNA and LUNA2

Nuclear physics has very important roles in astrophysics and in cosmology, for example in the creation of the primordial light elements three minutes after the so-called big-bang and in the formation, at much later epochs of the stars, of the galaxies and of the matter we are made of. To understand these phenomena, we must study and measure the nuclear processes at the relevant energy scales in nuclear physics laboratories on Earth. In several astrophysical cases, the nuclear reactions take place between nuclei that move at thermal velocities with energies much smaller than the Coulomb barrier. The kinetic energy of a proton in a star similar to the Sun core, corresponding to their Maxwell-Boltzmann distribution at $T = 1.6 \times 10^7$ K, is 1.3 keV. In order to fuse, two protons - or two other nuclei - must tunnel through the Coulomb barrier. Its height is, depending on the reaction, between 1500 and 2500 keV, much larger than the kinetic energy. The cross sections are proportional to the tunnel probability, which decreases exponentially with decreasing energy. The interaction probability, obtained by convolution of the Boltzmann energy distribution with the Coulomb penetration probability, is a bell-shaped curve, called Gamow peak. The maximum of the peak is typically at $E_0=20 - 25$ keV.

Fig. 14 shows an example of the dramatic decrease of the cross-section. To give two other examples, relevant for energy and neutrino production in the Sun, $\sigma(E_0)=0.7$ pb for ${}^3\text{He}+{}^3\text{He} \rightarrow 2\text{p}+{}^4\text{He}$ and $\sigma(E_0)=9$ fb for ${}^4\text{He}+{}^3\text{He} \rightarrow \gamma+{}^7\text{Be}$. Other cross sections are even smaller. One sees that sub-picobarn sensitivities are needed to reach the relevant energy regions. This was not possible until LUNA went into operation at LNGS and the cross sections were obtained by extrapolation from the measured values at higher energies.

To formally, but not substantially, avoid in the extrapolation the rapidly changing exponential factor, the "astrophysical factor" $S(E)$, shown in Fig. 14, is defined as

$$S(E) = E\sigma(E)\exp\left(31.3Z_1Z_2\sqrt{\frac{\mu}{E}}\right)$$

where μ is the reduced mass in units of amu, Z_1 and Z_2 are the charges of the nuclei and E is the centre of mass energy in keV. The extrapolation to E_0 is then done assuming a smooth behaviour of S . This procedure is clearly very risky in all cases and completely unreliable in presence of one or more resonances above or below threshold.

It is easy to calculate that in a reasonable target of a few $\mu\text{gr}/\text{cm}^2$, with beam currents of the order of a few mA (feasible in practice) and an efficiency of about 10%, the event rates are between 1 event/day and 1 event/month for cross sections between 1 nb and 1 pb. These must be compared with a rate of 2000 events a day due to cosmic rays in a 10 cm^2 detector. To measure such small cross sections, one needs an underground laboratory. This is why at Gran Sasso two Underground Laboratories for Nuclear Astrophysics, LUNA and LUNA2, have been built.

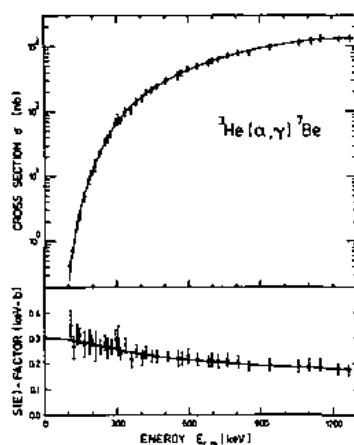


Fig. 14. A cross section and its astrophysical S factor

The two facilities are based on two low-energy, high intensity accelerators with associated detectors and targets construction capabilities. The first accelerator to be completed was LUNA with a 50 kV, 500 μA ion beam. LUNA2 employs a 400 kV, 650 μA accelerator with beam energy resolution better than 70 eV and long-term stability of 10 eV. A BGO-4 π -summing detector, consisting of six optically separated segments, each observed by two photomultipliers at either side is another important component of the facility. The gas target is located inside a bore-hole of the BGO detector. The high, 85%, efficiency allows to detect nearly all reaction products.

The experimental nuclear astrophysics program accessible to these - unique world-wide - facilities is very rich and challenging. Many important results have been obtained and more will certainly come in the next years. I'll review now the principal results.

Light, a surface phenomenon, is produced in the stars by nuclear reactions that take place in the star core. Two are the principal reaction chains, the *pp* cycle and the *CNO* (Carbon, Nitrogen, Oxygen) cycle, shown in Fig. 15. The relative importance of the two depends on the star mass and on the star evolution.

In the case of our Sun, the stars evolution theory, tells us that the largest fraction, 98%, of the energy is produced by the *pp* cycle, which is the overall reaction $4p \rightarrow ^4\text{He} + 2e^+ + 2\nu_e + 26.73 \text{ MeV}$, and by the following annihilation of the two positrons. If this is true, the electron neutrino flux at the sun core is known within 2% from the observed luminosity. Neutrino energies are relatively low, as shown in Fig. 16. Their observation became possible only with Gallium experiment, GALLEX at LNGS (and later SAGE at Baksan).

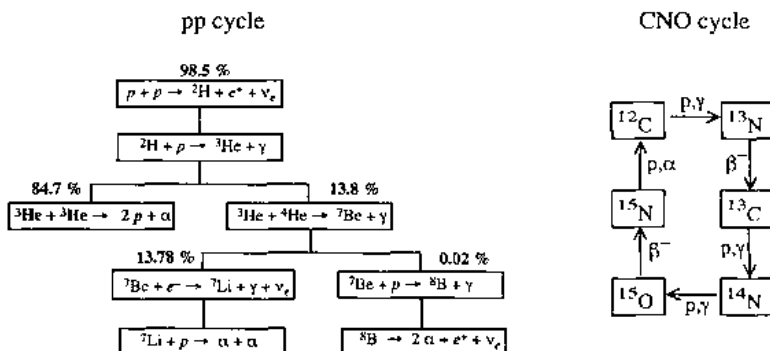


Fig. 15. The pp cycle and the simplified CNO cycle

Electron neutrinos absorption is completely negligible in the Sun, but their flux may be altered by flavour conversion into other neutrino flavours. This mechanism, the MSW effect, changes the electron neutrino flux but not the flux of all neutrino flavours.

The electron neutrino spectrum produced in the Sun core has been evaluated in 1964 and since then with increasing accuracy by J. Bahcall^[16]. (Solar Standard Model: SSM). One must consider not only the overall mentioned reaction, but all the details of the cycle shown in Fig. 15. Two other branches contribute only marginally to the electromagnetic energy output but produce electron neutrinos: the electron capture by ^7Be and by the ^8B decay, called "Beryllium neutrinos" and "Boron neutrinos" respectively. Their fluxes are low but their energies are much larger than those from the *pp* fusion. For the last reason they were observed historically first by the Chlorine (Homestake) and Cerenkov (KamiokaNDE) experiments. Fig. 16 shows the calculated electron neutrino flux at the Sun core. Its accurate and reliable knowledge is of fundamental importance not only for solar physics, but also

for neutrino physics: flavour conversion phenomena, both in matter and in vacuum, are in fact detected as a modification of the spectrum. The SSM calculations are based on extrapolations of the available cross-sections data, which should be measured in the relevant range. We will see later how.

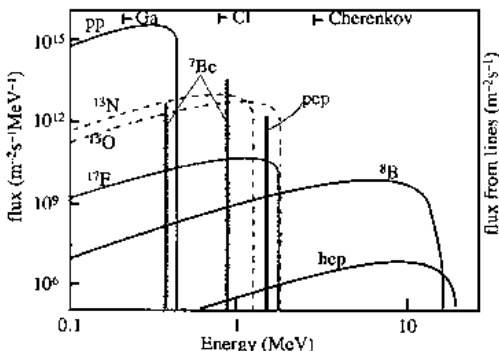


Fig. 16. The calculated solar neutrino spectrum and its components

$^3\text{He} + ^3\text{He} \rightarrow 2\text{p} + ^4\text{He}$ was the first reaction measured by LUNA with a 50 kV accelerator facility. Fig. 17a shows the LUNA results down to 17 keV⁽ⁿ⁾. At this energy the cross section is only 20 fb and the rate 2 events/month; the background rate was $< 10^{-2}$ counts/day. No extrapolation is needed anymore. Before these measurements, the hypothesis of a resonance close to the Gamow peak would have explained, increasing the rate of this process, the reduced Beryllium and Boron neutrinos fluxes observed by Homestake and KamiokaNDE. The non-observation of a resonance by LUNA eliminated the "nuclear solution" of the solar neutrino puzzle.

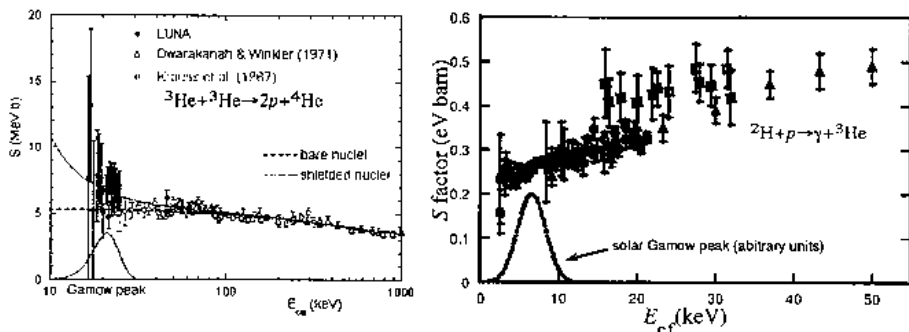


Fig. 17. Astrophysical factors measured by LUNA and LUNA2 at Gran Sasso for the reaction a) $^3\text{He} + ^3\text{He} \rightarrow 2\text{p} + ^4\text{He}$ b) $^2\text{H} + \text{p} \rightarrow \gamma + ^3\text{He}$. Higher energy data from other experiments are also reported

$^2\text{H} + p \rightarrow \gamma + ^3\text{He}$ was the second reaction measured (by LUNA2) below the Gamow peak, with a cross section of 10 fb at the lowest energy^[28]. The astrophysical factor is shown in Fig. 17b. The measurement is important for calculations of the equilibrium abundance of deuterium and for the evolution of proto stars.

The reaction $^{14}\text{N} + p \rightarrow \gamma + ^{15}\text{O}$ is extremely important in the theory of star evolution. Indeed, that evolution is determined largely by the CNO and by the pp cycles. The relative importance of each of them in the energy production depends on the temperature and on the age, two correlated quantities, of the star. The reaction $^{14}\text{N} + p \rightarrow \gamma + ^{15}\text{O}$ is the slowest one in the CNO cycle, the bottleneck that determines its speed and, as a consequence, its importance relative to pp . The extrapolation of this cross-section or, equivalently, of the astrophysical factor called $S_{14,1}$, to the Gamow peak region is strongly affected by the presence of a sub-threshold resonance, giving a factor 10 uncertainty in the extrapolated value.

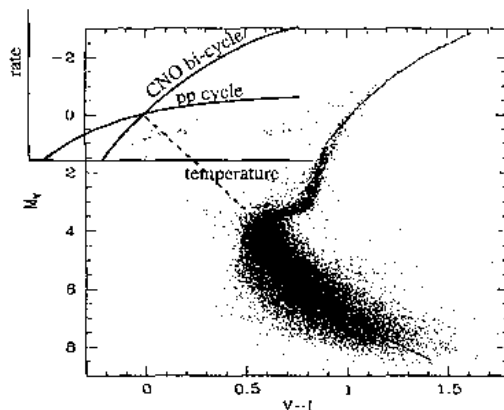


Fig. 18. The main sequence and its turning point, which is related, as shown in the insert to the crossover between CNO and pp cycles

Fig. 18 shows the main sequence of the stars evolution; the vertical axis is the magnitude, the horizontal the "colour", an observational quantity related to the temperature. The turnover point corresponds to the crossover between CNO and pp dominance, as schematically shown in the insert of the figure. From the corresponding magnitude the age of the star can be calculated; but, for that one needs $S_{14,1}$ at the Gamow peak. The above-mentioned uncertainties in the extrapolation reflect in uncertainties of 20-30% in the star age. This is the main reason why LUNA2 is presently measuring the cross section of the reaction $^{14}\text{N} + p \rightarrow \gamma + ^{15}\text{O}$ as a function of energy.

8. Conclusions

I have tried to show on three examples how experiments at LNGS give unique contributions to the progress of particle, nuclear and astro physics. Neutrino physics has already shown phenomena beyond the Standard Model and will certainly produce in the future more insight in the new physics. Dark matter search is showing tantalising evidence for new physics too. Nuclear astrophysics underground has moved only the first very important steps.

On more general grounds, while the experiments at present and future colliders are and will be extremely important for the advance in our understanding of the basic laws of Nature, they will not be enough. It is from experiments in underground laboratories that we have the first experimental evidence of physics beyond the standard model. Cross-fertilisation between particle and nuclear physics, astrophysics and cosmology finds a fertile environment at Gran Sasso. This give changeling opportunities in consideration of the basic fact that, curiously, the Standard Model that explains so accurately all data coming from accelerators, fails to explain not only neutrino masses and mixing, but also the main constituents of the Universe budget, gives a CP violation too small for baryogenesis, does not contain any dark matter particle, gives a wrong value for dark energy. We have tried to take seriously these opportunities and to gradually build a scientific programme that, with a bit of fortune and if sustained, may, complementing the experiments in the accelerator laboratories, lead to completely new grounds in physics.

References

- [1] A. Bettini. New Neutrino Physics, *Rivista del Nuovo Cimento*, **24**, n.11, 2002
- [2] G. L. Fogli. These proceedings
- [3] L. Wolfenstein, *Phys. Rev.* **D17**, (1978) 2369; *ibid D20*, (1979) 2634; S. P. Mikheyev and A. Yu. Smirnov, *Yad. Fiz.* **42**, (1985) 1441 [*Sov. J. of Nucl. Phys.* **42**, (1985) 913]; *Nuovo Cimento* **C9**, (1986) 17
- [4] D. N. Spergel et al., *ApJS*, **148**, 161 (2003)
- [5] J. Bonn et al. *Nucl. Phys. B* (Proc. Suppl.) **110**, 395 (2002); K. Hagihara et al. *Phys> Rev. D* **66**, 010001 (2002)
- [6] H.V. Klapdor-Kleingrothaus, "Sixty Years of Double Beta Decay – From Nuclear Physics to Beyond Standard Model Particle Physics", World Scientific, 2000
- [7] Feruglio, Strumia, Vissani; *Nucl. Phys.* **B637** (2002) 345-377; *Nucl. Phys.* **B659** (2003) 359-362
- [8] LNGS-LOI 12/98; LNGS-LOI 16/99; First results of CUORICINO, October 2003, LNGS-EXP 28/99 add. 4/03; CUORE: a Cryogenic Observatory for Rare Events, LNGS P32/03
- [9] LNGS-LOI 9/97; LNGS-LOI 9/97 add. 1; LNGS P23/2000 GENIUS MPI-Report MPI-H-V26-1999
- [10] Cappellaro and Turatto *astro-ph/0012455*
- [11] T. K. Kuo and J. Pantaleone; *Phys. Rev. D* **37** 298 (1988); G. Dutta, D. Indumathi, N. V. N. Murthy, G. Rajasekaran, *Phys. Rev. D* **61** 013009 (1999); A. Dinghe, A. Y. Smirnov; *Phys. Rev. D* **62**, 033007 (2000)

- [12] R. Bernabei et al. *Phys. Lett.* **B480** (2000) 23; *EPL* **C18** (2000) 283; *Phys. Lett.* **B509** (2001) 197. *Eur. Phys. J.* **C23** (2002) 61; hep-ph/0203242
- [13] R. Bernabei et al. *Rivista del Nuovo Cimento* **26** (2003) pag. 1 and references therein
- [14] A. Morales *Nucl. Phys. (Proc. Suppl.) B* **110** (2002) 39; Proceedings of the III International Meeting on Fundamental Physics, IMFP2002 to be published in *Nucl. Phys. (Proc. Suppl.)*
- [15] C. Bucci et al. "Update of the Proposal to the LNGS for a Second Phase of the CRESST Dark Matter Search". LNGS Proposal P24/2001, approved as CREEST2; MPI preprint MPI-PhE/2001-02
- [16] J. Bahcall; *Phys. Rev. Lett.* **12** (1964) 300-302; J. Bahcall, M. Piansonneault, S. Basu *Astrophys. J.* **555** (2001), 990-1012
- [17] R. Bonetti et al.; *Phys. Rev. Lett.* **82**, 26, (1999). 5205-5208
- [18] C. Casella et al. *Nucl. Phys.* **A706** (2002) 203-216

CHAIRMAN: A. BETTINI

Scientific Secretaries: M. Garbini, H. Menghetti

DISCUSSION

- *Cerri:*

In the DAMA experiment, is the relevant speed not the orbital velocity of the Sun around the galactic centre but the variations in the Earth speed when the Earth goes in one direction with respect to the other?

- *Bettini:*

The variation of the Earth speed relative to the Sun determines the modulation in the counting rate, a few percent of the total; the speed of the Sun determines the average counting rate.

- *Cerri:*

Can you clarify the statement that from the difference in arrival times of different neutrino species from a supernova you cannot draw information on neutrino masses?

- *Bettini:*

I said that you cannot get information on the masses of the flavour states and that this very concept is misleading. Suppose you detect an electron neutrino and after a certain delay a τ neutrino. This delay is not related to the so-called " v_ν mass". The states with definite mass, those that propagate in vacuum with different speeds are the mass eigenstates, v_1 , v_2 and v_3 . For each of them, there is a non-zero probability to observe a v_ν . Suppose v_3 has larger mass than v_1 : v_1 will arrive first but it has a component of each of the three flavour states, so you will detect each of them. Then v_3 will come and once again you will detect (different fractions of) v_e , v_μ and v_τ .

- *Cerri:*

So the issue is that you are measuring simultaneously the masses of the three mass eigenstates and the mixing of the three.

- *Bettini:*

The measured quantities depend in principle on all the parameters, masses and mixing angles.

- *Skinner:*

Some simulations of galaxies formation tend to find a very large clump of dark matter in the centre of galaxies. On the other hand, there are astrophysical experiments that seem to show that there is not much dark matter in the centre of our galaxy. In your talk you quoted an expected flux of dark matter particles of 10^{11} (GeV/M_W) $\text{m}^{-2}\text{s}^{-1}$. Can you explain where that number comes from?

- *Bettini:*

This number comes about in the simplest models of the WIMP density in the Galaxy halo (we are not in the centre). It is model-dependent: it might be larger or smaller. Strictly speaking, we do not even have any guarantee that dark matter is detectable.

- *Baldini:*

I was impressed by the DAMA results. Can you comment on other experiments in competition with DAMA?

- *Bettini:*

Traditionally, the results of the experiments on direct dark matter search are presented in the two-dimensional plot I have shown this morning: on the horizontal axis the WIMP mass (for an assumed mean velocity with respect to Galaxy), on the vertical axis the WIMP-nucleus cross-section times the ratio of the actual WIMP density to a standard assumed value. The DAMA result reported in this plot is an area that is model-dependent: it moves around and changes its shape, changing the assumptions of the model of WIMP distribution and of WIMP-nucleon interaction.

No other experiment has found positive evidence, but none of them looks for annual modulation. Each of them gives a lower limit reported as a curve in that plot. All these limits are model-dependent. In particular, notice that the WIMP couplings may be different in different nuclei.

- *Baldini:*

They do not exclude completely the DAMA result.

- *Bettini:*

As I said, one must be very careful in drawing conclusions from different experiments using different nuclei as targets. Anyway, even in a model-dependent comparison, the DAMA region is not completely excluded, even by EDELWEISS, which is the most sensitive experiment.

- *Cifarelli:*

Can you tell us more about the controversy on DAMA results? What is the reason why some people do not believe DAMA results?

- *Bettini:*

As a matter of fact I am not aware of any sound scientific argument, which can sustain these beliefs.

- *Cifarelli*

I am surprised, because I heard that there is a controversy still going on.

- *Bettini:*

I have already said the EDELWEISS result excludes a large fraction of the DAMA region. This is true within a definite set of assumptions. The controversy is largely due to the attitude of the lack of recognising this last point.

- *Cifarelli:*

I thought there was, maybe, some instrumental effect.

- *Bettini:*

These are claims, but nobody, to my knowledge, ever proposed a specific artefact to explain the observed modulation.

- *Rotaev:*

What kind of experiment could answer or could settle the question of which hierarchy, normal or inverted, is right?

- *Bettini:*

One possibility is given by the experiments on supernova neutrinos. In LVD, as I showed this morning, the ratio between the expected numbers of CC interactions on Carbon of ν_e and anti- ν_e , - which does not depend very much on the neutrino-sphere temperature - is about three times larger in the normal hierarchy with respect to the case of inverted hierarchy. So this is a possibility; optimistically, because expected rates are small and because neutrino and antineutrino interactions can be distinguished only statistically by LVD. On the other hand, other experiments, SK and SNO with different sensibility, will contribute.

Other possibilities are double-beta decay, a next generation atmospheric neutrino experiment sensitive to the muon charge and experiments on high intensity neutrino beams and, of course, combination of the information coming from all of them.

- *Rotaev:*

In order to distinguish the hierarchies, should we measure not only the amount of neutrinos and antineutrinos interactions but also the temperature?

- *Bettini:*

LVD can give information on the neutrino temperature by measuring the number of NC interactions on Carbon nuclei, which depends on the temperature but is independent from the neutrino flavour.

- *Galletly:*

I am trying to understand how I should think of neutrinos propagating. Should I think of them as mass eigenstates (or linear superposition of), which then are seen as flavour eigenstates when observed?

- *Bettini:*

The states that propagate conserving their identity are the mass eigenstates. Their velocities, for a given energy, are different because the masses are different. The states that interact with matter are the flavour eigenstates, each a different linear combination of the mass eigenstates.

Think, as an analogy, of a wave having three monochromatic components, propagating in a dispersive medium. Each of them moves without changing its shape but with a different velocity; as a consequence, the total wave changes in shape while it moves, and the probability to observe each flavour varies.

In this framework, let us make an exercise. For simplicity, suppose to have only two neutrinos and that the mixing is maximal. Call ν_1 and ν_2 the mass eigenstates and ν_μ and ν_τ the flavour states $\nu_\mu = \frac{1}{\sqrt{2}}(\nu_1 + \nu_2)$ and $\nu_\tau = \frac{1}{\sqrt{2}}(\nu_1 - \nu_2)$.

Suppose there is a meson that decays into a ν_μ and a μ . We have a sample of these mesons and we measure the energy of the muon for every decay. Then, knowing the mass M of the meson, we calculate the energy of the neutrino. The distribution of this energy shows, in principle, two peaks, say at $E_{\nu 1}$ and $E_{\nu 2}$ corresponding to the two neutrino masses m_1 and m_2 .

Now, if the energy resolution is indeed good enough to resolve the two peaks, we can tag, for example, those of energy $E_{\nu 1}$. In this way, we have a tagged pure ν_1 beam. When this beam interacts with a target, the relevant states are those of definite flavour, ν_μ and ν_τ . Considering that $\nu_1 = \frac{1}{\sqrt{2}}(\nu_\mu + \nu_\tau)$, we conclude that both muons and taus are produced, in equal numbers. In conclusion, from a pure ν_μ initial sample (resulting from the decay) one can produce taus, a process that does not conserve the (flavour) lepton number.

Is that absurd? In fact it is not, because remember that we need energy resolution and that energy resolution requires measuring time. An easy calculation shows that, for small energy differences, $E_{\nu 2} - E_{\nu 1} \sim \Delta m^2 / 4E_\nu$, where E_ν is an average energy.

Consider the following gedanke experiment. To measure the energies, we measure the frequencies of the two monochromatic waves. To do that, we count the number of periods, N_1 and N_2 respectively, in a chosen time interval τ . This time interval must be long enough if we want to distinguish the two numbers, say $N_2 - N_1 \geq O(1)$. Considering that $N_1 = \tau E_{\nu 1}$ and $N_2 = \tau E_{\nu 2}$, this condition reads $\tau(E_{\nu 2} - E_{\nu 1}) \geq O(1)$, which is the uncertainty relation.

And, with the above calculated energy difference, $\tau > \frac{1}{E_{\nu 2} \pm E_{\nu 1}} \sim \frac{E_\nu}{\Delta m^2}$ in order of magnitude. In conclusion, to produce taus from an originally pure ν_μ beam we must wait a time of the order of $\frac{E_\nu}{\Delta m^2}$.

In this time interval, the two components of the dichromatic wave, which initially are in phase, substantially go out of phase. But this, clearly, is just the oscillation

phenomenon. If we wait enough, taus are produced by an initially pure ν_μ beam hitting a target. Flavour lepton numbers are not conserved.

- *Krotov:*

I would like to ask about the solar neutrino experiments. So I see that the usual way is the following: we measure the neutrino flux of a certain flavour at the Earth. To infer that the flux is varied on its way to us, we should know the neutrino flux as originated in the Sun. How can we reconstruct the electron neutrino flux from the Sun without knowing the relevant internal parameters of the Sun? Surely the solar model needs the temperature in the centre of the Sun and all things like that? There should be some calculation and I believe they are not too exact. Can we absolutely exclude an explanation of the observed lack of neutrinos as a consequence of our incomplete knowledge of the structure of the Sun?

- *Bettini:*

In the Sun, the energy is produced by a chain of nuclear fusion reactions, known as the pp cycle, in the central part of the star. Overall four p nuclei fuse in a He nucleus, producing an energy of 27 MeV and two electron neutrinos (and two positrons that annihilate promptly). The energy spectrum of the electron neutrinos has been calculated by J. Bahcall since 40 years. The principal components are: the p-p branch at lower energies, the Be branch giving two monochromatic lines at intermediate energies and the Boron branch, which is the highest energy part of the spectrum. The pp component contributes with more than 98% to the energy flux and is known, from solar luminosity alone, within 1-2%. The calculated contributions of other two components strongly depend on the temperature in the core of the Sun. Gradually this quantity became known better and better, mainly from helioseismology data. The present uncertainty, less than a per mille, is completely irrelevant for the values of Be and B neutrino fluxes. The contributions of the uncertainties on the other physical parameters and on the structure of the Sun (a big hydrogen ball) are rather well known too.

All the experiments on solar neutrinos before SNO measured the ν_e flux (the water Cherenkov experiments, KamiokaNDE and Super-KamiokaNDE, have also a small sensitivity to ν_μ and ν_τ). As a consequence, they are ν_e disappearance experiments. Their energy thresholds are different, depending on the technique. The historically first experiments were sensitive to the higher energy part of the spectrum only: the Homestake Cl experiment to the B and Be components, the water Cherenkov experiments to the B components. The Ga experiments, Gallex and SAGE, have been designed with a very low threshold, 233 keV, in order to be sensitive to the pp neutrinos, whose flux is well-known independently on the model, as I said. When Gallex published in 1992 its first results, later confirmed by SAGE, it became clear that the "solar neutrino puzzle" did not have any astrophysical solution, and, as a consequence, that our concepts of neutrino physics had to be modified. Indeed the flux measured by Gallex is the sum of the pp, Be and B components but its value was

smaller than the sum of the B flux, as measured by KamiokaNDE and the pp flux, as calculated from the luminosity. This implies that the Be component should be negative (which is absurd) or, at maximum, zero, which is impossible because, in the nuclear reactions, chain B is produced by Be. Notice that this conclusion is independent of the solar model. By 1997, with the increased precision of Gallex and SAGE data, neutrino flavour conversion via oscillations in vacuum or MSW in the Sun has become the only reasonable explanation.

More recently, the SNO experiment has observed the appearance of ν_μ and ν_τ through their neutral currents interactions. These measurements, together with those of the previous experiments, made it possible to check completely the "standard solar model" of J. Bahcall, which was found in extremely good agreement with the data.

Finally, Kamland, measuring the (anti) electron neutrino flux from artificial sources (nuclear power reactors), confirmed exactly the oscillation parameters calculated by fitting the solar neutrinos data.

- *Lysov:*

What are the possibilities to obtain neutrino masses from cosmological observations? Could you make a short description of what we know?

- *Bettini:*

In the last several years, the progress in observational cosmology has been outstanding. A large quantity of data became available, with much better control of the systematic uncertainties and full consistency amongst observational data, within the framework of a "standard cosmological model". This is based on a flat (i.e. zero curvature), accelerating Universe in which all structures have been seeded by quantum fluctuations and which went through an early phase of inflation. The main parameters of the model are the Hubble constant, the age of the Universe and the densities of its components: total matter, baryons, dark ones and dark energy. We know that the Universe is flat, i.e. its matter-energy density has the critical value within 2%; matter gives about 1/4 of the budget, the remaining 3/4 is due to the cosmological constant (or dark energy).

The spectrum of the large structures is extremely important to check the model and to determine its parameters. The largest structures are the temperature fluctuations observed in the cosmic microwave background; their spectrum (their frequency as a function of the angular size) has been recently determined with unprecedented accuracy by the NASA WMAP experiment. We have access to somewhat smaller scales (10 – 100 Mpc) with the data on the clusters and superclusters of galaxies. At these scales, a galaxy is a physical point. The relevant function is the galaxy power spectrum, the Fourier transform of the two points correlation function between two galaxies divided by what is expected if everything is smooth. Data based on hundred thousands of galaxies have been published by surveys made with reduced systematic uncertainties. The 2DF collaboration has already published the data, while SDSS has recently published a first sample; the final

accuracy on the spectrum is expected to be around 1%. At still lower scales (less than 10 Mpc), the relevant data are those on the “Ly- α forest”. The galaxy power spectrum and the CMB one - evolved at the epoch of galaxies formation - overlap in an interval around 100 Mpc. This is important because it allows a relative normalisation.

Coming to neutrinos, we know from oscillations that they are massive. The two observed oscillation phenomena, the atmospheric and solar ones, give us the values of two differences between mass squared. As a consequence, we do not know the absolute neutrino mass scale but only a lower limit. This, in turn, gives a lower limit on the contribution of neutrinos to the budget of the Universe, which is about 0.15%; non-zero, but very small indeed.

On the other hand, neutrino masses, precisely the value of the sum of the masses of the three eigenstates (proportional to the neutrino density), as I said this morning, have an influence on the large-scale structures. Let us go a bit deeper. The structures seen in the cosmic microwave background are determined by the “cold” dark matter, where cold means non-relativistic at that time. But at that time, the temperature of the Universe was around 3000 K or 250 meV, and we can say that even neutrinos were not relativistic, as the rest of dark matter. As a consequence, the CMB spectrum is not very sensitive - at the angular scales observed so far - to neutrino masses below, say, one eV where they are indistinguishable, in their effects, from the rest. On the other hand, later on when galaxies are been formed, neutrinos, which do not interact with baryonic matter so much, have energies larger than the binding energies in galaxies and in their clusters. They hence freely stream over these structures and, proportionally to their mass, tend to erase them. In conclusion, neutrino masses reduce the power spectrum at the scales (order of 10 Mpc) of the galaxy clusters and lower; in this region we have information from the galaxies surveys and the Ly- α forest.

The limit I quoted this morning comes from a fit of the data with a given model containing the cosmological parameters. The accurate WMAP data are essential in reducing the uncertainties on all the parameters; then the limit on neutrino density (and masses) comes mainly from the galaxy power spectrum and from the Ly- α forest.

The limit on neutrino mass from cosmology is presently the best of all and it can improve in the future, as I will soon discuss, but there are a few caveats. First, the limit becomes weaker (by a factor 3) if Ly- α data are not included and these data are not, as far as I understand, as sure as the others. Second, the power spectrum needed by the theory is the matter spectrum, but experimentally only luminous matter is observed; from that the total matter density is inferred; this process, known as galaxy bias, has uncertainties. Third, theory has to calculate the mass spectrum starting from the initial fluctuations, those observed in the CMB. Now, in the first epochs, the density fluctuations are small and the system is linear, but later on fluctuations are of the order of unit and larger; calculations of the evolution of this non linear system are

based on computer codes and their result might have uncertainties larger than expected.

On the other hand, in the next years we expect new data, most important the SDSS data on the power spectrum with largely improved statistical and systematic accuracy and those of the ESA Planck mission on CMB, which with its unprecedented angular resolution, will have access at very small (relatively speaking) structures. Notice, in particular, that the expected decrease of the CMB power at these scales depends on neutrino mass in a less model-dependent way (no evolution calculation needed). Along with the presumable consolidation of the theoretical basis of the cosmological model, we can expect - with a bit of optimism - that the limit on neutrino mass sum might go close to the lower limit known from oscillations (50 meV for normal or 100 meV for inverted hierarchy), or that a reliable non zero effect be observed.

- *Wolf:*

A question about ICARUS. In order to reach the same sensitivity for proton decay as SuperKamiokaNDE, the experiment would need a sensitive mass well above 20 kt. When will ICARUS reach this tonnage?

- *Bettini:*

The present ICARUS proposal has a mass of 3 kt, which, as you say, is not competitive with SuperKamiokaNDE. On the other hand, ICARUS is sensitive to decays in more than one charged particle and SuperKamiokaNDE is not.

- *Wolf:*

But even in that case it would need 20000 t or more.

- *Bettini:*

Yes.

- *'t Hooft:*

You mentioned the cosmological limits on neutrino mass, but what limit on the absolute masses do you get from the SN's and how optimistic are you about possible improved observations in the future?

- *Bettini:*

First we need a time zero signal, for example a gravitational wave, which leaves the Supernova synchronous with the neutrino burst within a few milliseconds. The delay of the neutrino burst at 10 kpc distance - we cannot go much farther - is several milliseconds for 1 eV neutrino mass. You then see that for sub-eV neutrino masses, the delay in the arrival times is too small to be measured.

NEW TALENTS SESSIONS

A series of special sessions was devoted to young talents: those fellows who cannot be easily identified in the constantly increasing dimensions of experimental groups. The problem is less acute in the field of theoretical research. The results of the presentations follow.

Fast Automatic Systems for Nuclear Emulsion Scanning: Technique and Experiments

Cristiano Bozza, Salerno Emulsion Group, INFN and University of Salerno

Abstract:

The technique of nuclear emulsions has dramatically changed since the birth of automatic systems. General aspects of automatic systems are reviewed. The SySal system and its application in the CHORUS experiment are described in detail. This system has evolved into the European Scanning System for the OPERA experiment. Latest results and performances of the prototype are reported. An overview is given about the distributed computing model that allows the laboratories involved in OPERA to share the scanning load.

1 Nuclear Emulsions: Why?

Nuclear emulsions are a long-known detector for charged particles. They work on the same principle of photographic emulsions. A gel with interspersed AgBr crystals is prepared and often mounted on a transparent plastic support. During the exposure time, charged particles ionise the medium and some Ag ions along the path are displaced to the surface of the crystal and reduced to atoms. After the exposure, during the development process, the Ag atoms act as sites where the related AgBr crystal and its neighbours reduce to metallic Ag. Nearly spherical Ag grains with diameter of the order of $0.5\text{--}1\ \mu\text{m}$ grow up where the original ionisation took place. After the development, a 3D picture of the interaction is forever recorded in the emulsion plate.

As a detector, nuclear emulsions provide several specific features:

1. spatial resolution of the order of $0.07\ \mu\text{m}$;
2. continuous sensitivity (they cannot be triggered);
3. built-in data storage capability (they can be measured several times);
4. low cost.

The spatial resolution is presently better than any other detector. The number quoted above is obtained under special conditions. In normal operation, a precision of $0.3\ \mu\text{m}$ is easily achieved. This allows experimenters to use the event topology to identify interactions and particles. For instance, it is possible to separate the production and decay vertices of a charmed particle, and the visual features of the vertex itself carry information about the physical process (the vertex may show low energy fragments, secondary de-excitation products, or it might be completely "white", which is typical for decays of massive particles).

The continuous sensitivity is an advantage for certain tasks, but it is a problem in other cases. Emulsions store "pictures" of several events piled up. For this reason, nuclear emulsions can hardly be used for experiments at colliders. Even with lower statistics, at least one external triggerable electronic device is needed to disentangle several event pictures. Hybrid detectors are built, with nuclear emulsions used as a target or just for high precision tracking, and electronic detectors supplying additional information.

Nuclear emulsions can be exposed in several ways. However, the present common practice is to use doubly coated plates (i.e. transparent supports having both sides coated with emulsion layers), with the particle impinging on them mainly orthogonally to their plane. Plates can be stacked to obtain sizeable tracking volumes.

2 Automatic Scanning Systems

The biggest problem with nuclear emulsions before the '90s was that particle tracks had to be measured manually under a microscope by experienced human scanners. The work of recovering information was slow and prone to errors, so in many cases measurements had to be repeated.

Ideas to help human scanners had already been born in the late '70s but they had never received a systematic application, and indeed they were just oriented to "computer assisted manual scanning". The CHORUS experiment ($\nu_\mu \rightarrow \nu_e$, short baseline neutrino oscillation in the region of $\delta m^2 \approx 1\ \text{eV}^2$) really triggered the research for automatic scanning systems [1]. In its original proposal, CHORUS had to produce several hundred thousand interactions, but no more than 50,000 events should have been scanned, essentially by humans. At its end, the automatic systems developed in CHORUS have located and studied

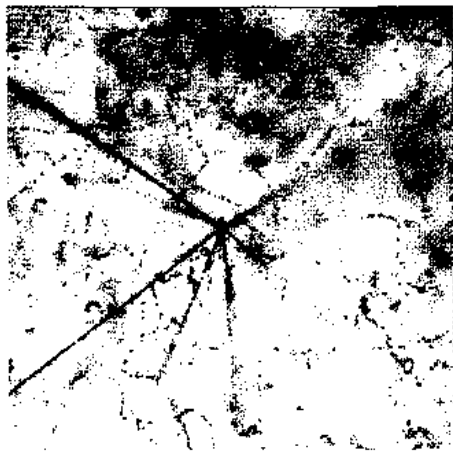


Fig. 1 Neutrino interaction in emulsion



Fig. 2 European Scanning System prototype (OPERA)

about 2×10^5 interactions over a total of about 10^6 triggers. The electronic detectors should have provided a very tight selection of interesting events; the emulsion scanning power available at the end was such that emulsion information was used to identify tracks of particles whose hits have then been searched in the raw data of the electronic detectors for confirmation, so in some cases the experiment detector had its logic reversed! In CHORUS, emulsions acted both as target and detector (neutrinos interacted mainly in the emulsion plates), so complete 3D pictures of the events are available. The total emulsion (target) mass was about 200 kg, with an intense neutrino beam whose average energy was 25 GeV.

The next large experiment with nuclear emulsions will be OPERA ($\nu_\mu \rightarrow \nu_\tau$, $\nu_\mu \rightarrow \nu_e$ long baseline neutrino oscillation in the region of $\delta m^2 \approx 10^{-3}$ eV 2) [2, 3]. It will have a 1.8 kton detector made of lead plates interleaved with thin emulsion plates that will only act as tracking planes, thus making an ECC (Emulsion Cloud Chamber) with the stopping power of lead and the precision of emulsions. $3 \cdot 4 \times 10^4$ neutrino interactions are expected in the volume, but they will be distributed over very large areas, so the scanning power needed will be much larger than for CHORUS.

Automatic scanning systems [4] in general include a motorized horizontal stage where the emulsion plates to be scanned are placed and held fixed by a vacuum system that squeezes it on the glass support. The emulsion is illuminated from below by normal or stroboscopic lamps, and the images are read by an optical system mounted along the same vertical axis. At the end of the optical tube a fast CCD or CMOS camera grabs the images that are then sent to electronic devices or computers for reconstruction and processing. The optical system can be moved along its axis to change the focal plane. In this way, a tomographic picture of the emulsion volume is obtained, and 3D track / event information can be reconstructed. It is impossible to cover the whole area of an emulsion plate by a single field of view, so after each tomography is complete the system moves to another field of view until the whole interesting area has been scanned. This basic idea of an automatic scanning system can then be realized in several ways.

One of the very first automatic scanning systems was built at the University of Nagoya (Japan) in the early '90s and was called Track Selector (TS) [5, 6]. It was able to detect tracks in the emulsion that were compatible with some predicted slope, so indeed the system "selected" tracks out of a background. Its working principle was very simple: for each field of view and for each emulsion layer, a tomography of 16 images was achieved; then, each image was processed by a simple (differential) filter and then binarized by means of a threshold; pixels were then classified as "white" or "black" (pixels that could possibly be part of a track image). The 16 images were shifted according to the predicted slope, and then they were summed up. Black pixels piled up, and real tracks emerged as "pulse peaks" over a background of random alignments. All this processing was obtained by a custom hardware device attached to a computer that was only used to dump the final track information (position, slope and pulse height). The TS was followed by the NTS (New Track Selector) in 1996 with higher scanning speed, and by the UTS (Ultra-Track-Selector)

in 1998 where parallel processing units allowed to give up the requirement of a predicted slope (all tracks in a proper angular region were detected). The Nagoya group is now working to produce the S-UTS (Super-UTS) [2, 3] that is expected to provide a scanning power one order of magnitude larger than the UTS. It will profit of a special mechanics with continuous constant speed motion along one horizontal axis, while a piezoelectric device will move the objective diagonally to produce a "vertical tomography" of the emulsion without having to stop the stage at each field of view.

The automatic system we will focus on is called SySal (**S**ystem of **S**alerno) and was conceived and realized at the University of Salerno since 1996 [7, 8]. The system and its evolution are discussed in detail in the next chapters, so only a few conceptual guidelines are given here. The basic idea of SySal is to extract the most detailed information emulsion can provide, namely the metallic Ag grains position, size and shape. This information should be processed at several levels in order to get tracks, vertices, full event reconstructions and Physics analysis. The system should be clever enough to automate analysis as well as scanning, leaving only the study of interesting situations to humans (of course, humans can modify any step of the processing if they want, but the system should not rely on manual help, and must be able to work on its own in normal duty). Another guiding principle in SySal is that commercial technology has to be used whenever possible, so that the developers can concentrate on experimental problems and on Physics rather than having to invent new devices when the market is already doing that research (e.g. the speed of commercial cameras has increased in the last two years by almost two orders of magnitude whereas the cost has fallen by one order of magnitude). Finally, flexibility in the scanning system must be such that it can be used in several situations just changing some tuneable parameters rather than having to modify the software or the hardware. SySal has successfully contributed to CHORUS, and its software has now been officially adopted to realize the European Scanning System for the OPERA experiment. Several laboratories are involved in this sub-collaboration (Bari, Bern, Bologna, Lyon, Münster, Napoli, Rome, Salerno).

Other scanning systems have been designed and in some cases put to work, but presently they are not going to be used in next-future experiments.

3 SySal and CHORUS

SySal is a completely software-based system. Real life installations do use sophisticated hardware, but that is always commercial, and SySal can run with minimum adaptation in several hardware configurations. When a piece of the hardware changes, no more than one driver module has to be modified accordingly, all the rest remaining identical. SySal is designed to run on Microsoft Windows NT/2000/XP/2003 on commercial PCs equipped with frame grabbers and motion control cards.

In the following, we will call a "microtrack" a sequence of grains left by a particle in one emulsion layer; in general, in a doubly coated plate, most particles leave two microtracks (one in each layer); by connecting, across the transparent base, the two microtracks associated to a particle, we get an entity that we call a "base track".

The process of data extraction from emulsion is divided in two stages: one is the direct interaction with the emulsion image to recognize particle tracks in the emulsion; the second is the organization of microtracks in coherent data structures from which Physics information can be easily retrieved.

3.1 From Emulsion Images to 3D Microtracks

Automatic microscope stages bear a camera mounted on the optical axis. A CCD camera (Hitachi KP-F110) is used with SySal. It provides primary images in the form of grey level maps of pixels (8 bits per pixel, 1024×1024 pixels / image) at a rate of 30 fps (frames per second). The image data rate is thus 30 MB/s. For each field of view, a tomographic sequence of 16–60 images (depending on the thickness of the emulsion) is taken with the focal plane of the objective in motion (an electronic shutter ensures that images are quasi-static). These images are seldom perfect, and SySal applies correction / compensation procedures on the fly. Among these procedures we recall:

1. spatial noise subtraction to equalize the grey level pedestal of each pixel;
2. 2D Finite Impulse Response filtering to enhance the images of grains in the emulsion;
3. filter output equalization to compensate astigmatism, non-uniform lighting, and differences in pixel sensitivity;
4. binarization using a proper threshold on the filter output.

The images are corrected while still on the frame grabber (Matrox Genesis). They are passed to the host PC RAM in a binary format. The host PC recognizes clusters of black pixels on a white background in these binary maps. For each cluster, the coordinates of its centre of gravity, its area and some shape

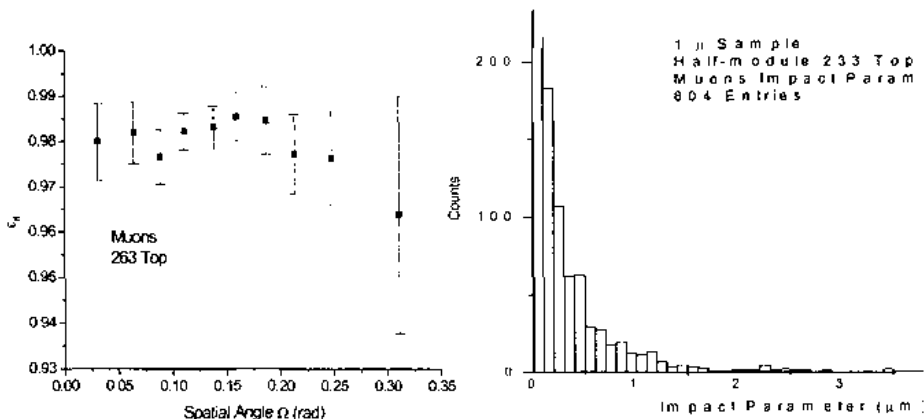


Fig. 3 Tracking efficiency in CHORUS

Fig. 4 Vertex reconstruction precision in CHORUS

parameters are stored. These parameters are then used to select the clusters that correspond to grains of metallic silver in the emulsion. In a typical 2D emulsion image, 1000 clusters pass the selection, and usually no more than 10 belong to real 3D tracks of high-energy particles, the others being just fog due to the chemical development process of the emulsion.

The next step is 3D tracking on the DAQ machine. The amount of grains is usually such that it is really impractical to store all of them for off-line analysis (indeed, this is done during set-up and optimisation, but not in mass data production). A considerable data rate reduction is obtained if the microtracks in the emulsion due to the passage of high-energy particles are recognised on-line. There are two compelling conditions that must be satisfied:

1. on-line tracking must be very efficient to avoid that good information is discarded;
2. on-line tracking must be very fast so that data taking process is not slowed down.

To accomplish this task, SySal runs dedicated tracking algorithms on the host PC CPU. In order to recognize 3D sequences of well-aligned grains, the 3D position of the centre of gravity of each grain is used. Because of emulsion fog, the combinatorial complexity is very high. To reduce the tracking time, some "tracking triggers" are set-up. Local sequences (3 consecutive layers) of well-aligned grains are detected, and they are used as nuclei to grow tracks. Grains are appended upwards and downwards starting from a track nucleus. After each new grain, the temporary track parameters (slope and position) are updated. Notice that the SySal tracking keeps the notion of a track as a sequence of grains, i.e. ionising events. It is even possible to detect small decay kinks on a track by using the grain information instead of global track parameters.

The 3D microtracks that have been recognised are periodically saved to local disk or network units; the first stage of emulsion data extraction is then complete.

3.2 From Microtracks to Volume Tracks

When the plastic base is much thicker than either emulsion layer, it is more convenient to use base tracks rather than microtracks as the unit information. They are reconstructed by associating pairs of microtracks detected on single emulsion layers within proper slope and position tolerances. In these conditions, base tracks have much better slope and position precision than microtracks in emulsion layers.

Since emulsion sheets are almost always exposed to beams in stacks, with the sheet plane orthogonal to the beam axis, physical events often involve a region in space that spans several plates. In other words, we are more interested in "volume tracks", i.e. tracks that extend in a volume, than in microtracks or base tracks. However, microtracks and base tracks contain all the available information about volume tracks. Indeed, volume tracks are formed by connecting several microtracks together (or base tracks, depending on the plate geometry). A very precise intercalibration between emulsion plates is needed to perform this connection in a meaningful way. The procedure requires two steps: pattern recognition and microtrack (or base track) linking.

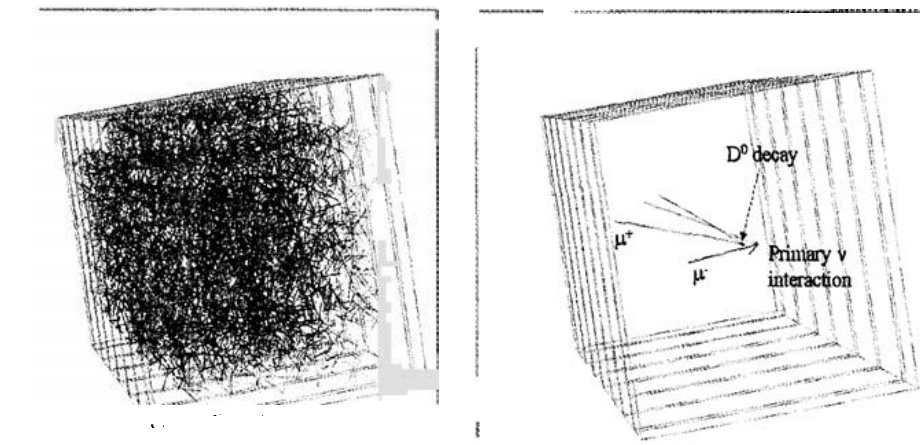


Fig. 5 Left: 10^4 emulsion microtracks from 8 stacked plates. Right: after fine alignment of the sheets, ~200 volume tracks are obtained and passing-through spectator tracks are removed. A clear event with charm production at the primary vertex and decay at a secondary vertex is reconstructed.

During pattern recognition, the off-line software tries to recognise the same pattern of tracks in two areas of contiguous plates. The outcome of this procedure is a translation or an affine transformation to be applied to one of the two areas to match the track pattern seen in the other area. This is a starting point to refine the alignment parameters iteratively. At the end of this iterative procedure, both a reliable set of alignment parameters and a reliable set of connections between microtracks (base tracks) in two contiguous sheets are obtained. Since inefficiencies in the data acquisition procedure must be tolerated (emulsion sheets can be damaged or defective), one recovery step is to try and connect microtracks (base tracks) across one or more sheets (i.e., "holes" are tolerated in a sequence of connected microtracks / base tracks).

If the momentum spectrum of the volume tracks is expected to be wide, it is possible to select only tracks left by high momentum particles for alignment. They are defined as the volume tracks that have similar slopes at the most upstream and most downstream points in the volume.

The outcome of this procedure is a precise alignment: residual alignment errors in tracks are of the order of $0.7 \mu\text{m}$ in CHORUS emulsions. With such a high precision, it is straightforward to automatically reconstruct interaction / decay vertices and decay kinks [9]. For each event, a "tree" of particle tracks gives the complete picture of the physical process, which can then be analysed.

3.3 The SySal contribution to CHORUS

Two research groups (University of Salerno and University of Roma) have used SySal to take part in the scanning of CHORUS emulsion plates. CHORUS has located and studied about 2×10^5 neutrino interactions in the emulsion target. 8×10^3 events of this data sample have been scanned by SySal (the remainder mainly by the Japanese system: see above TS, NTS, UTS). Although this might seem a small fraction, one should keep in mind that SySal was just beginning when the Japanese system had already been adopted officially by many laboratories. Indeed, the SySal data quality is comparable with that provided by the other system. Some of the performances of the system are reported in Figures 3 and 4. It is worth to notice how, by means of the very high alignment accuracy, it is possible to disentangle the relevant physical information from the mess of spectator tracks and generic background the emulsion have accumulated during two years' exposure (see Fig. 5).

CHORUS has been able to exclude a region in the space of parameters for neutrino oscillations [1] and has found and measured precisely many events with production and decay of charmed particles [10, 11, 12, 13, 14]. In addition, as a specific feature, SySal has produced a unique library of 3D neutrino interaction images. Thanks to the quasi-on-line analysis capabilities of the SySal software, as soon as events were scanned they were also recognised, and the scanning machines were directed to produce tomographic image sequences. This library can now be viewed and studied from everywhere in the world without a microscope.

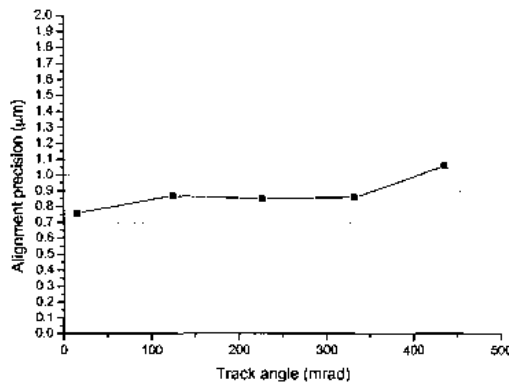


Fig. 6 Current alignment precision for tracks scanned by the prototype at $10 \text{ cm}^2/\text{h}$ on OPERA emulsion plates.

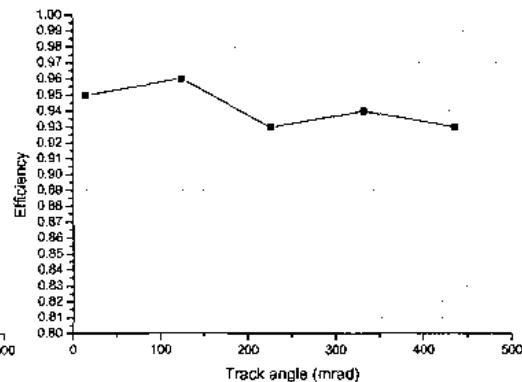


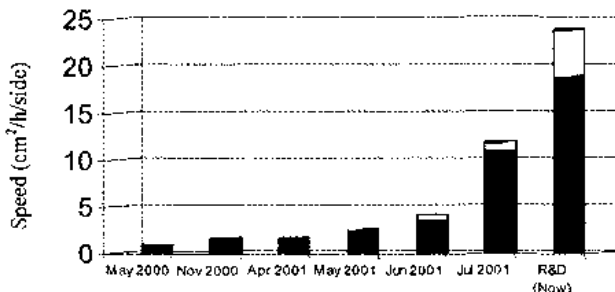
Fig. 7 Current tracking efficiency of the prototype at $10 \text{ cm}^2/\text{h}$ on OPERA emulsion plates.

4 The European Scanning System and OPERA

The performances of SySal were quite adequate to the needs of CHORUS. With OPERA [2, 3], a quantum leap in the scanning speed is needed. The target will be made of bricks of lead sheets interleaved with emulsion plates that act as tracking planes. The electronic tracker merely points to the brick to be scanned. The first (external) sheet, called Changeable Sheet (CS) is scanned to verify the tracker predictions. However, the area over which the tracks of the interaction products have to be searched is a considerable fraction of the sheet area (120 cm^2); it might well be the whole area in some cases. Automatic microscopes with scanning speed of $20 \text{ cm}^2/\text{h}/\text{side}$ will fit the needs, and that is the new frontier for the development of automatic systems. Another difficulty with OPERA emulsion plates is that the emulsion layers are very thin ($43 \mu\text{m}$ each).

In routine duty, European laboratories will scan half of the bricks ($15\text{--}20$ bricks / day), and the Japanese groups will scan the remainder.

Fig. 8 Evolution of the scanning speed of the European Scanning System prototypes. For each version of the prototype, the bar shows the minimum and maximum speed that can be obtained by slightly different hardware configurations.



Presentation date of the European Scanning System prototype

4.1 The European Scanning System DAQ

While the Japanese group from Nagoya is developing the S-UTS (see above), the European scanning laboratories involved in OPERA have agreed to build a new system (the European Scanning System) based on the SySal software and know-how. Although the concepts are still the same, the hardware is almost completely new:

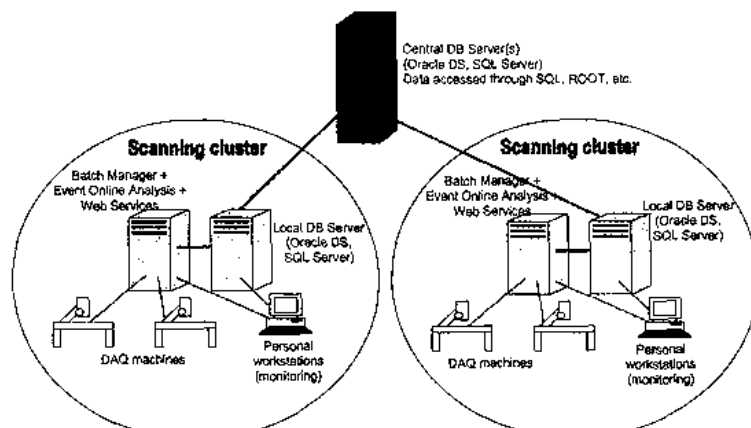
1. CMOS cameras with high resolution running at 150 fps and more are being tested;
2. a new stage has been built with improved dynamic performances (small and quickly damped vibrations): moving to one field to the next requires less than 80 ms, including the time to stop oscillating around the final position;
3. commercial optics has been adapted to obtain large, planar fields of view (360 μm and more);
4. the vision processor is now the Matrox Odyssey (a very new and very powerful image processing device, 6+16 times faster, depending on the operation, than the previous Matrox Genesis processor);
5. multiprocessor machines are being used for on-line computations.

All this new hardware required of course some new software to drive it. The overall architecture of SySal has not changed conceptually, but many features have been added. Heavy computations such as cluster finding and tracking can now be shared by several processors; image grabbing and processing are now asynchronous, which improves the CPU time usage and reduces the risk of missing frames essentially to zero. As a result the DAQ cycle for each field takes presently 210 ms (in the case of SySal on CHORUS emulsions it took more than 1 s). The fiducial field of view has also been enlarged from 250 \times 250 μm^2 to 330 \times 330 μm^2 (30 μm overlap between adjacent fields are needed to ensure that tracks are fully contained at least in one field). In Fig. 8 the evolution of speed vs. time is shown. A stable prototype exists that takes data at 10 $\text{cm}^2/\text{h}/\text{side}$. Another prototype that works at a speed between 20 and 25 $\text{cm}^2/\text{h}/\text{side}$ is already in the optimisation phase. The data in Fig. 6 and Fig. 7 show the efficiency and the precision for the prototype running at 10 $\text{cm}^2/\text{h}/\text{side}$. Such thin emulsion layers have also required a change in the tracking algorithm, to take into account the fact that the image of one grain can be "replicated" on several layers due to the nonvanishing focal depth. The precision is still sub-micron, and the efficiency is already high enough to perform tests of OPERA scanning strategies.

4.2 The European Scanning Computing Infrastructure

The European laboratories will share their scanning load for OPERA. However, this is not a simple passive sharing of tasks, but will need a tight interplay of several resources. OPERA will need a "quasi-on-line" scanning, i.e. triggered bricks will be extracted within a few hours since the interaction trigger, the associated Changeable Sheet will be developed and checked, and then the confirmed bricks will be developed and scanned. Thus, an immediate feedback from the scanning laboratories to the detector is needed. Moreover, in order to avoid unnecessary scanning, a continuous monitoring of partial results is

Fig. 9 Scheme of the European Scanning Computing Infrastructure for OPERA.



desirable: e.g. when studying an event the scanning zone might be enlarged to contain an electromagnetic shower, and kept small for events with fewer tracks. Last, but not least, some specific measurement could need special equipment and processing, so some events might need to undergo further analysis in some laboratory, so they have to be moved from one laboratory to another. These are some of the needs that require a careful, secure and safe way to share data and tasks. The backbone for the European Scanning Computing Infrastructure is an Oracle-based database system. A central cluster of database servers provides redundancy as well as quick response to queries. Database servers located in scanning laboratories contain copies of the locally produced portions of the whole data set to reduce the network traffic. Each laboratory is equipped with at least one machine acting as batch server, data processing server and web server. These are the three services that build up the Computing Infrastructure.

- The batch server schedules the various scanning tasks on the available microscopes.
- The data processing server performs on-line analysis on the output from scanning microscopes: e.g., it is possible to measure the momentum of a particle by estimating the effect of multiple Coulomb scattering; the energy of an electron can be estimated by the analysis of its shower.
- The web server acts as a standard graphical interface that can be accessed from everywhere in the world, with proper permissions, to drive the other services.

5 Conclusions

The European Scanning System looks in very good shape for the OPERA experiment. Three years before the beginning of the data taking, the performances needed for the normal mass data production are already at hand. Of course, when the minimal performances for OPERA will be reached, there is no reason to believe the development will stop. As technology improves, scanning systems are becoming faster and smarter. Nuclear emulsions are then regaining the interest and attractiveness they had in the old days. As the scanning power and precision increase, precise measurements that were impractical or difficult are now routinely performed. Modern systems that use commercial or slightly customised components increase their capabilities steadily with time. The adoption of a flexible software model makes it very easy to adapt the scanning system both to new hardware and to new needs and measurement techniques.

6 References

- 1 *New results from a search for $\nu_\mu \rightarrow \nu_\tau$ and $\nu_e \rightarrow \nu_\tau$ oscillations - CHORUS Collaboration - Phys. Lett. B* (2001) 7
- 2 *Experiment Proposal. OPERA: An appearance experiment to search for $\nu_\mu \rightarrow \nu_\tau$ oscillations in the CNGS beam. - OPERA Collaboration - CERN/SPSC 2000-028, SPSC/P318, LNGS P25/2000*
- 3 *Status Report on the OPERA experiment - CERN/SPSC 2001-025, SPSC/M668, LNGS-EXP 30/2001 Add. 1/01*
- 4 *Automatic microscope systems in the CHORUS experiment. C. Bozza, Presented at Vienna Conference on Instrumentation 2001, published in Nucl. Instr. Meth. Phys. Res. 2002 (478)*
- 5 S. Aoki et al, *NIM B51* (1990) 466-472
- 6 T.Nakano, *Ph.D thesis, Nagoya University 1998*
- 7 *Esperimenti sulle Oscillazioni di Neutrino con Emulsioni Nucleari. Tesi di Dottorato di Ricerca in Fisica XII Ciclo. 1999, C. Bozza*
- 8 *Automatic analysis of digitised TV-images by a computer-driven optical microscope. A. Di Bartolomeo, G. Grella, G. Romano, G. Rosa, Nucl. Instr. Meth. Phys. Res. A394 (1997) 357*
- 9 *Study of charmed particles production and decay in neutrino interactions, E. Barbuto, Fundamental Interactions (Proceedings of the XVII Lake Louise Winter Institute). World Scientific - 2003*
- 10 *Observation of weak neutral current neutrino production of J/ ψ - CHORUS Collaboration - Phys. Lett. B* (2001)
- 11 *Measurements of D⁺ production in neutrino charged-current interactions - CHORUS Collaboration - Phys. Lett. B* (2002)
- 12 *Determination of the semi-leptonic branching fraction of charm hadrons produced in neutrino charged-current interaction - CHORUS Collaboration - Phys. Lett. B 549 (2002)*
- 13 *Measurement of A_c production in neutrino charged-current interactions - CHORUS Collaboration - Phys. Lett. B* 555 (2003)
- 14 *Cross-section measurement for quasi-elastic production of charmed baryons in neutrino nucleus interactions - CHORUS Collaboration - accepted for publication in Phys. Lett. B*

Probing the QGP with charm at ALICE–LHC

Andrea Dainese

Università degli Studi di Padova, via Marzolo 8, 35131 Padova, Italy

e-mail: andrea.dainese@pd.infn.it

Abstract

The exclusive reconstruction of D^0 mesons in the ALICE experiment allows to study the QCD energy loss of charm quarks in the deconfined quark gluon plasma (QGP) medium expected to be produced in central nucleus–nucleus collisions at the Large Hadron Collider.

1 Introduction

The ALICE experiment [1] at the LHC will study nucleus–nucleus (AA) collisions at a centre-of-mass energy $\sqrt{s_{NN}} = 5.5$ TeV (for Pb–Pb) per nucleon–nucleon (NN) pair in order to investigate the properties of QCD matter at energy densities of few hundred times the density of atomic nuclei. In these conditions a deconfined state of quarks and gluons is expected to be formed [2].

Hard partons and heavy quarks, abundantly produced at LHC energies in initial hard scattering processes, are sensitive probes of the medium formed in the collision as they may lose energy by gluon bremsstrahlung while propagating through the medium itself. The attenuation (quenching) of leading hadrons and jets observed at RHIC [3] is thought to be due to such a mechanism. The large masses of the charm and beauty quarks make them qualitatively different probes, since, on well-established QCD grounds, in-medium energy loss off massive partons is expected to be significantly smaller than off ‘massless’ partons (light quarks and gluons). Therefore, a comparative study of the attenuation of massless and massive probes is a promising tool to test the coherence of the interpretation of quenching effects as energy loss in a deconfined medium and to further investigate the properties (density) of such medium.

In the first part of this paper, we shortly summarize one of the widely used models of parton energy loss and we discuss how we used it in our simulation. In the second part, we show that the exclusive reconstruction of

$D^0 \rightarrow K^- \pi^+$ decays with ALICE allows to carry out the mentioned comparative quenching studies by measuring the *nuclear modification factor* of the D mesons transverse momentum (p_t) distribution

$$R_{AA}(p_t) \equiv \frac{dN_{AA}/dp_t/\text{binary NN collision}}{dN_{pp}/dp_t}, \quad (1)$$

which would be 1 if the AA collision was a mere superposition of independent NN collisions without nuclear or medium effects, and the D/*charged hadrons* (D/h) ratio

$$R_{D/h}(p_t) \equiv R_{AA}^D(p_t) / R_{AA}^h(p_t). \quad (2)$$

2 Parton energy loss and the dead cone effect for heavy quarks

In this work we use the quenching probabilities (or weights) calculated by C.A. Salgado and U.A. Wiedemann [4] in the framework of the ‘BDMPS’ formalism [5], which we summarize in the following. The energy loss obtained with the quenching weights is presented in Section 3.

An energetic parton produced in a hard collision radiates a gluon with a probability proportional to its path length L in the dense medium. Then (Fig. 1, left) the radiated gluon undergoes multiple scatterings in the medium, in a Brownian-like motion with mean free path λ which decreases as the density of the medium increases. The number of scatterings of the radiated gluon is also proportional to L . Therefore, the average energy loss of the parton is proportional to L^2 .

The scale of the energy loss is set by the ‘maximum’ energy of the radiated gluons, which depends on L and on the properties of the medium:

$$\omega_c = \hat{q} L^2 / 2, \quad (3)$$

where \hat{q} is the *transport coefficient of the medium*, defined as the average transverse momentum squared transferred to the projectile per unit path length, $\hat{q} = \langle q_t^2 \rangle_{\text{medium}} / \lambda$ [4].

In the case of a static medium, the distribution of the energy ω of the radiated gluons (for $\omega \ll \omega_c$) is of the form:

$$\omega \frac{dI}{d\omega} \simeq \frac{2 \alpha_s C_R}{\pi} \sqrt{\frac{\omega_c}{2\omega}}, \quad (4)$$

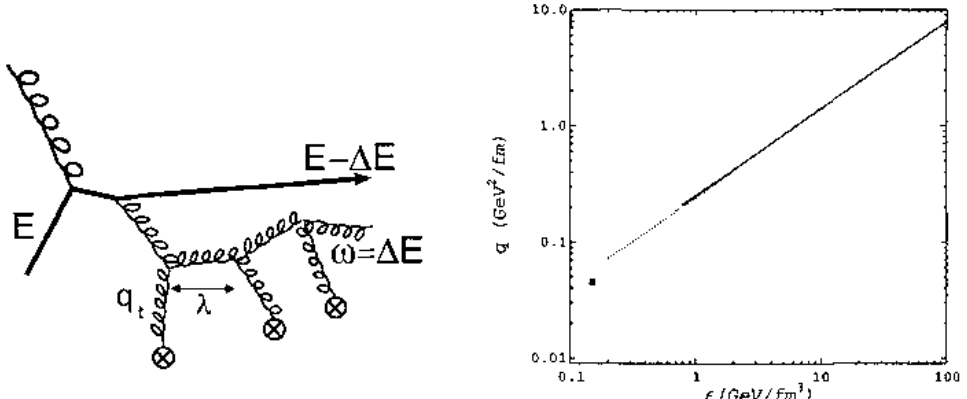


Figure 1: Typical gluon radiation diagram (left) and transport coefficient as a function of energy density (right) for different media: cold (marker), massless hot pion gas (dotted curve) and ideal QGP (solid curve) [6].

where C_R is the QCD coupling factor (Casimir factor), equal to $4/3$ for quark-gluon coupling and to 3 for gluon-gluon coupling. The integral of the energy distribution up to ω_c estimates the average energy loss of the initial parton:

$$\langle \Delta E \rangle = \int^{\omega_c} \omega \frac{dI}{d\omega} d\omega \propto \alpha_s C_R \omega_c \propto \alpha_s C_R \hat{q} L^2. \quad (5)$$

The average energy loss is therefore: proportional to $\alpha_s C_R$ and, thus, larger by a factor $9/4 = 2.25$ for gluons than for quarks; proportional to the transport coefficient of the medium; proportional to L^2 ; independent of the parton initial energy. The last point is peculiar to the BDMPS model. Other models [7, 8] consider an explicit dependence of ΔE on the initial energy E . However, there is always an intrinsic dependence of the radiated energy on the initial energy, determined by the fact that the former cannot be larger than the latter, $\Delta E \leq E$.

The transport coefficient is proportional to the density of the scattering centres and to the typical momentum transfer in the gluon scattering off these centres. Figure 1 (right) reports the estimated dependence of \hat{q} on the energy density ϵ for different equilibrated media [6]: for cold nuclear matter (marker) the estimate is $\hat{q}_{\text{cold}} \simeq 0.05 \text{ GeV}^2/\text{fm}$; for a QGP formed at the LHC with $\epsilon \sim 50-100 \text{ GeV}/\text{fm}^3$, \hat{q} is expected to be of $\simeq 5-10 \text{ GeV}^2/\text{fm}$.

In Ref. [9] Yu.L. Dokshitzer and D.E. Kharzeev argue that for heavy quarks, because of their large mass, the radiative energy loss should be lower

than for light quarks. The predicted consequence of this effect is an enhancement of the ratio of D mesons to pions (or hadrons in general) at moderately large (5–10 GeV/c) transverse momenta, with respect to that observed in the absence of energy loss (proton–proton collisions).

Heavy quarks with momenta up to 20–30 GeV/c propagate with a velocity which is smaller than the velocity of light. As a consequence, gluon radiation at angles Θ smaller than the ratio of their mass to their energy $\Theta_0 = m/E$ is suppressed by destructive quantum interference. The relatively depopulated cone around the heavy quark direction with $\Theta < \Theta_0$ is indicated as ‘dead cone’ [10].

In Ref. [9] the dead cone effect is assumed to characterize also in-medium gluon radiation and the energy distribution of the radiated gluons (4), for heavy quarks, is estimated to be suppressed by the factor:

$$\left. \frac{dI}{d\omega} \right|_{\text{Heavy}} \Big/ \left. \frac{dI}{d\omega} \right|_{\text{Light}} = \left[1 + \frac{\Theta_0^2}{\Theta^2} \right]^{-2} = \left[1 + \left(\frac{m}{E} \right)^2 \sqrt{\frac{\omega^3}{\hat{q}}} \right]^{-2} \equiv F_{\text{H/L}}, \quad (6)$$

where the expression for the characteristic gluon emission angle [9] $\Theta \simeq (\hat{q}/\omega^3)^{1/4}$ has been used. The heavy-to-light suppression factor $F_{\text{H/L}}$ in (6) increases (less suppression) as the heavy quark energy E increases (the mass becomes negligible) and it decreases at large ω , indicating that the high-energy part of the gluon radiation spectrum is drastically suppressed by the dead cone effect.

3 Simulation of energy loss

The Salgado Wiedemann (SW) quenching weight is defined as the probability that a hard parton radiates an energy ΔE due to scattering in spatially extended QCD matter. In Ref. [4], the weights are calculated on the basis of the BDMPS formalism, keeping into account both the finite in-medium path length L and the dynamic expansion of the medium after the nucleus–nucleus collision. The input parameters for the calculation are the length L , the transport coefficient \hat{q} and the parton species (light quark or gluon).

The distribution of the in-medium path length in the plane transverse to the beam line¹ for central Pb–Pb collisions (impact parameter $b < 3.5$ fm, corresponding to the 5% most central collisions) is calculated in the framework of the Glauber model of the collision geometry [11]. For a given impact parameter, hard parton production points are sampled according to the density $\rho_{\text{coll}}(x, y)$ of binary nucleon–nucleon collisions in the transverse plane

¹Partons produced at central rapidities propagate in the transverse plane.

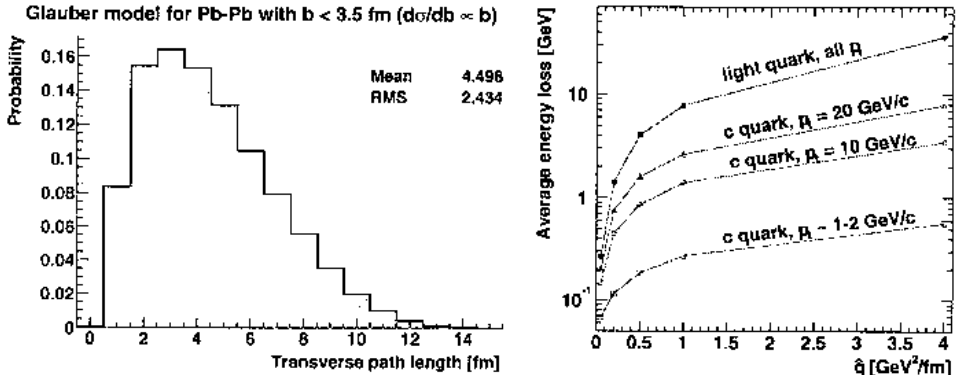


Figure 2: Distribution of the path lengths in the transverse plane for partons produced in Pb–Pb collisions with $b < 3.5$ fm (left). Average energy loss as a function of the transport coefficient (right).

and their azimuthal propagation directions are sampled uniformly. For a parton with production point (x_0, y_0) and azimuthal direction (u_x, u_y) , the path length is defined as:

$$L = \frac{\int_0^\infty dl l \rho_{\text{coll}}(x_0 + l u_x, y_0 + l u_y)}{0.5 \int_0^\infty dl \rho_{\text{coll}}(x_0 + l u_x, y_0 + l u_y)}. \quad (7)$$

Many sampling iterations are performed varying the impact parameter b from 0.25 fm to 3.25 fm in steps of 0.5 fm. The obtained distributions are given a weight b , since we verified that $d\sigma^{\text{hard}}/db \propto b$ for $b < 3.5$ fm, and added together. The result is shown in Fig. 2 (left). The average length is 4.5 fm, corresponding to about 70% of the radius of a Pb nucleus and the distribution is significantly accumulated towards low values of L because a large fraction of the partons are produced in the periphery of the superposition region of the two nuclei ('corona' effect).

For a given value of the transport coefficient \hat{q} and a given parton species, we use the routine provided in Ref. [4] to get the energy loss probability distribution $P(\Delta E; L)$ for the integer values of L up to 15 fm. Then, these 15 distributions are weighted according to the path length probability in Fig. 2 and added together to obtain a global energy loss probability distribution $P(\Delta E)$. The energy loss to be used for the quenching simulation can be directly sampled from the $P(\Delta E)$ distribution corresponding to the chosen \hat{q} and to the correct parton species.

The predicted lower energy loss for charm quarks is accounted for by multiplying the $P(\Delta E)$ distribution for light quarks with the dead cone

suppression factor $F_{H/L}$ in (6). It was verified that this approximation is equivalent to recalculating the SW quenching weights with the gluon energy distribution for heavy quarks as given in (6) [12, 13]. Since $F_{H/L}$ depends on the heavy quark energy, the product has to be done for each c quark or, more conveniently, in bins of p_t . Figure 2 (right) reports the average energy loss as a function of the transport coefficient for light quarks and for charm quarks ($m_c = 1.2$ GeV) with $p_t = 1\text{--}2, 10, 20$ GeV/c, as obtained with the described dead cone correction (p_t -dependent $P(\Delta E) \otimes F_{H/L}$ product). With $\hat{q} = 4$ GeV $^2/\text{fm}$, our estimated transport coefficient for the LHC (see next paragraph), the average energy loss for light quarks is $\langle \Delta E \rangle \simeq 35$ GeV (the effective value of $\langle \Delta E \rangle$ is lower by about a factor 2, due to the constraint $\Delta E \leq E$). For c quarks of 1–2, 10, 20 GeV/c $\langle \Delta E \rangle$ is about 2%, 10% and 20%, respectively, of the average loss for light quarks.

For the estimation of the transport coefficient \hat{q} for our simulation, we consider that it is reasonable to require for central nucleus–nucleus collisions at the LHC a quenching of hard partons at least of the same magnitude as that observed at RHIC. We, therefore, derive the nuclear modification factor R_{AA} for charged hadrons produced at the LHC and we choose the transport coefficient in order to obtain $R_{AA} \simeq 0.2\text{--}0.3$ in the range $p_t = 5\text{--}10$ GeV/c (for RHIC results see e.g. Refs. [3, 14]).

The transverse momentum distributions, for $p_t > 5$ GeV/c, of charged hadrons are generated by means of the chain:

1. generation of a parton, quark or gluon, with $p_t > 5$ GeV/c, using PYTHIA [15] proton–proton with $\sqrt{s} = 5.5$ TeV and CTEQ 4L parton distribution functions; with these parameters, the parton composition given by PYTHIA is 78% gluons and 22% quarks;
2. sampling of an energy loss ΔE according to $P(\Delta E)$ and calculation of the quenched transverse momentum of the parton, $p'_t = p_t - \Delta E$ (if $\Delta E > p_t$, p'_t is set to 0);
3. (independent) fragmentation of the parton to a hadron using the leading order Kniehl-Kramer-Pötter (KKP) fragmentation functions [16].

Quenched and unquenched p_t distributions are obtained including or excluding the second step of the chain. R_{AA} is calculated as the ratio of the p_t distribution with quenching to the p_t distribution without quenching. We find $R_{AA} \simeq 0.25\text{--}0.3$ in $5 < p_t < 10$ GeV/c for $\hat{q} = 4$ GeV $^2/\text{fm}$. This value is reasonable, as it corresponds, using the plot in Fig. 1, to an energy density $\epsilon \simeq 40\text{--}50$ GeV/fm 3 , which is about a factor 2 lower than the maximum energy density expected for central Pb–Pb collisions at the LHC.

Charm quarks are generated using PYTHIA, tuned in order to reproduce the single-inclusive c (and \bar{c}) p_t distribution predicted by the pQCD program HVQMNR [17] with $m_c = 1.2$ GeV and $\mu_{\text{Fact.}} = \mu_{\text{Renorm.}} = 2m_t \equiv 2\sqrt{m_c^2 + p_t^2}$ (the details on this tuning can be found in Ref. [18]). We use the CTEQ 4L parton distribution functions including the nuclear shadowing effect by means of the EKS98 parameterization [19] and the parton intrinsic transverse momentum broadening as reported in Ref. [18]. Energy loss for charm quarks is simulated following a slightly different procedure with respect to that for light quarks and gluons. Since the total number of $c\bar{c}$ pairs per event has to be conserved, in the cases where the sampled ΔE is larger than p_t , we assume the c quark to be thermalized in the medium and we give it a transverse momentum according to the distribution $dN/dm_t \propto m_t \exp(-m_t/T)$. We use $T = 300$ MeV as the thermalization temperature. The other difference with respect to the previous case is that we use the standard string model in PYTHIA for the c quark fragmentation.

4 Charm reconstruction with ALICE

The transverse momentum distribution of charm mesons produced at central rapidity, $|y| < 1$, can be directly measured with ALICE from the exclusive reconstruction of $D^0 \rightarrow K^-\pi^+$ (and charge conjugates). The displaced vertices of D^0 decays ($c\tau = 124 \mu\text{m}$) can be identified in the ALICE Inner Tracking System, that provides a measurement of the track impact parameters to the collision vertex with a resolution better than $50 \mu\text{m}$ for $p_t > 1 \text{ GeV}/c$. The low value of the magnetic field (0.4 T) and the K/π separation in the ALICE Time of Flight allow to extend the measurement of the D^0 production cross section down to almost 0 transverse momentum. The strategy for this analysis and the selection cuts to be applied were studied with a realistic and detailed simulation of the detector geometry and response, including the main background sources [13, 20].

The expected performance for central Pb-Pb ($b < 3.5$ fm) at $\sqrt{s_{\text{NN}}} = 5.5$ TeV and pp collisions at $\sqrt{s} = 14$ TeV, as obtained using the input production yields $N_{\text{Pb-Pb}}^{c\bar{c}} = 115$ and $N_{\text{pp}}^{c\bar{c}} = 0.16$ (see Ref. [18]), is summarized in Fig. 3. The accessible p_t range is 1–14 GeV/c for Pb-Pb and 0.5–14 GeV/c for pp. In both cases the statistical error (corresponding to 1 month of data-taking for Pb-Pb and to 9 months for pp) is better than 15–20% and the systematic error (acceptance and efficiency corrections, subtraction of the feed-down from $B \rightarrow D^0 + X$ decays, cross section normalization, centrality selection for Pb-Pb) is better than 20%. More details are given in Ref. [13].

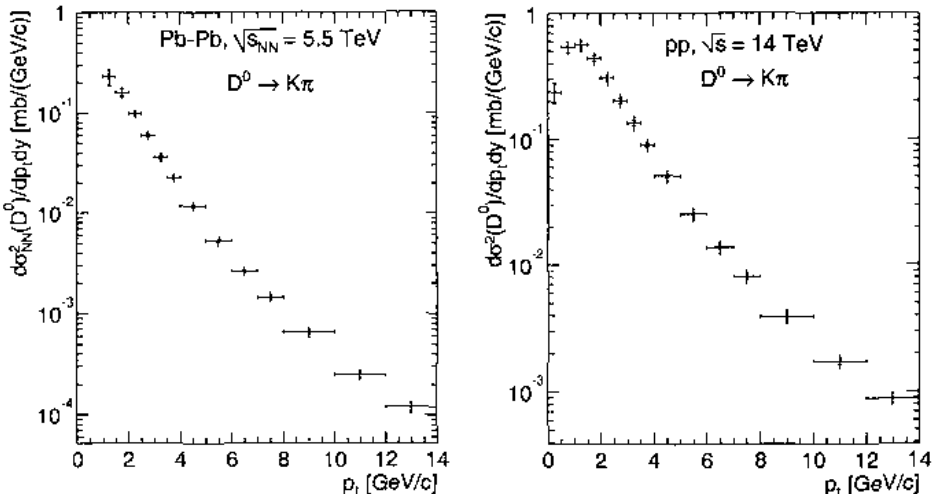


Figure 3: Double differential cross section per nucleon–nucleon collision for D^0 production as a function of p_t , as it can be measured with 10^7 central Pb–Pb events (left) and 10^9 pp minimum-bias events (right). Statistical (inner bars) and p_t -dependent systematic errors (outer bars) are shown. A normalization error of 11% for Pb–Pb and 5% for pp is not shown.

5 Results: R_{AA} and $R_{D/h}$

The nuclear modification factor for D^0 mesons is reported in Fig. 4. Nuclear shadowing, parton intrinsic transverse momentum broadening and energy loss are included. The dead cone effect is not included in the left-hand panel and included in right-hand panel. Different values of the transport coefficient are used for illustration; we remind that the value expected on the basis of the pion quenching observed at RHIC is $\hat{q} = 4 \text{ GeV}^2/\text{fm}$. The reported statistical (bars) and systematic (shaded area) errors are obtained combining the previously-mentioned errors in Pb–Pb and in pp collisions and considering that the contributions due to cross section normalization, feed-down from beauty decays and, partially, acceptance/efficiency corrections will cancel out in the ratio. An uncertainty of about 5% introduced in the extrapolation of the pp results from 14 TeV to 5.5 TeV by pQCD is also accounted for (see Ref. [13]).

The effect of shadowing, clearly visible for $\hat{q} = 0$ (no energy loss) as a suppression of R_{AA} , is limited to $p_t < 6\text{--}7 \text{ GeV}/c$. Above this region only (possible) parton energy loss is expected to affect the nuclear modification

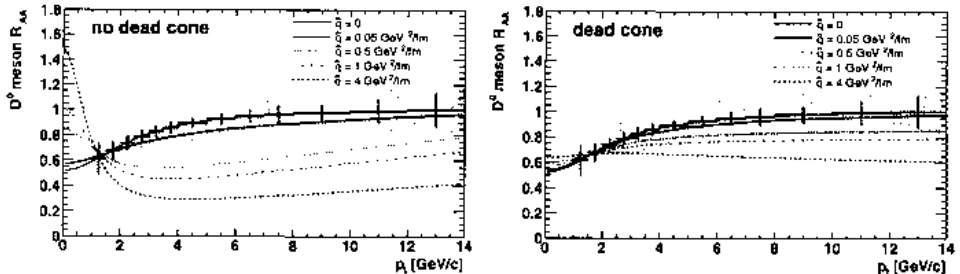


Figure 4: Nuclear modification factor for D^0 mesons with shadowing, intrinsic k_t broadening and parton energy loss. Left panel: without dead cone correction; right panel: with dead cone correction. Errors corresponding to the curve for $\hat{q} = 0$ are shown: bars = statistical, shaded area = systematic.

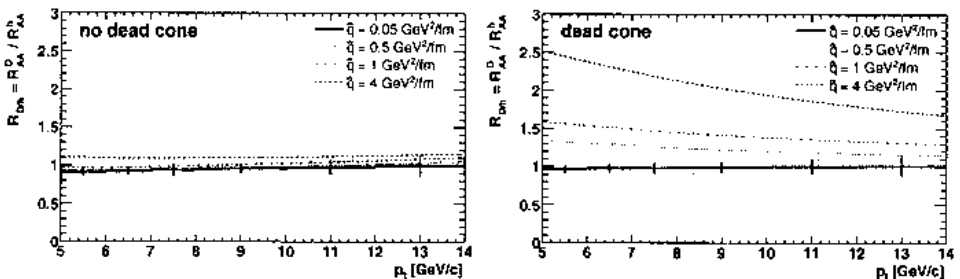


Figure 5: Ratio of the nuclear modification factors for D^0 mesons and for charged hadrons. Left panel: without dead cone correction; right panel: with dead cone correction. Errors corresponding to the curve for $\hat{q} = 0.05 \text{ GeV}^2/\text{fm}$ are shown: bars = statistical, shaded area = systematic.

factor of D mesons.

For $\hat{q} = 4 \text{ GeV}^2/\text{fm}$ and no dead cone, we find R_{AA} reduced, with respect to 1, by a factor about 3 and slightly increasing with p_t , from 0.3 at $6 \text{ GeV}/c$ to 0.4 at $14 \text{ GeV}/c$. Even for a transport coefficient lower by a factor 4, $\hat{q} = 1 \text{ GeV}^2/\text{fm}$, R_{AA} is significantly reduced (0.5–0.6). When the dead cone effect is taken into account, the R_{AA} reduction due to quenching is found to be lower by about a factor 1.5–2.5, depending on \hat{q} and p_t .

We point out that the estimated systematic uncertainty of about 18% may prevent from discriminating between a scenario with moderate quenching and negligible dead cone effect (e.g. $\hat{q} = 1 \text{ GeV}^2/\text{fm}$ in the left-hand panel of Fig. 4) and a scenario with large quenching but also strong dead cone effect (e.g. $\hat{q} = 4 \text{ GeV}^2/\text{fm}$ in the right-hand panel).

The comparison of the quenching of charm-quark-originated mesons and massless-parton-originated hadrons will be the best suited tool to disentangle the relative importance of energy loss and dead cone effects. The D/*charged hadrons* (D/h) ratio, defined as in (2), is presented in Fig. 5 for the range $5 < p_t < 14$ GeV/c. We used R_{AA}^h calculated as previously described and $R_{AA}^{D,h}$, without and with dead cone, as reported in Fig. 4. Being essentially a double ratio $Pb-Pb/Pb-Pb \times pp/pp$, this observable is particularly sensitive, as many systematic uncertainties cancel out (centrality selection and, partially, acceptance/efficiency corrections and energy extrapolation by pQCD). The residual systematic error is estimated to be of about 10–11%.

We find that, if the dead cone correction for c quarks is not included, $R_{D/h}$ is essentially 1 in the considered p_t range, independently of the value of the transport coefficient, i.e. of the magnitude of the energy loss effect. When the dead cone is taken into account, $R_{D/h}$ is enhanced of a factor strongly dependent on the transport coefficient of the medium: e.g. 2–2.5 for $\hat{q} = 4$ GeV²/fm and 1.5 for $\hat{q} = 1$ GeV²/fm. The enhancement is decreasing with p_t , as expected (the c quark mass becomes negligible).

The $R_{D/h}$ ratio is, therefore, found to be enhanced, with respect to 1, only by the dead cone and, consequently, it appears as a very clean tool to investigate and quantify this effect.

Since hadrons come mainly from gluons while D mesons come from (c) quarks, the D/h ratio should, in principle, be enhanced also in absence of dead cone effect, as a consequence of the larger energy loss of gluons with respect to quarks. Such enhancement is essentially not observed in the obtained $R_{D/h}$ because it is ‘compensated’ by the harder fragmentation of charm quarks with respect to light quarks and, particularly, gluons. With z the typical momentum fraction taken by the hadron in the fragmentation, $p_t^{\text{hadron}} = z p_t^{\text{parton}}$, and ΔE the average energy loss for the parton, $(p_t^{\text{parton}})' = p_t^{\text{parton}} - \Delta E$, we have

$$(p_t^{\text{hadron}})' = p_t^{\text{hadron}} - z \Delta E, \quad (8)$$

meaning that the energy loss observed in the nuclear modification factor is, indeed, $z \Delta E$. We have, thus, to compare $z_{c \rightarrow D} \Delta E_c$ to $z_{\text{gluon} \rightarrow \text{hadron}} \Delta E_{\text{gluon}}$. With $z_{\text{gluon} \rightarrow \text{hadron}} \approx 0.4$, $z_{c \rightarrow D} \approx 0.8$ for $p_t^{D,h} > 5$ GeV/c and $\Delta E_c = \Delta E_{\text{gluon}}/2.25$ (without dead cone), we obtain

$$z_{c \rightarrow D} \Delta E_c \approx 0.9 z_{\text{gluon} \rightarrow \text{hadron}} \Delta E_{\text{gluon}}. \quad (9)$$

This simple estimate confirms that the quenching for D mesons is almost the same as for (non-charm) hadrons, if the dead cone effect is not considered.

The errors reported in Fig. 5 show that ALICE is expected to have good capabilities for the study of $R_{D/h}$: in the range $5 < p_t < 10$ GeV/c the enhancement due to the dead cone is an effect of more than 3σ for $\hat{q} > 1$ GeV $^2/\text{fm}$. The comparison of the values for the transport coefficient extracted from the nuclear modification factor of charged hadrons and, *independently*, from the D/*hadrons* ratio shall provide an important test for the coherence of our understanding of the energy loss of hard probes propagating in the dense QCD medium formed in Pb–Pb collisions at the LHC.

Acknowledgements

I am grateful to F. Antinori, A. Morsch, G. Paic, K. Šafařík, C.A. Salgado and U.A. Wiedemann for many fruitful discussions and to Prof. A. Zichichi and Prof. G. 't Hooft for providing me with the opportunity to present my work in the New Talents session of the 41st International School of Subnuclear Physics in Erice.

References

- [1] ALICE Technical Proposal, CERN/LHCC 95-71 (1995).
- [2] F. Karsch, these proceedings.
- [3] T.W. Ludlam, these proceedings.
- [4] C.A. Salgado and U.A. Wiedemann, Phys. Rev. **D68** (2003) 014008.
- [5] R. Baier, Yu.L. Dokshitzer, A.H. Mueller, S. Peigné and D. Schiff, Nucl. Phys. **B483** (1997) 291; *ibidem* **B484** (1997) 265.
- [6] R. Baier, Nucl. Phys. **A715** (2003) 209c.
- [7] M. Gyulassy and X.N. Wang, Nucl. Phys. **B420** (1994) 583.
- [8] M. Gyulassy, P. Lévai and I. Vitev, Nucl. Phys. **B571** (2000) 197; Phys. Rev. Lett. **85** (2000) 5535; Nucl. Phys. **B594** (2001) 371.
- [9] Yu.L. Dokshitzer and D.E. Kharzeev, Phys. Lett. **B519** (2001) 199.
- [10] Yu.L. Dokshitzer, V.A. Khoze and S.I. Troyan, J. Phys. **G17** (1991) 1602.
- [11] R.J. Glauber and G. Matthiae, Nucl. Phys. **B21** (1970) 135.
- [12] C.A. Salgado and U.A. Wiedemann, private communication.
- [13] A. Dainese, Ph.D. Thesis, arXiv:nucl-ex/0311004.
- [14] J. Jia *et al.*, PHENIX Coll., Nucl. Phys. **A715** (2003) 769c.
- [15] T. Sjöstrand *et al.*, Computer Phys. Commun. **135** (2001) 238.
- [16] B.A. Kniehl, G. Kramer and B. Pötter, Nucl. Phys. **B582** (2000) 514.
- [17] M. Mangano, P. Nason and G. Ridolfi, Nucl. Phys. **B373** (1992) 295.
- [18] N. Carrer and A. Dainese, arXiv:hep-ph/0311225.
- [19] K.J. Eskola, V.J. Kolhinen, C.A. Salgado, Eur. Phys. J. **C9** (1999) 61.
- [20] N. Carrer, A. Dainese and R. Turrisi, J. Phys. **G29** (2003) 575.

Magnetic screening length in hot QCD

Pierre Giovannangeli

Centre Physique Théorique au CNRS,

Case 907, Campus de Luminy, F13288, Marseille, France

Abstract

In hot QCD, static chromomagnetic fields are screened, contrary to magnetic fields in electromagnetic plasmas. The inverse of the magnetic Debye mass measures the screening length. In this talk I reformulate a well-known definition of the magnetic Debye mass as a correlator between spin 0 operators. This means that the magnetic Debye mass -like its electric counterpart- is the mass of a state with the appropriate quantum numbers. This gives a useful consistency check in simulations.

1 Introduction

The plasma phase is one of the most wide-spread states of matter. Electromagnetic plasmas can be found in very different places in Nature like in the Sun or, artificially, in neon lights. Such a state of matter can be obtained by thermal ionisation of a gas. In QCD, the so-called plasma phase correspond to the state of matter where quarks are deconfined. This phase transition occurs at a temperature of about 170 Mev.

One of the most important parameters for characterizing such a phase is the Debye mass. It measures the screening of an external electric field in such a medium. For static electromagnetic fields, the electric potential is known to be screened. But it's not the case for the magnetic field. Indeed one observes in the Sun long range magnetic fields responsible for sunspots. In QCD the situation is thoroughly different. Static chromomagnetic fields are screened.

The purpose of this talk is to show how to measure this chromomagnetic Debye mass.

The first two section are introductory.

In section (2) I will remind the reader the physics of classical plasma and the perturbative computation of the electric Debye mass in scalar QED.

In section (3) I will show that perturbation theory has limited applicability in hot QCD. So I will give a nonperturbative definition of the electric Debye mass.

In the last section, by analogy with the chromoelectric case, I will give a nonperturbative definition of the chromomagnetic Debye mass.

2 The electric screening mass in hot scalar QED

2.1 Debye screening in a classical electromagnetic plasma

Let's consider a positive heavy charge Q in a ionized gaz of electrons and heavy ions at thermal equilibrium. The collective behaviour of electrons in this ionic background will be guided by two effects:

- the attractive electric potential created by the heavy charge.
- thermal excitations that forbid the overall cancellation of the electric potential created by the heavy charge.

The result of these two effects is that above a certain screening distance l_E the electric potential will be almost zero. Indeed in the limit of high T ($kT \gg eA_0$ with A_0 the electric potential) the electric potential created by the heavy charge will behave instead of a Coulomb law like Yukawa law i.e.:

$$\frac{1}{r} \rightarrow \frac{1}{r} \exp -\frac{r}{l_e} \quad (2.1)$$

Indeed if one computes the classical Green's function of the electric potential we will find a mass term. Precisely in the high T limit the Poisson law reads:

$$\Delta A_0 = m_E^2 A_0 - Q\delta(\vec{r}) \quad (2.2)$$

with the Debye mass $m_E = \frac{e^2 n}{T}$ where n is the density of electrons. It defines the screening length $l_e = \frac{1}{m_E}$.

2.2 Perturbative computation of the electric screening mass in Hot scalar QED

First of all let us recall how to describe a quantum field at thermal equilibrium [1].

The thermal average of an observable O reads:

$$\langle O \rangle_T = \text{Tr } O \exp(-H/T) / \text{Tr} \exp -H/T \quad (2.3)$$

In the imaginary time formalism one can express this thermal average in term of a path integral:

$$\langle O \rangle_T = \int D\phi D\psi O \exp -\frac{1}{g^2} S_E(\phi, \psi) / \int DA \exp -\frac{1}{g^2} S_E(\phi, \psi) \quad (2.4)$$

where S_E is the Euclidean action and the time direction in Euclidean spacetime being periodic of period $\frac{1}{T}$.

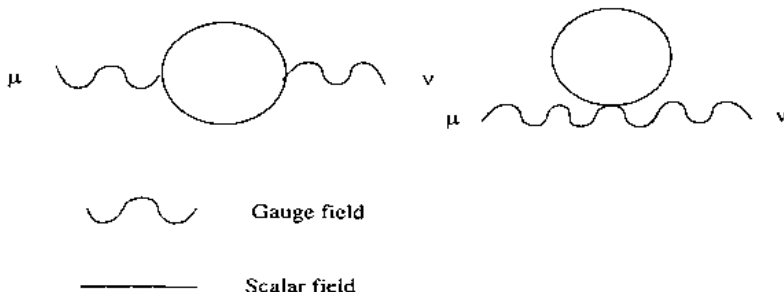


Figure 1: One loop contribution to the self energy in scalar QED.

ϕ and ψ are respectively bosonic field with time periodicity of $\frac{1}{T}$ and fermionic field with time antiperiodicity of $\frac{1}{T}$. Technically we are doing quantum field theory on a cylinder with a radius $\frac{1}{2\pi T}$ in the periodic time direction.

Physically what happens if one puts a heavy charge in the vacuum at temperature T is the following: thermal excitation of the vacuum will produce particles that as in the classical case are going to screen the potential created by the heavy charge.

Quantitatively, guided by the classical case, one likes to compute the mass term in the Green's function of the electric potential.

Let's take a look at the case of scalar QED because this theory has some common point with QCD at high temperature. The lagrangian for scalar QED reads:

$$\mathcal{L}_{SQED} = \frac{1}{4} F_{\mu\nu}^2 + D_\mu \phi D_\mu \phi^* + m^2 \phi \phi^* \quad (2.5)$$

We are going to work in the framework of perturbation theory. Let's compute the thermal contribution to the mass of the photon field. Up to one loop order, one has to compute the contribution to the selfenergy of the A_0 field. It consists of two graphs shown in fig.(1).

One has to find the location of the pole of the propagator in the static limit. It gives in coordinate space the mass term of the exponential fall-off of the field.

The one loop computation reads:

$$\frac{1}{\vec{p}^2} \rightarrow \frac{1}{\vec{p}^2 + m_e^2} \quad (2.6)$$

So after a Fourier transformation

$$\frac{1}{r} \rightarrow \frac{1}{r} \exp -\frac{r}{l_e} \quad (2.7)$$

with $m_e \equiv \frac{1}{l_e} = e^2 T^2 / 3$. This relation is similar to the classical one as $n \sim T^3$.

In conclusion, the thermal contribution will give a thermal mass to the A_0 and gives rise to a screened Coulomb potential. For higher orders, one can prove that the location of the pole is gauge-independent.

The question is, can we do the same in QCD? The answer is no.

3 The electric screening mass in hot QCD

3.1 The failure of perturbation theory.

Let's consider QCD with N colours and N_f fermions. The QCD lagrangian in imaginary time formalism reads:

$$\mathcal{L}_{QCD} = \frac{1}{2} Tr F_{\mu\nu}^2 + \sum_{i=1}^{N_f} \bar{\psi}_i (\gamma_\mu D_\mu + m_i) \psi_i \quad (3.1)$$

At very high T, because of asymptotic freedom, it's seems natural to work in the framework of perturbation theory. But there are two essential differences compared with scalar QED. First of all, the self energy is not gauge independent, even if the location of the pole is. Moreover, the perturbation theory fails up to two loop. A infinity of diagrams will contribute at two loop order [2]. The Debye mass reads:

$$m_D = \left(\frac{N}{3} + \frac{N_f}{6}\right)^{\frac{1}{2}} g T + \frac{g^2 N}{4\pi} T \left(\log\left(\frac{\frac{N}{3} + \frac{N_f}{6}}{g}\right)^{\frac{1}{2}} + 7.0\right) + O(g^3) \quad (3.2)$$

The log term is due to [3], the nonperturbative part of the $O(g^2)$ contribution is determined by lattice methods for $N = 2$ and $N = 3$ [4]. The physical reason of such a failure is the following: At very high temperature, despite the asymptotic freedom that renders the coupling constant small, QCD is described by a 3D lagrangian that is confining. As mentioned in the previous section, quantum field theory at thermal equilibrium is described by fields living in a periodic time direction space of period $\frac{1}{T}$. So at high T the effective theory is 3-dimensional. Quantitatively, one has, like in Kaluza Klein theory, integrated over heavy modes [5] [6]. The effective 3D electrostatic lagrangian reads:

$$\begin{aligned} \mathcal{L}_E &= Tr(\vec{D}(A)A_0)^2 + m_E^2 Tr A_0^2 + \lambda_E (Tr(A_0^2))^2 + \\ &+ \tilde{\lambda}_E (Tr(A_0)^4 - \frac{1}{2}(Tr A_0^2)^2) + \frac{1}{2} Tr F_{ij}^2 + \delta\mathcal{L}_E. \end{aligned} \quad (3.3)$$

with $\delta\mathcal{L}_E$ containing higher order operators. It is invariant under R-parity (A_0 goes to $-A_0$). This Lagrangian also exhibits invariance under the usual charge conjugaison C and parity P (y goes to $-y$).

Moreover one can also integrate over the massive A_0 field. The effective 3D magnetic lagrangian reads:

$$\mathcal{L}_{MQCD} = \frac{1}{2} Tr F_{ij}^2 + \delta\mathcal{L}_M \quad (3.4)$$

with $\delta\mathcal{L}_M$ containing higher order operators

So as T goes to infinity the physics is one of a purely magnetic Yang Mills theory It's a confining theory so even at high T there is a nonperturbative piece.

It contains a coupling constant $g_m^2(T)$ that has the dimension of a mass. It gives the magnetic mass scale of the theory. It is determined through perturbation theory to the coupling g_E in the Lagrangian (3.3). It is now known to two loop order [9].

3.2 Towards a nonperturbative and gauge invariant definition of the screening.

One has to consider a nonperturbative definition of the Debye mass. So the measurement of such a quantity will be done via lattice simulation. It renders mandatory the use of a gauge invariant operator.

Nevertheless, the physical idea is the same as that in section (2). One wants to know the behaviour of the electric potential in the hot QCD plasma. So let's consider two heavy static charges that propagate in the time direction.

Classically, such a source for an external field is given by the interaction term in the action $\int j_\mu A^\mu d^4r$. In the heavy static limit only j_0 is non zero and is given by $e\delta(r)$.

In non abelian gauge theory, a gauge invariant version of a static charge is known as the Wilson line or Polyakov loop. It reads:

$$P(A_0) \equiv \frac{1}{N} Tr \exp i \int_0^{\frac{1}{T}} g A_0 dt \quad (3.5)$$

where the trace is over colours.

So what we are going to consider is the correlator $\langle P(r)P(0)^\dagger \rangle$ between two heavy static electric charges [7].

Perturbatively it will give diagrams like in fig(1) when considering correlators of ImP^1 . Non perturbative aspect are measured by lattice simulation:

$$\langle ImP(r)ImP(0)^\dagger \rangle \sim \exp -\frac{\sigma r}{T} \quad (3.6)$$

for $T < T_c$

$$\langle ImP(r)ImP(0)^\dagger \rangle \sim \exp -m_e r \quad (3.7)$$

for $T > T_c$

In the deconfined phase, lattice simulations will give an exponential fall of that measures the electric Debye mass.

4 The magnetic Debye mass in hot QCD

4.1 The analogue of the Wilson line

One of the main features of hot QCD is the fact that there is a magnetic mass contrary to the electromagnetic case. This is an old idea of 't Hooft and

¹The exception is $SU(2)$, where the loop is real.

Mandelstam [8] and fits in the qualitative picture of confinement in term of a dual superconductor.

As this is a magnetic effect, its description is purely non-perturbative. The physics is mainly contained in the effective magnetic Lagrangian eq(3.4).

So we have to find an operator whose correlator is going to give us the magnetic mass. The idea is to take something like the correlator of a monopole and an antimonopole. The answer is take what is called the $Z(N)$ Dirac string. Dirac introduced monopoles in the 30's by considering a thin and infinite solenoid where the end point is the monopole.

On the wave function, such a candidate acts as a $U(1)$ gauge transformation with a discontinuity $2\pi n$ with n an integer.

In the case of a $SU(N)$ pure gauge theory, let's consider the center group $Z(N)$. It is the $SU(N)$ subgroup that contains all matrices that commute with every element of $SU(N)$. An element of $Z(N)$ is of the form of $\exp i \frac{2\pi k}{N} 1_{N \times N}$

The $Z(N)$ generalisation of the $U(1)$ Dirac string is represented on the Hilbert space by the following operator:

$$V_k = \exp i \int Tr \vec{D}(A)(v_k(x, y, z)) \cdot \vec{E} dx dy dz. \quad (4.1)$$

with $v_k(x, y, z) = \arctan(\frac{y}{x}) \Theta(z) \frac{1}{N} Y_k$ where Y_k is the k -hypercharge, i.e. an element of the Lie algebra of $SU(N)$ whose group value is in the center group.

With this definition, the monopole is created by V_k in the point $(x = 0, y = 0, z = 0)$

It has the good following properties:

- it's a gauge transformation with a $Z(N)$ discontinuity
- it carries a magnetic flux that is a $Z(N)$ value
- it can't be seen by scattering with adjoint fields as they do not feel $Z(N)$

Now that we have this monopole we just have to compute the correlation between a monopole and an antimonopole propagating in time

We have:

$$\langle Im V^\dagger(r) Im V(0) \rangle \sim \exp -M_m r \quad (4.2)$$

This correlation can be seen, like in the $U(1)$ case, as a string which begins by a monopole at 0 and ends with an antimonopole at r and carries a magnetic $Z(N)$ flux.

4.2 Lattice formulation

On the lattice, this object can be represented as a string which is going to add a $Z(N)$ extra factor at each plaquette pierced by this string, as shown in fig.(2). More precisely, $V_k(r)$ creates a vortex at the point r and the magnetic flux "twists" the plaquette by a factor $\exp i \frac{2\pi k}{N}$ considering the following commutation relation:

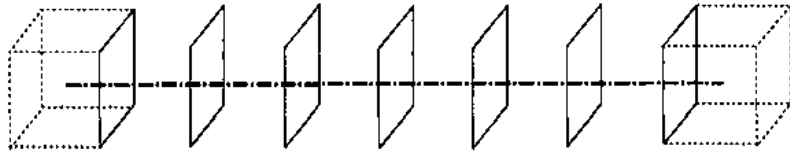


Figure 2: Monopole antimonopole pair induced by twisting the plaquettes pierced by the Dirac string.

$$V_k^\dagger W V_k = \exp i \frac{2\pi k}{N} W \quad (4.3)$$

where W is a plaquette (infinitesimal spatial Wilson Loop) pierced by the string.

So what the lattice has to compute is the partition function of the twisted action.

$$\langle \text{Im}V^\dagger(r)\text{Im}V(0) \rangle = \int DA \exp -S_{\text{twisted}} / \int DA \exp -S \sim \exp -M_m r \quad (4.4)$$

for large r

4.3 Behaviour of magnetic correlators

We can already parametrize the results in terms of the temperature. As the effective theory at high T is a 3D magnetic Yang Mills with a dimensionful coupling constant, the mass reads:

$$M_m = C g_m^2(T) \quad (4.5)$$

where C is to be determined.

As $g_m^2 \sim g^2 T$ with g^2 the QCD constant at a scale T when T goes to infinity. The behaviour of M_m and also m_e is shown in fig.(3).

One has to fit the curve via lattice simulation [10]. These authors have determined the mass for temperatures below $2T_c$.

4.4 Comparaison to mass levels of a fictitious Hamiltonian

The aim is to compute the correlator of two local operators $\langle \text{Im}V^\dagger(z)\text{Im}V(0) \rangle$. Let's introduce $\tilde{t} = z$ and $\tilde{r} = t$. Now we can see our correlation function as guided by the time evolution of a system described by a fictitious Hamiltonian that lives in a Euclidean space-time with a periodic spatial direction \tilde{z} . Formally:

$$\langle \text{Im}V^\dagger(z)\text{Im}V(0) \rangle \sim \exp -\tilde{H}\tilde{t} \quad (4.6)$$

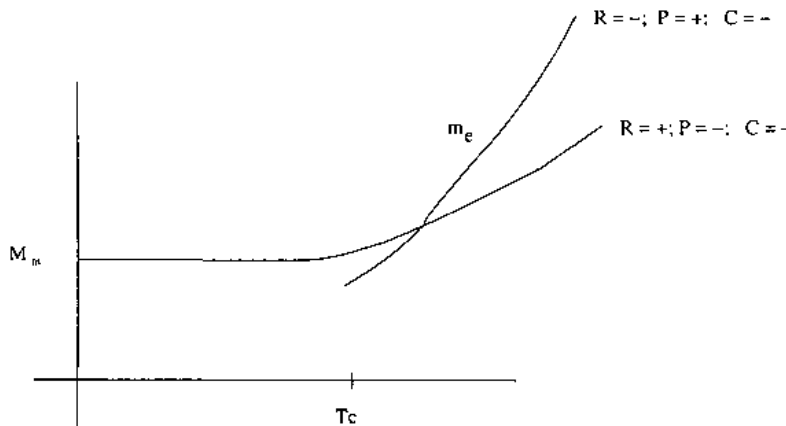


Figure 3: Schematic behaviour of the screening masses versus temperature.

The spectrum of \tilde{H} is not the same as the spectrum of the real Hamiltonian because of the periodic spatial direction. In the limit of zero T the spectra coincide of course. One has to find the lowest state of mass excited by ImV . The mass of this state can alternatively be determined by local glueball operators, with the same quantum number as the ImV operator.

5 Conclusion

In conclusion, we have constructed an operator that allows us to measure in an explicit gauge invariant way the magnetic mass. Moreover, compared to other methods [11], it really represents a spin 0 correlator and has a clear physical interpretation. We can now simulate the VV^\dagger correlator and compose it with the mass state in \tilde{H} . This is being done for infinite T in [12].

Acknowledgments I would like to thank A. Zichichi and G. 't Hooft for giving me the opportunity to present this material in the New Talents sessions in Erice. I thank Chris Korthals Altes for introducing me to the subject. I thank him and Christian Hoelbling for very useful discussions. I thank the MENESR for financial support.

References

- [1] M. Le Bellac "Thermal Field Theory", Cambridge University Press 96
- [2] A. Linde, Phys.Lett. B96 (1980) 289
- [3] A. Rebhan, Phys.Rev. D48 (1993) 3967-3970; hep-ph/9308232

- [4] K. Kajantie, M. Laine, J. Peisa, A. Rajantie, K. Rummukainen, M. Shaposhnikov, Phys.Rev.Lett. 79 (1997) 3130-3133; hep-ph/9708207; A. Hart, O. Philipsen Nucl.Phys. B572 (2000), 243-265; hep-lat/9908041; A. Hart, M. Laine, O. Philipsen, Nucl.Phys. B586 (2000) 443-474; hep-ph/0004060
- [5] E. Braaten, A. Nieto Phys.Rev. D51 (1995) 6990-7006; hep-ph/9501375
- [6] M. Shaposhnikov, Erice 96 lecture notes; hep-ph/9610247
- [7] P. Arnold L. Yaffe, Phys.Rev. D52 (1995) 7208-7219; hep-ph/9508280
- [8] G. 't Hooft, in High Energy Physics, ed. A. Zichichi (Editrice Compositori Bologna, 1976); S. Mandelstam, Phys. Rep. 23C (1976), 245
- [9] P. Giovannangeli; hep-ph/0312307
- [10] Ch. Hoelbling, C. Rebbi, V. A. Rubakov, Phys.Rev. D63 (2001) 034506; hep-lat/0003010
- [11] A. Cucchieri, F. Karsch, P. Petreczky Phys.Lett.B497:80-84,2001; hep-lat/0004027
- [12] P. De Forcrand, C. Hoelbling, C.P. Korthals Altes, O. Philipsen, in preparation.
- [13] C.P. Korthals Altes, Erice 2003 lecture notes; hep-ph/0308229

Non-supersymmetric deformation of the Klebanov-Strassler model and the related plane wave theory

Stanislav Kuperstein

*School of Physics and Astronomy
The Raymond and Beverly Sackler Faculty of Exact Sciences
Tel Aviv University, Ramat Aviv, 69978, Israel
E-mail: kopers@post.tau.ac.il*

We find a regular analytic 1st order deformation of the Klebanov-Strassler background. From the dual gauge theory point of view the deformation describes supersymmetry soft breaking gaugino mass terms. We calculate the difference in vacuum energies between the supersymmetric and the non-supersymmetric solutions and find that it matches the field theory prediction. We also discuss the breaking of the $U(1)_R$ symmetry and the space-time dependence of the gaugino bilinears two point function. Finally, we determine the Penrose limit of the non-supersymmetric background and write down the corresponding plane wave string theory. This string describes “annulons”-heavy hadrons with mass proportional to large global charge. Surprisingly the string spectrum has two fermionic zero modes. This implies that the sector in the non-supersymmetric gauge theory which is the dual of the annulons is supersymmetric.

1 Introduction

Since the formulation of the AdS/CFT conjecture [1], [2], [3] (see [4] for a review) there has been great progress in the study of theories with less supersymmetries and not necessarily conformal. There are several approaches one can use to break the $\mathcal{N} = 4$ supersymmetry down to $\mathcal{N} = 2$ or $\mathcal{N} = 1$.

A few years ago two important examples of supergravity duals of $\mathcal{N} = 1$ gauge theories have been provided by [5] and [6] (see [7] and [8] for recent reviews). The Maldacena-Nunez (MN) background consists of NS5-branes wrapped on an S^2 and based on the

solution of [9]. The supergravity dual of Klebanov-Strassler (KS) involves D5 branes wrapped around a shrinking S^2 . The metric has a standard D3-form with the 6d deformed conifold being the transversal part of the 10d space.

Non-supersymmetric deformations of the MN background have been studied by number of authors. In [10] the supersymmetry was broken completely by giving masses for some of the scalar fields. It was argued that the deformed non-supersymmetric background is guaranteed to be stable, since the original dual gauge theory had a mass gap. On other hand, the authors of [11] used the solution of [12] to study the supersymmetry breaking by the inclusion of a gaugino mass term and a condensate. Evidently, the global symmetry remains unbroken under this deformation.

Our main goal is to find a non-singular, non-supersymmetric deformation of the KS solution, which preserves the global symmetries of the original background and to study the Penrose limit of the new solution. The problem has been already attacked by different authors [13],[14]. The authors of [14] suggested a computational technique for studying the non-supersymmetric solution. The technique is based on the modification of the first order BPS equations, so that we might continue to use a superpotential even for a non-supersymmetric solution. In short, one obtains a set of sixteen 1st equations and one zero-order constraint instead of eight standard 2nd order differential equations.

In this paper (see [15] for more comprehensive discussion) we determine and describe a regular *analytic* solution of the 1st order equations similar to those appearing in [14]. We note that these equations are significantly simplified once we properly redefine the radial coordinate. (The equations transform non-trivially under the coordinate redefinition since one has to apply the “zero-energy” constraint, which removes the “gauge freedom” of the coordinate transformation). We also demonstrate how part of the 1st order equations can be re-derived using the usual 2nd order IIB equations of motion.

Our solution preserves the global symmetry and therefore describes a deformation corresponding to the inclusion of mass terms of the

two gaugino bilinears in the dual gauge theory.

We construct a Penrose limit (see [17], [18], [19], [20], [21] and [22]) of our non-supersymmetric KS background and obtain a pp-wave metric and a complex 3-form which are very similar to the PL limit [16] of the supersymmetric solution.

We also quantize the light-cone string Hamiltonian and determine the masses of the bosonic and fermionic modes. These masses, though different from the supersymmetric case, still obey the relation that the sum of the mass squared is the same for bosonic and fermionic modes. Again the string describes kinematics and excitations of heavy hadrons (called "annulons" [16]) with masses proportional to a large global symmetry charge $M_{\text{annulon}} = m_0 J$. The only difference between them and those of [16] is a modification of m_0 . A surprising feature of the string spectrum is that, like in the Penrose limit of the KS background, here as well, there are two fermionic zero modes. In the dual field theory this implies that even though the full theory is non-supersymmetric, the sector of states with large J charge admits supersymmetry. It is conceivable that in this limit of states of large mass the impact of the small gaugino mass deformations is washed away.

The authors of [23] used the solution of [13] to take the PL. The IR expansion of the fields given in [13] differs, however, from our solution (see later) and therefore the pp-wave background of [23] is also slightly different from the metric we have derived.

2 The Klebanov-Strassler model and beyond

Before reviewing the main features of the KS solution it will be worth to write down the type IIB equation of motion for a case of a constant dilaton ($\epsilon^\Phi = g_s$), a vanishing axion ($C_0 = 0$) and with the 10d metric and the 3-form flux having the structure of the D3-brane solution, namely:

$$ds^2 = h^{-1/2} dx_\mu^2 + h^{1/2} s_{M_6}^2 \quad (1)$$

and

$$\hat{F}_5 = \frac{1}{g_s} (1 + \star_{10}) dh^{-1} \wedge dx_0 \wedge \dots \wedge dx_3, \quad (2)$$

where M_6 is a 6d Ricci flat transversal space and the harmonic function h depends only on the coordinates on M_6 . We will denote the Hodge dual on M_6 by \star_6 . In order to find the connection between the 3-forms and the warp function h we have to use the 5-form equation. We end up with:

$$\begin{aligned} \hat{F}_5 &= B_2 \wedge F_3 + \star_{10} (B_2 \wedge F_3) \\ \text{or } dh &= -g_s \star_6 (B_2 \wedge F_3), \end{aligned} \quad (3)$$

where the 2nd equation is the integrated version of the first. Next we consider the 3-forms equations. Applying (3) and the relation between F_5 and \hat{F}_5 we get:

$$d \left[h^{-1} \left(\star_6 F_3 + \frac{1}{g_s} H_3 \right) \right] = 0 \quad (4)$$

and similarly for H_3 . In deriving this result we have used the fact that all the forms have their legs along the 6d space. Finally, calculating the Ricci scalar of the metric (1) we re-write the metric equation of motion:

$$d \star_6 dh = \frac{1}{2} \left[H_3 \wedge \star_6 H_3 + g_s^2 F_3 \wedge \star_6 F_3 \right]. \quad (5)$$

The equations we have written (3,4,5) as well as the the dilaton and the axion equations are easily solved by requiring that:

$$\star_6 F_3 = -g_s^{-1} H_3 \quad \text{and} \quad \star_6 H_3 = g_s F_3. \quad (6)$$

In this case the complex form $G_3 \equiv F_3 + \frac{i}{g_s} H_3$ is imaginary self dual $\star_6 G_3 = iG_3$.

Note that the equation for h is a first order differential equation, even though the solution is not supersymmetric in general.

The most important example of the supersymmetric solution is the Klebanov-Strassler model [6], where the 6d manifold is the deformed conifold space. The M fractional D5-branes wrapping the shrinking S^2 are introduced through the RR 3-form and on using the duality relations (6) one may also find the NS 3-form:

$$\begin{aligned} H_3 &= g_s M d \left[f(\tau) g^1 \wedge g^2 + k(\tau) g^3 \wedge g^4 \right], \\ F_3 &= M \left[g^5 \wedge g^3 \wedge g^4 + \right. \\ &\quad \left. + d \left(F(\tau) g^1 \wedge g^3 + g^2 \wedge g^4 \right) \right] \end{aligned} \quad (7)$$

where τ is the radial coordinate and the functions $f(\tau), k(\tau)$ and $F(\tau)$ satisfy a set of three

first order differential equations [6]. This set has three dimensional space of solutions. Using the complex structure of the deformed conifold space [24] the complex form $G_3 = F_3 + \frac{i}{g_s} H_3$ can be identified for the Klebanov-Strassler solution as a regular $(2, 1)$ form. There are also two additional solutions corresponding to a $(0, 3)$ form which breaks the supersymmetry and diverges at $\tau \rightarrow \infty$ and a $(2, 1)$ form which is singular at $\tau = 0$.

The dual field theory realized on the world-volume of the N physical and M fractional D3-branes is a 4d $\mathcal{N} = 1$ supersymmetric $SU(N+M) \times SU(N)$ gauge theory with a $SU(2) \times SU(2)$ global symmetry inherited from the conifold isometries. The gauge theory is coupled to two bi-fundamental chiral multiplets A and B , which transform as a doublet of one of the $SU(2)$'s each and are inert under the second $SU(2)$. This theory is believed to exhibit a cascade of Seiberg dualities reducing in the deep IR to pure $SU(M)$. On the supergravity side M is fixed by the charge of the RR 3-form, while N is encoded in the UV behavior of the 5-form. The sum of the gauging couplings is constant and the logarithmic running of the difference is determined by the NS 2-form.

Similarly to pure $SU(M)$ the theory confines. This is evident by virtue of the fact that the warp factor approaches a constant value $h_0 \sim a_0$ at $\tau \rightarrow 0$ and therefore the tension of the confining strings does not diverge. This conclusion is valid only for a non-zero value of the deformation parameter ϵ , since $a_0 \sim \epsilon^{-8/3}$. Note also that for $\epsilon \neq 0$ the $U(1)_R$ conifold symmetry is broken down to Z_2 . This is the symmetry preserved by the gaugino bilinear $\text{Tr}\lambda\bar{\lambda}(x)$. In the supergravity dual this gauge theory operator is associated with the form $C_2 = C_2^{RR} + iC_2^{NS}$ [25]. Subtracting the asymptotic value of $G_3 = dC_2$ we find at $\tau \rightarrow \infty$:

$$\begin{aligned} \Delta G_3 &\approx \frac{M}{2} \tau e^{-\tau} \omega_3, \quad \Delta C_2 \approx -\frac{M}{2} \tau e^{-\tau} \omega_2, \\ \omega_3 &= d\omega_2, \quad \omega_2 = \left[(g^1 \wedge g^3 + g^2 \wedge g^4) + \right. \\ &\quad \left. + ig_s (g^1 \wedge g^2 - g^3 \wedge g^4) \right], \end{aligned} \quad (8)$$

where we write only the polarization along $T_{1,1}$ and we see that ΔC_2 transforms under $U(1)_R$ by the same phase as $\text{Tr}(\lambda\bar{\lambda})$. Moreover, ΔG_3 has an asymptotic behavior we would expect from a scalar operator of dimension 3 and a non-zero VEV, namely: $\Delta G_3 \approx$

$\frac{1}{2} M \frac{m^3}{r^3} \ln \frac{r^3}{m^3} \omega_3$, where the deformation parameter is related to the 4d mass scale through $m \sim \epsilon^{2/3}$.

Finally, we will recall the identification of supergravity fields with gauge theory operators. In order to find this correspondence one writes the most general $SU(2) \times SU(2)$ invariant background ansatz, which includes the supersymmetric KS solution:

$$\begin{aligned} ds^2 &= 2^{1/2} 3^{3/4} \left[e^{-5q+2Y} (dx_\mu)^2 + \right. \\ &\quad + \frac{\epsilon^{3q-8p}}{9} (d\tau^2 + g_5^2) + \frac{\epsilon^{3q+2p+y}}{6} (g_1^2 + g_2^2) + \\ &\quad \left. + \frac{\epsilon^{3q+2p-y}}{6} (g_3^2 + g_4^2) \right], \quad \Phi = \Phi(\tau), \end{aligned} \quad (9)$$

with the 3-forms are given by (7) and the 5-form by (2). This general ansatz includes both the conformal solution with a singular geometry ($y = \tilde{f} - \tilde{k} = 0$) and the non-conformal case with regular deformed conifold ($y, \tilde{f} - \tilde{k} \neq 0$). Here \tilde{f}, \tilde{k} and \tilde{F} are the rescaled KS functions: $\tilde{f} = -2Pg_s f$, $\tilde{k} = -2Pg_s k$, $\tilde{F} = 2PF$ and the constant P is related to the number of fractional branes: $P = \frac{1}{4} M l_s^2$. Note that for the given structure of the 3-form F_3 the integral $\int_{S_3} F_3$ does not depend on $\tilde{F}(\tau)$. Moreover, the NS-NS 3-form has the same structure as in the KS solution as dictated by the equation for a vanishing axion: $H_3 \wedge F_3 = 0$.

Integration of the type IIB Lagrangian over the angular and the world-volume coordinates yields a 1d effective action:

$$S \sim \int d\tau \left(-\frac{1}{2} G_{ij} \dot{\phi}^i \dot{\phi}^j - V(\phi) \right), \quad (10)$$

and we refer the reader to [26],[27],[24],[28] for an explicit form of the metric and the potential $V(\phi)$. There is also a “zero-energy” constraint $\frac{1}{2} G_{ij} \dot{\phi}^i \dot{\phi}^j - V(\phi) = 0$. This Lagrangian admits a superpotential

$$\begin{aligned} V &= \frac{1}{8} G^{ij} \partial_i W \partial_j W \quad \text{for} \\ W &= -3e^{4Y+4p-4q} \cosh y - \\ &\quad - 2e^{4Y-6p-4q} - 3\sqrt{3}e^{4Y-10q}\tilde{L} \end{aligned} \quad (11)$$

and for supersymmetric solutions the second order equations of motion can be reduced to the first order ones:

$$\dot{\phi}^i = \frac{1}{2} G^{ij} \partial_j W. \quad (12)$$

The potential appearing in the action has an $\mathcal{N} = 1$ critical point corresponding to the

conformal background $AdS_5 \times T_{1,1}$ generated by physical D3-branes in absence of fractional branes ($P = 0$). Expanding the potential around the critical point and using the mass/dimension formula $\Delta = 2 + \sqrt{4 + m^2}$ one obtains the dimensions of the fields, which now can be identified with various gauge theory operators [29], [28]. Here we list two of them (both with $\Delta = 3$):

$$\begin{aligned}\xi_2 &\sim -F + \frac{k-L}{2} \rightarrow \text{Tr} \left(W_{(1)}^2 + W_{(2)}^2 \right), \\ y &\rightarrow \text{Tr} \left(W_{(1)}^2 - W_{(2)}^2 \right)\end{aligned}$$

There are also two massless fields. $s = f + k$ is associated with a marginal direction in the CFT and the corresponding operator is $\text{Tr} \left(F_{(1)}^2 - F_{(2)}^2 \right)$. Similarly, the dilaton Φ corresponds to $\text{Tr} \left(F_{(1)}^2 + F_{(2)}^2 \right)$.

In this paper we will focus on the non-supersymmetric deformation of the KS background by introducing mass terms of the gaugino bilinears associated with both ξ_2 and y . The former field is related to the SUGRA 3-forms and the latter is responsible for a deformation of the 6d metric. The expected UV behavior of the fields in the background deformed by the masses is $g(\tau) e^{-\tau/3}$, where $g(\tau)$ is a polynomial in τ .

3 Non-supersymmetric extension of KS

We start this section with a brief review of the method proposed by [14] (see also [30], [31], [32], [33], [34] and [35]) to study first order non-supersymmetric deformations of the KS background still making use of the superpotential. We expand the fields around a given supersymmetric solution derived from the superpotential $\phi^i = \phi_0^i + \delta \cdot \phi^i + O(\delta^2)$. Define new functions:

$$\begin{aligned}\xi_i &= G_{ij}(\phi_0) \left(\frac{d\bar{\phi}^j}{d\tau} - M_k^j(\phi_0) \bar{\phi}^k \right) \quad \text{where} \\ M_k^j &= \frac{1}{2} \frac{\partial}{\partial \phi^k} \left(G^{jl} \frac{\partial W}{d\phi^l} \right).\end{aligned}\quad (13)$$

Now one might represent the linearized equations of motion as a “double” set of first order equations (we refer the reader to [14] for the proof):

$$\frac{d\xi_i}{d\tau} + \xi_j M_k^j = 0, \quad \frac{d\bar{\phi}^i}{d\tau} - M_j^i \bar{\phi}^j = G^{ik} \xi_k \quad (14)$$

while the zero-energy condition can be rephrased as $\xi_k \partial_\tau \bar{\phi}^k = 0$.

An important remark is in order. One can use various definitions for the radial coordinate in the 1d effective action. This ambiguity is removed by applying the zero-energy constraint. The explicit form of the 1st order equations (14) is highly dependent on the radial coordinate choice. In our paper we will fix this “gauge freedom” by requiring that even in the deformed solution the G_{rr} and $G_{\theta\theta}$ entries of the metric will remain equal exactly as in the supersymmetric case. We will see that with this choice the set of the equations (14) possesses an analytic solution. On the contrary the radial coordinate (τ_*) of [14] is related to our coordinate (τ) via $d\tau_* = e^{4\bar{P}-4q} d\tau$. Note, however, that since both $\bar{p}(\tau)$ and $\bar{q}(\tau)$ are expected to vanish at $\tau \rightarrow 0$ and $\tau \rightarrow \infty$, the deep UV and IR expansions of the fields have to be the same in terms of τ and τ_* .

Let us first consider the equations of motion for ξ_i 's¹. Throughout this paper we will be interested in a solution satisfying: $\xi_Y = \xi_p = \xi_q = 0$. Under this assumption we get:

$$\begin{aligned}\dot{\xi}_y &= \xi_y \cosh y_0 + 2e^{2y_0} (2P - \bar{F}_0) \xi_{j+k} - \\ &- 2e^{-2y_0} \bar{F}_0 \xi_{\bar{k}}, \quad \dot{\xi}_{j+k} = 0, \\ \dot{\xi}_{\bar{P}} &= -\cosh(2y_0) \xi_{\bar{j}-\bar{k}} - \sinh(2y_0) \xi_{\bar{j}+\bar{k}}, \\ \dot{\xi}_{\bar{\Phi}} &= \left(e^{2y_0} (2P - \bar{F}_0) \xi_j + e^{-2y_0} \bar{F}_0 \xi_{\bar{k}} \right) - \\ &- \frac{\bar{k}_0 - \bar{J}_0}{2} \xi_{\bar{P}}, \quad \dot{\xi}_{\bar{j}-\bar{k}} = -\xi_{\bar{P}},\end{aligned}\quad (15)$$

where $\xi_{j\pm\bar{k}} = \xi_j \pm \xi_{\bar{k}}$. We have $\xi_{j+k} = X$ for constant X and from the equations for $\xi_{\bar{j}-\bar{k}}$ and $\xi_{\bar{P}}$ we obtain a 2nd order differential order equation for $\xi_{\bar{j}-\bar{k}}$. This equation has a two dimensional space of solutions. However, solving for ξ_y , plugging the result into the zero-energy constraint $\xi_i \phi_0^i = 0$ and requiring also regularity at $\tau \rightarrow 0$ we pick up a unique simple solution $\xi_{\bar{j}-\bar{k}}(\tau) = X \cosh \tau$ and therefore:

$$\begin{aligned}\xi_{\bar{P}} &= -X \sinh \tau, \quad \dot{\xi}_{\bar{\Phi}} = 0, \\ \xi_y &= 2PX(\tau \cosh \tau - \sinh \tau),\end{aligned}\quad (16)$$

Having determined the explicit form of ξ_i 's we can consider the equations for the fields $\bar{\phi}^i$'s. For \bar{y} we get:

$$\dot{\bar{y}} + \cosh(y_0) \bar{y} = \frac{2}{3} e^{4y_0 - 4p_0 - 4Y_0} \xi_y. \quad (17)$$

¹We will set $g_* = 1$ throughout this section

Using the result for ξ_y and substituting the expressions for $g_0(\tau)$, $p_0(\tau)$ and $Y_0(\tau)$ we may solve for $\bar{y}(\tau)$ fixing an integration constant by requiring regularity at $\tau \rightarrow 0$ (see [15]). In this review we will need an asymptotic behavior of $\bar{y}(\tau)$ at $\tau \rightarrow \infty$:

$$\bar{y} \approx \mu \left(\tau - \frac{5}{2} \right) e^{-\tau/3} + V e^{-\tau} + \dots, \quad (18)$$

where μ is a deformation parameter proportional to X and V is a numerical constant proportional to μ . Note that μ is a dimensionless parameter. Using the result for $\bar{y}(\tau)$ and the fact that $\xi_p = 0$ we may find the solution for $p(\tau)$. We refer the reader to the original paper [15] for a full analytic solution for $p(\tau)$ and other fields (in particular it appears that $\Phi = 0$). Here we will only review the derivation of the results for the 3-form fields. Using the expressions for $\xi_{f \pm k}$ and $\xi_{\bar{f}}$, passing from \bar{f} , k and \bar{F} to f , k and F we obtain and recalling that $\Phi = 0$:

$$\begin{aligned} \dot{\bar{f}} + e^{2y_0} \bar{F} - 2\dot{f}_0 \bar{y} &= -\frac{2X}{2P} h_0 (\cosh \tau - 1) \\ \dot{k} - e^{-2y_0} F + 2\dot{k}_0 \bar{y} &= \frac{2X}{2P} h_0 (\cosh \tau + 1) \\ \dot{\bar{F}} - \frac{1}{2}(\bar{k} - \bar{f}) &= -\frac{2X}{2P} h_0 \sinh \tau. \end{aligned} \quad (19)$$

Before discussing the explicit solution of this system it is worth to re-derive these equations using the 2nd order type IIB equations of motion. In the most general ansatz preserving the global symmetry the 5-form \bar{F}_5 is given by

$$\bar{F}_5 = \frac{1}{g_s} (1 + \star_{10}) d\varphi \wedge dx_0 \wedge \dots \wedge dx_3, \quad (20)$$

where $\varphi = \varphi(\tau)$. Supersymmetry requires $\varphi = h^{-1}$ (see [36] and [37]), but it does not necessarily hold in a non-supersymmetric case. In what follows we will demonstrate how assuming that $\Phi = 0$ and $\varphi = h^{-1}$ one may reproduce (19) from the usual 2nd order 3-forms equations of motion. Indeed, under these assumptions the type IIB 3-forms equations reduce to (4). Let us expand (4) around the supersymmetric KS solution. Note that the expansion includes also \star_6 due to the deformation of the 6d space. We will denote the modified Hodge star operation by $\star_6 = \star_6^{(0)} + \star_6$, where $\star_6^{(0)}$ corresponds to the supersymmetric configuration. After some algebra the linearized RR

3-form equation reduces to:

$$\begin{aligned} dZ_3 &= 0, \quad \text{where} \\ Z_3 &= \frac{1}{g_s} \bar{H}_3 + \star_6^{(0)} \bar{F}_3 + \star_6 F_3^{(0)}. \end{aligned} \quad (21)$$

where $F_3^{(0)}$ is the RR 3-form in the KS background. Similarly, from the NSNS 3-form equation we have:

$$d \star_6 Z_3 = 0. \quad (22)$$

Comparing this with (19) we see that the r.h.s. of (19) is exactly the components of the closed (and co-closed) form Z_3 . Notice that having $Z_3 \neq 0$ necessary means that the complex form $G_3 = F_3 + \frac{i}{g_s} H_3$ is not imaginary self dual and therefore the supersymmetry is broken [36], [37]. The most general solution of (21) and (22) has 3 integration constants and it appears in [15]. In particular, it turns out that the 3-form on the r.h.s. of (19) corresponds to the divergent $(0, 3)$ -form we have mentioned in the discussion following (7). Remarkably, this is the only solution for Z_3 , which is consistent with $\Phi = 0$. To find the solution for $F(\tau)$, $\bar{f}(\tau)$ and $k(\tau)$ note that the homogeneous part of (19) reduces to an equation of the form $dZ_3 = d \star_6 Z_3 = 0$ and as we have already mentioned the related 3-parameter solution appears in [15]. Using this solution we may easily find the solution of the three inhomogeneous equations (see [15]). In the UV we have:

$$\begin{aligned} F(\tau) &\approx \mu \left(\frac{3}{4}\tau - 3 \right) e^{-\tau/3} + \left(\frac{3}{2}V + V' \right) e^{-\tau} \\ \bar{f}(\tau) &\approx -\frac{27}{16}\mu e^{-\tau/3} + \left(\frac{V}{2} + V' \right) e^{-\tau} + \dots \\ \bar{k}(\tau) &\approx \frac{27}{16}\mu e^{-\tau/3} - \left(\frac{V}{2} + V' \right) e^{-\tau} + \dots \end{aligned}$$

where V' is a constant proportional to μ .

Let us summarize. The deformation is controlled by the single parameter μ and all the fields have a regular behavior in the UV and in the IR. There are two non-normalizable modes. The first one is $y(\tau)$ and it is related to the deformation of the 6d metric. The second one is ξ_2 and it is associated with the 3-forms. In the UV we have:

$$\xi_2 \sim -F + \frac{k - f}{2} \approx -\frac{3}{4}\mu \left(\tau - \frac{25}{4} \right) e^{-\tau/3}. \quad (23)$$

Both $y(\tau)$ and ξ_2 have dimension $\Delta = 3$ which matches perfectly with the asymptotic behavior of the fields. In the dual gauge theory

these operators are dual to the gaugino bilinears. The deformation also involves other fields like $s = f + k$ with a normalizable behavior at $\tau \rightarrow \infty$. For example, $s \approx e^{-4\tau/3}$ as expected for an operator with $\Delta = 4$.

4 Vacuum energy

To calculate the vacuum energy of the deformed non-supersymmetric theory we will use the standard AdS/CFT technique [4]. The supergravity dual of the gauge theory Hamiltonian is a G_{00} component of the 10d metric. The vacuum energy, therefore, can be found by variation of the type IIB SUGRA action with respect to G_{00} . This variation vanishes on-shell, except a boundary term. Looking at the supergravity action, it is clear that the only such a boundary term will appear from the curvature part of the action. Since the vacuum energy does not depend on the world-volume coordinates we might consider the metric variation in the form $G_{00} \rightarrow qG_{00}$. Here we only quote the final result for the vacuum energy (see [15] for the derivation):

$$E \sim \lim_{\tau \rightarrow \infty} \left(e^{n(\tau)} \partial_\tau \ln h(\tau) \right), \quad (24)$$

where $\bar{n} = -4q + 4p + 4\bar{Y}$. The divergent result we have found is expected to be canceled out when we compare the vacuum energies of our solution and of the KS background, which we take as a reference. Using that $h \rightarrow h_0 + \bar{h}$ and $n \rightarrow n_0 + \bar{n}$ we get:

$$\Delta E \sim \left[e^{n_0} \left(\partial_\tau \left(\frac{\bar{h}}{h_0} \right) + \bar{n} \partial_\tau (\ln h_0) \right) \right]_{\tau \rightarrow \infty}, \quad (25)$$

so that $\Delta E \sim \mu$. Here we used the asymptotic solutions for the fields at $\tau \rightarrow \infty$ from the previous section. In (25) the term $e^{n_0(\tau)}$ diverges at $\tau \rightarrow \infty$ as $e^{4\tau/3}$. This is suppressed by the $e^{-4\tau/3}$ term in the large τ expansion of the fields appearing in the parenthesis which multiply the $e^{n_0(\tau)}$ term. Furthermore, the term linear at τ cancels and we end up with a constant proportional to μ .

5 Dual gauge theory

As was announced in the introduction the deformation of the supergravity background corresponds to an insertion of

the soft supersymmetry breaking gaugino mass terms. The most general gaugino bilinear term has the form of $\mu_+ \mathcal{O}_+ + \mu_- \mathcal{O}_- + c.c$ where $\mathcal{O}_\pm \sim Tr[W_{(1)}^2 \pm W_{(2)}^2]$ and $W_{(i)}$, $i = 1, 2$ relate to the $SU(N + M)$ and $SU(N)$ gauge groups respectively. Namely, the general deformation is characterized by two complex masses. Our non-supersymmetric deformation of the KS solution derived above is a special case that depends on only one real parameter μ . Since the supergravity identification of the operators \mathcal{O}_\pm is known up to some constants of proportionality we can not determine the precise form of the soft symmetry breaking term.

In the non-deformed supersymmetric theory the $U(1)_R$ symmetry is broken [38], [39] first by instantons to Z_{2M} and then further spontaneously broken down to Z_2 by a VEV of the gaugino bilinear. Let us discuss first the latter breaking. We have already seen that on the SUGRA side this fact is manifest from the UV behavior of the complex 3-form $G_3 = F_3 + \frac{i}{g_s} H_3$. The sub-leading term in the expansion of G_3 preserves only the Z_2 part of the $U(1)_R$ symmetry and it vanishes at infinity like $e^{-\tau}$ matching the expectation from the scalar operator $Tr(\lambda \lambda)$ of dimension 3 with a non-zero VEV [25]. Plugging the non-supersymmetric solution into G_3 we find that the leading term breaking the $U(1)_R$ symmetry behaves like $\Delta G_3 = g(\tau) e^{-\tau/3}$, where $g(\tau)$ is some polynomial in τ . This is exactly what one would predict for an operator with $\Delta = 3$ and a non-trivial mass. The second combination of the gaugino bilinears is encoded in the 6d part of the metric. For the 6d metric in (9) to preserve the $U(1)_R$ one has to set $y = 0$. In the supersymmetric deformed conifold metric $y(\tau) = -2e^{-\tau} + \dots$ similarly to the behavior of the 3-form. In the non-supersymmetric solution $y(\tau)$ goes like $e^{-\tau/3}$ elucidating again that the gaugino combination gets a mass term. Notice also that the non-zero VEVs of the gaugino bilinears are modified by the SUSY breaking deformation. This is evident, for example, from the $V e^{-\tau}$ term in the UV expansion of $\bar{y}(\tau)$ in (18). Clearly, for $V \neq 0$ we have a correction to the VEV in the supersymmetric theory which was encoded in the expansion of $y_0(\tau)$. Similar $e^{-\tau}$ term appears also in the expansion of $\xi_2(\tau)$ and therefore the VEV of the second combination of the gauginos gets modified too.

The spontaneous breaking of the Z_{2M} discrete group down to the Z_2 subgroup by gaugino condensation results in an M -fold degenerate vacua. This degeneracy is generally lifted by soft breaking mass terms in the action. For small enough masses one can treat the supersymmetry breaking as a perturbation yielding (for a single gauge group) the well-known result [40] that the difference in energy between a non-supersymmetric solution and its supersymmetric reference is given by $\Delta E \sim \text{Re}(\mu C)$, where μ and C are the mass and the gaugino condensate respectively. For the gauge theory dual of the deformed KS solution the vacuum energy will in general be proportional to $\text{Re}(a_+ \mu_+ C_+ + a_- \mu_- C_-)$ where C_\pm are the expectation values of \mathcal{O}_\pm and a_\pm are some proportionality constants. In the special deformation we are discussing in this paper this reduces to $\mu \text{Re}(a_+ C_+ + a_- C_-)$. In the previous section we have derived a result using the SUGRA dual of the gauge theory which has this structure. For the softly broken MN background similar calculations were performed by [11]. In their case the explicit linear dependence on the condensate was demonstrated.

One of the properties of the supersymmetric gauge theory is the space-time independence of the correlation function of two gaugino bilinears. This appears from the supergravity dual description as follows [25]. Consider a perturbation of the complex 2-form:

$$C_2 \rightarrow C_2 + y\omega_2, \quad G_3 \rightarrow G_3 + y\omega_3 + dy \wedge \omega_2, \quad (26)$$

where $\omega_{2,3}$ are given by (8) and $y(x, \tau)$ has non-vanishing boundary values. Plugging this forms into the relevant part of the type IIB action and integration over τ will not lead to a kinematic term $dy(x_1)dy(x_2)$ and therefore the corresponding correlation function will be space-time independent. This derivation is only schematic since there is a mixing between the 3-form modes and the modes coming from metric as we have seen in Section 3. Notice, however that this simplified calculation will yield the kinetic term for the deformed non-supersymmetric background, since the complex 3-form is not imaginary self dual in this case. Thus in the non-supersymmetric theory the correlation function will be time-space dependent as one would expect.

6 The plane wave limit

In this section we will construct a Penrose limit of the non-supersymmetric background. Following [16] we will expand the metric around a null geodesic that goes along an equator of the S^3 at $\tau = 0$. The parameter ε appearing in the 6d metric of the deformed conifold and the gauge group parameter M are both taken to infinity in the PL limit, while keeping finite the mass of the glue-ball: $M_{gb} \sim \frac{\varepsilon^{2/3}}{g_s M \alpha'}$. The final result [15] is:

$$\begin{aligned} ds^2 = & -4dx_- dx_+ + dx_i^2 + dz^2 + du d\bar{u} + \\ & + dv d\bar{v} - m_0^2 [v\bar{v} + \left(\left(\frac{4a_1}{a_0} - \frac{4}{5} \right) - 8\frac{3^{2/3}}{135}\mu \right) z^2 \\ & + \left(\left(\frac{4a_1}{a_0} - \frac{3}{5} \right) + 4\frac{3^{2/3}}{135}\mu \right) u\bar{u}] dx_+^2, \end{aligned} \quad (27)$$

where

$$m_0^2 = \frac{3^{1/3} \varepsilon^{4/3}}{2(g_s M \alpha')^2 a_0} (1 + 2C_Y). \quad (28)$$

Recall that C_Y is a numerical constant proportional to μ . As expected for $\mu = 0$ we recover the result of the supersymmetric case [16]. We see that all the world-sheet masses (m_v, m_z and m_u) depend on the supersymmetry breaking parameter. Under the Penrose limit the 3-forms read:

$$\begin{aligned} (F_3)_{+v\bar{v}} &= \left(\frac{1}{3} + 4\gamma \right)^{-1} (F_3)_{+u\bar{u}} = \frac{3im_0}{\sqrt{2}g_s} \sqrt{\frac{a_1}{a_0}} \\ (H_3)_{+v\bar{v}} &= (H_3)_{+u\bar{u}} = \frac{im_0}{\sqrt{2}} \sqrt{\frac{a_1}{a_0}} (1 - 6\gamma). \end{aligned}$$

7 The plane wave string theory and the Annulons

The string theory associated with the plane wave background described in the previous section is quite similar to that associated with the PL limit of the KS background. The bosonic sector includes three massless fields that correspond to the spatial directions on the world-volume of the D3 branes. Their masslessness is attributed to the translational invariance of the original metric and the fact that the null geodesic is at constant τ . The rest five coordinates are massive. The only difference between the bosonic spectrum of the deformed model and that of [16] is the shift of the masses of the $z, v, \bar{v}, u, \bar{u}$ fields. The sum of the mass², however, of the individual fields $\sum m^2 = 12m_0^2 \frac{a_1}{a_0}$

still has the same form as the sum in the supersymmetric case apart from the modification of m_0 (28). The modification of m_0 is also responsible for the deviation of the deformed string tension with from the supersymmetric one since the string tension $T_s \sim g_s M m_0^2$. The fermionic spectrum takes the form ($k = 1, \dots, 4$ and $l = 1, 2$):

$$\begin{aligned}\omega_n^k &\approx \sqrt{n^2 + \hat{m}_B^2 (1 + 18\gamma)}, \\ \omega_n^l &= \sqrt{n^2 + \frac{1}{4} \hat{m}_B^2 \pm \frac{1}{2} \hat{m}_B}, \quad \text{where} \\ \hat{m}_B &= \sqrt{2} p^+ \alpha' m_0 \left(\frac{a_1}{a_0} \right)^{1/2} (1 - 6\gamma).\end{aligned}$$

Comparing the bosonic and fermionic masses we observe that like in the undeformed KS model there is no linearly realized world-sheet supersymmetry and the hence there is a non-vanishing zero point energy. However, up to deviations linear in μ the sum of the square of the frequencies of the bosonic and fermionic modes match. Since this property follows in fact from the relation between R_{++} and $(G_3)_{+ij} (G_3)_+^{ij}$ it should be a universal property of any plane wave background.

Surprisingly we find that the fermionic spectrum admits two fermionic zero modes $\omega_0^{l=1,2}$ exactly like in the supersymmetric case. The fermionic zero modes in the spectrum of the latter case were predicted [16] upon observing that the Hamiltonian still commutes with the four supercharges that correspond to the four dimensional $N = 1$ supersymmetric gauge theory. This implies that four supersymmetries out of the sixteen supersymmetries of plane wave solution commute with the Hamiltonian giving rise to the four zero-frequency modes and a four dimensional Hilbert sub-space of (two bosonic and two fermionic) degenerate states. One might have expected that in the PL of the deformed theory the fermionic zero modes will be lifted by an amount proportional to the supersymmetry breaking parameter. Our results, however, contradict this expectation. In the dual field theory this implies that even though the full theory is non-supersymmetric, the sector of states with large J charge admits supersymmetry. As will be discussed below these states are characterized by their large mass which is proportional to J . Presumably, in this limit of states of large mass

the impact of the small gaugino mass deformations is washed away. For instance one can estimate that the ratio of the boson fermion mass difference to the mass of the annulon scales like $\frac{\mu}{J}$ and since μ has to be small and $J \rightarrow \infty$ this ratio is negligible.

Note that the fermionic zero modes are in accordance with the criteria presented in [23]. However, the metric and the 3-form given in [23] do not coincide with our results, because of the factor of C_Y in the expression for m_0^2 .

Since apart from the modifications of the fermionic and bosonic frequencies the string Hamiltonian we find has the same structure as the one found for the KS case, the analysis of the corresponding gauge theory states also follows that of [16]. We will not repeat here this analysis, but rather just summarize its outcome:

- The ground state of the string corresponds to the *Annulon*. This hadron which carries a large J charge is also very massive since its mass is given by

$$M_{\text{annulon}} = m_0 J \quad (29)$$

Obviously, the only difference between the annulon of the deformed theory in comparison with the supersymmetric one is the modification of m_0 .

- The annulon can be described as a ring composed of J constituents each having a mass (in the mean field of all the others) of m_0 .
- The annulon which is a space-time scalar has a fermionic superpartner of the same mass. The same holds for the rest of the bosonic states.
- The string Hamiltonian has a term $\frac{P_J^2}{2m_0 J}$ that describes a non-relativistic motion of the annulons.
- The annulons admit stringy ripples. The spacing between these excitations are proportional to $\frac{T_s}{M_{\text{annulon}}}$.
- The string Hamiltonian describes also excitations that correspond to the addition of small number of different constituents on top of the J basic ones.

Acknowledgments

The author thanks G. 't Hooft for the opportunity to speak in the new talent sessions at the 41st International School on Subnuclear Physics in Erice, Italy.

References

- [1] J. M. Maldacena, *The large n limit of superconformal field theories and supergravity*, *Adv. Theor. Math. Phys.* **2** (1998) 231–252, [[hep-th/9711200](#)].
- [2] S. S. Gubser, I. R. Klebanov, and A. M. Polyakov, *Gauge theory correlators from non-critical string theory*, *Phys. Lett. B* **428** (1998) 105–114, [[hep-th/9802109](#)].
- [3] E. Witten, *Anti-de sitter space and holography*, *Adv. Theor. Math. Phys.* **2** (1998) 253–291, [[hep-th/9802150](#)].
- [4] O. Aharony, S. S. Gubser, J. M. Maldacena, H. Ooguri, and Y. Oz, *Large n field theories, string theory and gravity*, *Phys. Rept.* **323** (2000) 183–386, [[hep-th/9905111](#)].
- [5] J. M. Maldacena and C. Nunez, *Towards the large n limit of pure $n = 1$ super yang mills*, *Phys. Rev. Lett.* **86** (2001) 588–591, [[hep-th/0008001](#)].
- [6] I. R. Klebanov and M. J. Strassler, *Supergravity and a confining gauge theory: Duality cascades and chiral-resolution of naked singularities*, *JHEP* **08** (2000) 052, [[hep-th/0007191](#)].
- [7] M. Bertolini, *Four lectures on the gauge-gravity correspondence*, [hep-th/0303160](#).
- [8] F. Bigazzi, A. L. Cotrone, M. Petrini, and A. Zaffaroni, *Supergravity duals of supersymmetric four dimensional gauge theories*, *Riv. Nuovo Cim.* **25N12** (2002) 1–70, [[hep-th/0303191](#)].
- [9] A. H. Chamseddine and M. S. Volkov, *Non-abelian bps monopoles in $n = 4$ gauged supergravity*, *Phys. Rev. Lett.* **79** (1997) 3343–3346, [[hep-th/9707176](#)].
- [10] O. Aharony, E. Schreiber, and J. Sonnenschein, *Stable non-supersymmetric supergravity solutions from deformations of the maldacena-nunez background*, *JHEP* **04** (2002) 011, [[hep-th/0201224](#)].
- [11] N. Evans, M. Petrini, and A. Zaffaroni, *The gravity dual of softly broken $n = 1$ super yang-mills*, *JHEP* **06** (2002) 004, [[hep-th/0203203](#)].
- [12] S. S. Gubser, A. A. Tseytlin, and M. S. Volkov, *Non-abelian 4-d black holes, wrapped 5-branes, and their dual descriptions*, *JHEP* **09** (2001) 017, [[hep-th/0108205](#)].
- [13] R. Apreda, *Non supersymmetric regular solutions from wrapped and fractional branes*, [hep-th/0301118](#).
- [14] V. Borokhov and S. S. Gubser, *Non-supersymmetric deformations of the dual of a confining gauge theory*, *JHEP* **05** (2003) 034, [[hep-th/0206098](#)].
- [15] S. Kuperstein and J. Sonnenschein, *Analytic non-supersymmetric background dual of a confining gauge theory and the corresponding plane wave theory of hadrons*, [hep-th/0309011](#).
- [16] E. G. Gimon, L. A. Pando Zayas, J. Sonnenschein, and M. J. Strassler, *A soluble string theory of hadrons*, *JHEP* **05** (2003) 039, [[hep-th/0212061](#)].
- [17] R. Gueven, *Plane wave limits and t -duality*, *Phys. Lett. B* **482** (2000) 255–263, [[hep-th/0005061](#)].
- [18] M. Blau, J. Figueroa-O'Farrill, C. Hull, and G. Papadopoulos, *A new maximally supersymmetric background of iib superstring theory*, *JHEP* **01** (2002) 047, [[hep-th/0110242](#)].
- [19] R. R. Metsaev, *Type iib green-schwarz superstring in plane wave ramond-ramond background*, *Nucl. Phys.* **B625** (2002) 70–96, [[hep-th/0112044](#)].
- [20] D. Berenstein, J. M. Maldacena, and H. Nastase, *Strings in flat space and pp*

- waves from $n = 4$ super yang mills, *JHEP* **04** (2002) 013, [[hep-th/0202021](#)].
- [21] R. R. Metsaev and A. A. Tseytlin, *Exactly solvable model of superstring in plane wave ramond- ramond background*, *Phys. Rev.* **D65** (2002) 126004, [[hep-th/0202109](#)].
- [22] M. Blau, J. Figueroa-O'Farrill, and G. Papadopoulos, *Penrose limits, supergravity and brane dynamics*, *Class. Quant. Grav.* **19** (2002) 4753, [[hep-th/0202111](#)].
- [23] R. Apreda, F. Bigazzi, and A. L. Cotrone, *Strings on pp-waves and hadrons in (softly broken) $n = 1$ gauge theories*, [hep-th/0307055](#).
- [24] G. Papadopoulos and A. A. Tseytlin, *Complex geometry of conifolds and 5-brane wrapped on 2-sphere*, *Class. Quant. Grav.* **18** (2001) 1333–1354, [[hep-th/0012034](#)].
- [25] A. Loewy and J. Sonnenschein, *On the holographic duals of $n = 1$ gauge dynamics*, *JHEP* **08** (2001) 007, [[hep-th/0103163](#)].
- [26] I. R. Klebanov and A. A. Tseytlin, *Gravity duals of supersymmetric $su(n) \times su(n+m)$ gauge theories*, *Nucl. Phys.* **B578** (2000) 123–138, [[hep-th/0002159](#)].
- [27] L. A. Pando Zayas and A. A. Tseytlin, *3-branes on resolved conifold*, *JHEP* **11** (2000) 028, [[hep-th/0010088](#)].
- [28] F. Bigazzi, L. Girardello, and A. Zaffaroni, *A note on regular type 0 solutions and confining gauge theories*, *Nucl. Phys.* **B598** (2001) 530–542, [[hep-th/0011041](#)].
- [29] A. Ceresole, G. Dall'Agata, R. D'Auria, and S. Ferrara, *Spectrum of type IIB supergravity on $ads(5) \times t(11)$: Predictions on $n = 1$ scft's*, *Phys. Rev.* **D61** (2000) 066001, [[hep-th/9905226](#)].
- [30] S. Ferrara, R. Kallosh, and A. Strominger, *$N=2$ extremal black holes*, *Phys. Rev.* **D52** (1995) 5412–5416, [[hep-th/9508072](#)].
- [31] D. Z. Freedman, S. S. Gubser, K. Pilch, and N. P. Warner, *Renormalization group flows from holography supersymmetry and a c-theorem*, *Adv. Theor. Math. Phys.* **3** (1999) 363–417, [[hep-th/9904017](#)].
- [32] K. Skenderis and P. K. Townsend, *Gravitational stability and renormalization-group flow*, *Phys. Lett.* **B468** (1999) 46–51, [[hep-th/9909070](#)].
- [33] O. DeWolfe, D. Z. Freedman, S. S. Gubser, and A. Karch, *Modeling the fifth dimension with scalars and gravity*, *Phys. Rev.* **D62** (2000) 046008, [[hep-th/9909134](#)].
- [34] J. de Boer, E. Verlinde, and H. Verlinde, *On the holographic renormalization group*, *JHEP* **08** (2000) 003, [[hep-th/9912012](#)].
- [35] M. Wijnholt and S. Zhukov, *On the uniqueness of black hole attractors*, [hep-th/9912002](#).
- [36] M. Graña and J. Polchinski, *Supersymmetric three-form flux perturbations on $ads(5)$* , *Phys. Rev.* **D63** (2001) 026001, [[hep-th/0009211](#)].
- [37] S. S. Gubser, *Supersymmetry and f-theory realization of the deformed conifold with three-form flux*, [hep-th/0010010](#).
- [38] I. R. Klebanov, P. Ouyang, and E. Witten, *A gravity dual of the chiral anomaly*, *Phys. Rev.* **D65** (2002) 105007, [[hep-th/0202056](#)].
- [39] C. P. Herzog, I. R. Klebanov, and P. Ouyang, *D-branes on the conifold and $n = 1$ gauge / gravity dualities*, [hep-th/0205100](#).
- [40] A. Masiero and G. Veneziano, *Split light composite supermultiplets*, *Nucl. Phys.* **B249** (1985) 593.

Holographic Renormalization Made Simple: an example

Ioannis Papadimitriou^{*}

*Institute for Theoretical Physics, University of Amsterdam,
Valckenierstraat 65, 1018XE Amsterdam, The Netherlands*

March 17, 2004

Abstract

We present an alternative method to obtain the exact solution of the bulk field equations for a free scalar field in fixed Euclidean AdS_{d+1} with prescribed but arbitrary Dirichlet boundary conditions. We demonstrate that the Dirichlet boundary conditions allow for a reduction of the second order field equations to a first order problem. The approach is meant to highlight the key points underlying the general method we present in [1], which is a simpler version of what is known as ‘holographic renormalization’ in the context of the AdS/CFT correspondence. The example we discuss here is special in that an exact solution of the bulk field equations can be obtained and hence the full quantum effective action of the boundary theory can be calculated exactly.

1 Introduction

The AdS/CFT correspondence is so far the best understood example of a gravity/gauge theory duality. The duality asserts that string theory on an asymptotically anti-de Sitter spacetime (AAdS) times a compact manifold is equivalent to a quantum field theory (QFT) on the conformal boundary of AAdS. As string theory on AdS spacetimes is not well-understood, one often considers the low energy limit of string theory which is described in terms of some supergravity theory in the bulk and corresponds to the large ‘t Hooft limit, $\lambda = g_{YM}^2 N \gg 1$, of the boundary gauge theory. According to the duality then, for every bulk field Φ on the supergravity side there is a gauge invariant operator O_Φ in the boundary QFT. More precisely, the supergravity partition function with prescribed but arbitrary Dirichlet boundary conditions is identified with the generating functional of connected

^{*}ipapadim@science.uva.nl

correlators of the dual operator. The boundary values of the bulk fields are then interpreted as sources for the dual operators.

$$Z_{SUGRA}[\phi_{(0)}] = \int_{\Phi \sim \phi_{(0)}} [d\Phi] \exp(-S[\Phi]) = \langle \exp \left(- \int_{\partial AAdS} \phi_{(0)} O_\Phi \right) \rangle_{QFT}, \quad (1)$$

where $\partial AAdS$ denotes the boundary of the asymptotically AdS space. If one ignores quantum corrections on the supergravity side, which corresponds to taking the large N limit in the gauge theory, we have the saddle point approximation

$$S_{\text{on-shell}}[\phi_{(0)}] = -W_{QFT}[\phi_{(0)}]. \quad (2)$$

However, as is well known, both sides of the last equation are not well defined as they contain divergences. The QFT generating functional suffers from the usual UV divergences while the on-shell bulk action diverges due to the infinite volume of AAdS. We know that the UV divergences on the QFT side are independent of the IR physics and can be consistently removed by some renormalization scheme. Hence, on the basis of the gravity/gauge theory correspondence, one expects that the near boundary divergences of the bulk action should be completely determined from the asymptotic analysis and should not depend on the dynamics of the theory in the deep interior of the AAdS space. Moreover, there should be a systematic procedure that can be applied to consistently remove the divergences of the on-shell action by adding bulk-covariant counter terms.

A systematic method for consistently removing these divergences was developed in [2, 3, 4, 5]. The method relied on [6], in which the bulk metric was reconstructed in the form of an asymptotic solution from the boundary data. The same procedure was applied to scalar and vector fields and was shown that in addition to power-law divergences there are logarithmic divergences related to the conformal anomalies of the dual CFT. A review of this method can be found in [7] (which also contains a more complete set of references). The main idea is that all bulk fields, e.g. the metric, gauge fields or scalar fields, admit asymptotic expansions near the boundary of the AAdS space. Only a finite number of terms is relevant as higher order terms do not play any role in the boundary effective action. These asymptotic expansions are then inserted into the bulk Einstein's equations which then lead to a series of *algebraic* equations for the coefficients in the asymptotic expansions. Solving these algebraic equations one is able to determine all but one coefficient of each asymptotic expansion as *local* functionals of the boundary data. The undetermined coefficients are precisely the one-point functions in the presence of sources of the corresponding dual operators which necessarily contain information about the dynamics of the theory and hence cannot be determined by the asymptotic analysis alone. In the very few cases where the bulk equations can be solved exactly, these terms take the form of *non-local* functionals of the boundary data. Nevertheless, the coefficients that are determined by the near boundary analysis are sufficient for the construction of local covariant counterterms for the divergences of the on-shell action, since the undetermined coefficients do not lead to divergences of the on-shell action. In fact, it is precisely

these undetermined coefficients that survive on the boundary and lead to the quantum effective action of the boundary QFT. In order to find the covariant counterterms, however, one must first invert the asymptotic expansions of the bulk fields to express the boundary data as a local functional of the bulk fields. This rather tedious step has been actually shown to be unnecessary, but this can only be achieved if one starts with a slightly different formulation of the problem [1].

A second method using the Hamilton-Jacobi formalism for AdS gravity was proposed in [8]. The advantage of this method is that all the analysis is carried out in terms of bulk fields living on a regulating surface, thus avoiding the explicit breaking of bulk covariance introduced by the asymptotic expansions of the previous method. However, we know that the logarithmic term, whenever it does not vanish, does break the bulk covariance and so the analysis in terms of bulk fields only must break down exactly for the logarithmic terms. Indeed, the Hamilton-Jacobi approach to holographic renormalization proceeds by making an ansatz for the counterterm action in terms of bulk fields, which is then inserted into Hamilton's constraint to fix any arbitrariness in the ansatz. However, apart from the fact that one would prefer a method that does not require an ansatz at any stage, this approach is by construction missing the logarithmic counterterm of the on-shell action, while it says nothing about the exact one-point functions of the dual operators. Covariant counterterms for the on-shell action and the holographic stress tensor were also discussed in [9, 10, 11]. However, no logarithmic counterterms were obtained by these authors. A more recent comparison between the asymptotic expansion and the Hamilton-Jacobi approaches can be found in [12].

In [1] we propose an alternative method which in a certain sense combines the asymptotic expansion and the Hamilton-Jacobi approaches. The benefit of doing this is that we are able to carry out the analysis by minimally breaking the bulk covariance to account for the conformal anomalies. So in the cases where there are no conformal anomalies our analysis is manifestly bulk covariant, in contrast to the asymptotic expansion method, while we are still able to track the logarithmic counterterms when these do not vanish, in contrast to the Hamilton-Jacobi method. The main idea is to setup the problem using the Hamiltonian formulation of AdS gravity, with the AdS radius playing the role of the 'time' coordinate, and write the bulk Einstein's equations using the Gauss-Codacci relations as equations for the extrinsic curvature of hypersurfaces of constant AdS radius. The same setup was also used in [11]. The Hamilton-Jacobi method can be used to relate the on-shell action to the canonical momenta of the bulk fields. One then proceeds by expanding the canonical momenta as *functionals of the bulk fields*. The role of the radial coordinate in the asymptotic expansion method is now played by the total dilatation operator which schematically takes the form

$$\delta_D = \sum_I (d - \Delta_I) \Phi_I \frac{\delta}{\delta \Phi_I}, \quad (3)$$

where Δ_I is the scaling dimension of the dual operator. In fact, $d - \Delta_I$ is the scaling dimension of

the source. It is shown that this new approach is completely equivalent to the asymptotic expansion method, but one does not need to invert any expansions, since the expansions are already covariant. In fact, the covariant expansions of the canonical momenta turn out to be just a rearrangement of the original asymptotic expansions in such a way that each term is bulk covariant. The only place where this bulk covariance breaks down is at the logarithmic term as is expected. This method is general and rigorous and requires less labour than the asymptotic expansion method. It also provides a general formula for the on-shell action and the renormalized stress tensor in terms of certain coefficients of the extrinsic curvature, independent of what bulk fields there are.

In this note we will only consider a very special example, namely a free massive scalar in a fixed AdS background, in order to illustrate the new approach. This problem is special because it can be solved exactly and so an exact expression for the quantum effective action can be obtained.

2 Free scalar in fixed AdS

Consider a free scalar field Φ in a fixed (Euclidean) AdS_{d+1} background

$$ds^2 = g_{\mu\nu}dx^\mu dx^\nu = \frac{d\rho^2}{4\rho^2} + \frac{1}{\rho}dx^i dx^i = \frac{1}{4}d\eta^2 + e^{-\eta}dx^i dx^i. \quad (4)$$

The AdS boundary is located at $\rho = 0$. The appropriate action is

$$S = \frac{1}{2} \int d^{d+1}x \sqrt{g} (g^{\mu\nu} \partial_\mu \Phi \partial_\nu \Phi + m^2 \Phi^2). \quad (5)$$

The scaling dimension Δ of the dual operator is defined as the positive root of the equation

$$m^2 = \Delta(\Delta - d). \quad (6)$$

The equation of motion is

$$(-\square_g + m^2)\Phi = (2d\partial_\eta - 4\partial_\eta^2 - \square + m^2)\Phi = 0, \quad (7)$$

where $\square \equiv e^\eta \partial_i \partial_i$ is the covariant Laplacian with respect to the induced metric $h_{ij} = e^{-\eta} \delta_{ij}$. One can solve this equation by Fourier transforming in the transverse coordinates to obtain a solution $\tilde{\Phi}(\eta, \mathbf{k})$ in terms of modified Bessel functions (see, for instance, [7] for an example). However, given that our primary aim is to obtain an expression for the quantum effective action of the boundary theory, we will follow a different approach which immediately allows us to evaluate the effective action in full generality.

To this end we write the equation of motion in factorized form as

$$(\partial_\eta - f_+(-\square))(\partial_\eta - f_-(-\square))\Phi = 0. \quad (8)$$

This is equivalent to the original equation (7) provided the functions f_\pm satisfy

$$f_+ + f_- = d/2, \quad (9)$$

and

$$-4f'_-(-\square)\square + 4f_-(-\square)^2 - 2df_-(-\square) + \square - m^2 = 0. \quad (10)$$

To solve this equation introduce $y(x) = f_-(x) - d/4$ and let $k = \Delta - d/2$. With these definitions we obtain

$$xy'(x) + y^2 - \frac{1}{4}(k^2 + x) = 0. \quad (11)$$

This can now easily be related to the modified Bessel equation by introducing $\xi = \sqrt{x}$ and $p = \exp(2 \int^\xi d\xi' y(\xi'^2)/\xi')$. One then obtains

$$\xi^2 \frac{d^2 p}{d\xi^2} + \xi \frac{dp}{d\xi} - (k^2 + \xi^2)p = 0, \quad (12)$$

which is precisely the equation for modified Bessel functions of order k . We take k to be an integer. The linearly independent solutions are $K_k(\xi)$ and $I_k(\xi)$ but only the first has the desired asymptotic behavior $y(\xi^2) \sim -k/2$ as $\xi \rightarrow 0$. Therefore, we find

$$f_\pm(-\square) = \frac{d}{4} \mp \frac{d \log(K_k(\sqrt{x}))}{d \log x}, \quad (13)$$

or

$$f_\pm(-\square) \approx \partial_\eta \left[\frac{d}{2} \log \sqrt{-\square} \mp \log K_k(\sqrt{-\square}) \right], \quad (14)$$

where $K_k(x)$ is a modified Bessel function of order $k = \Delta - d/2$. At this point we have succeeded in factorizing the equation of motion as

$$Q_+ Q_- \Phi = 0, \quad (15)$$

where Q_\pm take the asymptotic form

$$Q_+ = \partial_\eta - f_+(-\square) \sim \partial_\eta - \frac{\Delta}{2} + \mathcal{O}(\rho) \quad (16)$$

$$Q_- = \partial_\eta - f_-(-\square) \sim \partial_\eta - \frac{d - \Delta}{2} + \mathcal{O}(\rho). \quad (17)$$

The general solution can then be written as

$$\Phi = \Phi_- + \Phi_+, \quad (18)$$

where $\Phi_\pm \in \ker Q_\pm$, with $\Phi_+ \notin \ker Q_-$. From the asymptotic form of the operators Q_\pm one sees that

$$\Phi_+ \sim \rho^{\Delta/2} \quad (19)$$

and hence, Φ_+ corresponds to the normalizable mode which is irrelevant for the near boundary analysis. The problem of finding the solution with the correct asymptotics is therefore reduced to the *first order* problem

$$Q_- \Phi = 0, \quad (20)$$

which immediately gives the momentum conjugate to Φ as

$$\varphi \equiv \dot{\Phi} = f_-(-\square)\Phi. \quad (21)$$

This is everything one needs to determine the covariant counterterms and the quantum effective action of the boundary CFT, since the regularized on-shell action is simply

$$S_{reg} = \int_{\rho=\epsilon} d^d x \sqrt{h} \Phi \dot{\Phi} = \int_{\rho=\epsilon} d^d x \sqrt{h} \Phi f_-(-\square)\Phi. \quad (22)$$

The covariant counterterms are obtained explicitly by expanding $f_-(x)$ for small x :

$$f_-(x) = \frac{(d-\Delta)}{2} - \frac{x}{2(2\Delta-d-2)} + \frac{x^2}{2(2\Delta-d-2)^2(2\Delta-d-4)} + \dots + \frac{(-1)^{k+1}}{2^{2k}\Gamma(k)^2} x^k \log x + \dots \quad (23)$$

In particular, the counterterm action is

$$S_{ct} = - \int_{\rho=\epsilon} d^d x \sqrt{h} \Phi \left[\frac{(d-\Delta)}{2} - \frac{-\square}{2(2\Delta-d-2)} + \frac{(-\square)^2}{2(2\Delta-d-2)^2(2\Delta-d-4)} + \dots + \frac{(-1)^{k+1}}{2^{2k}\Gamma(k)^2} (-\square)^k \log \epsilon \mu^2 \right] \Phi, \quad (24)$$

where we have introduced an arbitrary mass scale, μ , to make the argument of the logarithm dimensionless. Thus, $\square = \epsilon \square_{(0)} = \epsilon \mu^2 \square_{(0)} / \mu^2$. Using the asymptotic form

$$\Phi \sim \rho^{(d-\Delta)/2} \phi_{(0)}(x) \quad (25)$$

the quantum effective action becomes a functional of the boundary data $\phi_{(0)}$, namely

$$S_{ren}[\phi_{(0)}] \equiv \lim_{\epsilon \rightarrow 0} [S_{reg} + S_{ct}] = \frac{(-1)^{k+1}}{2^{2k}\Gamma(k)^2} \int d^d x \sqrt{h_{(0)}} \phi_{(0)} (-\square_{(0)})^k \log(-\square_{(0)} / \mu^2) \phi_{(0)}, \quad (26)$$

where $h_{(0)ij} = \delta_{ij}$ and $\square_{(0)}$ is the Laplacian with respect to the boundary metric $h_{(0)ij}$. This exact form of the quantum effective action enables us to calculate any correlation function of the dual QFT by taking the appropriate number of functional derivatives with respect to the boundary condition $\phi_{(0)}$.

It is important to realize that the information contained in equation (21) is no less than the full solution Φ with the prescribed boundary conditions. Indeed,

$$\Phi = \frac{2^{1-k}}{\Gamma(k)} (\sqrt{-\square})^{d/2} K_k(\sqrt{-\square}) (-\square_{(0)})^{(\Delta-d)/2} \phi_{(0)} \quad (27)$$

satisfies (21) and has the correct asymptotic behavior and hence, by the uniqueness of the solution, is precisely the solution one would obtain by solving directly the equations of motion. In fact, this is exactly the solution obtained in [7] for the case $k = 1$. What we have shown then, in this particular example, is that all information contained in a solution Φ of the bulk field equations with prescribed but arbitrary Dirichlet boundary conditions at the boundary of an AdS space can be expressed in terms of a functional relation between the canonical momenta and the bulk fields. This observation is key to the method presented in [1].

Acknowledgments

This work has been done in collaboration with Kostas Skenderis.

References

- [1] I. Papadimitriou and K. Skenderis, "Simplifications in Holographic Renormalization", in preparation.
- [2] M. Henningson and K. Skenderis, "The holographic Weyl anomaly," JHEP **9807** (1998) 023 [arXiv:hep-th/9806087]; M. Henningson and K. Skenderis, "Holography and the Weyl anomaly," Fortsch. Phys. **48** (2000) 125 [arXiv:hep-th/9812032].
- [3] S. de Haro, S. N. Solodukhin and K. Skenderis, "Holographic reconstruction of spacetime and renormalization in the AdS/CFT correspondence," Commun. Math. Phys. **217** (2001) 595 [arXiv:hep-th/0002230].
- [4] M. Bianchi, D. Z. Freedman and K. Skenderis, "How to go with an RG flow," JHEP **0108** (2001) 041 [arXiv:hep-th/0105276].
- [5] M. Bianchi, D. Z. Freedman and K. Skenderis, "Holographic renormalization," Nucl. Phys. B **631** (2002) 159 [arXiv:hep-th/0112119].
- [6] C. Fefferman and C. Robin Graham, "Conformal Invariants", in *Elie Cartan et les Mathématiques d'aujourd'hui* (Astérisque, 1985) 95.
- [7] K. Skenderis, "Lecture notes on holographic renormalization," Class. Quant. Grav. **19** (2002) 5849 [arXiv:hep-th/0209067].
- [8] J. de Boer, E. Verlinde and H. Verlinde, "On the holographic renormalization group," JHEP **0008** (2000) 003 [arXiv:hep-th/9912012].
- [9] V. Balasubramanian and P. Kraus, "A stress tensor for anti-de Sitter gravity," Commun. Math. Phys. **208**, 413 (1999) [arXiv:hep-th/9902121].
- [10] R. Emparan, C.V. Johnson and R.C. Myers, "Surface Terms as Counterterms in the AdS/CFT Correspondence", Phys.Rev. **D60** (1999) 104001, [arXiv:hep-th/9903238].
- [11] P. Kraus, F. Larsen and R. Siebelink, "The gravitational action in asymptotically AdS and flat spacetimes," Nucl. Phys. B **563** (1999) 259 [arXiv:hep-th/9906127].
- [12] D. Martelli and W. Muck, "Holographic renormalization and Ward identities with the Hamilton-Jacobi method," Nucl. Phys. B **654** (2003) 248 [arXiv:hep-th/0205061].

The KamLAND Impact on Neutrino Oscillations

ANNA MARIA ROTUNNO

Dipartimento di Fisica, Università di Bari, and Sezione INFN di Bari, Via Amendola 173, I-70126 Bari, Italy

1. – Introduction

The hypothesis of neutrino masses and flavour mixing [1] has been confirmed by several experiments. The first generation of solar ν experiments [2] have narrowed the allowed solutions to a few isolated regions in the $(\sin^2 2\vartheta_{12}, \delta m_{21}^2)$ ⁽¹⁾ parameter space relevant for $\nu_e \rightarrow \nu_x$ oscillations ($x = \mu, \tau$). The Small Mixing Angle (SMA) ($\sin^2 2\vartheta_{12} \sim 10^{-3}$ and $\delta m_{21}^2 \sim 10^{-5} \text{ eV}^2$) and the "just-so" ($\delta m_{21}^2 < 10^{-9} \text{ eV}^2$) solutions have been disfavoured by the Super-Kamiokande and SNO results, while the Large Mixing Angle (LMA) ($\sin^2 2\vartheta_{12} > 0.3$ and $\delta m_{21}^2 \sim 10^{-5} \text{ eV}^2$) emerges as the favorite solution [3, 4]. After the first results from the Kamioka Liquid scintillator AntiNeutrino Detector (KamLAND) [5], all solutions to the solar neutrino problem except for the LMA region have been excluded, in the context of two-flavour neutrino oscillations with CPT invariance. Furthermore, the allowed region has been split by KamLAND into two sub-regions, usually named LMA-I and LMA-II.

The present work illustrates the impact of KamLAND on the neutrino oscillation problem, and discusses the discrimination of the two surviving solutions, LMA-I and LMA-II. We consider two possible approaches. First, we study the role of other long baseline reactor antineutrino experiments, BOREXINO [6] (as a reactor experiment) and HLMA [7] (proposed). We compute the expected signals for these experiments, in order to determine the new informations that they will be able to provide. We produce the sensitivity plots in the solar-neutrino parameter space and show that, with just these experiments, we will hopefully solve the solar neutrino problem conclusively. Second, we study the position of the KamLAND spectrum peak. We analyze the different cases for LMA-I/II solution, above and below the energy threshold. Finally, we discuss the problem of the Earth antineutrino detection, relevant for LMA-I/II discrimination and for the determination of the Earth radiogenic heat.

⁽¹⁾ Mass mixing parameters: $\delta m_{21}^2 = m_2^2 - m_1^2$, ϑ_{12} = mixing angle.

2. – Long-Baseline Reactor Experiments: KamLAND

In the framework of two-flavour neutrino mixing, the ν_e survival probability at the detector (in vacuum or for negligible Earth effects) is given by:

$$(1a) \quad P_{ee} = P(\nu_e \rightarrow \nu_e) = P(\bar{\nu}_e \rightarrow \bar{\nu}_e) \\ = 1 - \sin^2 2\vartheta_{12} \sin^2 \left(1.27 \frac{\delta m_{21}^2 [\text{eV}^2] L [\text{m}]}{E_\nu [\text{MeV}]} \right)$$

where L is the source-detector distance, and E_ν is the (anti)neutrino energy. The oscillation phase is of $O(1)$ if

$$(2a) \quad L(\text{km}) \sim 10^{-3} \frac{E_\nu(\text{MeV})}{\delta m_{21}^2 (\text{eV}^2)} \\ \sim 10^2 E_\nu(\text{MeV}),$$

where the second line refers to the LMA parameter values. For reactor antineutrino energies $O(\text{MeV})$ [8], observable oscillation phenomena are thus expected over a distance $L \sim 10^2$ km, implying the need for long baselines, just as in the KamLAND and BOREXINO experiments.

The Kamioka Liquid scintillator AntiNeutrino Detector (KamLAND) [9, 5] is located at the Kamiokande site. With low energy neutrinos, it can only measure $\bar{\nu}_e$ disappearance and is thus suited to test relatively large mixing angles, $\sin^2 2\vartheta_{12} > 0.1$. The detector collects $\bar{\nu}_e$ from 16 commercial nuclear power plants, that supply about one third (130 GW) of the total electric power in Japan. About 95% of the $\bar{\nu}_e$ flux at KamLAND comes from reactors located between 80–350 km from the detector, making the baseline long enough to provide a sensitive probe of the LMA solution. Specifically, the highest sensitivity to the mass-square difference lies in the range $10^{-5} < \delta m^2 < 10^{-4}$ eV².

The target consists of a spherical transparent balloon filled with 1000 tons of non-doped liquid scintillator. The antineutrinos are detected via the inverse β -decay process:



The e^+ is directly observable and gives a prompt signal. The neutron is captured on a time scale of ~ 200 μsec by a proton in the nearby liquid, according to the reaction $n + p \longrightarrow d + \gamma$ (2.2 MeV). The antineutrino events have a clear signature of a delayed coincidence between the (prompt) positron signal and the (delayed) neutron capture gamma-ray. The neutrino energy threshold of the reaction is $E_{vis}^{thr} = 1.8$ MeV [10], where the total visible energy corresponds to $E_{vis} = E_{e^+} + m_{e^+}$. The statistical significance of the signal crucially depends on the background reduction.

In the framework of two-flavour neutrino mixing, we compute the KamLAND positron spectrum by using the Vogel and Engel parametrization [11] for the original reactor $\bar{\nu}_e$ spectrum.

Figure 1 shows the KamLAND positron spectrum calculated for different δm_{21}^2 values and $\sin^2 \vartheta_{12} = 0.31$, compared with the no-oscillation case. Energy spectrum distortions can give a strong evidence for neutrino oscillations and a specific signature for parameter estimation. For a deeper analysis and related bibliography we refer to [12], in which we studied the accuracy of parameter reconstruction in KamLAND, with an estimate of statistical and systematic errors.

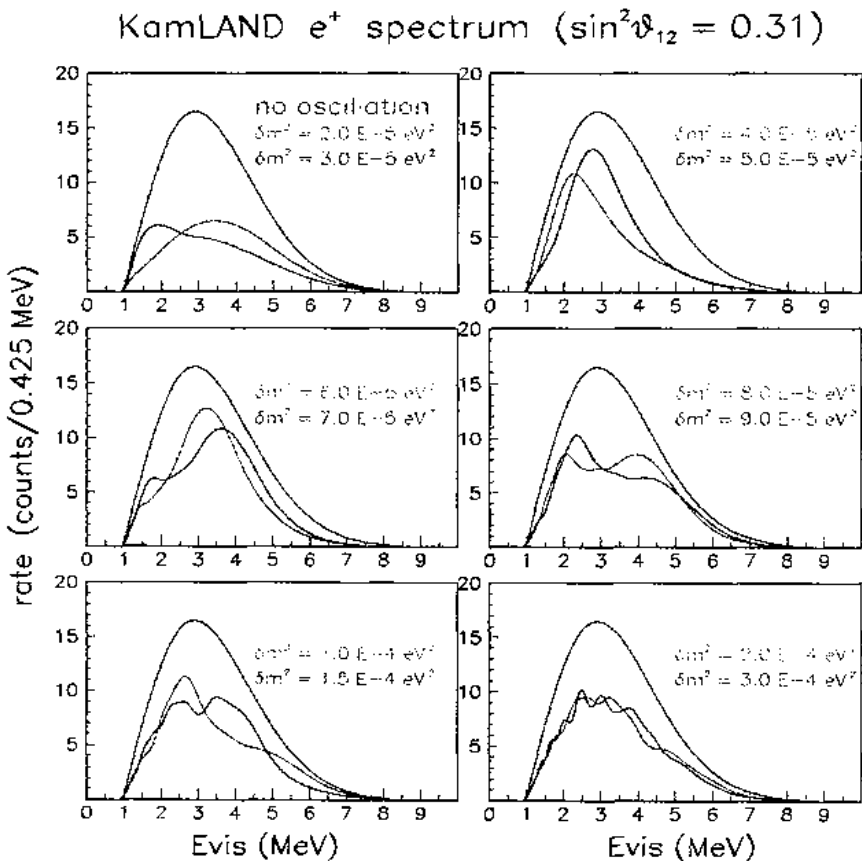


Fig. 1. - KamLAND positron spectrum (two-neutrino mixing) with and without oscillations. Energy resolution used: $\sigma(E)/E = 7.5\%$ (at $E = 1$ MeV).

3. - Solar Neutrino Problem After First KamLAND results

KamLAND has measured the flux of antineutrinos from distant nuclear reactors. The observed reactor antineutrino events are significantly less than those expected in the absence of neutrino oscillations [5]:

$$(4a) \quad \frac{N_{obs} - N_{BG}}{N_{expected}} = 0.611 \pm 0.085(\text{stat}) \pm 0.041(\text{syst}),$$

for $E_{vis} > 2.6$ MeV and an exposure of 162 ton·yr (145.1 day lifetime).

Figure 2 shows the ratio of measured to expected $\bar{\nu}_e$ events for KamLAND, as well as for previous reactor experiments [13], as a function of the average distance from the source. The solid circle is the KamLAND result plotted at a flux-weighted average distance of about 180 km. The dotted curve is representative of a best-fit LMA prediction [4], and the dashed curve is expected for no oscillations.

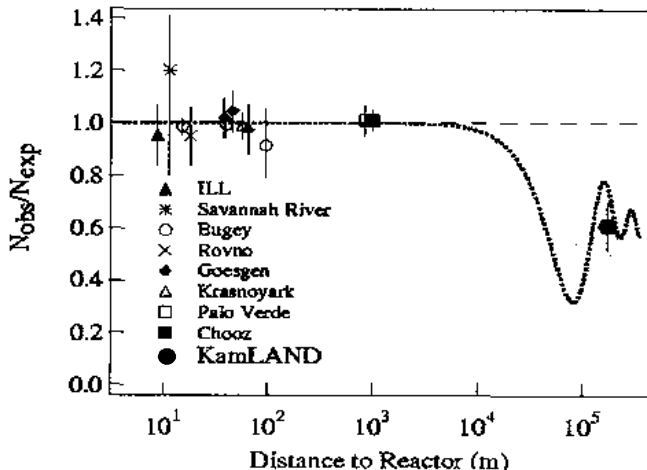


Fig. 2. - The ratio of measured to expected $\bar{\nu}_e$ flux from reactor experiments. Taken from [5].

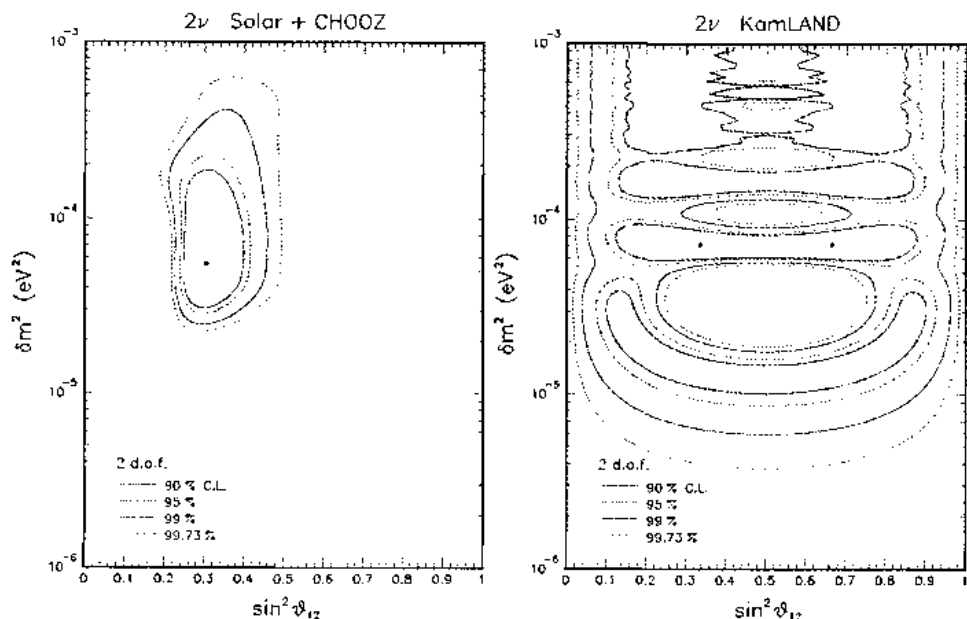


Fig. 3. - Left panel: Global analysis of Solar and CHOOZ neutrino data in the $(\delta m_{21}^2, \sin^2 \vartheta_{12})$ parameter space, restricted to the LMA region, in two flavor active neutrino oscillation frame. The black dot indicates the best fit solution. Right panel: Analysis of KamLAND energy spectrum data above the visible energy threshold $E_{\text{vis}}^{\text{thr}} = 2.6$ MeV in the $(\delta m_{21}^2, \sin^2 \vartheta_{12})$ parameter space, for 2ν active neutrino oscillations. The black dots indicate the (symmetric) best fit points, the left one being remarkably close to the solar best fit point (from [14]).

In the case of two flavor active neutrino oscillations, the global analysis of solar and CHOOZ data, restricted to the LMA solution, provides the results shown in the left panel of Fig. 3 [12]. A similar analysis of the KamLAND data is shown in the right panel of Fig. 3 [14]. A "tower" of octant-symmetric regions is allowed at different values of δm_{21}^2 . The three lower regions with $\delta m_{21}^2 \leq 2 \cdot 10^{-4}$ eV 2 are well separated at 90% C.L., while the upper ones tend to merge in a continuum. The symmetric best fits are represented by black dots. The left dot is remarkably close to the solar best fit point in the left panel, indicating a very good agreement between solar and KamLAND results.

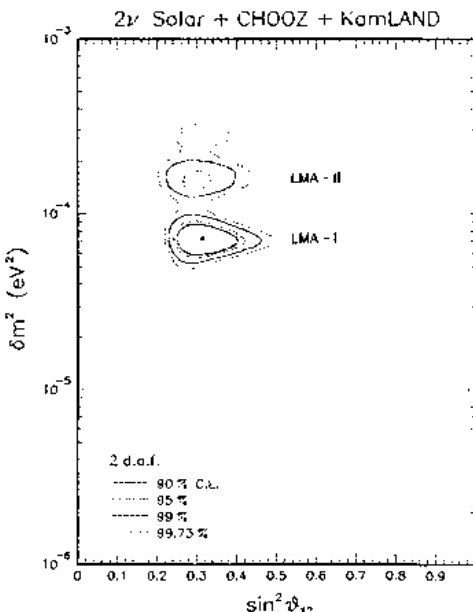


Fig. 4. – Global analysis of solar, CHOOZ and KamLAND neutrino data in the $(\delta m_{21}^2, \sin^2 \vartheta_{12})$ parameter space, in two flavor active neutrino oscillation frame. The LMA region is significantly constrained and is split into two sub-regions, LMA-I and LMA-II (from [14]).

Fig. 4 illustrates the combination of the Solar+CHOOZ results (Fig. 3 - left panel) with the KamLAND results (Fig. 3 - right panel), [14]. After the inclusion of KamLAND first data, the LMA region is more constrained and shows a "fine structure": it is basically split into two sub-regions at "small" and "large" δm_{21}^2 , the so called LMA-I and LMA-II solutions respectively (the LMA-I being preferred by the data). At 99.73% C.L. the two solutions merge into a single one, which extends towards $\delta m_{21}^2 \sim 3 \cdot 10^{-4}$ eV 2 .

In conclusion, the KamLAND experiment has not only been able to confirm the LMA region as solution to the Solar Neutrino Problem, but has constrained the corresponding oscillation parameter space, which now exhibits a sub-structure. The refinement of the $(\delta m_{21}^2, \sin^2 \vartheta_{12})$ parameter estimate needs higher statistics and a better control of systematics.

4. - LMA-I/LMA-II Discrimination

A very important task for the next future is the confirmation of one of the two solutions, LMA-I or LMA-II. In this section we discuss some methods which can be useful to discriminate between them. First: experimental evidence from other reactor antineutrino experiments, such as BOREXINO and the HLMA project. Second: the study of the KamLAND spectrum peak.

4.1. BOREXINO and HLMA implications. - The BOREXINO experiment [6] is located in the Gran Sasso Laboratories (Italy). The detector is similar in structure to KamLAND. Built as a solar neutrino experiment, BOREXINO is also able to detect $\bar{\nu}_e$ coming from the nuclear reactor plants located in Europe, characterized by an average distance of ~ 800 km (to be compared with ~ 160 km in KamLAND). Therefore, BOREXINO is expected to have a lower statistics as compared with KamLAND, and a lower sensitivity to the mass-mixing parameter. Although with a lower sensitivity, BOREXINO can confirm the KamLAND reactor results in an independent way.

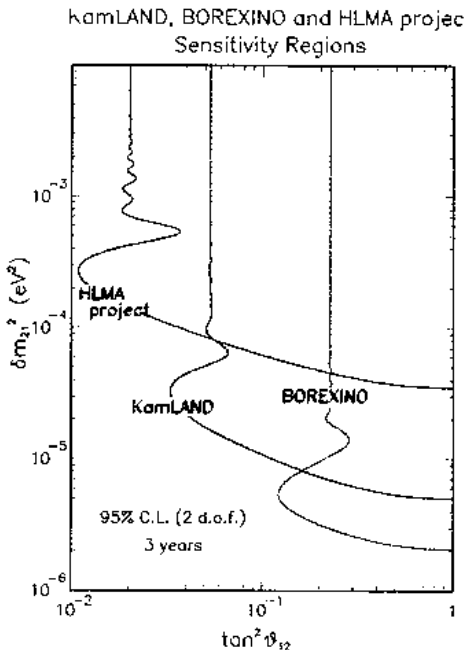


Fig. 5. - Sensitivity plot for KamLAND and BOREXINO experiments and HLMA project, for 3 years and 95 % C.L.

If the solution is such that $\delta m_{21}^2 \geq 2 \cdot 10^{-4}$ eV 2 , i.e. the LMA-II solution, KamLAND will only observe a rate suppression but no spectral distortions, and thus will not have the optimal sensitivity to measure the oscillation parameters. In this case there is a proposal [7] for a new medium baseline reactor experiment located at Heilbronn (Germany), to get the precise value of δm_{21}^2 . The detector for the determination of δm_{21}^2 in the HLMA parameter range consists of ~ 100 ton liquid scintillator, and the experiment is similar

in structure to KamLAND. All relevant European nuclear plants would marginally contribute to the $\bar{\nu}_e$ flux at the Heilbronn site, since $\sim 92\%$ of the total rate will come from only five of them (at a medium distance of ~ 20 km). This distance makes the HLMA project suited to study relatively high values of δm_{21}^2 ($> 2 \cdot 10^{-4}$ eV 2).

In Fig. 5 we show the sensitivity plot for KamLAND, BOREXINO and the HLMA project, at 95% C.L. and assuming three years of data taking. For δm^2 between 10^{-5} and 10^{-4} eV 2 , KamLAND is able to observe a suppression of the rate and a deformation of the spectrum. For values larger than $\sim 2 \cdot 10^{-4}$ eV 2 the oscillation signal is smeared out, and only a lower limit on δm^2 can be given by KamLAND. The sensitivity region for BOREXINO is lower than for KamLAND, but it will give an independent experimental result. The HLMA project sensitivity region is instead maximal in the LMA-II region.

These experiments can thus complete the information on the LMA solution, and give a chance to discriminate the LMA subregions, up to the upper limit fixed by the CHOOZ experiment, which is about $\delta m^2 < 7 \cdot 10^{-4}$ eV 2 .

4.2. KamLAND Positron Spectrum for LMA-I and LMA-II. – Fig. 6 shows the absolute KamLAND energy spectra of reactor events, predicted for the LMA-I and LMA-II global best-fit points, and for no oscillations, together with the KamLAND experimental data (black dots) above the analysis threshold (2.6 MeV).

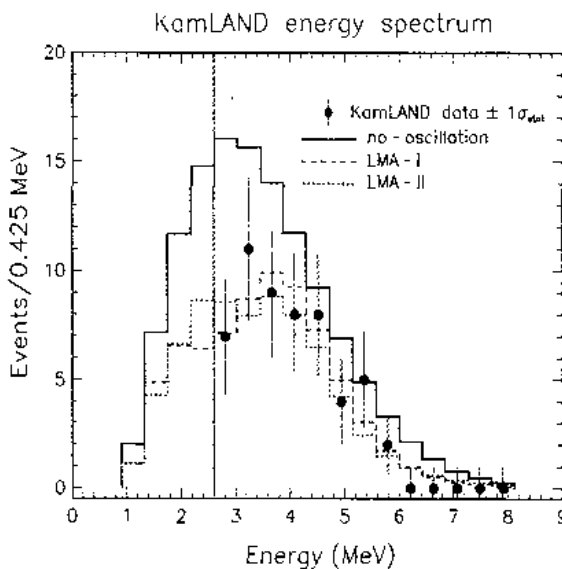


Fig. 6. Absolute KamLAND positron energy spectra for the LMA-I and LMA-II best fit solutions, and for the no oscillation case. The black dots represent the current KamLAND data (above the analysis energy threshold). From [14].

The main difference between the two oscillated spectra is the position of the spectrum peak, that is shifted at higher energies for the LMA-I solution, and is aligned with the no-oscillation position for the LMA-II solution. This difference may be useful as a discrimination tool between the two solutions in the next future. Fig. 6 also shows that the greatest difference appears in the first bin below the current experimental threshold.

In this region the geoneutrino contribution is relevant. Therefore, an accurate study in this region requires a higher statistics and a deeper understanding of geoneutrino modeling.

5. – GeoNeutrinos

The Earth radiates about 40 TW of heat from its surface. About 40 % of this energy (~ 16 TW) is believed to have radiogenic origin, mainly from ^{238}U and ^{232}Th decays inside the crust and mantle of Earth. The radiogenic heat is therefore an essential component of the present dynamics of our planet. These phenomena could be directly studied by detecting the antineutrinos deriving from the β -decays of these actinides, the terrestrial antineutrinos, or the so called "geoneutrinos" ($\bar{\nu}_{geo}$). KamLAND will be able to detect the $\bar{\nu}_{geo}$ for the first time and thus open a new field in geophysics.

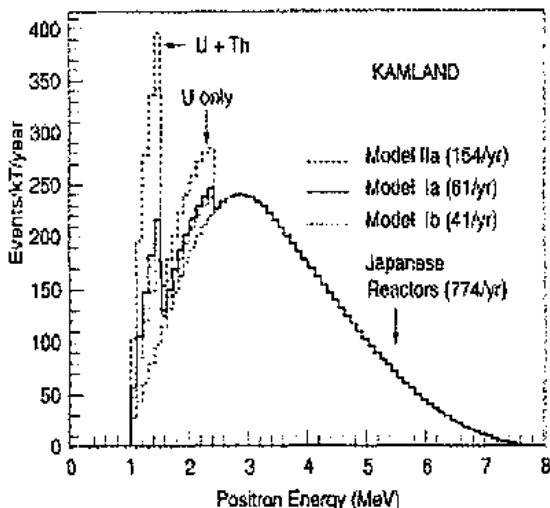


Fig. 7. – Energy spectrum from terrestrial antineutrino and nuclear reactor spectrum as expected at KamLAND. The different geophysical models are shown for the terrestrial antineutrinos and no oscillations are assumed for all the spectra shown. The signal rates point to several years of measurements for data of statistical significance to different aspects of geophysical interpretation. Taken from [15].

Geoneutrinos produce events with $E_{\nu_{geo}} < 2.49$ MeV. The expected observed energy spectrum will have a characteristic "double hump" structure, as shown in Fig. 7. Such feature is useful to separate the reactor antineutrino signal from the terrestrial $\bar{\nu}_{geo}$ signal.

The two lower spectra (Ia and Ib), superimposed in Fig. 7, correspond to two different geophysical models of the heavy element concentration in the oceanic and continental crusts [15]. In one year of data taking, model Ia would give an integral of 61 events, while model Ib would give only 41 events. When these events will be measured and subtracted

from the total spectrum, a better determination of the spectrum peak will be possible, and thus the LMA-I and LMA-II solutions will be more easily separated.

6. – Conclusions

KamLAND demonstrated reactor antineutrino disappearance over long baselines at high confidence level (99.95 %) for the first time. The LMA region is the only remaining oscillation solution to the solar neutrino problem. KamLAND has split such solution into two sub-regions, LMA-I and LMA-II.

Future KamLAND measurements with improved statistical precision and reduced systematic errors will provide precision determinations of neutrino oscillation parameters. Other reactor antineutrino experiments (BOREXINO and HLMA project) can be useful as independent experimental confirmation and will allow to discriminate between the two solutions, LMA-I/LMA-II. Finally, geo-neutrino studies will be important also to discriminate LMA-I/II and to give total Earth radiogenic heat, thus opening a new field in geophysics.

7. – Acknowledgments

A.M. R. is sincerely grateful to Prof. Antonino Zichichi and Prof. Gerardus t'Hooft for their kind hospitality to the International School of Subnuclear Physics, 41st course and for their interest in my work. This work has been done in collaboration with Prof. G.L. Fogli, Dr. E. Lisi, Dr. A. Marrone, Dr. A. Palazzo, of the Dipartimento di Fisica, Università di Bari, and Sezione INFN di Bari, Italy, and Dr. D. Montanino of the Dipartimento di Scienza dei Materiali, Università di Lecce, and Sezione INFN di Lecce, Italy.

REFERENCES

- [1] PONTECORVO B., *J. Exptl. Theoret. Phys.*, **34** (1958) 247 [*Sov. Phys. JETP*, **7** (1958) 172]; PONTECORVO B., *Zh. Eksp. Teor. Fiz.*, **53** (1967) 1717 [*Sov. Phys. JETP*, **26** (1968) 984; MAKI Z., NAKAGAWA M. and SAKATA S., *Prog. Theor. Phys.*, **28** (1962) 870.
- [2] HOMESTAKE COLLABORATION, CLEVELAND B. et al., *Astrophys. J.*, **496** (1998) 505; SAGE COLLABORATION, ABDURASHITOV J. et al., *Phys. Rev. C*, **60** (1999) 055801; GALLEX COLLABORATION, HAMPEL W. et al., *Phys. Lett. B*, **447** (1999) 127; KAMIOKANDE COLLABORATION, FUKUDA Y. et al., *Phys. Rev. Lett.*, **77** (1996) 1683; SUPERKAMIOKANDE COLLABORATION, FUKUDA Y. et al., *Phys. Rev. Lett.*, **82** (1999) 1810; *Phys. Rev. Lett.*, **82** (1999) 2430.
- [3] FOGLI G.L., LISI E., MONTANINO D. and PALAZZO A., *Phys. Rev. D*, **64** (2001) 093007; BAHCALL J.N., KRASTEV P.I. and SMIRNOV A.YU., *Phys. Rev. D*, **60** (1999) 093001.
- [4] FOGLI G.L., LISI E., MARRONE A., MONTANINO D. and PALAZZO A., *Phys. Rev. D*, **66** (2002) 053010.
- [5] KAMLAND COLLABORATION, EGUCHI K. et al., *Phys. Rev. Lett.*, **90** (2003) 021802. Additional information available at the sites:
hep.stanford.edu/neutrino/KamLAND/KamLAND.html and kamland.lbl.gov.
- [6] BOREXINO COLLABORATION, SCHÖNERT S., *Nucl. Phys. B (Proc. Suppl.)*, **70** (1999) 195; arXiv: hep-ex/0202021 (v1).
- [7] SCHÖNERT S., LASSEUR T. and OBERAUER L., *Astropart. Phys.*, **18** (2003) 565.
- [8] BEMPORAD C., GRATTA G. and VOGEL P., *Rev. Mod. Phys.*, **74** (2002) 297.
- [9] KAMLAND COLLABORATION, BUSENITZ J. et al., *Proposal for US Participation in KamLAND* (Unpublished), March 1999. See: <http://bsfk0.lbl.gov/kamland/>.

- [10] VOGEL P. and BEACOM J., *Phys. Rev. D*, **60** (1999) 053003.
- [11] VOGEL P. and ENGEL J., *Phys. Rev. D*, **39** (1989) 3378.
- [12] FOGLI G.L., LETTERA G., LISI E., MARRONE A., PALAZZO A. and ROTUNNO A.M., *Phys. Rev. D*, **66** (2002) 093008.
- [13] PARTICLE DATA GROUP, *Phys. Rev. D*, **66** (2002) 010001.
- [14] FOGLI G.L., LISI E., MARRONE A., MONTANINO D., PALAZZO A., ROTUNNO A.M., *Phys. Rev. D*, **67** (2003) 073002.
- [15] RAGHAVAN R.S. et al., *Phys. Rev. Lett.*, **80** (1998) 635.

Particle Identification with the ALICE TOF Detector at Very High Particle Multiplicity

Chiara Zampolli

University and INFN, Bologna, Italy

1 Introduction

ALICE (A Large Ion Collider Experiment) [1], together with CMS, ATLAS and LHCb, will be one of the experiments at the CERN LHC (Large Hadron Collider). It will study Pb-Pb collisions with a centre-of-mass energy $\sqrt{s} = 5.5$ TeV/nucleon pair, (~ 30 times higher than RHIC energies) in order to explore the behaviour of nuclear matter in extreme density and temperature conditions. As a matter of fact, such an energy should make nuclear matter undergo a QCD phase transition which, in turn, should result in the formation of a state where quarks and gluons are almost free, the so-called Quark-Gluon Plasma (QGP). This state is what is supposed to have existed very little after the Big Bang, and is thought to be now present in the heart of Neutron stars. However, if the QGP is actually produced during Pb-Pb collisions, it will last only for a very small fraction of a second after which it will expand into a dilute hadronic state.

Besides the QGP formation, another important goal of the ALICE experiment is to study whether a partial restauration of the chiral symmetry, with quark masses reduced to the bare ones, will occur.

In order to face the extremely compelling task of understanding and analyzing such a system, ALICE will concentrate on the study of a large number of observables [2], such as particle multiplicities, particle spectra, the production of jets and direct photons, and many others, relying especially on an excellent power of separation among pions, kaons and protons in the momentum range from 0.5 GeV/c up to a few GeV/c, where a large fraction of the primary charged hadrons are expected to be produced. For this reason, an effective Particle IDentification (PID) based on a powerful Time Of Flight (TOF) system, is of undoubtful importance.

2 The Time of Flight system

The ALICE Time of Flight (TOF) system [1], [3], [4], [5] has been thought of in order to be eligible for the precise particle identification required by the goals of the experiment itself. Since it will have to deal with a very large amount of particles ($dN_{ch}/dy \leq 8000$), a high segmentation is definitely needed. For this reason, the TOF set up is based on a modular arrangement of a basic unit, the MRPC (Multigap Resistive Plate Chamber),

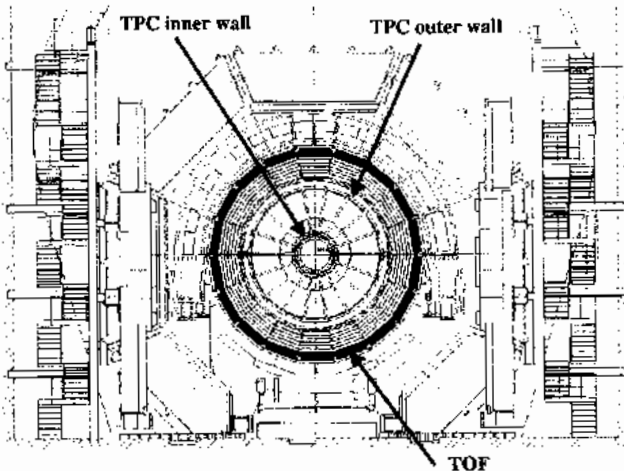


Figure 1: Transverse view of the ALICE detector, where the 18 sectors of the TOF system can be seen. The inner and the outer walls of the TPC are indicated.

which is characterized by an excellent intrinsic resolution of $50 \div 60$ ps, and an overall resolution of 120 ps, necessary in order to be able to efficiently separate kaons from pions in the momentum range under study. The MRPCs will be overlapped and tilted in space in order to reduce the dead space and the traversal path of the particles through the chambers themselves.

The TOF will work in presence of a solenoidal magnetic field $B = 0.2 \div 0.5$ T and under extremely high multiplicity (and background) conditions. The most pessimistic hypothesis predicts ~ 8000 charged particles per rapidity unit (in fact, $3000 \leq dN_{ch}/dy \leq 8000$, [2]). However, the detector will rely on 160000 read out pads (thanks to the MRPC technology), and to an occupancy of $\leq 15\%$.

In this paper, we will describe a track matching procedure which concerns the TOF and the ALICE central tracker, the TPC [6] (see Figure 1 for a transverse view of the ALICE detector), and we will then present two different approaches to the particle identification problem. For all the calculations presented herein, the AliROOT package [7] has been used (developed in the framework of the ALICE Software Project) which is based on ROOT [8] and GEANT3 [9], and is interfaced with several event generators, such as HIJING [10] and SHAKER [1], [3].

3 Track matching

The track matching procedure involves contiguous subdetectors. In the case of the TOF, the TPC (Time Projection Chamber) and the TRD (Transition Radiation Detector) [11] are the subdetectors which must be taken into account.

3.1 The “probe-track method”

In order to match the tracks in the TPC with the pads producing signals in the TOF, the “probe-track method” has been developed. The starting point of this method is a particle tracked/reconstructed in the TPC. For this particle, 20 probe tracks are then generated and extrapolated to the TOF surface. This amount has been chosen as a good compromise between computational time and statistics. The probe tracks are generated from the last TPC pad row and then Gaussianly deviated in such a way as to simulate the multiple scattering which the particle should undergo on its way to the TOF pad¹. To each of these probe tracks, a weighting contribution is assigned according to whether a sensitive pad hit actually fired or not: in the first case, $weight_1 = \epsilon_{eff}$, while in the second case $weight_1 = 1 - \epsilon_{eff}$, where ϵ_{eff} is the TOF efficiency and is equal to 99%.

A signal on one pad could sometimes generate a signal on the neighbouring pad(s) which would be slightly delayed in time according to the amount of charge induced (the smaller the charge, the longer the delay). In order to minimize this double-signal effect, another weight is defined for each track: $weight_2 = q_{induced}^2$, where $q_{induced}$ is the normalized charge induced on the pad. The total weight is then defined as the product of the two contributions, $weight_{pr} = weight_1 \times weight_2$. The weight of each pad then becomes the sum of the weights of the probe tracks which fall in that pad, $Weight_{pad} = \sum weight_{pr}$. Finally, the pad to which the maximum value of the quantity $Weight_{pad}$ corresponds is chosen to be the TOF match for the initial TPC track.

3.2 The TPC-TOF matching efficiency

The efficiency of the track matching procedure is defined as

$$efficiency = \frac{N_{match}^t(i)}{N(i)}$$

where $N(i)$ is the total number of particles of type i ($i = \pi, K, p$) extrapolated to the TOF sensitive-pad surface, and $N_{match}^t(i)$ is the number of correctly matched particles of type i . Table 1 shows the value of the efficiency for the three types of hadrons obtained from 100 HIJING² events at $B = 0.2$ T and, in brackets, at $B = 0.4$ T. This efficiency is mostly

¹Multiple scattering takes place in the TPC outer wall, throughout the TRD (which is considered here as passive material) and in the TOF inner wall.

²HIJING is an event generator which is based on the results of current heavy ion experiments [10].

influenced by the effect of multiple scattering rather than by the level of occupancy. One can see that while the magnetic field increases, the efficiency significantly increases only for pions as a consequence of the fact that the pion is the lightest particle among the three types of hadrons considered. Very low momentum pions (the matching of which is the most critical because of multiple scattering) are swept away when the field is stronger and do not reach the TOF surface.

Primary hadron	Efficiency
π^\pm	38 (42)
K^\pm	37 (36)
$p(\bar{p})$	35 (32)

Table 1: TPC-TOF matching efficiencies (%) for primary hadrons extrapolated to the TOF sensitive-pad surface with $B = 0.2$ T and, in brackets, with $B = 0.4$ T (100 HIJING events).

4 Particle identification

After matching the track between the TPC and the TOF, it is necessary to identify the particle which has been tracked. For this reason, its mass must be determined according to the formula:

$$m = p(t^2/l^2 - 1)^{1/2} \quad (1)$$

which gives the mass of the particle as a function of its momentum, time of flight, and track length.

In order to identify particles, two methods have been studied, the “contour method”, and the “probability method”. They will be presented in Subsections 4.1 and 4.2.

4.1 The “contour method”

This method consists in using the data obtained after the reconstruction in the TPC and the matching in the TOF to fill a momentum versus mass plot where the particles are then identified according to some appropriate contour cuts. Figure 2 shows how the identification of pions, kaons and protons can be performed for a set of 25 SHAKER³ “a

³SHAKER is an event generator developed to describe the central rapidity region of heavy ion events at LHC [1], [3]. This generator has been modified in the present exercise (SHAKER “à la RHIC”) in order to reproduce the experimental p_t distributions measured at RHIC for π , K , p .

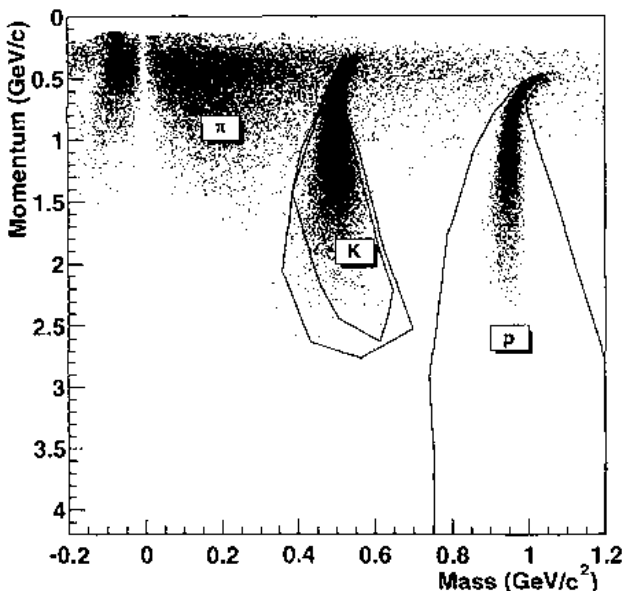


Figure 2: Mass separation with the TOF detector (overall time resolution: 120 ps) as a function of momentum for 25 SHAKER "à la RHIC" events, with $B=0.2$ T.

"à la RHIC" [12] events, applying cuts only for kaons and protons. In particular, for kaons two examples of possible contour cuts are drawn. Besides these contour cuts, some other selection cuts have been used during the matching phase. The most stringent cut has been applied to kaons (because of the large pion contamination): only pads matched with single tracks have been chosen. For protons, instead, also pads with more than one track have been considered. In Figure 2 any particle that was not identified as a kaon or a proton (even if mismatched) was then considered to be a pion.

The plot in Figure 2 shows very clearly some clusters which correspond to the three different types of hadrons. A broad horizontal band stands out as well, which is due to background contamination accounted for by the mismatched tracks. At small momenta, it is possible to notice a distortion in the clusters, which then deviate towards larger masses. This is an effect of the energy loss in this momentum range. On the other hand, at large momenta the clusters become wider because the mass resolution decreases (especially as a consequence of the errors on the time of flight and track length determination, rather than those on the momentum).

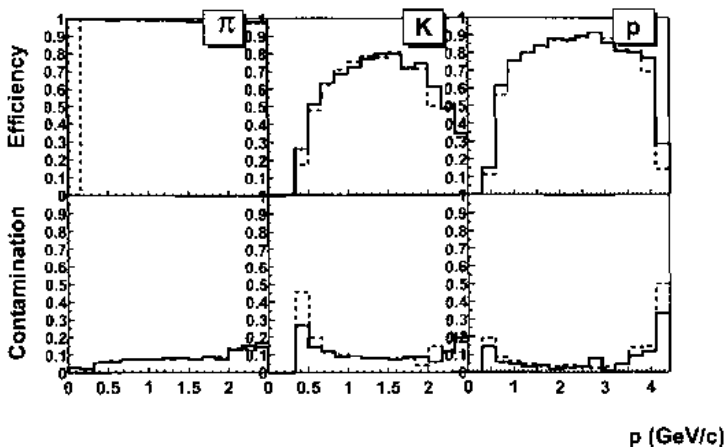


Figure 3: PID efficiencies and contaminations vs. momentum for primary charged particles of different species matched with fired TOF pads (100 HIJING events), tracked with $B = 0.2$ T (solid-line histograms) and $B = 0.4$ T (dashed-line histograms).

The negative mass values in Figure 2 correspond to negative square root arguments in the mass determination formula, due to the above-mentioned errors.

4.1.1 PID efficiency and contamination

Similarly to what is done for the track matching procedure, also for the particle identification (PID) step we can define an efficiency and a contamination:

$$\text{efficiency} = \frac{N_{id}^t(i)}{N(i)}, \quad \text{contamination} = \frac{N_{id}^w(i)}{N_{id}(i)}$$

where $N_{id}(i)$ is the number of identified particles of type i ($i = \pi, K, p$) and so it is the sum of two contributions, $N_{id}^t(i)$ and $N_{id}^w(i)$, that is, the number of i particles well-identified and mis-identified. $N(i)$ is, in turn, the total number of particles of type i in the $m - p$ scatter plot (reconstructed in the TPC, and then track-matched in the TOF).

Figure 3 shows the values of the efficiency and contamination obtained for 100 HIJING events both in the case of $B = 0.2$ T and $B = 0.4$ T. At large momenta, since the mass resolution decreases, the contamination increases, even though it remains low ($\leq 10\%$) up to $p \simeq 2$ GeV/c for pions and kaons, and up to $p \simeq 4$ GeV/c, for protons. This is a very important result, since it underlines the effectiveness of the method in the momentum range under study. On the other hand, at low momenta, where track mismatching becomes significant, the kaon and proton contaminations increase again.

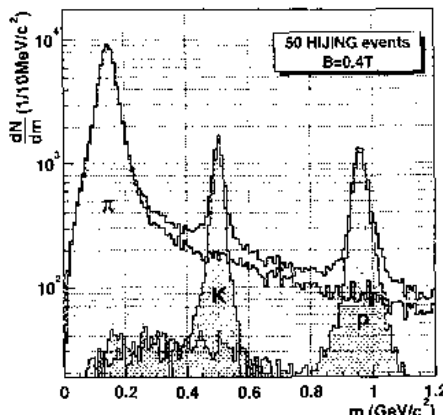


Figure 4: Reconstructed mass with the TOF detector (overall TOF system resolution: 120 ps) in the momentum range $0.5 \leq p \leq 2.5$ GeV/c, for 50 HIJING events at $B = 0.4$ T. The grey- and dashed-area histograms superimposed show the individual mass distributions of the true pions, kaons and protons associated with the fired TOF pads.

Figure 4 shows the reconstructed particle mass⁴ for TOF-identified primaries. The values of the overall efficiency and of the contamination for the three types of hadrons are given (both $B = 0.2$ T and $B = 0.4$ T have been taken into account) in table 2, relatively to the momentum ranges meaningful for them. In particular, the overall efficiency includes all the acceptance and efficiency factors involved in the analysis. Notwithstanding the uncertainties at the present stage, we can confidently conclude that in each Pb-Pb final state the ALICE TOF detector will be able to identify thousands of pions, and hundreds of kaons and protons, with low contamination in the momentum range exceeding ≈ 2 GeV/c for kaons, and extending up to ≈ 4 GeV/c for protons.

4.2 The “probability method”

Another method has been developed in order to identify the particles which have been tracked and matched to the TOF, the so-called “probability method”. This method has already been used in the STAR experiment at RHIC [13]. For each type of particle, starting from the appropriate Monte Carlo simulated distribution, it is possible to derive a probability density function (p.d.f.) based on a separation parameter, such as the mass. The probability to be a particle of type i having a mass m so depends on the values of

⁴Tracks with “negative” mass enter the histogram in correspondence to $|m|$.

Primary hadron	Momentum range	Overall efficiency	Contamination
π^\pm	(*) $p < 2.5$	63 (48)	7 (9)
K^\pm	(*) $p < 2.5$	14 (13)	13 (15)
$p(\bar{p})$	(*) $p < 4.5$	27 (24)	5 (7)
π^\pm	$0.5 < p < 2$	74 (72)	11 (12)
K^\pm	$0.5 < p < 2$	23 (21)	11 (12)
$p(\bar{p})$	$0.5 < p < 2$	37 (33)	5 (7)

Table 2: Overall PID efficiencies (%) and contaminations (%) in different momentum (GeV/c) ranges, relative to all primary hadrons generated in the $|\theta - 90^\circ| < 45^\circ$ region (100 HIJING events), tracked with $B = 0.2 \text{ T}$ and, in brackets, with $B = 0.4 \text{ T}$.
(*) [Identified pions, kaons and protons have respectively: $p \geq 0.15$ (0.2), 0.25 (0.3) and 0.35 (0.4) GeV/c , at $B = 0.2$ (0.4) T.]

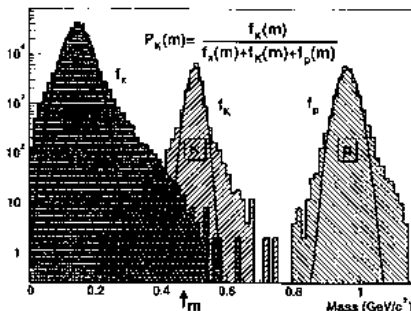


Figure 5: Examples of mass probability density functions for pions, kaons and protons, obtained as mass spectra of unambiguously TPC-TOF matched primary tracks with $0.5 \leq p \leq 2.5 \text{ GeV}/c$ (100 HIJING events at $B = 0.4 \text{ T}$). Superimposed, some Gaussian fits to guide the eye.

the three p.d.f.'s (electrons are excluded) at that particular m -value, $f_i(m)$, $i = \pi, K, p$. For example, this probability could be defined as:

$$P_i(m) = \frac{f_i(m)}{(f_\pi(m) + f_K(m) + f_p(m))}.$$

Each p.d.f. is normalized to the corresponding particle yield.

Figure 5 shows some examples of probability density functions obtained for simulated

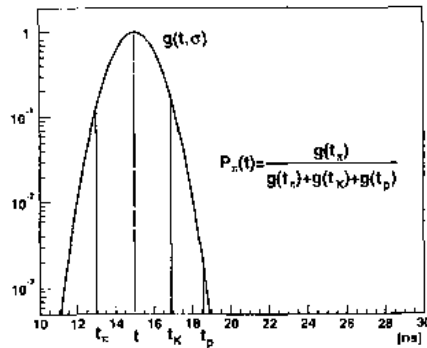


Figure 6: Example of flight-time probability density function. The standard deviation σ_{TOF} of this Gaussian function, centred at the measured track time t , has been enlarged by an arbitrary factor for the sake of clarity.

mass distributions. Obviously, the more different sets of mass distributions (corresponding to different appropriate momentum bins) are simulated, the more accurate the p.d.f.'s will be.

Since the p.d.f.'s as a function of the mass are not Gaussian (as a consequence of the mass determination formula (1)), another approach, based on the time of flight, may be preferable. In this case, for a track measured with a time of flight t , the probability to be a particle with mass m_i ($i = \pi, K, p$) depends on the now Gaussian p.d.f. $g(t_i)$ (with mean value equal to t and standard deviation σ_{TOF}) calculated at the time t_i derived from the momentum and the track length measurements with mass hypothesis m_i (see Fig. 6):

$$P_i(t) = \frac{g(t_i)}{(g(t_\pi) + g(t_K) + g(t_p))}.$$

Here a weighting procedure is applied to take into account the different particle yields.

Figure 7 shows the time-based probability as a function of the mass.

This kind of approach to the particle identification problem is extremely important, and could become even more powerful when combining the probability information from different sub-detectors providing PID with multidimensional distributions.

5 Conclusions

Since it has to suit and face extreme conditions (very high multiplicity, severe background level, etc.), the particle identification procedure for the TOF detector in the ALICE ex-

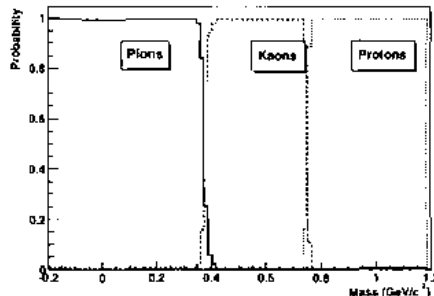


Figure 7: Time-based PID probability distributions versus mass, for pions, kaons and protons, corresponding to unambiguously TPC-TOF matched primary tracks with $0.5 \leq p \leq 2.5$ GeV/c (50 HIJING events at $B = 0.4$ T).

periment has to be very powerful. The method presented herein starts from a track matching procedure between the TPC and the TOF. This track matching, which is called "probe-track approach", is a compromise between statistical requirements and computational time, and has given satisfactory results even in the extreme conditions simulated for ALICE Pb-Pb collisions.

As regards the actual PID procedure, two different approaches have been discussed. The first, the so-called "contour method", is a two-dimensional treatment which works in the mass-momentum plane. Thanks to the TOF-MRPC technology, and especially to its extraordinary efficiency and time resolution, this method has shown to be very effective. The second approach is a "probability method": it relies on only one separation parameter (mass or time) and has given very good results as well.

It is obviously worth to say that PID efficiencies, contaminations and probabilities are influenced by and strongly depend on the model assumed. In particular, the Monte Carlo physics input acts as a bias especially for what concerns the particle ratios. Nevertheless, whenever the model is reasonable, the results obtained from simulations could safely be considered reliable.

References

- [1] ALICE Collaboration, Technical Proposal, CERN/LHCC/95-71.
- [2] B. Alessandro et al., ALICE Internal Note 2002-025.

- [3] ALICE Collaboration, Time of Flight System, Technical Design Report, CERN/LHCC 2000-12, ALICE TDR 8, 16 February 2000.
- [4] ALICE Collaboration, Answers to the Questions of LHCC Referees, CERN/ALICE, 5 May 2000.
- [5] ALICE Collaboration, Addendum to ALICE TDR 8, CERN/LHCC 2002-16, 24 April 2002.
- [6] ALICE Collaboration, Time Projection Chamber, Technical Design Report, CERN/LHCC 2000-001, ALICE TDR 7, 7 January 2000.
- [7] <http://AliSoft.cern.ch/offline>.
- [8] R. Brun, *et al.*, <http://root.cern.ch>.
- [9] R. Brun, *et al.*, GEANT3, CERN program library Q123.
- [10] X. N. Wang and M. Gyulassy, Phys. Rev. D44(1991) 3501;
X. N. Wang and M. Gyulassy, Phys. Rev. D45 (1992) 844;
X. N. Wang and M. Gyulassy, Comp. Phys. Comm. 83(1994) 307.
- [11] ALICE Collaboration, Transition Radiation Detector, Technical Design Report, CERN/LHCC 2001-21, ALICE TDR 9, 3 October 2001.
- [12] K. Adcox *et al.*, PHENIX Collaboration, Phys. Rev. Lett. 88, 242301 (2002).
- [13] <http://www.star.bnl.gov/comp/pkg/dev/StRoot/StPsdAmpMaker/doc>.

SUPERPOTENTIALS OF $\mathcal{N} = 1$ SUSY GAUGE THEORIES

B. M. GRIPAIOS

*Department of Physics - Theoretical Physics,
University of Oxford,*

1, Keble Road,

Oxford,

OX1 3NP,

United Kingdom.

E-mail: b.gripaios1@physics.ox.ac.uk

An introduction to recent advances in computing effective superpotentials of four dimensional $\mathcal{N} = 1$ SUSY gauge theories coupled to matter is presented. The correspondence with matrix models and two proofs of this are discussed and a novel derivation of the Veneziano-Yankielowicz superpotential for a pure gauge theory is given using the generalized Konishi anomaly. Re-printed from European Physical Journal C.

1. Introduction

This work provides a brief introduction to recent advances in the study of four-dimensional gauge theories with the minimal amount (that is $\mathcal{N} = 1$) of supersymmetry. We consider general theories of this type, with arbitrary gauge group coupled to matter in an arbitrary representation, and with an arbitrary superpotential for the matter. The aim is to compute the effective superpotential for the gauge superfields obtained by integrating out the matter. Minimising this effective superpotential then yields the quantum vacua of the theory. In doing so, one discovers two remarkable things. The first remarkable thing is that the ‘integrating out’ part, which involves evaluating Feynman diagrams in superspace, reduces to the computation of planar diagrams in a matrix model. That is, the entire dependence on (super)space ‘disappears’!¹ The second remarkable thing is that, having done the perturbative computation in this way to n loops, one finds (upon minimising the effective superpotential) that one has calculated the n -instanton correction to the vacuum structure. Thus, a *perturbative* computation leads to *non-perturbative* information about the physics!

Before we see how all of this comes about, let us make a rather simple, but nonetheless important remark about symmetries in physics in general. In any phys-

¹The disappearance is not a straightforward dimensional reduction however. If it were, the arguments presented here would hold in arbitrary dimensions; in fact they are specifically four-dimensional.

ical system, the presence of a symmetry (an invariance of the system) places a constraint on the possible dynamics of the system, and thus results in a simplification: in a sense, one of the reasons why we are so obsessed with symmetries in theoretical physics is because they simplify things. Ideally, one would like to consider systems with no symmetry at all. The set of such systems contains all more symmetric systems as a subset and so *general* statements made about *less* symmetric theories hold for all *more* symmetric theories. Unfortunately making such statements can be rather difficult.

Supersymmetries in gauge quantum field theories are no different. One can make general statements about gauge theories with no supersymmetry (for example the renormalisation group) and such statements are very powerful. What if we require our theory to have the *minimal* amount ($\mathcal{N} = 1$) of SUSY? Can we make even stronger general statements? Supersymmetry places rather strong constraints on a theory and we shall see (as we have claimed above) that it is possible to make stronger statements in this case. Moreover, because the statements apply to arbitrary $\mathcal{N} = 1$ theories, they apply equally to the subset of all theories with extended ($\mathcal{N} > 1$) SUSY, and it is interesting to see how results obtained previously in such theories (e.g. Seiberg-Witten duality in $\mathcal{N} = 2$ [1] and corollaries of Olive-Montonen duality in $\mathcal{N} = 4$ [2]) can be reproduced in the framework presented here [3].

We stress that although the methods apply to general minimally supersymmetric four-dimensional gauge theories, they do not tell us *everything* about such theories. A complete specification of the theory is given by the effective action; here one is only able to calculate the so-called *F*-terms (the effective superpotential) in the effective action. The Kähler, or *D*-terms (which lack the strong constraint of holomorphy) are not determined.

In the next section, we *sketch* two proofs [4, 5] of the gauge theory/matrix model correspondence (conjectured in [3]) and show how the superpotentials are calculated in each case. We then show that there are matter-independent (i.e. pure gauge) contributions to the effective superpotential which are undetermined. These contributions turn out to be non-perturbative and provide the bridge between the perturbative computation and the non-perturbative physics mentioned above. In section 3 we show that that these contributions can in fact be determined in this framework [6], and we do this.

2. The Gauge Theory/Matrix Model Correspondence

We employ $\mathcal{N} = 1$ superspace notations (see e.g. [7]). The gauge fields (and their superpartners) are written as components of a real vector superfield V ; by acting with superspace covariant derivatives, one can form the analogue of the gauge field strength, $W_\alpha \sim \bar{D}^2 e^{-V} D_\alpha e^V$ and the gauge-invariant glueball chiral superfield $S \sim \text{tr} W^\alpha W_\alpha$. The matter is represented by chiral superfields Φ with a tree-level

matter superpotential in the action which is polynomial in the matter superfields^b

$$\int d^4x d^2\theta W_{\text{tree}} = \int d^4x d^2\theta g_k \Phi^k. \quad (1)$$

Here, the coefficients g_k are called the tree-level matter couplings. We consider integrating out the matter Φ in some *background* glueball field S to obtain an effective superpotential W_{eff} , which depends on S , the g_k , and the gauge coupling (which we write in terms of the dimensionally-transmuted scale Λ).

It was claimed in the introduction that the perturbative computation of W_{eff} reduces to the evaluation of planar diagrams in a bosonic matrix model, and one might well ask how this can be demonstrated. Two proofs have appeared. The first [4] simply considers the contributing Feynman diagrams in superspace and shows that the momentum dependence of the bosons and their fermion superpartners cancels in all such diagrams. The only things left to consider are insertions of S , factors of g_k coming from the vertices, and numerical symmetry factors. One can show that these can be obtained from planar diagrams of the matrix model

$$\exp \frac{F(S)}{g_s^2} = \int d\phi \exp \frac{W_{\text{tree}}(\phi)}{g_s}, \quad (2)$$

where ϕ are $N' \times N'$ bosonic matrices and $S = g_s N'$. The restriction to planar diagrams is enforced by taking the 't Hooft limit: $N' \gg 1$ and $g_s \ll 1$, with S fixed. The action of the matrix model is given by the tree-level matter superpotential W_{tree} with the matter superfields Φ replaced by bosonic matrices ϕ .

To compute the perturbative computation to W_{eff} obtained by integrating out the matter (e.g. for gauge group $SU(N)$), one evaluates

$$N \frac{\partial F(S)}{\partial S}, \quad (3)$$

where $F(S)$ is the perturbative free energy of the matrix model in the planar limit.

The second proof [5] is rather different. One considers the effect of general chiral changes of variables $\delta\Phi = \epsilon f(\Phi, W_\alpha)$ in the path integral. These lead to anomalous Ward identities generalizing the Konishi anomaly [8, 9]. For example, the variation $\delta\Phi = \epsilon\Phi'(\Phi)$ yields

$$\left\langle \Phi' \frac{\partial W_{\text{tree}}}{\partial \Phi} - S \frac{\partial \Phi'}{\partial \Phi} \right\rangle = 0. \quad (4)$$

From the general chiral change of variables specified by f , one obtains a complete set of anomalous Ward identities for the chiral matter fields, and one can show that these are in one-to-one correspondence with the complete set of Ward identities in the matrix model (which, since the matrix model partition function (2) is just

^bOnly polynomials of degree three or less are renormalizable. However, since we claim that the computation of the effective superpotential reduces to a matrix model, the results must be independent of the momenta and any momentum cutoff. The results are thus independent of the UV completion of the theory and one is free to consider 'non-renormalizable' tree-level superpotentials.

an integral, correspond to integration by parts identities). This establishes the correspondence between the SUSY gauge theory and the bosonic matrix model.

Having established the correspondence, one can go on and calculate the effective superpotential for any given theory. To do this, one needs to solve the complete set of Ward identities to obtain the expectation values $\langle \Phi^k \rangle$ appearing in the tree-level matter superpotential in terms of the background glueball superfield S and the couplings g_k . The effective superpotential can then be determined from the partial differential equations

$$\frac{\partial W_{\text{eff}}}{\partial g_k} = \langle \Phi^k \rangle, \quad (5)$$

which follow from standard supersymmetry and holomorphy arguments.

We note that these partial differential equations only specify the effective superpotential up to a term which is independent of the matter couplings g_k , but which may depend on both S and the gauge coupling scale Λ . This term must contain any contribution to the effective superpotential coming from the *pure* gauge theory *without* matter. So let us ask the question: is there a pure gauge theory contribution? It turns out that there is, as was shown many years ago by Veneziano and Yankielowicz [10, 11] using the $U(1)_R$ symmetry of the pure gauge theory. For the gauge group $SU(N)$, for example, the pure gauge theory superpotential is

$$W_{\text{eff}}(S, \Lambda) = N \left(-S \log \frac{S}{\Lambda^3} + S \right). \quad (6)$$

Such terms are non-perturbative. One way to see this is to minimise W_{eff} with respect to S . This reproduces the vacuum condensate $S^N = \Lambda^{3N}$, due to (non-perturbative) instantons [12]. In the next section, we show how such terms can be derived using the generalized Konishi anomaly in the presence of matter discussed above [6]. This then renders the above approach self-contained, as well as providing an independent derivation of the Veneziano-Yankielowicz terms.

Before doing so, one might ask where the missing terms are hidden in the perturbative approach using Feynman diagrams. One might assume that they correspond to diagrams with gauge superfields in the loops; this is not really correct, since the missing terms are non-perturbative and thus cannot show up in any diagram. Intriguingly, these terms can be generated by the measure of the matrix model (i.e. the volume of the gauge group) [3, 13], though it is not at all clear why.

3. Pure Gauge Terms

In order to derive the pure gauge theory contributions, we determine the effective superpotential in the case where the matter sector consists of F flavours of ‘quarks’ transforming in the fundamental representation of the gauge group, which we take to be $SU(N)$ (though the argument can be applied to any classical Lie group). Furthermore, we choose a tree-level superpotential in which the quarks can have either

zero or non-zero classical expectation values at the minima. If a quark has a non-zero vev, then since the quarks transform non-trivially under the gauge group, the gauge group must be spontaneously broken via the Higgs mechanism. By putting each of the F quarks at zero or non-zero minima, we can *engineer* the gauge symmetry breaking such that the unbroken gauge group is anything from $SU(N)$ down to $SU(N - F)$. We then solve the Konishi anomaly Ward identities (4) and the resulting partial differential equations (5), determining the effective superpotential in each vacuum, up to a constant term (by ‘constant’ we mean ‘independent of the tree-level matter couplings’).

The tree-level matter couplings are free parameters in the theory. We vary them such that both the quark masses and the Higgs vevs (which determine the masses of the massive gauge bosons) become large. In that limit, the massive matter decouples from the unbroken low energy gauge group, and the effective superpotential contains a sum of contributions from the decoupled matter and the low energy gauge group. Once we have identified the contribution of the massive matter and discarded it, we are left with the superpotential of the low energy gauge group. This includes the constant term.

Now any two distinct vacua have different unbroken gauge groups, but the same constant term. If we subtract the two superpotentials (with the massive matter discarded), the constant cancels and we are left with a difference equation for the pure gauge theory superpotential. The solution to this difference equation yields precisely the Veneziano-Yankielowicz terms (6). To determine the constant term in any theory, one then demands that $W_{\text{eff}}(S, g_k, \Lambda)$ reproduces the correct decoupled contributions of the unbroken gauge group and massive matter in any vacuum in the massive limit [14]. Incidentally, the fact that the matching in one vacuum correctly reproduces the superpotential in all vacua justifies *a posteriori* the assumption that the constant term is the same for each vacuum branch.

Having explained the argument, let us now carry it out. Since quarks are Dirac fermions and chiral supermultiplets contain Weyl fermions, we represent F flavours of quarks by F chiral superfields Q_i transforming in the fundamental representation of $SU(N)$ and a further F chiral superfields \tilde{Q}^j transforming in the anti-fundamental representation. The tree-level matter superpotential is written in terms of the gauge invariant mesons $M_i^j = Q_i \tilde{Q}^j$ as

$$W_{\text{tree}} = m \text{tr} M - \lambda \text{tr} M^2. \quad (7)$$

The classical vacua are then

$$m M_i^j - 2\lambda M_i^k M_k^j = 0, \quad (8)$$

with F_- eigenvalues at $M_i^j = 0$ and $F_+ = F - F_-$ eigenvalues at $M_i^j = m/2\lambda$. If M_i^j has a non-zero vev, then so have Q_i and \tilde{Q}^j , and the gauge symmetry is broken. The low energy gauge group is thus broken down to $SU(N - F_+)$. The quantum

theory has the Konishi anomaly and the classical vacua are modified to (4)

$$m\langle M_i^j \rangle - 2\lambda\langle M_i^k M_k^j \rangle = \delta_i^j S, \quad (9)$$

with F_{\pm} eigenvalues at

$$\langle M_i^j \rangle = \frac{m}{4\lambda} \left(1 \pm \sqrt{1 - \frac{8\lambda S}{m^2}} \right). \quad (10)$$

The partial differential equations following from holomorphy and supersymmetry are [5]

$$\begin{aligned} \frac{\partial W_{\text{eff}}}{\partial m} &= \langle \text{tr} M \rangle, \\ \frac{\partial W_{\text{eff}}}{\partial \lambda} &= -\langle \text{tr} M^2 \rangle. \end{aligned} \quad (11)$$

We shall not write here the expression for the effective superpotential W_{eff} which is obtained by integrating these equations (it is rather cumbersome). Taking the limit of W_{eff} in which the quark mass m and Higgs vev $\sqrt{m/2\lambda}$ become large and subtracting the superpotentials for the vacua in which the number of Higgsed quarks is $F_{1,2}$, one obtains

$$W_{\text{eff},1} - W_{\text{eff},2} \rightarrow (F_1 - F_2) \frac{m^2}{4\lambda} + (F_1 - F_2) \left[S \log \frac{S}{m^2/2\lambda} - S \right]. \quad (12)$$

The first term represents the decoupled matter: it is given (according to the non-renormalization theorem) by the classical expectation value of W_{tree} . The second term must therefore represent the contribution of the low energy pure gauge group $SU(N - F_{1,2})$.^c It seems peculiar that what we have identified as the superpotential of the low energy gauge group contains the matter couplings m and λ . However, these are precisely the factors needed to convert the $SU(N)$ gauge coupling scale Λ to the $SU(N - F_{1,2})$ scales $\Lambda_{1,2}$ via the scale-matching relation

$$\Lambda_1^{3(N-F_1)} \left(\frac{m^2}{2\lambda} \right)^{F_1} = \Lambda^{3N-F} m^F = \Lambda_2^{3(N-F_2)} \left(\frac{m^2}{2\lambda} \right)^{F_2}. \quad (13)$$

This relation comes from requiring that the coupling constants of the high energy theory (with dynamic matter) and the low energy theory (with matter integrated out) match at the Higgs and quark mass scales (see e.g. [15]). Replacing the matter couplings by the appropriate gauge coupling scales in this way (and discarding the massive matter) leads to the difference equation

$$\begin{aligned} W_{\text{eff},1} - W_{\text{eff},2} &= \\ (N - F_1) \left(-S \log \frac{S}{\Lambda_1^3} + S \right) - (N - F_2) \left(-S \log \frac{S}{\Lambda_2^3} + S \right), \end{aligned} \quad (14)$$

^cThere is a subtlety here: the glueball superfield S includes the massive gauge bosons, which should be integrated out by replacing them with their vevs. However, in the decoupled limit, the massive gauge bosons have zero vevs, so the field S is equivalent to the glueball superfield of the low energy gauge group once the massive gauge bosons have been integrated out.

with solution

$$W_{\text{eff}}(S, \Lambda) = N \left(-S \log \frac{S}{\Lambda^3} + S \right) + f(S). \quad (15)$$

Here, $f(S)$ is an arbitrary function of S alone; it is independent of all other parameters. On dimensional grounds, $f(S) \propto S$ and one sees that the ambiguity in f (which can be re-written as a pure number multiplying Λ^{3N}) corresponds to the freedom to choose a renormalisation group scheme [15].

4. Discussion

The methods summarised above provide a very powerful framework in which to study gauge theories with $N = 1$ SUSY, and it is certainly of interest to go on and study the vacuum structure and phases of specific models.

More general extensions to this work include the question of whether similar results hold in dimensions other than four [16], the extension to supergravity (rather than supergauge) backgrounds [3, 17–20] and whether dynamical breaking of supersymmetry may be studied in this framework.

Acknowledgement

The author is supported by a PPARC studentship.

References

1. N. Seiberg and E. Witten, *Electric-magnetic duality, monopole condensation, and confinement in $n=2$ supersymmetric Yang-Mills theory*, *Nucl. Phys.* **B426** (1994) 19–52, [[hep-th/9407087](#)].
2. C. Montonen and D. I. Olive, *Magnetic monopoles as gauge particles?*, *Phys. Lett.* **B72** (1977) 117.
3. R. Dijkgraaf and C. Vafa, *A perturbative window into non-perturbative physics*, [hep-th/0208048](#).
4. R. Dijkgraaf, M. T. Grisaru, C. S. Lam, C. Vafa, and D. Zanon, *Perturbative computation of glueball superpotentials*, [hep-th/0211017](#).
5. F. Cachazo, M. R. Douglas, N. Seiberg, and E. Witten, *Chiral rings and anomalies in supersymmetric gauge theory*, *JHEP* **12** (2002) 071, [[hep-th/0211170](#)].
6. B. M. Gripaios and J. F. Wheater, *Veneziano-Yankielowicz superpotential terms in $N = 1$ SUSY gauge theories*, [hep-th/0307176](#).
7. S. J. Gates, M. T. Grisaru, M. Rocek, and W. Siegel, *Superspace, or one thousand and one lessons in supersymmetry*, *Front. Phys.* **58** (1983) 1–548, [[hep-th/0108200](#)].
8. K. Konishi, *Anomalous supersymmetry transformation of some composite operators in SQCD*, *Phys. Lett.* **B135** (1984) 439.
9. K.-i. Konishi and K.-i. Shizuya, *Functional integral approach to chiral anomalies in supersymmetric gauge theories*, *Nuovo Cim.* **A90** (1985) 111.
10. G. Veneziano and S. Yankielowicz, *An effective Lagrangian for the pure $N=1$ supersymmetric Yang-Mills theory*, *Phys. Lett.* **B113** (1982) 231.
11. T. R. Taylor, G. Veneziano, and S. Yankielowicz, *Supersymmetric QCD and its massless limit: An effective Lagrangian analysis*, *Nucl. Phys.* **B218** (1983) 493.

12. V. A. Novikov, M. A. Shifman, A. I. Vainshtein, and V. I. Zakharov, *Instanton effects in supersymmetric theories*, *Nucl. Phys.* **B229** (1983) 407.
13. H. Ooguri and C. Vafa, *Worldsheet derivation of a large N duality*, *Nucl. Phys.* **B641** (2002) 3–34, [[hep-th/0205297](#)].
14. A. Brandhuber, H. Ita, H. Nieder, Y. Oz, and C. Romelsberger, *Chiral rings, superpotentials and the vacuum structure of $N = 1$ supersymmetric gauge theories*, [hep-th/0303001](#).
15. J. Terning, *Tasi-2002 lectures: Non-perturbative supersymmetry*, [hep-th/0306119](#).
16. R. Dijkgraaf and C. Vafa, *$N = 1$ supersymmetry, deconstruction, and bosonic gauge theories*, [hep-th/0302011](#).
17. A. Klemm, M. Marino, and S. Theisen, *Gravitational corrections in supersymmetric gauge theory and matrix models*, *JHEP* 03 (2003) 051, [[hep-th/0211216](#)].
18. R. Dijkgraaf, A. Sinkovics, and M. Temurhan, *Matrix models and gravitational corrections*, [hep-th/0211241](#).
19. J. R. David, E. Gava, and K. S. Narain, *Konishi anomaly approach to gravitational F -terms*, [hep-th/0304227](#).
20. B. M. Gripaios, *Superpotentials of glueball and supergravity backgrounds*, to appear.

Measurement of the Proton Structure Function F_2 in QED Compton Scattering at HERA

V. Lendermann

Deutsches Elektronen-Synchrotron (DESY)

Notkestr. 85, D-22607 Hamburg, Germany; e-mail: victor@mail.desy.de

Abstract. QED Compton scattering at HERA is proposed for a measurement of the proton structure function F_2 at low momentum transfers Q^2 . It is shown that the analysis of inelastic QED Compton events allows the extension of present HERA structure function measurements to a kinematic domain, which up to now was only accessed in fixed target data. Preliminary results of such a measurement performed by the H1 Collaboration are presented. The results are in good agreement with the measurements from fixed target experiments wherever they overlap.

PACS: not given

1 Introduction

Measurements of deep inelastic lepton-proton scattering (DIS) provide information which is crucial to our understanding of proton structure and which has played a decisive role in the development of the theory of strong interactions, Quantum Chromodynamics (QCD). Since the discovery of Bjorken scaling [1] and its violation [2, 3] at fixed target experiments, much progress has been made in extending the kinematic range of measurements in terms of the Bjorken variable x and the negative four-momentum transfer squared Q^2 . In particular, the H1 and ZEUS experiments, running since 1992 at the HERA ep collider, have shown that the Q^2 evolution of the proton structure function $F_2(x, Q^2)$ is well described by perturbative QCD throughout a wide range in x and Q^2 [4–7]. However, at small Q^2 deviations from pQCD predictions are observed [7, 8], indicating the transition into a regime in which non-perturbative effects dominate and the data can only be described by phenomenological models such as those derived from the Regge approach [9].

In order to study this non-perturbative regime, the structure function F_2 has been measured at very low values of Q^2 , which are accessible at HERA via special devices mounted close to the outgoing electron beam direction [8], thus facilitating measurements of the scattered electron at very low angles. These devices, however, do not cover the transition region around $Q^2 \sim 1 \text{ GeV}^2$, which up to now has only been investigated using “shifted vertex” [10, 11] and Initial State Radiation [12, 13] data. In this article a new approach for an F_2 measurement in the low Q^2 domain is discussed, which utilises ep data with wide angle hard photon radiation, so called QED Compton events. First results of such a measurement performed by the H1 Collaboration are presented.

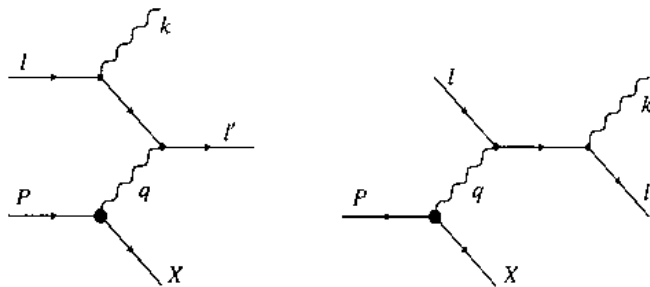


Fig. 1. Lowest order Feynman diagrams for the radiative process $ep \rightarrow e\gamma X$ with photon emission from the electron line. l, P represent the four-momenta of the incoming electron and the incoming proton, while l' , k and X are the four-momenta of the scattered electron, the radiated photon and the hadronic final state, respectively

2 QED Compton Scattering

Radiative processes in ep scattering, as depicted in Fig. 1, may be split into three different classes [14, 15] with (i) the bremsstrahlung or Bethe-Heitler process corresponding to small virtualities of both the exchanged electron and the exchanged photon, (ii) the QED Compton (QEDC) process with a low exchanged photon and a large exchanged electron virtuality and finally (iii) the radiative DIS process where the photon is collinear either with the incoming (Initial State Radiation, ISR) or the outgoing (Final State Radiation, FSR) electron. All three classes correspond to distinct experimental signatures. For the QEDC scattering process the final state topology is given by an azimuthal back-to-back configuration of the outgoing electron and photon detected under rather large scattering angles. In this configuration their transverse momenta balance such that very low values of the exchanged photon virtuality Q^2 are experimentally accessible.

To correctly describe the process $ep \rightarrow e\gamma X$ the standard kinematic variables x and Q^2 , used to describe inclusive deep inelastic scattering, have to be redefined in order to account for the additional photon in the final state

$$Q^2 = -q^2 = -(l - l' - k)^2, \quad x = \frac{Q^2}{2P \cdot (l - l' - k)}. \quad (1)$$

Here l and P are the four-momenta of the incoming electron and the incoming proton, and l' and k represent the momenta of the scattered electron and the radiated photon, respectively (Fig. 1), and $s = (l + P)^2$ is the ep centre-of-mass energy squared. On the other hand, the definitions remain unchanged if these variables are calculated using the four-momentum of the hadronic final state, X :

$$Q^2 = -q^2 = -(X - P)^2, \quad x = \frac{Q^2}{2P \cdot (X - P)}. \quad (2)$$

Three further non-trivial degrees of freedom have to be taken into account for a full description of the differential QEDC scattering cross section. In the

formalism presented in [14] the Lorentz invariant scale variable $x_\gamma = (q \cdot l)/(P \cdot l)$ and the scattering solid angle Ω^* defined in the centre-of-mass frame of the virtual Compton process and encapsulating two degrees of freedom are employed for this purpose. The cross section is then given by [14]

$$\frac{d^4\sigma^{ep \rightarrow e\gamma X}}{dx dx_\gamma dQ^2 d\Omega^*} = f_{\gamma^*/p}^T(x, x_\gamma, Q^2) \left[\frac{d\sigma}{d\Omega^*} \right]^T + f_{\gamma^*/p}^L(x, x_\gamma, Q^2) \left[\frac{d\sigma}{d\Omega^*} \right]^L, \quad (3)$$

where $[d\sigma/d\Omega^*]^{T,L}$ are the differential cross sections of the process $e\gamma^* \rightarrow e\gamma$ for transverse and longitudinal polarised photons, fully calculable in the framework of QED [14], and $f_{\gamma^*/p}^{T,L}$ represent the corresponding virtual photon spectra, which may be expressed in terms of the photo-absorption cross sections $\sigma_{\gamma^* p}^{T,L}$. Depending on the value of the invariant mass of the hadronic final state, $W = [Q^2(1-x)/x + m_p^2]^{1/2}$, one has to consider three separate contributions, in order to specify $\sigma_{\gamma^* p}^{T,L}$:

1. Elastic scattering, for which the proton stays intact ($W = m_p$, $x = 1$). This channel is well measured, and the cross section is given by the electric and magnetic form factors G_E and G_M ;
2. Resonance production, where the total mass of the hadronic final state X lies in the range $m_p + m_\pi \lesssim W \lesssim 2 \text{ GeV}$;
3. Continuum inelastic scattering at $W \gtrsim 2 \text{ GeV}$. In this region the $\gamma^* p$ cross section is defined through the structure functions F_2 and F_L .

It is proposed in [16], to employ the latter contribution for a measurement of F_2 .

3 Experimental Technique

The H1 measurement is performed on 9.25 pb^{-1} of $e^+ p$ data with centre-of-mass energy $\sqrt{s} = 301 \text{ GeV}$, which were collected at HERA in 1997.

The outgoing electron and photon in QEDC events are selected in the H1 detector [17] by requiring two energy depositions (clusters) in the electromagnetic part of the backward¹ lead-fibre calorimeter SpaCal [18]. The Backward Drift Chamber (BDC) [19] situated in front of the SpaCal is employed as a pre-shower detector to increase the precision of the cluster position measurement for electrons and converted photons. In events with the electron scattered in the inner part of the SpaCal, the Backward Silicon Tracker (BST) [20] is used to measure the electron polar angle and to reconstruct the interaction vertex position. In events in which the electron is scattered out of the BST acceptance, the Central Inner Proportional Chamber (CIP) [17] is employed in conjunction with BDC and SpaCal to determine the vertex coordinates. The hadronic final state is measured in the Liquid Argon Calorimeter (LAr) [17].

¹The z axis of the right-handed coordinate system used by H1 is defined to lie along the direction of the incident proton beam and the origin to be at the nominal ep interaction vertex. The backward direction is thus defined through $z < 0$

4 Event Simulation

The cross section expression (3) is implemented in the COMPTON Monte Carlo event generator [14, 21]. The program also calculates higher order corrections for Initial State Radiation in the peaking approximation [22, 23]. However, as this generator was primarily written for use in analyses of elastic QECD events, in the original version a rather crude approach is employed to describe the resonance region and only simple scale invariant F_2 parameterisations are used to model the continuum inelastic domain. Furthermore, no hadronisation of the final state X is performed.

For the investigation of inelastic QECD events a new version of the COMPTON generator was developed [24] which includes detailed parameterisations for the resonance [25] and the continuum [26] regions. In addition, several packages for a complete simulation of the hadronic final state have been interfaced to the program. For the present study the SOPHIA package [27] is used in the range of low Q^2 ($Q^2 < 2 \text{ GeV}$) or low masses of the hadronic final state ($W < 5 \text{ GeV}$), while the Quark Parton Model with subsequent Lund string fragmentation [28] is employed at higher W and higher Q^2 .

The SOPHIA model provides a minimum bias description of photoproduction processes reproducing a large set of available data. The simulation includes production of major baryon resonances, direct pion production, multiparticle production based on the Dual Parton Model [29] with subsequent Lund string fragmentation, as well as the diffractive production of light vector mesons.

5 Background Processes

A prominent background to inelastic QECD scattering arises from inclusive DIS events in which one particle from the hadronic final state (typically a π^0) fakes the outgoing photon, producing a cluster in the electromagnetic SpaCal. Such events are modelled using the DJANGO MC generator [30]. At high $y = Q^2/xs$, where the hadronic final state lies mostly in the hemisphere of the scattered electron and photon, this process dominates the QECD signal, hampering a clean QECD event selection.

Another source of significant background is Deeply Virtual Compton Scattering (DVCS), in which the final state photon is produced in the virtual photon proton collision. DVCS and QECD are indistinguishable experimentally, and differ only in the kinematic distributions of the outgoing electron and photon. Nevertheless, both processes can be simulated separately, as the interference between them does not influence the energy and polar angle distributions of the final state particles in the leading twist approximation. Elastic DVCS events were simulated by the TINTIN generator [31] and the cross section was normalised to the H1 results [32]. At present there is neither a theoretical prediction, nor a measurement for the inelastic DVCS cross section. The ratio of the inelastic to elastic scattering cross section was therefore estimated experimentally to be of a similar size to that for diffractive vector meson electroproduction.

Further background sources considered are comparatively small.

6 Details of the Measurement

The phase space covered by a QEDC MC sample after the experimental event selection is shown in Fig. 6. Compared to the kinematic range accessed at HERA via standard deep inelastic scattering, the QEDC events clearly extend to lower Q^2 . For inclusive DIS the outgoing electron is not detected for such low values of Q^2 as it is scattered at small angles, escaping unseen through the beam pipe. QEDC events, however, with the electron and photon in the final state balancing in transverse momentum, reach into the transition region below $Q^2 < 1.5 \text{ GeV}^2$, which otherwise is only accessed through ISR [12, 13] (not shown), shifted vertex [10, 11] and BPT [8] data. However, these latter data do not extend the low $Q^2 F_2$ measurements to such high x as QEDC events. It is therefore the range of medium to high x which is of special interest when analysing QEDC scattering.

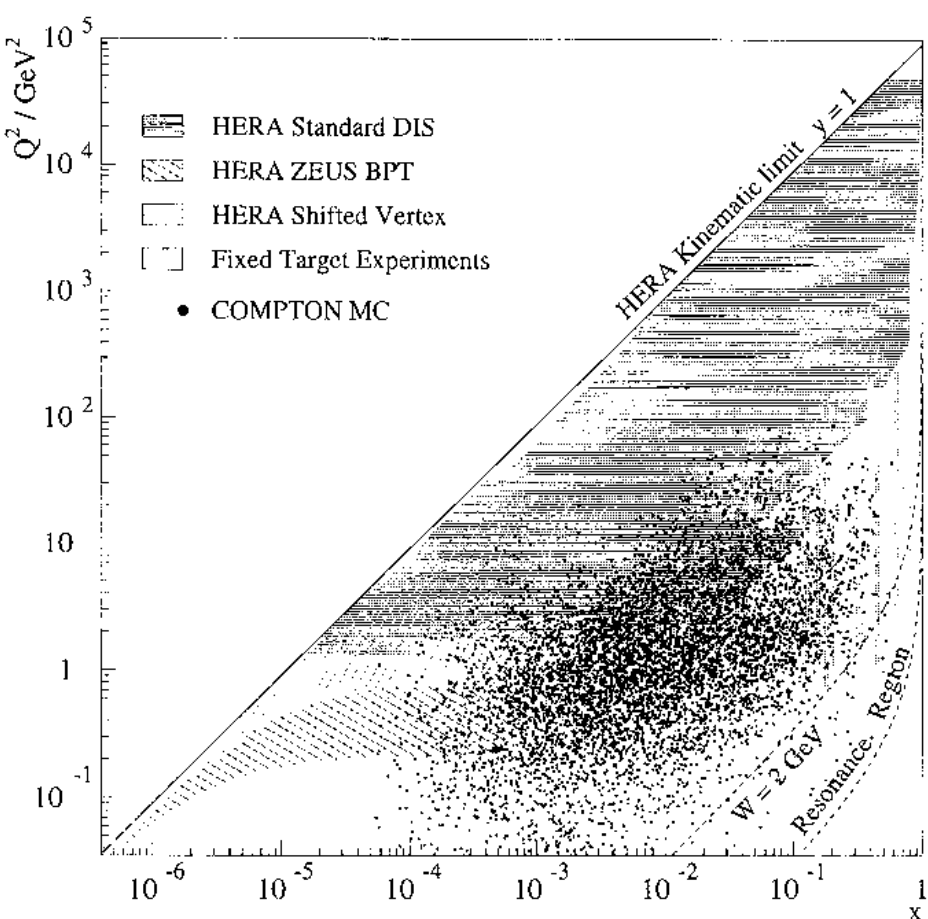


Fig. 2. Kinematic domain of inelastic QED Compton events in comparison to the regions covered by inclusive DIS measurements at HERA and fixed target experiments

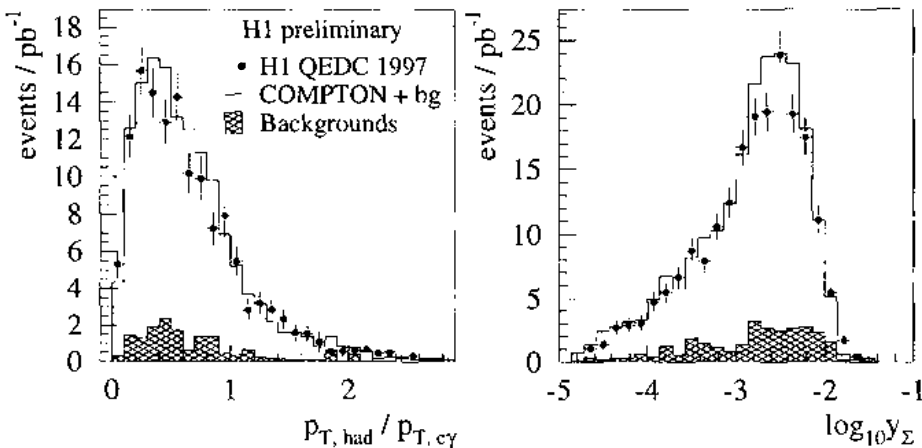


Fig. 3. a) Ratio of the total measured transverse momentum of hadrons to the total transverse momentum of the $e\gamma$ system; b) y_Σ distribution. H1 data are depicted by the closed circles. The solid histogram represents the sum of COMPTON MC events with all background contributions added. The hatched histogram denotes the sum of all background contributions

In QEDC events at HERA the kinematic variables Q^2 , x and y can be reconstructed using the parameters of the outgoing electron and photon or those of the hadronic final state. However, for the kinematic range in question, the variables x and y cannot be determined solely from the measured electron and photon four-momenta, since the resolution deteriorates as $1/y$. Therefore, these variables are reconstructed using the so-called Sigma method [33] which employs both hadrons as well as the electron and the photon. As low y corresponds to low scattering angles of the final state hadrons, one of the main challenges for the analysis is a good understanding of the hadronic energy flow and the acceptance corrections in the forward region of the detector. This requires a good modelling of hadronisation processes at low invariant masses W , for which the SOPHIA package (see Sect. 4) is employed in this analysis.

The quality of the description of the hadronic final state, comprising both the hadron distribution modelled by the SOPHIA package and the subsequent simulation of the detector response, is illustrated in Fig. 3a, in which the ratio of the total transverse momentum of measured hadrons $p_{t,\text{had}}$ to the total transverse momentum of the $e\gamma$ system $p_{t,e\gamma}$ is plotted. The simulation provides a very good description of data. Due to losses in the very forward region, outside the acceptance of the LAr calorimeter, the distribution peaks at values smaller than one. One should note, however, that for the calculation of the kinematic variables y and x with the Sigma method, the total $E - p_z$ of hadrons is used, which is much less sensitive to the losses in the beam pipe than the transverse momentum.

The event distribution in y shown in Fig. 3b demonstrates the good quality of both the hadronic simulation and the cross section description given by the COMPTON program down to the lowest y values, even beyond the range used

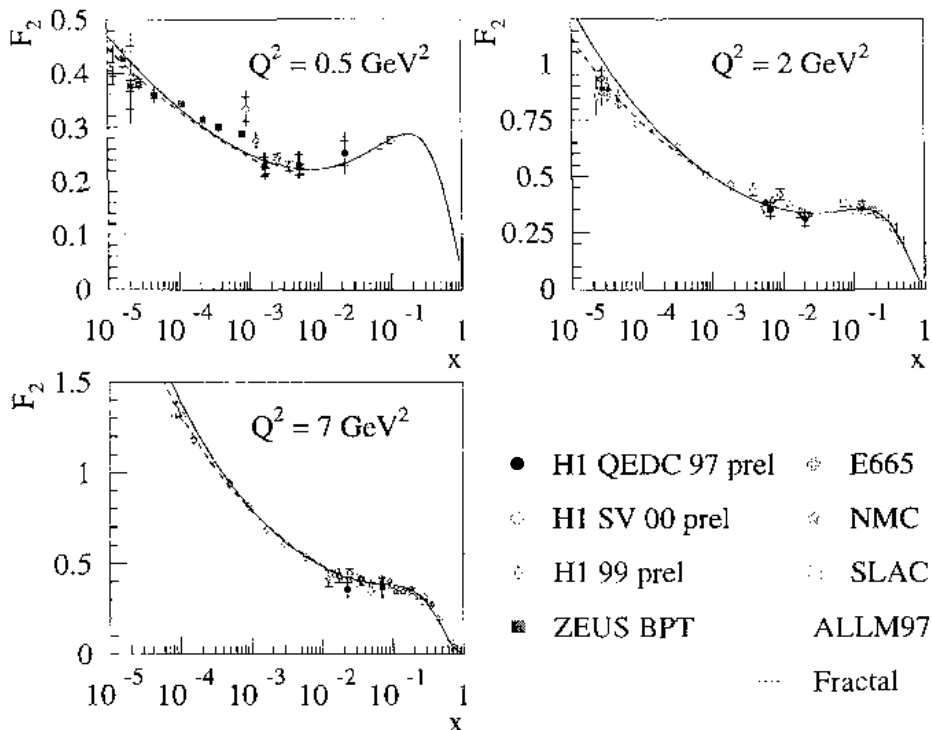


Fig. 4. Preliminary results of an F_2 measurement in QED Compton scattering by H1 (closed circles), compared with other measurements at HERA (closed squares [8], open diamonds [34] and open circles [35]) and fixed target experiments (open squares [36], open stars [37] and open crosses [38]). The solid line depicts the ALLM97 parameterisation [26], while the dashed line represents a 'Fractal' fit [39], which is plotted in the range $y > 0.003$

for the measurement.

7 First Results of the H1 Measurement

The preliminary F_2 values measured in QED Compton scattering by H1 are shown in Fig. 4 as a function of x at fixed Q^2 and compared to other HERA [8, 34, 35] and fixed target [36–38] data. Both the statistical and the systematic errors of the H1 measurement lie in the range 8–13% such that the total error lies between 12% and 18%.

The present analysis extends the kinematic range of HERA at very low Q^2 towards higher x values, thus complementing standard inclusive and shifted vertex measurements. The region covered mostly overlaps with the domain of fixed target experiments. A good agreement with their results is observed.

References

1. E. D. Bloom *et al.* [SLAC-MIT collaboration], Phys. Rev. Lett. **23** (1969) 930
2. D. J. Fox *et al.*, Phys. Rev. Lett. **33** (1974) 1504
3. J. G. de Groot *et al.*, Z. Phys. C **1** (1979) 143
4. C. Adloff *et al.* [H1 Collaboration], Eur. Phys. J. C **21** (2001) 33
5. C. Adloff *et al.* [H1 Collaboration], Eur. Phys. J. C **30** (2003) 1
6. S. Chekanov *et al.* [ZEUS Collaboration], Eur. Phys. J. C **21** (2001) 443
7. C. Adloff *et al.* [H1 Collaboration], Phys. Lett. B **393** (1997) 452
8. J. Breitweg *et al.* [ZEUS Collaboration], Phys. Lett. B **487** (2000) 53
9. P. D. Collins, *An Introduction To Regge Theory And High-Energy Physics*, Cambridge, 1977, 445p
10. M. Derrick *et al.* [ZEUS Collaboration], Z. Phys. C **69** (1996) 607
11. C. Adloff *et al.* [H1 Collaboration], Nucl. Phys. B **497** (1997) 3
12. ZEUS Collaboration, contributed paper to International Conference on High Energy Physics, ICHEP 2002, Amsterdam, abstract **771**
13. H1 Collaboration, contributed paper to International Conference on High Energy Physics, ICHEP 2002, Amsterdam, abstract **976**
14. A. Courau and P. Kessler, Phys. Rev. D **46** (1992) 117
15. T. Ahmed *et al.* [H1 Collaboration], Z. Phys. C **66** (1995) 529
16. V. Lendermann, H.-C. Schultz-Coulon and D. Wegener, accepted by Eur. Phys. J. C, DESY-03-085, hep-ph/0307116
17. I. Abt *et al.* [H1 Collaboration], Nucl. Instrum. Meth. A **386** (1997) 310 and 348
18. R. D. Appuhn *et al.* [H1 SpaCal Group], Nucl. Instrum. Meth. A **374** (1996) 149, A **382** (1996) 395 and A **386** (1997) 397
19. B. Schwab, Doctoral Thesis, Ruprecht Karl University of Heidelberg, 1996
20. W. Eick *et al.*, Nucl. Instrum. Meth. A **386** (1997) 81
21. T. Carli, A. Courau, S. Kermiche and P. Kessler, in **Proceedings of the Workshop "Physics at HERA", Hamburg, 1991**, DESY, 1992, Vol. 2, p. 902 and Vol. 3, p. 1468
22. E. Etim, G. Pancheri and B. Touschek, Nuovo Cim. B **51S10** (1967) 276
23. G. Pancheri, Nuovo Cim. B **60S10** (1969) 321
24. V. Lendermann, Doctoral Thesis, University of Dortmund, 2002
25. F. W. Brasse *et al.*, Nucl. Phys. B **110** (1976) 413
26. H. Abramowicz and A. Levy, DESY-97-251, hep-ph/9712415
27. A. Mücke *et al.*, Comput. Phys. Commun. **124** (2000) 290
28. T. Sjöstrand *et al.*, Comput. Phys. Commun. **135** (2001) 238
29. A. Capella, U. Sukhatme, C. Tan and J. Tran Thanh Van, Phys. Rept. **236** (1994) 225
30. G. A. Schuler and H. Spiesberger, in *Proceedings of the Workshop "Physics at HERA", Hamburg, 1991*, DESY, 1992, Vol. 3, p. 1419
31. R. Stamen, Doctoral Thesis, University of Dortmund, 2001
32. C. Adloff *et al.* [H1 Collaboration], Phys. Lett. B **517** (2001) 47
33. U. Bassler and G. Bernardi, Nucl. Instrum. Meth. A **361** (1995) 197
34. H1 Collaboration, contributed paper to the International Europhysics Conference on High Energy Physics, EPS 2001, Budapest; Abstract **799**
35. H1 Collaboration, contributed paper to the International Europhysics Conference on High Energy Physics, EPS 2003, Aachen; Abstract **082**
36. L. W. Whitlow *et al.*, Phys. Lett. B **282** (1992) 475
37. M. Arneodo *et al.* [New Muon Collaboration], Nucl. Phys. B **483** (1997) 3
38. M. R. Adams *et al.* [E665 Collaboration], Phys. Rev. D **54** (1996) 3006
39. T. Laštovička, Eur. Phys. J. C **24** (2002) 529

Yang-Mills effective action at high temperature

M. Oswald

Niels Bohr Institute, Blegdamsvej 17, 2100 Copenhagen, Denmark:
e-mail: oswald@alf.nbi.dk

Abstract. Yang-Mills theory undergoes a transition from a confined to a deconfined phase in the intermediate temperature regime, where perturbation theory fails. In order to approach this phase transition from the high temperature side we study the effective action for the eigenvalues of the order parameter, the Polyakov loop, in the whole range of its possible variation. By means of a covariant derivative expansion we integrate out fast varying quantum fluctuations around background gluon fields and assume that these are slowly varying, but that the amplitude of A_4 is arbitrary. Our results can be used to study correlation functions of the order parameter at high temperatures.

PACS: 11.15.-q, 11.10.Wx, 11.15.Tk

1 Introduction

The equilibrium behavior of quantum field theories at finite temperature is described through the grand canonical partition function. This introduces a compactification of the imaginary time direction in the Euclidean formulation of the theory. The partition function of a statistical system is defined as a sum over physical states n :

$$Z = \sum_{n_{\text{phys}}} \langle n | e^{-\beta \mathcal{H}} | n \rangle, \quad (1)$$

where $\beta = 1/T$ and \mathcal{H} is the Hamiltonian of the system. In Yang-Mills theory physical states are those which are gauge-invariant, i.e. invariant under gauge transformation of the gluon fields:

$$\begin{aligned} A_\mu(x) \rightarrow [A_\mu(x)]^{\Omega(x)} &= \Omega(x)^\dagger A_\mu(x) \Omega(x) + i \Omega(x)^\dagger \partial_\mu \Omega(x), \\ \Omega(x) &= \exp\{i \omega_a(x) t^a\}. \end{aligned} \quad (2)$$

The partition function in its Euclidean-invariant form is given by

$$Z = \int D A_\mu \exp \left\{ -\frac{1}{4g^2} \int_0^{\beta=\frac{1}{T}} dt \int d^3 x F_{\mu\nu}^a F_{\mu\nu}^a \right\}. \quad (3)$$

Due to the compactified time direction the gluon fields obey periodic boundary conditions in time

$$A_\mu(0, x) = A_\mu(\beta, x). \quad (4)$$

There are special gauge transformations, which leave the periodic boundary conditions for the gluons intact, but which themselves are only periodic up to an

element of the center of the gauge group. The center group $Z(N_c)$ is a discrete one and has the elements

$$z_k = e^{2\pi i k / N_c} \quad \text{where} \quad k \in \{0, N_c - 1\}. \quad (5)$$

In particular for the gauge group $SU(2)$, which we will use for our calculations, the elements of $Z(2)$ are

$$z_0 = \begin{pmatrix} 1 & 0 \\ 0 & 1 \end{pmatrix}, \quad z_1 = \begin{pmatrix} -1 & 0 \\ 0 & -1 \end{pmatrix}. \quad (6)$$

The center group is of relevance for the order parameter of the confinement-deconfinement phase transition. It is given by $\langle \text{Tr } P \rangle$ where P is the Polyakov line

$$P(x) = \mathcal{P} \exp \left(i \int_0^{1/T} dt A_4 \right). \quad (7)$$

Here \mathcal{P} stands for path ordering. The Polyakov line is not invariant under $Z(N_c)$ transformations but transforms as

$$P(x) \rightarrow z_k^{-1} P(x). \quad (8)$$

One sees immediately that a manifest $Z(N_c)$ symmetry implies $\langle \text{Tr } P \rangle = 0$. This corresponds to the confined phase. If $\langle \text{Tr } P \rangle \neq 0$ then the symmetry must have been broken spontaneously. This corresponds to the deconfined phase. (In the presence of fermions the symmetry gets broken explicitly.) At very high temperatures the potential energy of the Polyakov line (or of A_4) has its zero-energy minima for values of $P(x)$ at the center of the gauge group (or for quantized values of A_4). High temperature perturbation theory hence corresponds to the system oscillating around these trivial values of the Polyakov line, *i.e.* $\langle \text{Tr } P \rangle \neq 0$. As the temperature decreases, however, the fluctuations of the Polyakov line increase and eventually at the critical temperature T_c the system undergoes a phase transition from a deconfined to a confined phase which has $\langle \text{Tr } P \rangle = 0$. In order to approach this phase transition from the high-temperature side, one needs to study the Polyakov line in its whole range of possible variation. In our recent paper [1] we worked with static and diagonal A_4 gluon fields and the gauge group $SU(2)$. In this case the Polyakov line

$$P(x) = \exp \left(i \frac{A_4(x)}{T} \right) \quad (9)$$

has the gauge invariant eigenvalues

$$e^{\pm i\pi\nu} \quad \text{where} \quad \nu = \sqrt{A_4^a A_4^a} / 2\pi T. \quad (10)$$

We assume that the gluons are varying slowly, but we allow for an arbitrary amplitude of the A_4 fields. We then find the non-trivial effective action for the eigenvalues of the Polyakov line, interacting in a covariant way with the spatial gluon fields A_i .

2 Energy scales at high temperatures

Since the gluon fields are periodic in time one can make a Fourier decomposition:

$$A_\mu(t, x) = \sum_{k=-\infty}^{\infty} A_\mu(\omega_k, x) e^{i\omega_k t}, \quad \omega_k = 2\pi k T, \quad (11)$$

where the Matsubara frequencies ω_k are the quantized values for the energies. The energy scales that show up in the theory are at the tree level the temperature T , on the quantum level the Debye mass scale gT which arises from screening effects for the color-electric gluons, and $g^2 T$, which is the (non-perturbative) scale of the color-magnetic gluons. The first step on the way to an effective theory is to integrate out the non-zero Matsubara modes, since they become very heavy at high temperatures. This reduces the original 4D Euclidean symmetry to a 3D static one, and is exact in the $T \rightarrow \infty$ limit. The next step is to include quantum fluctuations. There all Matsubara modes show up in loops again and produce infinitely many effective vertices. In [1] we obtained all these vertices, but restricted to low momenta $p < T$.

3 The 1-loop action

We use the so-called background field method where the gluon fields are decomposed into a background component (denoted by a bar) and quantum fluctuations around them:

$$A_\mu = \bar{A}_\mu + a_\mu. \quad (12)$$

For the quantum fluctuations we choose the background Lorenz gauge $D_\mu^{ab}(\bar{A}) a_\mu^b = 0$, where D_μ is the covariant derivative in the adjoint representation. A one loop calculation corresponds to expanding the action to quadratic power in a_μ . This results in the following effective theory for the background \bar{A} fields:

$$Z(\bar{A}) = e^S \int D a D \chi D \chi^+ \exp \left[-\frac{1}{2g^2(M)} \int d^4 x a_\mu^b W_{\mu\nu}^{bc} a_\nu^c - \int d^4 x \chi^{+\mu} D^2 \chi^\mu \right]. \quad (13)$$

Here χ, χ^+ are the ghost fields and

$$\bar{S} = -\frac{1}{4g^2(M)} \int d^4 x F_{\mu\nu}^a(\bar{A}) F_{\mu\nu}^a(\bar{A}) \quad (14)$$

is the action of the background fields. The quadratic form for a_μ is given by

$$W_{\mu\nu}^{ab} = -[D^2(\bar{A})]^{ab} \delta_{\mu\nu} - 2f^{acb} F_{\mu\nu}^c(\bar{A}). \quad (15)$$

Integrating out a , χ and χ^+ provides us with the 1-loop action

$$S_{1\text{-loop}} = \log (\det W)^{-1/2} + \log \det (-D^2). \quad (16)$$

Since the only gluon fields which are left are the background fields we will omit the bar from now on.

4 Gradient expansion of $S_{\text{1-loop}}$

For the background $A_4(x)$ fields one can always choose a gauge where they are static and diagonal in the fundamental representation, while the spatial $A_i(t, x)$ fields have to remain time dependent. In our calculation, however, it turns out to be easy to reconstruct the results for a time dependent $A_i(t, x)$ from an original ansatz where the spatial components are static as well. We shall hence assume that all background fields are static and reconstruct the more general results later. We then expand the 1-loop action in powers of the spatial covariant derivative D_i and obtain the kinetic energy by identifying the electric and magnetic fields as

$$[D_i, D_4] = -iF_{i4} = -iE_i, \quad B_i = \frac{1}{2}\epsilon_{ijk}F_{jk} = \frac{i}{2}\epsilon_{ijk}[D_j, D_k]. \quad (17)$$

For $SU(2)$ there are only two independent color vectors in the electric (magnetic) sector, E_i (B_i) and A_4 , and we thus expect the following structure for the result

$$S_{\text{1-loop}} = \int \frac{d^3x}{T} \left[-T^4 V(A_4^2) + E_i^2 f_1(A_4^2) + \frac{(E_i A_4)^2}{A_4^2} f_2(A_4^2) + B_i^2 h_1(A_4^2) + \frac{(B_i A_4)^2}{A_4^2} h_2(A_4^2) + \dots \right]. \quad (18)$$

The potential energy $V(A_4^2)$ has long been known [2, 3], the functions $f_{1,2}, h_{1,2}$ from the kinetic energy were newly obtained in [1].

4.1 The proper time formalism

The functional determinants in the 1-loop action eq. (16) are UV divergent which reflects the running of the coupling constant. As a regularization we hence introduce a Pauli-Villars cutoff M . In addition we want to normalize the functional determinants with respect to the free theory. This can be done with a method introduced by Schwinger [4], which yields for the ghost functional determinant

$$\begin{aligned} \log \det(-D^2)_{\text{Norm, Reg}} &= \log \frac{\det(-D_\mu^2)}{\det(-\partial_\mu^2)} \frac{\det(-\partial_\mu^2 + M^2)}{\det(-D_\mu^2 + M^2)} \\ &= - \int_0^\infty \frac{ds}{s} \text{Sp} \left[\left(1 - e^{-sM^2} \right) \left(e^{sD_\mu^2} - e^{s\partial_\mu^2} \right) \right], \end{aligned} \quad (19)$$

where Sp denotes a functional trace. The trace can be taken by inserting a plane wave basis:

$$\begin{aligned} \log \det(-D^2)_{\text{Norm, Reg}} &= - \int d^3x \sum_{k=-\infty}^{\infty} \int \frac{d^3p}{2\pi^3} \int_0^\infty \frac{ds}{s} \left(1 - e^{-sM^2} \right) \\ &\times \text{Tr} \left\{ \exp \left[s(\mathcal{A}^2 + (D_i + ip_i)^2) \right] - \exp \left[-s(\omega_k^2 + p^2) \right] \right\}, \end{aligned} \quad (20)$$

where we defined the adjoint matrix $\mathcal{A}^{ab} = f^{abc}A_4^c + i\omega_k\delta^{ab}$. A similar result can be found for the ghost functional determinant, see [1] for details.

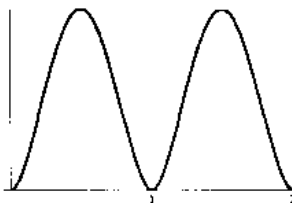


Fig. 1. The periodic potential V with period 1 in units of ν .

4.2 The effective potential

We find the potential $V(A_4^2)$ at zeroth order in D_i . This corresponds to $\mathbf{E} = \mathbf{B} = \mathbf{0}$ and

$$\det^{-\frac{1}{2}} W_{\mu\nu} = \det^{-2}(-D_\mu^2). \quad (21)$$

We choose the gauge where A_4 is diagonal in the fundamental representation:

$$A_4^a = \delta^{a3} \phi = \delta^{a3} 2\pi T \nu \quad , \quad \nu = \frac{\sqrt{A_4^a A_4^a}}{2\pi T}. \quad (22)$$

The resulting potential is well known [2, 3] and reads

$$V = \frac{1}{3(2\pi)^4 T^4} \phi^2 (2\pi T - |\phi|)^2 |_{\text{mod } 2\pi T} = \frac{(2\pi)^2}{3} \nu^2 (1 - \nu)^2 |_{\text{mod } 1}. \quad (23)$$

It is shown in Fig. (1). The potential is clearly periodic in ν with period one, which means that it is center-symmetric. At the minima of the potential A_4 has quantized values. For the Polyakov line this means that it assumes values of $Z(2)$. In particular for $SU(2)$ with

$$P = \exp\left(i A_4^a \frac{\tau^a}{2T}\right) = \cos \frac{|A_4|}{2T} + i \frac{A_4^a \tau^a}{|A_4|} \sin \frac{|A_4|}{2T}, \quad (24)$$

the minima correspond to

$$\nu = 0, 2, \dots \rightarrow P = \begin{pmatrix} 1 & 0 \\ 0 & 1 \end{pmatrix}, \quad (25)$$

$$\nu = 1, 3, \dots \rightarrow P = \begin{pmatrix} -1 & 0 \\ 0 & -1 \end{pmatrix}. \quad (26)$$

At the minima one hence has $\langle \text{Tr } P \rangle \neq 0$, and at high temperatures perturbation theory around one of these minima is performed. At lower temperatures, however, the fluctuations of $\langle \text{Tr } P \rangle$ increase and eventually at the phase transition point $\langle \text{Tr } P \rangle \rightarrow 0$ and the center symmetry is broken. It is hence of interest to study the fluctuations of the Polyakov line beyond the perturbative minima. This is tantamount to calculating the kinetic energy, which we shall do by means of an expansion in higher powers of the covariant derivative.

4.3 Higher powers of the covariant derivative

For the kinetic energy we encounter structures of the type

$$\exp s(A^2 + (D_i + ip_i)^2), \quad A^{ab} = f^{abc} A_4^c + i\omega_k \delta^{ab} \quad (27)$$

which we have to expand in powers of D_i . This can be done by using

$$\begin{aligned} e^{A+B} &= e^A + \int_0^1 d\alpha e^{\alpha A} B e^{(1-\alpha)A} \\ &+ \int_0^1 d\alpha \int_0^{1-\alpha} d\beta e^{\alpha A} B e^{\beta A} B e^{(1-\alpha-\beta)A} + \dots, \end{aligned} \quad (28)$$

and dragging $B = D_i, D_i^2$ to the right with the help of

$$[B, e^A] = \int_0^1 d\gamma e^{\gamma A} [B, A] e^{(1-\gamma)A}. \quad (29)$$

Then we have to evaluate all the integrals over $\alpha, \beta, \gamma, \dots, p, s$ and sum over the Matsubara frequencies $\omega_k = 2\pi kT$. This should be done separately for the ghost and gluon determinants. For the electric sector one has to go to second order in D , and for the magnetic sector to the quartic order. We will only show the results of the calculations. The details can be found in [1].

4.4 Results for the electric sector

We indeed find the structure for the kinetic energy that was outlined in eq. (18) with the functions given by

$$\begin{aligned} f_1(\nu) &= \frac{11}{48\pi^2} \left[2(\log \mu - \gamma_E) - \psi\left(-\frac{\nu}{2}\right) - \psi\left(\frac{\nu}{2}\right) + \frac{20}{11\nu} \right], \quad \nu = \frac{\sqrt{A_4^a A_4^a}}{2\pi T} \\ f_2(\nu) &= \frac{11}{48\pi^2} \left[\psi\left(-\frac{\nu}{2}\right) + \psi\left(\frac{\nu}{2}\right) - \psi(\nu) - \psi(1-\nu) - \frac{20}{11\nu} \right]. \end{aligned} \quad (30)$$

Here ψ is the digamma function,

$$\psi(z) = \frac{\partial}{\partial z} \log \Gamma(z), \quad (31)$$

γ_E is the Euler constant and μ is a UV cutoff that we introduced in the sum over Matsubara frequencies. It is related to the Pauli-Villars mass as

$$\mu = \frac{M}{4\pi T} e^{\gamma_E}. \quad (32)$$

This scale has been previously found in [5] for the running coupling constant in the dimensionally reduced theory, and our result agrees. At this point we shall also reconstruct the more general results for a time dependent background $A_i(t, x)$ field. In the calculations we identified the electric field as

$$[D_i, \mathcal{A}] = [D_i, D_4] = -iF_{i4} = -iE_i. \quad (33)$$

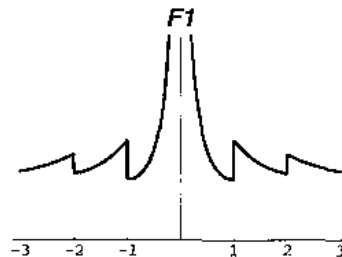


Fig. 2. The function $f_1(\nu)$ with the constant part subtracted, in different intervals.

Now it is easy to see that since $\mathcal{A}^{ab} = D_4^{ab} + i\omega_k \delta^{ab}$, reintroducing time dependence is tantamount to using the full covariant time derivative $D_4^{ab} = \partial_4 \delta^{ab} + f^{acb} A_4^c$. The functions eq. (30) remain unaltered, only from now on we have the full time dependent electric field

$$E_i^a = D_i^{ab} A_4^b - \dot{A}_i^a = \partial_i A_4^a + \epsilon^{acb} A_i^c A_4^b - \dot{A}_i^a. \quad (34)$$

Since there is no explicit time dependence in the magnetic field, the results for the magnetic sector will remain the same. It should be noted here that the above results are valid for $0 \leq \nu \leq 1$. In other intervals the functional forms of f_1 and f_2 are different. We show the results for f_1 for a broader range of ν in Fig. (2). One can clearly see that this result is not $Z(2)$ symmetric, the same is true for f_2 . However, one particular combination, namely

$$f_3(\nu) \equiv f_1(\nu) + f_2(\nu) = \frac{11}{48\pi^2} [2(\log \mu - \gamma_E) - \psi(\nu) - \psi(1-\nu)] \quad (35)$$

turns out to be periodic. We plot it in Fig. (3). The reason for this is the following: We chose the gauge for the A_4 fields where they are static and diagonal in the fundamental representation. This leaves certain residual gauge symmetries:

$$A_\mu \rightarrow S^\dagger A_\mu S + iS^\dagger \partial_\mu S, \quad S(x, t) = \exp \left\{ -i \frac{\tau^3}{2} [\alpha(x) + 2\pi t T n] \right\}. \quad (36)$$

Our invariants in the electric sector can be expressed as

$$E_i^a E_i^a f_1 + \frac{(E_i^a A_4^a)^2}{A_4^b A_4^b} f_2 = E_i^{\parallel} E_i^{\parallel} f_3 + E_i^{\perp} E_i^{\perp} f_1 \quad (37)$$

where $E_i^{\parallel} E_i^{\parallel} = (E_i^1)^2 + (E_i^2)^2$ and $E_i^{\perp} E_i^{\perp} = (E_i^3)^2$ denote the structures parallel and orthogonal to A_4^2 .

The time-dependent gauge transformations eq. (36) now introduce large time derivatives in the $A_i^{1,2}$ but not in the A_i^3 fields. The time-dependent part of the electric field eq. (34) enters in $E_i^{\perp} E_i^{\perp}$, but not in $E_i^{\parallel} E_i^{\parallel}$. Hence one should not expect gauge-invariance in the structure $E_i^{\perp} E_i^{\perp} f_1$, since it is only quadratic in $\dot{A}_i^{1,2}$. In order to have gauge invariance one would have to sum over all powers $\dot{A}_i^{1,2}/T$, which would result in a non-local effective action.

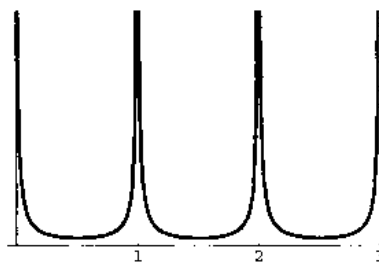


Fig. 3. The symmetric function in f_3 , $h_{1,2}$ without the constant part, in different intervals.

4.5 Results for the magnetic sector

In order to obtain the functions $h_{1,2}$ from eq. (18) we have to go to quartic order in D_i . At this order there are also mixing terms between the electric and the magnetic field. We ignore these since we are only interested in the kinetic energy in the magnetic sector. Again the functional form of $h_{1,2}$ depends on the interval that we choose for A_4 . For $0 \leq \nu \leq 1$ we find

$$h_1(\nu) = -\frac{11}{96\pi^2} \left[4 \left(\log \frac{M}{4\pi T} + \frac{\gamma_E}{2} \right) - \psi(\nu) - \psi(1-\nu) \right], \quad (38)$$

$$h_2(\nu) = -\frac{11}{96\pi^2} [2\gamma_E + \psi(\nu) + \psi(1-\nu)]. \quad (39)$$

In Fig. (3) we plot the constant part (which is the same as for f_3) for different intervals. The result is obviously center-symmetric.

4.6 Renormalization

The functions f_1 and h_1 are UV divergent, they contain the Pauli-Villars cutoff M in the subtraction scale μ , see eq. (32). This divergence is expected and necessary to cancel the tree level divergence from the running coupling constant:

$$-\frac{F_{\mu\nu}^a F_{\mu\nu}^a}{4g^2(M)} = -F_{\mu\nu}^a F_{\mu\nu}^a \frac{11}{3} N_c \frac{1}{32\pi^2} \log \frac{M}{A}. \quad (40)$$

If we evaluate the coupling constant at the scale M and add the tree level action eq. (40) to our 1-loop action, then we obtain a finite result. In the effective action the scale M in μ gets replaced by A . This yields the following logarithm in the kinetic energy:

$$\frac{11}{24\pi^2 T} \log \frac{A}{4\pi T} (E_i^a E_i^a + B_i^a B_i^a). \quad (41)$$

5 Comparison to previous work

In reference [6] a covariant derivative expansion of the 1-loop Yang-Mills action is performed. While we keep all powers of the background A_4 field the author of [6]

goes only to quadratic order. For a comparison we have to expand our functions $f_{1,2}$ and $h_{1,2}$ to quadratic order in ν and we find that the results agree.

We mentioned in the section on the electric sector that one combination of our functions, namely $f_3 = f_1 + f_2$ is $Z(2)$ symmetric. This function has been obtained in [7] in the context of a calculation of the interface tension of $Z(N)$ instantons, and our result again agrees.

6 Summary

In our recent paper [1] we studied the effective action for the eigenvalues of a static $SU(2)$ Polyakov line at high temperatures. In the $T \rightarrow \infty$ limit perturbation theory works and dimensional reduction takes place. The Polyakov loop has values at the center of the gauge group. If one lowers the temperature, however, the fluctuations of the Polyakov loop around these perturbative values increase. We studied the fluctuations of P in the whole range of its possible variation and found the 1-loop effective action for its eigenvalues, interacting in a covariant way with the A_i fields. We found that while the kinetic energy in the magnetic sector is center-symmetric, the kinetic energy in the electric sector is not. If one wishes to preserve this symmetry one has to sum over all powers of the electric field, which results in a non-local effective theory. For small values of A_4 all functions are singular and behave as $1/A_4$, which is due to the contribution of the zero Matsubara frequency.

ACKNOWLEDGMENTS:

I would like to thank Prof. 't Hooft for the opportunity to speak in the new talents sessions at the "Ettore Majorana" International School of Subnuclear Physics 2003 in Erice, Italy. And I am grateful to my supervisor Dmitri Diakonov for providing me with this interesting problem for my PhD thesis and for innumerable helpful and useful discussions.

References

1. D. I. Diakonov and M. Oswald, Phys. Rev. D **68**, 025012 (2003).
2. D. J. Gross, R. D. Pisarski and L. G. Yaffe, Rev. Mod. Phys. **53**, 43 (1981).
3. N. Weiss, Phys. Rev. D **24**, 475 (1981), Phys. Rev. D **25**, 2667 (1982).
4. J. Schwinger, Phys. Rev. **82**, 664 (1951).
5. S. Huang and M. Lissia, Nucl. Phys. B **438**, 54 (1995); K. Kajantie, M. Laine, K. Rummukainen and M.E. Shaposhnikov, Nucl. Phys. B **458**, 90 (1996), *ibid.* **503**, 357 (1997).
6. S. Chapman, Phys. Rev. D **50**, 5308 (1994).
7. T. Bhattacharya, A. Gocksch, C. Korthals Altes and R.D. Pisarski, Nucl. Phys. B **383**, 497 (1992).

The Time Of Flight (TOF) system of the ALICE experiment

G. Sciolli^{1,2}

¹ Dipartimento di Fisica dell'Università, Bologna, Italy

² INFN, Bologna, Italy

15/11/2003

Abstract. The double-stack Multigap Resistive Plate Chamber (MRPC) is the detector chosen for the large Time-Of-Flight system of the ALICE experiment at CERN LHC. The TOF barrel has to cover an area of 160 m^2 and has to be highly segmented ($160,000$ readout pads of $2.5 \times 3.5 \text{ cm}^2$) in order to keep the occupancy at the 15% level. In this article recent results on several prototype MRPCs are presented, with particular emphasis on the study of the uniformity of these devices.

PACS. XX.XX.XX No PACS code given

1 Introduction

ALICE (A Large Ion Collider Experiment) [1] is one of the four experiments at the CERN Large Hadron Collider (LHC). ALICE will study Pb-Pb collisions at a centre-of-mass energy of 5.5 TeV per nucleon pair. The aim of the experiment is to investigate the behaviour of nuclear matter at extreme densities and temperatures. In particular ALICE will study the QCD phase transition of nuclear matter into a deconfined state of quarks and gluons, i.e. the QGP (Quark-Gluon-Plasma) state, with partial chiral symmetry restoration and quark masses reduced to the small bare ones.

Particle identification is a key element to study the QGP. The event-by-event hadron identification will allow to measure, with high statistics, the shape of the p_t distributions of π , K and p , their average p_t and the $\pi/K/p$ ratios. It will provide information on possible thermodynamical instabilities during the phase transition, on the degree of thermal equilibrium and on expansion dynamics. Moreover the kaon identification will provide information on:

- the level of s-quark density, which is expected to be large due to the partial chiral symmetry restoration in a QGP;
- the identification of the $\phi \rightarrow K^+K^-$ decays. The measurement of the ϕ resonance provides more stringent constraints on the origin of the observed flavour composition, as compared to the K/π ratio.
- the open charm decays. The detection of open charm will be very important for cross-section normalization, necessary in the study of J/ψ suppression, one of the basic QGP probes.

The Time of Flight detector [2] [3], presently under construction, will allow hadron identification in the momentum range from $0.5 \text{ GeV}/c$ up to a few GeV/c .

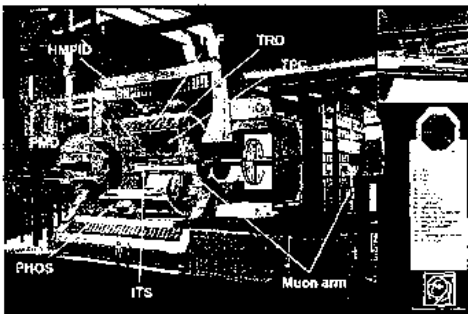


Fig. 1. Layout of the ALICE detector

The TOF surrounds the whole ALICE central barrel (see fig.1), equivalent to an area of 160 m^2 . In the ALICE experiment up to 8000 primary charged particles will be produced per unit of rapidity, therefore a high segmentation is required. In particular, Monte Carlo simulations [2] [3] [4] indicate that, in order to have an occupancy of about 15%, $160,000$ individual channels of $2.5 \times 3.5 \text{ cm}^2$ read-out pads are necessary.

2 The TOF system

The TOF detector is internal to the ALICE solenoid, it has a polar acceptance $|\theta - 90^\circ| < 45^\circ$ and full coverage in ϕ . The inner radius of the TOF cylinder is 3.70 m from the beam axis.

The TOF is divided into 18 azimuthal sectors, as shown in fig.2. Each sector is made of five modules of three differ-

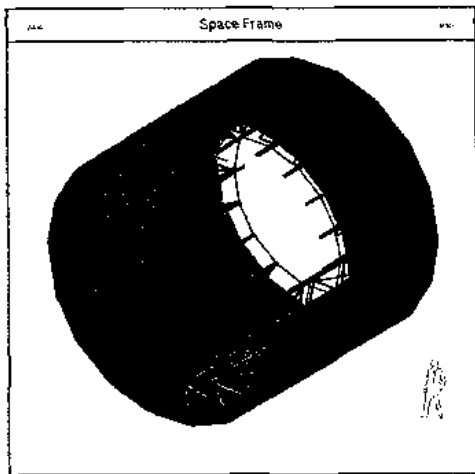


Fig. 2. Time of Flight (TOF) detector layout on the ALICE-spaceframe structure.

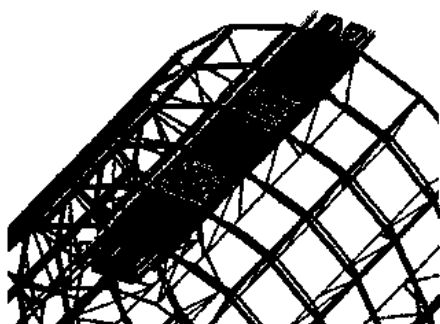


Fig. 3. A detail of one sector with 5 modules: one central, two intermediate and two external. The three types of modules have different lengths and contain different numbers of MRPC strips: there are 15 MRPCs in the central module, 19 in the intermediate and outer ones.

ent types (see fig.3). Each module consists of two separate volumes: a gas region containing the Multigap Resistive Plate Chambers (MRPCs) and a second one containing the Front End Analogue (FEA) cards.

The MRPC strips (each of $120 \times 7.4 \text{ cm}^2$ active area) will be placed orthogonally with respect to the beam direction (z -axis) and tilted in such a way as to be perpendicular to the particle trajectory from the interaction point in

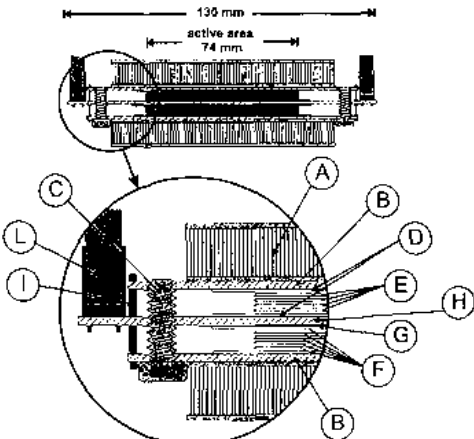


Fig. 4. Cross-section of the double-stack MRPC of the ALICE-TOF system. A: 10 mm thick honeycomb panel; B: PCB with cathode pick-up pads; C: M5 nylon screw to hold the fishing-line spacer; D: 550 μm thick external glass plates; E: four 400 μm thick internal glass plates; F: five gas gaps of 250 μm ; G: 250 μm thick mylar film; H: central PCB with anode pick-up pads; I: pin to bring cathode signals to central read-out PCB; L: flat-cable connector (for MRPC signal transmission to the front-end electronics).

the r - z plane¹. To minimize the dead area, adjacent strips inside the modules will be overlapped by about 2 mm.

3 The double-stack MRPC

The double-stack MRPC represents an evolution of the detector developed in [5] and consists of two stacks of equally spaced resistive plates, creating a series of gas gaps. High voltage is applied to the outer surfaces of the stack of resistive plates while all the internal plates are electrically floating. In this way the internal plates take voltage given by electrostatics and they are kept at the correct voltage values by the flow of positive ions and electrons created in the avalanches.

Two external and one central printed circuit boards (PCBs) contain the cathode and anode readout pads. Each stack has 5 gas gaps of 250 μm ; this distance is guaranteed by a fishing-line spacer held around a series of nylon screws, fixed in pre-drilled holes in one of the two external PCBs.

Due to the stack structure, the avalanches produced in different gaps by through-going particles ionizing the gas are independent and the signal is the sum of all gaps. A cross-section of the MRPC is shown in fig.4.

¹ r is the track projection in the longitudinal view.



Fig. 5. Photograph of the first prototype of fishing-line stretching machine.

During last year, a first prototype of fishing-line stretching machine was built (see fig. 5) and used to run the spacer across the surface of the glass plates, around the screws. This machine is very useful to automate, simplify and speed up the MRPC assembling procedure. In fact it takes only a few minutes to place each fishing-line layer.

The resistive plates are made of 'soda-lime' glass manufactured by Glaverbel²; the internal plates are 400 μm thick while the outer plates are 550 μm thick. The external surface (facing the PCB) of the outer plate, painted with a resistive coating of few $M\ \Omega/\square$ (acrylic paint loaded with metal oxides),³ is used to apply the voltage. Figure 6 shows a MRPC during the assembly.

To guarantee a good mechanical rigidity, two honeycomb panels are glued on the external PCBs. Connecting pins are soldered across the 3 PCBs in order to bring the cathode signals from the external PCBs to the central one (providing the anode signals). Moreover these pins are also used to keep the stacks compressed. The connectors used to transmit the differential signals to the front-end electronics are soldered on the central PCB.

Due to the geometry of this detector, the voltage is applied differentially to the resistive coatings.

4 The experimental set-up

The experimental set-up was located at the PS-T10 beam line of the CERN Proton Synchrotron. As illustrated in fig. 7 it consisted of:

- a small MRPC (SMRPC), made of a single stack of glasses defining 5 gaps, each of 230 μm with 10 cm^2 active area, which acts as pre-trigger providing the start to the TDCs and the gate to the ADCs;

² Glaverbel VERTEC sales, 166 Chaussée de La Hulpe, 1170 Brussels, Belgium

³ DETEC di Orietti M.L., viale E. Thovez 16/a, 10131 Torino, Italy



Fig. 6. Photographs of the MRPC during the assembly. The upper picture shows an open MRPC strip. The lower picture shows the positioning of the central PCB, with two external glasses glued on both sides of it.

- three tracking chambers (TC1, TC2, TC3), each consisting of 2 plates ($10 \times 20 \text{ cm}^2$) of strips with 4 mm pitch, to provide information on the position of the beam. The precision of the TCs is about 1 mm in both the coordinates;
- two pairs (P1-P2 and P3-P4) of crossed scintillators, whose coincidence defines a 1 cm^2 area and provides the trigger;
- two fast scintillator bars ($2 \times 2 \times 10 \text{ cm}^3$), each equipped with two photomultipliers (S1, S2, S3 and S4), discriminated by Constant Fraction Discriminators, to provide an accurate time reference;
- the device under test (DUT), i.e. up to 5 MRPC strips, closed in an aluminium box with external dimensions of $19.5 \text{ cm} \times 48 \text{ cm} \times 129 \text{ cm}$.

The chambers were filled with a gas mixture of 90 % $C_2F_4H_2$, 5 % SF_6 and 5 % C_4H_{10} . The measurements have been made using a 7 GeV/c beam of negative particles (π and μ).

A mechanical frame was used to move the aluminium box with relative millimetric accuracy. This allowed to position the beam on different pads by remote control.

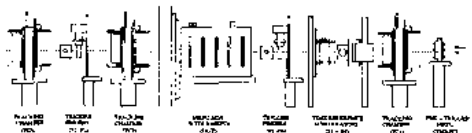


Fig. 7. Schematic layout of the experimental set-up at the T10 beam line.

5 Results

During autumn 2002, seventeen double-stack MRPCs were tested at the T10 beam line. Particular care was devoted to the study of the uniformity of response of the devices by centering the beam on many different pads, randomly distributed along each MRPC strip. Figure 8 shows the efficiencies and the time resolutions of over 100 pads belonging to the 17 chambers, measured at a fixed high voltage value of 13 kV. The upper histogram shows the distribution of the efficiency values, with a mean of 99.6 %, the lower one refers to the distribution of the time resolution values, with a mean of 62.9 ps.

Figure 9 shows an example of high voltage scan along one MRPC: the two plots show, respectively, the efficiency and the time resolution as a function of high voltage, for different beam positions along the strip. It should be noted that each curve corresponds to a different read-out pad.

In the HV range between 12 and 13 kV, the mean efficiency is 99.9 % and the mean time resolution is 50 ps. All the tested MRPCs showed a very good uniformity and a long streamer-free plateau.

To collect these data, a front-end electronics based on the commercial MAXIM 3760 amplifier and MAXIM 9691 ECL comparator was used.

To obtain a very good time resolution, a very fast front-end electronics is mandatory. Although the MAXIM 3760 gave good results, this kind of amplifier has the following drawbacks:

- it is a high power device (300 mW per channel);
- its input is not differential;
- it has a low input capacitance (1 pF).

The idea was then to design an ultra fast ASIC amplifier solution. The advantages of this choice are several:

- it has a differential input;
- it has to operate with a large input capacitance (30 pF);
- it is very fast, with a jitter less than 25 ps;
- it has a low input impedance;
- it is a low power device (about 30 mW per channel).

The new NINO-ASIC (see fig.11) is an excellent amplifier/discriminator to fully exploit the MRPC intrinsic performances. It was used during a beam test in May 2003, with different MRPC strips. Figure 10 shows the efficiency and time resolution versus high voltage for different chambers. As it can be seen, the uniformity is very satisfactory; in fact the mean efficiency is close to 100 % and the mean time resolution is 50 ps in the plateau region.

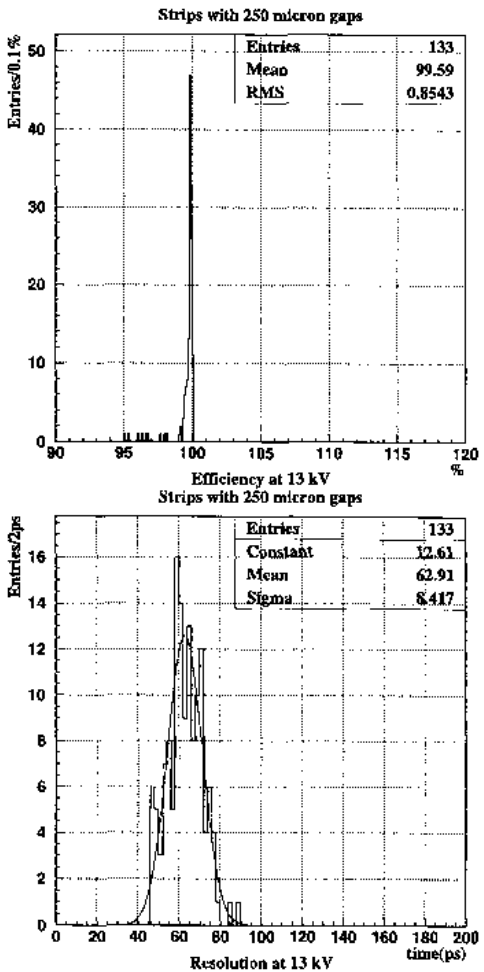


Fig. 8. Efficiency and time resolution distributions for all 17 MRPCs tested in October 2002.

The ALICE experiment will run for many years and the detectors will be irradiated by a very large number of particles. Hence ageing tests are required to study a possible degradation of the behaviour of the MRPCs. During last year, two detectors (CH1 and CH2) were irradiated at the CERN Gamma Irradiation Facility (GIF), located in the X5 area of the West Hall. This facility allows a device to be irradiated with 662 keV photons from a 740 GBq ^{137}Cs source.

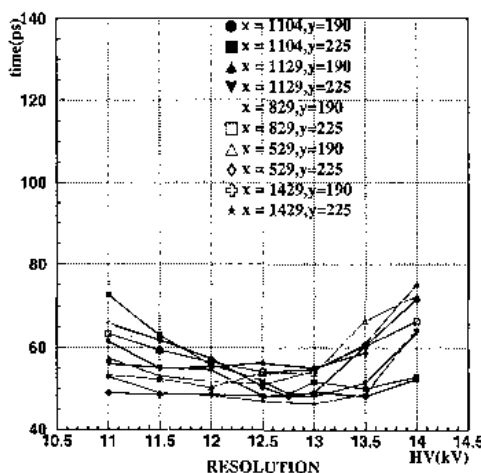
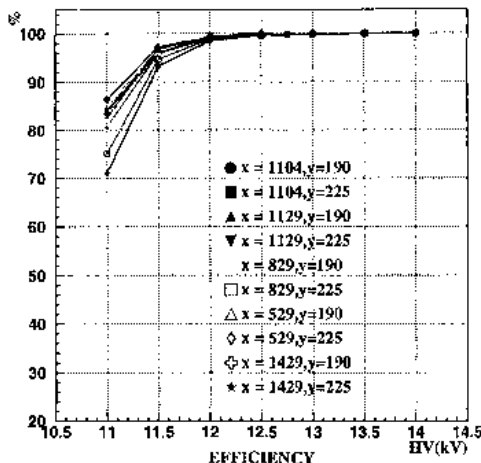


Fig. 9. Example of uniformity study along one MRPC strip in terms of efficiency and time resolution measured in different positions along the strip.

CH1 and CH2 were irradiated for a total equivalent of about 1000 days of Pb-Pb run at 50 Hz/cm²⁴. These two MRPCs were tested at the T10 beam line before and after the irradiation at Gif and no ageing effect was observed.

⁴ According to the present LHC running scenario, Pb-Pb collision runs will last about 1 month per year.

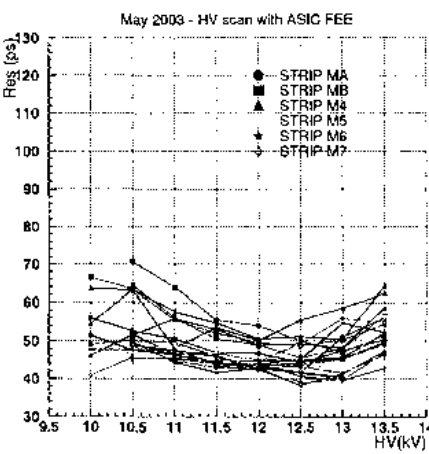
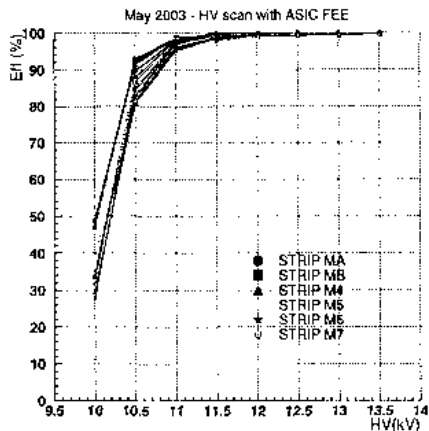


Fig. 10. Results of May 2003 beam test, using the new NINO-ASIC FEE card for different MRPCs.

6 Conclusion

All the tests presented herein clearly show that the double-stack MRPC of the ALICE-TOF system is an outstanding detector. This device has a very good uniformity, a long streamer-free plateau, an excellent efficiency of 99.9 % and an excellent time resolution of ~50 ps. Moreover, after a long period of irradiation corresponding to 17 years of ALICE activity, the MRPC has proved to be a radiation-hard device.



Fig. 11. Photograph of the new FEE card with 3 NINO-ASIC amplifiers/discriminators used to collect data during May 2003 beam test.

References

1. ALICE Collaboration, Technical Proposal, CERN/LHCC/95-71.
2. ALICE Collaboration, Time of Flight System, Technical Design Report, CERN/LHCC 2000-12 ALICE TDR 8, 16 February 2000.
3. ALICE Collaboration, Addendum to ALICE TDR 8, CERN/LHCC 2002-16, 24 April 2002.
4. ALICE TOF GROUP (A. Akindinov et al.), European Physical Journal C Direct, 10.1140/epjcd/s2003-01-0013-5.
5. E. Cerron Zeballos, I. Crotty, D. Hatzifotiadou, J. Lamas Valverde, S. Neupane, M.C.S. Williams and A. Zichichi, Nucl. Instr. Meth. A374(1996)132.

ALMOST PRODUCT MANIFOLDS AS THE LOW ENERGY GEOMETRY OF DIRICHLET BRANES*

FREDERIC P. SCHULLER

*Department of Applied Mathematics and Theoretical Physics,
University of Cambridge, Cambridge CB3 0WA, United Kingdom
and*

*Perimeter Institute for Theoretical Physics,
Waterloo Ontario N2J 2W9, Canada;
E-mail: fschuller@perimeterinstitute.ca*

Any candidate theory of quantum gravity must address the breakdown of the classical smooth manifold picture of space-time at distances comparable to the Planck length. String theory, in contrast, is formulated on conventional space-time. However, we show that in the low energy limit, the dynamics of generally curved Dirichlet p -branes possess an extended local isometry group, which can be absorbed into the brane geometry as an almost product structure. The induced kinematics encode two invariant scales, namely a minimal length and a maximal speed, without breaking general covariance. Quantum gravity effects on D-branes at low energy are then seen to manifest themselves by the kinematical effects of a maximal acceleration. Experimental and theoretical implications of such new kinematics are easily derived. We comment on consequences for brane world phenomenology.

1. Introduction

The formulation of a relativistic theory of quantum gravity is one of the key open questions in fundamental physical theory today. Attempts to reconcile the principles of general relativity and quantum theory by employing otherwise tried-and-tested methods indeed face severe difficulties, suggesting that a considerable departure from the standard space-time picture may be inevitable. This becomes dramatically clear in a simple gedankenexperiment. Assume we want to probe the space-time structure down to arbitrarily small distances. The position-momentum uncertainty relation predicts that this can only be done at the cost of increasingly large fluctuations of the energy-momentum tensor. These directly translate into fluctuations of the geometry via Einstein's field equations. A simple calculation shows that if one aims at resolving lengths on the order of the Planck length $\ell_P = \sqrt{\hbar G/c^3}$, the described mechanism significantly disturbs the very space-time distance that one attempts to resolve. Any candidate theory of quantum gravity is therefore expected to conceptually involve a fundamental length scale of order ℓ_P . Due to the rôle of

*reprinted from European Physical Journal C

ℓ_P as the minimum resolvable length in the above reasoning, it indeed appears appropriate to look for a space-time structure in which the Planck length joins the speed of light as a geometrical invariant. Thus, it seems inevitable that quantum gravity should be based on such new kinematics with two invariant scales, at least in the low energy limit.

The conceptual basis of string theory is apparently in direct opposition to the above reasoning. Standard semi-Riemannian space-time is upheld as the geometry underlying the formulation of the theory. A length scale, however, is subtly implemented in the dynamics. The fundamental objects of the classical theory are assumed to be strings of characteristic length ℓ . A geometrical action proportional to the world-sheet surface area swept out by the string in space-time then features the length scale as an overall factor for dimensional reasons. However, the simple geometrical formulation of the theory comes at a price. The corresponding quantum theory is only consistent in 26-dimensional space-time for the bosonic string, or 10 dimensions if one includes fermions and supersymmetry. This result challenges phenomenological models to provide a compelling reasoning of how the observable 4-dimensional universe is supposed to emerge from such a picture. Proposals to resolve this question have experienced valuable new input from the discovery of Dirichlet- p -branes¹ as non-perturbative solutions in string theory. D p -branes are $(p + 1)$ -dimensional sub-manifolds of the 10- or 26-dimensional string target space, defined by the property that open strings can end on them. Their phenomenological significance arises from ideas to devise models of the observable universe as a D3-brane propagating in the higher dimensional space-time². The dynamics of (and the new physics seen on) such brane-worlds originate from the interaction with the strings propagating in the higher dimensional space-time. It is therefore of utmost interest to study and understand the properties of D-branes, as they constitute the fundamental building blocks of all such brane world theories. Properties of these building blocks have an impact on any phenomenological scenario in which they are involved, and are hence largely model-independent.

The key observation of this paper is that the low energy dynamics of D p -branes possess a hidden invariance, which can be absorbed into the world-volume geometry of the brane. This geometry can be viewed, alternatively, either as a module bundle over a semi-Riemannian manifold³, or as a tangent bundle of the standard space-time sub-manifold with an almost product structure. New geometry is synonymous with new kinematics⁴. In the present case, the local Lorentz symmetry remains intact, but is extended to a larger local gauge group, by transformations to rotating and sub-maximally accelerated frames, with the maximum acceleration given by the inverse $1/\ell$ of the string length scale. In other words, the original *dynamical* encoding of a length scale in string theory finally implies a particular *kinematical* implementation on $(p + 1)$ -dimensional manifolds, as it is expected of a candidate theory of quantum gravity.

2. Pseudo-complex module bundles over D_p-branes

The exact dynamics of D_p-branes is determined by the interaction of the open strings ending on the brane with any other strings in the theory. The analysis of the resulting dynamics is, of course, prohibitively difficult. In the low energy limit, however, only the massless string modes contribute. For technical simplicity, we consider in this article the toy model of bosonic string theory. The quantum spectrum of bosonic string theory contains a tachyon, which renders Dirichlet branes unstable. We will ignore this issue altogether, but remark that the following developments can be extended in a straightforward manner to type I superstring theory. The irreducible components of the second rank tensor modes of massless closed bosonic strings give rise to effective background fields $G_{(MN)}$, $B_{[MN]}$ and Φ , where $M, N = 0, \dots, 25$. These can be identified as the classical target space metric, Neveu-Schwarz two-form potential, and the dilaton. The massless vector modes of open strings ending on the D_p-brane produce an effective gauge field A_μ , where $\mu = 0, \dots, p$. It has been shown that in the low energy limit, the dynamics of this gauge field A is given by the Dirac-Born-Infeld (DBI) action ⁵

$$\int_{\text{brane}} \sqrt{\det(g_{\mu\nu})} dx^0 \wedge \cdots \wedge dx^p e^{-\Phi} \sqrt{\det(\delta^\mu{}_\nu + B^\mu{}_\nu + \ell^2 F^\mu{}_\nu)}, \quad (1)$$

where $F_{\mu\nu} = \partial_{[\mu} A_{\nu]}$, and $g_{\mu\nu}$ and $B_{\mu\nu}$ are the pull-backs to the brane of the target space fields g_{MN} and B_{MN} , respectively. Indices μ, ν are lifted and lowered using the induced metric on the brane. Note that (1) can be viewed as a theory of non-linear electrodynamics ⁶, and has in fact been devised as such in the 1930s ⁷ in order to covariantly regularize the energy divergence of the electrostatic field of a charged point particle in Maxwell theory. Expansion of the determinant, using the identity $\det(1 + \mathcal{F}) = \exp \text{tr} \ln(1 + \mathcal{F})$, with $\mathcal{F} = B + \ell^2 F$, shows that only even powers of \mathcal{F} contribute to the action. We can hence multiply \mathcal{F} by a number I satisfying $I^2 = +1$, without changing the action (1) at all. In order to clear up the notation, we use the shorthand $\omega = \sqrt{\det(g_{\mu\nu})} dx^0 \wedge \cdots \wedge dx^p$ for the volume form on the brane, so that we have

$$\int_{\text{brane}} \omega e^{-\Phi} \sqrt{\det(\delta^\mu{}_\nu + \mathcal{F}^\mu{}_\nu)} = \int_{\text{brane}} \omega e^{-\Phi} \sqrt{\det(\delta^\mu{}_\nu + I \mathcal{F}^\mu{}_\nu)}. \quad (2)$$

Note that $\mathcal{F}_{\mu\nu}$ are the components of a $(0, 2)$ -tensor field on the brane Σ , i.e., $\mathcal{F}(p)$ is a linear map $T_p \Sigma \otimes T_p \Sigma \rightarrow \mathbb{R}$ for any point $p \in \Sigma$. The addition on the left hand side of Eq. (2) is the addition in the vector space of real $(0, 2)$ tensors. If we assume that $I \in \mathbb{R}$ (i.e. $I = \pm 1$) then the addition on the right hand side is the same, and also well-defined. It will turn out to be enlightening, however, to take $I \notin \mathbb{R}$ and to define an algebraic extension

$$\mathbb{P} := \{a + Ib | a, b \in \mathbb{R}\} \quad (3)$$

of \mathbb{R} , where we identify $\mathbb{R} \equiv \{a + Ib | a \in \mathbb{R}, b = 0\}$. The set \mathbb{P} equipped with the addition and multiplication inherited from \mathbb{R} fails to be a field due to the existence

of zero-divisors of the form $\lambda(1 \pm I)$, where $\lambda \in \mathbb{R}$, which do not possess multiplicative inverses. However, $(\mathbb{P}, +, \cdot)$, to whose elements we will refer as pseudo-complex numbers, is a commutative ring. One also finds the terms double numbers, hyperbolic complex or para-complex numbers for the ring \mathbb{P} in the literature, indicating that this simple structure has ample applications⁸, but is little known and hence re-invented time and again. The commutativity of the ring \mathbb{P} allows, in particular, for the construction of Lie algebras over \mathbb{P} . Note that in accordance with the mathematical literature, vector space like structures over a ring R rather than a number field will be called R -modules in this paper. Taking $I \notin \mathbb{R}$ therefore enforces the pseudo-complexification $(T_p\Sigma)_{\mathbb{P}} := \{v + Iw \mid v, w \in T_p\Sigma\}$ of the real tangent spaces, such that tensors of type (r, s) are now \mathbb{R} -linear maps

$$\bigotimes_s (T_p\Sigma)_{\mathbb{P}} \longrightarrow \bigotimes_r (T_p\Sigma)_{\mathbb{P}}, \quad (4)$$

constituting a real vector space for each pair (r, s) . This renders the addition on the right hand side of Eq. (2) well-defined if $I \notin \mathbb{R}$. In summary, the insertion of the pseudo-imaginary unit I into the DBI action is valid if one extends the tangent bundle $T\Sigma$ of the brane world-volume to a \mathbb{P} -module bundle over Σ with typical fiber \mathbb{P}^{p+1} . In like fashion, the frame bundle $L(\Sigma)$ of the real manifold Σ is replaced by the pseudo-complexified frame bundle $L_{\mathbb{P}}(\Sigma)$. In general relativity, an observer is given by a curve $e : \mathbb{R} \longrightarrow L(\Sigma)$ in the frame bundle, where the metric g on Σ is used to orthonormalize the frame such that $g(e_a, e_b) = \eta_{ab}$, where $a, b = 0, \dots, p$ and η is the Minkowski metric. The local $O(1, p)$ gauge group the Lorentzian manifold Σ parameterizes the freedom to choose equivalent orthonormal frames. The frame vector e_0 is taken to be the unit tangent to the curve $\pi(e)$ on Σ , where π is the canonical bundle projection. The covariant change of the frame along the observer's world-line $\pi(e)$ is then parameterized by an anti-symmetric Lorentz tensor Ω_{ab} , such that

$$\nabla_{e_0} e_a = \Omega_a^{b} e_b. \quad (5)$$

The translational p -acceleration of the observer is $\Omega_{0\alpha}$, with $\alpha = 1, \dots, p$. With respect to an observer whose spatial frame vectors e_α are parallelly transported along $\pi(e)$, our observer e possess angular velocity $\Omega_{\alpha\beta}$ in the $\alpha\beta$ -plane⁹.

The Frenet-Serret tensor Ω is therefore implicitly contained in the choice of any given observer e . When extending the real frame bundle $L(\Sigma)$ to the pseudo-complexified one $L_{\mathbb{P}}(\Sigma)$, we choose to explicitly encode the Frenet-Serret tensor in the pseudo-imaginary part of a pseudo-complex frame $E : \mathbb{R} \longrightarrow L_{\mathbb{P}}(\Sigma)$,

$$E_a := \gamma_a^{b} (\delta_b^c + I\ell\Omega_b^{c}) e_c, \quad (6)$$

where we have included the length scale ℓ for later interpretational convenience. The overall tensor factor γ is a normalization factor such that

$$g(E_a, E_b) = \eta_{ab}. \quad (7)$$

The freedom of choice for such frames is now obviously parameterized by the gauge group $O_{\mathbb{P}}(1, p) \cong O(1, p) \times O(1, p)$. This decomposition of the pseudo-complex Lorentz group $O_{\mathbb{P}}(1, p)$ into two copies of the real Lorentz group is easily seen in the zero-divisor decomposition of \mathbb{P} . The real Lorentz group presents a proper subgroup of $O_{\mathbb{P}}(1, p)$, and is diagonally embedded in this decomposition. Note that this means that the standard local Lorentz symmetry is fully preserved by the pseudo-complexification of the frame bundle. Thus we can identify the inertial frames of general relativity with those of the pseudo-complexified theory, which allows to maintain the strong equivalence principle.

In order to exhibit the physical interpretation of the action of $O_{\mathbb{P}}(1, p)$, first note the following polarization formula. Any $A \in O_{\mathbb{P}}(1, p)$ can be written as a unique product of a real Lorentz transformation $L \in O(1, p)$ and a pseudo-complex Lorentz transformation K with purely pseudo-imaginary coefficients,

$$A^a{}_b = K^a{}_m L^m{}_b, \quad (8)$$

as can be easily shown in the zero-divisor decomposition. As the action of real Lorentz transformations L is well-understood, the polarization formula allows to analyze the meaning of general $O_{\mathbb{P}}(1, p)$ transformations by study of transformations of type $K = \exp(\omega_{mn} IM^{mn})$, i.e., transformations with purely pseudo-imaginary coefficients. Consider an unaccelerated and non-rotating observer at time τ , so that $\Omega(\tau) = 0$. The pseudo-complex frame at this instant is then simply $E_a = e_a$. A real Lorentz transformation L will simply re-define the real frame and, of course, map the real Lorentz tensor $\Omega = 0$ onto itself. A pseudo-complex Lorentz transformation of type K , however, will yield a transformed frame

$$E = \cosh(\omega_{mn} M^{mn}) (1 + I \tanh(\omega_{mn} M^{mn})) e, \quad (9)$$

corresponding to mapping the Frenet-Serret tensor $\Omega = 0$ to

$$\Omega \rightarrow \ell^{-1} \tanh(\omega_{mn} M^{mn}). \quad (10)$$

This corresponds to a transformation to a non-inertial frame, with the values for the p -acceleration and the angular velocities to be read off from the corresponding components of Ω . In the following, we will only consider pseudo-complex frames that are locally continuously connected to inertial frames, i.e., frames E_a such that $E_a = \Lambda^m{}_a e_m$ for some real frame e , and Λ an element of the connection component of the identity of the pseudo-complex Lorentz group. We call such frames admissible. Now consider the phenomenologically interesting case $p = 3$. There are two real Lorentz invariants encoded in the Frenet-Serret tensor,

$$I_1 = \frac{1}{2} \Omega_{ab} \Omega^{ab} = \mathbf{a}^2 - \mathbf{L}^2, \quad (11)$$

$$I_2 = \frac{1}{2} \Omega_{ab} (*\Omega)^{ab} = 2\mathbf{a} \cdot \mathbf{L}, \quad (12)$$

where $*\Omega$ denotes the Hodge dual of the two-form Ω . The 3-vectors \mathbf{a} and \mathbf{L} are the translational acceleration and angular velocity of the observer. Restricting

attention to observers with admissible frames, we can always apply local $O_{\mathbb{P}}^e(1,3)$ transformations to obtain a Fermi-Walker transported observer, i.e., $\mathbf{L} = \mathbf{0}$. For such non-rotating observers, it is easy to see by direct calculation that the condition that the frame be admissible corresponds to requiring a covariant upper limit on scalar accelerations,

$$\mathbf{a}^2 < 1/\ell^2, \quad (13)$$

given by the inverse of the string length scale. The fact that a maximal acceleration arises as a consequence of a minimal length scale, through the above relation, is not too surprising. Consider the following simple causality argument: A relativistic observer of scalar acceleration g cannot set up, in an operationally well-defined manner, a coordinate system that extends more than a distance $1/g$ in any spatial direction, because the Rindler horizon makes him causally disconnected from certain regions of space-time. Now if there is a spatially extended object of characteristic minimal length ℓ , then uniform acceleration of the whole object, at a value larger than $1/\ell$, would causally disconnect parts of this object.

Before pressing on with the application to the Dp-brane geometry, we list the irreducible second rank tensor representations of the pseudo-complex Lorentz group. Of immediate physical interest is the connection component of the identity of the pseudo-complexified Lorentz group, which we denote by $O_{\mathbb{P}}^e(1,p)$. Any element Λ of the defining vector representation \mathcal{R}_v of $O_{\mathbb{P}}^e(1,p)$ can be generated by exponentiation of the standard Lorentz generators $(M^{mn})^a{}_b = \eta^{ma}\delta_b^n - \eta^{na}\delta_b^m$ with pseudo-complex parameters $\omega_{mn} \in \mathbb{P}$,

$$\Lambda(\omega) = \exp(\omega_{mn} M^{mn}), \quad m, n = 0, \dots, p. \quad (14)$$

It can be shown³ that the pseudo-complex conjugate representation \mathcal{R}_v^* is equivalent to \mathcal{R}_v over \mathbb{R} , but inequivalent over \mathbb{P} . All irreducible second rank tensors are therefore contained in

$$\mathcal{R}_v \otimes_{\mathbb{R}} \mathcal{R}_v \cong \mathcal{R}_t \oplus \mathcal{R}_a \oplus \mathcal{R}_s \oplus \mathcal{R}_H \oplus \mathcal{R}_{\bar{H}}, \quad (15)$$

if we use a tensor product over \mathbb{R} , or

$$\mathcal{R}_v \otimes_{\mathbb{P}} \mathcal{R}_v \cong \mathcal{R}_t \oplus \mathcal{R}_a \oplus \mathcal{R}_s, \quad (16)$$

$$\mathcal{R}_v \otimes_{\mathbb{P}} \mathcal{R}_v^* \cong \mathcal{R}_H \oplus \mathcal{R}_{\bar{H}}, \quad (17)$$

if we use a tensor product over \mathbb{P} . Elements of the representation spaces \mathcal{R}_t , \mathcal{R}_a , \mathcal{R}_s , \mathcal{R}_H , $\mathcal{R}_{\bar{H}}$ can be concisely encoded in a pseudo-complex trace, and pseudo-complex symmetric, anti-symmetric, hermitian or anti-hermitian matrices. Both methods to take tensor products yield the same irreducible representations finally. We mention both in order to illustrate that care must be taken in specifying of whether one deals with \mathbb{R} -linear or \mathbb{P} -linear structures. From the tensor product (17), we read off the transformation behavior of hermitian second rank tensors $H \in \mathcal{R}_H$ as

$$H_{ab} \longrightarrow \Lambda^m{}_a \Lambda^{*n}{}_b H_{mn} \quad (18)$$

under $O_{\mathbb{P}}(1, p)$ -transformations, where $\Lambda \in \mathcal{R}_v$. Rewriting the Dirac–Born–Infeld action in terms of the pseudo-hermitian tensor H , whose local frame components are given by $H^a{}_b := E_\mu^a E_b^{*\nu} (B^\mu{}_\nu + I\ell^2 F^\mu{}_\nu)$, yields

$$\int_{\Sigma} w e^{-\Phi} \sqrt{\det(E_a^\mu E_\nu^{*\mu} H^a{}_b)}. \quad (19)$$

This expression is manifestly invariant under $O_{\mathbb{P}}(1, p)$ transformations. Let us briefly summarize what we have achieved by casting the Dirac–Born–Infeld action into the form (19). In its original form (1), the length scale ℓ appears as a numerical constant, without any geometrical meaning. Extending the real frame bundle of the brane to its pseudo-complexified version allows to re-write the DBI action in the fully equivalent form (19). The length scale ℓ , however, now appears as an invariant of the orthogonal group $O_{\mathbb{P}}^*(1, p)$, formally on an equal footing with the invariant speed of light. The kinematical interpretation of pseudo-complex Lorentz transformations identifies $1/\ell$ as the maximum admissible (Lorentz-)scalar acceleration for a non-rotating observer. For a rotating observer with angular velocity \mathbf{L} , the maximal acceleration is shifted up to $\sqrt{\ell^{-2} + \mathbf{L}^2}$. We have thus achieved our goal of geometrizing the length scale ℓ , in a way that is consistent with the low energy dynamics of Dirichlet p -branes.

3. Almost product manifolds

So far, we considered a semi-Riemannian manifold Σ with pseudo-complexified tangent spaces. From a mathematical point of view, this is a somewhat hybrid structure, and therefore leads us to the natural question of whether this pseudo-complex structure of the tangent spaces can be absorbed into the manifold structure itself. The purpose of the present section is to cast this question into a precise form, and to find to which extent such a reformulation is possible. From a physical point of view, we might want to restrict our attention to Fermi–Walker transported observers, as we can always arrange for such systems experimentally by means of gyroscopes. Consider the frame vector E_0 of an observer on a low energy Dp-brane with $\Omega_{\alpha\beta} = 0$ for $\alpha, \beta = 1, \dots, p$. Using Eq. (6), we find an expression for this frame vector in terms of the $(p+1)$ -velocity u and covariant acceleration $a = \nabla_u u$ of the observer’s world-line x ,

$$E_0 = \frac{u + I\ell a}{\sqrt{1 - \ell^2 a^2}}. \quad (20)$$

Representing the unit 1 and pseudo-imaginary unit I in $\mathbb{IP} = \mathbb{IR} \oplus \mathbb{IR}$ by matrices

$$1 = \begin{pmatrix} 1 & 0 \\ 0 & 1 \end{pmatrix}, \quad I = \begin{pmatrix} 0 & 1 \\ 1 & 0 \end{pmatrix}, \quad (21)$$

and identifying the pseudo-complex module \mathbb{P}^n with $\mathbb{R}^n \oplus \mathbb{R}^n$, the normalization condition $g(E_0, E_0) = 1$ can be written as the two conditions

$$\gamma^2(g \otimes 1)(u \oplus \ell a, u \oplus \ell a) = 1, \quad (22)$$

$$\gamma^2(g \otimes I)(u \oplus \ell a, u \oplus \ell a) = 0, \quad (23)$$

where $\gamma = 1/\sqrt{1 - \ell^2 a^2}$. Now consider the natural lift of the curve x in Σ to the curve $X = x \oplus \ell u$ on the tangent bundle $T\Sigma$. If τ is the natural parameter of the curve x with respect to the metric g on Σ , then define the new parameter $\omega = \tau/\gamma$, which we will soon identify as the natural parameter of the lifted curve X with respect to a particular metric on $T\Sigma$. It is easily shown that in terms of the lifted curve X , the normalization conditions read

$$g^D\left(\frac{dX}{d\omega}, \frac{dX}{d\omega}\right) = 1, \quad (24)$$

$$g^H\left(\frac{dX}{d\omega}, \frac{dX}{d\omega}\right) = 0, \quad (25)$$

where g^D and g^H are the so-called diagonal and horizontal lifts of the space-time metric g to the tangent bundle¹⁰. Note that $dX/d\omega = \gamma(u \oplus \ell du/d\tau)$ is not identical to $E_0 = \gamma(u \oplus \ell \nabla_u u)$. However, the connection coefficients in $\nabla_u u$ are absorbed into the definition of g^D and g^H , whose components in the induced frame on $T\Sigma$ can be easily derived from the stated equivalence of (22-23) to (24-25). As is shown in differential geometry, both g^D and g^H are globally defined semi-Riemannian metrics on $T\Sigma$. From Eq. (24), we see that the parameter ω is the natural parameter of the curve X with respect to the metric g^D , as anticipated above. We hence obtain a bi-metric tangent bundle picture $(T\Sigma, g^D, g^H)$ for the Dirichlet brane geometry, equivalent to the module-bundle approach for non-rotating observers.

The question of whether the pseudo-complex structure of the tangent spaces ultimately originates from a manifold with pseudo-complex coordinates, can now be rigorously addressed. The bi-metric structure $(T\Sigma, g^D, g^H)$ can be reconstructed from a metric tangent bundle

$$(T\Sigma, g^D, F) \quad (26)$$

with a globally defined almost product structure $F := (g^D)^{-1} g^H$. An almost product structure is a $(1, 1)$ tensor F , such that F^2 is the identity transformation on the tangent spaces $T_Q T\Sigma$ of the tangent bundle $T\Sigma$ for all $Q \in T\Sigma$. Product and almost product manifolds have been explored in the mathematical literature, and there exist integrability theorems analogous to those for complex and almost complex manifolds. In particular, the vanishing of the Nijenhuis tensor

$$N_{LM}{}^J := (\partial_K F^J{}_L - \partial_L F^J{}_K) F^K{}_M - (L \leftrightarrow M), \quad J, K, L, M = 0, \dots, 2p+1 \quad (27)$$

is necessary and sufficient¹¹ for the almost product structure to be induced from a manifold with pseudo-complex local charts \mathbb{P}^{p+1} . However, for the almost product structure at hand, $F = (g^D)^{-1} g^H$, the Nijenhuis tensor can be calculated explicitly

and is seen to vanish if and only if the base manifold Σ is flat. This is, of course, not the generic case for a Dirichlet brane. This answers our question, of whether the pseudo-complex structure of the tangent spaces can be fully absorbed into pseudo-complex coordinates, to the negative. However, in the tangent bundle formulation, the normalization conditions (24–25) provide a clear physical interpretation for the rôles of the metrics g^D and g^H . The requirement that tangent bundle curves are null with respect to g^H is simply a reformulation of the orthogonality of covariant velocity and acceleration, $g(u, a) = 0$ for any timelike world-line. The normalization of the tangent bundle vector $dX/d\omega$ with respect to g^D is equivalent to requiring that there is an upper bound on admissible covariant accelerations, $g(a, a) < 1/\ell^2$.

The partial geometry $(T\Sigma, g^D)$ has been studied before^{12,13} as a maximal acceleration geometry, but without contact to any well-studied candidate theory of quantum gravity. It is remarkable that the low energy dynamics of Dirichlet branes imply just this geometry, and completes it by requiring that the tangent bundle is further equipped with a second metric g^H , or, equivalently an almost product structure F . Indeed, analogy with the symplectic structure of classical phase space would apparently rather suggest almost complex tangent bundles $(T\Sigma, g^D, J)$, with $J^2 = -1$. There is, however, a theorem due to Tachibana and Okumura¹⁴, that shows that simultaneous covariant constancy of both structures, $\nabla g^D = 0$ and $\nabla J = 0$ (which would be required if one wants to invoke a strong principle of equivalence), is possible if and only if the base manifold Σ is flat. In contrast, there is a connection ∇^H on $T\Sigma$, the horizontal lift¹⁰ of the Levi-Civita connection on (Σ, g) , which renders both the metric g^D and the almost product structure F simultaneously covariantly constant. The structure of low energy Dirichlet branes therefore induces a geometry that is consistent with the strong principle of equivalence. We have seen this compatibility of the maximal acceleration/minimal length geometry with the strong equivalence principle before in the module bundle picture, and thus the automatic circumvention of the Tachibana-Okumura theorem in the tangent bundle approach provides a non-trivial consistency check on that result.

4. Applications

We give two examples for applications of the Dirac–Born–Infeld kinematics, one each for the module bundle picture and almost product manifold picture, respectively. The Thomas precession of the spatial frame of a observer in circular motion with respect to an inertial frame is a standard result in special relativity. It is brought about essentially by the structure of the real Lorentz algebra, in particular the commuting of two independent boost generators up to a rotation generator,

$$[M^{0\alpha}, M^{0\beta}] = c^{-2} M^{\alpha\beta}. \quad (28)$$

As the orbiting observer has non-constant velocity, one must perform successive infinitesimal Lorentz boosts, in order to analyze the parallel transport of the spatial frames attached to the observer, using the above commutation relations. In the non-

relativistic limit $c \rightarrow \infty$, the effect vanishes. Such an observer in circular motion also undergoes a non-constant acceleration. In the presence of a length scale ℓ , changes to accelerating frames are generated by $IM^{0\alpha}$, as we saw from Eq. (10). Successive infinitesimal transformations of this type also effect a rotation of the spatial frame,

$$[IM^{0\alpha}, IM^{0\beta}] = \ell^2 M^{\alpha\beta}. \quad (29)$$

The corrected Thomas precession rate for an observer performing circular motion of radius R and angular velocity ω is found¹⁵ to be

$$\left(\sqrt{(1 - R^2\omega^2/c^2)(1 - R^2\ell^2\omega^4/c^2)} - 1 \right) \omega, \quad (30)$$

deforming the standard result by the length parameter ℓ . However, the real Lorentz algebra $so(1, p)$ is unaffected by the presence of the length scale. This shows, as a corollary, that high precision measurements of the Thomas precession in atomic physics cannot possibly falsify Lorentz symmetry, as is often assumed. Such experiments rather yield a lower bound on the hypothetical maximal acceleration.

The second example is more of theoretical interest, and uses the above result that in the case of a flat space-time Σ , the almost product structure on $T\Sigma$ is integrable, i.e., can be absorbed into pseudo-complex coordinates. A careful study¹⁷ of free quantum field theory on pseudo-complexified Minkowski space \mathbb{IP}^{p+1} shows that the propagators of any tensor field are automatically Pauli–Villars regularized with the regularization parameter given by the inverse length scale $1/\ell$. From a representation theoretical point of view, this result is understood from the fact that an irreducible representation of the pseudo-complexified Poincaré group (being the isometry group on \mathbb{IP}^{p+1}) accommodates two irreducible representations of the real Poincaré group, of equal spin (helicity) but generically different mass. Invoking a correspondence principle to standard quantum field theory in the limit $\ell \rightarrow 0$, one then observes that one of these real particles acts as a Pauli–Villars regulating Weyl ghost of the other proper particle. Taking the standard relativistic limit $\ell \rightarrow 0$ after, rather than before, the construction of a quantum field theory therefore corresponds exactly to the Pauli–Villars regularization prescription. The isometry group $O_{\mathbb{IP}}(1, p)$ apparently captures the regularization of the classical Dirac–Born–Infeld dynamics in a kinematical way.

5. Conclusion

Starting from the Dirac–Born–Infeld action as the low energy dynamics of a gauge field A on a Dirichlet p -brane in bosonic string theory, we found that the length scale appearing in the fundamental string dynamics finally gives rise to relativistic kinematics on the brane that preserve this length scale as a geometrical invariant. This finding implies, independently of string theory, two equivalent techniques for the extension of Lorentzian manifolds such as to encode a length scale as a geometrical invariant. The first technique consists in the pseudo-complexification of the

individual tangent spaces of the space-time manifold. The resulting module bundle structure is particularly well-suited for the discussion of observers in the new geometry. These still enjoy local Lorentz symmetry, but the extended local isometry group further contains transformations to rotating and accelerated frames. For non-rotating observers, however, only frames of sub-maximal acceleration are continuously connected to inertial frames. The maximal acceleration scale is given by the inverse length scale that originally entered the string action. A surprising immediate consequence of these minimal length/maximal acceleration kinematics is a correction to the Thomas precession. The module bundle formalism naturally allows for the discussion of rotating coordinate systems, but as we can always arrange for Fermi-Walker transported spatial frames by the use of gyroscopes, one can focus one's attention to non-rotating observers. Such a restriction permits to cast the new geometry into the form of a metric structure on the space-time tangent bundle, additionally equipped with a particular almost product structure. Both the tangent bundle metric and the almost product structure are globally defined lifts of the space-time metric. This lift of the metric structure to the tangent bundle presents the second technique for a geometrical implementation of a fundamental length scale, applicable to any Lorentzian manifold. The tangent bundle picture is particularly adapted to answer geometrical questions about the theory, as the whole apparatus of differential geometry on the tangent bundle is available. In particular, the theory of product manifolds shows that the pseudo-complex structure on the tangent spaces does not derive from a manifold with pseudo-complex coordinates in the presence of gravity. In the absence of gravity, however, the kinematical group reduces to the isometry group of pseudo-complexified space-time, allowing for the definition of sub-maximally accelerated quantum particles as irreducible representations of the pseudo-complexified Poincaré group. In this setting, a conjecture¹⁶ on the regularizing effect of a maximal acceleration in quantum field theory can be made precise and proved¹⁷.

In particular on D3-branes, the exhibited string theoretically induced maximal acceleration kinematics are of direct interest for brane world phenomenology. As is illustrated by the case of the Thomas precession, the mathematically simple structure of the theory allows its ready application. The merit of the presented approach to minimal length kinematics roots in the following facts. Any generically curved Lorentzian manifold can be extended such as to geometrically encode a minimal length scale in a covariant way. The employed mathematics consists of standard techniques in differential geometry and linear algebra. The preservation of the local Lorentz symmetry allows to maintain the strong equivalence principle, while the extended local isometry group makes non-trivial predictions for accelerated observers. Finally, its derivation from the low energy dynamics of Dirichlet branes makes rigorous contact with string theory, with implications for string phenomenology and the prospect of future insights into the presented questions inspired by string theory.

Acknowledgments

The author thanks G. 't Hooft for the opportunity to speak in the new talent sessions at the 41st International School on Subnuclear Physics in Erice, Italy, and the University of Cambridge for financial support.

References

1. J. Polchinski, Phys. Rev. Lett. **75**, 4724 (1995)
2. L. Randall and R. Sundrum, Phys. Rev. Lett. **83**, 4690 (1999)
3. F. P. Schuller and H. Pfeiffer, arXiv:hep-th/0307247.
4. F. P. Schuller, Annals Phys. **299**, 174 (2002)
5. R. G. Leigh, Mod. Phys. Lett. A **4**, 2767 (1989).
6. G. W. Gibbons and K. Hashimoto, JHEP **0009**, 013 (2000)
7. M. Born and L. Infeld, Proc. Roy. Soc. Lond. A **144**, 425 (1934).
8. J. Hucks, J. Math. Phys. **34**, 5986 (1993).
9. C. W. Misner, K. S. Thorne and J. A. Wheeler, *Gravitation*, W. H. Freeman 1973
10. K. Yano and S. Ishihara, *Tangent and Cotangent Bundles*, Marcel Dekker New York 1973
11. K. Yano, *Differential Geometry on complex and almost complex spaces* vol. 49 Macmillan Intl. Series of monographs in pure and appl. math., New York 1965
12. H. E. Brandt, Found. Phys. Lett. **2**, 39 (1989).
13. E. R. Caianiello, Lett. Nuovo Cim. **32**, 65 (1981).
14. S. Tachibana and M. Okumura, Tohoku Math. Jour., **14**, 156-161 (1962)
15. F. P. Schuller, Phys. Lett. B **540**, 119 (2002)
16. V. V. Nesterenko, A. Feoli, G. Lambiase and G. Scarpetta, Phys. Rev. D **60**, 065001 (1999)
17. F. P. Schuller, M. Wohlfarth and T. Grimm, Class. Quant. Grav. **20**, 4269 (2003)

DIPLOMAS

Eighteen Diplomas were open for competition among the participants. They have been awarded as follows:

- John S. BELL Diploma to:

Ioannis PAPADIMITRIOU
Universiteit Van Amsterdam, The Netherlands

- Patrik M.S. BLACKETT Diploma to:

Wolfgang MENGES
DESY, Hamburg, Germany

- James CHADWICK Diploma to:

Sebastian SCHÄTZEL
DESY, Hamburg, Germany

- Paul A.M. DIRAC Diploma to:

Tomas SYKORA
Università degli Studi di Salerno, Italy

- Vladimir N. GRIBOV Diploma to:

Pierre GIOVANNANGELI
Centre de Physique Théorique, CNRS Luminy, Marseille, France

- Robert HOFSTADTER Diploma to:

Paul LAYCOCK
DESY, Hamburg, Germany

- Gunnar KÄLLEN Diploma to:

David GALLETTY
The University of Edinburgh, UK

- Giuseppe P.S. OCCHIALINI Diploma to:

Cristiano BOZZA
Università degli Studi di Salerno, Italy

- Bruno PONTECORVO Diploma to:
Anna Maria ROTUNNO
Università degli Studi di Bari, Italy
- Oreste PICCIONI Diploma to:
David d'ENTERRIA
Brookhaven National Laboratory, Upton, USA
- Isidor I. RABI Diploma to:
Olga SHEKHOVTSOVA
Kharkov Physics and Technology Institute, Kharkov, Ukraine
- Giulio RACAH Diploma to:
Stanislav KUPERSTEIN
Tel-Aviv-University, Tel-Aviv, Israel
- Bruno ROSSI Diploma to:
Alessandro CERRI
Lawrence Berkeley National Laboratory, Berkeley, USA
- Andreij D. SAKHAROV Diploma to:
Vyacheslav LYSOV
Institute for Theoretical and Experimental Physics (ITEP), Moscow, Russia
- Victor F. WEISSKOPE Diploma to:
Dmitri KROTOV
Institute for Theoretical and Experimental Physics (ITEP), Moscow, Russia
- Eugene P. WIGNER Diploma to:
Jorge CASALDERREY-SOLANA
State University of New York at Stony Brook, USA
- Biorn H. WIJK Diploma to:
Ivan NIKOLAEV
Budker Institute of Nuclear Physics, Novosibirsk, Russia
- Chien Shiung WU Diploma to:
Andrea DAINES
CERN, Geneva, Switzerland

AWARDS

The Award for the best “New Talents”-“Speaker” is divided into three parts:

- i) for the best theoretical presentation:

Michaela OSWALD

Brookhaven National Laboratory, Upton, USA

- ii) for the best experimental presentation, to:

Gilda SCIOLI

Università degli Studi di Bologna, Italy

- iii) for the original work, to:

A) Ben M. GRIPAIOS

Oxford University, UK

Motivation:

For a novel derivation of the effective potential in supersymmetric gauge theories first proposed by Yankielowicz and Veneziano.

for the original work, to:

B) Frederic Paul SCHULLER

University of Cambridge, UK

Motivation:

For original work exploring the consequences of relativistic kinematics with an invariant acceleration scale as might be expected from D-brane physics.

for the original experimental work, to:

C) Victor LENDERMANN

DESY, Hamburg, Germany

Motivation:

For proposing a method to measure the proton structure function at low resolving scales, in QED Compton scattering, otherwise used for luminosity calibration in e-p interactions.

- Award for BEST SCIENTIFIC SECRETARY given to:

Mikhail ROTAEV

Institute for Theoretical and Experimental Physics (ITEP), Moscow, Russia

- Award for BEST STUDENT given to:

David SKINNER

Oxford University, UK

This page intentionally left blank

PARTICIPANTS

Marco ALBERICI Italy	Dipartimento di Fisica Università degli Studi Via Irnerio 46 – 40126 BOLOGNA, Italy
Ignatios ANTONIADIS Greece	Centre de Physique Théorique Ecole Polytechnique 48 route de Saclay F-91128 PALAISEAU, France
Halina ABRAMOWICZ Israel	Faculty of Exact Sciences Tel Aviv University Ramat Aviv - 69978 TEL AVIV, Israel
Roberto BALBINOT Italy	Dipartimento di Fisica Università degli Studi Via Irnerio 46 – 40126 BOLOGNA, Italy
Rinaldo BALDINI Italy	Enrico Fermi Centre Via Panisperna, 89/A 00184 ROMA, Italy
Anton BAUSHEV Russia	Space Research Institute 84/32 Profsoyuznaya Street RU-117997 MOSCOW, Russia
Giampaolo BEI Italy	Dipartimento di Fisica Università degli Studi Piazzale Aldo Moro, 5 – 00183 ROMA
Alessandro BETTINI Italy	Dipartimento di Fisica Università degli Studi Via Marzolo 8 – 35131 PADOVA, Italy
Aleksei BOGDANOV Russia	Dept. of Physics Moscow Engineering Physics Institute Kashirskoe Shosse 32 RU-115409 Moscow, Russia
Cristiano BOZZA Italy	Dipartimento di Fisica “E.R. Caianiello” Università di degli Studi Via S. Allende 84081 BARONISSI (Salerno), Italy
Fabrizio CANFORA Italy	Dipartimento di Fisica “E.R. Caianiello” Università di degli Studi Via S. Allende 84081 BARONISSI (Salerno), Italy
Riccardo CAPRA Italy	Istituto di Scienze Fisiche Università degli Studi Via Dodecaneso 33 16146 GENOVA, Italy

Marco CARIGLIA Italy	DAMPT, CMS - University of Cambridge Wilberforce Road CAMBRIDGE, CB3 OWA, UK
Jorge CASALDERREY-SOLANA Spain	Department of Physics and Astronomy State University of New York at Stony Brook STONY BROOK, NY 11794, USA
Alessandro CERRI Italy	Lawrence Berkeley National Laboratory 1 Cyclotron Road BERKELEY, CA 94720, USA
Luisa CIFARELLI Italy	Dipartimento di Fisica Università degli Studi Via Irnerio 46 – 40126 BOLOGNA, Italy
Andrea DAINESI Italy	PH Division – CERN CH-1211 GENEVE 23, Switzerland Dipartimento di Fisica “G. Galilei” Via Marzolo 8 – 35131 PADOVA, Italy
Richard Henry DALITZ UK	Department of Theoretical Physics University of Oxford 1 Keble Road - OXFORD, OX1 3NP, UK
Abilio DE FREITAS Venezuela	Theory Group DESY Platanenallee 6 D-15738 ZEUTHEN, Germany
Michel GOURDIN France	Laboratoire de Physique Théorique et Hautes Énergies Université Pierre et Marie Curie 4 Place Jussieu F-75252 PARIS Cedex 05, France
David d'ENTERRIA Spain	Physics Department Brookhaven National Laboratory UPTON, NY 11973-5000, USA
Vyacheslav DIDENKO Russia	Lebedev Institute P.N. Lebedev Institute of Physics - FIAN Leninsky Prospect 53 RU-117924 MOSCOW, Russia
Robbert H. DIJKGRAAF The Netherlands	Korteweg-de Vries Institute for Mathematics Universiteit van Amsterdam Plantage Muidergracht 24 1018 TV AMSTERDAM, The Netherlands
Michael James DUFF USA	Michigan Center for Theoretical Physics Department of Physics University of Michigan ANN ARBOR, MI 48109-1120, USA

Bruno DURIN
France

LPTHE, Université Paris 6
4 Place Jussieu
F-75252 PARIS Cedex 05, France

Gianluigi FOGLI
Italy

Sezione INFN di Bari
Università degli Studi
Via Orabona 4 - 70126 BARI, Italy

Harald FRITZSCH
Germany

Sektion Physik
Ludwig-Maximilians-Universität München
Theresienstrasse 37A
D-80333 MÜNCHEN, Germany

David GALLETTY
UK

Department of Physics and Astronomy
The University of Edinburgh
EDINBURGH, EH4 3JZ, UK

Marco GARBINI
Italy

Dipartimento di Fisica
Università degli Studi
Via Irnerio 46 - 40126 BOLOGNA, Italy

Marcello GIORGI
Italy

Università di Pisa & INFN
Viale Buonarroti 2
56100 PISA, Italy

Pierre GIOVANNANGELI
France

Centre de Physique Théorique
CNRS Luminy
F-13288 MARSEILLE Cedex 9, France

Ben M. GRIPAIOS
UK

Department of Physics
Theoretical Physics, Oxford University
I, Keble Road – OXFORD, OX1 3NP, UK

Alan Harvey GUTH
USA

Centre for Theoretical Physics
Department of Physics
Massachusetts Institute of Technology
77 Massachusetts Avenue
CAMBRIDGE, MA 02139-4307, USA

Andrew HAMILTON
Canada

FERMILAB
Mail Station 318
P.O. Box 500
BATAVIA, IL 60510-0500, USA

Dieter HAIDT
Germany

EPJC - DESY
Notkestrasse 85
D-22607 HAMBURG, Germany

Francesco IACHELLO
Italy

Center for Theoretical Physics
Sloane Physics Laboratory
Yale University
217 Prospect Street - P.O. Box 208120
NEW HAVEN, CT 06520-8120, USA

Frithjof KARSCH Germany	Fakultät für Physik Universität Bielefeld Universitätsstrasse 25 D-33615 BIELEFELD, Germany
Richard D. KENWAY UK	School of Physics and Astronomy The University of Edinburgh The King's Buildings EDINBURGH, EH9 3JZ, Scotland, UK
Dong Hyun KIM South Korea	PH Division CERN CH-1211 GENEVE 23, Switzerland
Edward W. KOLB USA	Department of Theoretical Astrophysics, Fermi National Accelerator Laboratory P.O. Box 500 BATAVIA, IL 60510-0500, USA
Christian P. KORTHALS-ALTES The Netherlands	Centre de Physique Théorique CNRS-Luminy 163 avenue de Luminy F-13288 MARSEILLE Cedex 9, France
Dmitri KROTOV Russia	ITEP B. Cheremushkinskaya 25 RU-117259 MOSCOW, Russia
Stanislav KUPERSTEIN Israel	Department of Physics Tel-Aviv-University Ramat Aviv P.O. Box 39040 TEL AVIV, 69978, Israel
Paul LAYCOCK UK	DESY Notkestrasse 85 D-22607 HAMBURG, Germany
Victor LENDERMANN Germany	DESY Notkestrasse 85 D-22607 HAMBURG, Germany
Aharon LEVY Israel	School of Physics and Astronomy Tel Aviv University 69978 TEL AVIV, Israel
Lev N. LIPATOV Russia	Lab. de Physique Theorique et Hautes Energies Université Pierre et Marie Curie Tour 16, 1-er etage, 4 Place Jussieu F-75252 PARIS Cedex 05, France
Thomas W. LUDLAM USA	Brookhaven National Laboratory Physics Department, Building 510A P.O. Box 5000 - UPTON, NY 11973, USA

Vyacheslav LYSOV Ukraine	M. Physics Group ITEP B. Cheremushkinkaya 25 RU-117259 MOSCOW, Russia
Luciano MAIANI Italy	Director-General CERN 1211 Geneva 23, Switzerland
John (Yannis) MALAMOS Greece	Physics Department University of Athens, Panepistimiopolis, Ilissia ATHENS 15771, Greece
Vladimir MARKOV Russia	Theoretical Physics Department Petersburg Nuclear Physics Institute Orlova Roscha, Gatchina RU-188300 ST. PETERSBURG, Russia
Anna MASTROBERARDINO Italy	Dipartimento di Fisica Università della Calabria Campus di Arcavacata - Ponte Pietro Bucci 87036 ARCAVACATA DI RENDE, Italy
Wolfgang MENGES Germany	DESY Notkestrasse 85 D-22607 HAMBURG, Germany
Helenia Menghetti Italy	Dipartimento di Fisica Università degli Studi Via Irnerio 46 - 40126 BOLOGNA, Italy
Konstantin MIKHIN Russia	ITEP B. Cheremushkinkaya 25 RU-117259 MOSCOW, Russia
Alessandro MIRIZZI Italy	Dipartimento Interateneo di Fisica Università degli Studi – Politecnico di Bari Via Amendola 173 – 70126 BARI, Italy
Dominik NICKEL German	Institut für Kernphysik Schloßgartenstrasse 9 D-64289 DARMSTADT, Germany
Ivan NIKOLAEV Russia	Budker Institute of Nuclear Physics Academy of Sciences 11 Lavrentyev Ave. RU-630090 NOVOSIBIRSK 90, Russia
Francesco NOFERINI Italy	Dipartimento di Fisica Università degli Studi Via Irnerio 46 – 40126 BOLOGNA, Italy
James O'DWYER UK	Trinity College CAMBRIDGE CB2 1TQ, UK

Michaela OSWALD Austria	Department of Physics Brookhaven National Laboratory UPTON, 11973-5000 NY, USA
Polina OTIOUGOVA Russia	PH Division CERN CH-1211 GENEVE 23, Switzerland
Ioannis PAPADIMITRIOU Greece	Institute for Theoretical Physics Universiteit Van Amsterdam Valckenierstraat 65 1018 XE, AMSTERDAM, The Netherlands
Stephen PARKE USA	Theoretical Physics Department Fermi National Accelerator Laboratory, P.O. Box 500 BATAVIA, IL 60510-0500, USA
Agostino PATELLA Italy	Scuola Normale Superiore Piazza dei Cavalieri - 56100 PISA, Italy
James PINFOLD Canada	Department of Physics Director of the Centre for Subatomic Research University of Alberta EDMONTON, Alberta T6G 2N5, Canada
Martin POGHOSYAN Armenia	Physics Department Yerevan State University 1 A. Manukian Street AM-375 049 YEREVAN 36, Armenia
Roberto PREGHENELLA Italy	Dipartimento di Fisica Università degli Studi Via Irnerio 46 - 40126 BOLOGNA, Italy
Mauro RAGGI Italy	Dipartimento di Fisica Università degli Studi Via A. Pascoli - 06126 PERUGIA, Italy
Verónica RIQUER Mexico	Theory Division CERN CH-1211 GENEVE 23, Switzerland
Oana RISTEA Romania	Department of Atomic and Nuclear Physics University of Bucharest P.O. Box MG-11 76900 BUCUREST-MAGURELE, Romania
Catalin Lucian RISTEA Romania	Department of Atomic and Nuclear Physics University of Bucharest P.O. Box MG-11 76900 BUCUREST-MAGURELE, Romania

Mikhail ROTAEV
Russia

ITEP
M Physics Group
B. Cheremushkinskaya 25
RU-117259 MOSCOW, Russia

Anna Maria ROTUNNO
Italy

Dipartimento Interateneo di Fisica
Università degli Studi – Politecnico di Bari
Via Amendola 173 – 70126 BARI, Italy

Dmitriy RUSINOV
Russia

ITEP
B. Cheremushkinkaya 25
RU-117259 MOSCOW, Russia

Fabio SCARDIGLI
Italy

Institut für Theoretische Physik
Freie Universität Berlin
Arnimallee 14
D-14195 BERLIN, Germany

Sebastian SCHÄTZEL
German

DESY
Notkestrasse 85
D-22607 HAMBURG, Germany

Wolf-Dieter SCHLATTER
Germany

PH Division
CERN
CH-1211 GENEVE 23, Switzerland

Frederic Paul SCHULLER
Germany

DAMPT - University of Cambridge
Wilberforce Road
CAMBRIDGE, CB3 OWA, UK

Gilda SCIOLI
Italy

Dipartimento di Fisica
Università degli Studi
Via Irnerio 46 - 40126 BOLOGNA, Italy

Olga SHEKHOVTSOVA
Ukraine

Kharkov Physics and Technology Institute
Akademicheskaya st. 1
61108 KHARKOV, Ukraine

David SKINNER
UK

Department of Theoretical Physics
Oxford University
1 Keble Road - OXFORD OX1 3NP, UK

Tomas SYKORA
Czech

Dipartimento di Fisica "E.R. Caianiello"
Università di degli Studi
Via S. Allende
84081 BARONISSI (Salerno), Italy

Gerardus 't HOOFT
The Netherlands

Department of Theoretical Physics
Spinoza Institute - Utrecht University
NL-3508 TD UTRECHT, The Netherlands

Samuel Chao Chung TING
China

Laboratory for Nuclear Science
Massachusetts Institute of Technology
Vassar Street
CAMBRIDGE, MA 02139, USA

Wei-yuan TING
Canada

Centre for Subatomic Research
University of Alberta
EDMONTON, Alberta T6G 0V1, Canada

Enrico TRINCERINI
Italy

Dipartimento di Fisica
Università degli Studi di Milano "Bicocca"
Piazza delle Science 3 – 20100 MILANO

Alessandro TRONCONI
Italy

Dipartimento di Fisica
Università degli Studi
Via Irnerio 46 - 40126 BOLOGNA, Italy

Kirill VOLOSHIN
Russian

ITEP
B. Cheremushkinkaya 25
RU-117259 MOSCOW, Russia

Gunther WOLF
Germany

DESY
Notkestrasse 85
D-22607 HAMBURG, Germany

Chiara ZAMPOLLI
Italy

Dipartimento di Fisica
Università degli Studi
Via Irnerio 46 – 40126 BOLOGNA, Italy

Yufeng ZHOU
China

Sektion Physik
Ludwig-Maximilians-Universität München
Theresienstrasse 37
D-80333 MÜNCHEN, Germany

Antonino ZICHICHI
Italy

CERN
CH-1211 GENEVA 23, Switzerland
Dipartimento di Fisica
Università di Bologna
Via Irnerio 46 – 40126 BOLOGNA, Italy